Universitat Politècnica de Catalunya
Escola Tècnica Superior d'Enginyers
de Camins, Canals i Ports

Departament de Resisténcia de Materials
i Estructures a l'Enginyeria

GEOMETRIC AND CONSTITUTIVE NONLINEAR DYNAMIC ANALYSIS OF BEAM STRUCTURES WITH LOCAL IRREGULARITIES

Doctoral Thesis

Pablo Liver Mata Almonacid

Advisors:

Dr. **Alex H. Barbat**

Dr. **Sergio Oller M**

Barcelona, March, 2008.

ACTA DE QUALIFICACI DE LA TESI DOCTORAL

Reunit el tribunal integrat pels sota signants per jutjar la tesi doctoral:

Ttol de la tesi: Geometric and Constitutive Nonlinear Dynamic Analysis of Beam Structures with Local Irregularities

Autor de la tesi: Pablo Liver Mata Almonacid

Acorda atorgar la qualificaci de:

- ☐ No apte
- ☐ Aprovat
- ☐ Notable
- ☐ Excel·lent
- ☐ Excel·lent Cum Laude

Barcelona, ... de/d' ..... de .....

El President | El Secretari

..... (nom i cognoms) | ..... (nom i cognoms)

El vocal | El vocal | El vocal

..... (nom i cognoms) | ..... (nom i cognoms) | ..... (nom i cognoms)

Dedico este trabajo a la memoria

de mi abuela,

la señora Petronila Mansilla Hernandez.

Agradecimientos

Primeramente, deseo expresar mi más sincero agradecimiento a mis directores de tesis, los profesores Alex Barbat y Sergio Oller por sus invaluables contribuciones en mi proceso de formación como investigador, la permanente orientación, guía y paciencia durante el desarrollo de este trabajo; y por facilitar el soporte necesario poder dedicarme a las actividades de investigación con tranquilidad.
Seguidamente, deseo agradecer a mis padres Sonia Almonacid y Victor Mata por brindarme su incondicional apoyo, confianza y preocupación durante todo este tiempo. También deseo agradecer a todas las demás personas, tanto del entorno de la Universidad como de otros ámbitos, que me han dado su amistad y afecto de manera desinteresada a lo largo de estos años.
Finalmente, deseo agradecer el apoyo proporcionado por el Centro Internacional para Métodos Numéricos en Ingeniería, CIMNE, que a proporcionado todo tipo de medios materiales y humanos, además de un entorno motivante, para llevar a cabo esta investigación[1].

[1]Particularmente, deseo agradecer la financiación obtenida a partir de los proyectos:
European Integrated Project CEE–FP6-50544(GOCE) *Risk Mitigation for Earthquakes and Landslides* (LESS-LOSS); Ministerio de Educación y Ciencia de España, Project REN2002-03365/RIES *Development and application of advanced approaches for the evaluation of the seismic vulnerability and risk of structures* (EVASIS), Project BIA2003-08700-C03-02 *Numerical simulation of the seismic behavior of structures with energy dissipation devices.*

Abstract

In this work a formulation for rod structures able to consider coupled geometric and constitutive sources of nonlinearity in both the static and the dynamic range is developed. Additionally, it is extended for allowing the inclusion of passive energy dissipating elements as a special rod element and geometric irregularities as a full three-dimensional body connected to the framed structure by means of a two-scale model.

The proposed formulation is based on the Reissner-Simo geometrically exact formulation for rods considering an initially curved reference configuration and extended to include arbitrary distribution of composite materials in the cross sections. Each material point of the cross section is assumed to be composed of several simple materials with their own thermodynamically consistent constitutive laws. The simple mixing rule is used for treating the resulting composite. Cross sections are meshed into a grid of quadrilaterals, each of them corresponding to a fiber directed along the axis of the beam. A mesh independent response is obtained by means of the regularization of the energy dissipated at constitutive level considering the characteristic length of the mesh and the fracture energy of the materials. Local and global damage indices have been developed based on the ratio between the visco elastic and nonlinear stresses.

The consistent linearization of the weak form of the momentum balance equations is performed considering the effects of rate dependent inelasticity. Due to the fact that the deformation map belongs to a nonlinear manifold, an appropriated version of Newmark's scheme and of the iterative updating procedure of the involved variables is developed. The space discretization of the linearized problem is performed using the standard Galerkin finite element approach. A Newton-Raphson type of iterative scheme is used for the step-by-step solution of the discrete problem.

A specific element for energy dissipating devices is developed, based on the rod model but releasing the rotational degrees of freedom. Appropriated constitutive relations are given for a wide variety of possible dissipative mechanisms.

A two–scale, global and local, approach is used for considering local geometric irregularities. At global scale level, all the elements of the model are prismatic rods. For the geometric irregularity, an amplified view of the corresponding element is carried out, constructing a fully three-dimensional model which constitutes the local scale level. The dimensional–coupling between scales is performed through surface–interfaces. An iterative Newton–Raphson scheme which considers the interaction between scales is developed even in the nonlinear dynamic range.

Several numerical examples have been included for the validation of the proposed formulation. The examples include elastic and inelastic finite deformation response of framed structures with initially straight and curved beams. Comparisons with existing literature is performed for the case of plasticity and new results are presented for degrading and composite materials. Those examples show how the present formulation is able to capture different complex mechanical phenomena such as the uncoupling of the dynamic response from resonance due to inelastic incursions and suppression of the high frequency content. The study of realistic flexible pre-cast and cast in place reinforced concrete framed structures subjected to static and dynamic actions is also carried out. Detailed studies regarding to the evolution of local damage indices, energy dissipation and ductility demands are presented. The studies include the seismic response of concrete structures with energy dissipating devices. Advantages of the use of passive control are verified. Finally, examples showing the capabilities of the developed two–scale approach in predicting the elastic and inelastic dynamic responses of structures with local irregularities are included.

Table of Contents

List of Figures

List of Tables

Chapter 1

Introduction

The three dimensional nonlinear analysis of rod structures has captured the interest of many researchers and practitioners during the past decades and currently it still constitutes a very active branch of research in structural analysis [81]. In the case of civil engineering structures and some flexible mechanical components, *reduced* or one–dimensional (1D) formulations for structural elements appear as a solution combining both, numerical precision and reasonable computational costs [258, 260] when compared with fully three-dimensional (3D) descriptions of the structures.

Many contributions have been focused on the formulation of geometrically consistent models of beams undergoing large displacements and rotations, but considering that the material behavior remains elastic and, therefore, employing simplified linear constitutive relations in terms of cross sectional forces and moments [299, 174]. Most of the recent works in this field invoke the formulation and the numerical implementation proposed Simo *et al.* [362, 363, 365], which generalize to the three-dimensional dynamic case, by means of an appropriated parametrization of the rotational part of the kinematics, the formulation originally developed by Reissner [333, 332]. This formulation employs a *director type* approach in describing the configuration of the beam cross sections during the motion, considering finite shearing and finite extension, as described by Antman in Ref. [11]. The so called Reissner–Simo geometrically exact rod theory consider a straight and unstressed rod as reference configuration and the hypothesis of plane cross sections. The resulting deformation map can be identified with elements belonging to the differential manifold obtained from the *rotation group* $SO(3)$ and the canonical vector space $\mathbb{R}^3$. Posteriorly, other authors have contributed in different manners to the enrichment of the finite deformation theory of rods and also have applied it in a wide number of fields[1]; in this sense it is possible to quote [89, 178, 187, 207, 198, 388] among many others.

On the contrary, constitutive nonlinearity in numerical models for beam structures has been described by means of *concentrated* and *distributed* models, both of them formulated, in the most cases, for small strain and small displacement kinematics hypothesis. In the first case, inelasticity in a beam element is concentrated in springs located at the ends of a linear elastic element [354]. Among the most common drawbacks in concentrated plasticity models, one has to considers that transversal force-moment interaction is ignored. Moreover, the cross sectional properties of the rod elements require a calibration based on experiments and usually the range of application of the obtained constitutive relations is rather limited due to the fact that specific hysteretic rules have to be defined for each type of cross section. If a new cross sectional shape or reinforcement configuration is employed in a structure, additional hysteretic models have to be

[1] A more complete review of the state of the art in the topics here mentioned is given in §2 of the present work.

provided. In the second case, distributed models alow to spread the inelastic behavior along the element, evaluating the constitutive equations at a fixed number of cross sections along the rod's axis. Further enhancement in the analysis of the mechanical response of structures is obtained considering inhomogeneous distributions of materials on arbitrarily shaped cross sections [113]. In this case, the procedure consists into obtaining the constitutive relationship at cross sectional level by means of integrating on a selected number of points corresponding to *fibers* directed along the beam's axis [390]. Thus, the mechanical behavior of beams with complex combinations of materials can be simulated [36]. The employment of fibers allows predicting a more realistic strain-stress state at the cross sectional level, but it requires the definition of uniaxial constitutive laws for each material point. In most cases, both types of models, the concentrated and the distributed ones, have been formulated under the hypothesis of infinitesimal deformation and commonly, inelasticity in the fibers is restricted to the component of the stress tensor acting perpendicular to the cross section; maintaining the other components (shear stresses) in the elastic range. Moreover, the thermodynamical basis of the constitutive equations are usually ignored [36]. In general, when materials with softening are considered, the numerical solutions are affected by strain localization. A technique based on the regularization of the energy dissipated at any material point [258] ensures that the whole structural response remains objective, but the length of the zone where softening occurs is still mesh dependent. Other approaches based on the use of strong discontinuities at a micro-scale have been recently considered [25]. Only a few works have been carried out using fully geometric and constitutive nonlinear formulations for beams, but they have been mainly focused on perfect plasticity [347, 361] and on the static analysis of the structures [151].

An important effort has been devoted to develop time–stepping schemes for the integration of the nonlinear dynamic equations of motion involving finite rotations. The main difficulty arises in the fact that the deformation map takes values in the differentiable manifold $S0(3) \times \mathbb{R}^3$ and not in a linear space, as it is the case in classical dynamics. An *implicit* time–stepping algorithm is developed in Ref. [365] extending the classical Newmark's scheme to $S0(3)$, obtaining a formulation similar to that of the linear case. In the same work, the consistent linearization of the weak form of the balance equations yields to a tangential inertia tensor, nonsymmetric in the rotational components. Again, additional research have been carried out by a number of authors in this field *e.g.* [183, 245, 244].

Newmark's family of implicit schemes fails to preserve certain conservation laws of the motion, such as the total energy and momentum of nonlinear *Hamiltonian systems*, producing numerical (fictitious) dissipation [82, 371]. A further improvement in the development of robust time–stepping schemes is provided by the *energy-momentum conserving* algorithms [372]. These algorithms have been extended to the rotation group by Simo *et al.* in Ref. [373] and applied to the nonlinear dynamic problems of rods, shells and rigid bodies. The attention recently captured by these methods rely on the potential applications and the algorithmic stability gained with them. For example, a list of representative works could be [23, 21, 46, 182, 189, 340] (see also §2.1.3).

More recently, attention have been turned towards *variational integrators i.e.* algorithms formed from a discrete version of Hamilton's variational principle [226]. For conservative systems usual variational principles of mechanics are used, while for dissipative or forced systems, the *Lagrange-d'Alembert* principle is preferred. The main properties that make them attractive are: for the conservative case they are *symplectic* [252] and momentum conserving and permit the systematic construction of higher order integrators with remarkably good energy behavior. A summary can be found in [227, 253, 254]. At the author's knowledge, this type of methods have not been formally applied to the present rod theory.

The above topics about nonlinear problems in rod theories can be seen as *free of local irregularities* in the sense explained in the following section.

Local irregularities

On one hand, modern practice in engineering permits designing structures for forces lower than those expected from the elastic response on the premise that the structural design assures significant energy dissipation potential and, therefore, the survival of the structures when subjected to severe accidental loads such as those derived from earthquakes [161]. Frequently, the dissipative zones are located near the beam–column joints and, due to cyclic inelastic incursions, some structural members can suffer a great amount of damage. A limited level of structural damage dissipates part of the energy induced by earthquakes and uncouples the dynamic response from resonance offering a certain protection [260], however, the large displacements can also increase the second order effects such as the so called P–Δ effect in seismic engineering. Moreover, these deformations can produce irreparable damage in those members.
Additionally, in the last decades new concepts for the design of building, based on the manipulation of the energy dissipation, have improved the behavior of the structures providing higher levels of safety for the occupants and the buildings. The new techniques are based on adding devices to the buildings with the main objective of dissipating the energy demand imposed by the dynamic actions alleviating the ductility demand on primary structural elements and decreasing the dynamic response [161, 382]. The devices can be installed in new or in existing structures and can be used in seismic design or rehabilitation. The purpose is to *control* the dynamics response of the buildings by means of a set of dissipating devices which constitutes the *control system*, adequately located in the structure.
In general, control systems can be classified in four groups detailed in §2.3.1. However, in this work attention is focused on *passive energy dissipating devices* (EDDs) which is a well understood technique and its use is widely accepted by the engineering community. EDDs are devices located throughout the structure to absorb and dissipate an important part of the energy input induced in the structure by earthquakes or other dynamic actions (see Fig. 1.1a). EDDs are considered as a local irregularity due to the fact that energy dissipation has place on a specific point in the element and the dissipative characteristic are designed in a manner that it permits to improve the global dynamics of the whole structure.

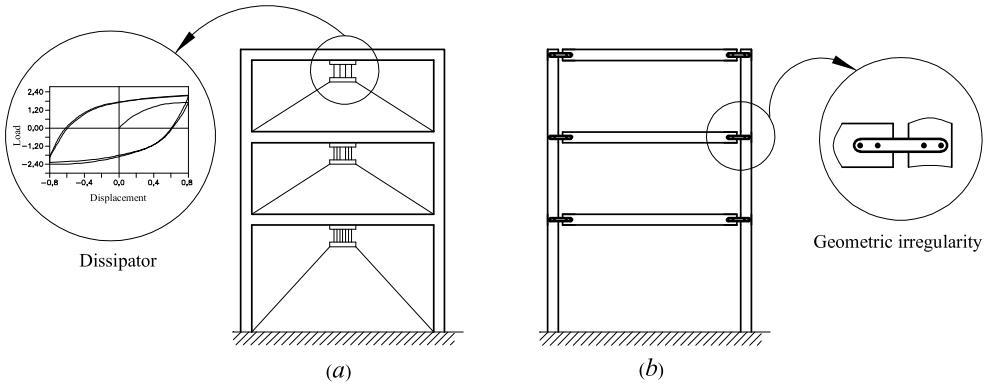

Figure 1.1: Local irregularities. (a): Energy dissipating devices added as diagonal elements to the bare frame. (b): Geometric irregularity constituted by the non-monolithic connecting joint.

On the other hand, fully 3D numerical technics provide the most precise tools for the simula-

tion of the nonlinear behavior of RC buildings, although the computing time required for real structures makes their applications unpractical. Considering that a great part of the elements in buildings are prismatic, one–dimensional formulations appear as a solution combining both, numerical precision and reasonable computational costs [258, 260]. However, in spite of the fact that a great amount of work has been devoted to the development of refined nonlinear models for beam structures, almost (if not all) of them are subjected to the following limitations: (i) beam structures present either fully monolithic connections among elements [200]. Therefore, structural failures due to damage inside of the nodes, such as those occurred in poorly designed RC buildings [54, 55] or in the so called *semi–rigid* connections of steel structures [17], often are not properly considered. (ii) The shape and the mechanical properties of the cross sections present smooth variations along an element and, therefore, they show serious difficulties in reproducing structural behaviors dominated by *local changes* in the geometry *e.g.* those in the connecting joints of precast structures [315, 316], (see Fig. 1.1*b*).
Some authors model the effects of local irregularities employing plastic hinge models reflecting the mechanical characteristics of the connecting joints [221], although this approach has the previously described limitations. An alternative approach, combining precision, generality and computational efficiency consists of coupling reduced 1D and full 3D numerical models for different parts of the structure. The connection between models of different dimensions is done through *interface–surfaces*. Some research in this direction have been carried out by in *et al.* [158, 280, 359, 358] among others.

1.1 Problem statement

In Summary, a modern numerical approach to the structural analysis and design of three-dimensional rod–like engineering structures should take into account the following aspects:

(i) *Geometric nonlinearity.* Changes in the configuration of rod–like in structures (and flexible mechanisms) due to the action of static and/or dynamic actions produces additional stress fields which should be considered in a coupled manner with

(ii) *Constitutive nonlinearity.* In this case, inhomogeneous distribution of inelastic materials can appear in many structures. The obtention of the reduced cross sectional forces and moments as well as the estimation of the dissipated energy should be considered in a manner consistent with the thermodynamic basis of the constitutive theory. The success in determining the energy dissipation for softening structures constitutes an excellent point of departure for the application of

(iii) *Modern control techniques*, which allows to improve the dynamic response of structures by means of the strategic incorporation of devices contributing to the control of displacements and to the alleviation of the ductility demand on primary structural elements.

(iv) *Geometric irregularities.* In the case that geometric irregularities in framed structures are detected it should be desirable to have an appropriated and efficient numerical tool able to determine their effects on the global structural response.

At the author's knowledge the present state of the art in rod analysis have provided a set of partial solutions to the above mentioned requirements, however, there is not an unified approach covering all the aspects in a manner consistent with the principles of the continuum mechanics. The following list addresses in a summarized manner (see §2 for a more complete survey) the main lacks and drawbacks in the existing developments:

(i) Finite deformation models for rod–like structures, particularly the geometrically exact ones, even when are highly sophisticated and strongly founded formulations, in most of the cases have been restricted to the elastic case or when they consider inelasticity it corresponds to plasticity in the static case.

(ii) Most of the formulations for considering inelasticity in rods are developed under the small strain assumption, constitutive laws are valid for specific geometries of the cross sections or the thermodynamical basis of the constitutive theories are violated; limiting severely the possibility of obtaining good characterizations of the mechanical properties of the structures in the nonlinear dynamic range.

(iii) Several research and commercial codes have included special elements for EDDs, however, the obtained formulations inherit the drawbacks of points (i) and (ii) of the present list.

(iv) In general, a not too much large list of works can be said to be advocated to the numerical treatment of geometric irregularities in a manner consistent with the continuum mechanics. The references provided in §2.3.2 permit to affirm that most of the works are restricted to the static and elastic analysis of problems under infinitesimal deformation.

Taking into account the above list the following section presents the objectives of the present work, which tries to be a contribution to the improvement of those aspects in a unified form consistent with the laws of the continuum mechanics and oriented to the obtention of a software package able to be applied in practical (realistic) cases of study.

1.2 Objectives

The main purpose of this thesis consists in developing a formulation for rod structures able to consider in a coupled manner geometric and constitutive sources of nonlinearity in both static and dynamic range. Additionally, the same formulation must be extended for allowing the inclusion of passive energy dissipating elements as a special case of rods and geometric irregularities as a full three-dimensional body connected to the framed structure.
To this end, the initially curved and twisted version of the Reissner–Simo geometrically exact formulation for rods is expanded to consider an inhomogeneous distribution of inelastic, probably rate dependent, composite materials on arbitrarily shaped, but planar[2], cross sections. Constitutive laws for the materials should be developed consistently with the kinematics of the rod model and with the thermodynamical laws[3]. A particular case of this model for rods is considered for the development of specific elements representing energy dissipating devices. Additionally, if local geometric irregularities appear in the structure, a two–scale approach (global and local) is developed in order to study the nonlinear response of RC framed buildings. At global scale level, all the elements of the finite element model are rods; however, if (locally) geometric irregularities appear, a *zoom view* of the corresponding element is performed, consisting in a fully 3D model which constitutes the local scale level. The dimensional–coupling between scales is performed through *surface–interfaces* imposing the kinematic hypothesis assumed for the beam model.
In this sense, the following list of objectives can be defined according to their nature:

(i) **Theoretical objectives**

[2]Cross sectional warping is not considered, avoiding to include additional warping variables in the formulation or iterative procedures for recovering the corrected cross sectional strain and stress fields.

[3]This aspect can be exceptionally important in procedures currently applied in the earthquake resistant design of structures.

(i.1) To preform a deep study and theoretical analysis of the continuum based theory of rods under the Reissner–Simo hypothesis.

(i.2) To deduce explicit expressions for the strain measure and for the objective measure of the strain rate acting on each material point of the cross section, in terms of the variables defining the deformation map, its derivatives and the geometry of the beam cross section.

(i.3) Based on (i.1) develop rate dependent and independent inelastic constitutive laws for simple materials lying on points on the cross sections in terms of the First Piola Kirchhoff stress tensor and the corresponding energetically conjugated strain measure. The developed laws have to be consistent with the kinematics of the rod model and the laws of the thermodynamics, and allow to describe plastic deformations and damage.

(i.4) To include several simple materials as the components of a *composite* associated to a point of the cross section. To this end, an appropriated version of the *mixing theory* for composites has to be deduced for the case of the present rod theory.

(i.5) To develop explicit expressions for the stress resultant and stress couples which consider inelasticity.

(i.6) To propose local and global *damage indices* able to describe the evolution of the remaining load carrying capacity of complex structures.

(i.7) To carry out the consistent linearization of the weak form of the balance equations including the effects of the rate dependent inelasticity existing at material point level considering both, the spatial and material updating rules for the rotational field (see §A). In this way, the corresponding rate dependent and independent parts of the tangential stiffness should be deduced and added to the loading and geometric terms.

(i.8) To develop a specific rod element adapted for modeling the mechanical behavior of energy dissipating devices incorporated to the full geometric and constitutive rod theory.

(i.9) To provide appropriated one–dimensional force-displacement and/or moment-curvature relations for the description of the nonlinear hysteretic behavior of EDDs.

(i.10) To develop an appropriated theoretical framework for the construction of a two–scale model of rod structures with local geometric irregularities. To this end, the formal definition of the scales of the problem as well the hypothesis for the interaction between them have to be provided.

(ii) **Numerical objectives**

(ii.1) To provide numerical algorithms for the integration of the constitutive laws developed for simple materials as well as for the obtention of the mechanical behavior of composites.

(ii.2) To perform the time discretization according to the Newmark's method of the linearized problem defined in (i.7). Newmark's scheme has been preferred due to the fact that the present study is focused on dissipative structures and its implementation in a standard finite element code is rather straightforward. Additionally, considering that the key idea in numerics is to implement the solution procedure in an iterative Newton–Raphson scheme, iterative updating procedures, consistent with the nonlinear nature of the manifold $\mathbb{R}^3 \times SO(3)$, have to be developed for the strain and strain rate measures defined in (i.2).

(ii.3) In the category of an additional proposal, some theoretical development about the application of variational integrators for the time discretization of the action integral of the system is presented.

(ii.4) To develop an appropriated cross sectional analysis, based on the fiber discretization of the cross sections. Each fiber must has associated a composite (probably with one or more inelastic components) material. The calculation of the damage indices at material point and cross sectional level should also developed at this stage. Moreover, the procedure for obtaining the cross sectional tangential stiffness should be provided.

(ii.5) To perform the discretization in space of the linearized problem using the *Galerkin* finite element interpolation of the deformation variables and their linearized forms. Both, spatial and material updating rule for rotations should be analyzed.

(ii.6) To provide the explicit expression for the iterative Newton–Raphson scheme which includes the cross sectional analysis and the Newmark's updating scheme for the dynamic variables.

(ii.7) To develop an integration algorithm for the constitutive relation assigned to the energy dissipating devices and a method for obtaining the total force or the total moment in the devices for a given strain field.

(ii.8) To implement the numerical coupling between scales for the two–scale approach developed, for the case when local geometric irregularities are present. Starting from the full 3D stress state existing in the local model, cross sectional forces and moments, required at global level, should be recovered by integrating at the surface–interface in an analogous manner as for the cross sectional analysis of beams.

(ii.9) To develop an iterative Newton–Raphson scheme based on the displacement method, which considers the interaction between scales to obtain the response at global level even in the nonlinear dynamic range. The tangential stiffness of the local model should be obtained numerically applying the perturbation method and obtaining the corresponding reaction forces reduced to the degree of freedom of the global level.

(ii.10) To implement (computationally) a parallelized version of the *master–slave* approach for managing the two–scale problem, where the global scale problem acts as the master, sending a *trial* displacement field to the local scale models (slaves) and then receives the corresponding internal forces and tangential tensors. The iterative process is finished when the global convergence is achieved. The communication between processes should be carried out by mean of an appropriated library of communication. In this way, minimal intervention on existing codes specific for beams and solids should be required.

(iii) **Practical objectives**

(iii.1) To validate the proposed formulation through a set of linear elastic numerical examples in the static and dynamic cases which are compared with results provided in existing literature.

(iii.2) To validate the proposed formulation throughout an extensive set of numerical examples (statics and dynamics) covering inelastic constitutive equations. The results should be compared with those provided in existing literature when possible.

(iii.3) To validate the obtention of a mesh independent response when materials presenting softening are considered.

(iii.4) To verify the ability of the proposed model for predicting the ultimate load, ductility and other relevant engineering parameters when compared with experimental tests on real structures.

(iii.5) To evaluate the ability of the proposed damage indices for predicting the load carrying capacity of structures.

(iii.6) To study the static and dynamic (even seismic) response of real two and three-dimensional reinforced concrete structures comparing the results obtained when full nonlinearity is not considered in the numerical simulations.
(iii.7) To study the possibility of improving the dynamic (seismic) response of real civil engineering structures by means of using energy dissipating devices.
(iii.8) To study the nonlinear static and dynamic response of precast concrete structures including EDDs.
(iii.9) To investigate the nonlinear static and dynamic response of a precast concrete structure with non ductile connecting joints using the developed two–scale approach.

1.3 Layout

The organization of the present document is as follows:
Chapter 2 is regarded to perform a state of the art review in nonlinear analysis of rod–like structures. Section 2.1 is dedicated to the formulations developed for the treatment of geometric nonlinearity; in §2.1.1, §2.1.2 and §2.1.3 material related to large rotations, research related to rod models and time–stepping schemes on the rotational manifold are reviewed. §2.2 is devoted to the constitutive nonlinearity in rod–like structures including §2.2.2 about cross sectional analysis. Section 2.3 is dedicated to local irregularities. The review of nonlinear methods for the determination of the response of engineering structures equipped with energy dissipating devices is performed in §2.3.1 including a characterization of the most commonly used types of devices. §2.3.2 is dedicated to the review of the approaches followed for the numerical treatment of local geometric irregularities.
Chapter 3 is devoted to the presentation of a geometrically exact formulation for rods capable of undergoing finite deformation based on that originally proposed by Reissner [333, 332] and Simo [362]. In Section 3.1 a detailed description of the kinematic of the model is carried out with special attention paid on the formal definition of the configuration and placement manifolds as well as their tangent spaces. In §3.2 to §3.3, after calculating the deformation gradient tensor, the strain and strain rate measures at both, material point and dimensionally reduced levels, are described along with the corresponding conjugated stress measures deduced using the power balance condition in §3.4. The rod's equations of motion are deduced starting from the local form of the linear and angular balance conditions. An appropriated (weak) form for numerical implementations is deduced in §3.5 and §3.6, for the nonlinear functional corresponding to the virtual work principle. Finally, hyperelastic cross sectional constitutive laws and load types are treated in §3.7 and §3.8, respectively.
Chapter 4 treats on constitutive nonlinearity. Section 4.1 provides the a general view of the approach followed for considering softening materials and strain localization in rod elements. Sections 4.2.2 to 4.2.3 are devoted to the development of specific damage and plasticity models for rods including viscosity which are formulated in terms of the material forms of the strain and stress vectors existing on the face of a given cross section. In §4.3 the mixing rule (in its parallel version) for composite materials is presented in a way such that it is able to be included for simulating arbitrary distributions of inelastic materials on the cross section. In §4.4 the explicit expressions for the calculation of the stress resultant and stress couples (cross sectional forces) are given along with the deduction of the corresponding cross sectional tangential stiffness which includes rate dependent effects. In §4.5 local and global damage indices able to estimate the remaining load carrying capacity of damaged structures are described.
Nonlinear problems in continuum mechanics are solved by linearizing an appropriated form of nonlinear equilibrium equations and iteratively solving the resulting linear systems. Chapter 5

is concerned with the linearization of the virtual work functional, in a manner consistent with the geometry of the configurational manifold. Formally, the linearization procedure is carried out using the directional derivative. In Section 5.1.1 some basic linear forms are calculated, in §5.1.2, §5.1.3 and §5.1.4 the consistent linearization of the strain, spin variables and strain rate measures is performed. Section 5.2 is devoted to the linearization of the stress resultant and couples considering rate dependent inelastic constitutive equations for composite materials. Finally, in §5.3 to §5.4 the consistent linearization of the virtual work functional is deduced, which yields to the consistent tangential tensors including rate dependent (viscous) and rate independent contributions. In all the cases, linearization is preformed considering both the material and the spatial rule for updating rotations.
Chapter 6 concerns with the presentation of a time–stepping scheme consistent with the kinematic assumptions made for the present rod model. In the case of the rotational part of the motion, explanations and new developments follow the procedures originally proposed by Simo and Vu-Quoc [365]. In Section 6.1 the formulation of the problem is presented along with the Newmark algorithm for rotational variables (§6.1.1), the iterative updating procedure for the configuration variables and their related kinematical objects (§6.1.2, §6.1.3) as well as the strain and strain rate measures §6.1.4 (§6.1.4.a – §6.1.4.d) are presented. Section 6.2 is dedicated to obtain the semi–discrete version of the linearized form of the virtual work principle. The (semi) discrete out of balance force terms are given in §6.2.1 and the discrete tangential stiffness are obtained in §6.2.2.a to §6.2.2.c. More modern energy-momentum conserving methods are reviewed in §6.4 in view of obtaining a dissipative scheme based on constitutive damping. Finally, in Section 6.5 the possibility of applying variational integrators obtained from the Hamilton principle for developing time–stepping schemes is explored.
Chapter 7 describes the spatial discretization based on the Galerkin isoparametric finite element (FE) approximation of the time discretization presented in §6 for the variational equations described in §5.3.3. The applied procedure yields to a system of nonlinear algebraic equations well suited for the application of the Newton iterative method. Sections 7.5 to 7.3 are dedicated to the spatial updating of the rotational field. While, in §7.4 to §7.6 the material updating rule is used. In both cases, the obtained inertial and viscous tangential matrices are consistent with the Newmark procedure previously described. Finally, Section 7.7 is devoted to the implementation of the iterative Newton–Raphson scheme and the cross sectional analysis.
In §8 the inclusion of local irregularities in the full constitutive and geometric nonlinear rod model is considered. Section 8.1 is devoted to the development of a special FE for energy dissipating devices and §8.2 covers the development of a two–scale (global in and local; see §8.3 and §8.4, respectively) approach for the numerical treatment of geometric irregularities. In the second case, the resulting step-by-step iterative algorithm is implemented in a multiprocessor scheme in §8.5. In both cases, advantages and limitations of the proposed approaches are discussed in §8.5.4.
Chapter 9 presents the results obtained from numerical simulations showing the ability of the developed formulations in simulating the full geometric and constitutive nonlinear dynamics of rod–like structures including local irregularities. §9.1, §9.2 and §9.3 are devoted to the validation of the present version of the geometrically exact rod model in the linear elastic and inelastic cases. The following sections cover studies of real engineering structures including reinforced concrete structures in §9.4, precast structures with EDDs subjected to earthquake excitation in §9.5 and local irregularities in §9.6.
Finally, in Chapter 10 conclusions abut the works performed are presented. A detailed survey is given in §10.1 and an additional section (§10.2) is included for considering further lines of research born from the results of the present work.

The present work is complemented with the Appendix A including technical details pertaining to the large rotations theory, which are necessaries for the formulation of geometrically exact models for rod, therefore, for readers non necessarily familiarized with that theory it should be recommendable to read it before the rest of the work.

Notation

Scalar quantities are denoted using lightfaced letters with italic or calligraphic style or lightfaced mathematical symbols. First order tensors are denoted using lightfaced letters or symbols but equipped with the over-head hat $\hat{\bullet}$. Tensors of greater order are written in boldface. A special case are skew–symmetric tensors which boldfaced and equipped with an over-head tilde $\tilde{\bullet}$. Upper or lower case letters are used for scalars, vectors or tensors, but subjected to the previously defined convention. The symbol $\mathrm{Diag}[a_1, a_2, a_3]$ is used to denote a diagonal matrix constructed from the values $a_1, a_2, a_3 \in \mathbb{R}$. The superscript T is used to denote the transpose of a given quantity. The superscripts 'm' and 's' are used for distinguish quantities in the material or spatial description, respectively. In the same manner, the superscripts 'me', 'mt' are used for denoting the material description of the elastic and tangential version of a tensorial quantity, respectively. Analogously, the superscripts 'se', 'st' are used for denoting the spatial description of the elastic and tangential version of tensorial quantities. Other sub and superscripts are employed in several quantities through the text, but they are defined the first time they are used. Summation index convention applies through the text. Latin indices, such as i, j, range over the values: $\{1, 2, 3\}$ and Greek indices, such as α, β, range over the values: $\{2, 3\}$. If it is not the case, specific ranges are given in the text. The absolute value is denoted by $\mathrm{Ab}(\bullet)$ and the symbol $\langle \pm \bullet \rangle = 1/2(\mathrm{Ab}(\bullet) \pm \bullet)$ denotes the McAuley's function. The inner (dot), cross, and tensorial products are denoted by means of the symbols $(\cdot)$, $(\times)$ and $(\otimes)$, respectively. Partial differentiation of the quantity $(\bullet)$ with respect to the variable x is denoted as $(\bullet)_{,x}$ and the overhead dot is used to denote the time derivative *i.e.* $\dot{(\bullet)}$. Other operators and specific symbols are introduced in Appendix A.

Chapter 2

State of the art review

The three dimensional nonlinear dynamic analysis of beam structures currently constitutes a very active branch of research in structural analysis [81]. In the case of engineering structures and flexible components of mechanical systems, one–dimensional formulations for structural elements appear as a solution combining both, numerical precision and reasonable computational costs [258, 260]. Numerous contributions have been devoted to the formulation of geometrically consistent models of beams undergoing finite deformation, but employing simplified linear cross sectional constitutive relations. By the other hand, constitutive nonlinearity has been described by means of concentrated and distributed models, formulated in the most cases, considering the small strain hypothesis. Works coupling geometric and constitutive nonlinearity have been mainly focused on plasticity.

Moreover, modern engineering permits designing structures on the premise that the design assures significant energy dissipation potential and, therefore, the survival of the structure when subjected to severe accidental loads [161]. Frequently, the dissipative zones are located near the beam-column joints and, due to dynamic cyclic inelastic incursions, some structural members can be be severely damaged. If the damage is limited, it contributes to dissipate a part of the energy induced by the action and prevents resonance offering a certain protection, however, larger displacements can also increase the second order effects.

Recently, new design concepts for building based on the manipulation of the dissipation, have provided higher levels of safety for the occupants and the buildings. The new techniques are based on adding devices to the buildings with the main objective of dissipating the energy demand imposed by the dynamic actions alleviating the ductility demand on primary structural elements [382].

In what regard to beam models, the following limitations can be mentioned: (i) they usually present fully monolithic connections among elements [200]. Therefore, structural failures due to damage inside of the nodes often are not properly considered. (ii) The shape and the mechanical properties of the cross sections present smooth variations along an element and then, structural behaviors dominated by local changes in the geometry are not well reproduced.

In Summary, a modern approach to the analysis and design of framed structures should take into account in a coupled manner, geometric and constitutive sources of nonlinearity in both static and dynamic ranges. Additionally, it should be possible to describe, include and analyze local irregularities such as sudden changes in the geometry or elements specifically designed to act as dissipative points in the structure.

The present chapter deals with an extensive (as much as possible) state of the art review in several topics of the nonlinear analysis of rod structures and the treatment given to the local irregularities. As it can be though, this review does not intend to be exhaustive due to the large

amount of works existing in most of the topics here covered, however, the provided reference list naturally complements the works quoted throughout the text. The exposition is given in such a way that its reading, along with the reviewing of the quoted works, should provide an acceptable basis for the compression of the new contributions of the present work, which are declared in the objectives of Chapter 1.

2.1 Geometric nonlinearity

Geometric nonlinearity in rod elements has been developed by two different approaches:

(i) The so called *inexact* or *co–rotational* formulations which considers arbitrarily large displacements and rotations but infinitesimal strains and

(ii) the *geometrically exact* formulations obtained from the full three dimensional problem by a reduction of the dimensions by means of the imposition of appropriated restrictions on the kinematics of the displacement field.

A complete survey about the co–rotational techniques for rod elements is carried out in the textbooks of Crisfield [107] Ch. 7 and [108] Ch. 17 for static problems and 24 for dynamic problem, it also includes in Ch. 16 a complete review of the mathematical treatment for large rotations from an engineering point of view. Other classical textbooks such as [42, 170] consider the formulation of beam elements with different degrees of detail. Specific research papers are also available *e.g.* in [106] the dynamics of the co–rotated beam models is investigated. Hsiao *et al.* in [169] develop a consistent co–rotational finite element formulation for geometrically nonlinear dynamic analysis of 3D beams. An application to the three-dimensional continua is given in [290]. Behdinans and Tabarrok [53] use the updated Lagrangian method to obtain a finite element solution for flexible sliding beams. In [424] Xue and Meek study the dynamic response and instability of frame structures using a co–rotational formulation for beams and columns. Battini and Pacoste in [45] develop co–rotational beam elements with warping effects for the study of instabilities problems.
On the other hand, attending to the number of works devoted to the topic and the wide range of the applications, probably the more successful formulations are the geometrically exact ones [256]. The theoretical basis for the process that allows to make the dimensional reduction for obtaining rod models (independent of the specific constraints imposed on the 3D displacement field) can be consulted in the book of Antman [11]. Additional works of the same author covering invariant dissipative mechanism for the motion of artificially damped rods and visco elastic rods can be reviewed in [13, 12] and references therein. A theoretical discussion about the dimensional reduction using nonconvex energy is given in [85]. Additionally, a complete work about the exact theory of stress and strain in rods and shells can be consulted in the text of Ericksen and Truesdell [124].
Other approaches such as the core-congruential formulation for geometrically nonlinear beam finite elements can also be consulted, for example in the work of Felippa *et al.* [131]. In [243] a force formulation for non–prismatic Timoshenko beams is presented. Healey and Mehta in [162] study the computation of the spatial equilibria of geometrically exact Cosserat rods. Zupan and Saje in [429] develops a finite-element formulation of geometrically exact rods based on interpolation of strain measures; in [432] the linearized theory is considered and in [430] a rod's formulation based on curvature is presented. In [353] a rod element based on the interpolation of the curvature is developed. Hjelmstad and Taciroglu [165] develop a mixed variational methods for finite element analysis of geometrically nonlinear Bernoulli-Euler beams. Complementarily,

theoretical works are also available: Izzuddin in [197] analyzes some conceptual issues in geometrically nonlinear analysis of rod structures. In [220] the dynamics of stretchable rods in the inertial case is studied and in [233] Liu and Hong also study the finite deformation dynamics of three-dimensional beams. Łuczko [242] investigates the bifurcations and internal resonances in rods. Friedemann in [136] presents a variational approach to obstacle problems for shearable nonlinearly elastic rods. Rey [334] study the mathematical basis of the symmetry breaking, averaging and elastic rods with high intrinsic twist. The nonlinear equations for thin and slender rods are developed in [326, 331], respectively. Rosen *et al.* [342] develop a general nonlinear structural model of a multirod systems. Wisniewski [404] uses a finite rotation quadrilateral element for multi-layer beams. A theoretical work about constitutive relations for elastic rods is developed by O'Reilly in [311]. Simmonds [360] discusses about the possibility of developing a nonlinear thermodynamic theory of arbitrary elastic beams which including the mathematical requirements for the constitutive relations.
Moreover, the most invoked geometrically exact formulation is that originally proposed by Simo [362] which generalize to the three dimensional dynamic case the formulation originally developed by Reissner [333, 332] for the plane static problem. According to the author, this formulation should be regarded as a convenient parametrization of a three-dimensional extension of the classical Kirchhoff–Love[1] [234] rod model due to Antman [11], employing a *director type* approach for describing the configuration of the beam cross sections during the motion, which allows to consider finite shearing and finite extension. In this formulation, the concepts of rotations and moments have the classical meanings. Rotations are actions of the orthogonal group on the Euclidean space, which do not commute. This formulation avoids the alternative approach employing *semi tangential* rotations and *moments* (see Ref. [321]). Posteriorly, Simo and Vu-Quoc [363, 365] implemented the numerical integration of the equations of motion of rods in the context of the finite element framework for the static and dynamic cases. They have considered a straight and unstressed rod as reference configuration and the hypothesis of planar sections, neglecting any kind of warping.
One of the main conceptual difficulties arising in the Reissner–Simo formulation is given by the fact that the resulting configuration space for the rod in no longer a linear space but a infinite-dimensional nonlinear differentiable manifold. Concretely, the mentioned manifold is obtained by the pairing $\mathbb{R}^3 \times SO(3)$, where $SO(3)$ is the rotation group [16] (see Appendix A). Therefore, the application of the standard techniques of continuum mechanics and numerical methods has to be carried out taking into account the intrinsic non–additive nature of a part of the kinematics of the rods. For example, after the linearization of the weak form of the equilibrium equations, the resulting geometric stiffness is non-symmetric away from equilibrium but symmetry is recovered in the equilibrium configuration [391]. A deep analysis about this and other aspects were provided by Simo in [371]. Other earlier works on finite deformation of rod elements can be found in the works of Atluri and Vasudevan [29], Bathe and Bolourchi [41], Iaura and Atluri [174, 173] and Meek and Loganathan [282] among others.

2.1.1 Large rotations

The fact that the configuration manifold of the rod model involves large rotations become strongly desirable (if not compulsory) to dispose of an acceptable background in mathematics of Lie groups, its associated Lie algebras and other topics related to rotations such as: parametriza-

[1]The Kirchhoff–Love formulation can be seen as the finite strain counterpart of the Euler formulation for beams frequently employed in structural mechanics and civil and earthquake engineering application as it can be reviewed in Refs. [36, 113].

tion [394], linearization, configurational description of rotational motion, time derivatives [425] and so on (see Appendix A).
Literature about the parametrization of the rotational motion can be found *e.g.* in the papers of Bauchau and Trainelli [48], Trainelli [394], Bauchau and Choi [49], Argyris [15], Argyris and Poterasu [16] and Grassia [148], among many others; about the coupling between large displacements and rotations of displacement fields in solid mechanics in [28]; on the Lie group[2] methods for rigid body dynamics in [92]. A survey about integration of differential equations on manifolds[3] can be reviewed in [68, 84]. A Lie-group formulation of kinematics and dynamics of constrained multi-body systems is presented in [294].
Works about the parametrization of finite rotations in computational mechanics can be reviewed in [58, 71, 246, 283], for the specific case of shells Refs. [76, 104, 105, 188] are available. Ibrahimbegović presents a discussion about the choice of finite rotation parameters in [181] and the computational aspects of vector–like parametrization of three-dimensional finite rotations are analyzed in [179]. Rhim and Lee [336] follow a similar approach for the vectorial approach and the computational modeling of beams undergoing finite rotations. A formulation of the rotational dynamics of rigid bodies using the Cayley Klein parametrization is presented in the work of Cottingham and Doyle [103]. Gerardin and Cardona [142] employ a Quaternion algebra for parameterizing the kinematics and dynamics of rigid and flexible mechanisms. Mcrobie and Lasenby [281] review the J. Simo-Vu Quoc rods but using so called Clifford algebra. Park and Ravani in [319] develop a smooth invariant interpolation of rotations. In [426] the representation of finite rotation in nonlinear field theory of continuum mechanics is discussed.
In most of the works about parametrization of finite rotations, different versions of the so called Rodrigues's formula for the exponentiation of a vectorial quantity are presented. For example, Ritto-Corrëa and Camotin in [338] develop a complete survey about the differentiation of this formula and its significance for the vector-like parametrization of Reissner–Simo beam theory. A careful analysis about the interpolation of rotations and its application to geometrically exact rods is given by Romero in [341]. Sansour and Wagner [350] use a path independent approach for the multiplicative updating of the rotation tensor in the analysis of rods and shells. A classical work about the parametrization of the three-dimensional rotation group is provided by Stuelpnagel in Ref. [389].

2.1.2 Research related to the Reissner–Simo rod theory

A great amount of works on both theoretical and numerical implementation of the geometrically exact formulations for beams have been developed starting from the Reissner–Simo works [380]. Particularly, interesting developments have been carried out by Ibrahimbegović and Frey to extend the formulation given in Ref. [362] to the case of a two dimensional curved reference configuration of the rod in [175] and by Ibrahimbegović[4] [178] in the three dimensional case; proposing alternative numerical treatments for the parametrization of rotations [181] and applications to the optimal design and control of structures [193, 192]. Li [228] and Kapania and Li [207, 208] develop a careful presentation of the initially curved and twisted rod theory based on the principles of the continuum mechanics. Mäkinen [247] presents a total Lagrangian formulation for geometrically exact rod elements, which does not presents singularities in the rotational manifold.

[2]More theoretical works in the context of differential geometry can be consulted for *e.g.* [99] or the textbooks of Dubrokin *et al.* [119] and Marsden and Ratiu [255].

[3]More specific works can also be consulted, *e.g.* Borri *et al.* in [67] presents general variational formulations for dynamical problems, which are well suited to be implemented numerically.

[4]Both authors have also make contributions in the theory of shells with finite rotations [176, 177].

Jelenić and Saje [198] develop a formulation based on the so called generalized principle of virtual work, eliminating the displacement variables of the model and retaining only rotational degrees of freedom, avoiding thus the shear locking phenomenon, previously investigated in [202], in the numerical simulations. The same phenomenon has also been studied by Rubin [343] for thin beams based on the Cosserat point theory. The usual discretization procedures applied in implementing the strain measures in the finite element method violates the objectivity condition of this tensor; Jelenić and Crisfield in Refs. [110, 199] propose a remedy for this problem. In [190] several improvements in finite element implementations are addressed to ensure the invariance of the continuum problem. Additional numerical work to obtain frame indifference of the strain measurements in the numerical implementations have been carried out by Betsch and Steinmann in [57], details about this specific subject can be found in Refs. [198, 199, 110].
A formulation equivalent to that proposed by Simo has been employed by Cardona and Gerardin in [88] using an total Lagrangian updating rule for the rotational components. Cardona and Huespe [89] have used this formulation for evaluating the bifurcation points along the nonlinear equilibrium trajectory of flexible mechanisms with large rotations. Ibrahimbegović *et al.* in [187, 180] for studying the buckling and post buckling behavior of framed structures. Nadler and Rubin study the post buckling behavior of rods and frames using the theory of Cosserat point in [295]. A comparative study between tangent and secant formulations of *Cosserat* beams for the study of critical points is carried out by Pérez Morán [321] along with a generalization of the original formulations allowing to use any kind of suitable parametrization for the rotational field. By other hand, Sansour *et al.* in [349] develop a finite element approach for studying the in plane chaotic motion of geometrically exact rods. Vu-Quoc and Li in [421] use the Reissner–Simo formulation for studying the some complex phenomenon in the dynamics of sliding geometrically-exact beams. Further, Vu-Quoc *et al.* [423, 422] extend the formulation for considering the dynamics of geometrically exact sandwich beams/1D plates. Saje *et al.* [348] study the instability of rod–like systems.
A very active research area closely connected to the development of geometrically exact rod formulations is given by the analysis of flexible multi-body systems [328]. Advances in both fields usually provide shearable results [33]. For example, Ambrósio [10] develops efficient descriptions for the kinematics of joints for flexible multi-body systems and the same scheme can be applied to rods; alternatively, [133] can also be consulted. In [185] rigid components and joint constraints in dynamics of flexible multi-body systems with 3D rods is studied.
An additional improvement in reproducing more realistic strain fields on the cross section is obtained starting from enhanced (more complex) kinematical hypothesis. For example, other works based on alternative kinematic hypothesis allow to consider the *warping* of the cross section [151, 372]. Particularly, Simo and Vu-Quoc in [370] develop a geometrically exact rod model incorporating torsion-warping deformation. In spite of the fact that the mentioned theory is exact, at cross sectional level the warping functions are taken from the small strain theory as deduced in [195] starting from the Saint-Venànt's principle. Petrov and Géradin in two works develop a finite element theory for rods based on exact solutions for three-dimensional solids. In [323] they present the geometrically exact nonlinear formulation and in [324] extend the previous work to the anisotropic case. However, even when the authors claim that the proposed formulation is geometrically exact, *i.e.* without assumptions added to the kinematical ones, at cross sectional level the small strain hypothesis is used for constructing the displacement field.
Another active research area is focused on designing time-integration schemes for nonlinear dynamics of flexible structural systems undergoing large overall motion. Taking the flexibility into account allows a better representation of system behavior at higher operating speeds and controlling the corresponding stress states [189]. By one hand, in certain circumstances it is de-

sirable to develop time–stepping schemes able to reproduce conserved quantities of the motion (see *e.g.* [252] and references herein) and by the other hand, considering that the finite element method provides a poor estimate of the higher frequencies, for certain systems, it is desirable to eliminate or reduce the contribution of higher frequencies in computed response of a system. This is the main motivation for introducing numerical dissipation on higher modes. The next section is devoted to the review of a number of relevant works related to the design and the numerical implementation of time–stepping schemes applied to the dynamic of geometrically exact rods undergoing finite deformations.

2.1.3 Time–stepping schemes on the rotational manifold

An important effort has been devoted to develop time–stepping schemes for the integration of the nonlinear dynamic equations of motion involving finite rotations [87]. As in the static case, the basic difficulty arises in the noncommutative nature of the group $SO(3)$ [365]. A general view of numerical integration schemes for both explicit and semi–implicit methods applied to rotational motion can be consulted in [216, 217].
Simo and Vu-Quoc in [365] develop an implicit transient algorithm that extends the classical Newmark formulae, stated in $\mathbb{R}^3$, to the rotation group $S0(3)$, obtaining a formulation similar to that of the linear case. In the same work, the consistent linearization of the weak form of the balance equations yields to a tangential inertia tensor, nonsymmetric in the rotational components. A comparison among implicit time–stepping schemes according to different choices of rotational parameters can be reviewed in Ref. [183] and in [182] Ibrahimbegović and Mazen discusses about the parametrization of finite rotations in dynamics of beams and implicit time–stepping schemes (see also [184]). Recently, Mata *et al.* [260] present the inclusion of viscous and rate independent dissipation in the Reissner–Simo rod model considering a thermodynamically consistent visco damage model on each material point of the cross section. Details about its numerical implementation in a Newmark time–stepping scheme are also addressed. Rubin in [344] provides a simplified implicit Newmark integration scheme for finite rotations.
Even though Newmark's scheme has been widely applied to the study of the dynamic response of structures, rigid bodies and flexible mechanisms, Mäkinen states in Ref. [245] that it only constitutes an approximated version of the corrected formulae, which are given in his work for the spatial and material descriptions. The main reasons are that material descriptions of the spin and acceleration vectors involved in the updating procedures, belong to different tangent spaces at different times. Additionally, a critical study of Newmark's scheme on the manifold of finite rotations is given by the same author in [244].
On the other hand, Newmark's family of implicit schemes fails to preserve certain conservation laws of the motion, such as the total energy and momentum of nonlinear Hamiltonian systems, producing numerical (fictitious) dissipation [82]. Algorithms which inherit the conservation properties of the Hamiltonian dynamical system are attractive due to the fact that conserved quantities often capture important qualitative characteristics of the long-term dynamics [82] and numerically, conservation the total energy lead to convenient notions of algorithmic stability [145]. A further improvement in the development of robust time–stepping schemes is provided by the energy-momentum conserving algorithms. One of the pioneering works in constructing one of such of that algorithms is due to Simo *et al.* [372] which also develops symplectic schemes for nonlinear dynamics including an extension to the rotational motion. A recent survey on algorithms inheriting conservation properties for rigid and elastic bodies as well as constrained mechanical systems can be consulted in the works of Betsch and Steinmann [59, 60, 61]. Simo *et al.* in [373] provide a detailed formulation and the numerical implementation of a time–stepping

algorithm designed to conserve exactly the total energy, the linear and the angular momentum for 3D rods.
Some additional enhancements have been carried out, for example: Armero and Romero develops an energy–dissipating momentum–conserving time–stepping algorithms for nonlinear rods in [23]. A survey abut second order methods for high–frequency dissipative algorithms is given by the same authors in [21]. Bauchau and Theron [46] present an energy–decaying scheme for beams. It is worth to note that, finite elements based on the space interpolation of rotational variables may be afflicted with problems such as nonobjective and path-dependent solutions; in [340] Romero and Armero develop an objective FE approach for the energy-momentum conserving dynamics of geometrically exact rods. Betsch and Steinmann [62] avoid the use of rotational variables regarding nonlinear beams from the outset as constrained mechanical systems. An energy–decaying scheme constructed as an extension of the energy–conserving schemes proposed by Simo [373] is presented by Ibrahimbegović and Mamouri in [189]. Jelenič and Crisfield [201] analyzes the problems associated with the use of *Cayley* transform and tangent scaling for energy and momenta conservation in the Reissner–Simo theory for rods.
Closely related applications of the previous time–stepping schemes are found in the field of multi-body dynamics. Bauchau and Bottasso [47] design an energy preserving and decaying scheme for flexible multi-body systems. An application of the geometrically exact theory of rods to multi-body dynamics with holonomic constrains and energy conserving schemes can be reviewed in Ibrahimbegović *et al.* [186]. In Refs. [182] and [189] a complete study of the general dynamics of flexible mechanisms is carried out and an energy conserving/decaying time–stepping scheme is proposed for eliminating the high frequency content in the response of flexible structures. In [70] Bottasso *et al.* develop conserving/dissipating numerical schemes for the integration of elastic multi-body systems. The specific case of rods is covered in [69]. Shell elements have been also investigated see *e.g.* [80, 79, 77] for the application of the Newmark scheme with finite rotations and [376] for energy-momentum conserving schemes. In [144] the dynamic analysis of rigid and deformable multi-body systems with penalty methods and energy-momentum schemes is considered and in [225, 298] energy preserving implicit and explicit integrators for constrained multi-body systems are developed. A survey about non–linear dynamics of flexible multi-body systems is given in [191].
More recently, attention have been turned towards *variational integrators i.e.* algorithms formed from a discrete version of Hamilton's variational principle [226]. For conservative systems usual variational principles of mechanics are used, while for dissipative or forced systems, the Lagrange-d'Alembert principle is preferred. The main properties that make these algorithms attractive are: for the conservative case variational integrators are, *symplectic* [252] and momentum conserving. These methods also permit the systematic construction of higher order integrators. Variational integrators also have remarkably good energy behavior. A summary can be reviewed in [227, 254]. An extensive treatment for the case of the continuum mechanics can be reviewed in [253].
Additionally, in [206] Kane *et al.* discuse about variational integrators and the Newmark algorithm for conservative and dissipative mechanical systems. Marsden and Wendlandt [252] present a nice overview on mechanical systems with symmetry, variational principles, and integration algorithms. An application to the design of variational integrators on the Lie group for the full body problem is given in [222]. At the author's knowledge, this type of methods have not been formally applied to the Reissner–Simo's rod theory.

2.2 Constitutive nonlinearity

2.2.1 Inelasticity in rod elements

In spite of the great capacity of the mentioned formulations, works considering both constitutive and geometric nonlinearity are rather scarce. Research on constitutive nonlinearity have progressed based on a different approaches, that's, *lumped* and *distributed* plasticity models [317]. Experimental evidence shows that inelasticity in beam elements can be formulated in terms of cross sectional quantities and, therefore, the beams's behavior can be described by means of *concentrated* (lumped) models, some times called *plastic hinges*, which focalizes all the inelastic behavior at the ends of linear elastic structural elements by means of *ad-hoc* force-displacement or moment-curvature relationships (see *e.g.* Bayrak and Sheikh [50] or Lubliner [239], among many others). Mitsugi in [286] proposes a method for the measurement of strains develop in a finite deformation formulation for hinge connected beam structures. Some of these models have been extended for considering a wide variety of failure criteria; an example is shown in the work of Hyo-Gyoung Kwank and Sun-Pil Kim [219] where a moment-curvature relationship for the study of reinforced concrete (RC) beams subjected to cyclic loading is defined. This method is recommended by certain authors due to its numerical efficiency when compared with the full three-dimensional formulation of the nonlinear problem. It is important to note that the nonlinear constitutive laws are valid only for specific geometries of the cross section and that usually, the thermodynamical basis of the material behavior are violated [159]. Moreover, some components of the reduced forces and/or moments are frequently treated elastically [113, 160, 296].
A further refinement in the analysis of the mechanical response of beam structures is obtained considering inhomogeneous distributions of materials on arbitrarily shaped cross sections [113]. In the case of distributed plasticity models, the constitutive nonlinearity is evaluated at a fixed number of cross sections along the beam axis, allowing to obtain a distributed nonlinear behavior along the structural elements. In this case, the usual procedure consists into obtaining the constitutive relationship at cross sectional level by integrating on a selected number of points corresponding to *fibers* directed along the beam's axis [355, 390]. Thus, the mechanical behavior of beams with complex combinations of materials can be simulated [36, 102]. Fiber models fall into the category known as *distributed* beam models [155] due to the fact that inelasticity spreads along the beam element axis [317]. The employment of fibers allows predicting a more realistic strain-stress state at the cross sectional level, but it requires the definition of uniaxial constitutive laws for each material point. A combination of both models, applied to the study of the collapse loads of RC structures, is proposed by Kim and Lee [214]. Another example is given in the work of Mazars *et al.* [278] where a refined fiber models is used for the analysis of concrete elements including torsion and shear. Monti and Spacone use a fiber beam element for considering the *bond-slip* effect in reinforced concrete structural elements in [293]. In most cases, both types of models, the concentrated and the distributed ones, have been formulated under the hypothesis of infinitesimal deformation.
Two versions of the distributed plasticity models can be found in literature: the *stiffness* (displacement based) and *flexibility* (force based) methods [317]. The first one is based on the interpolation of the strain field along the elements. A precise representation of forces and moments requires a refined FE mesh for each structural element in which nonlinear constitutive behavior is expected to appear. In the flexibility method, the cross sectional forces and moments are obtained interpolating the nodal values and satisfying the equilibrium equations even in the nonlinear range [354]. Examples of flexibility based finite elements for the geometrically nonlinear analysis of beams structures can be found in the work of Neuenhofer and Filippou

[297] and Barham *et al.* [39] for elastic perfectly plastic beam structures.
Both approaches are affected by the *strain localization* phenomenon when materials with softening behavior are employed. A extensive review of the strain localization in force-based frame elements is presented by Coleman and Spacone in [98]. A more theoretical work about this topic is given by Armero and Ehrlich in [24] and Ehrlich and Armero [121] for a plastic hinge model incorporated into a infinitesimal formulation for Euler-Bernoulli rods and frames. In the stiffness method, localization occurs in a specific element and, in the case the flexibility method, nonlinearity is concentrated in the volume associated to a specific cross section of the element undergoing strain softening. In any case, the whole structural response becomes mesh dependent if no appropriate corrections are considered. Several techniques have been proposed for ensuring *objectivity*[5] of the structural element response: Scott and Fenves [354] develop a new integration method based on the Gauss-Radau quadrature that preserve the objectivity for force based elements; Hanganu *et al.* [159] and Barbat *et al.* [36] regularize the energy dissipated at material point level, limiting its value to the specific fracture energy of the material [301]. These methods ensure that the whole structural response remains objective, but the length of the zone where softening occurs is still mesh dependent. Recently, some developments employing *strong discontinuities*[6] have been applied to the study of beam models but considering constitutive laws in terms of cross sectional forces and infinitesimal deformations, as it can be seen in Armero and Ehrlich [25, 26] and in references therein. The characterization of localized solutions in a softening bar using an analysis of the propagation of waves is presented by Armero in Ref. [22].
One of the most common limitation of distributed formulations arises from fact that constitutive nonlinearity is defined for the component of the strain acting in the direction normal to the face of the cross section and, therefore, the shearing components of the stress are treated elastically. This assumption does not allows to simulate the nonlinear coupling between different stress components at constitutive level, resulting in models where cross sectional shear forces and torsion moments are transmitted elastically across then elements [113, 296]. This assumption predefines the way in which the failure of the members occurs, limiting severely the participation of shear forces to the equilibrium. A comparative study of different plasticity models applied to earthquake analysis of buildings can be consulted in [117].
Most of the geometrically nonlinear models are limited to the elastic case [362, 363]. Works considering both constitutive and geometric nonlinearity are scarce and the inelastic behavior has been mainly restricted to plasticity [347, 372]. In [64, 65] and [118] a higher order approximation is used for the calculation of the axial strain in truss elements and uniaxial constitutive descriptions are used for different material behaviors. Simo *et al.* in [361] extends the formulation of rod elements with warping of arbitrary cross sections for considering a small strain formulation for elastic visco plastic constitutive materials. An outstanding work considering the warping of cross sections made of elastic plastic materials is due to Gruttmann *et al.* [151]. Additionally, Wagner and Gruttmann in [398] develop the finite element analysis of the Saint-Venànt torsion problem considering the exact integration of the elastic plastic constitutive equations. Nukala and White [299] develop a mixed finite element for studying the stability behavior of steel structures. Pi and Bradford [325] study the coupled elastic plastic buckling and the post buckling evolution of arches subjected to central loads. In [284] a method for studying the large deflection

[5]Note that in this case, the term *objectivity* is used for referring to a mesh independent response of the structure in stead of the usual sense in continuous mechanics where it refers to an invariant response under rigid body motions.

[6]For an extensive review about the employment of the strong discontinuity approach for the treatment of localized dissipative mechanisms in a local continuum see Armero [18]; the theoretical basis of these methods in the three dimensional version of fracture in mechanics can be found in [303, 302, 417] and references therein.

of three-dimensional steel frames is proposed. Gebbeken [141] develop a numerical approach for the (static) ultimate load analysis of steel framed structures. Isotropic hardening is included in the model presented by Park and Lee in [318] which is based on the work of Simo [363] for considering geometric nonlinearity. A kinematically exact formulation of elastic plastic frames is presented in [346] by Saje *et al.* , however, results are restricted to the plane case.
Recently, Mata *et al.* [258, 260] have extended the geometrically exact formulation for rods due to Reissner, Simo and others [178, 199, 207] to include an arbitrary distribution of composite materials with inelastic constitutive laws on the cross sections for the static and dynamic cases; thermodynamically consistent constitutive laws of visco damage and plasticity are developed in terms of the material form *first Piola Kirchhoff* stress vector in the framework of the *mixing theory* for composites. Some basic requirements, such as the objectivity of the response when strain localization for softening materials occurs is also considered by means of a regularization of the energy dissipated by the materials [36, 160].
Alternative approaches are also available, *e.g.* in [167, 168] Hori and Sasagawa develop a large deformation model based on subelements for inelastic analysis of large space frames. Examples of application of the proposed model are given in the second paper. In all the above references, examples are restricted to the static case. In the dynamic case, Galucio *et al.* [139] employ the finite element method for the study of the mechanical response of a infinitesimal deformation version of visco elastic sandwich beams using fractional derivative operators. Turkalj *et al.* [396] uses the external stiffness approach for large displacement analysis of elastic plastic framed structures. Shi and Atluri [357] employ a plastic hinge formulation for the elastic plastic analysis of space–frames considering large deformation. Battini and Pacoste in [44] study the plastic instability of beam structures using the co–rotational technique.
Other kind of research has been conducted toward the more precisely estimation of the constitutive behavior of rod–like structures, it corresponds to the employment of the homogenization theory at material point level on the cross section (see *e.g.* [224, 427]) or the *asymptotic cross sectional analysis* [410]. This last type of approximation can give a very precise simulation of the behavior of the materials but they have the inconvenient that it is very expensive in computing time. In distributed models for the coupled constitutive and geometric nonlinear analysis of rod–like structures, the cross sectional analysis became a crucial step. According to the hypothesis assumed, several degrees of refinement can be obtained. This specific topic is covered in the next section.

2.2.2 Cross sectional analysis

The cross sectional analysis in a *strain driven* numerical method can be defined as the set of procedures used for determining: (i) the stress distribution in a cross section for a given strain field; (ii) the stress resultant and stress couples (see §3 for formal definitions) and (iii) the reduced (cross sectional) tangential stiffness if inelastic materials are considered. All these procedures are usually dependent on the shape of the cross section and, the distribution and the constitutive relation of the involved materials.
Therefore, a large amount of research have been concentrated on this topic. The significance of the techniques developed for the precise cross sectional analysis arises on the accuracy of the stress field assigned to point on the rod. Special attention has been directed to the determination of the shear stress and the shear strain distribution on arbitrarily shaped cross sections. Gruttmann *et al.* in [150] develop a refined method based on the finite element for shear stresses in prismatic beams and Gruttmann and Wagner [153] use the same method for calculating the *shear correction factors* in Timoshenko's beams. An analytical study about the shear coefficients

is performed by Hutchinson in [171]. Jiang and Henshall [203] present a finite element model coupled with the cross sectional analysis for the torsion problem in prismatic bars. Similarly, Petrolo and Casciaro in [322] develop 3D beam element based on the Saint Venànt's rod theory. Specific efforts have been oriented to the case of thin walled (closed or not) cross sections; For example, Freddi *et al.* [135] analyze the case of thin-walled beams of rectangular shape. Beams made of composite materials have received great attention due to the fact that failure in this type of structures is closely related to the shear distribution between layers. For example, Reznikov in [335] develops a method for the analysis of the nonlinear deformation of composites including finite rotations. An application to the analysis of sections of rotor blades made of composite materials can be reviewed in [204]. Ovesy *et al.* [312] perform the geometric nonlinear analysis of channel sections using the so called finite strip method. Mokos and Sapountzakis in [289] propose the use of the *boundary element method* [351] for obtaining a solution to the transverse shear loading of composite beams.
An innovative procedure for the precise analysis of stresses in arbitrary cross sections is given by the *asymptotic variational methods* which take advantage of certain small parameters inherent to beam-like structures [412]. Several works can be quoted in this line of research, *e.g.* Cesnik *et al.* in [93] analyze the role of the short–wavelength extrapolation in a refined theory of composite beams. Popescu and Hodges [327] uses the method for deducing an asymptotically correct version of the Timoshenko anisotropic beam theory. Yu and Hodges compares the elasticity solutions with those obtained from asymptotic analysis for prismatic beams in [414] and in [413] Yu *et al.* apply the method to initially curved and twisted composite beams. Additional works can be reviewed *e.g.* in [399, 420].
Most of the previous mentioned references are restricted the small strain deformation or to the elastic case. In several areas of engineering the inelastic response of the structures is required, as is the case of earthquake engineering. Moreover, several modern techniques of characterizing structures are based on nonlinear analysis *e.g.* [395] or the work of Fantilli *et al.* [127] about flexural deformability of concrete beams. Complex phenomenons such as the effect of confinement in shear dominated failures of civil engineering structures have received increasing research efforts [329]. Burlion *et al.* [86] analyze the compaction and tensile damage in concrete including the development of constitutive relations in the dynamic range. In [288] Mohd Yassina and Nethercotb develop a procedure for the calculation of the key cross sectional properties of steelconcrete composite beams of complex cross sections. In [406] Yang and Leu develop constitutive laws and a force recovery procedure for the nonlinear analysis of trusses. Thanoon *et al.* [392] propose a method for estimating the inelastic response of composite sections. Ayoub and Filippou [30] employ a mixed formulation for structures with composite steel and concrete cross sections. In the work of Bentz [56] an intend to develop a method for the cross sectional analysis is presented. The reference list is extensive, with works covering from specific aspects to more general procedures. Recently, Bairan and Mari [31, 32] present a coupled model for the nonlinear analysis of anisotropic sections. In §7.7.1 of the present work, a method for the cross sectional analysis consistent with the Reissner–Simo rod hypothesis is developed. The present procedure tries to combine simplicity and the sophistication required by composite materials.

2.3 Local Irregularities

As explained in §1 two types of singularities are considered: (i) energy dissipating devices and (ii) local geometric irregularities. In following a state of the art review of both topics is presented.

2.3.1 Energy dissipating devices

Conventional seismic design practice permits designing reinforced concrete, steel and composite structures for forces lower than those expected from the elastic response on the premise that the structural design assures significant energy dissipation potential and, therefore, the survival of the building when subjected to severe earthquakes [161]. Normally, energy dissipation during seismic or other dynamic actions, occurs in critical zones of the structure specially designed to admit large ductility demands [74]. Frequently, the dissipative zones are located near the beam-column joints and, due to cyclic inelastic incursions during earthquakes, several structural members can suffer a great amount of damage with irreversible degradation of the mechanical properties of the materials, cracking and yielding of the steel reinforcements etc. For a complete survey about reinforced concrete structures subjected to seismic actions see Fardis [128].
Even if a limited level of structural damage dissipates part of the energy induced by the action and uncouples the dynamic response from resonance offering a certain level of protection against seismic actions [260], the large displacements required for developing hysteretic cycles in dissipative zones can cause severe damage to non structural components. Particularly, in earthquake engineering, these deformations can produce irreparable damage in those members, but this situation is generally considered economically acceptable if life safety and collapse prevention are achieved.
In the last decades, new concepts for the design of building, based on the manipulation of the energy dissipation, have improved the seismic behavior of the structures providing higher levels of safety for the occupants, the buildings and the nonstructural components. The new techniques are based on adding devices to the buildings with the main objective of dissipating the energy demand imposed by the dynamic loading, alleviating the ductility demand on primary structural elements, such as beams, columns or walls and decreasing the acceleration response [161, 382]. The devices can be installed in new or in existing structures and can be used in seismic design or rehabilitation. The purpose is to *control* the dynamic response of the buildings by means of a set of dissipating devices which constitutes the *control system*, adequately located in the structure.
In general, control systems can be classified in four major groups:

(i) *Active control systems.* These systems work measuring, by means of sensors, the external excitation and/or the structural response. Then, based on those data and using algorithms, compute the control forces needed to improve the seismic response of the building. Control forces are applied to the structure by means of actuators, which take the energy from an external supply. (see [14, 35, 229, 385] among others).

(ii) *Passive control systems.* In this case, the *passive energy dissipating devices* (EDD) work dissipating the energy of the earthquake, localizing and concentrating the nonlinear phenomena of the structure and thus the damage in the devices without the need of an external energy supply [163, 382, 393].

(iii) *Semi active systems.* In this case the control algorithm changes some of the properties of the EDD in order to obtain a better seismic performance of the structure. In this category of control systems, control actuators do not add energy directly to the structure and EDD can be seen as *controllable* passive devices. [95, 248, 383, 387, 407].

(iv) *Hybrid systems.* This systems are typically defined as a combination of different active and/or passive systems. A comparative study of the response of structures for different control systems can be reviewed in [40, 330]. A rather brief state of the art review about theory and practice using control techniques in civil engineering structures can be found in Ref. [383].

Today, the passive control of structures is a well understood technique and its use is widely accepted by the engineering community even in the case when passive EDDs are not able to adapt their behavior to the seismic response of the building [385]. The passive control systems most used in reducing the seismic response of buildings are: *base isolation* and EDDs.
By one hand, base isolation uncouples the structure from the soil introducing flexible supports between foundations and the rest of the structure. The isolation system transforms the building into a rigid body moving over flexible supports, shifting thus the fundamental period of the structure and enhancing the energy dissipating characteristics of the isolation-superstructure system [4]. A detailed presentation of theory, numerical analysis and of the practical applications of base isolation systems can be reviewed in [211]. More specific aspects of this technique, such as analytical models for bearings, linear equivalent models for practical design of structures, etc. can be consulted in [5, 213, 75, 212] and references therein.
By the other hand, passive EDDs, also called *supplemental dampers*, are devices located throughout the structure to absorb and dissipate an important part of the energy input induced in the structure by earthquakes or other dynamic actions (*e.g.* hurricanes or machinery induced vibrations). Figs. 2.1*a-c* 2.2*a-b* show the location of several types of energy dissipating devices. They are applicable to a wider range of structures than base isolation but the benefits obtained in reducing the seismic response of the structure are usually less significative.

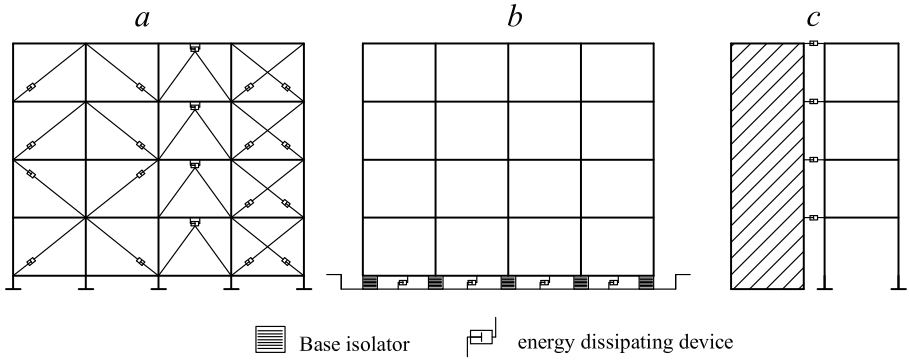

Figure 2.1: Energy dissipating devices location in buildings. (a): Diagonal elements. (b): Base level elements. (c): Connecting elements.

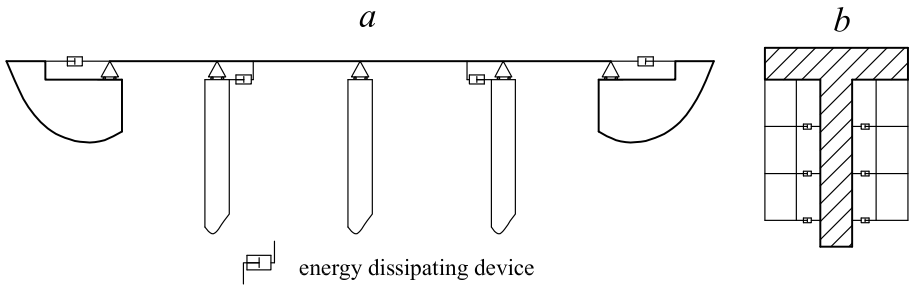

Figure 2.2: Energy dissipating devices location in a bridge. (a): Longitudinal direction. (b): Transversal direction.

Many practical application of EDDs to real structures are summarized in [4]. The effectiveness of the implementation of EDDs in engineering structures can be analyzed starting from the

energy balance equation [8] as

$$E_I = E_K + E_S + E_D + E_\pi \tag{2.1}$$

where E_I is the absolute earthquake energy input, E_K is the absolute kinetic energy, E_S is the elastic strain energy, E_D is the energy dissipation due to inelastic behavior in the structure (including viscous effects) and E_π is the contribution of energy dissipation due to the addition of EDDs.
Using the assumption that the term E_π has no influence on E_I, it is possible to see from Eq. (2.1) that increments of the contribution of $E_D + E_\pi$ implies reductions of $E_K + E_S$ and, therefore, lower displacements and velocities are obtained when extra energy dissipation is provided [4, 382]. The main objective of designers when applying passive control in improving the seismic behavior of the structures, is defining appropriately the properties of the EDDs in such way that the inelastic demand on primary structural members E_D be transferred to the term E_π. After severe loadings, EDDs can be replaced by new ones if necessary.
EDDs can be classified according to the nature of their dissipative mechanism in (i) *displacement dependent*, *e.g.* friction, metallic and extrusion devices, (ii) *velocity dependent e.g.* viscous, (iii) *mixed e.g.* visco elastic and others such as tuned liquid and tuned mass dampers; each of these types is described in further sections. A great amount of works comparing the ability of different passive EDDs in controlling the seismic response of structures is available in the literature, for example in [137] is compared the response of frame structures equipped with visco elastic and viscous devices; in Ref. [210] an approximated method is used to carry out a comparative study considering metallic and viscous devices. Guidelines and methods for testing and characterizing the different types of EDDs can be consulted in [163, 164, 337].
Other points of view are admissible for considering the incorporation of passive control in RC structures, for example Aiken presents in Ref. [4] the contribution of the extra energy dissipation due to EDDs as an *equivalent damping* added to the linear bare structure and *displacement reduction factors* are given as a function of the damping ratio added to buildings by means of the EDDs. A critical review of the reduction factors and design force levels can be consulted in [230]. In Ref. [100] Connor *et al.* propose a method for a preliminary design of passively controlled buildings under the hypothesis that the structure is composed of two systems, the bare frame and the dissipative one, that work together to satisfy a design criterium. In Ref. [143] the optimal control theory is use to design supplemental viscous and visco elastic passive damping systems in seismic control. In [231, 232] Lin and Copra study the accuracy in estimating the dynamic response of asymmetric one-story buildings equipped with EDDs, when the dissipating devices are replaced by their energetic equivalent linear viscous dampers; a correction factor is provided estimating the maximum forces in the EDDs. Other procedures for the analysis and design of structures with EDDs can be consulted in [96].
Today, only a few countries have codes for designing RC buildings with EDDs; one of them is United States, where there are several codes that provide procedures and requirements for the design of passive energy dissipating devices. Particularly, the US *Federal Emergency Management Agency* (FEMA) proposes code provisions and standards along with other references pertaining to the design of EDDs for use in buildings. The document includes *Prestandard and Commentary for the Seismic Rehabilitation of Buildings* (FEMA 356)[129] and NEHRP *Recommended Provisions for Seismic Regulations for New Buildings and Other Structures* (FEMA 368)[130], which covers the detailed design of EDDs in an Appendix to Chapter 13.
As it is mentioned in Ref. [279] in the case of Europe, efforts have been focused in developing codes for base isolation in some countries such as Italy or the Soviet Union. In the case of EDDs

the developments have been limited to guidelines rather that codes or official standards. The last (draft) version of Eurocode 8 of the year 2003 (Ref. No: prEN 1998-1:2003 E) [125] contains the Chapter 10 devoted to base isolation systems, but no guidelines or recommendations are made for other kind of passive control. In the case of Japan a fully review of the state of the art in passive control of structures is reviewed in [397], however, no mentions are given in this work to available codes, standards or guidelines for practitioners.
As it can be concluded from the existing codes, guidelines and technical literature, a great part of the design methods proposed for RC (or steel) structures are based on supposing that the behavior of the bare structure remains in the elastic range, concentrating the energy dissipation demands on the control system. However, even though this assumption can be useful for a preliminary design, experimental and theoretical evidence show that inelastic behavior will occur in the main structural elements during severe strong motion as noted by Shen and Soong in [356]. Therefore, these authors recommend to eliminate the assumption of linear structural response and propose a design method based on the damage control. However, it is widely recognized that nowadays it is possible to carry out nonlinear time history analysis, which can provide a most precise and complete evaluation of the responde of structural systems incorporating EDDs (see [261, 262, 416]); but it also requires relatively large amounts of analysis expertise and computational time and effort. It is also recognized that equivalent linear static or dynamic procedures require the least amount of time and computational effort, but they are not able to represent the fully complexity of the nonlinear dynamic behavior of structures. This situation regarding to the most appropriated kind of analysis for simulating the response of engineering building with dissipators is taken into account in the FEMA code, which recommends the use of a combination of rationality and an admissible computational cost. The code describes four different analysis procedures: (1) linear static; (2) linear dynamic; (3) nonlinear static; and (4) nonlinear dynamic analysis. Linear methods are based on force reduction factors and can be applied subjected to limitations specified in the code [393], in other cases nonlinear analysis have to be carried out.
Independently of the type of analysis chosen, it is clear that the nonlinear time history analysis has gained space in the passive control of structures subjected to great dynamic actions, therefore, sophisticated numerical tools became more necessary for both academics and practitioners. For example, in Ref. [235] Lu presents a comparative study between numerical simulations and experimental test carried out on scaled RC structures. During the last decades, great efforts have been done in developing numerical formulations and their implementation in computer codes for the simulation of the nonlinear dynamic response of RC structures, for example a recent state of the art review for the case of concrete structures can be found in [384].
The engineering community agrees with the fact that the use of general fully 3D numerical technics, such as finite elements with appropriated constitutive laws, constitute the most precise tools for the simulation of the the behavior of RC buildings subjected to earthquakes [196, 382, 386] to other kind of loads [218] or even for the simulation of the mechanisms that produce earthquakes itself [1]. However, usually the computing time required when using full models of real structures became their application unpractical. Several approaches have been developed to overcome this difficulty; some authors propose the use of the so called *macro–elements*, which provide simplified solutions for the analysis of large scale problems [114, 115, 126]. Considering that most of the elements in RC buildings are columns or beams, one–dimensional formulations for structural elements, obtained trough the reduction of spatial dimensions by means of kinematic assumptions [11, 85], appear as a solution combining both numerical precision and reasonable computational costs [258]. Experimental evidence [50] shows that nonlinearity in beam elements can be formulated in terms of cross sectional forces and/or moments and displacements and/or curvatures, which is frequently quoted in literature as plastic hinges models

[98] (see §2.2). Some formulations of this type have been extended to take into account geometric nonlinearities [314, 378, 418, 419] allowing to simulate the P–Δ effect, which occurs due to the changes of configuration of the structure during the earthquake [83, 152, 378, 403]. Several limitations have been reported to this kind of models, specially for the modeling of RC structures with softening behavior in the dynamic range [390] (this aspect is covered in §4.1). A discussion about topics such as step-by-step methods, path bifurcation, overall stability, limit and deformation analysis in the context of the plastic hinges formulation for beam structures can be consulted in [97].
An additional refinement is obtained considering inhomogeneous distributions of materials on arbitrarily shaped beam cross sections [299, 416]. Specific numerical models based on a secondary discretization of the beam cross sections have been developed allowing to include multiple materials. In this case, the constitutive force-displacement and/or moment-curvature relationship at cross sectional level is deduced by integrating over the selected points on the cross section [155]. Therefore, using this approach the mechanical behavior of beams constituted by complex combinations of materials, such it is the case of RC beams, can be simulated [156, 157, 43]. In general, the engineering community agree with the fact that although this models are more expensive, in terms of computational cost, than the plastic hinges ones, they allow to estimate more precisely the response nonlinear response of RC and other kind of structures [34, 113, 390]. Formulations of this type, considering both constitutive and geometric nonlinearity are rather scarce [118]; moreover, most of the geometrically nonlinear models for beams are limited to the elastic range of materials, as it can be consulted for example in Refs. [178, 256, 362] and the treatment of constitutive nonlinear behavior has been mainly restricted to plasticity [64, 151]. In reference [134] a theory for the stress analysis of composite beams is presented, however the formulation is only valid for moderated rotations and the behavior of the materials remain in the elastic range. Recently, Mata *et al.* [258, 260] has extended the geometrically exact formulation for beams due to Reissner–Simo [333, 332, 362, 363, 365] for considering and arbitrary distribution of composite materials con the cross sections for the static and dynamic cases.
From the numerical point of view, the nonlinear behavior of EDDs usually has been described in a global sense by means of force-displacement or moment-curvature relationships [382] which intend to capture appropriately the force/moment level and the energy dissipating capacity existing in the devices. That is to say that, a rather simplified description appears to be enough for the mechanical characterization of the EDDs, independently of the micro-mechanisms involved in the energy dissipation or the stress distribution in each of their components [259].
The inclusion of EDDs in a software package for the seismic analysis of RC structures is frequently done by means of using link elements equipped with the mentioned nonlinear relationships [382]. In this way, the link elements connect the different points of the model of structure which represent the anchorage point of the EDDs in the real buildings. During the seismic event the relative displacement and/or rotation between the anchorage points activates the dissipative mechanisms of the devices [397].
Nowadays, there are several numerical codes available for the study of the nonlinear dynamic response of engineering structures with EDDs. For example, in Ref. [416] a detailed presentation of a computer program able to simulate the static and dynamic (seismic) behavior of different types of buildings with EDDs is presented. Other professional (commercial) softwares such as those described in references [111, 112, 132] have incorporated different kind of inelastic analysis including beam element with plastic hinges and specific link elements for EDDs. A comparative study of the performance of different commercial software packages for simulation the P–Δ effect in structures can be consulted in [352]. In any case, the mentioned softwares show a balance between capabilities and limitations.

2.3.1.a EDDs in RC building structures

There are a great number of EDDs developed, however, a tentative classification can be constructed following Soong and Dargush [382] where the following types are identified according to their working mechanism:

(i) *Metallic devices*

In this type of devices, energy dissipation depends upon plastic deformation of metallic materials, such as mild steel or aluminium [382]. A large set of possible geometries have been used as tentative devices, which includes torsional beams, U-strips, braced systems etc. As an example, Fig 2.3*a*-*b* show the geometric characteristics of X-shaped (ADAS) devices and 2.3*c* a torsional beam.

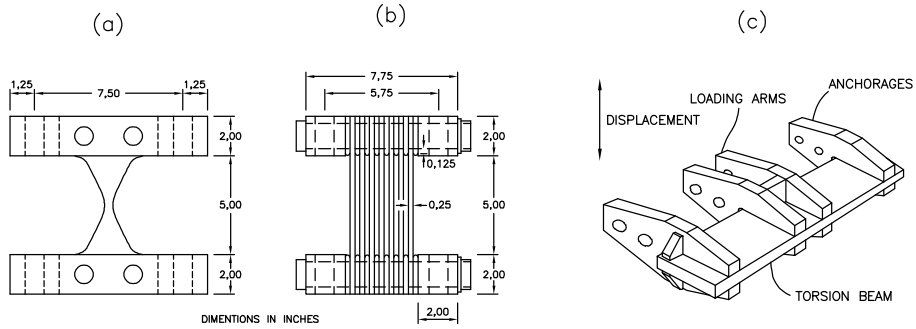

Figure 2.3: Plastic devices. (a, b): ADAS devices, front and lateral views. (c): Torsion beam.

A large set of mathematical models have been developed for describing the force-displacement relationship in metallic devices *e.g.* [401]. In any case, classical plasticity models can produce good results [239, 377]. Specific design methods for incorporating metallic dissipators in structures can be consulted *e.g.* in [287]. An example of the effects of several types of devices, including metallic, is presented in [249].

(ii) *Visco elastic devices*

Visco elastic dampers (VDE) use polymeric materials which dissipate energy when subjected to shear deformations. Originally, applications for controlling vibration were focused in the aircraft and aerospace industry and more recently in seismic engineering. The main effects and benefices are obtained due to the fact that VEDs increases the global damping of the structure [212].

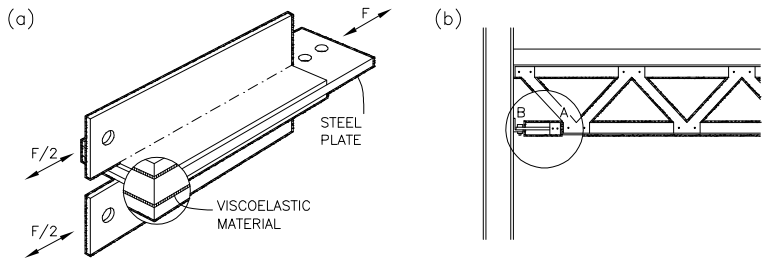

Figure 2.4: Visco elastic dampers. (a): Device. (b): Location in a building.

A typical device is depicted in Fig. 2.4*a* which consists of visco elastic layers bounded

with steel plates and a typical building's location is shown in 2.4*b*. Dissipation in the VE layers reduces the relative motion between elements of the structure.
In general terms, the shear stress-strain relationship is frequency and temperature dependent as it can be consulted in [259, 382]. In [3] a detailed study about the modeling of the dynamic properties of filled rubber is presented. Asano *et al.* [27] carry out the experimental study on visco elastic dampers and the formulation of an analytical model. Kojima and Yoshihide [215] present a survey about the performance, and durability of high damping rubber bearings for earthquake protection. Other analytical models for visco elastic materials can be consulted in [172, 273, 267, 265] and references therein. Design recommendations for building incorporating VE–EDDs can be consulted in [211, 382].

(iii) *Friction Devices*

Friction dampers (FD) dissipate energy through the friction that develops between two solid bodies sliding one relative to the another. The force developed in the device depends on the friction coefficient between the materials and the normal force, according to the well known Coulomb's law [382]. Several geometric choices have been proposed; for example, in Fig. 2.5*a* a FD based on the relative motion of two diagonal element enclosed by two steel plates is presented; Fig. 2.5*b* shows the location of the devices in a typical portal frame.
The numerical modeling of the device's behavior is commonly based on the use of bilinear hysteretic rules, however, more complications appears in the (nonlinear) studies covering the seismic analysis of buildings with FDs, *e.g.* Aiken *et al.* in [6] study the seismic response of a nine-story steel frame with FD located in the cross-bracing system. Ryan and Chopra [345] estimate the seismic displacement of friction pendulum isolators based on time history responses obtained from nonlinear analysis. Additional references can be consulted in the same works.

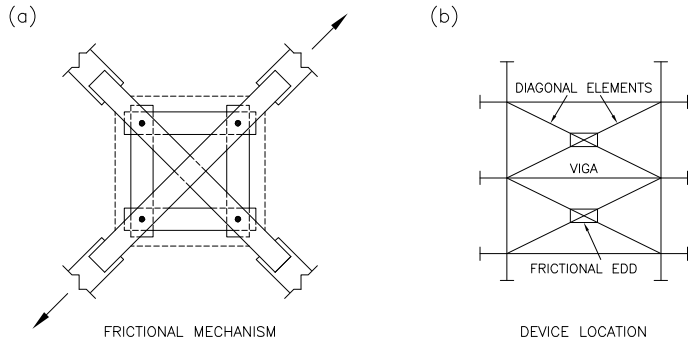

Figure 2.5: Frictional damper. (*a*): Device. (*b*): Location on a typical RC building.

(iv) *Fluid based devices*

Fluids can also be used as basic material in order to control the seismic response of flexible structures. The original efforts have been oriented to convert the applications developed for the military and heavy industry to the civil engineering field. Several application of this kind of devices have been focused on the control of vibrations derived from shock and ambient excitations. For example, in [223] the fluid damper technology is described in a wide context.
Viscous fluid dampers (VFD) dissipate energy when subjected to a velocity input. Usually,

dissipation has place due to the conversion of the mechanical work of a piston moving in a highly viscous fluid, such as silicon gel, into heat. Larger viscosity values implies a greater energy dissipation. Currently, materials which exhibits both frequency and temperature dependency are used.

Several kinds of devices have been proposed as VFD, for example in [408] the behavior and effectiveness of viscous–damping walls [287] in controlling wind-induced vibrations in multi-story buildings investigated. Other applications combine base isolation systems with VFD for controlling the lateral displacement of base isolated building. In this case, the VFDs increase the damping of the isolation system. Figure 2.1*b* shows several VFDs working in parallel with the base isolation system.

The most common types of VFDs are based on the flow of the fluid in a closer container. In general these devices acts forcing the fluid to pass through small orifices by mean of a piston [382]. Greater levels of energy dissipation can be obtained using this kind of devices, however, a more complex mechanical design of the damper is needed.

Fig. 2.6 show two typical cross sections of VFDs. They both consist of a stainless steel piston with an orifice head and are filled with viscous liquid, such as silicon oil. One of them has an accumulator while the other has a run-through rod instead. The difference of pressure between each side of the piston head result in the damping force, and the damping constant of the damper can be determined by adjusting the configuration of the orifice of the piston head. The device of Fig. 2.6*a* contains compressible silicone oil.

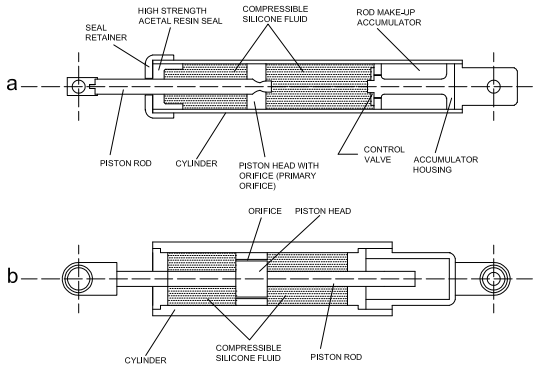

Figure 2.6: Typical VFD. (*a*): Device based on a highly compressible fluid. (*b*): device based on the flow of fluid through orifices.

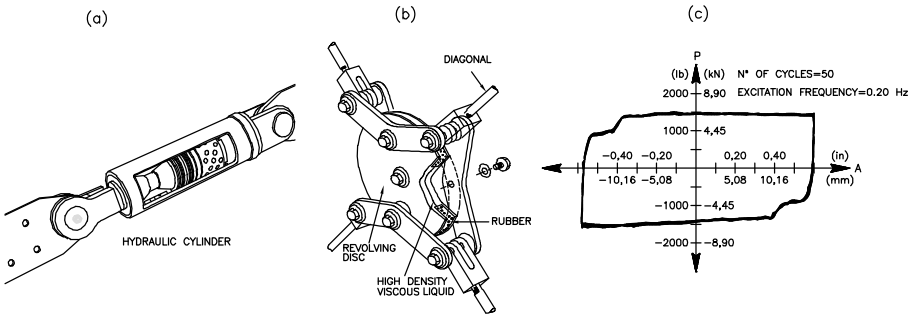

Figure 2.7: Hydraulic dampers. (*a*): Cylinder. (*b*): Revolving disc device. (*c*): Force-displacement characteristic curve.

Practical applications of this kid of EDD can be reviewed in [415, 409]. In Ref. [405] analytical and experimental studies to evaluate a strategy for structural health monitoring of nonlinear viscous dampers are presented. In [7] an extensive overview of the testing program for the viscous dampers used in the retrofit of the Golden Gate Bridge is provided, including four devices from U.S. manufacturers and two from European ones.

(v) *Extrusion devices*

A particular case of metallic devices is given by the extrusion ones (ED). In this case energy dissipation is produced due to the rearrangement of the crystalline red of special metals (such as lead) due to the imposition of a deformation (extrusion) but maintaining confined the dissipative nucleus of the device.

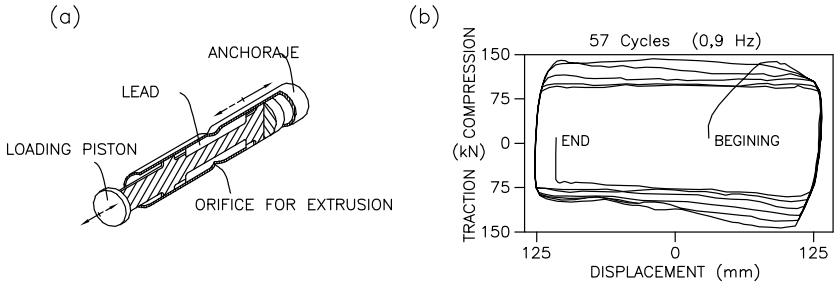

Figure 2.8: Lead extrusion dampers. (a): Device. (b): Force-displacement characteristic curve.

Fig. 2.8a shows a typical ED and in 2.8a the experimental force-displacement hysteretic curve is presented. Applications of these devices can be reviewed in [320, 339] and references therein.

(vi) *Other types*

Additional types of devices can be added to the present list, however, and by briefly, here only three additional typologies, which are treated in passive as well as active control fields, are mentioned: (a): *Smart materials*: This materials are incorporated to structural elements along with a set of sensors and actuator and are able to change their mechanical properties according to the dynamics of the structure were they are located. In this category are included *shape memory alloys* and devices based on *piezoelectric materials*. (b): *Tuned mass dampers*: These devices are added to the structures with the objective of receive and dissipate a part of the vibrational energy. They can be seen in the simplest case as a spring–dashpot system attached to the main structure. Usually, tuned mass dampers contribute to decrease the response of a particular mode and, therefore, for environmental actions with a wide frequency content, they are used in combination with other type of devices. For a more complete review of these types of devices see [382, 383] and references there quoted.

2.3.2 Complex geometric details

As it has been explained, although a great amount of work has been devoted to the development of refined nonlinear models for beam structures, all of them are subjected to the following limitations:

(i) Beam structures present either fully monolithic connections among elements or some of their degree of freedoms are released [200] (*e.g.* pinned connections). Therefore, structural

failures due to damage inside of the nodes, such as those occurred in poorly designed RC buildings [54] or in the so called *semi–rigid* connections of steel or composite structures [17], often are not properly considered.

(ii) The shape and the mechanical properties of the cross sections are considered constants in an element (or they have smooth variations) and, therefore, the beam models show serious difficulties in reproducing structural behaviors dominated by *local changes* in the geometry such as those observed in the connecting joints of precast concrete structures [315, 316].

Several attempts have been carried out for modeling the effects of local irregularities or local complex stress concentrations in framed structures. Probably, the most common approach consists in employing plastic hinge models with moment-curvature relations reflecting the mechanical characteristics of the connecting joints [221], although this approach has the previously described limitations. Other authors have focused their efforts towards developing specific solid-to-beam transition elements *e.g.* [428]. More realistic numerical studies of beam–column connections involve fully 3D finite element models as it is shown by Fu *et al.* in [138]; however, in their work the purpose still is obtaining simpler moment-curvature relationship of the connecting joints.
An alternative approach, combining precision, generality and computational efficiency consists of coupling reduced 1D and full 3D numerical models for different parts of the structure. In this case, most of the elements are prismatic rods and local irregularities or zones corresponding to the connecting joints receive a more detailed geometric description. The connection between models of different dimensions is done through *interface–surfaces*. Some research in this direction have been carried out by McCune *et al.* [280] where a scheme for establishing displacement compatibility and stress equilibrium at the interface is developed. The results are finally implemented as *multi–point constraint* equations relating the displacement field of the beam's node (which includes rotations) with the corresponding of the nodes of the solid at the interface. A similar approach is followed by Shim *et al.* [359, 358] and an application to earthquake engineering can be reviewed in [154]. The kinematic restrictions for a consistent beam-to-shell transition element in finite deformation is presented in [400]. Garusi and Tralli [140] develop hypostatic *transition* solid-to-beam and plate-to-beam elements following a stress assumed method. In [158], the dimensional–coupling is obtained applying the Lagrange multiplier's method. Göttlicher and Schweizerhof in [147] present the analysis of flexible structures with occasionally rigid parts under dynamics actions. Monaghan *et al.* in Ref. [291] develops a method for the dimensional–coupling between 1D beams and full 3D bodies. Blanco *et al.* [63] develop a unified variational approach for coupling 3D–1D models and show an application to the blood flow. In [146] a displacement based super–element is used for studying the propagation of waves in structures with singularities. In all the cases, the numerical examples are limited to the linear elastic case.
In this work, a two–scale approach (global and local) is developed in order to study the nonlinear response of RC framed buildings. At *global* scale level, all the elements of the FE model are rods; however, if (locally) geometric irregularities appear, a *zoom view* of the corresponding element is performed, consisting in a fully 3D model which constitutes the *local* scale level. The dimensional–coupling between scales is performed through *surface–interfaces* imposing the kinematic hypothesis assumed for the beam model. This method avoids the use of multi-points constraints or Lagrange multipliers. Starting from the full 3D stress state existing in the local model, cross sectional forces and moments, required at global level, are recovered by integrating at the surface–interface in an analogous manner as for the cross sectional analysis of beams [258]. Force and displacement equilibrium is checked local and global levels, ensuring that compatible configurations are reached for the whole problem. Computationally, the problem is managed by

means of a *master–slave* approach, where the global scale problem acts as the master, sending a *trial* displacement field to the local scale models (slaves) and then receives the corresponding internal forces, moments and tangential tensors estimated by means of integration on the surface interfaces. The proposed approach is well suited to be implemented in a *parallelized algorithm*, where the mater and slave problems are solved independently by different programs [379]. All the details are presented in §8.2.
An important branch of civil engineering structures presenting local geometric irregularities is that including the precast ones. In this case, irregularities are mainly located in the connecting joints which are, by constructive reasons, non-monolithic. The following section is devoted to give an overview of the main characteristics and limitations of the precast concrete structures.

2.3.2.a Precast structures

Precast concrete structures has been categorized in three types: (i) *skeletal frames*, (ii) *portal frames* and (iii) *wall frames*. Of these, the skeletal frame is the most challenging, both structural and architectonically, and therefore, they have attracted the most attention in research and development. This kind of structures has transformed passing since heavy-mass-produced elements to streamlined, long-span, lightweight, thermally and acoustically efficient free-maintenance structures of today. Many engineers, builders and researchers consider that precast concrete is the most versatile building material available, (see *e.g.* [122] and references therein). The other two kind of precast concrete structures, *i.e.* portal and wall frames, have limited applications to modular-like structures, however, the skeletal ones may be adapted for a wide range of multi-storey offices, car parks, shopping etc. The main feature being the versatile use of large open spaces. In general, the mass of skeletal structures is about a 5% of its volume with about a 2/3 of this in the floors[7].
Among the main reasons that have contributed to increase the market participation of the precast concrete are the high velocity of erection with a minimum site presence getting construction rates of 1000-2000 m^2 per week with a fixing team of around six persons. To achieve this rates, structural elements, (beams, columns, floors and walls), must be erected simply and safely, through efficient connector designs [315].
The global stiffness of precast frames is highly dependant on the local stiffness of the connectors between elements, often 5-10 times that of the elements. A very important aspect of the structural design of precast structures is that connections possess adequate strength and ductility specially when the whole structure undergoes large displacements, [122]. In this sense the most important connections are the column-foundation and column-beam joints. Most of the research work in the present is given by the study of the behavior of connecting joints, possibly at the expense of the structural elements itself which has been optimized in-house by the precast manufacturer. The lack of specific codes providing technical specifications about the design of precast structures with different connecting systems has carry to the employment pejorative rules that must be applied to concrete columns in unbraced frames, requiring lateral bracing to stabilize be used to stabilize skeletal frames of more than three storeys.
Precast shear walls, cores, masonry infill walls and cross bracing provide lateral stability and different degrees of stiffness but nonlinear interaction between stabilizing elements and the skele-

[7]This fact has motivated a large amount of research in pre-tensioned floors for both gravity and horizontal loads. Today there are a wide variety of engineering solutions providing light weight floors based on precast prestressing concrete unit and high strength concrete [122], which are one of the most economical flooring systems worldwide.

tal elements take place[8]. Some unbraced structures frames are stabilized by columns acting as moment-resisting cantilevers or by frame action via rigid or semi-rigid connections. Some designers prefer the pinned connections because of the perceived view that a semi-rigid connection could if not properly detailed and constructed, soften at loads near ultimate failure.
Pinned connections are easier to assemble, but rarely behave as perfect hinges because of the need of continuity tie steel, which rather destroy the intended notion. In any case unbraced frames frequently are designed as pinned joined structures [122].
Until recent years only a little effort in research and development on the global structural behavior of precast structures has been done. Probably, the most challenging initiative in this way has been the US-Japanese PRESSS project [122], but in any case a lot of work is necessary in development of specific tools in numerical analysis and design codes.
By other hand, braced frames are stabilized laterally by strategically positioned walls, cores or diagonals struts and ties. Many times these elements are in conflict with the architectural requirements limiting enormously their positions in the structure. The addition of bracing elements can produce extraordinarily high stress concentration when connected to the flexible pinned jointed frame and, therefore, the major part of the research has been focused on the localized behavior of such frames, particulary on cyclic or reversal loads in large displacement conditions, simulating the behavior expected during earthquakes. The need to develop hysteretic energy dissipaters has concentrated on attempting to satisfy the requirements of strength, stiffness and toughness simultaneously.
After several collapses of precast structures during recent earthquakes and other failures, the design criteria has been enhanced and innovative methods such as the *alternative load path* has been developed as a means of bypassing damaged elements or connections. In general, research activity on precast concrete frames can be subdivided in [122]:

(i) Studies on global precast frame behavior, focusing on the influence of connections. The profession agree that this type of research contribute to enhance the status of precast demonstrating their unquestionable structural integrity. Studies have been focused on the continuity of connections rather than on the elements themselves.
(ii) Sub-structuring the precast frames into appropriated two-dimensional cruciform or floor bay assemblies for the convenient experimental testing and/or numerical modeling.
(iii) Optimization of precast elements, in particular lightweight prestressed floor systems.
(iv) Vertical and horizontal stability systems, such as infill shear walls and precast floor diaphragms with out cast in situ structural toppings.
(v) Connections and joints.
(vi) Structural integrity. The collective issues of ductility, toughness and robustness.

Even when in the last 15 years the research on precast carried out in United States, Japan, the European Union and other countries has been increased notably, the percentage of the total resources invested in research on concrete structures destined to precast is about 2-3 %.
In view of the above list it is clear that numerical research and particularly, the development of robust numerical techniques for modeling and simulating the nonlinear response of precast structures considering local geometric irregularities, appears as a very important need for improving the mechanical response of this type of structures when subjected to accidental actions.

[8] A widespread amount of research is being done to know more about structural interaction between frame elements and the stabilization system [166].

Chapter 3

Geometrically exact formulation for rods

This chapter is devoted to the presentation of a geometrically exact formulation for rods capable of considering large displacements and rotations. The present formulation is based on that originally proposed by Simo [362] and extended by Vu-Quoc [363, 365], which generalize to the full three-dimensional dynamic case the formulation originally developed by Reissner [333, 332] for the plane static problem. These works are based on a convenient parametrization of the three-dimensional extension of the classical Kirchhoff–Love[1] [234] model. The approach can be classified as a *director type*'s one according to Antman [11, 13], which allows to consider finite shearing, extension, flexure and torsion. In the present case, an initially curved and unstressed rod is considered as the reference configuration in an analogous approach as Ibrahimbegović *et al.* [178, 182].

First, a detailed description of the kinematic assumptions of the rod model is carried out in the framework of the configurational description of the mechanics. Due to its importance in the development of time–stepping schemes in next chapters, special attention is paid to the formal definition of the nonlinear differentiable manifolds that constitute the configuration, placement and their tangent spaces. After defining translational and rotational strain vectors and calculating the deformation gradient tensor, a set of strain measures at material point level on the cross section are described following the developments of Kapania and Li [207, 208]. However, the developments are not limited to the static case and explicit expressions for the material, spatial and co–rotational versions of the strain rate vectors as functions of the spin variables are also provided. At material point level, the conjugated stress measures are deduced from the principles of continuum mechanics and using the power balance condition for deducing the stress measure energetically conjugated to the cross sectional strain measures.

The equations of the motion of the rod are deduced starting from the local form of the linear and angular balance conditions and integrating over the rod's volume. A form (weak) appropriated for the numerical implementation is deduced for the nonlinear functional corresponding to virtual work principle, considering the noncommutative nature of a part of the admissible variation of the displacement field.

Finally, a discussion about the deduction of reduced constitutive relations considering hyperelastic materials is presented, leaving the detailed treatment of the rate dependent and independent constitutive nonlinearity for the next chapter.

[1] The Kirchhoff–Love formulation can be seen as the finite strain counterpart of the Euler formulation for beams frequently employed in structural engineering [36, 113].

3.1 Kinematics

For an appropriated description of the three-dimensional motion of rods and shells in finite deformation (and in the rigid body dynamics [11, 62, 108, 188]) it is necessary to deal with the (finite) rotation of a unit triad and therefore, the results of Appendix A will be used repeatedly here to describe the Reissner–Simo geometrically exact formulation for rods.
First, it is necessary to define the orthogonal frame $\{\hat{E}_i\}$ which corresponds to the *material* reference frame of the configurational description of the mechanic, and it is defined to be coincident with the *fixed spatial* frame $\{\hat{e}_i\}$ by convenience. The concept of *spatially fixed* means that the corresponding spatially fixed objects are fixed in an arbitrarily chosen orthogonal frame[2] $\{\hat{e}_i\}$ that has no acceleration nor rotation in the 3D inertial physical space [365].

3.1.1 Initially curved and twisted reference rod

The configuration of a physically *unstrained*, *unstressed*, *curved* and *twisted* rod, simply called *curved reference rod*, is defined by a smooth and *spatially* fixed reference curve with its position vector given by

$$\hat{\varphi}_0 = \hat{\varphi}_0(S_0) \in \mathbb{R}^3 = \varphi_{0i}\hat{e}_i \in \mathbb{R}^3, \quad S_0 \in [0, L_0] \tag{3.1}$$

where reference curve is parameterized by its real *arch–length* coordinate $S_0 \in [0, L_0] \subset \mathbb{R}$ with $L_0 \in \mathbb{R}$ being the total real arch–length of the initially curved and twisted reference curve.
The reference curve also correspond to the line of *centroid* connecting a family of *cross sections* through the geometry, mass or elasticity [228, 362]. Formally, plane cross sections are defined considering the local *orthogonal* frame $\{\hat{t}_{0i}(S_0)\}$, which is rigidly attached to each $S_0 \in [0, L_0]$ with its origin at $\hat{\varphi}_0(S)$. It is explicitly given by

$$\hat{t}_{0i} = \hat{t}_{0i}(S_0) = t_{0ij}\hat{e}_j \in \mathbb{R}^3, \quad \hat{t}_{0i} \cdot \hat{t}_{0j} = \delta_{ij} \tag{3.2}$$

where the components of the vectors $\hat{t}_{0i}$ are given referred to the spatial frame $\{\hat{e}_i\}$.
Considering the coordinate system $\xi_\beta \in \mathbb{R}$, $(\beta = 2, 3)$ defined along the base vectors $\{\hat{t}_{0\beta}\}$ it is possible to construct a compact subset of $\mathbb{R}^2$ defining the shape and size of the rod cross section, which is obtained by means of selecting an appropriated set of pairs $(\xi_\beta) \in \mathbb{R}^2$. This set is designed as $\mathcal{A}_0 = \mathcal{A}_0(S_0) \subset \mathbb{R}^2$ and in following it will be identified with the corresponding plane rod cross section at S_0. An additional assumption is that $\mathcal{A}_0$ vary smoothly along the material points on the reference curve $\hat{\varphi}_0$, but it is invariant under any deformation. Thats to say, material points attached to a given cross section are always the same. Since, the curved reference rod is considered to be free of either strain nor stress, it is conventionally assumed that the cross section planes of the curved reference rod are normal to the unit tangent vector[3] $\hat{\varphi}_{0,S_0} \in \mathbb{R}^3$ at the point $S_0 \in [0, L_0]$ [178, 228, 362] and, therefore, we have

$$\hat{\varphi}_{0,S_0} = \hat{t}_{01} \tag{3.3a}$$

$$\hat{\varphi}_{0,S_0} \cdot \hat{t}_{0i} = \delta_{1i} \tag{3.3b}$$

$$\|\hat{t}_{0i}\| = 1. \tag{3.3c}$$

[2] The base vector $\{\hat{e}_i\}$ is such that $\hat{e}_i \cdot \hat{e}_j = \delta_{ij}$; $(i, j = 1 \dots 3)$.
[3] The symbol $(\bullet)_{,x}$ denotes partial differentiation with respect to the variable x *i.e.* $\partial(\bullet)/\partial x$.

In this manner, we have that the position vector of any *material point* $\hat{x}_0 = \hat{x}_0(S_0, \xi_\beta) \in \mathbb{R}^3$ on the curved reference rod[4] is described by

$$\hat{x}_0 = \hat{\varphi}_0(S_0) + \xi_\beta \hat{t}_{0\beta}(S_0) = \hat{\varphi}_0 + \xi_2 \hat{t}_{02} + \xi_3 \hat{t}_{03} \tag{3.4}$$

where $(S_0, \xi_\beta) \in ([0, L_0] \times \mathcal{A}_0) \subset (\mathbb{R} \times \mathbb{R}^2)$. It is worth to note that the reference curve $\hat{\varphi}_0$ corresponds to the set of material points of the form described by the family of vectors $\hat{x}(S_0, \xi_\beta = 0)$. Therefore, the kinematic assumptions imply that an *admissible configuration* of the curved reference rod is formed by material points as those described by Eq. (3.4).
Due to the fact that $\{\hat{E}_i\}$ and $\{\hat{e}_i\}$ are orthogonal frames, there exist an orthogonal tensor $\mathbf{\Lambda}_0 = \mathbf{\Lambda}_0(S_0) \in SO(3)$ relating $\hat{t}_{0i}$ and $\hat{E}_i$ by

$$\hat{t}_{0i} = \mathbf{\Lambda}_0 \hat{E}_i \quad \Leftrightarrow \quad \mathbf{\Lambda}_0 \equiv \hat{t}_{0i} \otimes \hat{E}_i = t_{0ji} \hat{e}_i \otimes \hat{E}_j = \Lambda_{0ij} \hat{e}_i \otimes \hat{E}_j. \tag{3.5}$$

Therefore, the components of $\mathbf{\Lambda}_0$ referred to the basis $\{\hat{e}_i \otimes \hat{E}_j\}$ are given by

$$[\mathbf{\Lambda}_0]_{\hat{e}_i \otimes \hat{E}_j} = [\Lambda_{0ij}]_{\hat{e}_i \otimes \hat{E}_j} = \begin{bmatrix} t_{011} & t_{021} & t_{031} \\ t_{012} & t_{022} & t_{032} \\ t_{013} & t_{023} & t_{033} \end{bmatrix}. \tag{3.6}$$

Hence, considering that $t_{0ij} = \hat{t}_{0i} \cdot \hat{e}_j$ gives the *director cosine* of $\hat{t}_{0i}$ with respect to $\hat{e}_j$, we have that the orthogonal tensor $\mathbf{\Lambda}_0 \in SO(3)$ determines the orientation of the cross sections of the curved reference rod. For this reason the rotation tensor $\mathbf{\Lambda}_0 = \hat{t}_{0i} \otimes \hat{E}_j$ is usually referred as the *orientation tensor* of the curved reference rod cross section [228, 362].
By the other hand, $\mathbf{\Lambda}_0$ corresponds to a *two-point* tensor relating vectors belonging to the *material space vector*, obtained by the expansion of the material reference frame $\{\hat{E}_i\}$ and vectors belonging to the *spatial space vector* obtained expanding the spatial reference frame $\{\hat{t}_{0i}\}$. In this way, it is possible to say that $\mathbf{\Lambda}_0$ has 'one leg' in the material reference configuration and the another in the spatial one.
The above results imply that the *configuration* of the curved reference rod is completely determined by the family of position vectors of the centroid curve $\hat{\varphi}_0$ and the family of orthogonal rotation tensors $\mathbf{\Lambda}_0$ [246, 362, 363]. Moreover, taking into account the results of §A.3 to §A.5 of Appendix A, it is possible to construct the following definitions:

Definition 3.1. ***Curved reference configuration***

In this way, it is possible to define the *curved reference configuration* by the following manifold

$$\mathcal{C}_0 := \{(\hat{\varphi}_0, \mathbf{\Lambda}_0) : [0, L_0] \to \mathbb{R}^3 \times SO(3) \;\big|\; \hat{\varphi}_{,S_0} \cdot \hat{t}_{01} > 0\} \tag{3.7}$$

which is the set composed by the family of pairs $(\hat{\varphi}_0, \mathbf{\Lambda}_0)$ that define the initial geometry of the curved reference rod ■

Definition 3.2. ***Material placement***

The *material placement* of the curved reference rod is defined as

$$\mathcal{B}_0 := \{\hat{x}_0(S_0, \xi_\beta) \in \mathbb{R}^3 \;\big|\; \hat{x}_0 = \hat{\varphi}_0(S_0) + \xi_\beta \mathbf{\Lambda}(S_0) \hat{E}_\beta; \quad (S_0, \xi_\beta) \in [0, L_0] \times \mathcal{A}_0\} \tag{3.8}$$

constituted by all the physical points of the space which are occupied by material points at the

[4]It has been identified each material point or particle on the rod with its corresponding coordinate coordinate values *i.e.* $(S_0, \xi_\beta) \in [0, L_0] \times \mathcal{A}(S_0)$ along the spatial frame $\{\hat{t}_{0i}\}$ or equivalently $\{\hat{e}_i\}$.

initial time, conventionally designed by t_0 ■

Definition 3.3. ***Tangent bundle***

The *tangent space* to the material placement of the curved reference rod is given by

$$T\mathcal{B}_0 := \{(\hat{U}_{x_0}, \hat{x}_0) \in \mathbb{R}^3 \otimes \mathcal{B}_0 \subset \mathbb{R}^3 \otimes \mathbb{R}^3 \;\big|\; \hat{U}_{x_0} \in \mathbb{R}^3; \quad \hat{x}_0 \in \mathcal{B}_0\}. \tag{3.9}$$

That is to say, the tangent space to $\mathcal{B}_0$ corresponds to the set of vectors belonging to $\mathbb{R}^3$ (or an isomorphic linear space) with base points on the elements of $\mathcal{B}_0$ ■

Definitions 3.1 and 3.2 correspond to nonlinear differentiable manifolds. If one takes a fixed point $\hat{x}_0$, by analogy with Eq. (3.9), it is possible to define the tangent space to the material placement with base point $\hat{x}_0$ denoted by $T_{\hat{x}_0}\mathcal{B}_0$. Moreover, one have

$$T\mathcal{B}_0 \equiv \bigcup_{\hat{x}_0 \in \mathcal{B}_0} T_{\hat{x}_0}\mathcal{B}_0.$$

3.1.2 Straight reference rod

Additionally, a spatially fixed, straight, unstrained and untwisted reference rod can be defined, whose the centroid line is given by the position vector

$$\hat{\varphi}_{00}(S_{00}) = S_{00}\hat{E}_1 = S_{00}\hat{e}_1 \tag{3.10}$$

with its arch–length coordinate S_{00} and total arch–length L_{00} exactly the same as in the case of the curved reference rod *i.e.* $S_{00} \equiv S_0$ and $L_{00} \equiv L_0$. The corresponding local frames $\{\hat{t}_{00i}\}$ of the cross sections are given by $\hat{t}_{00i} \equiv \hat{E}_i = \hat{e}_i$.
By analogy with the case of the curved reference rod, the position vector $\hat{x}_{00} = \hat{x}_{00}(S_{00}, \xi_\beta)$ of any material point (S_{00}, ξ_β) for $S_{00} \equiv S_0 \in [0, L_{00}]$ and $(\xi_\beta) \in \mathcal{A}_{00}(S_{00})$ on the cross section, can be described by

$$\hat{x}_{00} = \hat{\varphi}_{00}(S_{00}) + \xi_\beta \hat{t}_{00\beta}(S_{00}) = S_0\hat{E}_1 + \xi_2\hat{E}_2 + \xi_3\hat{E}_3. \tag{3.11}$$

Following analogous procedures as for $\mathbf{\Lambda}_0$, the corresponding *orientation tensor* (or rotation tensor) for the straight reference rod is simply given by

$$\mathbf{\Lambda}_{00} \in SO(3) \equiv \hat{t}_{00i} \otimes \hat{E}_i = \hat{E}_i \otimes \hat{E}_i = \mathbf{I} \tag{3.12}$$

where $\mathbf{I}$ is the second–order identity tensor of dimension three on the material vector space spanned by $\{\hat{E}_i \otimes \hat{E}_j\}$. The configuration of the straight reference rod is completely determined by the family of the arch–length coordinates S_{00} and orthogonal rotation tensors $\mathbf{\Lambda}_{00}$, therefore, it is possible to define the following mathematical objects:

Definition 3.4. ***Straight reference configuration***

The *straight reference configuration space* is defined by

$$\mathcal{C}_{00} := \{(S_{00}, \mathbf{\Lambda}_{00} = \mathbf{I}) : [0, L_{00}] \to \mathbb{R} \times SO(3)\} \tag{3.13}$$

which is fixed in space and time ■

Definition 3.5. ***Material placement***

The *material placement* of the straight reference rod is defined as

$$\mathcal{B}_{00} := \{\hat{x}_{00}(S_{00}, \xi_\beta) \in \mathbb{R}^3 \;\big|\; \hat{x}_{00} = S_{00}\hat{E}_1 + \xi_\beta \hat{E}_\beta; \quad (S_{00}, \xi_\beta) \in [0, L_{00}] \times \mathcal{A}_{00}\} \tag{3.14}$$

which is equivalent to the set of material points of the rod at the fictitious time t_{00} ■

Definition 3.6. ***Tangent bundle***

The *tangent bundle* to the material placement of the straight reference rod is given by

$$T\mathcal{B}_{00} := \{(\hat{U}_{x_{00}}, \hat{x}_{00}) \in \mathbb{R}^3 \otimes \mathcal{B}_{00} \subset \mathbb{R}^3 \otimes \mathbb{R}^3 \;\big|\; \hat{U}_{x_{00}} \in \mathbb{R}^3; \quad \hat{x}_{00} \in \mathcal{B}_{00}\}. \tag{3.15}$$

Therefore, the tangent bundle to $\mathcal{B}_0$ corresponds to the set of vectors belonging to $\mathbb{R}^3$ (or an isomorphic linear space) with base points on the elements of $\mathcal{B}_{00}$ ■

As before in the curved reference rod, definitions 3.5 and 3.6 correspond to nonlinear differentiable manifolds. The tangent space to the material placement with base point $\hat{x}_{00} = \hat{X}$ denoted by $T_{\hat{X}}\mathcal{B}_{00}$ and one has

$$T\mathcal{B}_{00} \equiv \bigcup_{\hat{X} \in \mathcal{B}_{00}} T_{\hat{X}}\mathcal{B}_{00}.$$

3.1.3 Current rod

During the motion the rod deforms from the curved reference rod configuration at time t_0 to the *current rod configuration* at time t. The position vector of any material point initially located on the curved reference rod with coordinate $S_0 \equiv S \in [0, L_0]$ moves from $\hat{\varphi}_0 \in \mathbb{R}^3$ to $\hat{\varphi} \in \mathbb{R}^3$ at time t throughout the addition of the translational displacement $\hat{u} = \hat{u}(S) \in \mathbb{R}^3$ *i.e.*

$$\hat{\varphi}(S) = \hat{\varphi}_0(S) + \hat{u}(S) \tag{3.16}$$

during the same motion, the initial local orientation frame $\mathbf{\Lambda}_0$ is rotated, along with the plane cross section, from $\hat{t}_{0i} \in \mathbb{R}^3$ at time t_0 to $\hat{t}_i \in \mathbb{R}^3$ at time t, which stays orthogonal and unitary ($\hat{t}_i \cdot \hat{t}_j = \delta_{ij}$), by means of the orthogonal *incremental rotation tensor* $\mathbf{\Lambda}_n \in SO(3)$ in the following way

$$\hat{t}_i \equiv \mathbf{\Lambda}_n \hat{t}_{0i} = \mathbf{\Lambda}_n \mathbf{\Lambda}_0 \hat{E}_i. \tag{3.17}$$

The term $\mathbf{\Lambda} = \mathbf{\Lambda}_n \mathbf{\Lambda}_0 \in SO(3)$ corresponds to a compound rotation as it as been defined in Eq. (A.3). In Eq. (3.17) the spatial updating rule for rotations has been used; if the material updating is preferred Eq. (3.17) transforms to the equivalent $\mathbf{\Lambda} = \mathbf{\Lambda}_0 \mathbf{\Lambda}_n^{\mathrm{m}}$ with $\mathbf{\Lambda}_n^{\mathrm{m}} = \mathbf{\Lambda}^T \mathbf{\Lambda}_n \mathbf{\Lambda}$. By simplicity in the exposition, for the moment the spatial rule will be used in most of the cases; on the contrary it will be clearly indicated.
In the configurational description of the motion, the rotation tensor $\mathbf{\Lambda}$ can be seen as a two-point operator that maps vectors belonging the space spanned by the material reference frame $\{\hat{E}_i\}$ to vectors belonging the space spanned by the current spatial frame $\{\hat{e}_i\}$. Furthermore, $\mathbf{\Lambda}$ can be seen as a linear application as follows

$$\begin{aligned} \mathbf{\Lambda} : \{\hat{E}_i\} &\rightarrow \{\hat{e}_i\} \\ \hat{V} &\mapsto \mathbf{\Lambda}\hat{V} = \hat{v} \end{aligned} \tag{3.18}$$

where $\hat{V}$ and $\hat{v}$ are two generic vectors belonging to the spaces spanned by $\{\hat{E}_i\}$ and $\{\hat{e}_i\}$, respectively. The components of $\mathbf{\Lambda}$ in those two reference systems are simply given by

$$\mathbf{\Lambda} \equiv \hat{t}_i \otimes \hat{E}_i \in SO(3). \tag{3.19}$$

By the other hand, the incremental rotation tensor $\mathbf{\Lambda}_n$ maps the base vectors $\{\hat{t}_{0i}\}$ to the base vectors $\{\hat{t}_i\}$ and the components of $\mathbf{\Lambda}_n$ given in those reference systems are given by

$$\mathbf{\Lambda}_n \equiv \hat{t}_i \otimes \hat{t}_{0i} \in SO(3). \tag{3.20}$$

Considering that $\hat{t}_i = t_{ij}\hat{e}_j$, it is possible to observe that the component representation of the orthogonal tensor $\mathbf{\Lambda}$, referred to the bases $\{\hat{e}_i \otimes \hat{E}_j\}$, is

$$[\mathbf{\Lambda}]_{\hat{e}_i \otimes \hat{E}_j} = [\Lambda_{ij}]_{\hat{e}_i \otimes \hat{E}_j} = \begin{bmatrix} t_{11} & t_{21} & t_{31} \\ t_{12} & t_{22} & t_{32} \\ t_{13} & t_{23} & t_{33} \end{bmatrix} = [\hat{t}_1, \hat{t}_2, \hat{t}_3]. \tag{3.21}$$

In this manner, the orthogonal tensor $\mathbf{\Lambda}$ determines the orientation of the moving rod cross section at time t. Similar to $\mathbf{\Lambda}_0$, the rotation tensor $\mathbf{\Lambda}$ is frequently called the *orientation tensor* of the current rod cross section at the material point $(S, \xi_\beta = 0)$.
It is worth to note that the rotation operator $\mathbf{\Lambda}(S,t)$ can be minimally parameterized (see Appendix A, Section A.2) using the material or spatial description of the rotation vector $\hat{\Psi}(S,t) \in T^{\text{mat}}_{\mathbf{I}}$, $\hat{\psi}(S,t) \in T^{\text{spa}}_{\mathbf{I}}$, respectively.

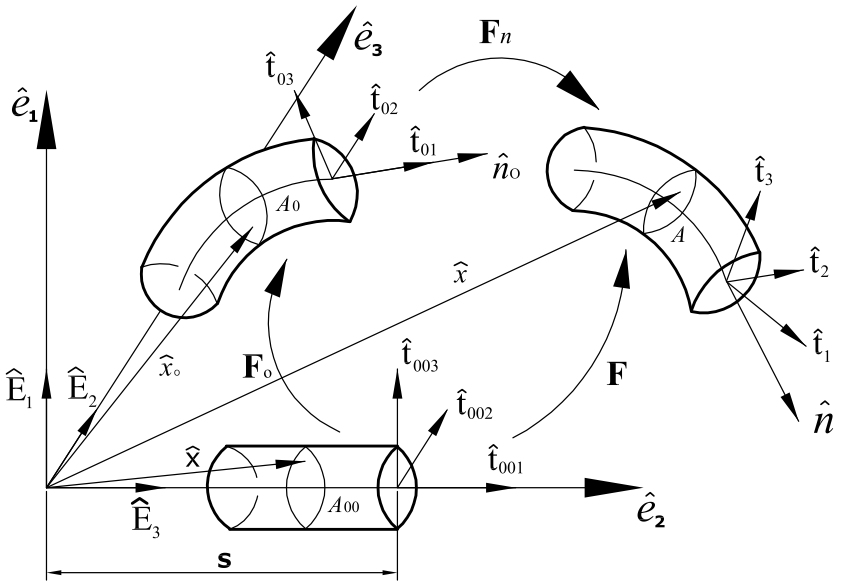

Figure 3.1: Configurational description of the rod model.

The position vector $\hat{x} \equiv \hat{x}(S, \xi_\beta, t) \in \mathbb{R}^3 \times \mathbb{R}^+$ of any material point $(S, \xi_\beta) \in [0, L] \times \mathcal{A}$ on the moving rod cross section at time t is

$$\hat{x}(S, \xi_\beta, t) = \hat{\varphi}(S,t) + \xi_\beta \hat{t}_\beta(S,t) = \hat{\varphi}(S,t) + \xi_\beta \mathbf{\Lambda}(S,t)\hat{E}_\beta. \tag{3.22}$$

Eq. (3.22) realizes the Reissner–Simo hypothesis for rods [332, 362], hence it is a parametrization of the constraint infinite–dimensional manifold that arise from the hypothesis that the config-

uration of the rod is described by means of the displacement of a centroid line more the rigid body-rotation of the cross sections attached to it.
The position vector field $\hat{x}$ can also be viewed as an one–dimensional solid, *i.e.* an internally one–dimensional vector bundle constituted by the cross section planes of the rod; and time t is considered as an independent parameter. For a more complete review of this point of view of the rod theory it is convenient to consult the works of Mäkinen *et al.* [246, 245].
The above results imply that the *moving rod configuration* at time $t \in \mathbb{R}^+$ can be completely determined by the position vector of the centroid curve $\hat{\varphi} \in \mathbb{R}^3$ and the family of orthogonal rotation tensors $\mathbf{\Lambda} \in SO(3)$ of the rod cross section [246, 362, 363]. The following definitions complete the kinematical hypothesis for the current rod:

Definition 3.7. ***Current configuration space***

In this way, it is possible to define the *current configuration space* at time t by

$$\mathcal{C}_t := \{(\hat{\varphi}, \mathbf{\Lambda}) : [0, L_0] \to \mathbb{R}^3 \times SO(3) \;\Big|\; \hat{\varphi}_{,S_0} \cdot \hat{t}_{01} > 0,\ (\hat{\varphi}_0, \mathbf{\Lambda}_0)|_{\partial_\Phi \hat{\varphi}_0} = (\hat{\varphi}_{0\Phi}, \mathbf{\Lambda}_{0\Phi})\} \tag{3.23}$$

subjected to have prescribed values $(\hat{\varphi}_{0\Phi}, \mathbf{\Lambda}_{0\Phi})$ on a subset $\partial_\Phi \hat{\varphi}_0$ of the two end points of the rod defined by the set $\partial \hat{\varphi}_0 = \{\hat{\varphi}_0(0), \hat{\varphi}_0(L_0)\}$. The manifold $\mathcal{C}_t$ is called the abstract configuration space of the rod. Note that $\partial_\Phi \hat{\varphi}_0 = \emptyset$ implies the *free fly* of a rod [373] ■

Particular cases are $\mathcal{C}_0$ of Eq. (3.7), at time t_0 when the moving rod coincides with the spatially fixed curved reference rod and $\mathcal{C}_{00}$ of Eq. (3.13), at 'time' t_{00} when it coincides with the spatially fixed straight reference rod configuration[5]. Therefore, the configuration space can be globally included in the Cartesian product $\mathbb{R}^3 \times SO(3)$ where $\mathbb{R}^3$ refers to the translational displacement and $SO(3)$ to the rotational displacement.

Definition 3.8. ***Spatial placement of the rod***

The *spatial placement of the rod* is defined as

$$\mathcal{B}_t := \{\hat{x}(S, \xi_\beta, t) \in \mathbb{R}^3 \;\big|\; \hat{x} = \hat{\varphi}(S, t) + \xi_\beta \mathbf{\Lambda}(S, t) \hat{E}_\beta; \quad (S, \xi_\beta, t) \in [0, L_0] \times \mathcal{A} \times \mathbb{R}\} \tag{3.24}$$

which can be seen as the set of the point in the ambient space which are occupied by the material points of the rod at time t ■

Definition 3.9. ***Tangent bundle***

The *tangent bundle* to the spatial placement is given by

$$T\mathcal{B}_t := \{\delta(\hat{x}) \in \mathbb{R}^3 \;\big|\; \delta(\hat{\varphi}) + \delta(\mathbf{\Lambda}) \xi_\beta \hat{E}_\beta,\ \hat{x} \in \mathcal{B}\} \tag{3.25}$$

where the variation $\delta(\bullet)$ can also be replaced by other vectors with base point on material points of the rod at the current configuration ■

Again, one has that $\mathcal{C}_t$ and $\mathcal{B}_t$ are differentiable manifolds. The *tangent space* to $\mathcal{B}_t$ at base point $\hat{x}$ is denoted by $T_{\hat{x}}\mathcal{B}_t$ and the following relation holds

$$T\mathcal{B}_t \equiv \bigcup_{\hat{x} \in \mathcal{B}_t} T_{\hat{x}}\mathcal{B}_t.$$

[5]Note that both curved and straight reference rod configurations are spatially fixed and independent of time though moving rod configuration may coincide with these by respectively taking pre–subscripts '0' and '00'.

If the material updating rule is used for compound rotations, we have that the *variation field* $\delta\hat{x} \in T\mathcal{B}_t$, which define the elements of the tangent space to the spatial placement $\mathcal{B}_t$ in Eq. (3.24), can be written in material representation as

$$\delta\hat{x} = \delta\hat{\varphi} + \mathbf{\Lambda}\delta\widetilde{\mathbf{\Theta}}\xi_\beta\hat{E}_\beta \quad \in \quad T_{\hat{x}}\mathcal{B}_t \tag{3.26}$$

where $\mathbf{\Lambda}\delta\widetilde{\mathbf{\Theta}} \in T^{\text{mat}}_{\mathbf{\Lambda}}SO(3) = T_{\hat{X}}\mathcal{B}_{00}\otimes T^*_{\hat{X}}\mathcal{B}_{00}$ corresponds to the variation of the rotation operator $\mathbf{\Lambda}$ given in Eq. (A.98a). By the other hand, if $\mathbf{\Lambda}$ is updated using the spatial rule *i.e.* $\hat{\theta} = \mathbf{\Lambda}\hat{\Theta}$, it is also possible to represent the variation field $\delta\hat{x}$ in spatial form as

$$\delta\hat{x} = \delta\hat{\varphi} + \delta\widetilde{\boldsymbol{\theta}}\mathbf{\Lambda}\xi_\beta\hat{E}_\beta = \delta\hat{\varphi} + \delta\widetilde{\boldsymbol{\theta}}\xi_\beta\hat{t}_\beta \quad \in \quad T_{\hat{x}}\mathcal{B}_t \tag{3.27}$$

where $\delta\widetilde{\boldsymbol{\theta}}\mathbf{\Lambda} \in T^{\text{spa}}_{\mathbf{\Lambda}}SO(3) = T_{\hat{x}}\mathcal{B}_t \otimes T^*_{\hat{x}}\mathcal{B}_t$. One of the main advantages of choosing the material representation for the rotation tensor and their variation field is avoiding the employment of Lie derivatives in the linearization of the virtual work functional and, therefore, avoiding certain complications related with the obtention of the tangent stiffness tensor for numerical calculations, as it will be explained in next chapters.
The straight and curved reference configurations as well as the current configuration have been drawn in Fig. 3.1. All the above described tangent spaces have associated the corresponding *dual tangent spaces*[6]: $T^*_{(\bullet)}\mathcal{B}$, $T^*_{(\bullet)}\mathcal{B}_0$ and $T^*_{(\bullet)}\mathcal{B}_{00}$ respectively, spanned by the co–vector base $\{\hat{E}^*_i\}$. Considering that the material reference frame $\{\hat{E}_i\}$ is an Euclidean spatially fixed basis, it is possible to assume that the associated dual basis $\{\hat{E}^*_i\}$ is coincident with it, *i.e.* $\{\hat{E}_i\} \cong \{\hat{E}^*_i\}$; therefore, strictly no differentiation is needed between $T_{(\bullet)}(\bullet)$ and $T^*_{(\bullet)}(\bullet)$.

3.1.4 Geometric interpretation of elongation and shearing

The arch–element ds of the current rod centroid line corresponding to the material point at $S \in [0, L]$ on the curved reference rod is $ds = \mathcal{J}dS$, where $\mathcal{J} \equiv \|\hat{\varphi}_{,S}\|_{L_2}$[7]. Then the *elongation* or *elongation ratio* of the centroid line of the moving rod at time t is defined by [228]

$$e(S) = \frac{ds}{dS} - 1 = \mathcal{J} - 1. \tag{3.28}$$

Thus, the *unit tangent vector* of the centroid curve of the moving rod at time t corresponding to the material point $S \in [0, L]$ on the rod centroid curve is calculated as

$$\hat{\varphi}_{,s} = \frac{d\hat{\varphi}}{dS}\frac{dS}{ds} = \frac{1}{\mathcal{J}}\hat{\varphi}_{,S} = \frac{1}{1+e}\hat{\varphi}_{,S}\,. \tag{3.29}$$

In the general case, the unit normal vector $\hat{t}_1$ of the deformed rod cross section does not coincide with the unit tangent vector $\hat{\varphi}_{,s}$ because of the shearing; the angle changes between the tangent vector of the centroid curve and $\hat{t}_1$ and away from orthogonal to $\hat{t}_2$ and $\hat{t}_3$ are the angles of shearing, denoted by γ_{1i} and determined (see [228, 207, 174]) by

$$\hat{\varphi}_{,s}\cdot\hat{t}_1 = \frac{1}{1+e}\hat{\varphi}_{,S}\cdot\hat{t}_1 = \cos\gamma_{11}$$

[6]Some times called *co–vector* spaces or space of the one forms [245].
[7]The L_2 norm of a vector is $\|\hat{v}\|_{L_2} = (\hat{v}\cdot\hat{v})^{\frac{1}{2}}$ for any vector $\hat{v} \in \mathbb{R}^n$.

$$\begin{aligned}\hat{\varphi}_{,s}\cdot\hat{t}_2 &= \frac{1}{1+e}\hat{\varphi}_{,S}\cdot\hat{t}_2 = \cos(\frac{\pi}{2}-\gamma_{12}) = \sin\gamma_{12}\\ \hat{\varphi}_{,s}\cdot\hat{t}_3 &= \frac{1}{1+e}\hat{\varphi}_{,S}\cdot\hat{t}_3 = \cos(\frac{\pi}{2}-\gamma_{13}) = \sin\gamma_{13}.\end{aligned} \tag{3.30}$$

At time t_0 the moving rod coincides with the curved reference rod. Similarly, it is possible to rewrite Eqs. (3.30) for the curved reference rod throughout the corresponding elongation and shearing as

$$\begin{aligned}\frac{1}{1+e_0}\hat{\varphi}_{0,S}\cdot\hat{t}_{01} &= \cos\gamma_{011}\\ \frac{1}{1+e_0}\hat{\varphi}_{0,S}\cdot\hat{t}_{02} &= \sin\gamma_{012}\\ \frac{1}{1+e_0}\hat{\varphi}_{0,S}\cdot\hat{t}_{03} &= \sin\gamma_{013}, \quad e_0=0,\ \gamma_{01i}=0.\end{aligned}$$

3.1.5 Time derivatives, angular velocity and acceleration

Considering the spatial updating of the compound rotation $\boldsymbol{\Lambda}=\boldsymbol{\Lambda}_n\boldsymbol{\Lambda}_0$ we have that the velocity of a material point in the current configuration is calculated as the following material time derivative [251]:

$$\dot{\hat{x}} = \frac{\mathrm{d}\hat{x}}{\mathrm{d}t} = \dot{\hat{\varphi}} + \widetilde{\boldsymbol{v}}\hat{\mathscr{T}} = \boldsymbol{\Lambda}\big[\boldsymbol{\Lambda}^T\dot{\hat{\varphi}} + \widetilde{\boldsymbol{V}}\hat{\mathscr{E}}\big] \qquad \in \quad T_{\hat{x}}\mathcal{B}_t \tag{3.31a}$$

where $\hat{\mathscr{T}} \triangleq \xi_\beta\hat{t}_\beta$, $\hat{\mathscr{E}} \triangleq \xi_\beta\hat{E}_\beta$ and the spatial *angular velocity* tensor $\widetilde{\boldsymbol{v}} = \dot{\boldsymbol{\Lambda}}\boldsymbol{\Lambda}^T \in T^{\mathrm{spa}}_{\boldsymbol{\Lambda}}SO(3)$ of the current cross section is referred to the straight reference configuration and it is calculated employing the result of Eq. (A.113) as

$$\widetilde{\boldsymbol{v}} = \widetilde{\boldsymbol{v}}_n + \boldsymbol{\Lambda}_n\widetilde{\boldsymbol{v}}_0\boldsymbol{\Lambda}_n^T = \widetilde{\boldsymbol{v}}_n \quad \in \quad T^{\mathrm{spa}}_{\boldsymbol{\Lambda}_n}SO(3) \tag{3.31b}$$

where $\widetilde{\boldsymbol{v}}_0 = \dot{\boldsymbol{\Lambda}}_0\boldsymbol{\Lambda}_0^T = 0$ due to the fact that $\boldsymbol{\Lambda}_0$ is a spatially fixed tensor[8]. In Eq. (3.31a) the angular velocity tensor is also phrased in terms of the material angular velocity tensor referred to the straight reference rod, which is explicitly given by

$$\widetilde{\boldsymbol{V}} = \boldsymbol{\Lambda}^T\dot{\boldsymbol{\Lambda}} = \boldsymbol{\Lambda}^T\widetilde{\boldsymbol{v}}_n\boldsymbol{\Lambda} = \boldsymbol{\Lambda}_0^T\widetilde{\boldsymbol{V}}_n\boldsymbol{\Lambda}_0 \quad \in \quad T^{\mathrm{mat}}_{\boldsymbol{\Lambda}}SO(3) \tag{3.31c}$$

where $\widetilde{\boldsymbol{V}}_n = \boldsymbol{\Lambda}_n^T\dot{\boldsymbol{\Lambda}}_n \in T^{\mathrm{mat}}_{\boldsymbol{\Lambda}_n}SO(3)$ and in an analogous manner as with the spatial case we have that $\widetilde{\boldsymbol{V}}_0 = 0$. The corresponding axial vectors are: $\hat{v} = \hat{v}_n \in T^{\mathrm{spa}}_{\boldsymbol{\Lambda}}$, $\hat{V} \in T^{\mathrm{mat}}_{\boldsymbol{\Lambda}}$ and $\hat{V}_n \in T^{\mathrm{mat}}_{\boldsymbol{\Lambda}_n}$. Taking an additional material time derivative on Eq. (3.31a) we obtain the acceleration of a material point on the current configuration as

$$\ddot{\hat{x}} = \frac{\partial^2\hat{x}}{\partial t^2} = \ddot{\hat{\varphi}} + \dot{\widetilde{\boldsymbol{v}}}\hat{\mathscr{T}} + \widetilde{\boldsymbol{v}}\dot{\hat{\mathscr{T}}} = \ddot{\hat{\varphi}} + [\dot{\boldsymbol{\Lambda}}\widetilde{\boldsymbol{V}} + \boldsymbol{\Lambda}\boldsymbol{\Lambda}_0^T\dot{\widetilde{\boldsymbol{V}}}_n\boldsymbol{\Lambda}_0]\hat{\mathscr{E}} \qquad \in \quad T_{\hat{x}}\mathcal{B}_t \tag{3.32a}$$

where the time derivative of $\widetilde{\boldsymbol{v}}$, $\dot{\widetilde{\boldsymbol{V}}}_n$ and $\hat{\mathscr{T}}$ are calculated as

$$\begin{aligned}\dot{\widetilde{\boldsymbol{v}}} = \dot{\widetilde{\boldsymbol{v}}}_n &= \frac{\mathrm{d}}{\mathrm{d}t}(\dot{\boldsymbol{\Lambda}}_n\boldsymbol{\Lambda}_n^T) = \ddot{\boldsymbol{\Lambda}}_n\boldsymbol{\Lambda}_n^T + \dot{\boldsymbol{\Lambda}}_n(\dot{\boldsymbol{\Lambda}_n^T})\\ &= \ddot{\boldsymbol{\Lambda}}_n\boldsymbol{\Lambda}_n^T - \widetilde{\boldsymbol{v}}_n\widetilde{\boldsymbol{v}}_n = \widetilde{\boldsymbol{\alpha}}_n = \widetilde{\boldsymbol{\alpha}} \quad \in T^{\mathrm{spa}}_{\boldsymbol{\Lambda}_n}\end{aligned} \tag{3.32b}$$

[8] Detailed definitions of the material and spatial tangent spaces to $SO(3)$ at the base point $\boldsymbol{\Lambda}$ and their associated linear spaces, are given in Appendix A, Section A.4.

$$\dot{\widetilde{\boldsymbol{V}}} = \dot{\widetilde{\boldsymbol{V}}}_n = \frac{\mathrm{d}}{\mathrm{d}t}(\boldsymbol{\Lambda}_n^T\dot{\boldsymbol{\Lambda}}_n) = (\dot{\boldsymbol{\Lambda}_n^T})\dot{\boldsymbol{\Lambda}}_n + \boldsymbol{\Lambda}_n^T\ddot{\boldsymbol{\Lambda}}_n = -\boldsymbol{\Lambda}_n^T\widetilde{\boldsymbol{v}}_n\dot{\boldsymbol{\Lambda}}_n + \boldsymbol{\Lambda}_n^T\ddot{\boldsymbol{\Lambda}}_n$$
$$= -\boldsymbol{\Lambda}_n^T\widetilde{\boldsymbol{v}}_n\widetilde{\boldsymbol{v}}_n\boldsymbol{\Lambda}_n + \boldsymbol{\Lambda}_n^T\ddot{\boldsymbol{\Lambda}}_n = \widetilde{\boldsymbol{A}}_n = \widetilde{\boldsymbol{A}} \quad \in T^{\mathrm{spa}}_{\boldsymbol{\Lambda}_n}SO(3) \tag{3.32c}$$
$$\dot{\hat{\mathscr{T}}} = \widetilde{\boldsymbol{v}}_n\hat{\mathscr{T}}. \tag{3.32d}$$

Considering Eqs. (3.32b) to (3.32d) and the fact that $\boldsymbol{\Lambda}\boldsymbol{\Lambda}_0^T\dot{\widetilde{\boldsymbol{V}}}_n\boldsymbol{\Lambda}_0 = -\boldsymbol{\Lambda}\widetilde{\boldsymbol{V}}\widetilde{\boldsymbol{V}}$ and $\dot{\boldsymbol{\Lambda}} = \boldsymbol{\Lambda}\widetilde{\boldsymbol{V}}$ we obtain that

$$\ddot{\hat{x}} = \frac{\partial^2\hat{x}}{\partial t^2} = \ddot{\hat{\varphi}} + [\widetilde{\boldsymbol{\alpha}}_n + \widetilde{\boldsymbol{v}}_n\widetilde{\boldsymbol{v}}_n]\hat{\mathscr{T}} = \boldsymbol{\Lambda}[\boldsymbol{\Lambda}^T\ddot{\hat{\varphi}} + [\widetilde{\boldsymbol{A}}_n + \widetilde{\boldsymbol{V}}_n\widetilde{\boldsymbol{V}}_n\hat{\mathscr{E}}] \tag{3.33}$$

with the corresponding axial vectors $\hat{\alpha}_n \in T^{\mathrm{spa}}_{\boldsymbol{\Lambda}_n}$, $\hat{A}_n \in T^{\mathrm{mat}}_{\boldsymbol{\Lambda}_n}$.

REMARK 3.1. If the material updating rule for rotations is preferred *i.e.* $\boldsymbol{\Lambda} = \boldsymbol{\Lambda}_0\boldsymbol{\Lambda}_n^{\mathrm{m}}$ ($\boldsymbol{\Lambda}_n^{\mathrm{m}} = \boldsymbol{\Lambda}^T\boldsymbol{\Lambda}_n$), an entirely equivalent set of equations is obtained, which are summarized as

$$\dot{\hat{x}} = \dot{\hat{\varphi}} + \boldsymbol{\Lambda}_0\widetilde{\boldsymbol{v}}_n^{\mathrm{m}}\boldsymbol{\Lambda}_0^T\hat{\mathscr{T}} = \dot{\hat{\varphi}} + \widetilde{\boldsymbol{v}}^{\mathrm{m}}\hat{\mathscr{T}} = \boldsymbol{\Lambda}[\boldsymbol{\Lambda}^T\dot{\hat{\varphi}} + \widetilde{\boldsymbol{V}}_n^{\mathrm{m}}\hat{\mathscr{E}}] \tag{3.34}$$
$$\ddot{\hat{x}} = \ddot{\hat{\varphi}} + \boldsymbol{\Lambda}_0[\widetilde{\boldsymbol{\alpha}}_n^{\mathrm{m}} + \widetilde{\boldsymbol{v}}_n^{\mathrm{m}}\widetilde{\boldsymbol{v}}_n^{\mathrm{m}}]\boldsymbol{\Lambda}_0^T\hat{\mathscr{T}} = \ddot{\hat{\varphi}} + [\widetilde{\boldsymbol{\alpha}}^{\mathrm{m}} + \widetilde{\boldsymbol{v}}^{\mathrm{m}}\widetilde{\boldsymbol{v}}^{\mathrm{m}}]\hat{\mathscr{T}} = \boldsymbol{\Lambda}[\boldsymbol{\Lambda}^T\dot{\hat{\varphi}} + \widetilde{\boldsymbol{A}}_n^{\mathrm{m}}\hat{\mathscr{E}}] \tag{3.35}$$

where $\widetilde{\boldsymbol{v}}_n^{\mathrm{m}} = \dot{\boldsymbol{\Lambda}}_n^{\mathrm{m}}\boldsymbol{\Lambda}_n^{\mathrm{m}T}$, $\widetilde{\boldsymbol{\alpha}}_n^{\mathrm{m}} = \dot{\widetilde{\boldsymbol{v}}}_n^{\mathrm{m}} \in T^{\mathrm{spa}}_{\boldsymbol{\Lambda}_n}$, $\widetilde{\boldsymbol{V}}_n^{\mathrm{m}} = \boldsymbol{\Lambda}_n^{\mathrm{m}T}\widetilde{\boldsymbol{v}}_n^{\mathrm{m}}\boldsymbol{\Lambda}_n^{\mathrm{m}}$, $\widetilde{\boldsymbol{A}}_n^{\mathrm{m}} = \boldsymbol{\Lambda}^T\widetilde{\boldsymbol{\alpha}}^{\mathrm{m}}\boldsymbol{\Lambda} \in T^{\mathrm{mat}}_{\boldsymbol{\Lambda}_n}$; with the corresponding axial vectors $\hat{v}_n^{\mathrm{m}}$, $\hat{\alpha}_n^{\mathrm{m}} \in T^{\mathrm{spa}}_{\boldsymbol{\Lambda}_n}$ and $\hat{V}_n^{\mathrm{m}}$, $\hat{A}_n^{\mathrm{m}} \in T^{\mathrm{mat}}_{\boldsymbol{\Lambda}_n}$ ■

3.1.6 Curvature vectors and tensors

Employing identical procedures as for the case of time derivatives of the rotation tensor in the preceding section, (see also §A.5.7), it is possible to construct the curvature tensors for the spatial and material configurations as

$$\widetilde{\boldsymbol{\omega}}_0 \equiv \boldsymbol{\Pi}[\hat{\omega}_0] = \boldsymbol{\Lambda}_{0,S}\,\boldsymbol{\Lambda}_0^T \quad \in T^{\mathrm{spa}}_{\boldsymbol{\Lambda}_0}SO(3) \tag{3.36a}$$
$$\widetilde{\boldsymbol{\Omega}}_0 \equiv \boldsymbol{\Pi}[\hat{\Omega}_0] = \boldsymbol{\Lambda}_0^T\boldsymbol{\Lambda}_{0,S} = \overleftarrow{\boldsymbol{\Lambda}_0}\,(\widetilde{\boldsymbol{\omega}}_0) = \boldsymbol{\Lambda}_0^T\widetilde{\boldsymbol{\omega}}_0\boldsymbol{\Lambda}_0 \quad \in T^{\mathrm{mat}}_{\boldsymbol{\Lambda}_0}SO(3) \tag{3.36b}$$

and

$$\widetilde{\boldsymbol{\omega}} \equiv \boldsymbol{\Pi}[\hat{\omega}] = \boldsymbol{\Lambda}_{,S}\,\boldsymbol{\Lambda}^T = \widetilde{\boldsymbol{\omega}}_n + \boldsymbol{\Lambda}_n\widetilde{\boldsymbol{\omega}}_0\boldsymbol{\Lambda}_n^T \quad \in T^{\mathrm{spa}}_{\boldsymbol{\Lambda}}SO(3) \tag{3.37a}$$
$$\widetilde{\boldsymbol{\Omega}} \equiv \boldsymbol{\Pi}[\hat{\Omega}] = \boldsymbol{\Lambda}^T\boldsymbol{\Lambda}_{,S} = \overleftarrow{\boldsymbol{\Lambda}}\,(\widetilde{\boldsymbol{\omega}}) = \boldsymbol{\Lambda}^T\widetilde{\boldsymbol{\omega}}\boldsymbol{\Lambda} = \widetilde{\boldsymbol{\Omega}}_n + \widetilde{\boldsymbol{\Omega}}_0 \quad \in T^{\mathrm{mat}}_{\boldsymbol{\Lambda}}SO(3) \tag{3.37b}$$

where $\widetilde{\boldsymbol{\omega}}_n$ and $\widetilde{\boldsymbol{\Omega}}_n$ are given by

$$\widetilde{\boldsymbol{\omega}}_n \equiv \boldsymbol{\Pi}[\hat{\omega}_n] = \boldsymbol{\Lambda}_{n,S}\,\boldsymbol{\Lambda}_n^T \quad \in T^{\mathrm{spa}}_{\boldsymbol{\Lambda}}SO(3) \tag{3.38a}$$
$$\widetilde{\boldsymbol{\Omega}}_n \equiv \boldsymbol{\Pi}[\widehat{\Omega}_n] = \overleftarrow{\boldsymbol{\Lambda}}\,(\widetilde{\boldsymbol{\omega}}_n) = \boldsymbol{\Lambda}^T\boldsymbol{\Lambda}_{n,S}\,\boldsymbol{\Lambda}_0$$
$$= \boldsymbol{\Lambda}^T\widetilde{\boldsymbol{\omega}}_n\boldsymbol{\Lambda} = \boldsymbol{\Lambda}^T\boldsymbol{\Lambda}_{,S} - \boldsymbol{\Lambda}_0^T\boldsymbol{\Lambda}_{0,S} \quad \in T^{\mathrm{mat}}_{\boldsymbol{\Lambda}_n}SO(3). \tag{3.38b}$$

By simplicity, it is possible to say that the skew–symmetric tensors $\widetilde{\boldsymbol{\omega}}_0$, $\widetilde{\boldsymbol{\omega}}_n$, $\widetilde{\boldsymbol{\omega}}$, $\widetilde{\boldsymbol{\Omega}}_0$, $\widetilde{\boldsymbol{\Omega}}_n$ and $\widetilde{\boldsymbol{\Omega}}$ belongs to $so(3)$[9], with their corresponding associated axial vectors, Eq. (A.100), given by

$$\hat{\omega} \equiv \omega_j\hat{e}_j = \Omega_j\hat{t}_j \quad \in T^{\mathrm{spa}}_{\boldsymbol{\Lambda}} \tag{3.39a}$$

[9] In the corresponding spatial and material tangent spaces according to Eqs. (3.36a), (3.37a) and (3.38a).

$$\hat{\omega}_0 \equiv \omega_{0j}\hat{e}_j = \Omega_{0j}\hat{t}_{0j} \quad \in T^{\text{spa}}_{\mathbf{\Lambda}_0} \tag{3.39b}$$
$$\hat{\omega}_n \equiv \omega_j\hat{e}_j = \Omega_j\hat{t}_j \quad \in T^{\text{spa}}_{\mathbf{\Lambda}_n} \tag{3.39c}$$

for the spatial form and

$$\widehat{\Omega} \equiv \Omega_j\hat{E}_j = \mathbf{\Lambda}^T\hat{\omega} \quad \in T^{\text{mat}}_{\mathbf{\Lambda}} \tag{3.39d}$$
$$\widehat{\Omega}_0 \equiv \Omega_{0j}\hat{E}_j = \mathbf{\Lambda}_0^T\hat{\omega}_0 \quad \in T^{\text{mat}}_{\mathbf{\Lambda}_0} \tag{3.39e}$$
$$\hat{\Omega}_n \equiv \Omega_{nj}\hat{E}_j = \mathbf{\Lambda}^T\hat{\omega}_n = \widehat{\Omega} - \widehat{\Omega}_0 \quad \in T^{\text{mat}}_{\mathbf{\Lambda}_n} \tag{3.39f}$$

for the material forms.
The terms $\hat{\omega}_0$ and $\widehat{\Omega}_0$ are the *curvature vectors* of the curved reference rod configuration in the spatial and material descriptions, they measure the *orientation change rate* of the cross section with respect to the arch–length coordinate S. The component Ω_{01} is the *twist rate* around the *tangent* vector $\hat{t}_{01}$, and Ω_{02} and Ω_{03} are the corresponding curvature components around $\hat{t}_{02}$ and $\hat{t}_{03}$, respectively.
Similarly, we also call $\hat{\omega}$ and $\widehat{\Omega}$ the *curvature vectors* of the current rod in spatial and material forms; they denote the *orientation change rate* of the cross section of the current rod with respect to the arch–length coordinate S. Analogously, the component Ω_1 is the *twist rate* around the *normal* vector $\hat{t}_1$, and Ω_2 and Ω_3 are the corresponding curvature components around $\hat{t}_2$ and $\hat{t}_3$, respectively.
It is interesting to note that, according to the result of Eq. (A.100) of §A.5.6 of Appendix A, the components of the spatial curvature vectors in the spatial moving frame $\{\hat{t}_{0i}\}$ or $\{\hat{t}_i\}$ are identical to the components of the material curvature vectors in the material reference frame $\{\hat{E}_i\}$ *i.e.*

$$\begin{aligned} \Omega_{0j} &= \widehat{\Omega}_0 \cdot \hat{E}_j = \hat{\omega}_0 \cdot \hat{t}_{0j} \\ \Omega_j &= \widehat{\Omega} \cdot \hat{E}_j = \hat{\omega} \cdot \hat{t}_j. \end{aligned} \tag{3.40}$$

Additionally, it is possible to call $\hat{\omega}_n$ and $\widehat{\Omega}_n$ the *curvature change vectors* in spatial and material forms, of the current rod relative to the curved reference rod, and they denote *orientation change* of the cross sections of the current rod relative to the curved and twisted reference configurations with respect to the arch–length coordinate $S \in [0, L]$. The component Ω_{n1} is the *twist rate change* around the *normal* vector $\hat{t}_1$, and Ω_{n2} and Ω_{n3} are the corresponding curvature components around $\hat{t}_2$ and $\hat{t}_3$, respectively. In this manner, the *elongation, shearing* and *curvature change* have been described.
The fact that the cross section rotates away from the orthogonality with the tangent vector of the rod mid–curve is considered as *shearing*[10]. While *relative orientation angle* of the cross section as the material point $S \in [0, L]$ varies along the rod mid–curve determines the *curvature change* of a curved rod.

3.2 Strain measures

For deducing explicit expressions for the strain measures some preliminary results are required; the calculation of the co-rotated derivative of the orientation frames of a cross section of the current and curved reference rods.

[10]Shearing can be expressed in terms of the distortion angle as it has been described in §3.1.4. This measurement of shear or elongation is obtained from the *engineering* point of view; consult *e.g.* [228, 207, 208].

3.2.1 Co–rotated derivative of the orientation triads

Explicit expressions for the spatial derivative of the orientation triads $\{\hat{t}_{0i}\}$ and $\{\hat{t}_i\}$ can be calculated taking their co–rotated derivative with respect to the arch–length coordinate $S \in [0, L]$, recovering the *Frenet–Serret* formulae in the original sense as explained in Ref. [228]. They read as (see Def. A.27 of Appendix A, pp. 285)

$$\begin{aligned} [\overset{\triangledown}{\hat{t}_{0i}}],_S &\equiv L_{\mathbf{\Lambda}_0}(\hat{t}_{0i}) = \hat{t}_{0i},_S - \widetilde{\boldsymbol{\omega}}_0 \hat{t}_{0i} = \mathbf{\Lambda}_0(\mathbf{\Lambda}_0^T \hat{t}_{0i}),_S = \mathbf{\Lambda}_0(\hat{E}_i),_S = 0 \\ [\overset{\triangledown}{\hat{t}_i}],_S &\equiv L_{\mathbf{\Lambda}}(\hat{t}_i) = \hat{t}_i,_S - \widetilde{\boldsymbol{\omega}} \hat{t}_i = \mathbf{\Lambda}(\mathbf{\Lambda}^T \hat{t}_i),_S = \mathbf{\Lambda}(\hat{E}_i),_S = 0 \end{aligned}$$

what imply that

$$\hat{t}_{0i},_S = \widetilde{\boldsymbol{\omega}}_0 \hat{t}_{0i} = \hat{\omega}_0 \times \hat{t}_{0i} \tag{3.41a}$$

$$\hat{t}_i,_S = \widetilde{\boldsymbol{\omega}} \hat{t}_i = \hat{\omega} \times \hat{t}_i \tag{3.41b}$$

considering that $\hat{\omega}_0 = \Omega_{0j} \hat{t}_{0j}$ and writing for each component one obtains

$$\hat{t}_{01},_S = \Omega_{03}\hat{t}_{02} - \Omega_{02}\hat{t}_{03}; \quad \hat{t}_{02},_S = -\Omega_{03}\hat{t}_{01} + \Omega_{01}\hat{t}_{03}; \quad \hat{t}_{03},_S = \Omega_{02}\hat{t}_{01} - \Omega_{01}\hat{t}_{02},$$

for the curved reference orientation triad and considering $\hat{\omega} = \Omega_j \hat{t}_j$, one has that

$$\hat{t}_1,_S = \Omega_3\hat{t}_2 - \Omega_2\hat{t}_3; \quad \hat{t}_2,_S = -\Omega_3\hat{t}_1 + \Omega_1\hat{t}_3; \quad \hat{t}_3,_S = \Omega_2\hat{t}_1 - \Omega_1\hat{t}_2, \tag{3.41c}$$

for the current orientation triad.

3.2.2 Deformation gradient tensor

The *deformation gradient* can be defined as the *material gradient* of the deformation $\hat{x}(S, \xi_\beta, t)$ and it can be calculated with the aid of the formula $\mathbf{F} = \nabla_{\hat{X}} \hat{x}$. However, the deformation $\hat{x} : \mathcal{B}_{00} \to \mathcal{B}_t$ is more like a point mapping than a vector. Hence, the deformation gradient tensor can be defined as the tangent field of the deformation mapping [246, 245] *i.e.*

$$\mathbf{F} := T_{\hat{X}} \hat{x} \quad \in \quad T_{\hat{x}}\mathcal{B}_t \otimes T^*_{\hat{X}}\mathcal{B}_{00} \tag{3.42}$$

where $\mathbf{F}$ is also a linear application $T_{\hat{X}} \in \mathcal{L}(T_{\hat{x}}\mathcal{B}_t \otimes T_{\hat{X}}\mathcal{B}_{00})$ is formally defined as

$$T_{\hat{X}} \hat{x} := \frac{\partial x_i}{X_j} X_j = \mathbf{F}\hat{X}.$$

In Eq. (3.42) it has been assumed that $\hat{x}$ is a tensor of rank one *i.e.* a vector. The study of the deformation gradient helps to determine the strain measures at any material point of the current cross section of the rod [363, 207]. In this section, we will indirectly obtain the *deformation gradient tensor* of the current rod configuration relative to the curved reference rod configuration by means of obtaining the deformation gradient tensors of the two curved rod configurations relative to the straight reference rod configuration followed by a change of reference configuration[11] (see Ogden [300]).
Considering the expression for the position vector of material points on the curved and current rods, $\hat{x}_0$ and $\hat{x}$, given by Eqs. (3.4) and (3.22) respectively, and the result of §3.1.6, it is possible

[11] Avoiding use covariant and contra–variant reference frames.

to calculate the following derivatives:

$$\begin{aligned}\hat{x}_{0,S} &= \hat{\varphi}_{0,S} + \widetilde{\boldsymbol{\omega}}_0 \hat{\mathscr{T}}_0 = \hat{\epsilon}_0 + \hat{t}_{01} && (3.43a)\\ &= \boldsymbol{\Lambda}_0[\boldsymbol{\Lambda}_0^T \hat{\varphi}_{0,S} + \widetilde{\boldsymbol{\Omega}}_0 \hat{\mathscr{E}}] = \boldsymbol{\Lambda}_0[\hat{\mathcal{E}}_0 + \hat{E}_1] && (3.43b)\\ \hat{x}_{0,\beta} &= \hat{t}_{0\beta} = \boldsymbol{\Lambda}_0 \hat{E}_\beta && (3.43c)\end{aligned}$$

where we have denoted $\hat{\mathscr{E}} := \xi_\beta \hat{E}_\beta \in T_{\hat{X}}\mathcal{B}_{00}$ and $\hat{\mathscr{T}}_0 := \xi_\beta \hat{t}_{0\beta} \in T_{\hat{x}_0}\mathcal{B}_0$ by simplicity and the vectors $\hat{\epsilon}_0 \in T_{\hat{x}_0}\mathcal{B}_0$ and $\hat{\mathcal{E}}_0 \in T_{\hat{X}}\mathcal{B}_{00}$ are given by

$$\begin{aligned}\hat{\epsilon}_0 &\equiv \mathcal{E}_{0j}\hat{t}_{0j} = \hat{\gamma}_0 + \widetilde{\boldsymbol{\omega}}_0 \hat{\mathscr{T}}_0 && (3.44a)\\ \hat{\mathcal{E}}_0 &\equiv \mathcal{E}_{0j}\hat{E}_j = \hat{\Gamma}_0 + \widetilde{\boldsymbol{\Omega}}_0 \hat{\mathscr{E}} && (3.44b)\end{aligned}$$

with $\hat{\gamma}_0 \in T_{\hat{x}_0}\mathcal{B}_0$ and $\hat{\Gamma}_0 \in T_{\hat{X}}\mathcal{B}_{00}$ given by

$$\begin{aligned}\hat{\gamma}_0 &\equiv \Gamma_{0j}\hat{t}_{0j} = \hat{\varphi}_{0,S} - \hat{t}_{01} && (3.45a)\\ \hat{\Gamma}_0 &\equiv \Gamma_{0j}\hat{E}_j = \boldsymbol{\Lambda}_0^T \hat{\varphi}_{0,S} - \hat{E}_1 && (3.45b)\end{aligned}$$

for a point on the curved reference rod and

$$\begin{aligned}\hat{x}_{,S} &= \hat{\varphi}_{,S} + \widetilde{\boldsymbol{\omega}} \hat{\mathscr{T}} = \hat{\epsilon} + \hat{t}_1 && (3.46a)\\ &= \boldsymbol{\Lambda}[\boldsymbol{\Lambda}^T \hat{\varphi}_{,S} + \widetilde{\boldsymbol{\Omega}} \hat{\mathscr{E}}] \\ &= \boldsymbol{\Lambda}[\hat{\mathcal{E}} + \hat{E}_1] && (3.46b)\\ \hat{x}_{,\beta} &= \hat{t}_\beta = \boldsymbol{\Lambda} \hat{E}_\beta && (3.46c)\end{aligned}$$

where we have denoted $\hat{\mathscr{T}} := \xi_\beta \hat{t}_\beta \in T_{\hat{x}}\mathcal{B}_t$ by simplicity and the vectors $\hat{\epsilon} \in T_{\hat{x}}\mathcal{B}_t$ and $\hat{\mathcal{E}} \in T_{\hat{X}}\mathcal{B}_{00}$ are given by

$$\begin{aligned}\hat{\epsilon} &\equiv \mathcal{E}_j \hat{t}_j = \hat{\gamma} + \widetilde{\boldsymbol{\omega}} \hat{\mathscr{T}} && (3.47a)\\ \hat{\mathcal{E}} &\equiv \mathcal{E}_j \hat{E}_j = \hat{\Gamma} + \widetilde{\boldsymbol{\Omega}} \hat{\mathscr{E}} && (3.47b)\end{aligned}$$

with $\hat{\gamma} \in T_{\hat{x}}\mathcal{B}_t$ and $\hat{\Gamma} \in T_{\hat{X}}\mathcal{B}_{00}$ given by

$$\begin{aligned}\hat{\gamma} &\equiv \Gamma_j \hat{t}_j = \hat{\varphi}_{,S} - \hat{t}_1 && (3.48a)\\ \hat{\Gamma} &\equiv \Gamma_j \hat{E}_j = \boldsymbol{\Lambda}^T \hat{\varphi}_{,S} - \hat{E}_1 && (3.48b)\end{aligned}$$

for a material point on the current rod.
Therefore, employing the results of Eqs. (3.5) and (3.19) for rotation tensors, the deformation gradient tensors $\mathbf{F}_0 \in T_{\hat{x}_0}\mathcal{B}_0 \otimes T_{\hat{X}}\mathcal{B}_{00}$ and $\mathbf{F} \in T_{\hat{x}}\mathcal{B}_t \otimes T_{\hat{X}}\mathcal{B}_{00}$, of the curved reference rod and the current rod relative to the straight reference rod, respectively; are determined by

$$\begin{aligned}\mathrm{d}\hat{x}_0 &\equiv \mathbf{F}_0 \mathrm{d}\hat{x}_{00} \\ \mathbf{F}_0 &= \hat{x}_{0,S} \otimes \hat{E}_1 + \hat{x}_{0,\beta} \otimes \hat{E}_\beta = \hat{\epsilon}_0 \otimes \hat{E}_1 + \hat{t}_{0i} \otimes \hat{E}_i = \mathcal{E}_{0i}\hat{t}_{0i} \otimes \hat{E}_1 + \hat{t}_{0i} \otimes \hat{E}_i \\ &= \hat{\epsilon}_0 \otimes \hat{E}_1 + \boldsymbol{\Lambda}_0 = \boldsymbol{\Lambda}_0 \bar{\mathbf{F}}_0 && (3.49a)\end{aligned}$$

$$\begin{aligned} \mathrm{d}\hat{x} &\equiv \mathbf{F}\mathrm{d}\hat{x}_{00} \\ \mathbf{F} &= \hat{x}_{,S}\otimes\hat{E}_1 + \hat{x}_{,\beta}\otimes\hat{E}_\beta = \hat{\epsilon}\otimes\hat{E}_1 + \hat{t}_i\otimes\hat{E}_i = \mathcal{E}_i\hat{t}_i\otimes\hat{E}_1 + \hat{t}_i\otimes\hat{E}_i \\ &= \hat{\epsilon}\otimes\hat{E}_1 + \boldsymbol{\Lambda} = \boldsymbol{\Lambda}\bar{\mathbf{F}} \end{aligned} \tag{3.49b}$$

with $\bar{\mathbf{F}}_0, \bar{\mathbf{F}} \in T_{\hat{X}}\mathcal{B}_{00}\otimes T_{\hat{X}}\mathcal{B}_{00}$ given by

$$\bar{\mathbf{F}}_0 = \hat{\mathcal{E}}_0\otimes\hat{E}_1 + \mathbf{I} = \mathcal{E}_{0i}\hat{E}_i\otimes\hat{E}_1 + \hat{E}_i\otimes\hat{E}_i \tag{3.50a}$$

$$\bar{\mathbf{F}} = \hat{\mathcal{E}}\otimes\hat{E}_1 + \mathbf{I} = \mathcal{E}_i\hat{E}_i\otimes\hat{E}_1 + \hat{E}_i\otimes\hat{E}_i, \tag{3.50b}$$

respectively. Considering Eqs. (3.30) and (3.31) for the *elongation* and *shearing* of the curved reference rod and the current rod configuration, it is possible to obtain the components of $\hat{\gamma}_0(S)$ and $\hat{\gamma}(S)$ referred to the local frames as

$$\gamma_{0j} = \Gamma_{0j} = \hat{\varphi}_{0,S}\cdot\hat{t}_{0j} - \hat{t}_{01}\cdot\hat{t}_{0j} = \hat{\varphi}_{0,S}\cdot\hat{t}_{0j} - \delta_{1j}; \quad e_0 = 0; \quad \gamma_{01i} = 0 \tag{3.51a}$$

$$\gamma_j = \Gamma_j = \hat{\varphi}_{,S}\cdot\hat{t}_j - \hat{t}_1\cdot\hat{t}_j = \hat{\varphi}_{,S}\cdot\hat{t}_j - \delta_{1j}. \tag{3.51b}$$

Then the components of $\hat{\epsilon}_0(S,\xi_\beta)$ and $\hat{\epsilon}(S,\xi_\beta)$ in Eqs. (3.44a), (3.44b), (3.47a) and (3.47b) referred to their local frames are

$$\mathcal{E}_{01} = \gamma_{01} + \xi_3\Omega_{02} - \xi_2\Omega_{03}; \quad \mathcal{E}_{02} = \gamma_{02} - \xi_3\Omega_{01}; \quad \mathcal{E}_{03} = \gamma_{03} + \xi_2\Omega_{01}, \tag{3.52a}$$

and

$$\mathcal{E}_1 = \gamma_1 + \xi_3\Omega_2 - \xi_2\Omega_3; \quad \mathcal{E}_2 = \gamma_2 - \xi_3\Omega_1; \quad \mathcal{E}_3 = \gamma_3 + \xi_2\Omega_1. \tag{3.52b}$$

Note that the *component representation* of $\mathbf{F}_0$ and $\mathbf{F}$ in the *spatial form* as well as $\bar{\mathbf{F}}_0$ and $\bar{\mathbf{F}}$ in the material form (see §A.3.1) can be identified from Eqs. (3.49a), (3.49b), (3.50a) and (3.50b) as [207]

$$[\mathbf{F}_0]_{\hat{t}_{0i}\otimes\hat{E}_j} = [\bar{\mathbf{F}}_0]_{\hat{E}_i\otimes\hat{E}_j} = \begin{bmatrix} 1+\mathcal{E}_{01} & 0 & 0 \\ \mathcal{E}_{02} & 1 & 0 \\ \mathcal{E}_{03} & 0 & 1 \end{bmatrix} \tag{3.53a}$$

and

$$[\mathbf{F}]_{\hat{t}_i\otimes\hat{E}_j} = [\bar{\mathbf{F}}]_{\hat{E}_i\otimes\hat{E}_j} = \begin{bmatrix} 1+\mathcal{E}_1 & 0 & 0 \\ \mathcal{E}_2 & 1 & 0 \\ \mathcal{E}_3 & 0 & 1 \end{bmatrix}. \tag{3.53b}$$

The determinants of $\bar{\mathbf{F}}_0(S,\xi_\beta)$ and $\bar{\mathbf{F}}(S,\xi_\beta)$ can be obtained from Eqs. (3.53a) and (3.53b) as

$$\begin{aligned} g_0 &\equiv \mathrm{Det}[\mathbf{F}_0] = \mathrm{Det}[\boldsymbol{\Lambda}_0]\mathrm{Det}[\bar{\mathbf{F}}_0] = \mathrm{Det}[\bar{\mathbf{F}}_0] \\ &= 1+\mathcal{E}_{01} = 1+\Gamma_{01}+\xi_3\Omega_{02}-\xi_2\Omega_{03} \end{aligned} \tag{3.54a}$$

$$\begin{aligned} g &\equiv \mathrm{Det}[\mathbf{F}] = \mathrm{Det}[\boldsymbol{\Lambda}]\mathrm{Det}[\bar{\mathbf{F}}] = \mathrm{Det}[\bar{\mathbf{F}}] \\ &= 1+\mathcal{E}_1 = 1+\Gamma_1+\xi_3\Omega_2-\xi_2\Omega_3 \end{aligned} \tag{3.54b}$$

respectively, and the inverses of $\mathbf{F}_0$ and $\mathbf{F}$ are

$$\begin{aligned} \mathbf{F}_0^{-1} &= (\boldsymbol{\Lambda}_0\bar{\mathbf{F}}_0)^{-1} = \bar{\mathbf{F}}_0^{-1}\boldsymbol{\Lambda}_0^T = (-\frac{1}{g_0}\hat{\mathcal{E}}_0\otimes\hat{E}_1 + \mathbf{I})\boldsymbol{\Lambda}_0^T \\ &= [\mathcal{E}_{0i}\hat{E}_i\otimes\hat{E}_1 + \hat{E}_i\otimes\hat{E}_i]^{-1}\boldsymbol{\Lambda}_0^T \\ &= -g_0^{-1}\hat{\mathcal{E}}_0\otimes\hat{t}_{01} + \boldsymbol{\Lambda}_0^T = \boldsymbol{\Lambda}_0^T(-g_0^{-1}\hat{\epsilon}_0\otimes\hat{t}_{01} + \mathbf{I}) \ \in T_{\hat{X}}\mathcal{B}_{00}\otimes T^*_{\hat{x}_0}\mathcal{B}_0 \end{aligned} \tag{3.55a}$$

$$\begin{aligned}
\mathbf{F}^{-1} &= (\boldsymbol{\Lambda}\bar{\mathbf{F}})^{-1} = \bar{\mathbf{F}}^{-1}\boldsymbol{\Lambda}^T = (-\frac{1}{g}\hat{\mathcal{E}}\otimes\hat{E}_1 + \mathbf{I})\boldsymbol{\Lambda}^T \\
&= [\mathcal{E}_i\hat{E}_i\otimes\hat{E}_1 + \hat{E}_i\otimes\hat{E}_i]^{-1}\boldsymbol{\Lambda}^T \\
&= -\frac{1}{g}\hat{\mathcal{E}}\otimes\hat{t}_1 + \boldsymbol{\Lambda}^T = \boldsymbol{\Lambda}^T(-\frac{1}{g}\hat{\epsilon}\otimes\hat{t}_1 + \mathbf{I}) \qquad \in T_{\hat{X}}\mathcal{B}_{00}\otimes T^*_{\hat{x}}\mathcal{B}_t. \qquad (3.55b)
\end{aligned}$$

Taking into account the definitions given for $\mathbf{F}_0$ and $\mathbf{F}$ in Eqs. (3.49a) and (3.49b) as well as (3.55a) and (3.55b), it is possible to obtain the deformation gradient tensor of the current beam relative to the curved reference rod through a change of reference configuration, following the procedure described in Ref. [300].
As it has been previously explained the gradient tensor $\mathbf{F}_0 \in T_{\hat{x}_0}\mathcal{B}_0\otimes T^*_{\hat{X}}\mathcal{B}_{00}$ maps differential elements of length from the straight reference configuration $\mathcal{B}_{00}$ to the curved reference configuration $\mathcal{B}_0$, *i.e.* $\mathbf{F}_0(\mathrm{d}\hat{X}_{00}) \to \mathrm{d}\hat{x}_0$. By other hand, the gradient tensor $\mathbf{F} \in T_{\hat{x}}\mathcal{B}_t\otimes T^*_{\hat{X}}\mathcal{B}_{00}$ maps differential elements of length from the straight reference configuration $\mathcal{B}_{00}$ to the current placement of the body $\mathcal{B}_t$ *i.e.* $\mathbf{F}(\mathrm{d}\hat{X}_{00}) \to \mathrm{d}\hat{x}$. Considering that both gradient tensors are invertible

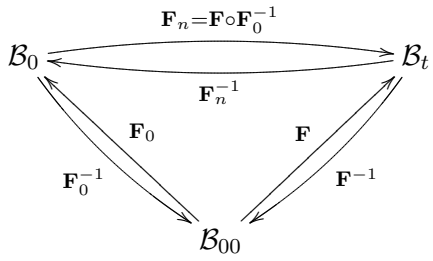

Figure 3.2: Diagram of domains and ranges for the gradient tensor $\mathbf{F}_n$.

applications it is possible to construct a third gradient tensor $\mathbf{F}_n \in T_{\hat{x}_0}\mathcal{B}_0\otimes T^*_{\hat{x}}\mathcal{B}_t$ relating differential elements of length between the curved reference placement $\mathcal{B}_0$ and the current placement $\mathcal{B}_t$ as

$$\begin{aligned}
\mathbf{F}_n := \mathbf{F}\circ\mathbf{F}_0^{-1} &\in T_{\hat{x}}\mathcal{B}_t\otimes T^*_{\hat{x}_0}\mathcal{B}_0; \qquad \text{such that} \\
\mathbf{F}_n : T_{\hat{x}_0}\mathcal{B}_0 &\to T_{\hat{x}}\mathcal{B}_t \qquad (3.56) \\
\mathrm{d}\hat{x}_0 &\mapsto \mathbf{F}_n(\mathrm{d}\hat{x}_0) = \mathrm{d}\hat{x}
\end{aligned}$$

The scheme of Fig. 3.2 shows the vector fields where the gradient tensor $\mathbf{F}_n$ acts. An explicit expression for the deformation gradient tensor $\mathbf{F}_n$ can be calculated as

$$\begin{aligned}
\mathrm{d}\hat{x} &\equiv \mathbf{F}_n\mathrm{d}\hat{x}_0 \\
\mathbf{F}_n &= \mathbf{F}\mathbf{F}_0^{-1} = (\mathcal{E}_i\hat{t}_i\otimes\hat{E}_1 + \hat{t}_i\otimes\hat{E}_i)(-g_0^{-1}\mathcal{E}_{0j}\hat{E}_j\otimes\hat{t}_{01} + \hat{E}_j\otimes\hat{t}_{0j}) \\
&= -g_0^{-1}\mathcal{E}_i\mathcal{E}_{0j}\delta_{1j}\hat{t}_i\otimes\hat{t}_{01} - g_0^{-1}\mathcal{E}_{0j}\delta_{ij}\hat{t}_i\otimes\hat{t}_{01} + \mathcal{E}_i\hat{t}_i\otimes\delta_{1j}\hat{t}_{0j} + \hat{t}_i\otimes\delta_{ij}\hat{t}_{0j} \\
&= -\frac{(\mathcal{E}_i\mathcal{E}_{01} + \mathcal{E}_{0i} - \mathcal{E}_{01}\mathcal{E}_i - \mathcal{E}_i)}{\mathcal{E}_{01}+1}\hat{t}_i\otimes\hat{t}_{01} + \hat{t}_i\otimes\hat{t}_{0i} \\
&= g_0^{-1}\mathcal{E}_{ni}\hat{t}_i\otimes\hat{t}_{01} + \hat{t}_i\otimes\hat{t}_{0i} \\
&= \frac{1}{g_0}\hat{\epsilon}_n\otimes\hat{t}_{01} + \boldsymbol{\Lambda}_n = \boldsymbol{\Lambda}\bar{\mathbf{F}}_n\boldsymbol{\Lambda}_0^T \qquad \in \quad T_{\hat{x}}\mathcal{B}_t\otimes T^*_{\hat{x}_0}\mathcal{B}_0 \qquad (3.57a) \\
\bar{\mathbf{F}}_n &= \frac{1}{g_0}\hat{\mathcal{E}}_n\otimes\hat{E}_1 + \mathbf{I} = \frac{1}{g_0}\mathcal{E}_{ni}\hat{E}_i\otimes\hat{E}_1 + \hat{E}_i\otimes\hat{E}_i \qquad \in \quad T_{\hat{X}}\mathcal{B}_{00}\otimes T_{\hat{X}}\mathcal{B}_{00} \qquad (3.57b)
\end{aligned}$$

where, employing Eqs. (3.44a) to (3.52b), and noting that $\widetilde{\mathbf{\Omega}}_n(\bullet) = \hat{\Omega}_n \times (\bullet)$ we have

$$\begin{aligned}
\hat{\mathcal{E}}_n &\equiv \mathcal{E}_{nj}\hat{E}_j \quad \in \quad T_{\hat{X}}\mathcal{B}_{00} \\
&\equiv \hat{\mathcal{E}} - \hat{\mathcal{E}}_0 = \hat{\Gamma}_n + \widetilde{\mathbf{\Omega}}_n\hat{\mathscr{E}} = \hat{\Gamma}_n + (\xi_3\Omega_{n2} - \xi_2\Omega_{n3})\hat{E}_1 + \Omega_{n1}(\xi_2\hat{E}_3 - \xi_3\hat{E}_2) \qquad (3.58) \\
\hat{\epsilon}_n &= \mathbf{\Lambda}\hat{\mathcal{E}}_n = \hat{\epsilon} - \mathbf{\Lambda}_n\hat{\epsilon}_0 = \hat{\gamma}_n + \widetilde{\boldsymbol{\omega}}_n\hat{\mathscr{T}} \quad \in \quad T_{\hat{x}}\mathcal{B}_t \\
&= \hat{\gamma}_n + (\xi_3\Omega_{n2} - \xi_2\Omega_{r3})\hat{t}_1 - \xi_3\Omega_{n1}\hat{t}_2 + \xi_2\Omega_{n1}\hat{t}_3 = \mathcal{E}_{nj}\hat{t}_j \qquad (3.59)
\end{aligned}$$

with

$$\begin{aligned}
\mathcal{E}_{nj} &\equiv \mathcal{E}_j - \mathcal{E}_{0j} = \hat{x}_{,S}\cdot\hat{t}_j - \hat{x}_{0,S}\cdot\hat{t}_{0j} \qquad (3.60a) \\
\mathcal{E}_{n1} &= \Gamma_{n1} + \xi_3\Omega_{n2} - \xi_2\Omega_{n3}) \\
\mathcal{E}_{n2} &= \Gamma_{n2} - \xi_3\Omega_{n1}) \\
\mathcal{E}_{n3} &= \Gamma_{n3} + \xi_2\Omega_{n1}) \\
\Gamma_{nj} &\equiv \Gamma_j - \Gamma_{0j} = \hat{\varphi}_{,S}\cdot\hat{t}_j - \hat{\varphi}_{0,S}\cdot\hat{t}_{0j} = \hat{\varphi}_{,S}\cdot\hat{t}_j - \delta_{1j} \qquad (3.60b)
\end{aligned}$$

and

$$\begin{aligned}
\hat{\Gamma}_n &\equiv \hat{\Gamma} - \hat{\Gamma}_0 = \Lambda^T\hat{\varphi}_{,S} - \Lambda_0^T\hat{\varphi}_{0,S} = \Gamma_{nj}\hat{E}_j \qquad (3.61a) \\
\hat{\gamma}_n &= \mathbf{\Lambda}\hat{\Gamma}_n = \hat{\varphi}_{,S} - \mathbf{\Lambda}_n\hat{\varphi}_{0,S} = \hat{\gamma} - \mathbf{\Lambda}_n\hat{\gamma}_0 = \hat{\varphi}_{,S} - \hat{t}_1 = \mathcal{E}_{rj}\hat{t}_j \qquad (3.61b)
\end{aligned}$$

where $\gamma_{0j} = \Gamma_{0j} = 0$, considering that the curved reference configuration $\hat{x}_0$ is unstressed and unstrained.
The determinant of $\mathbf{F}_n$ can be obtained employing Eqs. (3.53a) and (3.55a) [228] as

$$g_n = \mathrm{Det}[\mathbf{F}_n] = \mathrm{Det}[\mathbf{F}\mathbf{F}_0^{-1}] = \mathrm{Det}[\mathbf{F}]\mathrm{Det}[\mathbf{F}_0^{-1}] = \frac{\mathrm{Det}[\mathbf{F}]}{\mathrm{Det}[\mathbf{F}_0]} = \frac{g}{g_0} = 1 + \frac{\mathcal{E}_{n1}}{g_0} \qquad (3.62)$$

and, using Eqs. (3.49a) and (3.55b), it is possible to obtain the inverse of $\mathbf{F}_n$ as

$$\mathbf{F}_n^{-1} = (\mathbf{F}\mathbf{F}_0^{-1})^{-1} = \mathbf{F}_0\mathbf{F}^{-1} = \mathbf{\Lambda}_n^T(-\frac{1}{g}\hat{\epsilon}_n \otimes \hat{t}_1 + \mathbf{I}). \qquad (3.63)$$

It is important to note that $\hat{\epsilon}_0$, $\hat{\epsilon}$, $\hat{\mathcal{E}}_0$ and $\hat{\mathcal{E}}$ (in the spatial and material forms, respectively) are the *strain vectors* at any point of the cross section and $\hat{\gamma}_0$, $\hat{\gamma}$, $\hat{\Gamma}_0$ and $\hat{\Gamma}$ are the *strain vectors* on the centroid-curve for the curved reference rod and the current rod relative to the straight reference configuration. They determine the corresponding *elongation* and *shearing* relative to the straight reference rod [178, 188, 362].
Fig. 3.3 show a schematic representation of the these strain measurements expressing their components in the material reference frame by simplicity; additionally, the material form of the curvature vector has been draw to highlight the relation between $\hat{\epsilon}$, $(\hat{\mathcal{E}})$, and $\hat{\gamma}$, $(\hat{\Gamma})$, given in Eqs. (3.58) to (3.61a).
Noting the similarity between Eqs. (3.57b) and (3.50b), one may intuitively choose $\hat{\epsilon}_n/g_0$, $\hat{\mathcal{E}}_n/g_0$ as the *right strain vector* of the current rod configuration relative to the curved reference rod that is conjugated to the *First Piola Kirchhoff*[12] stress vector.
The term $g_0 = |\mathbf{F}_0|$, given in Eq. (3.54a), is the scale factor between the differential volumes of

[12] More details about stress measurements will be given in the next section.

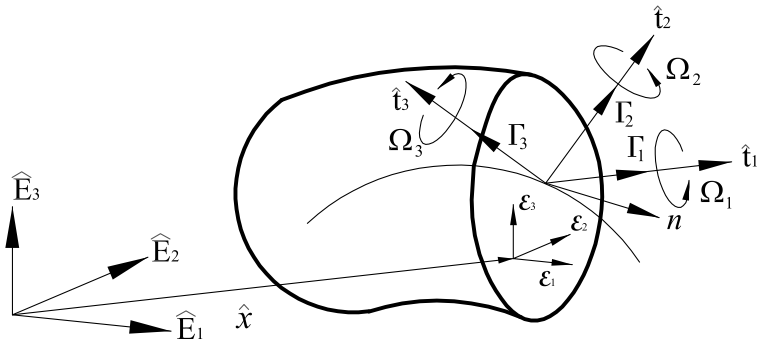

Figure 3.3: Geometric representation of the reduced strain vectors.

the curved reference rod and the straight reference rod at any material point (S, ξ_β)

$$\mathrm{d}V_0 = g_0 \mathrm{d}V_{00} = g_0 \mathrm{d}S\mathrm{d}\xi_2\mathrm{d}\xi_3 \tag{3.64a}$$

$$\mathrm{d}V_{00} = \mathrm{d}S\mathrm{d}\xi_2\mathrm{d}\xi_3 \tag{3.64b}$$

where V_0 and V_{00} are the volume domains of the curved reference rod and straight reference rod configurations, respectively. Additionally, the following relation holds for the current differential element of volume

$$\mathrm{d}V = g\mathrm{d}V_{00} = g_n \mathrm{d}V_0. \tag{3.64c}$$

An unit–length fiber parallel to $\hat{E}_1$, the normal to the straight reference rod cross section is *stretched* to be g_0 in the direction of $\hat{t}_{01}$, the normal of the curved reference rod cross section, if the rod moves from the straight reference configuration to the curved reference configuration. In fact, using Eq. (3.49a) for the *deformation*[13] gradient tensor $\mathbf{F}_0$ of the curved reference rod relative to the straight reference rod and Eq. (3.54a) for g_0, one has

$$(\mathbf{F}_0\hat{E}_1\mathrm{d}S)\cdot\hat{t}_{01} = (\hat{\epsilon}_0 + \hat{t}_{01})\cdot\hat{t}_{01} = (\hat{\epsilon}_0\cdot\hat{t}_{01} + \hat{t}_{01}\cdot\hat{t}_{01})\mathrm{d}S = (\mathcal{E}_{01}+1)\mathrm{d}S \equiv g_0\mathrm{d}S \tag{3.65}$$

which is dependent on the curvature of the curved reference rod configuration but not on the twist for a given point on the cross section, see Eq. (3.52b). This result is in agreement with the assumption that the rod cross section remains plane and undeformed during the motion. If in stead, an unit–length fiber along $\hat{E}_\beta$ is chosen we have that

$$(\mathbf{F}_0\mathrm{d}\xi_\beta\hat{E}_\beta)\cdot\hat{t}_{0\beta} = ((\hat{\epsilon}\otimes\hat{E}_1 + \mathbf{\Lambda})\mathrm{d}\xi_\beta\hat{E}_\beta)\cdot\hat{t}_{0\beta} = (\hat{\epsilon}\delta_{1\beta} + \mathrm{d}\xi_\beta\hat{t}_{0\beta})\cdot\hat{t}_{0\beta} = \mathrm{d}\xi_\beta \tag{3.66}$$

which is in conformity with the kinematic assumption that suppose that cross sections remain planes and undeformed. The same result is obtained if in Eq. (3.66) $\mathbf{F}_0$ and $\hat{t}_{0\beta}$ are replaced by $\mathbf{F}$ and $\hat{t}_\beta$, respectively. Therefore, one have the following result for elements of differential area

$$\mathrm{d}\mathcal{A}_{00} = \mathrm{d}\mathcal{A}_0 = \mathrm{d}\mathcal{A}. \tag{3.67}$$

Eq. (3.64b) also implies that any 'cut' slide of the curved reference rod through two cross section planes with differential length $\mathrm{d}S$, at any point on the mid–curve, is *linearly tapered* and its thickness in direction $\hat{t}_{01}$ varies according to $g_0\mathrm{d}S$ as the material point varies on the curved reference rod cross section [228]. Any fiber parallel to $\hat{t}_{01}$ has a real length $g_0\mathrm{d}S$ at (S, ξ_β) if a

[13]Here the term *deformation* has been used instead of *gradient* to highlight that $\mathbf{F}_0$ contains all the information relative to stretches and rotations of differential length elements [251, 300].

fiber parallel to $\hat{t}_{01}$ has a real length $\mathrm{d}S$ at S on the mid–curve.
The factor g_0^{-1} (in front of $\hat{\epsilon}_n$) in the deformation gradient tensor $\mathbf{F}_n$ of Eq. (3.57a), appears due to the fact that variations are taken with respect to the real undeformed fiber's length [228]. The same conclusion can be reached from the relation $\mathrm{d}\hat{x} \equiv \mathbf{F}_n \mathrm{d}\hat{x}_0$ in the same set of equations, in which $\mathrm{d}\hat{x}_0$ and $\mathrm{d}\hat{x}$ are the spatial vectors of an oriented differential fiber element with real length *before* and *after* deformation with the *orthonormal* reference frame $\{\hat{e}_i\}$ or $\{\hat{t}_i\}$.
The term g_0 ca be identified with the *initial curvature correction term*, whose effect may be significant for thick and moderately thick curved rods and small for slender rods. Similar explanations may be made for $g = |\mathbf{F}|$ as defined in Eq. (3.54b) and $g_n = |\mathbf{F}_n|$ in Eq. (3.62).

3.2.3 Other strain measurements

In continuous mechanics different strain measurements can be defined; Crisfield in reference [107], (Chapters 1–5), shows a good introduction to different measurement of strains in the one–dimensional case. For the 3D case it is possible to consult [251, 300].
The importance of studying several strain measurements is due to the fact that some of them are *energetically conjugated* to stress measurements although there are some exceptions.
Starting from $\mathbf{F}_n$ and removing the rigid body component $\mathbf{\Lambda}_n$ it is possible to define the following spatial strain tensor $\boldsymbol{\epsilon}_n$ (or $\boldsymbol{\mathcal{E}}_n$ in the material form):

$$\begin{aligned}
\boldsymbol{\epsilon}_n &\equiv (\mathbf{F}_n \hat{t}_{0i} - \mathbf{\Lambda}_n \hat{t}_{0i}) \otimes \hat{t}_{0i} = \mathbf{F}_n - \mathbf{\Lambda}_n \\
&= \frac{1}{g_0} \hat{\epsilon}_n \otimes \hat{t}_{01} = \frac{1}{g_0} \mathcal{E}_{ni} \hat{t}_i \otimes \hat{t}_{01} \\
&= \mathcal{E}_{nij} \hat{t}_i \otimes \hat{t}_{0j} \quad \in \quad T_{\hat{x}}\mathcal{B}_t \otimes T_{\hat{x}_0}\mathcal{B}_0 \qquad (3.68a) \\
\boldsymbol{\mathcal{E}}_n &\equiv (\bar{\mathbf{F}}_n \hat{E}_i - \mathbf{I}\hat{E}_i) \otimes \hat{E}_i = \bar{\mathbf{F}}_n - \mathbf{I} \\
&= \frac{1}{g_0} \hat{\mathcal{E}}_n \otimes \hat{E}_1 = \frac{1}{g_0} \mathcal{E}_{ni} \hat{E}_i \otimes \hat{E}_1 \\
&= \mathcal{E}_{nij} \hat{E}_i \otimes \hat{E}_j \quad \in \quad T_{\hat{X}}\mathcal{B}_{00} \otimes T_{\hat{X}}\mathcal{B}_{00} \qquad (3.68b)
\end{aligned}$$

which, as it will shown in next sections, is the energetically conjugated strain measurement to the *First Piola Kirchhoff* stress tensor. The component form of this strain measurement is

$$[\boldsymbol{\epsilon}_n]_{\hat{t}_i \otimes \hat{t}_{0j}} = [\boldsymbol{\mathcal{E}}_n]_{\hat{E}_i \otimes \hat{E}_j} = \frac{1}{g_0} \begin{bmatrix} \mathcal{E}_{n1} & 0 & 0 \\ \mathcal{E}_{n2} & 0 & 0 \\ \mathcal{E}_{n3} & 0 & 0 \end{bmatrix} = \frac{1}{g_0} \big[\hat{\mathcal{E}}_n \ \hat{0} \ \hat{0}\big]. \qquad (3.69)$$

In fact, as it has been previously described, the vector $g_0^{-1}\hat{\mathcal{E}}_n = \boldsymbol{\mathcal{E}}_n \cdot \hat{E}_1$ corresponds to the *right strain measurement* acting on the face of the cross section of the current rod configuration relative to the curved reference rod. The geometrical meaning of the strain vector $g_0^{-1}\hat{\epsilon}_n$ can be appreciated from the alternative definition:

$$\frac{1}{g_0} \hat{\epsilon}_n \equiv \mathbf{F}_n \hat{t}_{01} - \mathbf{\Lambda}_n \hat{t}_{01} \quad \in \quad T_{\hat{x}}\mathcal{B}_t \qquad (3.70)$$

which is the *stretching* of an oriented unit length fiber $\hat{t}_{01}$ of the curved reference rod at any material point to $\mathbf{F}_n \hat{t}_{01}$ with the rigidly rotated part $\hat{t}_1 = \mathbf{\Lambda}_n \hat{t}_{01}$ *removed*. The component $g_0^{-1}\epsilon_{n1}$ along $\hat{t}_1$ may be called the *extensional strain*, and the components $g_0^{-1}\epsilon_{n2}$ and $g_0^{-1}\epsilon_{n3}$ along $\hat{t}_2$ and $\hat{t}_3$ respectively, called the *shear strains*. For small strain problems the three components of the strain vector $g_0^{-1}\hat{\epsilon}_n$ become the extensional and shear strains in the classical or engineering

sense [300].
Taking advantage of the standard theory of continuum mechanics [251, 300], it is possible to construct the following definitions for the present theory:

Definition 3.10. ***Symmetric Green strain tensor***

Taking into account the result of Eq. (3.57a), the *symmetric Green strain tensor* in spatial and material forms are defined as [228]

$$\begin{aligned}
\boldsymbol{\epsilon}_G &\equiv \frac{1}{2}(\mathbf{F}_n^T\mathbf{F}_n - \mathbf{I}) = \frac{1}{2}\big((g_0^{-1}\mathcal{E}_{ni}\hat{t}_{01}\otimes\hat{t}_i + \hat{t}_{0i}\otimes\hat{t}_i)(g_0^{-1}\mathcal{E}_{nk}\hat{t}_k\otimes\hat{t}_{01} + \hat{t}_k\otimes\hat{t}_{0k}) - \mathbf{I}\big)\\
&= \frac{1}{2}\big(g_0^{-2}\mathcal{E}_{nk}\mathcal{E}_{nk}\hat{t}_{01}\otimes\hat{t}_{01} + g_0^{-1}\mathcal{E}_{nk}\hat{t}_{01}\otimes\hat{t}_{0k} + g_0^{-1}\mathcal{E}_{nk}\hat{t}_{0k}\otimes\hat{t}_{01} + \hat{t}_{0k}\otimes\hat{t}_{0k} - \mathbf{I}\big)\\
&= (\frac{g_0^{-2}}{2}\hat{\mathcal{E}}_n\cdot\hat{\mathcal{E}}_n + g_0^{-1}\mathcal{E}_{n1})\hat{t}_{01}\otimes\hat{t}_{01} + \frac{g_0^{-1}}{2}\mathcal{E}_{n\beta}(\hat{t}_{01}\otimes\hat{t}_{0\beta} + \hat{t}_{0\beta}\otimes\hat{t}_{01})\\
&= \mathcal{E}_{Gij}\hat{t}_{0i}\otimes\hat{t}_{0j} \quad \in \quad T_{\hat{x_0}}\mathcal{B}_0\otimes T_{\hat{x_0}}\mathcal{B}_0 \qquad (3.71a)\\
\boldsymbol{\mathcal{E}}_G &= (\frac{g_0^{-2}}{2}\hat{\mathcal{E}}_n\cdot\hat{\mathcal{E}}_n + g_0^{-1}\mathcal{E}_{n1})\hat{E}_1\otimes\hat{E}_1 + \frac{g_0^{-1}}{2}\mathcal{E}_{n\beta}(\hat{E}_1\otimes\hat{E}_\beta + \hat{E}_\beta\otimes\hat{E}_1)\\
&= \mathcal{E}_{Gij}\hat{E}_i\otimes\hat{E}_j \quad \in \quad T_{\hat{X}}\mathcal{B}_{00}\otimes T_{\hat{X}}\mathcal{B}_{00} \qquad (3.71b)
\end{aligned}$$

where the material form is obtained by means of the pullback operation by the rotation tensor $\boldsymbol{\Lambda}_0$ as $\boldsymbol{\mathcal{E}}_G = \boldsymbol{\Lambda}_0^T\boldsymbol{\epsilon}_G\boldsymbol{\Lambda}_0$ ■

The corresponding component form is

$$[\boldsymbol{\epsilon}_G]_{\hat{t}_{0i}\otimes\hat{t}_{0j}} = [\boldsymbol{\mathcal{E}}_G]_{\hat{E}_i\otimes\hat{E}_j} = \frac{1}{2g_0}\begin{bmatrix} 2\mathcal{E}_{n1} + g_0^{-1}\hat{\mathcal{E}}_n\cdot\hat{\mathcal{E}}_n & \mathcal{E}_{n2} & \mathcal{E}_{n3}\\ \mathcal{E}_{n2} & 0 & 0\\ \mathcal{E}_{n3} & 0 & 0\end{bmatrix} \qquad (3.72)$$

which is conjugated to the *Second Piola Kirchhoff* stress tensor.

Definition 3.11. ***Symmetric Eulerian strain tensor***

The spatial and material forms of the *symmetric Eulerian* strain tensor are defined as

$$\begin{aligned}
\boldsymbol{\epsilon}_E &\equiv \frac{1}{2}(\mathbf{I} - \mathbf{F}_n^{-T}\mathbf{F}_n^{-1}) \equiv \mathbf{F}_n^{-T}\boldsymbol{\epsilon}_G\mathbf{F}_n^{-1}\\
&= \frac{1}{2}\big(\mathbf{I} - (g^{-1}\mathcal{E}_{nk}\hat{t}_1\otimes\hat{t}_{ok} + \hat{t}_k\otimes\hat{t}_{ok})(g^{-1}\mathcal{E}_{nj}\hat{t}_{oj}\otimes\hat{t}_1 + \hat{t}_{oj}\otimes\hat{t}_j)\big)\\
&= \frac{1}{2}\big(\mathbf{I} - \hat{t}_k\otimes\hat{t}_k - g^{-2}\mathcal{E}_{nk}\mathcal{E}_{nk}\hat{t}_1\otimes\hat{t}_1 - g^{-1}\mathcal{E}_{nk}\hat{t}_1\otimes\hat{t}_k - g^{-1}\mathcal{E}_{nk}\hat{t}_k\otimes\hat{t}_1\big)\\
&= -\frac{g^{-1}}{2}\big((g^{-1}|\hat{\mathcal{E}}_n|^2 + 2\mathcal{E}_{nk})\hat{t}_1\otimes\hat{t}_1 + \mathcal{E}_{n\beta}(\hat{t}_1\otimes\hat{t}_\beta + \hat{t}_\beta\otimes\hat{t}_1)\big)\\
&= \mathcal{E}_{Eij}\hat{t}_i\otimes\hat{t}_j \quad \in \quad T_{\hat{x}}\mathcal{B}_t\otimes T_{\hat{x}}\mathcal{B}_t \qquad (3.73a)\\
\boldsymbol{\mathcal{E}}_E &= -\frac{g^{-1}}{2}\big((g^{-1}|\hat{\mathcal{E}}_n|^2 + 2\mathcal{E}_{nk})\hat{E}_1\otimes\hat{E}_1 + \mathcal{E}_{n\beta}(\hat{E}_1\otimes\hat{E}_\beta + \hat{E}_\beta\otimes\hat{E}_1)\big)\\
&= \mathcal{E}_{Eij}\hat{E}_i\otimes\hat{E}_j \quad \in \quad T_{\hat{X}}\mathcal{B}_{00}\otimes T_{\hat{X}}\mathcal{B}_{00}, \qquad (3.73b)
\end{aligned}$$

respectively. In Eq. (3.73b) the material form is obtained by means of the pullback operation by $\boldsymbol{\Lambda}$ as $\boldsymbol{\mathcal{E}}_G = \boldsymbol{\Lambda}^T\boldsymbol{\epsilon}_G\boldsymbol{\Lambda}$ ■

This stress tensor does not have an energetically conjugated strain measure. The corresponding component form is

$$[\boldsymbol{\epsilon}_E]_{\hat{t}_{0i}\otimes\hat{t}_{0j}} = [\boldsymbol{\mathcal{E}}_E]_{\hat{E}_i\otimes\hat{E}_j} = -\frac{1}{2g_0g_r}\begin{bmatrix} 2\mathcal{E}_{n1}+(g_rg_0)^{-1}\hat{\mathcal{E}}_n\cdot\hat{\mathcal{E}}_n & \mathcal{E}_{n2} & \mathcal{E}_{n3} \\ \mathcal{E}_{n2} & 0 & 0 \\ \mathcal{E}_{n3} & 0 & 0 \end{bmatrix}. \tag{3.74}$$

Both the Green strain tensor $\boldsymbol{\mathcal{E}}_G$ and the Eulerian strain tensor $\boldsymbol{\mathcal{E}}_E$ consist of those of the symmetric part of the engineering strain tensor $\boldsymbol{\mathcal{E}}_n$[14]. Writing both the Green and the Eulerian strain tensors in terms of the components of $\boldsymbol{\mathcal{E}}_n$, one obtains that the they consist of the following nonlinear quadratic term:

$$(\frac{1}{2g_0^2})\hat{\mathcal{E}}_n\cdot\hat{\mathcal{E}}_n = (\frac{1}{2g_0^2})\mathcal{E}_{ni}\mathcal{E}_{ni}.$$

3.2.4 Material time derivative of $\mathbf{F}_n$ and strain rates

In this section we calculate the material time derivative of $\mathbf{F}_n$, that will be used in next sections for the presentation of the balance laws for rod–like bodies. Noticing Eqs. (3.31b), (3.32b) for the angular velocity of the cross section, Eq. (A.105) for the co–rotated derivative of a second order tensor and Eqs. (3.57a) and (3.57b) for the spatial and material forms of the gradient tensor $\mathbf{F}_n$, we have

$$\begin{aligned} \dot{\mathbf{F}}_n &= \frac{\mathrm{d}}{\mathrm{d}t}(\boldsymbol{\Lambda}\bar{\mathbf{F}}_n\boldsymbol{\Lambda}_0^T) = \dot{\boldsymbol{\Lambda}}\bar{\mathbf{F}}_n\boldsymbol{\Lambda}_0^T + \boldsymbol{\Lambda}\dot{\bar{\mathbf{F}}}_n\boldsymbol{\Lambda}_0^T + \boldsymbol{\Lambda}\bar{\mathbf{F}}_n(\dot{\boldsymbol{\Lambda}}_0)^T \\ &= \widetilde{\boldsymbol{v}}\mathbf{F}_n - \mathbf{F}_n\dot{\widetilde{\boldsymbol{v}}}_0 + \overset{\triangledown}{[\dot{\mathbf{F}}_n]} \\ &= \widetilde{\boldsymbol{v}}\mathbf{F}_n + \overset{\triangledown}{[\dot{\mathbf{F}}_n]} \end{aligned} \tag{3.75}$$

where it has been used the fact that $\dot{\boldsymbol{\Lambda}}_0 = 0$ (spatially fixed) and the co–rotated time derivative of the deformation tensor $\overset{\triangledown}{[\dot{\mathbf{F}}_n]}$ is calculated considering $\boldsymbol{\Lambda} = \hat{t}_k\otimes\hat{E}_k$ and $\boldsymbol{\Lambda}_0^T = \hat{E}_p\otimes\hat{t}_{0p}$, as

$$\begin{aligned} \overset{\triangledown}{[\dot{\mathbf{F}}_n]} &= \underset{\rightarrow}{\boldsymbol{\Lambda}}(\dot{\mathbf{F}}_n) = \boldsymbol{\Lambda}\dot{\bar{\mathbf{F}}}_n\boldsymbol{\Lambda}_0^T \\ &= \frac{1}{g_0}(\hat{t}_k\otimes\hat{E}_k)\cdot\dot{\hat{\mathcal{E}}}\otimes\hat{E}_1\cdot(\hat{E}_p\otimes\hat{t}_{0p}) \\ &= \frac{1}{g_0}\dot{\mathcal{E}}_{ni}\hat{t}_k\delta_{ik}\otimes\delta_{1p}\hat{t}_{0p} = \frac{1}{g_0}\dot{\mathcal{E}}_{ni}\hat{t}_i\otimes\hat{t}_{01} = g_0^{-1}\boldsymbol{\Lambda}\dot{\hat{\mathcal{E}}}\otimes\hat{t}_{01} \\ &= \frac{1}{g_0}\overset{\triangledown}{[\dot{\epsilon}_n]}\otimes\hat{t}_{01} \qquad \in \quad T_{\hat{x}}\mathcal{B}_t\otimes T_{\hat{x}_0}\mathcal{B}_0 \end{aligned} \tag{3.76}$$

where the explicit explicit expression for the time derivative of the material form of the deformation gradient is calculated as

$$\dot{\bar{\mathbf{F}}}_n = \frac{1}{g_0}\dot{\hat{\mathcal{E}}}_n\otimes\hat{E}_1 \tag{3.77}$$

[14] Another researchers [174, 173], prefer to use $g_0\mathcal{E}_{nij} = \hat{x}_{,S}\cdot\hat{t}_j - \hat{x}_{0,S}\cdot\hat{t}_{0j}$ as the strain measure which is conjugated to the First Piola Kirchhoff stress tensor divided by the term g_0.

with

$$\hat{\mathcal{S}}_n = \dot{\hat{\mathcal{E}}}_n = \dot{\hat{\Gamma}}_n + \dot{\widetilde{\mathbf{\Omega}}}_n \hat{\mathscr{E}} \tag{3.78a}$$

$$\hat{s}_n = \overset{\triangledown}{[\dot{\hat{\epsilon}}_n]} = \mathbf{\Lambda}\dot{\mathcal{E}}_n\mathbf{\Lambda}^T = \overset{\triangledown}{[\dot{\hat{\gamma}}_n]} + \overset{\triangledown}{[\dot{\widetilde{\boldsymbol{\omega}}}_n]}\hat{\mathscr{T}}. \tag{3.78b}$$

Explicit formulae for the co–rotated *strain rate* vector, Eq. (3.78b), of any material point (S, ξ_β) on the current rod can be deduced with the aid of the expressions given for the spatial, material and co–rotated forms of the translational and rotational strain rates, as follows:

$$\dot{\hat{\gamma}}_n = \frac{\mathrm{d}}{\mathrm{d}t}\big(\hat{\varphi}_{,S} - \hat{t}_1\big) = \dot{\hat{\varphi}}_{,S} - \widetilde{\boldsymbol{v}}_n \hat{t}_1 \tag{3.79a}$$

$$\dot{\hat{\Gamma}}_n = \frac{\mathrm{d}}{\mathrm{d}t}\big(\mathbf{\Lambda}^T\hat{\gamma}_n\big) = \dot{\mathbf{\Lambda}}^T\hat{\varphi}_{,S} + \mathbf{\Lambda}^T\dot{\hat{\varphi}}_{,S} = \mathbf{\Lambda}^T\big(\dot{\hat{\varphi}}_{,S} - \widetilde{\boldsymbol{v}}_n\hat{\varphi}_{,S}\big) \tag{3.79b}$$

$$\overset{\triangledown}{[\dot{\hat{\gamma}}_n]} = \mathbf{\Lambda}\dot{\hat{\Gamma}}_n = \dot{\hat{\varphi}}_{,S} - \widetilde{\boldsymbol{v}}_n\hat{\varphi}_{,S} \tag{3.79c}$$

for the reduced translational strain rate vectors and

$$\begin{aligned}\dot{\widetilde{\boldsymbol{\omega}}}_n &= \frac{\mathrm{d}}{\mathrm{d}t}\big(\mathbf{\Lambda}_{n,S}\,\mathbf{\Lambda}_n^T\big) = (\dot{\mathbf{\Lambda}_n})_{,S}\,\mathbf{\Lambda}_n^T + \mathbf{\Lambda}_{n,S}\,(\dot{\mathbf{\Lambda}_n})^T \\ &= \big(\widetilde{\boldsymbol{v}}_{n,S}\,\mathbf{\Lambda}_n + \widetilde{\boldsymbol{v}}_n\mathbf{\Lambda}_{n,S}\big)\mathbf{\Lambda}_n^T - \mathbf{\Lambda}_{n,S}\,\mathbf{\Lambda}_n^T\widetilde{\boldsymbol{v}}_n \\ &= \widetilde{\boldsymbol{v}}_{n,S} + \widetilde{\boldsymbol{v}}_n\widetilde{\boldsymbol{\omega}}_n - \widetilde{\boldsymbol{\omega}}_n\widetilde{\boldsymbol{v}}_n \end{aligned} \tag{3.80a}$$

$$\begin{aligned}\dot{\widetilde{\mathbf{\Omega}}}_n &= \frac{\mathrm{d}}{\mathrm{d}t}\big(\mathbf{\Lambda}_0^T\mathbf{\Lambda}_n^T\mathbf{\Lambda}_{n,S}\,\mathbf{\Lambda}_0\big) = \mathbf{\Lambda}_0^T\big[(\dot{\mathbf{\Lambda}_n})^T\mathbf{\Lambda}_{n,S} + \mathbf{\Lambda}_n^T(\dot{\mathbf{\Lambda}_n})_{,S}\big]\mathbf{\Lambda}_0 \\ &= \mathbf{\Lambda}_0^T\big[-\mathbf{\Lambda}_n^T\widetilde{\boldsymbol{v}}_n\mathbf{\Lambda}_{n,S} + \mathbf{\Lambda}_n^T\big(\widetilde{\boldsymbol{v}}_{n,S}\,\mathbf{\Lambda}_n + \widetilde{\boldsymbol{v}}_n\mathbf{\Lambda}_{n,S}\big)\big]\mathbf{\Lambda}_0 \\ &= \mathbf{\Lambda}^T\widetilde{\boldsymbol{v}}_{n,S}\,\mathbf{\Lambda} \end{aligned} \tag{3.80b}$$

$$\overset{\triangledown}{[\dot{\widetilde{\boldsymbol{\omega}}}_n]} = \mathbf{\Lambda}\dot{\widetilde{\mathbf{\Omega}}}_n\mathbf{\Lambda}^T = \widetilde{\boldsymbol{v}}_{n,S} \tag{3.80c}$$

for the spatial, material and co–rotated descriptions of the rotational strain rate tensors, respectively. Therefore, the spatial, material and co–rotated descriptions of their associated rotational strain rate vectors are given by

$$\dot{\hat{\omega}}_n = \hat{v}_{n,S} - \widetilde{\boldsymbol{\omega}}_n\hat{v}_n = \hat{v}_{n,S} + \widetilde{\boldsymbol{v}}_n\hat{\omega}_n \tag{3.81a}$$

$$\dot{\hat{\Omega}}_n = \frac{\mathrm{d}}{\mathrm{d}t}\big(\mathbf{\Lambda}^T\hat{\omega}_n\big) = \dot{\mathbf{\Lambda}}^T\hat{\omega}_n + \mathbf{\Lambda}^T\big(\hat{v}_{n,S} + \widetilde{\boldsymbol{v}}_n\hat{\omega}_n\big) = \mathbf{\Lambda}^T\hat{v}_{n,S} \tag{3.81b}$$

$$\overset{\triangledown}{[\dot{\hat{\omega}}_n]} = \mathbf{\Lambda}\dot{\hat{\Omega}}_n = \hat{v}_{n,S} = \dot{\hat{\omega}}_n + \widetilde{\boldsymbol{\omega}}_n\hat{v}_n. \tag{3.81c}$$

Finally, Eq. (3.78b) can be rewritten as

$$\hat{s}_n = \overset{\triangledown}{[\dot{\hat{\epsilon}}_n]} = \overset{\triangledown}{[\dot{\hat{\gamma}}_n]} + \overset{\triangledown}{[\dot{\widetilde{\boldsymbol{\omega}}}_n]}\,\hat{\mathscr{T}} = \dot{\hat{\varphi}}_{,S} - \widetilde{\boldsymbol{v}}_n\hat{\varphi}_{,S} + \widetilde{\boldsymbol{v}}_{n,S}\,\hat{\mathscr{T}}. \tag{3.82}$$

As it has been noted by Simo [362], Eq. (3.82) corresponds to the strain rate measured by an observer located on the current reference system $\{\hat{t}_i\}$.

3.3 Stress measures and stress resultants

In the general theory of continuous mechanics several stress measurements can be constructed (see *e.g.* [251, 300, 388]). In this work only the *Cauchy*, the *First Piola Kirchhoff* and the *Second Piola Kirchhoff* stress tensors will be presented and deduced for a material point on the current cross section of the rod. Then, the *stress resultants* and *stress couples* will be defined in the classical sense [11, 333, 332, 362].

3.3.1 Cauchy stress tensor

The definition of the *Cauchy stress tensor*[15] starts from the postulation of the existence of a vector field $\hat{\mathfrak{t}}(\hat{x}, \hat{k}, t)$, depending on time t, the spatial point $\hat{x}(\hat{X}, t)$ and the unit vector $\hat{k}$. Physically, $\hat{\mathfrak{t}}$ represents the force per unit area exerted on a surface element oriented with normal $\hat{k}$. It is also called the *Cauchy* stress vector (see Fig. 3.4).
Assuming that the *balance of momentum*[16] holds, that $\hat{x}$ is C^1 and $\hat{\mathfrak{t}}$ is a continuous function of its arguments; then, there is a unique $\mathfrak{F}(2,0)$ *tensor field* (see §A.3.1 of Appendix A) denoted $\boldsymbol{\sigma} \in T_{\hat{x}}\mathcal{B}_t \otimes T_{\hat{x}}\mathcal{B}_t$, depending on $\hat{x}$ and t such that

$$\hat{\mathfrak{t}} = \langle \boldsymbol{\sigma}, \hat{k} \rangle \leftrightarrow \mathfrak{t}^i = \sigma^{ij} g_{qj} k^q = \sigma^i_j k^j. \tag{3.83}$$

In Eq. (3.83) the component form of the stress vector $\hat{\mathfrak{t}}$ has been expressed in terms of the tensor field $\boldsymbol{\sigma}$ associated to a general curvilinear coordinate system on $\mathcal{B}_t$ with metric tensor $\boldsymbol{g}$. Therefore, two equivalent expressions are obtained: $\boldsymbol{\sigma} = [\sigma^{ij}]_{\hat{t}_i \otimes \hat{t}_j} = [\sigma^i_j]_{\hat{t}_i \otimes \hat{t}^*_j}$, considering that $\sigma^{ij} g_{kj} = \sigma^i_k$. As it can be consulted in [251] the Cauchy stress tensor is symmetric.

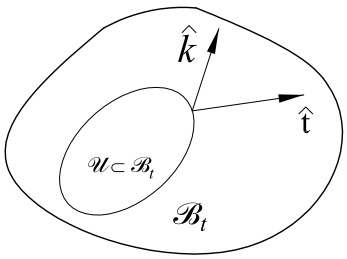

Figure 3.4: Geometric interpretation of the Cauchy stress vector.

In the case of the rod theory presented in this work, the Cauchy stress tensor $\boldsymbol{\sigma}$ at any material point (S, ξ_β) referred to a differential volume of the current rod cross section is given by

$$\boldsymbol{\sigma} \equiv \hat{\sigma}_j \otimes \hat{t}_j = \Sigma_{ji} \hat{t}_i \otimes \hat{t}_j \in T_{\hat{x}}\mathcal{B}_t \otimes T_{\hat{x}}\mathcal{B}_t \tag{3.84a}$$

$$\boldsymbol{\Sigma} = \Sigma_{ji} \hat{E}_i \otimes \hat{E}_j \in T_{\hat{X}}\mathcal{B}_{00} \otimes T_{\hat{X}}\mathcal{B}_{00} \tag{3.84b}$$

[15] The *Cauchy* stress tensor is some times called the *right* or *true* Cauchy stress tensor [251].

[16] Given $\hat{x}(\hat{X}, t)$, $\rho(\hat{x}, t)$, $\hat{\mathfrak{t}}(\hat{x}, \hat{k}, t)$ the motion function, density in the spatial form, the stress vector defined as before and $\hat{b}(\hat{x}, t)$ the body force, we say that the balance of momentum is satisfied provided that for every nice open set $\mathcal{U} \subset \mathcal{B}$:

$$\frac{\mathrm{d}}{\mathrm{d}t} \int_{\hat{x}_t(\mathcal{U})} \rho v \mathrm{d}V = \int_{\hat{x}_t(\mathcal{U})} \rho \hat{b} \mathrm{d}V + \int_{\partial \hat{x}_t(\mathcal{U})} \hat{\mathfrak{t}} \mathrm{d}a.$$

Where $v = \partial \hat{x} / \partial t$, $\hat{\mathfrak{t}}$ is evaluated on the unit outward normal $\hat{k}$ to $\partial \hat{x}_t(\mathcal{U})$ at the point $\hat{x}$ [251, 300].

in the spatial and material descriptions, respectively. The term $\hat{\sigma}_j$ is the stress vector acting on the current face and referred to the *real* area of the same face of the current rod with $\hat{t}_j$ as unit normal vector. Explicit expressions are

$$\begin{aligned} \hat{\sigma}_j &\equiv \Sigma_{ji}\hat{t}_j \quad \in \quad T_{\hat{x}}\mathcal{B}_t && \text{(3.85a)} \\ \hat{\Sigma}_j &= \Sigma_{ji}\hat{E}_j \quad \in \quad T_{\hat{X}}\mathcal{B}_{00} && \text{(3.85b)} \\ \Sigma_{ji} &\equiv \Sigma_{ij} \end{aligned}$$

3.3.2 First Piola Kirchhoff stress tensor

The *first Piola Kirchhoff* (FPK) stress tensor $\mathbf{P} \in T_{\hat{x}}\mathcal{B}_t \otimes T_{\hat{X}}\mathcal{B}_{00}$ is usually defined by means of the relation[17]

$$\hat{P}\mathrm{d}A_t = \mathbf{P} \cdot \hat{N}_0 \mathrm{d}A_0 \tag{3.86}$$

where $\hat{N}_0 \in T^*_{\hat{X}}\mathcal{B}_0$ is the unit normal co–vector belonging to the cotangent space of the material placement (see §A.3) $\mathrm{d}A_0$ and $\mathrm{d}A_t$ are the differential areas in the material and spatial placements and $\hat{P} \in T_{\hat{x}}\mathcal{B}_t$ is the FPK stress vector (see Fig. 3.4) that belongs to the tangent space of the spatial placement $\mathcal{B}_t$. We note that the basis vector $\{\hat{t}_i\}$ spans the tangent space $T_{\hat{x}}\mathcal{B}_t$. The FPK stress tensor $\mathbf{P}$ is an example of two point tensor in the sense that its stress vector belongs to the spatial vector space, its normal vector to the material vector space and its differential area to the material placement.

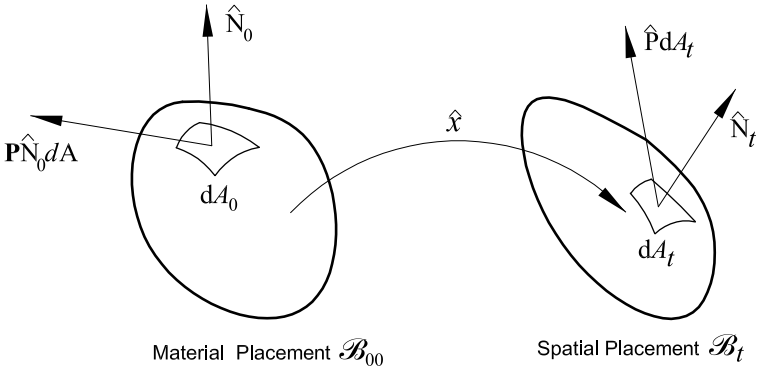

Figure 3.5: Geometric interpretation of the FPK stress tensor; note that $\mathbf{P} \cdot \hat{N}_0 \mathrm{d}A_0 \in T_{\hat{x}}\mathcal{B}_t$ although it is drawn on the material placement.

Moreover, it is possible to write the FPK stress tensor as a linear combination of stress vectors as

$$\mathbf{P} = \hat{P}_1 \otimes \hat{E}_1 + \hat{P}_2 \otimes \hat{E}_2 + \hat{P}_3 \otimes \hat{E}_3 \qquad \in \quad T_{\hat{x}}\mathcal{B}_t \otimes T_{\hat{X}}\mathcal{B}_{00} \tag{3.87}$$

where $\hat{P}_i = \hat{P}_i(\hat{x}, t)$ is the spatial stress vector belonging to the tangent space of spatial placement $\mathcal{B}_t$ and $\{\hat{E}_i\}$ is the material basis. Material and spatial place vector are related by Eq. (A.60). For the case of the present rod theory, using Eq. (3.63) for the inverse of the deformation tensor $\mathbf{F}_n^{-1} = \mathbf{\Lambda}_n^T(-g^{-1}\hat{\epsilon}_n \otimes \hat{t}_1 + \mathbf{I})$, the fact that $\mathbf{F}_n^{-T} = -g^{-1}\hat{t}_1 \otimes \mathcal{E}_{n1k}\hat{t}_{0k} + \hat{t}_k \otimes \hat{t}_{0k}$, the relation $g_n = 1 + g_0^{-1}\hat{\mathcal{E}}_{rj}$ as given in Eq. (3.62) and taking into account the definition given by Ogden [300], one obtains that the asymmetric FPK stress tensor $\mathbf{P}$ referred to a differential volume of

[17] A more formal definition of the FPK stress tensor require the definition of the *Piola transform* and it can be consulted in [251].

the curved reference rod is obtained as

$$\begin{aligned}
\mathbf{P} &\equiv g_n\boldsymbol{\sigma}\mathbf{F}_n^{-T} \\
&= \frac{-g_n}{g}\big[\Sigma_{ij}\hat{t}_j\underbrace{\otimes\hat{t}_i\cdot\hat{t}_1}_{\delta_{i1}}\otimes\mathcal{E}_{nk1}\hat{t}_{0k}\big] + g_n\big[\Sigma_{ij}\hat{t}_j\underbrace{\otimes\hat{t}_i\cdot\hat{t}_k}_{\delta_{ik}}\otimes\hat{t}_{0k}\big] \\
&= -g_0^{-1}\Sigma_{1i}\hat{t}_i\otimes\mathcal{E}_{nk1}\hat{t}_{0k} + g_n\Sigma_{ki}\hat{t}_i\otimes\hat{t}_{0k} \\
&= \big[g_n\hat{\sigma}_k - \frac{\mathcal{E}_{nk1}}{g_0}\hat{\sigma}_1\big]\otimes\hat{t}_{0k} \\
&= \hat{P}_k\otimes\hat{t}_{0k} = P^{\mathrm{m}}_{ki}\hat{t}_i\otimes\hat{t}_{0k} \qquad \in \quad T_{\hat{x}}\mathcal{B}_t\otimes T_{\hat{x}_0}\mathcal{B}_0 \qquad (3.88a)\\
\mathbf{P}^{\mathrm{m}} &\equiv \boldsymbol{\Lambda}^T\mathbf{P}\boldsymbol{\Lambda}_0^T = P^{\mathrm{m}}_{ki}\hat{E}_i\otimes\hat{E}_k \qquad \in \quad T_{\hat{X}}\mathcal{B}_{00}\otimes T_{\hat{X}}\mathcal{B}_{00} \qquad (3.88b)\\
\hat{P}_k &= P^{\mathrm{m}}_{ki}\hat{t}_i = g_n\hat{\sigma}_k - \frac{\hat{\mathcal{E}}_{nk1}}{g_0}\hat{\sigma}_1 \qquad \in \quad T_{\hat{x}}\mathcal{B}_t \qquad (3.88c)\\
\hat{P}^{\mathrm{m}}_k &= P^{\mathrm{m}}_{ki}\hat{E}_i \qquad \in \quad T_{\hat{X}}\mathcal{B}_{00} \qquad (3.88d)\\
P^{\mathrm{m}}_{ki} &= g_n\Sigma_{ki} - \frac{\mathcal{E}_{nk1}}{g_0}\Sigma_{1i} \neq P^{\mathrm{m}}_{ik} \qquad \in \quad \mathbb{R} \\
\hat{P}_1 &= \hat{\sigma}_1 \qquad (3.88e)
\end{aligned}$$

where $\hat{P}_j$ is the FPK stress vector acting on the deformed face in the current rod placement corresponding to the reference face with normal $\hat{t}_{0j}$ in the curved reference configuration and referred to the real area of the same reference face.
Additionally, considering $\mathbf{F}_n^T = g_0^{-1}\mathcal{E}_{ni1}\hat{t}_{01}\otimes\hat{t}_i + \hat{t}_{0i}\otimes\hat{t}_i$ one obtains

$$\begin{aligned}
\mathbf{P}\mathbf{F}_n^T &\equiv \big[g_n\Sigma_{ki} - \frac{1}{g_0}\Sigma_{1i}\mathcal{E}_{nk1}\big]\frac{1}{g_0}\mathcal{E}_{np1}\hat{t}_i\otimes\hat{t}_{0k}\cdot\hat{t}_{01}\otimes\hat{t}_p \\
&\quad + \big[g_n\Sigma_{ki} - \frac{1}{g_0}\Sigma_{1i}\mathcal{E}_{nk1}\big]\hat{t}_i\otimes\hat{t}_{0k}\cdot\hat{t}_{0p}\otimes\hat{t}_p \\
&= \big[\frac{g_n}{g_0}\Sigma_{1i}\mathcal{E}_{np1} - \frac{1}{g_0^2}\Sigma_{1i}\mathcal{E}_{np1}\mathcal{E}_{n11} + g_n\Sigma_{pi} - \frac{1}{g_0}\Sigma_{1i}\mathcal{E}_{np1}\big]\hat{t}_i\otimes\hat{t}_p \\
&= \big[\frac{1+(\mathcal{E}_{n11}/g_0)}{g_0}\Sigma_{1i}\mathcal{E}_{np1} - \frac{1}{g_0^2}\Sigma_{1i}\mathcal{E}_{np1}\mathcal{E}_{n11} + g_n\Sigma_{pi} - \frac{1}{g_0}\Sigma_{1i}\mathcal{E}_{np1}\big]\hat{t}_i\otimes\hat{t}_p \\
&= g_n\Sigma_{pi}\hat{t}_i\otimes\hat{t}_p = g_n\Sigma_{pi}\hat{t}_p\otimes\hat{t}_i; \qquad \text{(Symmetry of } \boldsymbol{\Sigma}\text{)}. \qquad (3.88f)
\end{aligned}$$

On the other hand, one has

$$\begin{aligned}
\mathbf{F}_n\mathbf{P}^T &\equiv \frac{1}{g_0}\mathcal{E}_{np1}\big[g_n\Sigma_{ki} - \frac{1}{g_0}\Sigma_{1i}\mathcal{E}_{nk1}\big]\hat{t}_p\otimes\hat{t}_{01}\cdot\hat{t}_{0k}\otimes\hat{t}_i \\
&\quad + \big[g_n\Sigma_{ki} - \frac{1}{g_0}\Sigma_{1i}\mathcal{E}_{nk1}\big]\hat{t}_p\otimes\hat{t}_{0p}\cdot\hat{t}_{0k}\otimes\hat{t}_i \\
&= \big[\frac{1+(\mathcal{E}_{n11}/g_0)}{g_0}\Sigma_{1i}\mathcal{E}_{np1} - \frac{1}{g_0^2}\Sigma_{1i}\mathcal{E}_{np1}\mathcal{E}_{n11} + g_n\Sigma_{pi} - \frac{1}{g_0}\Sigma_{1i}\mathcal{E}_{np1}\big]\hat{t}_p\otimes\hat{t}_i \\
&= g_n\Sigma_{pi}\hat{t}_p\otimes\hat{t}_i, \qquad (3.88g)
\end{aligned}$$

comparing the result of Eq. (3.88g) with the one of Eq. (3.88f) one obtains the identity $\mathbf{P}\mathbf{F}_n^T = \mathbf{F}_n\mathbf{P}^T$. Inversely, noticing Eq. (3.57b) for $\mathbf{F}_n$, we have

$$\boldsymbol{\sigma} \equiv \frac{1}{g_n}\mathbf{P}\mathbf{F}_n^T = \frac{1}{g_r}(P^{\mathrm{m}}_{ji} + \frac{\mathcal{E}_{nj1}}{g_0}P^{\mathrm{m}}_{1i})\hat{t}_i \otimes \hat{t}_j = \frac{1}{g_n}(P^{\mathrm{n}}_{ij} + \frac{\mathcal{E}_{ni1}}{g_0}P^{\mathrm{m}}_{1j})\hat{t}_i \otimes \hat{t}_j. \tag{3.89}$$

Similarly, for later reference, the FPK stress tensor $\mathbf{P}^0$ referred to a differential volume of the straight reference configuration is given by

$$\begin{aligned}
\mathbf{P}^0 &\equiv g\boldsymbol{\sigma}\mathbf{F}^{-T} = g_0\mathbf{P}\mathbf{F}_0^{-T} \\
&= g\Sigma_{jk}\hat{t}_k \otimes \hat{t}_j \cdot \big(-\frac{1}{g}\mathcal{E}_{i1}\hat{t}_1 \otimes \hat{E}_i + \hat{t}_i \otimes \hat{E}_i\big) \\
&= g\Sigma_{jk}\hat{t}_k \otimes \hat{E}_j - \Sigma_{1k}\hat{t}_k \otimes \mathcal{E}_{i1}\hat{E}_i \\
&= g\hat{\sigma}_j \otimes \hat{E}_j - \hat{\sigma}_1 \otimes \hat{\mathcal{E}}_1 = \hat{P}_i \otimes \hat{E}_i \quad \in \quad T_{\hat{x}}\mathcal{B}_t \otimes T_{\hat{X}}\mathcal{B}_{00} \qquad (3.90a) \\
\hat{P}^0_1 &= \hat{P}_1 = \hat{\sigma}_1 \quad \in \quad T_{\hat{x}}\mathcal{B}_t \\
\hat{P}^0_2 &= g_0\hat{P}_2 - \mathcal{E}_{021}\hat{P}_1 = g\hat{\sigma}_2 - \mathcal{E}_{21}\hat{\sigma}_1 \quad \in \quad T_{\hat{X}}\mathcal{B}_{00} \\
\hat{P}^0_3 &= g_0\hat{P}_3 - \mathcal{E}_{031}\hat{P}_3 = g\hat{\sigma}_3 - \mathcal{E}_{31}\hat{\sigma}_1 \quad \in \quad T_{\hat{X}}\mathcal{B}_{00} \\
\mathbf{P}^0\mathbf{F}^T &\equiv \mathbf{F}\mathbf{P}^{0T} \qquad (3.90b)
\end{aligned}$$

where $\hat{P}^{00}_i$ is the corresponding stress vector acting on the deformed face in the current placement corresponding to the reference face normal to $\hat{E}_i$ in the straight reference configuration and referred to the real area of the same reference face.
Correspondingly, the material form of $\mathbf{P}^0$ is given by

$$\begin{aligned}
\mathbf{P}^{0\mathrm{m}} &= \boldsymbol{\Lambda}^T\mathbf{P}^0 = g\Sigma_{jk}\hat{E}_k \otimes \hat{E}_j - \Sigma_{1k}\hat{E}_k \otimes \mathcal{E}_{i1}\hat{E}_i \\
&= g\hat{\Sigma}_j \otimes \hat{E}_j - \hat{\Sigma}_1 \otimes \hat{\mathcal{E}}_1 = \hat{P}_i \otimes \hat{E}_i \quad \in \quad T_{\hat{X}}\mathcal{B}_{00} \otimes T_{\hat{X}}\mathcal{B}_{00} \qquad (3.91)
\end{aligned}$$

REMARK 3.2. Note that the FPK stress vector referred to the cross section of any rod configuration is the same as the real Cauchy stress vector on the current cross section because it remains undeformed during the motion (see Eq. (3.67)) ■

3.3.3 Second Piola Kirchhoff stress tensor

Formally, the *Second Piola Kirchhoff* (SPK) stress tensor $\mathbf{S} \in T_{\hat{X}}\mathcal{B}_{00} \otimes T_{\hat{X}}\mathcal{B}_{00}$ is obtained by pulling the first leg of the FPK stress tensor $\mathbf{P}$ back by $\mathbf{F}$ (see the Section §A.5.2[18]). In coordinates,

$$\begin{aligned}
\mathbf{S} &\equiv \overleftarrow{\mathbf{F}}(\mathbf{P}) \\
S^{AB} &= (\mathbf{F}^{-1})^A_{\ a}P^{aB} = J(\mathbf{F}^{-1})^A_{\ a}(\mathbf{F}^{-1})^B_{\ b}\sigma^{ab} \qquad (3.92)
\end{aligned}$$

where J is the Jacobian of the map $\hat{x}$ and the coordinate systems $\{\hat{X}_A\}$ and $\{\hat{X}_a\}$ with their corresponding dual basis$\{\hat{X}^A\}$ and $\{\hat{X}^a\}$, are used to describe the material and spatial placements, respectively.
In the Reissner–Simo rod theory, $\mathbf{S}$ (see *e.g.* [251, 300]) is given in terms of the FPK and the

[18] For a detailed deduction of the SPK stress tensor see [251] Ch.2

Cauchy stress tensors as

$$\begin{aligned}
\mathbf{S} &\equiv g_n \mathbf{F}_n^{-1}\boldsymbol{\sigma}\mathbf{F}_n^{-T} = \mathbf{F}_n^{-1}\mathbf{P} \\
&= g_n(-\frac{1}{g}\mathcal{E}_{nj1}\hat{t}_{0j}\otimes\hat{t}_1 + \hat{t}_{0j}\otimes\hat{t}_j)\cdot\Sigma_{ik}\hat{t}_k\otimes\hat{t}_i\cdot(-\frac{1}{g}\hat{t}_1\otimes\mathcal{E}_{np1}\hat{t}_{0p} + \hat{t}_p\otimes\hat{t}_{0p}) \\
&= g_n(-\frac{1}{g}\mathcal{E}_{nj1}\hat{t}_{0j}\otimes\hat{t}_1 + \hat{t}_{0j}\otimes\hat{t}_j)\cdot(-\frac{1}{g}\Sigma_{1k}\mathcal{E}_{np1} + \Sigma_{pk})\hat{t}_k\otimes\hat{t}_{0p} \\
&= \Big[g_n\Sigma_{pj} - \Big(\frac{\mathcal{E}_{nj1}}{g_0}\Sigma_{p1} + \frac{\mathcal{E}_{np1}}{g_0}\Sigma_{1j}\Big) + \frac{1}{g_n}\Big(\frac{\mathcal{E}_{nj1}}{g_0}\Big)\Big(\frac{\mathcal{E}_{np1}}{g_0}\Big)\Sigma_{11}\Big]\hat{t}_{0j}\otimes\hat{t}_{0p} \\
&= \hat{S}_p\otimes\hat{t}_{0p} = S^{\mathrm{m}}_{pj}\hat{t}_{0j}\otimes\hat{t}_{0p} \qquad \in \quad T_{\hat{x}_0}\mathcal{B}_0\otimes T_{\hat{x}_0}\mathcal{B}_0
\end{aligned} \tag{3.93a}$$

with the corresponding material form given by

$$\begin{aligned}
\mathbf{S}^{\mathrm{m}} &= \boldsymbol{\Lambda}_0^T\mathbf{S}\boldsymbol{\Lambda}_0 = S^{\mathrm{m}}_{pj}\hat{E}_j\otimes\hat{E}_p \qquad \in \quad T_{\hat{X}}\mathcal{B}_{00}\otimes T_{\hat{X}}\mathcal{B}_{00} \\
\hat{S}_j &\equiv \mathbf{F}_n^{-1}\hat{P}_j = \mathbf{F}_n^{-1}(P^{\mathrm{m}}_{ji}\hat{t}_i) = P^{\mathrm{m}}_{ji}(\mathbf{F}_n^{-1}\hat{t}_i) = S^{\mathrm{m}}_{ji}\hat{t}_{0i} \qquad \in \quad T_{\hat{X}}\mathcal{B}_{00} \\
\hat{S}^{\mathrm{m}}_j &= S^{\mathrm{m}}_{ji}\hat{E}_i \qquad \in \quad T_{\hat{X}}\mathcal{B}_{00}
\end{aligned} \tag{3.93b}$$

$$S^{\mathrm{m}}_{ij} = P^{\mathrm{m}}_{ij} - \frac{\mathcal{E}_{ni1}}{g_n g_0}P^{\mathrm{m}}_{j1} = P^{\mathrm{m}}_{ij} - \frac{\mathcal{E}_{nj1}}{g_r g_0}P^{\mathrm{m}}_{i1}. \tag{3.93c}$$

In Eq. (3.93a) $\hat{S}_j$ is the stress vector acting on the deformed face in the current placement corresponding to the reference face normal to $\hat{t}_{0j}$ in the curved reference configuration and referred to the real area of the same reference face. That is equivalent to contract back $\hat{P}_j$ to the curved reference rod. It can be seen that the differences among the Cauchy stress and the FPK and SPK stresses are obvious for finite strain problems, though the differences tend to vanish for small strain problems (see Crisfield [107, 108]).

3.3.4 Stress resultants and stress couples

For the reduced one–dimensional rod model, it is convenient to define the *stress resultant* which is the internal force vector acting on the current cross section and the *stress couple i.e.* the internal moment vector acting on the same cross section.
The material form of the stress resultant $\hat{n}^{\mathrm{m}}(S,t)\in T^*_{\hat{X}}\mathcal{B}_{00}$ and stress couple $\hat{m}^{\mathrm{m}}(S,t)\in T^*_{\hat{X}}\mathcal{B}_{00}$ are defined by means of the following general formulas [245]:

$$\hat{n}^{\mathrm{m}} \triangleq \int_{\mathcal{A}_{00}}\boldsymbol{\Lambda}^T\hat{P}_1\mathrm{d}\mathcal{A}_{00} = \int_{\mathcal{A}_{00}}\hat{P}^{\mathrm{m}}_1\mathrm{d}\mathcal{A}_{00} \tag{3.94a}$$

$$\hat{m}^{\mathrm{m}} \triangleq \boldsymbol{\Lambda}^T\int_{\mathcal{A}_{00}}\widetilde{\boldsymbol{\mathscr{T}}}\hat{P}_1\mathrm{d}\mathcal{A}_{00} = \int_{\mathcal{A}_{00}}\widetilde{\boldsymbol{\mathscr{E}}}\hat{P}^{\mathrm{m}}_1\mathrm{d}\mathcal{A}_{00} \tag{3.94b}$$

where $\mathcal{A}_{00}(S)$ is the cross section at $S\in[0,L]$, $\widetilde{\boldsymbol{\mathscr{E}}}$ is the skew–symmetric tensor obtained from $\hat{\mathscr{E}}$ and $\hat{P}^{\mathrm{m}}_1$ is the FPK stress vector acting in the face of the cross sectional area with normal $\hat{E}_1$. The stress couple vector can be viewed as an element of the $T^{\mathrm{mat}*}_{\boldsymbol{\Lambda}}$ space that is the material co–vector space of rotation vectors.
For the formulation of the rod theory in terms of a straight and curved reference configurations it is necessary to define the spatial/material stress resultant and the spatial/material stress couple

vectors in following forms:

$$\begin{aligned}
\hat{n}(S) &= \int_{\mathcal{A}(S)} \boldsymbol{\sigma}\hat{t}_1 \mathrm{d}\xi_2\mathrm{d}\xi_3 = \int_{\mathcal{A}} \hat{\sigma}_1 \mathrm{d}\mathcal{A} \qquad \in \quad T_{\hat{x}}\mathcal{B}_t^* && \text{(3.95a)}\\
\hat{N}(S) &= \int_{\mathcal{A}_0(S)} \mathbf{P}\hat{t}_{01} \mathrm{d}\xi_2\mathrm{d}\xi_3 = \int_{\mathcal{A}_0} \hat{P}_1 \mathrm{d}\mathcal{A}_0 = \hat{n} \qquad \in \quad T_{\hat{x}_0}\mathcal{B}_0^* && \text{(3.95b)}\\
\hat{N}^0(S) &= \int_{\mathcal{A}_{00}(S)} \mathbf{P}^0\hat{E}_1 \mathrm{d}\xi_2\mathrm{d}\xi_3 = \int_{\mathcal{A}_{00}} \hat{P}_1^0 \mathrm{d}\mathcal{A}_{00} = \hat{n}^{\mathrm{m}} \qquad \in \quad T_{\hat{X}}\mathcal{B}_{00}^* && \text{(3.95c)}\\
\hat{n}^s(S) &= \int_{\mathcal{A}_0(S)} \mathbf{F}_n\mathbf{S}\hat{t}_{01} \mathrm{d}\xi_2\mathrm{d}\xi_3 = \int_{\mathcal{A}_0} \mathbf{F}_n\hat{S}_1 \mathrm{d}\mathcal{A}_0 \quad \in \quad T_{\hat{X}}\mathcal{B}_0^* && \text{(3.95d)}\\
&= N_i\hat{t}_i.
\end{aligned}$$

Considering that the rod has to maintain the internal force equilibrium in any configuration and neglecting the fact that all the stress resultant of Eqs. (3.95a) to (3.95d) are defined in their appropriated co–vector spaces, it is possible to write

$$\hat{n}(S) = \hat{N}(S) = \hat{N}^0(S) = \hat{n}^s(S) \tag{3.96}$$

with components $N_i = \int_{\mathcal{A}_{00}} P_{1i}^{\mathrm{m}} \mathrm{d}\mathcal{A}_{00}$.

For the case of the stress couple vector $\hat{m}(S)$, the following expressions are obtained [228]:

$$\begin{aligned}
\hat{m} &\equiv \int_{\mathcal{A}(S)} (\hat{x} - \hat{\varphi}) \times (\boldsymbol{\sigma}\hat{t}_1) \mathrm{d}\xi_2\mathrm{d}\xi_3 = \int_{\mathcal{A}} \widetilde{\boldsymbol{\mathscr{T}}}\hat{\sigma}_1 \mathrm{d}\mathcal{A} \qquad \in \quad T_{\hat{x}}\mathcal{B}_t^* && \text{(3.97a)}\\
\hat{M} &\equiv \int_{\mathcal{A}_0(S)} (\hat{x} - \hat{\varphi}) \times (\mathbf{P}\hat{t}_{01}) \mathrm{d}\xi_2\mathrm{d}\xi_3 = \int_{\mathcal{A}_0} \widetilde{\boldsymbol{\mathscr{T}}}\hat{P}_1 \mathrm{d}\mathcal{A}_0 = \hat{m} \qquad \in \quad T_{\hat{x}_0}\mathcal{B}_0^* && \text{(3.97b)}\\
\hat{M}^0 &\equiv \int_{\mathcal{A}_{00}(S)} \boldsymbol{\Lambda}^T(\hat{x} - \hat{\varphi}) \times (\mathbf{P}^0\hat{E}_1) \mathrm{d}\xi_2\mathrm{d}\xi_3 = \int_{\mathcal{A}_{00}} \widetilde{\boldsymbol{\mathscr{E}}}\hat{P}_1^0 \mathrm{d}\mathcal{A}_{00} = \hat{m}^{\mathrm{m}} \quad \in \quad T_{\hat{X}}\mathcal{B}_{00}^* && \text{(3.97c)}\\
\hat{m}^s &\equiv \int_{\mathcal{A}_0(S)} (\hat{x} - \hat{\varphi}) \times (\mathbf{F}_n\mathbf{S}\hat{t}_{01}) \mathrm{d}\xi_2\mathrm{d}\xi_3 = \int_{\mathcal{A}_0} \widetilde{\boldsymbol{\mathscr{T}}}\mathbf{F}_n S_1 \mathrm{d}\mathcal{A}_0 \qquad \in \quad T_{\hat{x}_0}\mathcal{B}_0^* && \text{(3.97d)}\\
&= M_i\hat{t}_i && \text{(3.97e)}
\end{aligned}$$

where $\widetilde{\boldsymbol{\mathscr{T}}}$ is the skew–symmetric tensors obtained from $\hat{\mathscr{T}}$. The component of Eqs. (3.97a) to (3.97d) are given by

$$M_1 = \int_{\mathcal{A}_{00}} \xi_2 P_{13}^{\mathrm{m}} - \xi_3 P_{12}^{\mathrm{m}} \mathrm{d}\mathcal{A}_{00}; \quad M_2 = \int_{\mathcal{A}_{00}} \xi_3 P_{11}^{\mathrm{m}} \mathrm{d}\mathcal{A}_{00}; \quad M_3 = -\int_{\mathcal{A}_{00}} \xi_2 P_{11}^{\mathrm{m}} \mathrm{d}\mathcal{A}_{00}. \tag{3.98}$$

In analogous manner to the case of the stress resultant, considering the equilibrium condition and the fact that all the tangent spaces to the material point on the body manifold in any configuration are isomorphic to $\mathbb{R}^3$, it is possible to write:

$$\hat{m}(S) = \hat{M}(S) = \hat{M}^0(S) = \hat{m}^s(S). \tag{3.99}$$

Given the stress resultant and the stress couple in their spatial forms $\hat{n}$ and $\hat{m}$ respectively, it is possible to obtain the corresponding material forms by means of pullback by $\boldsymbol{\Lambda}$ as

$$\hat{n}^{\mathrm{m}}(S) = \overleftarrow{\boldsymbol{\Lambda}}[\hat{n}] = \boldsymbol{\Lambda}^T\hat{n} = N_i\hat{E}_i \quad \in \quad T^*_{\hat{X}}\mathcal{B}_{00} \tag{3.100a}$$

$$\hat{m}^{\mathrm{m}}(S) = \overleftarrow{\boldsymbol{\Lambda}}[\hat{m}] = \boldsymbol{\Lambda}^T\hat{m} = M_i\hat{E}_i \quad \in \quad T^*_{\hat{X}}\mathcal{B}_{00}, \tag{3.100b}$$

respectively.
In Eqs. (3.95a) to (3.95d) and (3.97a) to (3.97d) $n_1 = N_1$ is the *normal* force component in the cross section with normal direction $\hat{t}_1$ while $n_2 = N_2$ and $n_3 = N_3$ are the *shear force* components in the directions $\hat{t}_2$ and $\hat{t}_3$, respectively. On the other hand, $m_1 = M_1$ is the *torque* component around the normal $\hat{t}_1$ while $m_2 = M_2$ and $m_3 = M_3$ are the *bending moment* components around $\hat{t}_2$ and $\hat{t}_3$, respectively. See Fig. 3.6 for a schematic representation of the stress resultant and the stress couple in the current configuration.

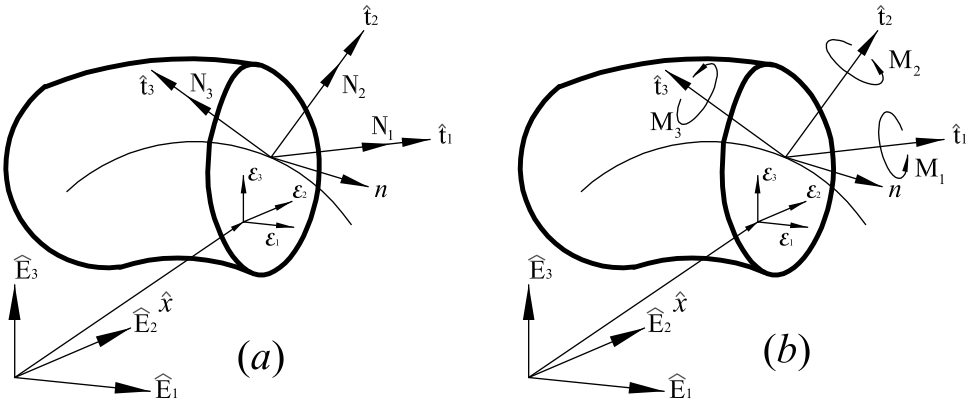

Figure 3.6: Geometric representation of (a): Stress resultant. (b): Stress couple.

3.4 Power balance condition

The purpose of this section is to formulate properly invariant reduced constitutive equations in terms of global kinetic and kinematical objects. The first step consists into obtain a reduced expression for the *internal power* from the general expression of three-dimensional theory, by means of introducing the kinematics assumptions of Eq. (3.22) [41, 62, 362]. This reduced expression yields the appropriated definition of strain measures conjugate to the resultant cross sectional forces and moments in the spatial as well as in the material descriptions.

3.4.1 Internal power

The general *power balance condition* can be stated as:

If the mechanical energy is conserved then, the power of the external loadings (surface traction and body force) is equal to the kinetic stress power plus the internal power for a given reference volume domain of the continuum using the Lagrangian description. The converse in also true.

The internal power per unit of reference volume of the continuum is

$$\mathfrak{P}_{\mathrm{int}} = \mathrm{Tr}\big[\mathbf{P}^T\dot{\mathbf{F}}_n\big] = g^{-1}\mathbf{P}^T(\widetilde{\boldsymbol{v}}_n(\delta_{i1}\hat{\epsilon}_n + \hat{t}_i) + \delta_{i1}[\overset{\triangledown}{\dot{\hat{\epsilon}}}_n]) \cdot \hat{t}_{0i} \tag{3.101}$$

where the trace operator has been used, Eq. (A.55), the internal power has been written in terms of the FPK stress tensor $\mathbf{P}$, Eq. (3.88a), and the material time derivative of the deformation gradient, $\dot{\mathbf{F}}_n$, which is an *objective scalar*, independent of the observer and the reference frame at a given material point. The objective of studying the internal power is to determine the strain measures that are conjugate to the FPK stresses for the curved reference rod.
Considering Eqs. (3.75) to (3.81c) for the material time derivative of the deformation tensor, $\dot{\mathbf{F}}_n$, and Eq. (A.56) for the trace of the product of two second order tensors, one obtains that the current rod internal power per unit of volume of the curved reference rod at any material point (S, ξ_β) is

$$\begin{aligned}\mathfrak{P}_{\text{int}}(S,\xi_\beta) &= \text{Tr}\big[\mathbf{P}^T\dot{\mathbf{F}}_n\big] = \text{Tr}\big[\mathbf{P}\dot{\mathbf{F}}_n^T\big] \\ &= \text{Tr}\big[\mathbf{P}^T\widetilde{\boldsymbol{v}}\mathbf{F}_n\big] + \text{Tr}\big[\mathbf{P}^T\big[\overset{\triangledown}{\mathbf{F}}_n\big]\big] = \text{Tr}\big[\mathbf{P}(\widetilde{\boldsymbol{v}}\mathbf{F}_n)^T\big] + \text{Tr}\big[\mathbf{P}^T\big[\overset{\triangledown}{\mathbf{F}}_n\big]\big]. \end{aligned} \tag{3.102}$$

The first term of the above equations is due to rigid–body rotation and should vanish. In fact, noticing Eq. (3.88a) for the relation between the FPK stress tensor and the Cauchy stress tensor as well as the symmetry of the Cauchy stress tensor and skew-symmetry of $\widetilde{\boldsymbol{v}}$, we have [228]

$$\begin{aligned}\text{Tr}\big[\mathbf{P}(\widetilde{\boldsymbol{v}}\mathbf{F}_n)^T\big] &= \text{Tr}\big[g_n\boldsymbol{\sigma}\mathbf{F}_n^{-T}\mathbf{F}_n^T\widetilde{\boldsymbol{v}}^T\big] = -g_n\text{Tr}\big[\boldsymbol{\sigma}\widetilde{\boldsymbol{v}}\big] \\ &= -g_n\text{Tr}\big[\boldsymbol{\sigma}^T\widetilde{\boldsymbol{v}}\big] = -g_n\text{Tr}\big[\boldsymbol{\sigma}\widetilde{\boldsymbol{v}}^T\big] \\ &= g_n\text{Tr}\big[\boldsymbol{\sigma}\widetilde{\boldsymbol{v}}\big] = 0 \end{aligned} \tag{3.103}$$

then, the second term become

$$\begin{aligned}\text{Tr}\big[\mathbf{P}^T\big[\overset{\triangledown}{\mathbf{F}}_n\big]\big] &= \text{Tr}\big[(\hat{t}_{0j}\otimes\hat{P}_j)(\frac{1}{g_0}\,\big[\overset{\triangledown}{\hat{\epsilon}_n}\big]\otimes\hat{t}_{01})\big] \\ &= \frac{1}{g_0}\text{Tr}\big[(\hat{P}_1\cdot\big[\overset{\triangledown}{\hat{\epsilon}_n}\big])(\hat{t}_{01}\otimes\hat{t}_{01})\big] \\ &= \frac{1}{g_0}\hat{P}_1\cdot\big[\overset{\triangledown}{\hat{\epsilon}_n}\big]\,. \end{aligned} \tag{3.104}$$

It follows that the current rod internal power per unit of the curved reference rod at any material point (S, ξ_β) is

$$\begin{aligned}\mathfrak{P}_{\text{int}} &= \text{Tr}\big[\mathbf{P}^T\dot{\mathbf{F}}_n\big] = \text{Tr}\big[\mathbf{P}^T\,\big[\overset{\triangledown}{\mathbf{F}}_n\big]\,\big] = \text{Tr}\big[\mathbf{P}^{\text{m}T}\dot{\tilde{\mathbf{F}}}_n\big] \\ &= \hat{P}_1\,\cdot(\frac{1}{g_0}\,\big[\overset{\triangledown}{\hat{\epsilon}_n}\big]) = \hat{P}_1^{\text{m}}\cdot(\frac{1}{g_0}\dot{\hat{\mathcal{E}}}_n). \end{aligned} \tag{3.105}$$

Therefore, $g_0^{-1}\hat{\epsilon}_n$ in the spatial form or $g_0^{-1}\hat{\mathcal{E}}_n$ in the material one is the strain vector at the material point (S, ξ_β) on the current cross section energetically conjugate to the FPK stress vector $\hat{P}_1$ in the spatial form or to $\hat{P}_1^{\text{m}}$ in the material description.
Additionally, it is possible to see that the strain tensors $\boldsymbol{\epsilon}_n$, $(\boldsymbol{\mathcal{E}}_n)$, Eqs. (3.68a) to (3.68b), are the energetically conjugated couples to the FPK strain tensors $\mathbf{P}$, $(\mathbf{P}^{\text{m}})$.
As it has been mentioned in §3.2.3 the Green strain tensors $\boldsymbol{\epsilon}_G$, $(\boldsymbol{\mathcal{E}}_G)$, are the energetically conjugated couples to the SPK stress tensors. Noting their relation with the FPK strain tensor,

Eq. (3.93a), it is possible to rewrite the internal power density as

$$\mathfrak{P}_{\rm int} \equiv {\rm Tr}\big[\mathbf{S}\dot{\boldsymbol{\epsilon}}_G\big] \equiv {\rm Tr}\big[\mathbf{P}\dot{\mathbf{F}}_n\big] = S^{\rm m}_{ij}\dot{\epsilon}_{Gij} = P^{\rm m}_{ij}\dot{\mathcal{E}}_{nij} = \hat{P}^{\rm m}_1 \cdot (\frac{1}{g_0}\dot{\hat{\mathcal{E}}}_n). \tag{3.106}$$

However, the symmetric Eulerian strain tensor $\boldsymbol{\epsilon}_E$, ($\boldsymbol{\mathcal{E}}_E$), does not have an energetically conjugated stress measure. In the case of the Cauchy stress tensor $\boldsymbol{\sigma}$, ($\boldsymbol{\Sigma}$), a conjugated strain rate tensor can by constructed in the following way [251, 300]

$$\mathfrak{P}_{\rm int} \equiv g_n {\rm Tr}\big[\boldsymbol{\sigma}\boldsymbol{\Sigma}^{\boldsymbol{*}}\big] \equiv {\rm Tr}\big[\mathbf{P}^T\dot{\mathbf{F}}_n\big] \equiv \Sigma_{ij}\Sigma^{*{\rm m}}_{ij} = \hat{\Sigma}_1 \cdot (\frac{1}{g_0}\dot{\hat{\mathcal{E}}}_n) = \mathbf{P}^{\rm m}_1 \cdot (\frac{1}{g_0}\dot{\hat{\mathcal{E}}}_n) \tag{3.107}$$

where

$$\boldsymbol{\Sigma}^* \equiv \mathbf{F}_n^{-T}\dot{\boldsymbol{\mathcal{E}}}_G\mathbf{F}_n^{-1} \equiv \Sigma^{*{\rm m}}_{ij}\hat{t}_{0i}\otimes\hat{t}_{0j} \tag{3.108a}$$

is the *Eulerian strain rate tensor*, which can not be obtained simply taking the material time derivative on $\boldsymbol{\epsilon}_E$ nor on $\boldsymbol{\mathcal{E}}_E$ in Eq. (3.73a). The component description of $\boldsymbol{\Sigma}^*$ is

$$[\boldsymbol{\Sigma}^*]_{\hat{t}_{0i}\otimes\hat{t}_{0j}} = \frac{1}{2g_0g_n}\begin{bmatrix} \dot{\mathcal{E}}_{n1} & \dot{\mathcal{E}}_{n2} & \dot{\mathcal{E}}_{n3} \\ \dot{\mathcal{E}}_{n2} & 0 & 0 \\ \dot{\mathcal{E}}_{n3} & 0 & 0 \end{bmatrix}. \tag{3.108b}$$

At cross sectional level, the current rod internal power per unit of arch–length of the curved reference rod is

$$\begin{aligned} \mathscr{P}_{\rm int}(S) &= \int_{\mathcal{A}(S)} \mathfrak{P}_{\rm int} g_0 {\rm d}\xi_2{\rm d}\xi_3 = \int_{\mathcal{A}(S)} \hat{P}_1 \cdot (\frac{1}{g_0}\overset{\triangledown}{[\hat{\mathcal{E}}_n]})g_0{\rm d}\mathcal{A} \\ &= \int_{\mathcal{A}(S)} \hat{P}_1 \cdot \big[\overset{\triangledown}{[\hat{\gamma}_n]} + \overset{\triangledown}{[\widetilde{\boldsymbol{\omega}}_n]}\,\hat{\mathscr{T}}\big]{\rm d}\mathcal{A} \\ &= \underbrace{\Big[\int_{\mathcal{A}(S)} \hat{P}_1 {\rm d}\mathcal{A}\Big]}_{\hat{n}(S)} \cdot \overset{\triangledown}{[\hat{\gamma}_n]} + \underbrace{\Big[\int_{\mathcal{A}(S)} \widetilde{\mathscr{T}}\hat{P}_1 \hat{d}\mathcal{A}\Big]}_{\hat{m}(S)} \cdot \overset{\triangledown}{[\hat{\omega}_n]}\,. \end{aligned} \tag{3.109}$$

The current rod internal power in spatial and material forms are

$$\mathscr{P}^{\rm spa}_{\rm int} = \hat{n}\cdot\overset{\triangledown}{[\hat{\gamma}_n]} + \hat{m}\cdot\overset{\triangledown}{[\hat{\omega}_n]} \tag{3.110a}$$

$$\mathscr{P}^{\rm mat}_{\rm int} = \hat{n}^{\rm m}\cdot\dot{\hat{\Gamma}}_n + \hat{m}^{\rm m}\cdot\dot{\hat{\Omega}}_n \tag{3.110b}$$

therefore, $\hat{\gamma}_n$ and $\hat{\omega}_n$ ($\hat{\Gamma}_n$ and $\hat{\Omega}_n$) are the strain measures conjugate to the stress resultant $\hat{n}(S)$ and stress couple $\hat{m}(S)$ ($\hat{n}^{\rm m}(S)$ and $\hat{m}^{\rm m}(S)$), respectively. These strain measures are summarized in Table 3.1.

Table 3.1: Reduced strain measures.

Strain measure	Spatial form	Material form
Translational	$\hat{\gamma}_n = \hat{\varphi}_{,S} - \hat{t}_1$	$\hat{\Gamma}_n = \boldsymbol{\Lambda}^T\hat{\gamma}_n$
Rotational	$\hat{\omega}_n = {\rm axial}[\boldsymbol{\Lambda}_{n,S}\,\boldsymbol{\Lambda}_n^T]$	$\hat{\Omega}_n = \boldsymbol{\Lambda}^T\hat{\omega}_n$

Once the reduced strain vectors are determined, the strain vector $g_0^{-1}\hat{\epsilon}_n$ at any material point (S, ξ_β) $(S \in [0, L];\ \xi_\beta \in \mathcal{A}(S))$ on the current rod cross section can be determined according to Eqs. (3.60a) and (3.54a). Having this information at hand, all the other strain measures reviewed in this work can be calculated using the equations of Section 3.2.3. Finally, the current rod internal power relative to the curved reference rod, Π_{int}, can be determined integrating along the length of the current rod as

$$\Pi_{\text{int}} \equiv \int_{\mathcal{A}(S)\times[0,L]} \text{Tr}\big[\mathbf{P}\mathbf{F}_n^T\big]\text{d}S\text{d}\xi_2\text{d}\xi_3 = \begin{cases} \int_0^L \big\{\hat{n}\cdot\big[\overset{\nabla}{\hat{\gamma}_n}\big] + \hat{m}\cdot\big[\overset{\nabla}{\hat{\omega}_n}\big]\big\}\text{d}S & \text{Spatial form} \\ \int_0^L \big\{\hat{n}^{\text{m}}\cdot\dot{\hat{\Gamma}}_n + \hat{m}^{\text{m}}\cdot\dot{\hat{\Omega}}_n\big\}\text{d}S & \text{Material form} \end{cases} \tag{3.111}$$

3.5 Equations of motion

The *Lagrangian differential equations of motion*[19] of a material point of the continuum without boundary conditions, can be written in terms of the FPK stress tensor referred to the curved reference configuration as

$$\begin{aligned} \nabla\cdot\mathbf{P} + \hat{b} &= \rho_0\ddot{\hat{x}} \\ \mathbf{P}\mathbf{F}_n^T &= \mathbf{F}_n\mathbf{P}^T \end{aligned} \tag{3.112}$$

where $\hat{b}$ and ρ_0 are the body force vector and the material density in the curved reference configuration, respectively. However, it is not convenient to work directly on the expression given in Eq. (3.112) because the divergence term is inconvenient to expand in the local frame $\{\hat{t}_{0i}\}$ along the mid–curve[20] [228, 207, 208].

As stated by Simo [362], it is possible to work on the straight reference configuration to obtain the equations of motion of the current rod. In this case, the equilibrium equations including boundary conditions are

$$\left.\begin{aligned} \nabla\cdot\mathbf{P}^0 + \hat{b}(\hat{X},t) &= \rho_{00}(\hat{X})\ddot{\hat{x}}(\hat{X},t) \\ \mathbf{P}^0\mathbf{F}^T &= \mathbf{F}\mathbf{P}^{0T} \end{aligned}\right\} \quad \text{in} \quad \mathcal{B}_{00} \tag{3.113a}$$

$$\mathbf{P}^0\hat{N}_{00} = \hat{\mathfrak{t}}_\sigma \quad \text{on} \quad \partial\mathcal{B}_{00\sigma} \tag{3.113b}$$

$$\hat{X} = \bar{\hat{X}} \quad \text{on} \quad \partial\bar{\mathcal{B}}_{00\sigma} \tag{3.113c}$$

where the boundary of the rod with applied initial conditions is defined by $\partial\mathcal{B}_{00} = \overline{\cup\partial\mathcal{B}_{00\sigma}\partial\bar{\mathcal{B}}_{00\sigma}}$, $\partial\mathcal{B}_{00\sigma}\cap\partial\bar{\mathcal{B}}_{00\sigma} = \emptyset$ and $\hat{b}$, $\rho_{00} = g_0\rho_0$, $\hat{N}_{00}$, $\hat{\mathfrak{t}}_\sigma$ and $\bar{\hat{x}}$ are the body force vector, the material density in the straight reference configuration, the vector normal to the traction boundary, the prescribed traction force vector and the prescribed placement vector, respectively. The base points are given in the material placement $\mathcal{B}_{00}$, but they occupy tangent spaces of the spatial placement $T_{\hat{x}}\mathcal{B}_t$ *i.e.* $\hat{b} := \hat{b}(\hat{x}) \in T_{\hat{x}}\mathcal{B}_t$ and $\mathbf{P}^0\mathbf{F}^T \in T_{\hat{x}}\mathcal{B}\otimes T_{\hat{x}}\mathcal{B}$.

According to Ogden [300] it is possible to work with the integral counterpart of Eq. (3.113a) yielding to the *Lagrangian field form* of the linear momentum balance equation written in term

[19] Alternatively, Iaura and Atluri [174, 173] work directly with the principle of virtual work for the reduced balance of equations of the initially curved/twisted rods.

[20] Taking directional derivatives can be a choice but more complicated algebraic developments are involved.

of integrals over $\mathcal{B}_{00}$ as

$$\int_{\mathcal{B}_{00}} \nabla \cdot \mathbf{P}^0 \mathrm{d}V_{00} + \int_{\mathcal{B}_{00}} \hat{b} \mathrm{d}V_{00} = \int_{\mathcal{B}_{00}} \rho_{00} \ddot{x} \mathrm{d}V_{00}. \tag{3.114}$$

By one hand, following analogous developments as those presented in [362] we have that $\nabla \cdot \mathbf{P}^0 = \hat{P}^0_{1},_S + \hat{P}^0_{\beta},_{\xi_\beta}$ and by Eqs. (3.95a), (3.95b), (3.97a) and (3.97b) we obtain

$$\hat{n},_S = \int_{\mathcal{A}_{00}} \hat{P}^0_{1},_S \, \mathrm{d}\mathcal{A}_{00} \tag{3.115}$$

where it has been taken into the fact that $\hat{P}^0_1 = \hat{\sigma}_1$; considering Eq. (3.113a) we have

$$\begin{aligned} \int_0^L \hat{n},_S \, \mathrm{d}S &= -\int_{V_{00}} \left\{ \hat{P}^0_{\beta},_{\xi_\beta} + \rho_{00} \hat{b} \right\} \mathrm{d}V_{00} + \int_{V_{00}} \rho_{00} \ddot{\hat{x}} \mathrm{d}V_{00} \\ &= -\Big\{ \int_{\mathcal{A}_{00*}} \hat{P}^0_{\beta} \nu_{00\beta} \mathrm{d}\mathcal{A}_{00*} + \int_{V_{00}} \rho_{00} \hat{b} \mathrm{d}V_{00} \Big\} + \int_{V_{00}} \rho_{00} \ddot{\hat{x}} \mathrm{d}V_{00} \end{aligned} \tag{3.116}$$

where $\mathcal{A}_{00*}$ is the arbitrarily chosen surface domain, $\hat{\nu}_{00} = \nu_{00\beta} \hat{E}_\beta$ the outward unit vector of the differential surface $\mathrm{d}\mathcal{A}_{00*}$ and V_{00} the corresponding volume domain surrounded by $\mathcal{A}_{00*}$. In Eq. (3.116) it has been used the divergence theorem to convert the volume integrals in area integrals.

Considering Eq. (3.33) it is possible to rewrite the last term in Eq. (3.116) as

$$\begin{aligned} \int_{V_{00}} \rho_{00} \ddot{\hat{x}} \mathrm{d}V_{00} &= \int_{[0,L]\times\mathcal{A}_{00}} \rho_{00} (\ddot{\hat{\varphi}} + [\widetilde{\boldsymbol{\alpha}}_n + \widetilde{\boldsymbol{v}}_n \widetilde{\boldsymbol{v}}_n] \hat{\mathscr{T}}) \mathrm{d}\mathcal{A}_{00} \mathrm{d}S \\ &= \int_0^L \ddot{\hat{\varphi}} [\int_{\mathcal{A}_{00}} \rho_{00} \mathrm{d}\mathcal{A}_{00}] \mathrm{d}S + \int_0^L \widetilde{\boldsymbol{\alpha}}_n [\int_{\mathcal{A}_{00}} \rho_{00} \hat{\mathscr{T}} \mathrm{d}\mathcal{A}_{00}] \mathrm{d}S \\ &+ \int_0^L \widetilde{\boldsymbol{v}}_n \widetilde{\boldsymbol{v}}_n [\int_{\mathcal{A}_{00}} \rho_{00} \hat{\mathscr{T}} \mathrm{d}\mathcal{A}_{00}] \mathrm{d}S \\ &= \int_0^L \ddot{\hat{\varphi}} \mathcal{A}_{\rho 00} \mathrm{d}S + \int_0^L \widetilde{\boldsymbol{\alpha}}_n \hat{\mathcal{S}}_{\rho 00} \mathrm{d}S + \int_0^L \widetilde{\boldsymbol{v}}_n \widetilde{\boldsymbol{v}}_n \hat{\mathcal{S}}_{\rho 00} \mathrm{d}S \\ &= \int_0^L [\ddot{\hat{\varphi}} \mathcal{A}_{\rho 00} + \widetilde{\boldsymbol{\alpha}}_n \hat{\mathcal{S}}_{\rho 00} + \widetilde{\boldsymbol{v}}_n \widetilde{\boldsymbol{v}}_n \hat{\mathcal{S}}_{\rho 00}] \mathrm{d}S \end{aligned} \tag{3.117}$$

where $\mathcal{A}_{\rho 00}(S) = \int_{\mathcal{A}_{00}} \rho_{00} \mathrm{d}\mathcal{A}_{00} \in \mathbb{R}$ and $\hat{\mathcal{S}}_{\rho 00} = \int_{\mathcal{A}_{00}} \rho_{00} \hat{\mathscr{T}} \mathrm{d}\mathcal{A}_{00} \in T_{\hat{x}} \mathcal{B}_t$.

If the Eq. (3.116) are applied to a parallel 'cut' slice through the straight reference configuration with differential length $\mathrm{d}S$ parallel to $\hat{E}_1$, defining the surface and volume integration domains (see Fig. 3.7), where $\mathrm{d}\mathcal{A}_{00*}$ is separated into the lateral surface $\mathrm{d}\mathcal{A}_{00L}$ and the cut surface $\mathrm{d}\mathcal{A}_{00N} = \mathrm{d}\mathcal{A}_{00N+} \cup \mathrm{d}\mathcal{A}_{00N-}$, and then using the variable and domain changes, one obtains the explicit expression for the *reduced external force* density per unit of arch–length of the curved reference rod as

$$\hat{\mathcal{N}}^* = \int_{\mathcal{A}_{00L}} \hat{P}^0_{\beta} \hat{\nu}_{00\beta} \mathrm{d}\mathcal{A}_{00L} + \int_{V_{00}} \rho_{00} \hat{b} \mathrm{d}\mathcal{A}_{00} \mathrm{d}S \tag{3.118}$$

and using Eq. (3.117) along with the preceding result one obtains the integral version of the *linear momentum balance equation* of the rod referred to the curved reference configuration,

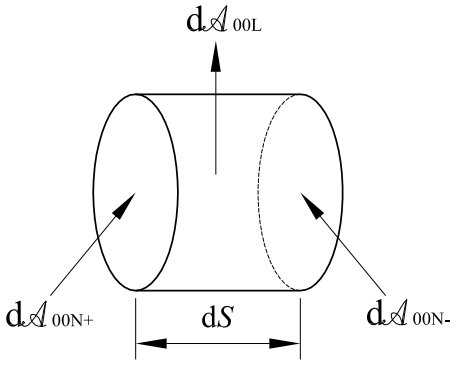

Figure 3.7: A differential slice for the straight reference configuration.

which read as

$$\int_0^L \{\hat{n}_{,S} + \hat{\mathcal{N}}^* - \mathcal{A}_{\rho 00}\ddot{\hat{\varphi}} - \widetilde{\boldsymbol{\alpha}}_n\hat{\mathcal{S}}_{\rho 00} - \widetilde{\boldsymbol{v}}_n\widetilde{\boldsymbol{v}}_n\hat{\mathcal{S}}_{\rho 00}\}\mathrm{d}S. \tag{3.119}$$

The local form of Eq. (3.119) constitutes the *linear momentum balance condition* and is given by

$$\hat{n}_{,S} + \hat{\mathcal{N}}^* = \mathcal{A}_{\rho 00}\ddot{\hat{\varphi}} + \widetilde{\boldsymbol{\alpha}}_n\hat{\mathcal{S}}_{\rho 00} + \widetilde{\boldsymbol{v}}_n\widetilde{\boldsymbol{v}}_n\hat{\mathcal{S}}_{\rho 00}. \tag{3.120}$$

Identical procedures allow to deduce the linear momentum balance condition when the reference configuration is the curved one. In this case one has

$$\hat{n}_{,S} + \hat{\mathcal{N}} = \mathcal{A}_{\rho_0}\ddot{\hat{\varphi}} + \underbrace{\hat{\alpha}_n \times \hat{\mathcal{S}}_{\rho_0} + \widetilde{\boldsymbol{v}}_n\widetilde{\boldsymbol{v}}_n\hat{\mathcal{S}}_{\rho_0}}_{\hat{\aleph}_1} \tag{3.121}$$

where the stress resultant $\hat{n} \in T^*_{\hat{x}}\mathcal{B}_t$ has been given in Eq. (3.95a), $\mathcal{A}_{\rho_0}$ is the reduced form of the translational mass density per unit of reference arch–length with explicit expression given by

$$\mathcal{A}_{\rho_0} = \int_{\mathcal{A}_0} g_0\rho_0\mathrm{d}\mathcal{A}_0 \tag{3.122}$$

$\hat{v}_n \in T^{\mathrm{spa}}_{\boldsymbol{\Lambda}}$ is the angular velocity vector of the current rod cross section; $\hat{\alpha} \in T^{\mathrm{spa}}_{\boldsymbol{\Lambda}}$ is the rotational acceleration of the current rod cross section and the *first mass moment density* vector $\hat{\mathcal{S}}_{\rho_0}$ per unit of arch–length of the curved reference rod mid–curve is

$$\begin{aligned}
\hat{\mathcal{S}}_{\rho_0} &= \int_{\mathcal{A}_0} \hat{\mathscr{T}} g_0\rho_0\mathrm{d}\mathcal{A}_0 = \bar{\mathcal{S}}_{\rho_0 3}\hat{t}_2 + \bar{\mathcal{S}}_{\rho_0 2}\hat{t}_3 \\
\bar{\mathcal{S}}_{\rho_0 3} &= \int_{\mathcal{A}_0} g_0\rho_0\xi_2\mathrm{d}\mathcal{A}_0, \qquad \bar{\mathcal{S}}_{\rho_0 2} = \int_{\mathcal{A}_0} g_0\rho_0\xi_3\mathrm{d}\mathcal{A}_0
\end{aligned} \tag{3.123}$$

and $\hat{\mathcal{N}} \in T^*_{\hat{x}}\mathcal{B}_t$ corresponds to the reduced form of the external applied forces calculated for the case of the curved reference rod as

$$\hat{\mathcal{N}} = \int_{\mathcal{A}_{00L}} \hat{P}^0_\beta\hat{\nu}_{00\beta}\mathrm{d}\mathcal{A}_{00L}) + \int_{V_{00}} \rho_{00}\hat{b}\mathrm{d}V_{00}\mathrm{d}S \tag{3.124a}$$

$$= \int_{\mathcal{A}_{0L}} (g_0\mathbf{P}\mathbf{F}_0^{-T})(g_0^{-1}\mathbf{F}_0^T\hat{\nu}_0\mathrm{d}\mathcal{A}_{0L}) + \int_{V_0} g_0\rho_0\hat{b}\mathrm{d}V_0 \tag{3.124b}$$

$$= \int_{\mathcal{A}_{0L}} \mathbf{P}\hat{\nu}_0 \mathrm{d}\mathcal{A}_{0L} + \int_{V_0} g_0\rho_0\hat{b}\mathrm{d}V_0 \tag{3.124c}$$

$$= \int_{\mathcal{C}_\mathcal{A}} \frac{g_0}{|\nu_0|^2\mathcal{C}_\mathcal{A}} \hat{P}_j\bar{\nu}_{0j}\mathrm{d}\mathcal{C}_\mathcal{A} + \int_{V_0} g_0\rho_0\hat{b}\mathrm{d}V_0 \quad \in \quad T^*_{\hat{x}}\mathcal{B}_t. \tag{3.124d}$$

The above expression for $\hat{\mathcal{N}}$ include the load boundary conditions for the lateral surface traction with outward unit vector $\hat{\nu}_0 = \bar{\nu}_{0j}\hat{t}_{0j}$ of the curved reference rod configuration; $\mathrm{d}\mathcal{C}_\mathcal{A}$ is the differential element of the contour line $\mathcal{C}_\mathcal{A}$ of the cross section domain $\mathcal{A}$ and $\hat{\nu}_{0\mathcal{C}_\mathcal{A}} = \bar{\nu}_{2\mathcal{C}_\mathcal{A}}\hat{t}_{02} + \bar{\nu}_{2\mathcal{C}_\mathcal{A}}\hat{t}_{02}$ the unit normal outward vector of $\mathcal{C}_\mathcal{A}$ in the cross section plane of the curved reference rod configuration [228].
Analogously, for the case of the *angular momentum balance* condition we have

$$\int_{V_{00}} (\hat{x} - \hat{\ell}) \times (\nabla \cdot \mathbf{P}^0)\mathrm{d}V_{00} + \int_{V_{00}} \rho_{00}(\hat{x} - \hat{\ell}) \times \hat{b}\mathrm{d}V_{00} = \int_{V_{00}} \rho_{00}(\hat{x} - \hat{\ell}) \times \ddot{\hat{x}}\mathrm{d}V_{00} \tag{3.125}$$

where $\hat{\ell} \in \mathbb{R}^3$ is and arbitrarily spatially fixed position vector. By one hand, developing for the right side of Eq. (3.125) and considering $\hat{\ell} = \hat{\varphi}$ by convenience along with the result of Eq. (A.21b) we obtain

$$\int_{V_{00}} \rho_{00}\hat{\mathscr{T}} \times \ddot{\hat{x}}\mathrm{d}V_{00} = \int_{V_{00}} \rho_{00}\hat{\mathscr{T}} \times \ddot{\hat{\varphi}}\mathrm{d}V_{00} + \int_{V_{00}} \rho_{00}\widetilde{\boldsymbol{\mathscr{T}}}\widetilde{\boldsymbol{\alpha}}_n\hat{\mathscr{T}}\mathrm{d}V_{00} + \int_{V_{00}} \rho_{00}\widetilde{\boldsymbol{\mathscr{T}}}\widetilde{\boldsymbol{v}}_n\widetilde{\boldsymbol{v}}_n\hat{\mathscr{T}}\mathrm{d}V_{00} \tag{3.126}$$

to develop an alternative expression for Eq. (3.126), it is necessary to take into account that

$$\begin{aligned}
\widetilde{\boldsymbol{\mathscr{T}}}\widetilde{\boldsymbol{v}}_n\widetilde{\boldsymbol{v}}_n\hat{\mathscr{T}} &= \widetilde{\boldsymbol{\mathscr{T}}}\hat{v}_n \times \widetilde{\boldsymbol{v}}_n\hat{\mathscr{T}} \\
&= -\mathbf{\Pi}[\widetilde{\boldsymbol{v}}_n\hat{\mathscr{T}}](\widetilde{\boldsymbol{\mathscr{T}}}\hat{v}_n) \\
&= -(\widetilde{\boldsymbol{v}}_n\widetilde{\boldsymbol{\mathscr{T}}} - \widetilde{\boldsymbol{\mathscr{T}}}\widetilde{\boldsymbol{v}}_n)(\widetilde{\boldsymbol{\mathscr{T}}}\hat{v}_n) \\
&= -\widetilde{\boldsymbol{v}}_n\widetilde{\boldsymbol{\mathscr{T}}}\widetilde{\boldsymbol{\mathscr{T}}}\hat{v}_n + (\widetilde{\boldsymbol{\mathscr{T}}}\hat{v}_n) \times (\widetilde{\boldsymbol{\mathscr{T}}}\hat{v}_n) \\
&= -\widetilde{\boldsymbol{v}}_n\widetilde{\boldsymbol{\mathscr{T}}}\widetilde{\boldsymbol{\mathscr{T}}}\hat{v}_n
\end{aligned}$$

which allows to rewrite Eq. (3.126) as

$$\begin{aligned}
\int_{V_{00}} \rho_{00}\hat{\mathscr{T}} \times \ddot{\hat{x}}\mathrm{d}V_{00} &= \int_{V_{00}} \rho_{00}\hat{\mathscr{T}} \times \ddot{\hat{\varphi}}\mathrm{d}V_{00} - \int_{V_{00}} \rho_{00}\widetilde{\boldsymbol{\mathscr{T}}}\widetilde{\boldsymbol{\mathscr{T}}}\hat{\alpha}_n\mathrm{d}V_{00} - \int_{V_{00}} \rho_{00}\widetilde{\boldsymbol{v}}_n\widetilde{\boldsymbol{\mathscr{T}}}\widetilde{\boldsymbol{\mathscr{T}}}\hat{v}_n\mathrm{d}V_{00} \\
&= \int_0^L \hat{S}_{\rho_{00}} \times \ddot{\hat{\varphi}}\mathrm{d}S + \int_0^L \boldsymbol{\mathcal{I}}_{\rho_{00}}\hat{\alpha}_n\mathrm{d}S + \int_0^L \widetilde{\boldsymbol{v}}_n\boldsymbol{\mathcal{I}}_{\rho_{00}}\hat{v}_n\mathrm{d}S
\end{aligned} \tag{3.127}$$

where the spatial inertial dyadic, $\boldsymbol{\mathcal{I}}_{\rho_{00}}$, with respect to the straight reference configuration is expressed by

$$\boldsymbol{\mathcal{I}}_{\rho_{00}} = -\int_{\mathcal{A}_{00}} \rho_{00}\widetilde{\boldsymbol{\mathscr{T}}}\widetilde{\boldsymbol{\mathscr{T}}}\mathrm{d}\mathcal{A}_{00} = \int_{\mathcal{A}_{00}} \rho_{00}(\|\hat{\mathscr{T}}\|^2\mathbf{I} - \hat{\mathscr{T}} \otimes \hat{\mathscr{T}})\mathrm{d}\mathcal{A}_{00} \tag{3.128}$$

the corresponding material form is obtained as $\mathbf{I}_{\rho_{00}} = \mathbf{\Lambda}^T\boldsymbol{\mathcal{I}}_{\rho_{00}}\mathbf{\Lambda}$. Before analyzing the left side of Eq. (3.125) we will present a previous result as follows: Considering Eq. (3.113c) and the

results given in Eqs. (A.21a) to (A.21g) of Appendix A, we have that

$$\begin{aligned}
\mathbf{P}^0\mathbf{F}^T &= \mathbf{F}\mathbf{P}^{0T}\\
\hat{P}_1^0\otimes\hat{x}_{,S}+\hat{P}_\beta^0\otimes\hat{x}_{,\xi_\beta} &= \hat{x}_{,S}\otimes\hat{P}_1^0+\hat{x}_{,\xi_\beta}\otimes\hat{P}_\beta^0\\
\leftrightarrow(\hat{P}_1^0\otimes\hat{x}_{,S}-\hat{x}_{,S}\otimes\hat{P}_1^0) &+ (\hat{P}_\beta^0\otimes\hat{x}_{,\xi_\beta}-\hat{x}_{,\xi_\beta}\otimes\hat{P}_\beta^0)=0\\
\leftrightarrow\mathbf{\Pi}[\hat{x}_{,S}]\mathbf{\Pi}[\hat{P}_1^0]-\mathbf{\Pi}[\hat{P}_1^0]\mathbf{\Pi}[\hat{x}_{,S}] &+ \mathbf{\Pi}[\hat{x}_{,\xi_\beta}]\mathbf{\Pi}[\hat{P}_\beta^0]-\mathbf{\Pi}[\hat{P}_\beta^0]\mathbf{\Pi}[\hat{x}_{,\xi_\beta}]=0\\
\leftrightarrow\quad \mathbf{\Pi}[\hat{x}_{,S}\times\hat{P}_1^0+\hat{x}_{,\xi_\beta}\times\hat{P}_\beta^0]&=0\\
\longrightarrow\quad \hat{x}_{,S}\times\hat{P}_1^0+\hat{x}_{,\xi_\beta}\times\hat{P}_\beta^0&=0.
\end{aligned}\tag{3.129}$$

By the other hand, the derivative with respect to the arch–length parameter S of the the cross sectional moment, Eq. (3.97b), is calculated considering Eqs. (3.125) and (3.129) as

$$\begin{aligned}
\hat{m}_{,S} &= \int_{\mathcal{A}_{00}}\hat{x}_{,S}\times\hat{P}_1^0\mathrm{d}\mathcal{A}_{00}-\hat{\varphi}_{,S}\times\int_{\mathcal{A}_{00}}\hat{P}_1^0\mathrm{d}\mathcal{A}_{00}+\int_{\mathcal{A}_{00}}\hat{\mathscr{T}}\times\hat{P}_1^0{}_{,S}\\
\longrightarrow\int_0^L(\hat{m}_{,S}+\hat{\varphi}_{,S}\times\hat{n})\mathrm{d}S &= \int_0^L(\hat{S}_{\rho_{00}}\times\ddot{\hat{\varphi}}+\boldsymbol{\mathcal{I}}_{\rho_{00}}\hat{\alpha}_n+\widetilde{\boldsymbol{v}}_n\boldsymbol{\mathcal{I}}_{\rho_{00}}\hat{v}_n)\mathrm{d}S\\
&- \int_0^L\int_{\mathcal{A}_{00}}\rho_{00}\hat{\mathscr{T}}\times\hat{b}\mathrm{d}\mathcal{A}_{00}\mathrm{d}S+\int_0^L\int_{\mathcal{A}_{00}}\hat{x}_{,S}\times\hat{P}_1^{00}\mathrm{d}\mathcal{A}_{00}\mathrm{d}S\\
&+ \int_0^L\int_{\mathcal{A}_{00}}\hat{\mathscr{T}}\times\hat{P}_{\beta,\xi_\beta}^0\,\mathrm{d}\mathcal{A}_{00}\mathrm{d}S
\end{aligned}$$

where, using the divergence theorem and the result of Eq. (3.129) allows to deduce the integral form of the *momentum balance condition* as

$$\begin{aligned}
\int_0^L(\hat{m}_{,S}+\hat{\varphi}_{,S}\times\hat{n})\mathrm{d}S &= \int_0^L(\hat{S}_{\rho_{00}}\times\ddot{\hat{\varphi}}+\boldsymbol{\mathcal{I}}_{\rho_{00}}\hat{\alpha}_n+\widetilde{\boldsymbol{v}}_n\boldsymbol{\mathcal{I}}_{\rho_{00}}\hat{v}_n)\mathrm{d}S-\int_0^L\int_{\mathcal{A}_{00}}\rho_{00}\hat{\mathscr{T}}\times\hat{b}\mathrm{d}\mathcal{A}_{00}\mathrm{d}S\\
&+\int_0^L\int_{\mathcal{A}_{00}}\underbrace{\{\hat{x}_{,S}\times\hat{P}_1^0+\hat{x}_{,\xi_\beta}\times\hat{P}_\beta^0\}}_{=0}\mathrm{d}\mathcal{A}_{00}\mathrm{d}S\\
&+\int_0^L\int_{\partial\mathcal{A}_{00}}\hat{\mathscr{T}}\times\hat{P}_\beta^0\nu_\beta\mathrm{d}\partial\mathcal{A}_{00}\mathrm{d}S\\
&= \int_0^L(\hat{S}_{\rho_{00}}\times\ddot{\hat{\varphi}}+\boldsymbol{\mathcal{I}}_{\rho_{00}}\hat{\alpha}_n+\widetilde{\boldsymbol{v}}_n\boldsymbol{\mathcal{I}}_{\rho_{00}}\hat{v}_n-\hat{\mathcal{M}}^*)\mathrm{d}S
\end{aligned}\tag{3.130}$$

where $\hat{\mathcal{M}}^*$ is the external applied moment per unit of reference arch–length, which reads

$$\hat{\mathcal{M}}^*=\int_{\partial\mathcal{A}_{00}}\hat{\mathscr{T}}\times\hat{P}_\beta^0\nu_\beta\mathrm{d}\partial\mathcal{A}_{00}-\int_{\mathcal{A}_{00}}\rho_{00}\hat{\mathscr{T}}\times\hat{b}\mathrm{d}\mathcal{A}_{00}.\tag{3.131}$$

The corresponding local form of the *momentum balance condition* is obtained from the previous equation as

$$\hat{m}_{,S}+\hat{\varphi}_{,S}\times\hat{n}+\hat{\mathcal{M}}^*=\hat{S}_{\rho_{00}}\times\ddot{\hat{\varphi}}+\boldsymbol{\mathcal{I}}_{\rho_{00}}\hat{\alpha}_n+\widetilde{\boldsymbol{v}}_n\boldsymbol{\mathcal{I}}_{\rho_{00}}\hat{v}_n.\tag{3.132}$$

Identical procedures allow to deduce the momentum balance condition when the reference configuration is the curved one. In this case, one obtains

$$\hat{m}_{,S} + \hat{\varphi}_{,S} \times \hat{n} + \hat{\mathcal{M}} = \underbrace{\hat{\mathcal{S}}_{\rho_0} \times \ddot{\hat{\varphi}}}_{\hat{\aleph}_2} + \boldsymbol{\mathcal{I}}_{\rho_0} \hat{\alpha}_n + \widetilde{\boldsymbol{v}}_n \big[\boldsymbol{\mathcal{I}}_{\rho_0} \hat{v}_n\big] \tag{3.133}$$

where the stress couple $\hat{m} \in T^*_{\hat{x}}\mathcal{B}_t$ has been given in Eq. (3.97a) and the *rotational mass* or *mass moment density* tensor $\boldsymbol{\mathcal{I}}_{\rho_0}$ per unit of arch–length of the curved reference rod is

$$\boldsymbol{\mathcal{I}}_{\rho_0} = -\int_{\mathcal{A}_0} g_0 \rho_0 \widetilde{\boldsymbol{\mathscr{T}}} \widetilde{\boldsymbol{\mathscr{T}}} \mathrm{d}\mathcal{A}_0 = \int_{\mathcal{A}_0} g_0 \rho_0 (\|\hat{\mathscr{T}}\|^2 \mathbf{I} - \hat{\mathscr{T}} \otimes \hat{\mathscr{T}}) \mathrm{d}\mathcal{A}_0 = \bar{\mathcal{I}}_{\rho_0 ij} \hat{t}_2 \otimes \hat{t}_3 \tag{3.134}$$

where

$$\begin{aligned}
\bar{\mathcal{I}}_{\rho_0 11} &= \bar{\mathcal{I}}_{\rho_0 22} + \bar{\mathcal{I}}_{\rho_0 33}, \quad \bar{\mathcal{I}}_{\rho_0 12} = \bar{\mathcal{I}}_{\rho_0 13} = \bar{\mathcal{I}}_{\rho_0 21} = \bar{\mathcal{I}}_{\rho_0 31} = 0 \\
\bar{\mathcal{I}}_{\rho_0 22} &= \int_{\mathcal{A}_0} g_0 \rho_0 (\xi_3)^2 \mathrm{d}\mathcal{A}_0, \quad \bar{\mathcal{I}}_{\rho_0 33} = \int_{\mathcal{A}_0} g_0 \rho_0 (\xi_2)^2 \mathrm{d}\mathcal{A}_0 \\
\bar{\mathcal{I}}_{\rho_0 23} &= \bar{\mathcal{I}}_{\rho_0 32} = -\int_{\mathcal{A}_0} g_0 \rho_0 \xi_2 \xi_3 \mathrm{d}\mathcal{A}_0
\end{aligned} \tag{3.135}$$

and the *reduced external moment* density per unit of arch–length of the curved reference rod mid–curve is

$$\begin{aligned}
\hat{\mathcal{M}} &= \int_{\mathcal{A}_{00L}} \hat{\mathscr{T}} \times \big[\mathbf{P}^0 \hat{\nu}_{00} d\mathcal{A}_{00L}\big] + \int_{\mathcal{A}} \rho_{00} \hat{\mathscr{T}} \times \hat{b} \mathrm{d}\mathcal{A} \\
&= \int_{\mathcal{A}_{0L}} \hat{\mathscr{T}} \times \mathbf{P} \nu_0 \mathrm{d}\mathcal{A}_{0L} + \int_{\mathcal{A}} g_0 \hat{\mathscr{T}} \times \rho_0 \hat{b} \mathrm{d}\mathcal{A} \\
&= \int_{\mathcal{C}_{\mathcal{A}}} \frac{g_0}{\hat{\nu}_0 \cdot \hat{\nu}_{0\mathcal{C}_{\mathcal{A}}}} \hat{\mathscr{T}} \times (\mathbf{P}^0_j \bar{\nu}_{0j}) d\mathcal{C}_{\mathcal{A}} + \int_{\mathcal{A}} g_0 \hat{\mathscr{T}} \times \rho_0 \hat{b} \mathrm{d}\mathcal{A} \quad \in \quad T^*_{\hat{x}}\mathcal{B}_t.
\end{aligned} \tag{3.136a}$$

The same equations of motion can be derived by very different principles and approaches as it can be reviewed in references [11, 174, 136]. It is worth to note that the linear and angular momentum balance equations for the case of the present initially curved and twisted rods is also a stress resultant formulation, consistent with the continuum mechanics at the resultant level [89, 142].

The system of nonlinear differential equations of Eqs. (3.121) and (3.133) have to be supplemented with the following boundary conditions:

$$(\hat{\varphi}_\Phi, \boldsymbol{\Lambda}_\Phi) \quad \in \quad \partial_\Phi \hat{\varphi} \times [0, T] \tag{3.137a}$$

$$(\hat{n}_\Sigma, \hat{m}_\Sigma) \quad \in \quad \partial_\Sigma \hat{\varphi} \times [0, T] \tag{3.137b}$$

with the standard conditions $\partial_\Phi \hat{\varphi}_0 \cup \partial_\Sigma \hat{\varphi}_0 = \partial \hat{\varphi}_0$ and $\partial_\Phi \hat{\varphi}_0 \cap \partial_\Sigma \hat{\varphi}_0 = \emptyset$ assumed to hold. The additional initial data are given by

$$\hat{\varphi}(S, 0) = \hat{\varphi}_0(S) \qquad \text{and} \qquad \boldsymbol{\Lambda}(S, 0) = \boldsymbol{\Lambda}_0(S), \qquad \forall S \in [0, L] \tag{3.137c}$$

$$\dot{\hat{\varphi}}(S, 0) = \dot{\hat{\varphi}}_0(S) \qquad \text{and} \qquad \dot{\boldsymbol{\Lambda}}(S, 0) = \boldsymbol{\Lambda}_0(S) \widetilde{\boldsymbol{V}}_{0n}(S), \qquad \forall S \in [0, L] \tag{3.137d}$$

where $(\dot{\hat{\varphi}}_0, \hat{V}_{0n}) : [0, L] \to \mathbb{R}^3 \times \mathbb{R}^3$ is a prescribed velocity field. The static version can be obtained ignoring the terms of Eqs. (3.137c) and (3.137d) and the corresponding inertial terms

in the equilibrium equations.

REMARK 3.3. For an untwisted straight rod made of homogeneous material with no initial elongation of the rod mid–curve, ($g_0 = 1$), the first mass moment density $\hat{\mathcal{S}}_{\rho_0}$ of Eq. (3.123) vanishes if the rod reference curve is chosen as the geometry centroid line of the rod cross section. In this case, the terms $\hat{\aleph}_1$ and $\hat{\aleph}_2$ of Eqs. (3.119) and (3.133) vanish and the balance equations reduce to the original forms given by Simo [362] and Simo and Vu-Quoc [363, 365]. In addition, if the rod is also uniform, Eqs. (3.124a) to (3.124d) and (3.136a) to (3.136a) also are reduced to those given by Simo *et al.* For initially curved rods, $g_0 \neq 1$, and if the rod reference curve is chosen as the geometric centroid line, $\hat{\mathcal{S}}_{\rho_0}$ does not vanish in general though its entries are small for slender rods. On other hand, if one choose the mass centroid line as the rod reference curve, $\hat{\mathcal{S}}_{\rho_0}$ also vanishes ■

3.6 Virtual work forms

In this section, we derive the *principle of virtual work* [201] for the Reissner–Simo rod theory. As stated by Mäkinen in Ref. [245] we state that the *virtual work* may be viewed as a linear form on the tangent field–bundle $T\mathcal{B}_0$ (see §A.5). This field bundle is also a tangent bundle of the placement manifold at fixed time. In following we give definitions for the virtual work in the finite–dimensional and infinite–dimensional cases. Moreover, it will be shown that the principle of virtual work constitutes a weak form of the linear and angular momentum balance equations recovering Eqs. (3.113a) to (3.113c) or equivalently Eqs. (3.121) and (3.133). Detailed explanations about virtual work forms on manifolds are given in Defs. A.18 and A.19 of §A.3.1 of Appendix A.

3.6.1 Principle of virtual work

The principle of virtual work states that at a dynamical equilibrium, the virtual work with respect to any virtual displacement, at time $t = t_0$ and place vector $\hat{x}_*$, vanishes *i.e.*

$$G(\hat{x}_*, \delta\hat{x}) := \int_{\mathcal{B}_{t_0}} \hat{f} \cdot \delta\hat{x} \mathrm{d}\mathcal{B}_{t_0} = 0 \quad \forall\, \hat{x}_* \in \mathcal{B}_{t_0}, \delta\hat{x} \in\ T_{\hat{x}_*}\mathcal{B}_{t_0} \tag{3.138}$$

where the virtual displacement field $\delta\hat{x} \in T\mathcal{B}_0$ and the force field $\hat{f} = \hat{f}(t_0, \hat{x}_*) \in T^*\mathcal{B}_{t_0}$ *i.e.* it belongs to the co–tangent field bundle.

3.6.2 Weak form of the balance equations

One choice for constructing a continuum based expression of the virtual work is given by taking as pair quantity the FPK stress tensor. This selection is very popular for the geometrically exact rod theories [174, 245, 362] since the work pair for the FPK stress tensor is the *virtual deformation gradient*, as it has been shown in §3.4, yielding rather a simple formulation. The virtual deformation gradient corresponds to the Lie variation (see §A.5.5) of the deformation gradient tensor, $\delta_{\mathbf{\Lambda}}(\mathbf{F}) \in T_{\hat{x}}\mathcal{B}_t \otimes T^*_{\hat{X}}\mathcal{B}_0$. Then, we write explicitly the virtual work principle and we show that it satisfies the balance equilibrium conditions given in Eqs. (3.113a) to (3.113a)

[245] as follows:

$$G(\hat{x},\delta\hat{x}) = \underbrace{\int_{\mathcal{B}_0}\langle\delta\hat{x},\hat{b}\rangle_{\boldsymbol{g}}\mathrm{d}V+\int_{\partial\mathcal{B}_0}\langle\delta\hat{x},\hat{\mathrm{t}}_\sigma\rangle_{\boldsymbol{g}}\mathrm{d}A}_{G_{\mathrm{ext}}}+\underbrace{\int_{\mathcal{B}_0}(\delta\overset{\triangledown}{[\mathbf{F}]}\colon\boldsymbol{g}\mathbf{P})\mathrm{d}V}_{G_{\mathrm{int}}}-\underbrace{\int_{\mathcal{B}_0}\langle\delta\hat{x},\rho_0\ddot{\hat{x}}\rangle_{\boldsymbol{g}}\mathrm{d}V}_{G_{\mathrm{ine}}}=0$$

$$= \int_{\mathcal{B}_0}\delta\hat{x}\cdot\hat{b}\mathrm{d}V+\int_{\partial\mathcal{B}_0}\delta\hat{x}\cdot\hat{\mathrm{t}}_\sigma\mathrm{d}A-\int_{\mathcal{B}_0}(\delta\overset{\triangledown}{[\mathbf{F}]}\colon\mathbf{P})\mathrm{d}V-\int_{\mathcal{B}_0}\rho_0\delta\hat{x}\cdot\ddot{\hat{x}}\mathrm{d}V=0. \quad (3.139)$$

In principle, in Eq. (3.139) a more general formulation, including the metric tensor $\boldsymbol{g}$, associated to the coordinate description of the current beam configuration, has been used (see §A.3 of Appendix A) by completeness. The formal definition for the inner product $\langle\bullet\rangle_{\boldsymbol{g}}\in\mathcal{L}(T_{\hat{x}_0}\mathcal{B}_{t_0}\times T^*_{\hat{x}_0}\mathcal{B}_{t_0},\mathbb{R})$ is given in the same appendix. The first two terms correspond to the *external* virtual work G_{ext} and to the *internal* virtual work G_{int}, respectively; and the last term to the *inertial* virtual work G_{ine}.
Note that the term $(\delta_{\boldsymbol{\Lambda}}\mathbf{F}:\mathbf{P})$ can be simplified into

$$\begin{aligned}\delta\overset{\triangledown}{[\mathbf{F}]}\colon\mathbf{P} &= \delta\mathbf{F}:\mathbf{P}-(\delta\widetilde{\boldsymbol{\theta}}\mathbf{F}):\mathbf{P}\\ &= (\nabla\delta\hat{x}):\mathbf{P}-\frac{1}{2}\big[(\delta\widetilde{\boldsymbol{\theta}}\mathbf{F}):\mathbf{P}-(\delta\widetilde{\boldsymbol{\theta}}^T\mathbf{F}):\mathbf{P}\big]\\ &= \nabla\cdot(\mathbf{P}^T\delta\hat{x})-\delta\hat{x}\cdot(\nabla\cdot\mathbf{P})-\frac{1}{2}\delta\widetilde{\boldsymbol{\theta}}:(\mathbf{P}\mathbf{F}^T-\mathbf{F}\mathbf{P}^T)\end{aligned} \quad (3.140)$$

where the skew–symmetry of $\delta\widetilde{\boldsymbol{\theta}}^T=-\delta\widetilde{\boldsymbol{\theta}}$ has been used together with the relation between divergence and gradient operators $(\nabla\delta\hat{\vartheta}):\boldsymbol{g}\boldsymbol{\vartheta}=\nabla\cdot(\boldsymbol{\vartheta}^*\boldsymbol{g}\delta\hat{\vartheta})-\boldsymbol{g}\delta\hat{\vartheta}\cdot(\nabla\cdot\boldsymbol{\vartheta}),\ \forall\hat{\vartheta}\in\mathbb{R}^3,\boldsymbol{\vartheta}\in\mathfrak{F}(0,2)$ with the metric tensor $\boldsymbol{g}=\mathbf{I}$ and $\mathbf{P}^*=\mathbf{P}^T$ (see §A.3).
Substituting the result of Eq. (3.140) in Eq. (3.139) we obtain

$$G=\int_{\mathcal{B}_0}\Big(\frac{1}{2}\delta\widetilde{\boldsymbol{\theta}}:(\mathbf{P}\mathbf{F}^T-\mathbf{F}\mathbf{P}^T)+\delta\hat{x}\cdot(\nabla\cdot\mathbf{P}+\hat{b}-\rho_0\ddot{\hat{x}})\Big)\mathrm{d}V+\int_{\partial\mathcal{B}_0}\delta\hat{x}\cdot(\hat{\mathrm{t}}_\sigma-\mathbf{P}\hat{N}_\sigma)\mathrm{d}A. \quad (3.141)$$

where it has been used the divergence theorem and $\hat{N}_\sigma$ is outward normal to the surface $\partial\mathcal{B}_0$ where traction forces are applied.
Comparing Eqs. (3.141) with (3.113a) to (3.113c) we found that the principle of virtual work of Eq. (3.139) satisfies the equations of motion for a kinematically admissible virtual displacement. The kinematically admissible virtual displacement field $\delta\hat{x}$ fulfills the essential boundary conditions by construction.

REMARK 3.4. It is worth to note that the term $\delta\overset{\triangledown}{[\mathbf{F}]}\colon\mathbf{P}$ also satisfies the balance equation of momentum $\mathbf{P}\mathbf{F}^T-\mathbf{F}\mathbf{P}^T$ but the term $\delta\mathbf{F}:\mathbf{P}$ does not [246] ■

REMARK 3.5. As it has been mentioned, the virtual work can be decomposed into three components: external, internal and inertial virtual works according to the following equation:

$$G=G_{\mathrm{ext}}+G_{\mathrm{int}}-G_{\mathrm{ine}}$$

where the minus sign indicate that the inertial forces act against the virtual displacements. Additionally, the inertial virtual work G_{ine} includes the minus sign inside its form. Sometimes it is convenient to avoid additional minus signs by introducing the virtual work of acceleration forces by the formula $G_{\mathrm{ine}}=-G_{\mathrm{acc}}$ ■

3.6.3 Reduced form virtual work principle

A dimensionally reduced version of the virtual work principle may also be obtained from the reduced linear and angular balance equilibrium equations [174, 198]. In this work an analogous procedure to these presented by Ibrahimbegović [178] will be used for the case of initially curved rods.

According to Eq. (3.27) taking an admissible variation of the position vector (consistent with the prescribed boundary conditions) in the current rod configuration $\delta\hat{x} = \delta\hat{\varphi} + \delta\hat{\theta} \times \hat{\mathscr{T}} \in T_{\hat{x}}\mathcal{B}_t$ *i.e.* a virtual displacement field, where $\delta\hat{\varphi} \in \mathbb{R}^3$ is an arbitrary but kinematically admissible variation of the translational field, $\delta\hat{\theta} = \delta\hat{\theta}_n \in T^{\text{spa}}_{\mathbf{\Lambda}}$ is an arbitrary but kinematically admissible rotation increment associated with the skew–symmetric tensor $\delta\widetilde{\boldsymbol{\theta}} = \delta\mathbf{\Lambda}_n\mathbf{\Lambda}_n^T \in T^{\text{spa}}_{\mathbf{\Lambda}}SO(3)$ thus, a virtual incremental rotation; taking the dot product of $\hat{\eta}^{\text{s}} = (\delta\hat{\varphi}, \delta\hat{\theta}) \in T\mathcal{C}_t \equiv \mathbb{R}^3 \times T^{\text{spa}}_{\mathbf{\Lambda}}$ with Eqs. (3.119) and (3.133) and integrating over the length of the curved reference rod we obtain the following contributions to the nonlinear functional corresponding to the *reduced virtual work principle*:

3.6.3.a Virtual work of external forces and moments

Considering the externally applied forces and moments we obtain the following expression for the virtual work of the external loading:

$$G_{\text{ext}}(\hat{\varphi}, \mathbf{\Lambda}, \hat{\eta}^{\text{s}}) = \int_0^L \left\langle \begin{bmatrix} \delta\hat{\varphi} \\ \delta\hat{\theta} \end{bmatrix}, \begin{bmatrix} \hat{\mathcal{N}}^* \\ \hat{\mathcal{M}}^* \end{bmatrix} \right\rangle_{\boldsymbol{g}} \mathrm{d}S = \int_0^L (\delta\hat{\varphi} \cdot \hat{\mathcal{N}}^* + \delta\hat{\theta} \cdot \hat{\mathcal{M}}^*)\mathrm{d}S. \tag{3.142}$$

It is worth noting that it has been carried out a separated integration for the translational part of the external work corresponding to the forces $\hat{\mathcal{N}}^* \in \mathbb{R}^{3*}$ and for the rotational part associated to the moments $\hat{\mathcal{M}}^* \in T^{\text{spa}*}_{\mathbf{\Lambda}}$ which is an element of the co–vector space of rotation and the work conjugated of the virtual incremental rotation vector $\delta\hat{\theta} \in T^{\text{spa}}_{\mathbf{\Lambda}}$.

3.6.3.b Virtual work of the internal forces and moments

The virtual work of the internal forces and moments can be computed in a similar way but taking the corresponding terms of Eqs. (3.119) and (3.133) as

$$\begin{aligned} G_{\text{int}}(\hat{\varphi}, \mathbf{\Lambda}, \hat{\eta}^{\text{s}}) &= \int_0^L \left\langle \begin{bmatrix} \delta\hat{\varphi} \\ \delta\hat{\theta} \end{bmatrix}, \begin{bmatrix} \hat{n}_{,S} \\ \hat{m}_{,S} + \hat{\varphi}_{,S} \times \hat{n} \end{bmatrix} \right\rangle_{\boldsymbol{g}} \mathrm{d}S \\ &= \int_0^L \Big[\delta\hat{\varphi} \cdot \hat{n}_{,S} + \delta\hat{\theta} \cdot \hat{m}_{,S} + \delta\hat{\theta} \cdot (\hat{\varphi}_{,S} \times \hat{n})\Big]\mathrm{d}S. \end{aligned} \tag{3.143}$$

3.6.3.c Virtual work of the inertial forces

The virtual work of the inertial forces can be computed in a similar way but taking the other terms of Eqs. (3.119) and (3.133) as

$$\begin{aligned} G_{\text{ine}}(\hat{\varphi}, \mathbf{\Lambda}, \hat{\eta}^{\text{s}}) &= \int_0^L \left\langle \begin{bmatrix} \delta\hat{\varphi} \\ \delta\hat{\theta} \end{bmatrix}, \begin{bmatrix} A_{\rho_0}\ddot{\hat{\varphi}} \\ \boldsymbol{\mathcal{I}}_{\rho_0}\hat{\alpha}_n + \widetilde{\boldsymbol{v}}_n\boldsymbol{\mathcal{I}}_{\rho_0}\hat{v}_n \end{bmatrix} \right\rangle_{\boldsymbol{g}} \mathrm{d}S \\ &= \int_0^L \Big[\delta\hat{\varphi} \cdot A_{\rho_0}\ddot{\hat{\varphi}} + \delta\hat{\theta} \cdot (\boldsymbol{\mathcal{I}}_{\rho_0}\hat{\alpha}_n + \widetilde{\boldsymbol{v}}_n\boldsymbol{\mathcal{I}}_{\rho_0}\hat{v}_n)\Big]\mathrm{d}S. \end{aligned} \tag{3.144}$$

Finally, the principle of virtual work for the Reissner–Simo rod's theory becomes

$$\begin{aligned} G(\hat{\varphi},\boldsymbol{\Lambda},\hat{\eta}^{\mathrm{s}}) &= [G_{\mathrm{int}}+G_{\mathrm{ine}}-G_{\mathrm{ext}}](\hat{\varphi},\boldsymbol{\Lambda},\hat{\eta}^{\mathrm{s}}) \\ &= \int_0^L \Big[\delta\hat{\varphi}\cdot\hat{n}_{,S}+\delta\hat{\theta}\cdot(\hat{m}_{,S}+\hat{\varphi}_{,S}\times\hat{n})\Big]\mathrm{d}S \\ &+ \int_0^L \Big[\delta\hat{\varphi}\cdot A_{\rho_0}\ddot{\hat{\varphi}}+\delta\hat{\theta}\cdot(\boldsymbol{\mathcal{I}}_{\rho_0}\hat{\alpha}_n+\widetilde{\boldsymbol{v}}_n\boldsymbol{\mathcal{I}}_{\rho_0}\hat{v}_n)\Big]\mathrm{d}S \\ &- \int_0^L (\delta\hat{\varphi}\cdot\hat{\mathcal{N}}^*+\delta\hat{\theta}\cdot\hat{\mathcal{M}}^*)\mathrm{d}S=0. \end{aligned} \tag{3.145}$$

From the above equation, taking integration by parts for the $\hat{n}_{,S}$ and $\hat{m}_{,S}$ terms and noticing $\delta\hat{\theta}\cdot(\hat{\varphi}_{,S}\times\hat{n})=(\delta\hat{\theta}\times\hat{\varphi}_{,S})\cdot\hat{n}$, one may easily obtains that

$$\begin{aligned} G(\hat{\varphi},\boldsymbol{\Lambda},\hat{\eta}^{\mathrm{s}}) &= \int_0^L \Big[(\delta\hat{\varphi}_{,S}-\delta\hat{\theta}\times\hat{\varphi}_{,S})\cdot\hat{n}+\delta\hat{\theta}_{,S}\cdot\hat{m}\Big]\hat{d}S \\ &+ \int_0^L \Big[\delta\hat{\varphi}\cdot A_{\rho_0}\ddot{\hat{\varphi}}+\delta\hat{\theta}\cdot(\boldsymbol{\mathcal{I}}_{\rho_0}\hat{\alpha}_n+\widetilde{\boldsymbol{v}}_n\boldsymbol{\mathcal{I}}_{\rho_0}\hat{v}_n)\Big]\mathrm{d}S \\ &- (\delta\hat{\varphi}\cdot\hat{n})\Big|_0^L-(\delta\hat{\theta}\cdot\hat{m})\Big|_0^L-\int_0^L(\delta\hat{\varphi}\cdot\hat{\mathcal{N}}^*+\delta\hat{\Theta}\cdot\hat{\mathcal{M}}^*)\mathrm{d}S=0. \end{aligned} \tag{3.146}$$

By this way it is possible to rewrite the external virtual work including the *natural boundary conditions*: $(\delta\hat{\varphi}\cdot\hat{n})|_0^L+(\delta\hat{\theta}\cdot\hat{m})|_0^L$ and an alternative (weak [363]) form of contribution, which constitutes spatial version of the *variational form of reduced internal power* as given in Eq. (3.111) *i.e.*

$$G(\hat{\varphi},\boldsymbol{\Lambda},\hat{\eta}^{\mathrm{s}})^{\mathrm{s}}_{\mathrm{int}}=\int_0^L(\delta[\overset{\triangledown}{\hat{\gamma}_n}]\cdot\hat{n}+\delta[\overset{\triangledown}{\hat{\omega}_n}]\cdot\hat{m})\mathrm{d}S \tag{3.147}$$

where $\delta[\overset{\triangledown}{\bullet}]$ is the Lie variation (or co–rotated variation) as it is explained in §A.5.5 of Appendix A. A deeper presentation of the calculation of the variations of mathematical quantities involved in the linearization of the weak form of the virtual work principle will be given in Chapter 5, for the moment it is sufficient to indicate that

$$\delta[\overset{\triangledown}{\hat{\gamma}_n}]=\delta\hat{\varphi}_{,S}-\delta\hat{\theta}\times\hat{\varphi}_{,S}\,;\qquad \delta[\overset{\triangledown}{\hat{\omega}_n}]=\delta\hat{\theta}_{,S}=\delta\hat{\theta}_{n,S}$$

Considering that in virtue of the results presented in Section A.5 one have that $\delta\hat{\Gamma}_n=\boldsymbol{\Lambda}^T\delta[\overset{\triangledown}{\hat{\gamma}_n}]$ and $\delta\hat{\Omega}_n=\boldsymbol{\Lambda}^T\delta[\overset{\triangledown}{\hat{\omega}_n}]$, therefore, Eq. (3.147) is completely equivalent to its material form which is given by

$$G(\hat{\varphi},\boldsymbol{\Lambda},\hat{\eta}^{\mathrm{s}})^{\mathrm{m}}_{\mathrm{int}}=\int_0^L(\delta\hat{\mathcal{E}}_n\cdot\hat{n}^{\mathrm{m}}+\delta\hat{\Omega}_n\cdot\hat{m}^{\mathrm{m}})\mathrm{d}S. \tag{3.148}$$

A formal demonstration of the mentioned equivalence is left to Section 5.3. In the more general term, the power balance equation in its variational form becomes the virtual work equation while the internal power becomes the internal virtual work.

REMARK 3.6. The superscripts 's' and 'm' has been added to the internal virtual work of Eqs. (3.147) and (3.148) to indicate that the corresponding scalar quantity G_{int} is phrased in terms of spatial (correspondingly material) quantities, although it is well known that a scalar by itself is independent of the reference system ■

3.7 Constitutive relations

In most of the cases in finite deformation theories for rods, hyper-elastic, isotropic and homogeneous materials have been assumed (see *e.g.* [73, 87, 131, 182, 363]) and therefore, the reduced constitutive equations become very simple. Other authors have extended the constitutive relations to the nonlinear case performing an integration of the constitutive equations at material point level and then obtaining the corresponding stress resultant and stress couple by mean of a second integration loop on the cross sectional area. Most of those works have been focused on plasticity [107, 118, 151, 299, 313, 318].
In the case that cross sections are composed by several materials, some authors prefer to work with 1D constitutive laws for the normal component of the stress tensor maintaining the shear behavior linear (see *e.g.* [113, 117, 214]). This last approach normally imply the violation of the law of thermodynamics [36, 307] conducing to *spurious energy dissipation.*
In the present work, cross sections are considered as formed by an inhomogeneous distribution of composite materials, each of them having several simple material components. Each simple material have associated its own constitutive law and the behavior of the composite is obtained using the *mixing rule theory* [90]. However, in this section only a brief overview of elastic constitutive relations for stress resultant and stress couples is discussed.

3.7.1 Hyperelastic materials

An elastic material is said to be a *hyperelastic* or a *Green–elastic* material if a *strain energy function* per unit volume $W_{\rm str}$ exist and the FPK stress tensor $\mathbf{P}^0$ can also be defined [300] as

$$\mathbf{P} := \frac{\partial W_{\rm str}(\mathbf{F})}{\partial \mathbf{F}} \qquad \in \quad T_{\hat{x}}\mathcal{B}_t \otimes T_{\hat{X}_{00}}\mathcal{B}_{00} \tag{3.149}$$

where it has been assumed that the strain energy function is frame–indifferent under orthogonal transformation *i.e.* $\mathbf{F}^+ = \mathbf{\Lambda F}$ by obeying the identity:

$$W_{\rm str}(\mathbf{F}^+) = W_{\rm str}(\mathbf{\Lambda F}) = W_{\rm str}(\mathbf{F})$$

with $\mathbf{\Lambda} \in SO(3)$. This means that the strain energy function is invariant under rigid–body rotations. The Lie variation by $\mathbf{\Lambda}$, Eq. (A.95), of the energy function $W_{\rm str}(\mathbf{F})$ can be written using Eqs. (3.149) as

$$\delta[\overset{\triangledown}{W_{\rm str}}] = \frac{\partial W_{\rm str}(\mathbf{F})}{\partial \mathbf{F}} : \delta[\overset{\triangledown}{\mathbf{F}}] = \mathbf{P} : \delta[\overset{\triangledown}{\mathbf{F}}] \qquad \in \quad \mathbb{R} \tag{3.150}$$

that is equal to the virtual work of internal forces $G_{\rm int}$ of Eq. (3.139). We get the same result for $W_{\rm str}(\mathbf{\Lambda}^T\mathbf{F})$. Employing the Lie variation, pullback and push–forward operators (see §A.5) it is possible to express Eq. (3.150) as

$$\delta[\overset{\triangledown}{W_{\rm str}}] = \mathbf{P} : \big(\mathbf{\Lambda}\delta(\mathbf{\Lambda}^T\mathbf{F})\big) = (\mathbf{\Lambda}^T\mathbf{P}) : \delta(\mathbf{\Lambda}^T\mathbf{F}) = (\mathbf{\Lambda}^T\mathbf{P}) : \delta(\mathbf{\Lambda}^T\mathbf{F} - \mathbf{I}). \tag{3.151}$$

Therefore the Lie variation of the strain energy function, Eq. (3.150), introduces the material strain and stress tensors defined by

$$\mathbf{\Sigma} := \mathbf{\Lambda}^T\mathbf{P} \qquad \in \quad T^*_{\hat{X}}\mathcal{B}_{00} \otimes T_{\hat{X}}\mathcal{B}_{00} \tag{3.152a}$$

$$\mathbf{H} := \mathbf{\Lambda}^T\mathbf{F} - \mathbf{I} \quad \in \quad T_{\hat{X}}\mathcal{B}_{00} \otimes T^*_{\hat{X}}\mathcal{B}_{00} \tag{3.152b}$$

The material stress tensor $\mathbf{\Sigma} = \Sigma_{ij}\hat{E}_i^* \otimes \hat{E}_j$ can be identified with the material form of the FPK stress tensor as given in Eq. (3.88b) and its work conjugated $\mathbf{H} = H_{ij}\hat{E}_i \otimes \hat{E}_j^*$ can be identified with the material form of the strain measure $\boldsymbol{\mathcal{E}}$ given in Eq. (3.68b). Both $\mathbf{\Sigma}$ and $\mathbf{H}$ are nonsymmetric tensors and are not named in continuum mechanics.
Let us to consider the constitutive relation between the components of the stress tensor $\mathbf{\Sigma}$ and the components of $\mathbf{H}$ given by

$$\mathbf{\Sigma} = \boldsymbol{\mathcal{C}}^{\mathrm{me}} : \mathbf{H} \tag{3.153}$$

where the *elasticity tensor* $\boldsymbol{\mathcal{C}}^{\mathrm{me}} \in T^*_{\hat{X}}\mathcal{B}_{00} \otimes T_{\hat{X}}\mathcal{B}_{00} \otimes T^*_{\hat{X}}\mathcal{B}_{00} \otimes T^*_{\hat{X}}\mathcal{B}_{00}$ is a fourth order tensor. For the purpose of establish a linear constitutive relation for the strain and stress measures acting on the face of the current cross section (see Fig. 3.3) we introduce the following simple linear constitutive relations in component form:

$$\Sigma_{11} = \mathrm{E}H_{11}; \qquad \Sigma_{21} = \mathrm{G}H_{21}; \qquad \Sigma_{31} = \mathrm{G}H_{31} \tag{3.154}$$

where E denote the elastic modulus and G the shear modulus. The constitutive relations of Eq. (3.154) correspond to commonly named the engineering approach. We note that the vector $\hat{H}_{i1}\hat{E}_i$ corresponds to $\hat{\mathcal{E}}$ as given in Eq. (3.68b). Thus, we could to express the material stress vector $\mathbf{\Sigma}_{i1}\hat{E}_i^*$ as

$$\mathbf{\Sigma}_{i1}\hat{E}_i^* = (\mathrm{E}\hat{E}_1^* \otimes \hat{E}_1^* + \mathrm{G}\hat{E}_2^* \otimes \hat{E}_2^* + \mathrm{G}\hat{E}_3^* \otimes \hat{E}_3^*)\hat{\mathcal{E}}. \tag{3.155}$$

Comparing the preceding equation with Eq. (3.87) and the material stress tensor $\mathbf{\Sigma}$, Eq. (3.152a), we get the material form of the stress vector at the current cross section

$$\mathbf{\Sigma}_{i1}\hat{E}_i^* = \mathbf{\Lambda}^T\hat{P}_1 = \hat{P}_1^{\mathrm{m}}. \tag{3.156}$$

Now we can substitute the above equation into the formula of the stress resultant vector $\hat{n}^{\mathrm{m}}$, obtained materializing Eq. (3.95c), that yields after integrating over the cross section to the following result:

$$\hat{n}^{\mathrm{m}} = \int_{\mathcal{A}_{00}} \mathbf{\Sigma}_{i1}\hat{E}_i^* \mathrm{d}\mathcal{A}_{00} = (\mathrm{E}\mathcal{A}_{00}\hat{E}_1^* \otimes \hat{E}_1^* + \mathrm{G}\mathcal{A}_{00}\hat{E}_\beta^* \otimes \hat{E}_\beta^*)\hat{\mathcal{E}} \quad \in T^*_{\hat{X}}\mathcal{B}_{00}. \tag{3.157}$$

Similarly, we may derive the stress couple vector $\hat{m}^{\mathrm{m}}$, obtained materializing Eq. (3.97c), as

$$\begin{aligned}
\hat{m}^{\mathrm{m}} &= \int_{\mathcal{A}_{00}} \widetilde{\boldsymbol{\mathcal{E}}}[\mathrm{E}\hat{E}_1^* \otimes \hat{E}_1^* + \mathrm{G}\hat{E}_\beta^* \otimes \hat{E}_\beta^*](\hat{\Gamma} + \widetilde{\mathbf{\Omega}}\hat{\mathscr{E}})\mathrm{d}\mathcal{A}_{00} \\
&= \Big[\int_{\mathcal{A}_{00}} \widetilde{\boldsymbol{\mathcal{E}}}\boldsymbol{\mathcal{C}}^{\mathrm{me}}\mathrm{d}\mathcal{A}_{00}\Big]\hat{\Gamma} - \Big[\int_{\mathcal{A}_{00}} \widetilde{\boldsymbol{\mathcal{E}}}\boldsymbol{\mathcal{C}}^{\mathrm{me}}\widetilde{\boldsymbol{\mathcal{E}}}\mathrm{d}\mathcal{A}_{00}\Big]\hat{\Omega} \\
&= \Big[(\mathrm{G}(-1)^\beta \int_{\mathcal{A}_{00}} \xi_\beta \mathrm{d}\mathcal{A}_{00})\hat{E}_1^* \otimes \hat{E}_\alpha^* + (\mathrm{E}(-1)^\alpha \int_{\mathcal{A}_{00}} \xi_\alpha \mathrm{d}\mathcal{A}_{00})\hat{E}_\beta^* \otimes \hat{E}_1^*\Big]\hat{\Gamma} \\
&\quad + \Big[\mathrm{GI}_{\rho_{00}11}\hat{E}_1^* \otimes \hat{E}_1^* + \mathrm{EI}_{\rho_{00}\alpha\beta}\hat{E}_\alpha^* \otimes \hat{E}_\beta^*\Big]\hat{\Omega}.
\end{aligned} \tag{3.158}$$

In Eq. (3.158) the formula for the material form second moment of inertia $\mathbf{I}_{\rho_{00}}$ given in Eqs. (3.134) and (3.135) has been used.

3.7.2 General formulation for the linear elastic case

Due to the fact that the reference configuration is describe using Euclidean coordinates, it will be assumed that $\{\hat{E}_i\} \cong \{\hat{E}_i^*\}$ by simplicity in the notation. A general expression for the

linear elastic relation between the material form of the FPK stress vector, $\hat{P}_1^{\mathrm{m}}$ given in Eq. (3.88c), and its energetically conjugate strain vector, $\hat{\mathcal{E}}_n$ given Eq. (3.69), at any material point $(S, \xi_\beta) \in [0, L] \times \mathcal{A}(S)$ on the current rod cross section for a hyperelastic but not necessarily isotropic nor homogeneous material can be given by

$$P_i^{\mathrm{m}} = [\mathbf{P}^{\mathrm{m}} \hat{E}_1] \cdot \hat{E}_i = \hat{P}_1^{\mathrm{m}} \cdot \hat{E}_i = g_0^{-1} \boldsymbol{\mathcal{C}}_{ij}^{\mathrm{me}} \mathcal{E}_{nj}; \qquad \boldsymbol{\mathcal{C}}_{ij}^{\mathrm{me}} = \bar{\alpha} \boldsymbol{\mathcal{C}}_{ij}^{0\mathrm{me}}; \qquad \bar{\alpha} = \bar{\alpha}(S, \xi_\beta) \tag{3.159}$$

where $\boldsymbol{\mathcal{C}}_{ij}^{\mathrm{me}} = \boldsymbol{\mathcal{C}}_{ji}^{\mathrm{me}}$ are the general elasticity constants for a given material point and they can vary over the material point considered; $\boldsymbol{\mathcal{C}}_{ij}^{0\mathrm{me}} = \boldsymbol{\mathcal{C}}_{ji}^{0\mathrm{me}}$ are the arbitrarily chosen reference material constants and do not vary over different material points; $\bar{\alpha}$ is a scalar factor between $\boldsymbol{\mathcal{C}}_{ij}^{\mathrm{me}}$ and $\boldsymbol{\mathcal{C}}_{ij}^{0\mathrm{me}}$ depending on the material point.
Then, the linear constitutive relation for a given material point on the current rod cross section may be described in the material and spatial settings as

$$\hat{P}_1^{\mathrm{m}} = g_0^{-1} \boldsymbol{\mathcal{C}}^{\mathrm{me}} \hat{\mathcal{E}}_n, \quad \boldsymbol{\mathcal{C}}^{\mathrm{me}} = \mathrm{C}_{ij}^{\mathrm{me}} \hat{E}_i \otimes \hat{E}_j \tag{3.160a}$$

$$\hat{P}_1 = g_0^{-1} \boldsymbol{\mathcal{C}}^{\mathrm{se}} \hat{\epsilon}_n, \quad \boldsymbol{\mathcal{C}}^{\mathrm{se}} = \mathrm{C}_{ij}^{\mathrm{se}} \hat{t}_i \otimes \hat{t}_j, \tag{3.160b}$$

respectively.
Substituting Eq. (3.160b) into the formulae for the components N_i and M_i of the stress resultant $\hat{n}$ and stress couple $\hat{m}$ vectors in Eqs. (3.95a) to (3.97d) and using the formulae for the components $\hat{\epsilon}_n$ without the initial curvature correction term in Eq. (3.59), it is possible to obtain, following analogous procedures as those given in Eqs. (3.157) and (3.158), the *reduced linear constitutive relations* as

$$\hat{n} = \mathbf{C}_{nn}^{\mathrm{se}} \hat{\gamma}_n + \mathbf{C}_{nm}^{\mathrm{se}} \hat{\omega}_n \tag{3.161a}$$

$$\hat{m} = \mathbf{C}_{mn}^{\mathrm{se}} \hat{\gamma}_n + \mathbf{C}_{mm}^{\mathrm{se}} \hat{\omega}_n \tag{3.161b}$$

for the spatial description, and

$$\hat{n}^{\mathrm{m}} = \mathbf{C}_{nn}^{\mathrm{me}} \hat{\Gamma}_n + \mathbf{C}_{nm}^{\mathrm{me}} \hat{\Omega}_n \tag{3.161c}$$

$$\hat{m}^{\mathrm{m}} = \mathbf{C}_{mn}^{\mathrm{me}} \hat{\Gamma}_n + \mathbf{C}_{mm}^{\mathrm{me}} \hat{\Omega}_n \tag{3.161d}$$

for the material description (see Eqs. (3.100a) and (3.100b)); where

$$\mathbf{C}_{pq}^{\mathrm{se}} = [\mathrm{C}_{pq}^{\mathrm{me}}]_{ij} \hat{t}_i \otimes \hat{t}_j; \qquad \mathbf{C}_{pq}^{\mathrm{me}} = [\mathrm{C}_{pq}^{\mathrm{me}}]_{ij} \hat{E}_i \otimes \hat{E}_j; \qquad \mathbf{C}_{pq}^{\mathrm{se}} = \boldsymbol{\Lambda} \mathbf{C}_{pq}^{\mathrm{me}} \boldsymbol{\Lambda}^T \tag{3.162}$$

and the subscripts $p, q \in \{m, n\}$. Explicit expressions for the general coefficients of Eqs. (3.161c) and (3.161c) are given in Appendix B.
The simplest case of the cross sectional elasticity constants is obtained when the rod material is isotropic and homogeneous

$$P_1^{\mathrm{m}} = g_0^{-1} \mathrm{E} \mathcal{E}_{n1}; \qquad P_2^{\mathrm{m}} = g_0^{-1} \mathrm{G} \mathcal{E}_{n2}; \qquad P_3^{\mathrm{m}} = g_0^{-1} \mathrm{G} \mathcal{E}_{n3} \tag{3.163}$$

i.e. $\bar{\alpha} = 1$ and $\mathcal{C}^{\mathrm{me}}_{11} = \mathrm{E}$, $\mathcal{C}_{22} = \mathrm{C}_{33} = \mathrm{G}$, $\mathrm{C}^{\mathrm{m}}_{ij} = \delta_{ij}$ otherwise. Then, the cross section elasticity constants became

$$[\mathrm{C}^{\mathrm{se}}_{nn}]_{\hat{t}_i\otimes\hat{t}_j} = [\mathrm{C}^{\mathrm{me}}_{nn}]_{\hat{E}_i\otimes\hat{E}_j} = \begin{bmatrix} \mathrm{E}\mathcal{A}_{00} & 0 & 0 \\ 0 & \mathrm{G}k_s\mathcal{A}_{00} & 0 \\ 0 & 0 & \mathrm{G}k_s\mathcal{A}_{00} \end{bmatrix} \tag{3.164a}$$

$$[\mathrm{C}^{\mathrm{se}}_{nm}]_{\hat{t}_i\otimes\hat{t}_j} = [\mathrm{C}^{\mathrm{me}}_{nm}]_{\hat{E}_i\otimes\hat{E}_j} = \begin{bmatrix} 0 & \mathrm{E}\bar{\mathcal{S}}_2 & -\mathrm{E}\bar{\mathcal{S}}_3 \\ -\mathrm{G}\bar{\mathcal{S}}_2 & 0 & 0 \\ \mathrm{G}\bar{\mathcal{S}}_3 & 0 & 0 \end{bmatrix} \tag{3.164b}$$

$$[\mathrm{C}^{\mathrm{se}}_{mm}]_{\hat{t}_i\otimes\hat{t}_j} = [\mathrm{C}^{\mathrm{me}}_{mm}]_{\hat{E}_i\otimes\hat{E}_j} = \begin{bmatrix} \mathrm{G}k_t\mathrm{I}_{11} & 0 & 0 \\ 0 & \mathrm{EI}_{22} & -\mathrm{EI}_{23} \\ 0 & -\mathrm{EI}_{32} & \mathrm{EI}_{33} \end{bmatrix} \tag{3.164c}$$

$$[\mathrm{C}^{\mathrm{se}}_{mn}]_{\hat{t}_i\otimes\hat{t}_j} = [\mathrm{C}^{\mathrm{me}}_{mn}]_{\hat{E}_i\otimes\hat{E}_j} = \begin{bmatrix} 0 & -\mathrm{G}\bar{\mathcal{S}}_2 & \mathrm{G}\bar{\mathcal{S}}_3 \\ \mathrm{E}\bar{\mathcal{S}}_2 & 0 & 0 \\ -\mathrm{E}\bar{\mathcal{S}}_3 & 0 & 0 \end{bmatrix} \tag{3.164d}$$

where

$$\mathcal{A}_{00} = \int_{\mathcal{A}_{00}} g_0^{-1}\mathrm{d}\mathcal{A}_{00} \qquad \bar{\mathcal{S}}_2 = \int_{\mathcal{A}} g_0^{-1}\xi_3 d\xi_2 d\xi_3; \qquad \bar{\mathcal{S}}_3 = \int_{\mathcal{A}} g_0^{-1}\xi_2 d\xi_2 d\xi_3$$

$$\bar{\mathcal{I}}_{22} = \int_{\mathcal{A}} g_0^{-1}(\xi_3)^2 d\xi_2 d\xi_3; \quad \bar{\mathcal{I}}_{33} = \int_{\mathcal{A}} g_0^{-1}(\xi_2)^2 d\xi_2 d\xi_3; \quad \bar{\mathcal{I}}_{23} = \int_{\mathcal{A}} g_0^{-1}\xi_2\xi_3 d\xi_2 d\xi_3$$

$$\bar{\mathcal{I}}_{11} = \bar{\mathcal{I}}_{22} + \bar{\mathcal{I}}_{33}; \qquad \bar{\mathcal{I}}_{23} = \bar{\mathcal{I}}_{32};$$

and k_s and k_t are the correction factors for shearing and torsion, respectively.
For slender curved rods or straight rods, we may let $g_0 \approx 1$ [228]. If the rods are further assumed to be built of isotropic, homogeneous and linear elastic material, we may take the rod cross section geometry centroid line as the rod reference curve and align $\hat{t}_2$ and $\hat{t}_3$ to coincide with the cross section principal axes. Then, $\mathbf{C}_{nn}$ and $\mathbf{C}_{mm}$ become diagonal, and $\mathbf{C}_{nm}$ and $\mathbf{C}_{mn}$ vanish. This last simple constitutive form has been used in most of the reviewed works (see *e.g.* [174, 190, 180, 228, 362] and references therein).

3.8 External loads

The applied external loads can be very complex in practice, for example when interaction between structure and environment is considered, such as the forces derived from fluid–structure interaction for aircrafts or the effects of earthquakes on civil engineering structures (see *e.g.* [117]) among many others. The complexity in the form of external forces acting on a given structure enforces to develop simplified models for simulating the real phenomena.

3.8.1 Point loads and concentrated moments

Clearly if a point load is applied in a globally fixed direction, the conventional procedures apply [108]. Consequently, we will concentrate on *follower* loads *i.e.* loads which maintain the position relative to the rod configuration. In general, this type of loads can be defined as referred to the

local frame $\{\hat{t}\}_i$, therefore, an applied point load can be described by

$$\hat{\mathrm{P}}_f = \mathrm{P}_{fi}\hat{t}_i \tag{3.165}$$

the corresponding contribution to the external virtual work of Eq. (3.142) is

$$G_{\text{ext}} = \delta\hat{\varphi} \cdot (\mathrm{P}_{fi}\hat{t}_i) \tag{3.166}$$

where the contribution to the external virtual work is configuration dependent due to the fact that the components of the follower point load are given with respect to a movable frame.
By the other hand, applied moments about fixed axes, $\hat{\mathrm{M}}_f = \mathrm{M}_{fi}\hat{e}_i$, are *non-conservative* (for a demonstration se *e.g.* [108, 190]) *i.e.* the work done by a mechanical system due to the application of a concentrated moment is *path–dependent*. The corresponding contribution to G_{ext} is

$$G_{\text{ext}} = \delta\hat{\theta} \cdot (\mathrm{M}_{fi}\hat{e}_i) \tag{3.167}$$

As it will be shown in a next chapter the non-conservative nature of concentrated moments leads to a non-symmetric tangent stiffness in the linearized problem.

3.8.2 Distributed loads

Three types of distributed loads, in the form of load densities, are considered, following the proposition given by Kapania and Li [207, 208]:

(**I**) The applied load density is given per unit of unstressed arch–length of curved configuration referred to the spatially fixed frame $\{\hat{e}_i\}$. One manner to define the *self–weight* of the structure is employing this kind of loads, but it has the disadvantage that is difficult to define for cross sections composed with different materials.
Therefore, the differential force $\mathrm{d}\hat{f}_g$ and moment $\mathrm{d}\hat{m}_g$, exerted on the differential element $\mathrm{d}S$ are calculated as:

$$\mathrm{d}\hat{f}_g = \lambda\hat{\mathcal{N}}_g(S)\mathrm{d}S \tag{3.168a}$$
$$\mathrm{d}\hat{m}_g = \lambda\hat{\mathcal{M}}_g(S)\mathrm{d}S, \tag{3.168b}$$

respectively; where $\hat{\mathcal{N}}_g(S)$ and $\hat{\mathcal{M}}_g(S)$ are the corresponding densities and $\lambda \in \mathbb{R}$ is a proportional loading factor. This type of loading is deformation invariant and usually conservative [228, 108].

(**II**) The applied load density is given as a constant in space in the sense that the load acting on unit projection length $\mathrm{d}s_d$ of the deformed arch–length ds corresponding to the undeformed arch–length $\mathrm{d}S$ at a material point S on the mid-curve onto any plane with normal $\hat{\mathrm{d}}_N = \hat{\mathcal{N}}_d/\|\hat{\mathcal{N}}_d\| \in \mathbb{R}^3$ is constant, given by

$$\mathrm{d}\hat{f}_d = \int_0^\lambda \hat{\mathcal{N}}_d \mathrm{d}s_d \mathrm{d}\lambda \tag{3.169}$$

where $\hat{\mathcal{N}}_d$ is constant with respect to both space and the rod itself; however, $\mathrm{d}s_d$ depends on the deformation and motion of the rod. $\mathrm{d}s_d$ relates the deformation and undeformed arch–length element $\mathrm{d}S$ as well as the direction of $\hat{\mathcal{N}}_d$ by

$$\mathrm{d}s_d = [(\hat{\mathrm{d}}_N \times \hat{\varphi}_{,s}) \times \hat{\mathrm{d}}_N] \cdot \hat{\varphi}_{,S}\,\mathrm{d}S = -[\widetilde{\mathbf{d}}_N^2\hat{\varphi}_{,s}] \cdot \hat{\varphi}_{,S}\,\mathrm{d}S.$$

Assuming that extension or elongation of the rod mid–curve is small and can be ignored, *i.e.* $\mathrm{d}s_d = \mathrm{d}S$, the above equation for $\mathrm{d}s_d$ can be simplified as

$$\mathrm{d}s_d = -[\widetilde{\mathbf{d}}_N^2 \hat{\varphi}_{,S}\,] \cdot \hat{\varphi}_{,S}\,\mathrm{d}S. \tag{3.170}$$

Therefore, Eq. (3.170) can be rewritten as [228]

$$\mathrm{d}\hat{f}_d = \hat{\mathcal{N}}_d \int_0^\lambda (-[\widetilde{\mathbf{d}}_N^2 \hat{\varphi}_{,S}\,] \cdot \hat{\varphi}_{,S}\,)\mathrm{d}\lambda\mathrm{d}S = \lambda c_N \hat{\mathcal{N}}_d \mathrm{d}S \tag{3.171}$$

where

$$c_N = -\frac{1}{\lambda}\int_0^\lambda [\widetilde{\mathbf{d}}_N^2 \hat{\varphi}_{,S}\,] \cdot \hat{\varphi}_{,S}\,\mathrm{d}\lambda.$$

Similarly, we may define the differential moment $\mathrm{d}\hat{m}_d$, exerted on the arc–element $\mathrm{d}S$ of the rod mid–curve, as

$$\mathrm{d}\hat{m}_d = \lambda c_M \hat{\mathcal{M}}_d \mathrm{d}S \tag{3.172}$$

where

$$\begin{aligned} \hat{\mathrm{d}}_M &= \hat{\mathcal{M}}_d / \|\hat{\mathcal{M}}_d\| \in \mathbb{R}^3 \\ c_M &= -\frac{1}{\lambda}\int_0^\lambda [\widetilde{\mathbf{d}}_M^2 \hat{\varphi}_{,S}\,] \cdot \hat{\varphi}_{,S}\,\mathrm{d}\lambda. \end{aligned}$$

Note that both $\mathrm{d}\hat{f}_d$ and $\mathrm{d}\hat{m}_d$ are dependent on deformation. The force density $\mathcal{N}_d$ may be a good approximation for loads acting on a uniform rod when loading process is addressed and the load itself can cause relatively large displacements/rotations. Therefore, this kind of loading can be non conservative.

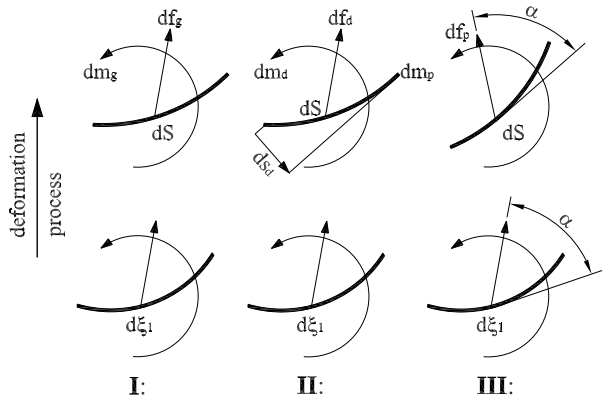

Figure 3.8: Different types of distributed applied loadings.

(**III**) The applied load density is given per unit unstressed arch–length of the rod mid–curve referred to the moving frame $\{\hat{t}_i\}$ invariant with respect to the deformation of the rod. Pressure and other *follower* loads belongs to this type if both the shear deformation and cross section variation along the rod axis are small and can be ignored.
The differential force $\mathrm{d}\hat{f}_p$, and moment, $\mathrm{d}\hat{m}_p$, exerted on the arch–length $\mathrm{d}S$ are calculated

as follows:

$$\mathrm{d}\hat{f}_p = \lambda\hat{\mathcal{N}}_p\mathrm{d}S = \lambda\mathbf{\Lambda}\hat{\bar{\mathcal{N}}}_p\mathrm{d}S \tag{3.173a}$$

$$\mathrm{d}\hat{m}_p = \lambda\hat{\mathcal{M}}_p\mathrm{d}S = \lambda\mathbf{\Lambda}\hat{\bar{\mathcal{M}}}_p\mathrm{d}S \tag{3.173b}$$

where $\hat{\bar{\mathcal{N}}}_p = \hat{\bar{\mathcal{N}}}_{pj}\hat{e}_j$ and $\hat{\bar{\mathcal{M}}}_p = \hat{\bar{\mathcal{M}}}_{pj}\hat{e}_j$ are given in the material form. This type of loads depends on the rotational displacements and, therefore, is non-conservative. In Fig. 3.8 are show the three types of applied distributed loads. Now it is possible to define

$$\hat{\mathcal{N}}_{\mathrm{dist}} = \lambda\big[\hat{\mathcal{N}}_g + c_N\hat{\mathcal{N}}_d + \hat{\mathcal{N}}_p\big] \tag{3.174a}$$

$$\hat{\mathcal{M}}_{\mathrm{dist}} = \lambda\big[\hat{\mathcal{M}}_g + c_M\hat{\mathcal{M}}_d + \hat{\mathcal{M}}_p\big] \tag{3.174b}$$

as the force density and the moment density along the rod mid–curve at current loading respectively.

Table 3.2 summarize the different types of loading. Note that all the components of the applied load densities are constant for given S in load types **I** and **III** and s_d in type **II**.

Table 3.2: Applied external load densities.

Load type	Force Density	Moment Density
I	$\hat{\mathcal{N}}_g(S) = \mathcal{N}_{gj}(S)\hat{e}_j$	$\hat{\mathcal{M}}_g(S) = \mathcal{M}_{gj}(S)\hat{e}_j$
II	$\hat{\mathcal{N}}_d(s_d) = \mathcal{N}_{dj}(s_d)\hat{e}_j$	$\hat{\mathcal{M}}_d(s_d) = \mathcal{M}_{dj}(s_d)\hat{e}_j$
III	$\hat{\mathcal{N}}_p(S) = \bar{\mathcal{N}}_{pj}(S)\hat{t}_j$	$\hat{\mathcal{M}}_p(S) = \bar{\mathcal{M}}_{pj}(S)\hat{t}_j$

3.8.3 Body loads

In Section 3.6 it has been written the balance law Eqs. (3.119) and (3.133), which include the external loads due to a body forces per unit of volume $\hat{b}$ in the terms $\hat{\mathcal{N}}$ and $\hat{\mathcal{M}}$. The evaluation of these external body forces at element level require the numerical integration of the following integrals

$$\hat{\mathcal{N}}_{\mathrm{bd}} = \int_0^L\int_{\mathcal{A}_0} g_0\big(\rho_0\hat{b}\big)(S,\xi_\beta)\mathrm{d}V_0 \qquad \in \quad T^*_{\hat{x}_0}\mathcal{B}_t \tag{3.175}$$

$$\hat{\mathcal{M}}_{\mathrm{bd}} = \int_0^L\int_{\mathcal{A}_0} \widetilde{\boldsymbol{\mathcal{F}}}\, g_0\rho_0\hat{b}(S,\xi_\beta)\mathrm{d}V_0 \qquad \in \quad T^*_{\hat{x}_0}\mathcal{B}_t \tag{3.176}$$

in analogous manner as explained in §3.6 if the mass centroid of the cross section is chosen as the reference curve for the rod, the term $\mathcal{M}_{\mathrm{bd}}$ in Eq. (3.176) vanish.

3.8.4 Seismic loading

If the structure is subjected to the base acceleration corresponding to a seismic input, the acceleration of each material point can be written as the sum of the acceleration of the material point with reference to the fixed inertial frame $\{\hat{E}_i\}$, Eq. (3.32a) or (3.31b), and the acceleration of the inertial frame itself. It worth to note that usually in earthquake engineering seismic inputs

are considered as a record of three base accelerations acting in three independent directions and, therefore, any rotational acceleration of the inertial frame itself have to be considered in the calculations. The resulting expression for the acceleration of the material point (S, ξ_β) in the spatial description is given by

$$\ddot{\hat{x}} = \ddot{\hat{\varphi}} + \ddot{\hat{a}} + \left[\widetilde{\alpha} + \widetilde{\boldsymbol{v}}\widetilde{\boldsymbol{v}}\right]\hat{\mathscr{T}} \quad \in \quad T_{\hat{x}}\mathcal{B}_t \tag{3.177}$$

where the vector $\ddot{\hat{a}}$ corresponds to the translational acceleration of the fixed reference frame $\{\hat{E}_i\}$ (see Fig. 3.9).

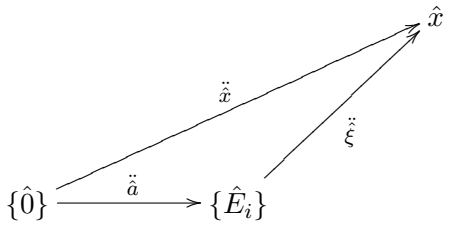

Figure 3.9: Seismic acceleration of the material point (S, ξ_β).

In this case Eqs. (3.119) and (3.119) are rewritten to consider the additional acceleration term $\ddot{\hat{a}}$ as

$$\hat{n}_{,S} + \hat{\mathcal{N}} = \mathcal{A}_{\rho_0}(\ddot{\hat{\varphi}} + \ddot{\hat{a}}) + \underbrace{\widetilde{\boldsymbol{\alpha}}_n\hat{\mathcal{S}}_{\rho_0} + \widetilde{\boldsymbol{v}}_n\widetilde{\boldsymbol{v}}_n\hat{\mathcal{S}}_{\rho_0}}_{\hat{A}_1} \tag{3.178}$$

$$\hat{m}_{,S} + \hat{\varphi}_{,S} \times \hat{n} + \hat{\mathcal{M}} = \underbrace{\hat{\mathcal{S}}_{\rho_0} \times (\ddot{\hat{\varphi}} + \ddot{\hat{a}})}_{\hat{A}_2} + \boldsymbol{\mathcal{I}}_{\rho_0}\hat{\alpha}_n + \widetilde{\boldsymbol{v}}_n\boldsymbol{\mathcal{I}}_{\rho_0}\hat{v}_n \tag{3.179}$$

As it has been said the terms $\hat{A}_1$ and $\hat{A}_2$ can be neglected if the reference curve of the rod coincide with the mass centroid or if the eccentricity between the mechanical center of the section and the mass centroid is small. In this case the seismic acceleration only affects to the linear momentum balance condition. The seismic acceleration vector $\ddot{\hat{a}}$ is independent of the material point and can be treated as an additional body force adding it to the term $\mathcal{N}$ on the right side of Eq. (3.178). Therefore, Eq. (3.175) can be employed to calculate the total body load acting on the rod.

Chapter 4

Constitutive nonlinearity

As it has been mentioned in previous sections, most of the works treating geometrically nonlinear rod theories have considered hyperelastic, isotropic and homogeneous material properties [131, 178, 362, 363] considering rather simple reduced constitutive equations. Normally, in engineering problems we are interested in knowing the behavior of the structures beyond the linear elastic case. Therefore, the assumption linearity of the constitutive relations may be in general not applicable in practical studies of engineering structures. Additionally, the viscous damping reduces the effects of the dynamic actions on structures, which has been considered, for example, in many seismic codes. Therefore, realistic studies focused on the simulation of the nonlinear dynamics of beam structures should consider inelastic rate dependent constitutive relations as well as geometric effects.

This chapter is focused on the treatment given in this work to constitutive nonlinearity. To this end, material points on the cross sections are considered as formed by a *composite material* corresponding to a homogeneous mixture of different *components*, each of them with its own constitutive law. The composite behavior is obtained by means of the *mixing theory* for composite materials. A schematic representation of these ideas is shown in Fig. 4.1 where a typical transversal cut throughout a cross section of a rod in the current configuration shows a material point that has associated a composite which is divided in a set of simple materials represented schematically in the zoom view by different zones hatched with points, lines, etc. The mechanical response of the composite is obtained supposing a rheological model where all the components work in parallel.

Two types of nonlinear constitutive models for simple materials are used in this work, corresponding to the *damage* and the *plasticity* models, both of then formulated in the rate independent and rate dependent forms and in a manner that is consistent with the laws of the thermodynamics for adiabatic processes [237, 236]. They have been chosen due to the fact that combining different parameters of the models a wide variety of mechanical behaviors can be reproduced, *e.g.* concrete, fiber reinforced composites and metals among others [160, 36, 309].

This chapter is organized starting with the formulation of the rate independent models for components; rate dependent behavior and viscosity is then included by means of a Maxwell model [307]. The mixing rule for composites is then introduced along with a continuum version of the cross sectional analysis.

Considering that the components of any spatial vector or tensor in the local frame $\{\hat{t}_i\}$ are the same as those of their corresponding material forms described in the material frame $\{\hat{E}_i\}$, in this section the constitutive models are formulated in terms of the material form of the FPK stress vector, $\hat{P}_1^{\mathrm{m}}$, and the strain and strain rate measures $\hat{\mathcal{E}}_n$ and $\hat{S}_n$, respectively.

We start assuming that each component of the composite associated to a material point is

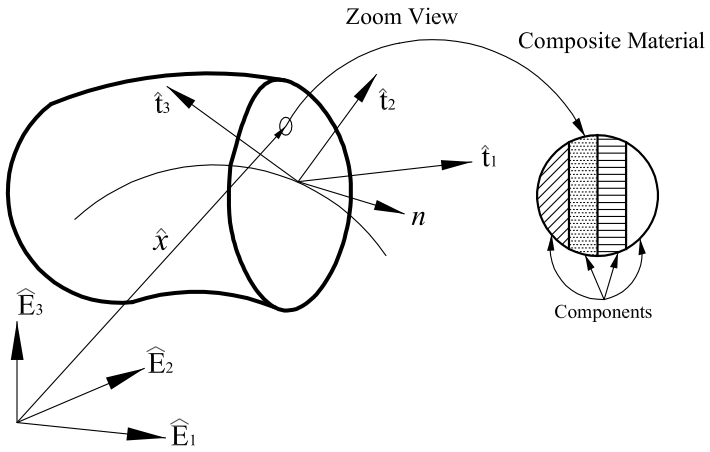

Figure 4.1: Each material point on the rod has associated a composite composed by a finite amount of simple materials.

described by means of a nonlinear strain-stress relation; by the moment this relation can be considered rate independent. Considering Eqs. (3.88a) to (3.88f) for the material form of the FPK stress vector referred to a differential volume of the curved reference rod, we can suppose a relation of the form

$$\hat{P}_1^{\mathrm{m}} = \hat{P}_1^{\mathrm{m}}(g_0^{-1}\hat{\mathcal{E}}_n). \tag{4.1}$$

It is also possible to assume that there exist a linearized relation between linear increments of the material forms of $\hat{P}_1^{\mathrm{m}}$ and $\hat{\mathcal{E}}_n$, given by the *tangential constitutive tensor* in material description $\boldsymbol{\mathcal{C}}^{\mathrm{mt}}$, as

$$\delta\hat{P}_1^{\mathrm{m}} = g_0^{-1}\boldsymbol{\mathcal{C}}^{\mathrm{mt}}\delta\hat{\mathcal{E}}_n; \qquad \boldsymbol{\mathcal{C}}_{ij}^{\mathrm{mt}} = g_0(\hat{P}_{1i}^{\mathrm{m}})_{,\hat{\mathcal{E}}_{nj}} \tag{4.2}$$

where the spatial form of the tangential constitutive tensor is obtained as $\boldsymbol{\mathcal{C}}^{\mathrm{st}} = \boldsymbol{\Lambda}\boldsymbol{\mathcal{C}}^{\mathrm{mt}}\boldsymbol{\Lambda}^T$. Explicit expressions for Eqs. (4.1) and (4.2) depend on the constitutive formulation assigned to the material considered. Additionally, taking into account the relation between material and co-rotated linear increments by means of employing the push–forward operation by the rotation tensor $\boldsymbol{\Lambda}$ we have that

$$\delta[\overset{\triangledown}{\hat{P}_1}] = \boldsymbol{\Lambda}\delta\hat{P}_1^{\mathrm{m}} = \boldsymbol{\Lambda}\big[g_0^{-1}\boldsymbol{\mathcal{C}}^{\mathrm{mt}}\delta\hat{\mathcal{E}}_n\big] = g_0^{-1}\boldsymbol{\mathcal{C}}^{\mathrm{st}}\delta[\overset{\triangledown}{\hat{\epsilon}_n}]\ . \tag{4.3}$$

However, attention should be paid that the stress vector must be determined according to the specific constitutive laws described in Eq. (4.1) for the general case.

4.1 Softening materials and strain localization

As noted by Armero and Ehrlich [25, 24] the failure of framed structures is normally determined by the localization of the degradation of the mechanical properties of the materials in critical cross sections. This process usually occurs when materials presenting softening are associated to the points on the cross section. Therefore, the *strain localization* phenomenon can occur on specific zones of the rod for certain loading levels [303]. Some authors have confined the dissipative zone to the existence of a band with defining a characteristic length of the material, which is called the *size effect* appearing in softening zones before the failure [51, 52] and have given correlations with complex redistribution of forces and moments in redundant structures. In any

case, softening behavior of points on the cross section implies the induction of a softer response at cross sectional level and, in this manner, the strain localization induced at material point level is translated to the cross sectional force-displacement and moment-curvature relationships leading to the classical concept of the formation of *plastic hinges* (see *e.g.* [97, 109, 117, 214] among many others).
Several approaches has been developed to treat the failure in framed structures, which cover from the theoretical studies to more practical engineering applications. By one hand, some classical techniques in structural analysis such as the limits analysis do not consider a softening response on the hinges after the yielding threshold of the cross section has been reached [239]. By the other hand, the inelastic analysis of rod structures in softening regime has been developed considering concentrated and distributed models (see §2 for a more complete survey about this topic).

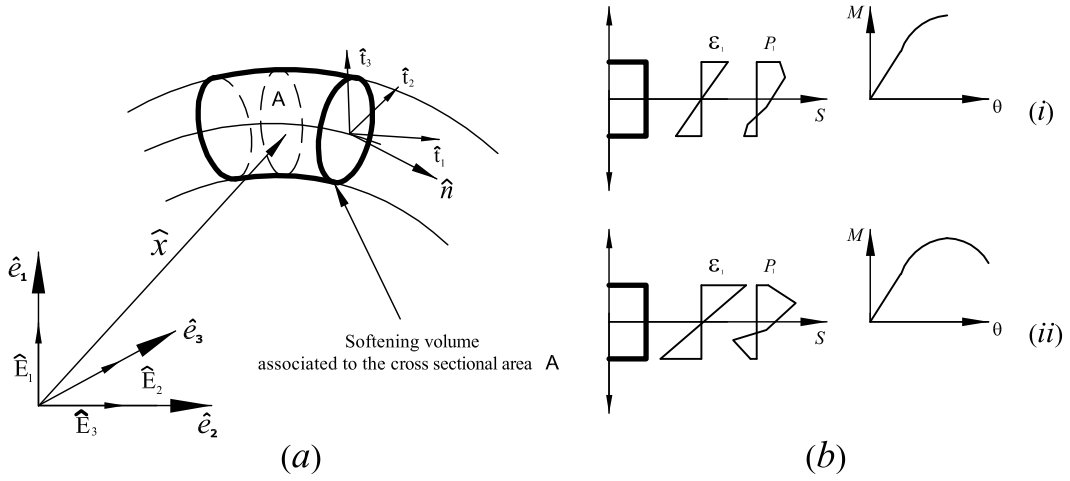

Figure 4.2: Softening volume in the rod element.

In this work, cross sectional degradation with softening is modeled considering that a specific length of the rod concentrates the large localized strains (see Fig. 4.2*a*) and the force-displacement and/or moment-curvature relations are estimated throughout cross sectional integration of the stress field (see Eqs. (3.94a) and (3.94b)). In this sense, the present approach fall in the category of distributed models, where inelasticity can occurs elsewhere in a given element. A similar approach has been followed by several authors in recent works as for example, Bratina *et al.* [81] or Coleman and Spacone [98] (and reference therein). Among the main advantages of this approach it is possible to mention:

(i) The definition of a finite length associated to the softening zone allows to simulate the distributed damage observed in some composite structures such as reinforced concrete in tension where numerous micro-cracks connect each with the others along a finite zone before the collapse of an element. In the case of compression a distributed damage zone appears before the shear band dominate the global response of the element [98].

(ii) The cross sectional force-displacement and/or moment-curvature relations are deduced *a posteriori* depending on the material distribution and their corresponding constitutive laws. In Fig. 4.2*b* a typical cross section associated to the volume of the beam where strain localization will have place has been depicted. The beam is subjected to a simple

flexural moment M. In the case (i) the stress distribution in the beam depth is irregular in the sense that it does not follows the same path as the strain according to the distribution of materials and their constitutive laws. On the right side it has been drawn the corresponding moment-curvature, $M-\theta$, relation. If M is increased, case (ii), the stress distribution changes and some points suffer a great degradation of their mechanical properties producing the softening branch in the corresponding $M-\theta$ diagram.

In general, the structural response becomes dependent on the mesh size and therefore, appropriated corrections has to be made. The *mesh independent response* of the structure is obtained regularizating the constitutive equations according to the energy dissipated in the corresponding softening volume, limiting this value to the specific fracture energy of the material [258]. Details about the regularization process can be consulted in [260, 307, 305]. Chapter 7 devoted to the finite element implementation of the present formulation allows to identify the mentioned specific length with the characteristic length associated to an integration point on a finite element. Some criticisms can be made to the present approach in what regards to treatment given to the softening response of rod structures, *e.g.* the fact that even in the case that the characteristic length of the materials exists (intrinsically, as a material property), this length should be largely smaller that the scales considered in the meshes [25]. However, among the above described capabilities, the present approach has been considered due to its versatility to be included in a standard finite element code for beam elements. Other alternative procedures based on considering the *strong discontinuity approach*[1] on the generalized displacement field of the beam can be consulted in [25, 24, 26]. In that case, the proposed approach leads to the regularization of the mathematical problem and to an solution with physical significance. However, at the author knowledge at the moment these results do not have been extended to cover some important characteristics of the mechanical behavior of the structures such as those described in (i) and (ii).

4.2 Constitutive laws simple materials

This section presents thermodynamically consistent formulations for the rate independent and rate dependent versions of the damage and plasticity models which allow their inclusion in the present geometrically exact rod model.

4.2.1 Degrading materials: damage model

The model here presented corresponds to an adaptation of the isotropic damage model proposed by Oliver *et al.* [301] and based on the early ideas of Kachanov [205]; in a way that it is consistent with the kinematic assumptions of the rod (see §3). The behavior of most of the degrading materials is presented attending to the fact that micro-fissuration in geomaterials occurs due to the lack of cohesion between the particles, among other processes. Different micro-fissures connect each with others generating a distributed damage zone in the material. After a certain loading level is reached a *fractured zone* is clearly defined[2] [159, 205]. In the 3D case, the directions of the dominating fissures are identified from the trajectories of the damaging points. Considering a *representative volume*[3] $\mathcal{B} \in \mathbb{R}^3$ of material in the reference configuration and an

[1] For a detailed treatment of this topics, consult [18, 303, 302] and references therein.

[2] In this sense, the fractured zone is composed by the geometric place of all completely damaged points.

[3] A volume big enough to contain a large number of defects but small enough to be considered representative of the behavior of a material point.

arbitrary cut with normal $\hat{k}$, as it has been shown in Fig. 4.4, the undamaged area is S_n and $\bar{S}_n$ is the effective area obtained subtracting the area of the defects from S_n. Therefore, the *damage variable* associated to this surface is

$$d_n = \frac{S_n - \bar{S}_n}{S_n} = 1 - \frac{\bar{S}_n}{S_n} \quad \in [0,1] \tag{4.4}$$

which measures the degradation level and is equal to zero before loading. When damage increases, the resisting area (also called effective) $\bar{S}_n \to 0$, which implies that $d_n \to 1$.

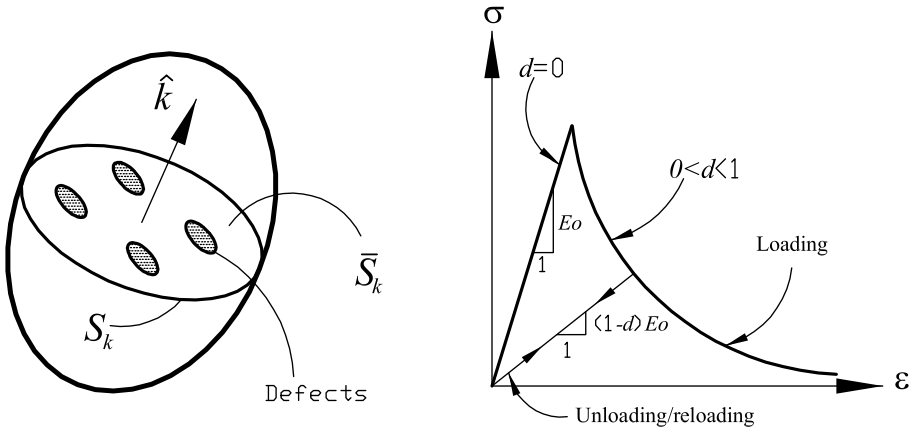

Figure 4.3: Schematic representation of the damage model.

The material form of the effective stress vector $\hat{\bar{P}}_1^{\mathrm{m}}$ is constructed from the material description of the FPK stress vector $\hat{P}_1^{\mathrm{m}}$ starting from the fact that the material form of the force $\hat{F}_k$ acting in the section S_n, can be written as [159]

$$\hat{F}_k = \hat{P}_1^{\mathrm{m}} S_n = \hat{\bar{P}}_1^{\mathrm{m}} \bar{S}_n \tag{4.5}$$

and considering Eq. (4.4) we have that

$$\hat{P}_1^{\mathrm{m}} = (1-d)\hat{\bar{P}}_1^{\mathrm{m}} = (1-d)\boldsymbol{\mathcal{C}}^{\mathrm{me}}\hat{\mathcal{E}}_n. \tag{4.6}$$

While damage is increasing, the effective area resists the external loads and, therefore, $\hat{\bar{P}}_1^{\mathrm{m}}$ is a quantity more representative of the physical phenomenon. Eq. (4.6) show that the material form of the FPK stress vector is obtained from its linear elastic counterpart (undamaged) $\boldsymbol{\mathcal{C}}^{\mathrm{me}}\hat{\mathcal{E}}_n$ by means of multiplying by degrading factor $(1-d)$. In this kind of models degradation is introduced by means of the internal state variable $d \in [0,1]$, called the *damage*, which measure the lack of secant stiffness of the material as it can be seen in Fig. 4.4.

In this work, a damage model consistent with the kinematic assumption of the rod theory and based on the 3D formulation presented by Oliver *et al.* [301] is developed. The model has only one internal variable (isotropic) employed for simulating the mechanical degradation of the material. The concept of *isotropic damage* is used to denote models that consider only one scalar damage parameter which affects to all the components of the elastic constitutive stress tensor avoiding to differentiate between preferential directions in space [159]. This model is based on the earlier ideas of Kachanov (1958) [205] and it presents a good equilibrium between the required complexity for modeling the behavior of softening materials and versatility for being used in large numerical simulations. In this case, fissuration is interpreted as a local effect

defined by means of the evolution of a set material parameters and functions which control the beginning and evolution of the damage [301].
One advantage of this kind of model is that it avoids the formulation in terms of *directional damage* and the fissuration paths are identified *a posteriori* from the damaged zones. The simple idea above explained allows to employ the damage theory for describing the mechanical behavior of even more complex degrading materials if a special damage function, which considers a differentiated material response for tension or compression, is included in the formulation of the model [159, 364].

4.2.1.a Secant constitutive equation and mechanical dissipation

In the case of thermally stable problems, with no temperature variation, the model has associated the following expression for the free energy density Ψ in terms of the material form of the elastic free energy density Ψ_0 and the damage internal variable d [250]:

$$\Psi(\hat{\mathcal{E}}_n, d) = (1-d)\Psi_0 = (1-d)(\frac{1}{2\rho_0}\hat{\mathcal{E}}_n \cdot (\boldsymbol{\mathcal{C}}^{\mathrm{me}}\hat{\mathcal{E}}_n)) \tag{4.7}$$

where $\hat{\mathcal{E}}_n$ is the material form of the strain vector, ρ_0 is the mass density in the curved reference configuration and $\boldsymbol{\mathcal{C}}^{\mathrm{me}} = \mathrm{Diag}[\mathrm{E}, \mathrm{G}, \mathrm{G}]$ is the material form of the *elastic constitutive tensor*, with E and G the Young and shear undamaged elastic modulus.
In this case, considering that the *Clausius Planck* (CP) inequality for the *mechanical dissipation* is valid, its local form [237, 250] can be written as

$$\begin{aligned} \dot{\Xi}_m &= \frac{1}{\rho_0}\hat{P}_1^{\mathrm{m}} \cdot \dot{\hat{\mathcal{E}}}_n - \dot{\Psi} \geq 0 \\ &= (\frac{1}{\rho_0}\hat{P}_1^{\mathrm{m}} - \frac{\partial \Psi}{\partial \hat{\mathcal{E}}_n}) \cdot \dot{\hat{\mathcal{E}}}_n - \frac{\partial \Psi}{\partial d}\dot{d} \geq 0 \end{aligned} \tag{4.8}$$

where $\dot{\Xi}_m$ is the dissipation rate.
For the unconditional fulfilment of the CP inequality and applying the Coleman's principle, we have that the arbitrary temporal variation of the free variable $\dot{\hat{\mathcal{E}}}_n$ must be null [237]. In this manner, the following constitutive relation for the material form of the FPK stress vector acting on each material point of the beam cross section is obtained:

$$\hat{P}_1^{\mathrm{m}} = (1-d)\boldsymbol{\mathcal{C}}^{\mathrm{me}}\hat{\mathcal{E}}_n = \boldsymbol{\mathcal{C}}^{\mathrm{ms}}\hat{\mathcal{E}}_n = (1-d)\hat{P}_{01}^{\mathrm{m}} \tag{4.9}$$

where $\boldsymbol{\mathcal{C}}^{\mathrm{ms}} = (1-d)\boldsymbol{\mathcal{C}}^{\mathrm{me}}$ and $\hat{P}_{01}^{\mathrm{m}} = \boldsymbol{\mathcal{C}}^{\mathrm{me}}\hat{\mathcal{E}}_n$ are the material form of the *secant constitutive tensor* and the *elastic* FPK stress vector, respectively.
Inserting the result of Eq. (4.9) into (4.8) the following expression is obtained for the dissipation rate

$$\dot{\Xi}_m = -\frac{\partial \Psi}{\partial d}\dot{d} = \Psi_0 \dot{d} \geq 0. \tag{4.10}$$

Eq. (4.9) shows that the FPK stress vector is obtained from its elastic (undamaged) counterpart by multiplying it by the degrading factor $(1-d)$. The internal state variable $d \in [0, 1]$ measures the lack of secant stiffness of the material as it can be seen in Fig. 4.4. Moreover, Eq. (4.10) shows that the temporal evolution of the damage $\dot{d}$ is always positive due to the fact that $\Psi_0 \geq 0$.

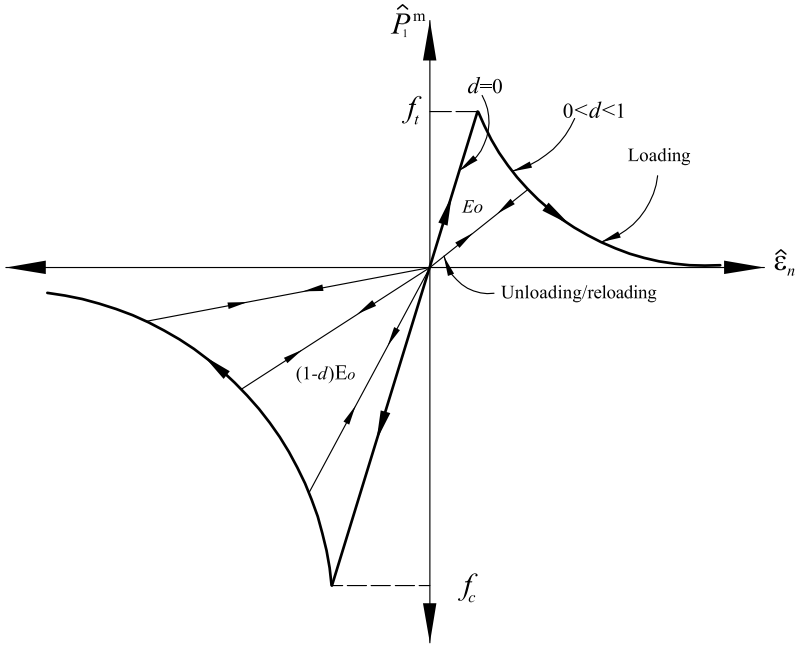

Figure 4.4: Differentiated traction compression behavior and evolution of the internal variable.

4.2.1.b Damage yield criterion

By analogy with the developments presented in [36, 160, 309], the damage yield criterion denoted by the scalar value $\mathcal{F}$ is defined as a function of the undamaged elastic free energy density and written in terms of the components of the material form of the undamaged principal stresses, $\hat{P}^{\mathrm{m}}_{p0}$, as

$$\mathcal{F} = \mathcal{P} - f_c = [1 + r(n-1)]\sqrt{\sum_{i=1}^{3}(P^{\mathrm{m}}_{p0i})^2} - f_c \leq 0 \tag{4.11a}$$

where $\mathcal{P}$ is the equivalent (scalar) stress and the parameters r and n given in function of the tension and compression strengths f_c and f_t, respectively; and the parts of the free energy density developed when the tension or compression limits are reached, $(\Psi^0_t)_L$ and $(\Psi^0_c)_L$, respectively. These quantities are defined as

$$(\Psi^0_{t,c})_L = \sum_{i=1}^{3}\frac{\langle \pm P^{\mathrm{m}}_{p0i}\rangle \mathcal{E}_{ni}}{2\rho_0}, \qquad \Psi^0_L = (\Psi^0_t)_L + (\Psi^0_c)_L \tag{4.11b}$$

$$f_t = (2\rho\Psi^0_t E_0)^{\frac{1}{2}}_L, \qquad f_c = (2\rho\Psi^0_c E_0)^{\frac{1}{2}}_L \tag{4.11c}$$

$$n = \frac{f_c}{f_t}, \qquad r = \frac{\sum_{i=1}^{3}\langle P^{\mathrm{m}}_{p0i}\rangle}{\sum_{i=1}^{3}|P^{\mathrm{m}}_{p0i}|} \tag{4.11d}$$

where $|u|$ is the absolute value function and $\langle \pm u\rangle = 1/2(|u| \pm u)$ is the McAuley's function defined $\forall\, u \in \mathbb{R}$.

REMARK 4.1. As it has been shown by Oliver *et al.* in [301], other kind of damage yield criteria can be used in substitution of $\mathcal{P}$ *e.g.* Mohr–Coulomb, Drucker–Prager, Von Mises etc, according to the mechanical behavior of the material (see also *e.g.* Hanganu *et al.* [160]) ■

A more general expression equivalent to that given in Eq. (4.11a) [36] is the following, which was originally proposed by Simo and Ju [364]:

$$\bar{\mathcal{F}} = \mathcal{G}(\mathcal{P}) - \mathcal{G}(f_c) \tag{4.12}$$

where $\mathcal{G}(\bullet)$ is a scalar monotonic function to be defined in such way to ensure that the energy dissipated by the material on an specific integration point is limited to the specific energy fracture of the material [301].

4.2.1.c Evolution of the damage variable

The evolution law for the internal damage variable d is given by

$$\dot{d} = \dot{\mu}\frac{\partial \bar{\mathcal{F}}}{\partial \mathcal{P}} = \dot{\mu}\frac{\partial \mathcal{G}}{\partial \mathcal{P}} \tag{4.13}$$

where $\dot{\mu} \geq 0$ is the *damage consistency* parameter. Additionally, a damage yield condition $\bar{\mathcal{F}} = 0$ and consistency condition $\dot{\bar{\mathcal{F}}} = 0$ are defined analogously as in plasticity theory [377]. By one hand, the yield condition implies that

$$\mathcal{P} = f_c \tag{4.14a}$$

$$\frac{\mathrm{d}\mathcal{G}(\mathcal{P})}{\mathrm{d}\mathcal{P}} = \frac{\mathrm{d}\mathcal{G}(f_c)}{\mathrm{d}f_c} \tag{4.14b}$$

and the consistency condition along with an appropriated definition of the damage variable expressed in terms of $\mathcal{G}$ *i.e.* $d = \mathcal{G}(f_c)$, allows to obtain the following expression for the damage consistency parameter:

$$\dot{\mu} = \dot{\mathcal{P}} = \dot{f}_c = \frac{\partial \mathcal{P}}{\partial \hat{P}^{\mathrm{m}}_{01}} \cdot \dot{\hat{P}}^{\mathrm{m}}_{01} = \frac{\partial \mathcal{P}}{\partial \hat{P}^{\mathrm{m}}_{01}} \cdot \boldsymbol{\mathcal{C}}^{\mathrm{me}} \dot{\hat{\mathcal{E}}}_n. \tag{4.15}$$

Details regarding the deduction of Eqs. (4.14b) to (4.15) can be consulted in Refs. [36, 160]. These results allow to rewrite Eqs. (4.10) and (4.13) as

$$\dot{d} = \frac{\mathrm{d}\mathcal{G}}{\mathrm{d}\mathcal{P}}\dot{\mathcal{P}} \tag{4.16a}$$

$$\dot{\Xi}_m = \Psi_0 \mathcal{G}(\dot{\mathcal{P}}) = \Psi_0 \Big[\frac{\mathrm{d}\mathcal{G}}{\mathrm{d}\mathcal{P}}\frac{\partial \mathcal{P}}{\partial \hat{P}^{\mathrm{m}}_{01}}\Big] \cdot \boldsymbol{\mathcal{C}}^{\mathrm{me}} \dot{\hat{\mathcal{E}}}_n. \tag{4.16b}$$

Finally, the Kuhn-Thucker relations: (a) $\dot{\mu} \geq 0$ (b) $\bar{\mathcal{F}} \leq 0$ (c) $\dot{\mu}\bar{\mathcal{F}} = 0$, have to be employed to derive the unloading–reloading conditions *i.e.* if $\bar{\mathcal{F}} < 0$ the condition (c) imposes $\dot{\mu} = 0$, on the contrary, if $\dot{\mu} > 0$ then $\mathcal{F} = 0$.

4.2.1.d Definition of $\mathcal{G}$

In an analogous manner as Barbat *et al.* in [36] and Oliver *et al.* [301], the following expression is employed for the function $\mathcal{G}$ of Eq. (4.12):

$$\mathcal{G}(\chi) = 1 - \frac{\bar{\mathcal{G}}(\chi)}{\chi} = 1 - \frac{\chi^*}{\chi} e^{\kappa(1-\frac{\chi}{\chi^*})} \tag{4.17}$$

where the term $\bar{\mathcal{G}}(\chi)$ gives the initial yield stress for certain value of the scalar parameter $\chi = \chi^*$ and for $\chi \to \infty$ the final strength is zero (see Fig. 4.5).

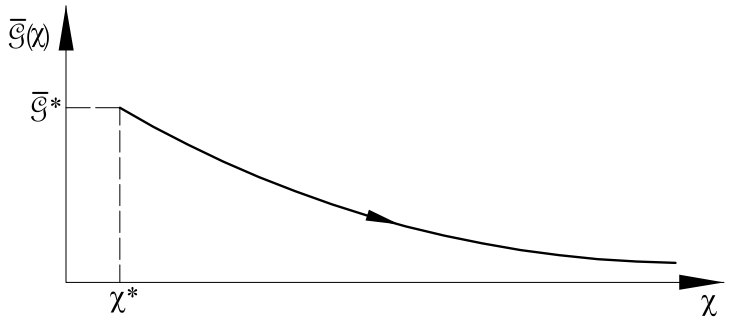

Figure 4.5: Function $\mathcal{G}(\chi)$.

The parameter κ of Eq. (4.17) is calibrated to obtain an amount of dissipated energy equal to the specific fracture energy of the material when all the deformation path is followed.
Integrating Eq. (4.8) for an uniaxial tension process with a monotonically increasing load, and considering that in this case the elastic free energy density can be written as $\Psi_0 = \mathcal{P}^2/(2n^2E_0)$ [36], it is possible to obtain that the total energy dissipated is [301]

$$\Xi_t^{\max} = \int_{\mathcal{P}^*}^{\infty} \underbrace{\frac{\mathcal{P}^2}{2\rho_0 n^2 E^0}}_{\Psi_0} \mathrm{d}\mathcal{G}(\mathcal{P}) = \frac{\mathcal{P}^{*2}}{2\rho_0 E^0}\big[\frac{1}{2} - \frac{1}{\kappa}\big]. \tag{4.18}$$

Therefore, the following expression is obtained for $\kappa > 0$

$$\kappa = \frac{1}{\frac{\Xi_t^{\max} n^2 \rho_0 E^0}{f_c^2} - \frac{1}{2}} \geq 0 \tag{4.19}$$

where it has been assumed that the equivalent stress tension $\mathcal{P}^*$ is equal to the initial damage stress f_c. The value of the maximum dissipation in tension $\Xi_t^{\max}$ is a material parameter equal to the corresponding fracture energy density g_f, which is derived from the fracture mechanics as

$$g_f^d = G_f^d / l_c \tag{4.20}$$

where G_f^d the tensile fracture energy and l_c is the characteristic length of the fractured domain employed in the regularization process [238]. Typically, in the present rod theory this length corresponds to the length of the fiber associated to a material point on the beam cross section (see §4.1).
An identical procedure gives the fracture energy density g_c^d for a compression process yielding to the following expressions for κ

$$\kappa = \frac{1}{\frac{\Xi_c^{\max} \rho_0 E^0}{f_c^2} - \frac{1}{2}} \geq 0. \tag{4.21}$$

Due to the fact that the value of κ have to be the same for a compression or tension test, we have that

$$\Xi_c^{\max} = n^2 \Xi_t^{\max}. \tag{4.22}$$

4.2.1.e Tangential constitutive tensor

Starting from Eq. (4.9) and after several algebraic manipulations which can be reviewed in [36, 160], we obtain that the material form of the *tangent constitutive* tensor $\boldsymbol{\mathcal{C}}^{\mathrm{mt}}$ can be calculated as

$$\delta\hat{P}_1^{\mathrm{m}} = \boldsymbol{\mathcal{C}}^{\mathrm{ms}}\delta\hat{\mathcal{E}}_n + \delta\boldsymbol{\mathcal{C}}^{\mathrm{ms}}\hat{\mathcal{E}}_n. \tag{4.23}$$

Considering

$$D\boldsymbol{\mathcal{C}}^{\mathrm{ms}}\cdot\delta d = \frac{\mathrm{d}}{\mathrm{d}\beta}\big[(1-(d+\beta\delta d))\boldsymbol{\mathcal{C}}^{\mathrm{me}}\big]\Big|_{\beta=0} = -\delta d\,\boldsymbol{\mathcal{C}}^{\mathrm{me}} \tag{4.24}$$

where $\beta\in\mathbb{R}$ and the definition of directional (Fréchet) derivative (see §A.21 of Appendix A) has been used to calculate the linear increment in the material form of the constitutive tensor. Using the results of Eqs. (4.13) and (4.15) in linearized form one obtains

$$\delta d\,\boldsymbol{\mathcal{C}}^{\mathrm{me}}\hat{\mathcal{E}}_n = \frac{\partial\mathcal{G}}{\partial\mathcal{P}}\Big[\frac{\partial\mathcal{P}}{\partial\hat{P}_{01}^{\mathrm{m}}}\cdot(\boldsymbol{\mathcal{C}}^{\mathrm{me}}\delta\hat{\mathcal{E}}_n)\Big]\hat{P}_{01}^{\mathrm{m}} \tag{4.25}$$

which after using Eq. (A.54) of Def. A.13 of Section A.3 and replacing in Eq. (4.23) yields to

$$\delta\hat{P}_1^{\mathrm{m}} = \boldsymbol{\mathcal{C}}^{\mathrm{mt}}\delta\hat{\mathcal{E}}_n = \big[(1-d)\mathbf{I} - \frac{\mathrm{d}\mathcal{G}}{\mathrm{d}\mathcal{P}}\hat{P}_{01}^{\mathrm{m}}\otimes\frac{\partial\mathcal{P}}{\partial\hat{P}_{01}^{\mathrm{m}}}\big]\boldsymbol{\mathcal{C}}^{\mathrm{me}}\delta\hat{\mathcal{E}}_n \tag{4.26}$$

where $\mathbf{I}$ is the identity tensor. It is worth noting that $\boldsymbol{\mathcal{C}}^{\mathrm{mt}}$ is nonsymmetric and it depends on the elastic FPK stress vector. Note that no explicit expression has been given for $\delta\hat{\mathcal{E}}_n$ what will be done in §5 devoted to linearization.
A backward Euler scheme is used for the numerical integration of the constitutive damage model. The flow chart with the step-by-step algorithm used in numerical simulations is shown in Table 4.1.

4.2.2 Rate dependent effects

In this section, the rate independent damage model presented in the previous section is extended to consider viscosity and, as it will be shown, the same formulation can be directly applied to visco elasticity neglecting the damage internal variable. For the case of materials with a visco plastic constitutive equation, reference [370] can be consulted and, therefore, those results are omitted here. In an analogous way as for the inviscid case, the formulation of the rate dependent damage model is carried out in terms of the material forms of the FPK stress vector $\hat{P}_1^{\mathrm{m}}$ and the strain and strain rate vectors $\hat{\mathcal{E}}_n$ and $\hat{\mathcal{S}}_n$, respectively.
The rate dependent behavior of a compounding material is considered by means of using the *Maxwell* model [159, 307]. In this case, the material form of the FPK stress vector $\hat{P}_1^{\mathrm{mt}}$ is obtained as the sum of a rate independent part $\hat{P}_1^{\mathrm{m}}$, see Eq. (4.9) and a viscous component $\hat{P}_1^{\mathrm{mv}}$ as

$$\hat{P}_1^{\mathrm{mt}} = \hat{P}_1^{\mathrm{m}} + \hat{P}_1^{\mathrm{mv}} = (1-d)\boldsymbol{\mathcal{C}}^{\mathrm{me}}\hat{\mathcal{E}}_n + \boldsymbol{\eta}^{\mathrm{sm}}\hat{\mathcal{S}}_n = (1-d)\boldsymbol{\mathcal{C}}^{\mathrm{me}}\big(\hat{\mathcal{E}}_n + \frac{\eta}{\mathrm{E}}\hat{\mathcal{S}}_n\big) \tag{4.27}$$

where $\hat{P}_1^{\mathrm{mt}}$ is the material form of the *total* FPK stress vector, $\hat{\mathcal{S}}_n$ is the material form of the strain rate vector given in Eq. (3.78b) and $\boldsymbol{\eta}^{\mathrm{sm}}$ is the material description of the *secant viscous* constitutive tensor defined from the material description of the secant constitutive tensor as

$$\boldsymbol{\eta}^{\mathrm{sm}} = \frac{\eta}{\mathrm{E}}\boldsymbol{\mathcal{C}}^{\mathrm{ms}} = \tau\boldsymbol{\mathcal{C}}^{\mathrm{ms}}. \tag{4.28}$$

Table 4.1: Flow chart for the damage model

1. INPUT: material form of the strain vector $\hat{\mathcal{E}}_n$ existing on a given integration point on the beam cross section

2. Compute the material form of the elastic (undamaged) FPK stress vector, at the loading step k and global iteration j as
$$(\hat{P}^{\rm m}_{01})^{(k)}_j = \boldsymbol{\mathcal{C}}^{\rm mt}(\hat{\mathcal{E}}_n)^{(k)}_j$$

3. Integration of the constitutive equation (Backward Euler scheme)
   Loop over the inner iterations: l^{th} iteration

For $l=1$	$\rightarrow$	$(\hat{P}^{\rm m}_1)^{(k,0)}_j = (\hat{P}^{\rm m}_{01})^{(k)}_j$
$(\star)$		$(\hat{P}^{\rm m}_1)^{(k,l)}_j = (1-d^{(k,l)}_j)(\hat{P}^{\rm m}_1)^{(k,0)}_j$
		$\mathcal{P}^{(k,l)}_j = \mathcal{P}((\hat{P}^{\rm m}_1)^{(k,l)}_j)$ Eq. (4.11a)
IF $\bar{\mathcal{F}}(\mathcal{P}^{(k,l)}_j, d^{(k,l)}_j) \leq 0$	$\rightarrow$	no damage $\rightarrow$ GOTO 4
ELSE	$\rightarrow$	Damage
		$(\Delta d)^{(k,l)}_j = \mathcal{G}(\mathcal{P}^{(k,l)}_j) - d^{(k,l-1)}_j$ Eq. (4.17)
		$d^{(k,l)}_j = (\Delta d)^{(k,l)}_j + d^{(k,l-1)}_j$
		$(\boldsymbol{\mathcal{C}}^{\rm mt})^{(k,l)}_j = \boldsymbol{\mathcal{C}}^{\rm me}\big[(1-d)\mathbf{I} - \frac{\mathrm{d}\mathcal{G}}{\mathrm{d}\mathcal{P}}\hat{P}^{\rm m}_{01} \otimes \frac{\partial \mathcal{P}}{\partial \hat{P}^{\rm m}_{01}}\big]^{(k,l)}_j$
		$l = l+1 \rightarrow$ GO BACK TO $(\star)$

4. OUTPUT: Updated values of the FPK stress vector and tangent constitutive tensor *i.e.*
$$(\hat{P}^{\rm m}_1)^{(k)}_j = (\hat{P}^{\rm m}_1)^{(k,l)}_j \text{ and } (\boldsymbol{\mathcal{C}}^{\rm mt})^{(k)}_j = (\boldsymbol{\mathcal{C}}^{\rm mt})^{(k,l)}_j$$
STOP.

The scalar parameter η is the *viscosity* and τ is the *relaxation time*, defined as the time required by the visco elastic system to reach a stable configuration in the undamaged configuration [159].

REMARK 4.2. It is interesting to note that in Eq. (4.27) for the case of a material completely damage ($d = 1$) the corresponding stresses are zero and for the case of an elastic material $\boldsymbol{\mathcal{C}}^{\rm ms} = \boldsymbol{\mathcal{C}}^{\rm me}$ and, therefore, the pure visco elastic behavior is recovered ■

In this case the dissipative power is given by

$$\dot{\Xi}_m = \Big[\Psi_0 + \frac{\tau}{\rho_0}\dot{\hat{\mathcal{E}}}_n \cdot \boldsymbol{\mathcal{C}}^{\rm me}\hat{\mathcal{E}}\Big]\frac{\mathrm{d}\mathcal{G}}{\mathrm{d}\mathcal{P}^{\rm m}}\frac{\partial \mathcal{P}^{\rm m}}{\partial \hat{P}^{\rm m}_1} \cdot \boldsymbol{\mathcal{C}}^{\rm ms}\dot{\hat{\mathcal{E}}}_n. \tag{4.29}$$

The linearized increment of the material form of the FPK stress vector is calculated as

$$\begin{aligned}
\delta\hat{P}^{\rm mt}_1 &= \delta\hat{P}^{\rm m}_1 + \delta\hat{P}^{\rm mv}_1 \\
&= \boldsymbol{\mathcal{C}}^{\rm mt}\delta\hat{\mathcal{E}}_n + \delta\boldsymbol{\eta}^{\rm sm}\hat{\mathcal{S}}_n + \boldsymbol{\eta}^{\rm sm}\delta\hat{\mathcal{S}}_n \\
&= \boldsymbol{\mathcal{C}}^{\rm mt}\delta\hat{\mathcal{E}}_n - \delta d\frac{\eta}{\mathrm{E}}\boldsymbol{\mathcal{C}}^{\rm me}\hat{\mathcal{S}}_n + \boldsymbol{\eta}^{\rm sm}\delta\hat{\mathcal{S}}_n \\
&= \boldsymbol{\mathcal{C}}^{\rm mt}\delta\hat{\mathcal{E}}_n - \delta d\hat{P}^{\rm mv}_{01} + \boldsymbol{\eta}^{\rm sm}\delta\hat{\mathcal{S}}_n \\
&= \boldsymbol{\mathcal{C}}^{\rm mv}\delta\hat{\mathcal{E}}_n + \boldsymbol{\eta}^{\rm sm}\delta\hat{\mathcal{S}}_n
\end{aligned} \tag{4.30}$$

where $\hat{P}^{\rm mv}_{01}$ is the material form of the FPK visco elastic stress vector, $\delta\hat{\mathcal{S}}_n$ is the linearized increment of the material description of the strain rate vector, which will be given in Chapter 5, and $\boldsymbol{\mathcal{C}}^{\rm mv}$ is the material description of the tangent constitutive tensor which considers the

viscous effects and is calculated in a completely analogous manner as Eq. (4.26) *i.e.*

$$\boldsymbol{\mathcal{C}}^{\mathrm{mv}} = (\mathbf{I} - \mathbf{D}^{\mathrm{mv}})\boldsymbol{\mathcal{C}}^{\mathrm{me}} = \Big[\mathbf{I} - \big(d\mathbf{I} + \frac{\mathrm{d}G}{\mathrm{d}\mathcal{P}^{\mathrm{m}}}(\hat{P}^{\mathrm{m}}_{01} + \hat{P}^{\mathrm{mv}}_{01}) \otimes \frac{\partial \mathcal{P}}{\partial \hat{P}^{\mathrm{m}}_{01}}\big)\Big]\boldsymbol{\mathcal{C}}^{\mathrm{me}}. \tag{4.31}$$

The co-rotated form of the linearized increment of the total FPK stress vector is obtained from Eq. (4.3) by means of the push-forward operation on Eq. (4.30) according to

$$\delta\, \overset{\triangledown}{[\hat{P}^{\mathrm{t}}_1]} = \boldsymbol{\Lambda}\delta\hat{P}^{\mathrm{mt}}_1 = \boldsymbol{\mathcal{C}}^{\mathrm{sv}}\delta\, \overset{\triangledown}{[\hat{\epsilon}_n]} + \boldsymbol{\eta}^{\mathrm{ss}}\delta\, \overset{\triangledown}{[\hat{s}_n]} \tag{4.32}$$

where $\boldsymbol{\mathcal{C}}^{\mathrm{sv}} = \boldsymbol{\Lambda}\boldsymbol{\mathcal{C}}^{\mathrm{mv}}\boldsymbol{\Lambda}^T$ and $\boldsymbol{\eta}^{\mathrm{ss}} = \boldsymbol{\Lambda}\boldsymbol{\eta}^{\mathrm{sm}}\boldsymbol{\Lambda}^T$ are the spatial descriptions of the rate dependent tangent and the secant viscous constitutive constitutive tensors, respectively.

4.2.3 Plastic materials

For case of a material which can undergo *non–reversible deformations*, the plasticity model formulated in the material configuration is used for predicting the corresponding mechanical response. The model here presented is adequate to simulate the mechanical behavior of metallic and ceramic materials as well as geomaterials [305]. Assuming a thermally stable process, small elastic and finite plastic deformations, we have that the free energy density Ψ is given by the addition of the elastic and the plastic parts [238] as

$$\Psi = \Psi^e + \Psi^P = \frac{1}{2\rho_0}(\hat{\mathcal{E}}^e_n \cdot \boldsymbol{\mathcal{C}}^{\mathrm{me}}\hat{\mathcal{E}}^e_n) + \Psi^P(k_p) \tag{4.33}$$

where the $\hat{\mathcal{E}}^e_n$ is the elastic strain vector calculated subtracting the plastic strain vector $\hat{\mathcal{E}}^P_n$ from the total strain vector $\hat{\mathcal{E}}_n$, Ψ^e and Ψ^P are the elastic and plastic parts of the free energy density, respectively, ρ_0 is the density in the material configuration and k_p is the *plastic damage* internal variable.

4.2.3.a Secant constitutive equation and mechanical dissipation

Following analogous procedures as those for the damage model *i.e.* employing the CP inequality and the Coleman's principle [237, 250], the secant constitutive equation and the mechanical dissipation take the following forms

$$\hat{P}^{\mathrm{m}}_1 = \rho_0 \frac{\partial \Psi(\hat{\mathcal{E}}^e_n, k_p)}{\partial \hat{\mathcal{E}}^e_n} = \boldsymbol{\mathcal{C}}^{\mathrm{ms}}\big(\hat{\mathcal{E}}_n - \hat{\mathcal{E}}^P_n\big) = \boldsymbol{\mathcal{C}}^{\mathrm{me}}\hat{\mathcal{E}}^e_n \tag{4.34a}$$

$$\dot{\Xi}_m = \frac{\hat{P}^{\mathrm{m}}_1 \cdot \dot{\hat{\mathcal{E}}}^P_n}{\rho_0} - \frac{\partial \Psi^P}{\partial k_p}\dot{k}_p \geq 0 \tag{4.34b}$$

where the material description of the secant constitutive tensor $\boldsymbol{\mathcal{C}}^{\mathrm{ms}}$ coincides with the elastic one $\boldsymbol{\mathcal{C}}^{\mathrm{me}} = \mathrm{Diag[E, G, G]}$. It is worth to note that Eqs. (4.34a) and (4.34b) constitute particular cases of a more general formulation of the so called coupled plastic–damage models as it can be reviewed in [305].

4.2.3.b Plastic yielding and potential functions

Both, the yield function, $\mathcal{F}_p$, and plastic potential function, $\mathcal{G}_p$, for the plasticity model, are formulated in terms of the material form of the FPK stress vector $\hat{P}^{\mathrm{m}}_1$ and the plastic damage

internal variable k_p as

$$\mathcal{F}_p(\hat{P}_1^{\mathrm{m}}, k_p) = \mathcal{P}_p(\hat{P}_1^{\mathrm{m}}) - f_p(\hat{P}_1^{\mathrm{m}}, k_p) = 0 \tag{4.35a}$$

$$\mathcal{G}_p(\hat{P}_1^{\mathrm{m}}, k_p) = \mathcal{K} \tag{4.35b}$$

where $\mathcal{P}_p(\hat{P}_1^{\mathrm{m}})$ is the (scalar) equivalent stress, which is compared with the *hardening* function $f_p(\hat{P}_1^{\mathrm{m}}, k_p)$ depending on the damage plastic internal variable k_p and on the current stress state, and $\mathcal{K}$ is a constant value [241, 305].

REMARK 4.3. Common choices for $\mathcal{F}_p$ and $\mathcal{G}_p$ are Tresca or Von Mises for metals, Mohr-Coulomb or Drucker-Prager for geomaterials ■

According to the evolution of the plastic damage variable, k_p, it is possible to treat materials considering *isotropic* hardening as in Refs. [151, 318, 372]. However, in this work k_p constitutes a measure of the energy dissipated during the plastic process and, therefore, it is well suited for materials with *softening*. In this case k_p is defined [238, 306] as

$$g_f^P = \frac{G_f^P}{l_c} = \int_{t=0}^{\infty} \hat{P}_1^{\mathrm{m}} \cdot \dot{\mathcal{E}}_n^P \mathrm{d}t \tag{4.36a}$$

$$0 \leq \left[k_p = \frac{1}{g_f^P} \int_{t=0}^{t} \hat{P}_1^{\mathrm{m}} \cdot \dot{\mathcal{E}}_n^P dt\right] \leq 1 \tag{4.36b}$$

where G_f^P is the specific plastic fracture energy of the material in tension and l_c is the length of the fractured domain defined in analogous manner as for the damage model. The integral term in Eq. (4.36b) corresponds to the energy dissipated by means of plastic work and, therefore, k_p constitutes a measure of the part of the fracture energy that has been consumed during the deformation. Similarly, it is possible to define the normalized plastic damage variable for the case of a compressive test related with g_c^P.

4.2.3.c Evolution laws for the internal variables

The flow rules for the internal variables $\hat{\mathcal{E}}_n^P$ and k_p are defined as usual for plastic models defined in the material configuration [238, 236] according to

$$\dot{\hat{\mathcal{E}}}_n^P = \dot{\lambda} \frac{\partial \mathcal{G}_p}{\partial \hat{P}_1^{\mathrm{m}}} \tag{4.37}$$

$$\dot{k}_p = \dot{\lambda}\, \hat{\varrho}(\hat{P}_1^{\mathrm{m}}, k_p, G_f^P) \cdot \frac{\partial \mathcal{G}_p}{\partial \hat{P}_1^{\mathrm{m}}} = \hat{\varrho}(\hat{P}_1^{\mathrm{m}}, k_p, G_f^P) \cdot \dot{\mathcal{E}}_n^P \tag{4.38}$$

where $\dot{\lambda}$ is the plastic consistency parameter and $\hat{\varrho}$ is the following *hardening* vector [238, 305]

$$\dot{k}_p = \left[\frac{r}{g_f^P} + \frac{1-r}{g_c^P}\right] \hat{P}_1^{\mathrm{m}} \cdot \dot{\mathcal{E}}_n^P = \widehat{\varrho} \cdot \dot{\mathcal{E}}_n^P \tag{4.39}$$

where term $\hat{P}_1^{\mathrm{m}} \cdot \dot{\hat{\mathcal{E}}}_n^P$ is the plastic dissipation and r is given in Eq. (4.11d). It is interesting to note that the proposed evolution rule allows to differentiate between tensile and compressive properties of the material, distributing the total plastic dissipation as weighted parts of the compressive and tensile fracture energy densities.
In what regards the hardening function of Eq. (4.35a), the following evolution equation has

been proposed [241]:

$$f_p(\hat{P}_1^{\mathrm{m}}, k_p) = r\sigma_t(k_p) + (1-r)\sigma_c(k_p) \tag{4.40}$$

where r has been defined in Eq. (4.11d) and the (scalar) functions $\sigma_t(k_p)$ and $\sigma_c(k_p)$ represent the evolution of the yielding threshold in uniaxial tension and compression tests, respectively. It is worth noting that in Eq. (4.40) a differentiated traction–compression behavior has been taken into account.

As it is a standard practice in plasticity, the loading/unloading conditions are derived in the standard form from the Kuhn-Tucker relations formulated for problems with unilateral restrictions, *i.e.* , (a) $\dot{\lambda} \geq 0$, (b) $\mathcal{F}_p \leq 0$ and (c) $\dot{\lambda}\mathcal{F}_p = 0$.

By other hand, starting from the plastic consistency condition $\dot{\mathcal{F}}_p = 0$ one has

$$\begin{aligned}
\dot{\mathcal{F}}_p &= \dot{\mathcal{P}}_p - \dot{f}_p = 0 \\
&= \frac{\partial \mathcal{P}_p}{\partial \hat{P}_1^{\mathrm{m}}} \cdot \dot{\hat{P}}_1^{\mathrm{m}} - \frac{\partial f_p}{\partial \hat{P}_1^{\mathrm{m}}} \cdot \dot{\hat{P}}_1^{\mathrm{m}} - \frac{\partial f_p}{\partial k_p}\dot{k}_p = 0 \\
&= (\frac{\partial \mathcal{P}_p}{\partial \hat{P}_1^{\mathrm{m}}} - \frac{\partial f_p}{\partial \hat{P}_1^{\mathrm{m}}}) \cdot (\boldsymbol{\mathcal{C}}^{\mathrm{me}}\dot{\mathcal{E}}_n - \dot{\mathcal{E}}_n^P) - \frac{\partial f_p}{\partial k_p}\dot{k}_p = 0
\end{aligned}$$

where it has been used the expression for the temporal variation of Eq. (4.34a). Considering the flow rules of Eqs. (4.37) and (4.38), it is possible to deduce the explicit form of $\dot{\lambda}$ as [305, 306]

$$\dot{\lambda} = -\frac{\frac{\partial \mathcal{F}_p}{\partial \hat{P}_1^{\mathrm{m}}} \cdot (\boldsymbol{\mathcal{C}}^{\mathrm{me}}\dot{\hat{\mathcal{E}}}_n)}{\{\frac{\partial \mathcal{F}_p}{\partial \hat{P}_1^{\mathrm{m}}} \cdot (\boldsymbol{\mathcal{C}}^{\mathrm{me}}\frac{\partial \mathcal{G}_p}{\partial \hat{P}_1^{\mathrm{m}}}) - \frac{\partial f_p}{\partial k_p}\hat{\underline{\varrho}} \cdot \frac{\partial \mathcal{G}_p}{\partial \hat{P}_1^{\mathrm{m}}}\}} \tag{4.41}$$

4.2.3.d Tangent constitutive tensor

The material form of the tangent constitutive tensor is calculated taking the time derivative of Eq. (4.34a), considering the flow rule of Eq. (4.37), replacing the plastic consistency parameter of Eq. (4.41), using Eq. (A.54) of Def. A.13 of Section A.3 and after several algebraic manipulations [305, 306], it is obtained as

$$\begin{aligned}
\delta\hat{P}_1^{\mathrm{m}} &= \boldsymbol{\mathcal{C}}^{\mathrm{me}}(\delta\hat{\mathcal{E}}_n - \delta\lambda\frac{\partial \mathcal{G}_p}{\partial \hat{P}_1^{\mathrm{m}}}) \\
&= \boldsymbol{\mathcal{C}}^{\mathrm{me}}\delta\hat{\mathcal{E}}_n - \boldsymbol{\mathcal{C}}^{\mathrm{me}}\Big[\frac{\frac{\partial \mathcal{F}_p}{\partial \hat{P}_1^{\mathrm{m}}} \cdot (\boldsymbol{\mathcal{C}}^{\mathrm{me}}\delta\hat{\mathcal{E}}_n)}{\{\frac{\partial \mathcal{F}_p}{\partial \hat{P}_1^{\mathrm{m}}} \cdot (\boldsymbol{\mathcal{C}}^{\mathrm{me}}\frac{\partial \mathcal{G}_p}{\partial \hat{P}_1^{\mathrm{m}}}) - \frac{\partial f_p}{\partial k_p}\hat{\underline{\varrho}} \cdot \frac{\partial \mathcal{G}_p}{\partial \hat{P}_1^{\mathrm{m}}}\}}\Big]\frac{\partial \mathcal{G}_p}{\partial \hat{P}_1^{\mathrm{m}}} \\
&= \Big[\boldsymbol{\mathcal{C}}^{\mathrm{me}} - \frac{(\boldsymbol{\mathcal{C}}^{\mathrm{me}}\frac{\partial \mathcal{G}_p}{\partial \hat{P}_1^{\mathrm{m}}}) \otimes (\boldsymbol{\mathcal{C}}^{\mathrm{me}}\frac{\partial \mathcal{F}_p}{\partial \hat{P}_1^{\mathrm{m}}})}{\frac{\partial \mathcal{F}_p}{\partial \hat{P}_1^{\mathrm{m}}} \cdot (\boldsymbol{\mathcal{C}}^{\mathrm{me}}\frac{\partial \mathcal{G}_p}{\partial \hat{P}_1^{\mathrm{m}}}) - \frac{\partial \mathcal{F}_p}{\partial k_p}\hat{\underline{\varrho}} \cdot (\frac{\partial \mathcal{G}_p}{\partial \hat{P}_1^{\mathrm{m}}})}\Big]\delta\hat{\mathcal{E}}_n \\
&= \Big[\boldsymbol{\mathcal{C}}^{\mathrm{me}} - \frac{(\boldsymbol{\mathcal{C}}^{\mathrm{me}}\frac{\partial \mathcal{G}_p}{\partial \hat{P}_1^{\mathrm{m}}}) \otimes (\boldsymbol{\mathcal{C}}^{\mathrm{me}}\frac{\partial \mathcal{F}_p}{\partial \hat{P}_1^{\mathrm{m}}})}{\frac{\partial \mathcal{F}_p}{\partial \hat{P}_1^{\mathrm{m}}} \cdot (\boldsymbol{\mathcal{C}}^{\mathrm{me}}\frac{\partial \mathcal{G}_p}{\partial \hat{P}_1^{\mathrm{m}}}) - \Phi_p}\Big]\delta\hat{\mathcal{E}}_n \\
&= \boldsymbol{\mathcal{C}}^{\mathrm{mt}}\delta\hat{\mathcal{E}}_n
\end{aligned} \tag{4.42}$$

where Φ_p is the so called *hardening parameter*.

4.2.3.e Perfect plasticity with Von Mises yield criterion

If the Von Mises criterion is chosen for the both the yielding and potential functions, equal tension/compression yielding thresholds are considered *i.e.* , $n = 1$ and $G_f = G_c \approx \infty$, one obtains that $k_p \approx 0$, $\dot{k}_p \approx 0$ and $f_p \sim f_c$ with σ^* being the characteristic yielding threshold of the material, the following expressions are obtained

$$\mathcal{F}_p = \mathcal{P}_p - f_p = \sqrt{\hat{P}_1^{\mathrm{m}} \cdot \boldsymbol{\mathcal{S}} \hat{P}_1^{\mathrm{m}}} - \sigma^*; \quad \boldsymbol{\mathcal{S}} = \mathrm{diag}[1,3,3] \tag{4.43a}$$

$$\frac{\partial \mathcal{F}_p}{\partial \hat{P}_1^{\mathrm{m}}} = \frac{\partial \mathcal{G}_p}{\partial \hat{P}_1^{\mathrm{m}}} = \frac{\boldsymbol{\mathcal{S}} \hat{P}_1^{\mathrm{m}}}{\mathcal{P}_p} := \hat{N}_1^{\mathrm{m}} \tag{4.43b}$$

$$\dot{\lambda} = -\frac{\hat{N}_1^{\mathrm{m}} \cdot (\boldsymbol{\mathcal{C}}^{\mathrm{me}} \dot{\hat{\mathcal{E}}}_n)}{\hat{N}_1^{\mathrm{m}} \cdot (\boldsymbol{\mathcal{C}}^{\mathrm{me}} \hat{N}_1^{\mathrm{m}})} \tag{4.43c}$$

$$\boldsymbol{\mathcal{C}}^{\mathrm{mt}} = \boldsymbol{\mathcal{C}}^{\mathrm{me}} - \frac{(\boldsymbol{\mathcal{C}}^{\mathrm{me}} \hat{N}_1^{\mathrm{m}}) \otimes (\boldsymbol{\mathcal{C}}^{\mathrm{me}} \hat{N}_1^{\mathrm{m}})}{\hat{N}_1^{\mathrm{m}} \cdot (\boldsymbol{\mathcal{C}}^{\mathrm{me}} \hat{N}_1^{\mathrm{m}})} \tag{4.43d}$$

In this particular case, more simple expressions are obtained as it can be seen in Eqs. (4.43a) to (4.43d) including a symmetric tangential tensor. Therefore, the perfect plasticity case can be considered as a limit case of the present formulation, for materials with an infinite fracture energy.
The backward Euler scheme is used for the numerical integration of the constitutive plasticity model [305]. A flow chart with the step-by-step algorithm used in numerical simulations is shown in Table 4.2.

4.3 Mixing theory for composite materials

4.3.1 Hypothesis

Each material point on the beam cross is treated as a composite material according to the *mixing theory* [258, 305], considering the following assumptions:

(i) Each composite has a finite number of simple materials (see Fig. 4.1).

(ii) Each component participate in the mechanical behavior according to its volumetric participation k_i defined as

$$k_q = V_q / V \rightarrow \sum_q k_q = 1$$

i.e. according to its proportional part V_i (in terms of volume) with respect to the total volume V associated to the material point.

(iii) All the components are subjected to the same strain field, what can be interpreted as a *rheological model* where each compounding substance works in parallel with the others.

Therefore, the interaction between all the components defines the overall mechanical behavior at material point level. Supposing that a generic material point, where coexist $N_c < \infty$ different components (hypothesis (i)), is subjected to a strain field described by the material strain vector $\hat{\mathcal{E}}_n$, according to hypothesis (iii) we have the following closing equation:

$$\hat{\mathcal{E}}_n \equiv (\hat{\mathcal{E}}_n)^1 = \cdots = (\hat{\mathcal{E}}_n)^j = \cdots = (\hat{\mathcal{E}}_n)^{N_c} \tag{4.44}$$

Table 4.2: Flow chart for the plasticity model

1. INPUT: material form of the strain vector $\hat{\mathcal{E}}_n$ existing on a given integration point on the beam cross section

2. Compute the material form of the predicted FPK stress vector, at the loading step k and global iteration j as
$$(\hat{P}_1^{\mathrm{m}})_j^{(k)} = \boldsymbol{\mathcal{C}}^{\mathrm{ms}}((\hat{\mathcal{E}}_n)_j^{(k)} - (\hat{\mathcal{E}}_n^P)_{(j-1)}^{(k)})$$

3. Integration of the constitutive equation (Backward Euler scheme)
Loop over the inner iterations: l^{th} iteration

For $l = 1$	$\rightarrow$	$(\hat{P}_1^{\mathrm{m}})_j^{(k,0)} = (\hat{P}_1^{\mathrm{m}})_j^{(k)}, \quad (\Delta\hat{\mathcal{E}}_n^P)_j^{(k,0)} = 0$
$(\star)$		$(\hat{P}_1^{\mathrm{m}})_j^{(k,l)} = (\hat{P}_1^{\mathrm{m}})_j^{(k,l-1)} - \boldsymbol{\mathcal{C}}^{\mathrm{ms}}(\Delta\hat{\mathcal{E}}_n^P)_j^{(k,l-1)}$
		$(\mathcal{P}_p)_j^{(k,l)} = \mathcal{P}_p((\hat{P}_1^{\mathrm{m}})_j^{(k,l)})$
IF $\mathcal{F}_p(\mathcal{P}_p, \hat{E}_n^P, k_p)_j^{(k,l)} \leq 0$	$\rightarrow$	elastic case $\rightarrow$ GOTO 4
ELSE	$\rightarrow$	plastic case
		$(\Delta\hat{\mathcal{E}}_n^P)_j^{(k,l)} = (\Delta\lambda)_j^{(k,l)}\left(\frac{\partial\mathcal{G}_p}{\partial\hat{P}_1^{\mathrm{m}}}\right)_j^{(k,l)}$ Eq. (4.41)
		$(\hat{\mathcal{E}}_n^P)_j^{(k,l)} = (\hat{\mathcal{E}}_n^P)_j^{(k,l-1)} + (\Delta\hat{\mathcal{E}}_n^P)_j^{(k,l)}$
		$(\Delta k_p)_j^{(k,l)} = (\hat{\varrho})_j^{(k,l)} \cdot (\Delta\hat{\mathcal{E}}_n^P)_j^{(k,l)}$ Eq. (4.39)
		$(k_p)_j^{(k,l)} = (k_p)_j^{(k,l-1)} + (\Delta k_p)_j^{(k,l)}$
		$l = l + 1 \rightarrow$ GO BACK TO $(\star)$

4. OUTPUT: Updated values of the FPK stress vector and tangent constitutive tensor *i.e.* $(\hat{P}_1^{\mathrm{m}})_j^{(k)} = (\hat{P}_1^{\mathrm{m}})_j^{(k,l)}$ and

$$(\boldsymbol{\mathcal{C}}^{\mathrm{mt}})_j^{(k)} = (\boldsymbol{\mathcal{C}}^{\mathrm{mt}})_j^{(k,l)} = \boldsymbol{\mathcal{C}}^{\mathrm{me}} - \left[\frac{\left(\boldsymbol{\mathcal{C}}^{\mathrm{ms}}\frac{\partial\mathcal{G}_p}{\partial\hat{P}_1^{\mathrm{m}}}\right)\otimes\left(\boldsymbol{\mathcal{C}}^{\mathrm{me}}\frac{\partial\mathcal{F}_p}{\partial\hat{P}_1^{\mathrm{m}}}\right)}{\left\{\left(\frac{\partial\mathcal{F}}{\partial\hat{P}_1^{\mathrm{m}}}\right)\cdot\left(\boldsymbol{\mathcal{C}}^{\mathrm{ms}}\frac{\partial\mathcal{G}_p}{\partial\hat{P}_1^{\mathrm{m}}}\right) - \frac{\partial\mathcal{F}_p}{\partial k_p}\hat{\varrho}\cdot\left(\frac{\partial\mathcal{G}_p}{\partial\hat{P}_1^{\mathrm{m}}}\right)\right\}} \right]_j^{(k,l)}$$

STOP.

which imposes the strain compatibility between components.

4.3.2 Free energy density of the composite

The free energy density of the composite is written for the adiabatic case as the weighted sum of the free energy of the components [305]

$$\Psi(\hat{\mathcal{E}}_n, \alpha_p) \equiv \sum_{q=1}^{N_c} k_q \Psi_q(\hat{\mathcal{E}}_n, \alpha_{p_q}) \tag{4.45}$$

where $\Psi_q(\hat{\mathcal{E}}_n, \alpha_{p_q})$ is the free energy of the q^{th} compounding substance with an associated constitutive model depending on p internal variables, α_{p_q}, and k_q is the volumetric fraction of the component. As it has been explained, in the present work only degrading and plastic materials are used as compounding substances, therefore, the values that the index p can take, is limited to 1 for the degrading materials, (the damage variable d), and to 2 for the plastic ones (the plastic strain vector $(\hat{\mathcal{E}}^P)_q$ and the plastic damage $(k_p)_q$. In any case, a generic notation has been preferred by simplicity, even though it is necessary to have in mind that different substances have associated a different number of internal variables.

4.3.3 Secant constitutive relation and mechanical dissipation

Starting from Eq. (4.45), it is possible to obtain the material form of the secant constitutive equation, the secant constitutive tensor, $\bar{\boldsymbol{\mathcal{C}}}^{\mathrm{ms}}$ and the mechanical dissipation $\dot{\bar{\Xi}}_m$ for the composite in analogous way as for simple materials *i.e.*

$$\hat{P}_1^{\mathrm{m}} \equiv \rho_0 \frac{\partial \Psi(\hat{\mathcal{E}}_n, \alpha_p)}{\partial \hat{\mathcal{E}}_n} = \sum_{q=1}^{N_c} (\rho_0)_q k_q \frac{\partial \Psi_q(\hat{\mathcal{E}}_n, \alpha_{p_q})}{\partial \hat{\mathcal{E}}_n} = \sum_{q}^{N_c} k_q (\hat{P}_1^{\mathrm{m}})_q \tag{4.46a}$$

$$\dot{\Xi}_m \equiv -\sum_{q=1}^{N_c} k_q (\dot{\Xi}_m)_q = -\sum_{q=1}^{N_c} k_q \Big[\sum_{j=1}^{p} \frac{\partial \Psi(\hat{\mathcal{E}}_n, \alpha_j)}{\partial \alpha_j} \dot{\alpha}_j \Big]_q \geq 0. \tag{4.46b}$$

where $(\hat{P}_1^{\mathrm{m}})_q$ and $(\dot{\Xi}_m)_q$, are the material form of the FPK stress vector and the mechanical dissipation of the q^{th} component, respectively. It is worth to comment the meaning of ρ_0 in Eq. (4.48) it corresponds to the average value of the material form of the density obtained as result of applying the mixing theory. Having calculated the material form of the FPK stress vector, the spatial form is obtained by $\hat{P}_1 = \boldsymbol{\Lambda} \hat{P}_1^{\mathrm{m}}$. From Eq. (4.48) it is possible to conclude that

$$\bar{\boldsymbol{\mathcal{C}}}^{\mathrm{ms}} \equiv \sum_{q=1}^{N_c} k_q (\boldsymbol{\mathcal{C}}^{\mathrm{ms}})_q \rightarrow \hat{P}_1^{\mathrm{m}} = \bar{\boldsymbol{\mathcal{C}}}^{\mathrm{ms}} (\hat{\mathcal{E}}_n - \hat{\mathcal{E}}_n^P) \tag{4.46c}$$

$$\hat{\mathcal{E}}_n^P = \sum_{q=1}^{N_c} k_q (\hat{\mathcal{E}}_n^P)_q \tag{4.46d}$$

where $(\boldsymbol{\mathcal{C}}^{\mathrm{ms}})^i$ and $(\hat{\mathcal{E}}_n^P)^i$, are the material form of the secant constitutive tensor and the (fictitious) material plastic strain vector, respectively. It is worth to comment the meaning of $\hat{\mathcal{E}}_n^P$ in Eq. (4.50), it corresponds to the average value of the material form of the plastic strain vector of the composite obtained using the mixing theory.

4.3.4 Tangent constitutive tensor

The material form of the tangent constitutive tensors, $\bar{\boldsymbol{\mathcal{C}}}^{\mathrm{mt}}$, of the composite is estimated in analogous way as for simple materials *i.e.*

$$\delta \hat{P}_1^{\mathrm{m}} = \bar{\boldsymbol{\mathcal{C}}}^{\mathrm{mt}} \delta \hat{\mathcal{E}}_n = \sum_{i=1}^{N_c} k_q (\boldsymbol{\mathcal{C}}^{\mathrm{mt}})_q \delta \hat{\mathcal{E}}_n \tag{4.47}$$

where $(\boldsymbol{\mathcal{C}}^{\mathrm{mt}})_q$, $\delta \hat{P}_1^{\mathrm{m}}$ and $\delta \hat{\mathcal{E}}_n$ are the material form of the tangent constitutive tensors and the variation of the material stress and strain vectors, respectively.

4.3.5 Rate dependent effects

Using the same reasoning as in Section 4.2.2, the participation of rate dependent effects in the composite can be considered in the following form:

$$\hat{P}_1^{\mathrm{mt}} \equiv \sum_{q}^{N_c} k_q (\hat{P}_1^{\mathrm{m}} + \hat{P}_1^{\mathrm{mv}})_q = \sum_{q}^{N_c} k_q \big[(1-d) \boldsymbol{\mathcal{C}}^{\mathrm{me}} \big(\hat{\mathcal{E}}_n + \frac{\eta}{\mathrm{E}} \hat{\mathcal{S}}_n \big) \big]_q$$

$$= \sum_{q}^{N_c} k_q(\boldsymbol{\mathcal{C}}^{\mathrm{ms}})_q \hat{\mathcal{E}}_n + \sum_{q}^{N_c} k_q(\boldsymbol{\eta}^{\mathrm{sm}})_q \hat{\mathcal{S}}_n = \bar{\boldsymbol{\mathcal{C}}}^{\mathrm{ms}} \hat{\mathcal{E}}_n + \bar{\boldsymbol{\eta}}^{\mathrm{sm}} \hat{\mathcal{S}}_n \tag{4.48}$$

where $\bar{\boldsymbol{\eta}}^{\mathrm{sm}}$ corresponds tho the viscous secant tensor of the composite.
By analogy with Eq. (4.30), the linearized relation between material forms of strain and stress vectors is given by

$$\delta \hat{P}_1^{\mathrm{mt}} = \bar{\boldsymbol{\mathcal{C}}}^{\mathrm{mv}} \delta \hat{\mathcal{E}}_n + \bar{\boldsymbol{\eta}}^{\mathrm{sm}} \delta \hat{\mathcal{S}}_n; \quad \bar{\boldsymbol{\mathcal{C}}}^{\mathrm{mv}} = \sum_{q}^{N_c} k_q(\boldsymbol{\mathcal{C}}^{\mathrm{mv}})_q, \quad \bar{\boldsymbol{\eta}}^{\mathrm{sm}} = \sum_{q}^{N_c} k_q(\boldsymbol{\eta}^{\mathrm{sm}})_q. \tag{4.49}$$

The co-rotated form of the linearized relation between strains and stresses for the composite material is based on the weighted sum of the spatial form of the tangent constitutive tensors $(\mathcal{C}^{\mathrm{mv}})^i$ plus the rate dependent tensors $(\eta^{\mathrm{ss}})^i$ of Eq. (4.31) for each one of the components and it is given by

$$\delta\, [\overset{\triangledown}{\hat{P}}_1^{\mathrm{t}}] = \sum_{q=1}^{N_c} k_q(\boldsymbol{\mathcal{C}}^{\mathrm{sv}})_q \delta\, [\overset{\triangledown}{\hat{\epsilon}}_n] + \sum_{q=1}^{N} k_q(\boldsymbol{\eta}^{\mathrm{ss}})_q \delta\, [\overset{\triangledown}{\hat{s}}_n] = \bar{\boldsymbol{\mathcal{C}}}^{\mathrm{sv}} \delta\, [\overset{\triangledown}{\hat{\epsilon}}_n] + \bar{\boldsymbol{\eta}}^{\mathrm{ss}} \delta\, [\overset{\triangledown}{\hat{s}}_n]\,. \tag{4.50}$$

Therefore, an entirely analogous formulation for composite materials is obtained considered the participation of the volumetric fraction of each component.

REMARK 4.4. An important aspect to consider is regarded to the total fracture energy of the composite, which is a experimental quantity. It is obtained as the sum of the fracture energy of the components *i.e.*

$$G^P_{(f,c)} = \sum_i G^{P(i)}_{(f,c)},$$

more details can be consulted in [90, 91] ■

4.4 Stress resultant, couples and related reduced tensors

As it has been explained in Section 4.2, the distribution of materials on the beam cross sections can be arbitrary (see Fig. 4.1). Considering Eqs. (3.100a) and (3.100b), one has that the material form of the cross sectional stress resultant and couples can be written as

$$\hat{n}^{\mathrm{m}} = \int_{\mathcal{A}_{00}} \hat{P}_1^{\mathrm{mt}} \mathrm{d}\mathcal{A}_{00} = \int_{\mathcal{A}_{00}} \bar{\boldsymbol{\mathcal{C}}}^{\mathrm{ms}} \hat{\mathcal{E}}_n \mathrm{d}\mathcal{A}_{00} + \int_{\mathcal{A}_{00}} \bar{\boldsymbol{\eta}}^{\mathrm{sm}} \dot{\hat{\mathcal{E}}}_n \mathrm{d}\mathcal{A}_{00} \hat{\mathcal{S}}_n \tag{4.51}$$

$$\hat{m}^{\mathrm{m}} = \int_{\mathcal{A}_{00}} \tilde{\boldsymbol{\mathcal{E}}} \hat{P}_1^{\mathrm{mt}} \mathrm{d}\mathcal{A}_{00} = \int_{\mathcal{A}_{00}} \tilde{\boldsymbol{\mathcal{E}}} \bar{\boldsymbol{\mathcal{C}}}^{\mathrm{ms}} \hat{\mathcal{E}}_n \mathrm{d}\mathcal{A}_{00} + \int_{\mathcal{A}_{00}} \tilde{\boldsymbol{\mathcal{E}}} \bar{\boldsymbol{\eta}}^{\mathrm{sm}} \dot{\hat{\mathcal{E}}}_n \mathrm{d}\mathcal{A}_{00} \tag{4.52}$$

where Eqs. (4.51) and (4.52) have been written in terms of the secant tensors for the composite even when there is not an explicit expression for them when plasticity is used (see §4.2.3.a). The numerical obtention of $\hat{n}^{\mathrm{m}}$ and $\hat{m}^{\mathrm{m}}$ will be explained in detail in §7.

4.4.1 Cross sectional tangential tensors

Taking into account the result of Eq. (4.49) it is possible to obtain the linearized relation between the material form of the stress resultant and couples and the corresponding linearized

forms of the reduced strain measures as

$$\begin{aligned}
\delta\hat{n}^{\mathrm{m}} &= \int_{\mathcal{A}_{00}} \delta\hat{P}_1^{\mathrm{mt}}\mathrm{d}\mathcal{A}_{00} = \int_{\mathcal{A}_{00}} \bar{\boldsymbol{\mathcal{C}}}^{\mathrm{mv}}\delta\hat{\mathcal{E}}_n\mathrm{d}\mathcal{A}_{00} + \int_{\mathcal{A}_{00}} \bar{\boldsymbol{\eta}}^{\mathrm{sm}}\delta\hat{\mathcal{S}}_n\mathrm{d}\mathcal{A}_{00} \\
&= \Big[\int_{\mathcal{A}_{00}} \bar{\boldsymbol{\mathcal{C}}}^{\mathrm{mv}}\mathrm{d}\mathcal{A}_{00}\Big]\delta\hat{\Gamma}_n - \Big[\int_{\mathcal{A}_{00}} \bar{\boldsymbol{\mathcal{C}}}^{\mathrm{mv}}\widetilde{\boldsymbol{\mathcal{E}}}\mathrm{d}\mathcal{A}_{00}\Big]\delta\hat{\Omega}_n \\
&\quad + \Big[\int_{\mathcal{A}_{00}} \bar{\boldsymbol{\eta}}^{\mathrm{sm}}\mathrm{d}\mathcal{A}_{00}\Big]\delta\dot{\hat{\Gamma}}_n - \Big[\int_{\mathcal{A}_{00}} \bar{\boldsymbol{\eta}}^{\mathrm{sm}}\widetilde{\boldsymbol{\mathcal{E}}}\mathrm{d}\mathcal{A}_{00}\Big]\delta\dot{\hat{\Omega}}_n \\
&= \bar{\mathbf{C}}^{\mathrm{mv}}_{nn}\delta\hat{\Gamma}_n + \bar{\mathbf{C}}^{\mathrm{mv}}_{nm}\delta\hat{\Omega}_n + \bar{\boldsymbol{\Upsilon}}^{\mathrm{sm}}_{nn}\delta\dot{\hat{\Gamma}}_n + \bar{\boldsymbol{\Upsilon}}^{\mathrm{sm}}_{nm}\delta\dot{\hat{\Omega}}_n \qquad (4.53a) \\
\delta\hat{m}^{\mathrm{m}} &= \int_{\mathcal{A}_{00}} \widetilde{\boldsymbol{\mathcal{E}}}\delta\hat{P}_1^{\mathrm{mt}}\mathrm{d}\mathcal{A}_{00} = \Big[\int_{\mathcal{A}_{00}} \widetilde{\boldsymbol{\mathcal{E}}}\bar{\boldsymbol{\mathcal{C}}}^{\mathrm{mv}}\mathrm{d}\mathcal{A}_{00}\Big]\delta\hat{\mathcal{E}}_n + \Big[\int_{\mathcal{A}_{00}} \widetilde{\boldsymbol{\mathcal{E}}}\bar{\boldsymbol{\eta}}^{\mathrm{sm}}\mathrm{d}\mathcal{A}_{00}\Big]\delta\hat{\mathcal{S}}_n \\
&= \Big[\int_{\mathcal{A}_{00}} \widetilde{\boldsymbol{\mathcal{E}}}\bar{\boldsymbol{\mathcal{C}}}^{\mathrm{mv}}\mathrm{d}\mathcal{A}_{00}\Big]\delta\hat{\Gamma}_n - \Big[\int_{\mathcal{A}_{00}} \widetilde{\boldsymbol{\mathcal{E}}}\bar{\boldsymbol{\mathcal{C}}}^{\mathrm{mv}}\widetilde{\boldsymbol{\mathcal{E}}}\mathrm{d}\mathcal{A}_{00}\Big]\delta\hat{\Omega}_n \\
&\quad + \Big[\int_{\mathcal{A}_{00}} \widetilde{\boldsymbol{\mathcal{E}}}\bar{\boldsymbol{\eta}}^{\mathrm{sm}}\mathrm{d}\mathcal{A}_{00}\Big]\delta\dot{\hat{\Gamma}}_n - \Big[\int_{\mathcal{A}_{00}} \widetilde{\boldsymbol{\mathcal{E}}}\bar{\boldsymbol{\eta}}^{\mathrm{sm}}\widetilde{\boldsymbol{\mathcal{E}}}\mathrm{d}\mathcal{A}_{00}\Big]\delta\dot{\hat{\Omega}}_n \\
&= \bar{\mathbf{C}}^{\mathrm{mv}}_{mn}\delta\hat{\Gamma}_n + \bar{\mathbf{C}}^{\mathrm{mv}}_{mm}\delta\hat{\Omega}_n + \bar{\boldsymbol{\Upsilon}}^{\mathrm{sm}}_{mn}\delta\dot{\hat{\Gamma}}_n + \bar{\boldsymbol{\Upsilon}}^{\mathrm{sm}}_{mm}\delta\dot{\hat{\Omega}}_n \qquad (4.53b)
\end{aligned}$$

where the *material* and *viscous* cross sectional tangential tensors $\bar{\mathbf{C}}^{\mathrm{mv}}_{ij}$ and $\bar{\boldsymbol{\Upsilon}}^{\mathrm{sm}}_{ij}$ $(i,j \in \{n,m\})$ are calculated in an completely analogous manner as for the elastic case but replacing the components of the elastic constitutive tensor by their tangent and viscous tangent counterparts (see §3.7.2).

It is worth noting that in Eqs. (4.53a) and (4.53b) the linearized material strain and strain rate vectors have been written as $\delta\hat{\mathcal{E}}_n = \delta\hat{\Gamma}_n - \widetilde{\boldsymbol{\mathcal{E}}}\delta\hat{\Omega}_n$ and $\delta\hat{\mathcal{E}}_n = \delta\hat{\Gamma}_n - \widetilde{\boldsymbol{\mathcal{E}}}\delta\hat{\Omega}_n$, however, by the moment we do not have explicit expressions for these linearized quantities. They will be calculated in great detail in §5.

Taking into account the results of §A.5.5 of Appendix A one has that the Lie variation (or co–rotated) variation of the stress resultant and couples are obtained as

$$\begin{aligned}
\delta\overset{\triangledown}{[\hat{n}]} = \boldsymbol{\Lambda}\delta\hat{n}^{\mathrm{m}} &= \bar{\mathbf{C}}^{\mathrm{sv}}_{nn}\delta\overset{\triangledown}{[\hat{\gamma}_n]} + \bar{\mathbf{C}}^{\mathrm{sv}}_{nm}\delta\overset{\triangledown}{[\hat{\omega}_n]} + \bar{\boldsymbol{\Upsilon}}^{\mathrm{ss}}_{nn}\delta\overset{\triangledown}{[\dot{\hat{\gamma}}_n]} + \bar{\boldsymbol{\Upsilon}}^{\mathrm{ss}}_{nm}\delta\overset{\triangledown}{[\dot{\hat{\Omega}}_n]} \qquad (4.53c) \\
\delta\overset{\triangledown}{[\hat{m}]} = \boldsymbol{\Lambda}\delta\hat{m}^{\mathrm{m}} &= \bar{\mathbf{C}}^{\mathrm{sv}}_{mn}\delta\overset{\triangledown}{[\hat{\gamma}_n]} + \bar{\mathbf{C}}^{\mathrm{sv}}_{mm}\delta\overset{\triangledown}{[\hat{\omega}_n]} + \bar{\boldsymbol{\Upsilon}}^{\mathrm{ss}}_{mn}\delta\overset{\triangledown}{[\dot{\hat{\gamma}}_n]} + \bar{\boldsymbol{\Upsilon}}^{\mathrm{ss}}_{mm}\delta\overset{\triangledown}{[\dot{\hat{\Omega}}_n]} \qquad (4.53d)
\end{aligned}$$

where the spatial form of the cross sectional tangential tensors $\bar{\mathbf{C}}^{\mathrm{sv}}_{ij}$ and $\bar{\boldsymbol{\Upsilon}}^{\mathrm{ss}}_{ij}$ $i,j \in \{n,m\}$ are obtained applying the push–forward by $\boldsymbol{\Lambda}$ *i.e.* $\bar{\mathbf{C}}^{\mathrm{sv}}_{ij} = \boldsymbol{\Lambda}\bar{\mathbf{C}}^{\mathrm{mv}}_{ij}\boldsymbol{\Lambda}^T$ and $\bar{\boldsymbol{\Upsilon}}^{\mathrm{ss}}_{ij} = \boldsymbol{\Lambda}\bar{\boldsymbol{\Upsilon}}^{\mathrm{sm}}_{ij}\boldsymbol{\Lambda}^T$, respectively. Additionally, the co–rotated linearized form of the reduced strain and strain rate vector has been included considering that $\delta\overset{\triangledown}{[\bullet]} = \boldsymbol{\Lambda}(\bullet)$, $\forall(\bullet) \in \mathbb{R}^3$. The above results can be summarized in matrix form as

$$\begin{bmatrix} \delta\hat{n}^{\mathrm{m}} \\ \delta\hat{m}^{\mathrm{m}} \end{bmatrix} = \begin{bmatrix} \bar{\mathbf{C}}^{\mathrm{mv}}_{nn} & \bar{\mathbf{C}}^{\mathrm{mv}}_{nm} \\ \bar{\mathbf{C}}^{\mathrm{mv}}_{mn} & \bar{\mathbf{C}}^{\mathrm{mv}}_{mm} \end{bmatrix}\begin{bmatrix} \delta\hat{\Gamma}_n \\ \delta\hat{\Omega}_n \end{bmatrix} + \begin{bmatrix} \bar{\boldsymbol{\Upsilon}}^{\mathrm{sm}}_{nn} & \bar{\boldsymbol{\Upsilon}}^{\mathrm{sm}}_{nm} \\ \bar{\boldsymbol{\Upsilon}}^{\mathrm{sm}}_{mn} & \bar{\boldsymbol{\Upsilon}}^{\mathrm{sm}}_{mm} \end{bmatrix}\begin{bmatrix} \delta\dot{\hat{\Gamma}}_n \\ \delta\dot{\hat{\Omega}}_n \end{bmatrix} \qquad (4.54)$$

$$\begin{bmatrix} \delta\overset{\triangledown}{[\hat{n}]} \\ \delta\overset{\triangledown}{[\hat{m}]} \end{bmatrix} = \begin{bmatrix} \bar{\mathbf{C}}^{\mathrm{sv}}_{nn} & \bar{\mathbf{C}}^{\mathrm{sv}}_{nm} \\ \bar{\mathbf{C}}^{\mathrm{sv}}_{mn} & \bar{\mathbf{C}}^{\mathrm{sv}}_{mm} \end{bmatrix}\begin{bmatrix} \delta\overset{\triangledown}{[\hat{\Gamma}_n]} \\ \delta\overset{\triangledown}{[\hat{\Omega}_n]} \end{bmatrix} + \begin{bmatrix} \bar{\boldsymbol{\Upsilon}}^{\mathrm{ss}}_{nn} & \bar{\boldsymbol{\Upsilon}}^{\mathrm{ss}}_{nm} \\ \bar{\boldsymbol{\Upsilon}}^{\mathrm{ss}}_{mn} & \bar{\boldsymbol{\Upsilon}}^{\mathrm{ss}}_{mm} \end{bmatrix}\begin{bmatrix} \delta\overset{\triangledown}{[\dot{\hat{\Gamma}}_n]} \\ \delta\overset{\triangledown}{[\dot{\hat{\Omega}}_n]} \end{bmatrix}. \qquad (4.55)$$

4.4.1.a Fiber reinforcements and structural damping

By one hand, the mixing rule provides an appropriated framework for simulating the mechanical behavior of some advanced composed materials such as: epoxy based materials with glass or carbon fibers or even reinforced concrete [305]. This behavior usually is based on the response of a *matrix* component which is reinforced with oriented fibres *e.g.* epoxy based materials with glass or carbon fibers or even reinforced concrete, where the usual steel bars and stirrups can be seen as embedded reinforcing fibers.[4]
The behavior behavior of fiber directed along the beam axis, *i.e. longitudinal reinforcements*, can be simulated by means of appropriated one–dimensional constitutive laws. Due to the limitations imposed by the assumption that plane cross section remain plane during the motion, the incorporation of stirrups or other kind of *transversal reinforcements* is not allowed in the present formulation. The reason is based on the fact that the mechanical effects of transversal reinforcements is due to the stretches of the fibers when the changes in cross sectional shape occurs (see §3.2.2 of Chapter 3 for a detailed discussion about the deformation of differential line elements in the rod). However, the simulation of the effect of this kind of reinforcement is carried out by means of modifying the fracture energy and the limit stress of the matrix material for increasing the cross sectional ductility, deformability, resistance and so on [258, 260, 261], even when this is an approximated method.
By the other hand, the employment of nonlinear constitutive equations at material point level implies that the global structural damping is added to the system in the term $G_{\text{int}}(\hat{\varphi}, \mathbf{\Lambda}, \hat{\eta}^{\text{s}})$ of the virtual work, Eq. (3.143), by means of the stress resultant and couples obtained trough the cross sectional integration of stresses according to Eqs. (4.51) and (4.52). These reduced quantities include the contribution of any kind of rate independent or viscous effects, according to the distribution of the materials on the cross section.
Some branches of engineering are focused on the dynamic response of damped system but considering that the material behavior remains within the linear elastic range, such as in robotics, in the study of flexible mechanisms and in earthquake engineering. Therefore, with this objective, several *ad hoc* approximations have been developed, most of them based on adding a damping term to the equilibrium equations, which is considered to be a function of the strain rates [189]. As it is well known, a widely used method in structural dynamics is *Rayleigh*'s method, which develops a damping matrix using a linear combination of potentials of the stiffness and mass matrices [94]. In this work, a constitutive approach using rate dependent constitutive models is preferred due to the fact that it avoids predefining the way in which the structural damping behaves. Therefore, the proposed method makes hypothesis only at constitutive level.

4.5 Damage indices

The estimation of damage indexes representative of the real remaining loading capacity of a structure has become a key issue in modern performance-based design approaches of civil engineering [209]. Several criteria have been defined for estimating the damage level of structures [160, 304]; some of them are defined for the global behavior of the structure, others can be applied to individual members or subparts of the structure [101].
The FPK stress vector at any material point on the cross section gives a suitable starting point for defining a damage index representative for the real remaining loading capacity of a structure [159]. The damage index developed in this work is based on an analogy with the problem at micro-scale (constitutive) level. A measure of the damage level of a material point can be

[4] A detailed presentation of the mixing rule applied to composites can be consulted the work of E. Car [91]

obtained as the ratio of the existing stress level, obtained applying the mixing rule, to its undamaged elastic counter part. Following this idea, it is possible to define the fictitious damage variable $\check{D}$ as follows:

$$\begin{aligned} \sum_{i=1}^{3} |P_{1i}^{\mathrm{mt}}| &= (1-\check{D}) \sum_{i=1}^{3} |P_{1i0}^{\mathrm{mt}}| = (1-\check{D}) \sum_{i=1}^{3} |(\boldsymbol{\mathcal{C}}^{\mathrm{m}} \hat{\mathcal{E}}_n)_i| \\ \check{D} &= 1 - \frac{\sum_{i=1}^{3} |P_{1i}^{\mathrm{mt}}|}{\sum_{i=1}^{3} |P_{1i0}^{\mathrm{mt}}|} \end{aligned} \tag{4.56}$$

where $|P_{1i}^{\mathrm{mt}}|$ and $|P_{1i0}^{\mathrm{mt}}|$ are the absolute values of the components of the existing and visco elastic stress vectors in material form, respectively. Observe that $|P_{1i}^{\mathrm{mt}}|$ can includes the viscous part of the stress. It is worth to note that $\check{D}$ considers any kind of stiffness degradation (damage, plasticity, etc.) at the material point level through the mixing rule and then it constitutes a measure of the remaining load carrying capacity. Initially, for low loading levels, the material remains elastic and $\check{D} = 0$, but when the entire fracture energy of the material has been dissipated $|P_{1i}^{\mathrm{m}}| \to 0$ and, therefore, $\check{D} \to 1$.
Eq. (4.56) can be extended to consider elements or even the whole structure by means of integrating the stresses over a finite volume of the structure. It allows defining the local and global damage indices as follows:

$$\check{D} = 1 - \frac{\int_{V_p} \left(\sum_i |P_{1i}^{\mathrm{m}}| \right) \mathrm{d}V_p}{\int_{V_p} \left(\sum_i |P_{1i0}^{\mathrm{m}}| \right) \mathrm{d}V_p} \tag{4.57}$$

where V_p is the volume of the part of the structure.
By one hand, the local/global damage index defined in Eq. (4.57) is a force-based criterium, which is able to discriminate the damage level assigned to a set of elements or to the whole structure, according to the manner in which they are loaded, in the same way as it has been explained in reference [160]. By the other hand, Eq (4.57) is easily implemented in an standard finite element code without requiring extra memory storage or time consuming calculations.

4.5.1 Cross sectional damage index

Considering Eq. (4.57) a *cross sectional* damage index, $\check{D}_{\mathcal{A}}(S)$, can be constructed restricting the integrations to the cross sectional area as

$$\check{D}_{\mathcal{A}}(S) = 1 - \frac{\int_{\mathcal{A}} \left(\sum_i |P_{1i}^{\mathrm{m}}| \right) \mathrm{d}\mathcal{A}}{\int_{\mathcal{A}} \left(\sum_i |P_{1i0}^{\mathrm{m}}| \right) \mathrm{d}\mathcal{A}} \quad \forall S \in [0, L]. \tag{4.58}$$

In this way, Eq. (4.57) can be rewritten as

$$\check{D} = \int_0^L \check{D}_{\mathcal{A}}(S) \mathrm{d}S. \tag{4.59}$$

The cross sectional damage index has the virtue of being a dimensionally reduced quantity that capture in a scalar the degradation level of the rod at the arch–length coordinate $S \in [0, L]$.

Chapter 5

Linearization of the virtual work principle

As stated by Marsden (see [256] Ch. 5), nonlinear problems in continuum mechanics are invariably solved by linearizing an appropriated form of nonlinear equilibrium equations and iteratively solving the resulting linear systems until a solution to the nonlinear problem is found. The Newton-Raphson method is the most popular example of such a technique [42]. Correct linearization of the nonlinear equations is fundamental for the success of such techniques.
As it has been demonstrated in §3.6 the virtual work principle is an equivalent representation of the equilibrium equations. For prescribed material and loading conditions, its solution is given by a deformed configuration fulfilling the equilibrium equations and the boundary conditions. Normally, the development of an iterative step-by-step procedure, such as the Newton-Raphson solution procedure, can be obtained based on the linearization, using the general directional derivative (see Def. A.22 in §A.5), of the virtual work functional, which is nonlinear with respect to the kinematic and kinetic variables, the loading and the constitutive behavior of the materials (see §4). Two approaches are available: (i) To discretize the equilibrium equations and then linearize with respect to the nodal positions or (ii) To linearize the virtual work statement and then discretize [66]. Here the later approach is adopted in Chapters 6 and 7 due to the fact that it is a more suitable for the solution of problems in solid mechanics.
This chapter is concerned with the linearization of the virtual work principle, in a manner consistent with the geometry of the configurational manifold where the involved kinetic and kinematical quantities belongs. The procedure requires an understanding of the directional derivative. The linearization procedure is carried out using the directional (Gâteaux) derivative considering it provides the change in an item due to a small change in something upon which item depends. For example, the item could be the determinant of a matrix, in which case the small change would be in the matrix itself.
The fact that the rotational part of the displacement field can be updated using two alternatively but equivalent rules, the material and the spatial one (see Appendix A), implies that two sets of linearized kinetic and kinematical quantities can be obtained, according to the selected updating rule. It is possible to show that both sets are also equivalent by mean of the replacement of the identities summarized in Eqs. (A.67a) to (A.67c) of §A.4. In any case and by completeness, both set of linearized expressions are obtained in the following sections of this chapter.

5.1 Consistent linearization: admissible variations

At it has been explained in Section 3.1.3 the *current configuration* manifolds of the rod at time t is specified by the position of its line of centroid and the corresponding field of orientation tensors, Eq. (3.23), explicitly $\mathcal{C}_t := \{(\hat{\varphi}, \mathbf{\Lambda}) : [0, L] \to \mathbb{R}^3 \times SO(3)\}$ which is a nonlinear differentiable manifold. Following the procedure presented in [363], where Simo and Vu-Quoc, according to the standard practice, carry out the linearization procedure based on using the *Gâteaux* differential (see Appendix A) as a way to approximate to the more rigorous Fréchet differential[1], it is possible to construct a *perturbed configuration* onto $\mathcal{C}_t$ as follows:

(i) Let $\beta > 0 \in \mathbb{R}$ be a scalar and $\delta\hat{\varphi}(S) = \delta\varphi_i(S)\hat{e}_i$ be a vector field (see Def. A.26 of Appendix A) considered as a *superimposed infinitesimal displacement* onto the line of centroid defined by $\hat{\varphi}$.

(ii) Let $\delta\widetilde{\boldsymbol{\theta}} = \delta\widetilde{\theta}_{ij}\hat{e}_i \otimes \hat{e}_j$ $(= \delta\widetilde{\theta}_{ij}\hat{e}_i \wedge \hat{e}_j \ (i < j))$ be the spatial version of a skew–symmetric tensor field interpreted, for $\beta > 0$, as a *superimposed infinitesimal rotation* onto $\mathbf{\Lambda}$, Eqs. (3.19) and (3.21), with axial vector $\delta\hat{\theta} \in T^{\text{spa}}_{\mathbf{\Lambda}}$ (see §A.4.4).

(iii) Let $\delta\widetilde{\mathbf{\Theta}} = \delta\widetilde{\Theta}_{ij}\hat{E}_i \otimes \hat{E}_j$ $(= \delta\widetilde{\Theta}_{ij}\hat{e}_i \wedge \hat{e}_j \ (i < j))$ be the material version of a skew–symmetric tensor field interpreted, for $\beta > 0$, as a *superimposed infinitesimal rotation* onto $\mathbf{\Lambda}$, Eqs. (3.19) and (3.21), with axial vector $\delta\hat{\Theta} \in T^{\text{mat}}_{\mathbf{\Lambda}}$.

(iv) Then, the perturbed configuration

$$\mathcal{C}_{t\beta} \triangleq \{(\hat{\varphi}_\beta, \mathbf{\Lambda}_\beta) : [0, L] \to \mathbb{R}^3 \times SO(3)\}$$

is obtained by setting[2]

$$\hat{\varphi}_\beta(S) = \hat{\varphi}(S) + \beta\delta\hat{\varphi}(S) \qquad \in \mathbb{R}^3 \tag{5.1a}$$

$$\mathbf{\Lambda}_\beta(S) = \exp\big[\beta\delta\widetilde{\boldsymbol{\theta}}(S)\big]\mathbf{\Lambda}(S) \qquad \in SO(3). \tag{5.1b}$$

The term $\mathbf{\Lambda}_\beta$ defined in Eq. (5.1b) is also a rotation tensor, due to the fact that it is obtained by means of the exponential map acting on the skew–symmetric tensor $\beta\delta\widetilde{\boldsymbol{\theta}} \in so(3)$ and, therefore, the perturbed configuration $\mathcal{C}_{t\beta}$ belongs to $\mathbb{R}^3 \times SO(3)$ as well as the current configuration $\mathcal{C}_t$ does ($\mathcal{C}_{t\beta} \subset \mathcal{C}_t$). It should be noted that the perturbed configuration also constitute a possible current configuration of the rod.
Note that in Eq. (5.1b) the spatial updating rule for compound rotations has been chosen for the superimposed infinitesimal rotation, *i.e.* $\beta\delta\widetilde{\boldsymbol{\theta}} \in T^{\text{spa}}_{\mathbf{\Lambda}}SO(3)$. If the material updating rule is preferred, Eq. (5.1b) has to be rewritten as

$$\mathbf{\Lambda}_\beta(S) = \mathbf{\Lambda}(S)\exp\big[\beta\delta\widetilde{\mathbf{\Theta}}(S)\big] \quad \in SO(3) \tag{5.2}$$

where $\beta\delta\widetilde{\mathbf{\Theta}}(S) \in T^{\text{mat}}_{\mathbf{\Lambda}}SO(3)$.
As it has been explained in Appendix A.4, both skew–symmetric tensors $\delta\widetilde{\boldsymbol{\theta}}$ and $\delta\widetilde{\mathbf{\Theta}}$ have associated the corresponding axial vectors $\delta\hat{\theta}$ and $\delta\hat{\Theta} \in \mathbb{R}^3$, respectively. Alternatively, it is possible to work with the field defined by the pair $\hat{\eta}(S) \triangleq (\delta\hat{\varphi}(S), \delta\hat{\theta}(S)) \in T\mathcal{C}_t \approx \mathbb{R}^3 \times \mathbb{R}^3$ and in this

[1] In reference [377] a rigorous foundation for this procedure can be found.

[2] Note that as it has been explained in §A, finite rotations are defined by orthogonal transformations, whereas *infinitesimal rotations* are obtained through *skew–symmetric* transformations. The exponentiation map (see §A.2.4) allows to obtain the finite rotation for a given skew–symmetric tensor.

case the definition for *admissible variation* given in §A.5.1 and §3.1.5 is recovered. The meaning for the two component of $\hat{\eta}(S)$ is analogous to those given for $(\delta\hat{\varphi}, \delta\widetilde{\boldsymbol{\Theta}})$ if the material updating rule of rotations is used[3].
Due to attention is focused on the boundary value problem in which displacements and rotations are the prescribed boundary data and starting from the previous definition for $\hat{\eta}$, it follows that the linear space of *kinematically admissible variations* is

$$\eta^{\mathrm{s}} = \{\hat{\eta}^{\mathrm{s}} = (\delta\hat{\varphi}, \delta\hat{\theta}) \in \mathbb{R}^3 \times \mathbb{R}^3 \ \mid \ \hat{\eta}^{\mathrm{s}}|_{\partial_\Phi \hat{\varphi}} = 0\} \subset T\mathcal{C}_t \tag{5.3}$$

if the spatial updating rule for rotations is used; if the material rule is preferred one has that

$$\eta^{\mathrm{m}} = \{\hat{\eta}^{\mathrm{m}} = (\delta\hat{\varphi}, \delta\hat{\Theta}) \in \mathbb{R}^3 \times \mathbb{R}^3 \ \mid \ \hat{\eta}^{\mathrm{s}}|_{\partial_\Phi \hat{\varphi}} = 0\} \subset T\mathcal{C}_t. \tag{5.4}$$

The above definitions allows to construct the expression given in Eq. (3.27) for the tangent space in the spatial form $T_{\hat{x}}\mathcal{B}_t$, which was originally developed following Ref. [245], Eqs. (A.85), (A.86), (A.87) and (A.88). Employing a slight abuse in the notation it is possible to write $\hat{\eta}^{\mathrm{s}}(S) \in T_\Phi \mathcal{C}_t$ *i.e.* the kinematically admissible variation belong to the tangent space to the current configuration $\mathcal{C}_t$ at the material point $\Phi = (\hat{\varphi}, \boldsymbol{\Lambda}) \in \mathcal{C}_t$.

5.1.1 Basic linearized forms

The basic set-up is: given the current configuration space $\mathcal{C}_t$, we consider the spatial description for the admissible variation field $\hat{\eta}^{\mathrm{s}} \in T_\Phi \mathcal{C}_t$ and the corresponding perturbed configuration $\mathcal{C}_{t\beta}$, Eqs. (5.1a) and (5.1b). For the case of the material representation we use $\hat{\eta}^{\mathrm{m}} \in T_\Phi \mathcal{C}_t$. To systematically carry out the linearization process [178, 251, 363, 377] we make use of the notion of directional (Gâteaux) derivative (see §A.5.1) as follows:

$$D\hat{\varphi} \cdot \delta\hat{\varphi} \ \triangleq \ \frac{\mathrm{d}}{\mathrm{d}\beta}\hat{\varphi}_\beta\Big|_{\beta=0} = \delta\hat{\varphi} \tag{5.5a}$$

$$D\boldsymbol{\Lambda} \cdot \delta\widetilde{\boldsymbol{\theta}} = \delta\boldsymbol{\Lambda} \ \triangleq \ \frac{\mathrm{d}}{\mathrm{d}\beta}\boldsymbol{\Lambda}_\beta\Big|_{\beta=0} = \delta\widetilde{\boldsymbol{\theta}}\boldsymbol{\Lambda} \tag{5.5b}$$

$$D\boldsymbol{\Lambda} \cdot \delta\widetilde{\boldsymbol{\Theta}} = \delta\boldsymbol{\Lambda} \ \triangleq \ \frac{\mathrm{d}}{\mathrm{d}\beta}\boldsymbol{\Lambda}_\beta\Big|_{\beta=0} = \boldsymbol{\Lambda}\delta\widetilde{\boldsymbol{\Theta}}. \tag{5.5c}$$

It is well known that the position vector and its linearized increment vector belong to the same vector space, $T_{\hat{x}}\mathcal{B}_t$, then the additive rule for vectors applies to them. Also it is interesting to note that Eqs. (5.5b) and (5.5c) recovers the spatial and material representations of the variation of the rotation tensor given in Eq. (A.98b) of §A.5.5.
Repeating the procedures followed in Eqs. (5.5b) and (5.5c) for the case of the rotation tensor from the curved reference rod to the current rod configuration, $\boldsymbol{\Lambda}_n$, we have the spatial and material representations of the corresponding admissible variation as

$$\delta\boldsymbol{\Lambda}_n = \frac{\mathrm{d}}{\mathrm{d}\beta}\Big|_{\beta=0}\big[\exp[\beta\delta\widetilde{\boldsymbol{\theta}}]\boldsymbol{\Lambda}_n\big] = \delta\widetilde{\boldsymbol{\theta}}\boldsymbol{\Lambda}_n \tag{5.6a}$$

$$\delta\boldsymbol{\Lambda}_n = \frac{\mathrm{d}}{\mathrm{d}\beta}\Big|_{\beta=0}\big[\boldsymbol{\Lambda}_n\exp[\beta\delta\widetilde{\boldsymbol{\Theta}}]\big] = \boldsymbol{\Lambda}_n\delta\widetilde{\boldsymbol{\Theta}}. \tag{5.6b}$$

[3]Note that $(\delta\hat{\varphi}, \delta\hat{\theta}) \approx (\delta\hat{\varphi}, \delta\widetilde{\boldsymbol{\theta}}) \equiv (\delta\hat{\varphi}, \boldsymbol{\Lambda}\delta\widetilde{\boldsymbol{\Theta}}\boldsymbol{\Lambda}^T)$ due to the fact that $(\mathbb{R}^3 \times T^{\mathrm{spa}}_{\boldsymbol{\Lambda}}) \approx (\mathbb{R}^3 \times T^{\mathrm{spa}}_{\boldsymbol{\Lambda}} SO(3)) \approx (\mathbb{R}^3 \times T^{\mathrm{mat}}_{\boldsymbol{\Lambda}} SO(3))$.

Note that in Eqs. (5.5a) and (5.6b) the symbol δ has been included to empathize the infinitesimal nature of the involved quantities. In analogous manner, the spatial and material forms of the admissible variation of the compound orientation tensor $\boldsymbol{\Lambda} = \boldsymbol{\Lambda}_n\boldsymbol{\Lambda}_0$ (see §3.1.1 and §3.1.3) is

$$\delta\boldsymbol{\Lambda} = \frac{\mathrm{d}}{\mathrm{d}\beta}\Big|_{\beta=0}\boldsymbol{\Lambda}_\beta = \Big[\frac{\mathrm{d}(\boldsymbol{\Lambda}_{n\beta}\boldsymbol{\Lambda}_0)}{\mathrm{d}\beta}\Big]\Big|_{\beta=0} = \delta\widetilde{\boldsymbol{\theta}}\boldsymbol{\Lambda}_n\boldsymbol{\Lambda}_0 = \delta\widetilde{\boldsymbol{\theta}}\boldsymbol{\Lambda} \tag{5.7a}$$

$$\delta\boldsymbol{\Lambda} = \frac{\mathrm{d}}{\mathrm{d}\beta}\Big|_{\beta=0}\boldsymbol{\Lambda}_\beta = \Big[\frac{\mathrm{d}(\boldsymbol{\Lambda}_{n\beta}\boldsymbol{\Lambda}_0)}{\mathrm{d}\beta}\Big]\Big|_{\beta=0} = \boldsymbol{\Lambda}_0\boldsymbol{\Lambda}_n\delta\widetilde{\boldsymbol{\Theta}} = \boldsymbol{\Lambda}\delta\widetilde{\boldsymbol{\Theta}} \tag{5.7b}$$

due to the fact that $\boldsymbol{\Lambda}_0$ is fixed in space and time.

5.1.2 Linearization of the strain measures

Since the admissible variations of the orthogonal tensor and the displacement fields of the current rod referred to the curved reference rod have been determined, other relevant linearized forms can be obtained using the chain rule for partial derivatives. An important aspect to be mentioned is given by the fact it has been assumed that variations and temporal derivatives commute, which is also a common assumption in continuum mechanics, however, it implies that all the considered restrictions are *holonomic*; more details can be consulted in [245]. In this section the admissible variations of strain measures given in Table 3.1 are calculated.

5.1.2.a Translational strains

Considering the spatial updating rule for rotations for the admissible variation field $\hat{\eta}^{\mathrm{s}} = (\delta\hat{\varphi}, \delta\hat{\theta}) \approx (\delta\hat{\varphi}, \delta\widetilde{\boldsymbol{\theta}})$, the spatial form of the translational strain vector, $\hat{\gamma}_n = \hat{\varphi}_{,S} - \hat{t}_1$, the results given in Eq. (5.6a) and the fact that $\hat{t}_1 = \boldsymbol{\Lambda}_n\hat{t}_{01}$, one has the following derivation for the linearized form of $\hat{\gamma}_n$:

$$\begin{aligned} D\hat{\gamma}_n\cdot\hat{\eta}^{\mathrm{s}} = \delta\hat{\gamma}_n &\triangleq \frac{\mathrm{d}}{\mathrm{d}\beta}\hat{\gamma}_{m\beta}\Big|_{\beta=0} \\ &= \delta(\hat{\varphi}_{,S} - \hat{t}_1) = \delta\hat{\varphi}_{,S} - \delta(\boldsymbol{\Lambda}_n\hat{t}_{01}) \\ &= \delta\hat{\varphi}_{,S} - \delta\boldsymbol{\Lambda}_n\hat{t}_{01} = \delta\hat{\varphi}_{,S} - \delta\widetilde{\boldsymbol{\theta}}\boldsymbol{\Lambda}_n\hat{t}_{01} = \delta\hat{\varphi}_{,S} - \delta\widetilde{\boldsymbol{\theta}}\hat{t}_1 \\ &= \delta\hat{\varphi}_{,S} + \widetilde{\boldsymbol{t}}_1\delta\hat{\theta} \end{aligned} \tag{5.8a}$$

where $\widetilde{\boldsymbol{t}}_1 = \boldsymbol{\Pi}[\hat{t}_1]$ is the skew–symmetric tensor obtained from $\hat{t}_1 \in \mathbb{R}^3$. In the case of the material form of the translational strain vector, $\hat{\Gamma}_n = \boldsymbol{\Lambda}^T\hat{\gamma}_n$, and noticing from Eq. (5.6a) the fact that $\delta\boldsymbol{\Lambda}^T = -\boldsymbol{\Lambda}^T\delta\widetilde{\boldsymbol{\theta}}$, one obtains that

$$\begin{aligned} D\hat{\Gamma}_n\cdot\hat{\eta}^{\mathrm{s}} = \delta\hat{\Gamma}_n &\triangleq \frac{\mathrm{d}}{\mathrm{d}\beta}\hat{\Gamma}_{n\beta}\Big|_{\beta=0} \\ &= \delta(\boldsymbol{\Lambda}^T\hat{\gamma}_n) = \delta\boldsymbol{\Lambda}^T\hat{\gamma}_n + \boldsymbol{\Lambda}^T\delta\hat{\gamma}_n \\ &= -\boldsymbol{\Lambda}^T\delta\widetilde{\boldsymbol{\theta}}(\hat{\varphi}_{,S} - \hat{t}_1) + \boldsymbol{\Lambda}^T(\delta\hat{\varphi}_{,S} - \delta\widetilde{\boldsymbol{\theta}}\hat{t}_1) \\ &= \boldsymbol{\Lambda}^T\big[-\delta\widetilde{\boldsymbol{\theta}}(\hat{\varphi}_{,S} - \hat{t}_1) + \delta\hat{\varphi}_{,S} - \delta\widetilde{\boldsymbol{\theta}}\hat{t}_1\big] = \boldsymbol{\Lambda}^T(\delta\hat{\varphi}_{,S} - \delta\widetilde{\boldsymbol{\theta}}\hat{\varphi}_{,S}) \\ &= \boldsymbol{\Lambda}^T(\delta\hat{\varphi}_{,S} + \boldsymbol{\Pi}[\hat{\varphi}_{,S}]\delta\hat{\theta}). \end{aligned} \tag{5.8b}$$

Employing the result of Eqs. (5.8a) and (5.8b) and the definition of Lie variation given in Eq. (A.96) it is possible to show that the Lie or co–rotated variation of the translational strain

vector, $\delta[\overset{\triangledown}{\hat{\gamma}}_n]$, is given by

$$\delta_{\mathbf{\Lambda}}[\hat{\gamma}_n] = \delta[\overset{\triangledown}{\hat{\gamma}}_n] = \mathbf{\Lambda}\delta\hat{\Gamma}_n = \delta\hat{\varphi}_{,S} + \widetilde{\boldsymbol{\varphi}}_{,S}\,\delta\hat{\theta} \tag{5.8c}$$

where $\widetilde{\boldsymbol{\varphi}}_{,S} = \mathbf{\Pi}[\hat{\varphi}_{,S}\,] \in so(3)$.

5.1.2.b Rotational strains

Similarly, considering the spatial form of the incremental curvature strain tensor, Eq. (3.38a), *i.e.* $\widetilde{\boldsymbol{\omega}}_n = \mathbf{\Lambda}_{n,S}\,\mathbf{\Lambda}_n^T$, (or equivalently its corresponding axial vector) and the fact that $\delta\mathbf{\Lambda}_n^T = -\mathbf{\Lambda}_n^T\delta\widetilde{\boldsymbol{\theta}}$, one obtains that

$$\begin{aligned}
D\widetilde{\boldsymbol{\omega}}_n\cdot\delta\widetilde{\boldsymbol{\theta}} = \delta\widetilde{\boldsymbol{\omega}}_n \;&\triangleq\; \frac{\mathrm{d}}{\mathrm{d}\beta}\widetilde{\boldsymbol{\omega}}_{n\beta}\Big|_{\beta=0} = \delta(\mathbf{\Lambda}_{n,S}\,\mathbf{\Lambda}_n^T)\\
&= \delta\mathbf{\Lambda}_{n,S}\,\mathbf{\Lambda}_n^T + \mathbf{\Lambda}_{n,S}\,\delta\mathbf{\Lambda}_n^T = (\delta\mathbf{\Lambda}_n)_{,S}\,\mathbf{\Lambda}_n^T + \mathbf{\Lambda}_{n,S}\,(-\mathbf{\Lambda}_n^T\delta\widetilde{\boldsymbol{\theta}})\\
&= (\delta\widetilde{\boldsymbol{\theta}}\mathbf{\Lambda}_n)_{,S}\,\mathbf{\Lambda}_n^T - \mathbf{\Lambda}_{n,S}\,\mathbf{\Lambda}_n^T\delta\widetilde{\boldsymbol{\theta}}\\
&= (\delta\widetilde{\boldsymbol{\theta}}_{,S}\,\mathbf{\Lambda}_n + \delta\widetilde{\boldsymbol{\theta}}\mathbf{\Lambda}_{n,S}\,)\mathbf{\Lambda}_n^T - \mathbf{\Lambda}_{n,S}\,\mathbf{\Lambda}_n^T\delta\widetilde{\boldsymbol{\theta}}\\
&= \delta\widetilde{\boldsymbol{\theta}}_{,S}\,\mathbf{\Lambda}_n\mathbf{\Lambda}_n^T + \delta\widetilde{\boldsymbol{\theta}}\mathbf{\Lambda}_{n,S}\,\mathbf{\Lambda}_n^T - \mathbf{\Lambda}_{n,S}\,\mathbf{\Lambda}_n^T\delta\widetilde{\boldsymbol{\theta}}\\
&= \delta\widetilde{\boldsymbol{\theta}}_{,S} + \delta\widetilde{\boldsymbol{\theta}}\widetilde{\boldsymbol{\omega}}_n - \widetilde{\boldsymbol{\omega}}_n\delta\widetilde{\boldsymbol{\theta}}\\
&= \delta\widetilde{\boldsymbol{\theta}}_{,S} + \mathbf{\Pi}[\delta\hat{\theta}\times\hat{\omega}_n] = \delta\widetilde{\boldsymbol{\theta}}_{,S} + [\delta\widetilde{\boldsymbol{\theta}},\widetilde{\boldsymbol{\omega}}_n].
\end{aligned} \tag{5.9a}$$

For the case of the material form of the incremental curvature tensor, we obtain

$$\begin{aligned}
D\widetilde{\mathbf{\Omega}}_n\cdot\delta\widetilde{\boldsymbol{\theta}} = \delta\widetilde{\mathbf{\Omega}}_n \;&\triangleq\; \frac{\mathrm{d}}{\mathrm{d}\beta}\widetilde{\mathbf{\Omega}}_{n\beta}\Big|_{\beta=0} = \mathbf{\Lambda}_0^T\delta(\mathbf{\Lambda}_n^T\mathbf{\Lambda}_{n,S}\,)\mathbf{\Lambda}_0\\
&= \mathbf{\Lambda}_0^T\Big[\mathbf{\Lambda}_n^T\delta\mathbf{\Lambda}_{n,S} + \delta\mathbf{\Lambda}_n^T\mathbf{\Lambda}_{n,S}\Big]\mathbf{\Lambda}_0\\
&= \mathbf{\Lambda}_0^T\Big[\mathbf{\Lambda}_n^T(\delta\mathbf{\Lambda}_n)_{,S} - \mathbf{\Lambda}_n^T\delta\widetilde{\boldsymbol{\theta}}\mathbf{\Lambda}_{n,S}\Big]\mathbf{\Lambda}_0\\
&= \mathbf{\Lambda}_0^T\Big[\mathbf{\Lambda}_n^T(\delta\widetilde{\boldsymbol{\theta}}\mathbf{\Lambda}_n)_{,S} - \mathbf{\Lambda}_n^T\delta\widetilde{\boldsymbol{\theta}}\mathbf{\Lambda}_{n,S}\Big]\mathbf{\Lambda}_0\\
&= \mathbf{\Lambda}_0^T\Big[\mathbf{\Lambda}_n^T(\delta\widetilde{\boldsymbol{\theta}}_{,S}\,\mathbf{\Lambda}_n + \delta\widetilde{\boldsymbol{\theta}}\mathbf{\Lambda}_{n,S}\,) - \mathbf{\Lambda}_n^T\delta\widetilde{\boldsymbol{\theta}}\mathbf{\Lambda}_{n,S}\Big]\mathbf{\Lambda}_0\\
&= \mathbf{\Lambda}^T\delta\widetilde{\boldsymbol{\theta}}_{,S}\,\mathbf{\Lambda}.
\end{aligned} \tag{5.9b}$$

Then, the co–rotated variation of the rotational strain tensor is then given by

$$\delta_{\mathbf{\Lambda}}[\widetilde{\boldsymbol{\omega}}_n] = \delta[\overset{\triangledown}{\widetilde{\boldsymbol{\omega}}}_n] = \mathbf{\Lambda}\delta\widetilde{\mathbf{\Omega}}_n\mathbf{\Lambda}^T = \delta\widetilde{\boldsymbol{\theta}}_{,S}\,. \tag{5.9c}$$

Employing the fact that for any two vectors $\hat{v}_1,\hat{v}_2 \in \mathbb{R}^3$ it is possible to define a third vector $\hat{v} = \hat{v}_1\times\hat{v}_2$ and to define the skew–symmetric tensor constructed from $\hat{v}$, $\mathbf{\Pi}[\hat{v}] \equiv \widetilde{\boldsymbol{v}}$, which has the following property: $\widetilde{\boldsymbol{v}} = \widetilde{\boldsymbol{v}}_1\widetilde{\boldsymbol{v}}_2 - \widetilde{\boldsymbol{v}}_2\widetilde{\boldsymbol{v}}_1 = [\widetilde{\boldsymbol{v}}_1,\widetilde{\boldsymbol{v}}_2]$ (Lie brackets, see Def. A.5 of Appendix A); then, we can rewrite Eq. (5.9a) in terms of axial vectors as

$$D\hat{\omega}_n\cdot\delta\hat{\theta} = \delta\hat{\omega}_n = \delta\hat{\theta}_{,S} + \delta\widetilde{\boldsymbol{\theta}}\hat{\omega}_n = \delta\hat{\theta}_{,S} - \widetilde{\boldsymbol{\omega}}_n\delta\hat{\theta}. \tag{5.10a}$$

Considering that the material form of the curvature vector is obtained by means of the pullback operator by the rotation tensor $\mathbf{\Lambda}$ acting on its spatial form as given by Eq. (3.39e), $\widehat{\Omega}_n = \mathbf{\Lambda}^T\hat{\omega}_n$,

one obtains that

$$\begin{aligned} D\hat{\Omega}_n \cdot \delta\hat{\theta} = \delta\hat{\Omega}_n &\triangleq \frac{\mathrm{d}}{\mathrm{d}\beta}\hat{\Omega}_{n\beta}\Big|_{\beta=0} = \delta(\boldsymbol{\Lambda}^T\hat{\omega}_n) \\ &= \delta\boldsymbol{\Lambda}^T\hat{\omega}_n + \boldsymbol{\Lambda}^T\delta\hat{\omega}_n \\ &= -\boldsymbol{\Lambda}^T\delta\widetilde{\boldsymbol{\theta}}\hat{\omega}_n + \boldsymbol{\Lambda}^T(\delta\hat{\theta}_{,S} - \widetilde{\omega}\delta\hat{\theta}) \\ &= \boldsymbol{\Lambda}^T\delta\hat{\theta}_{,S}\,. \end{aligned} \tag{5.10b}$$

The above results allow to obtain the co–rotated variation of the curvature strain vector as

$$\delta_{\boldsymbol{\Lambda}}[\hat{\omega}_n] = \delta[\overset{\triangledown}{\hat{\omega}_n}] = \boldsymbol{\Lambda}\delta\hat{\Omega}_n = \delta\hat{\theta}_{,S} \tag{5.10c}$$

and considering Eq. (5.10a) the following identity is obtained: $\delta\hat{\theta}_{,S} = \delta\hat{\omega}_n + \widetilde{\boldsymbol{\omega}}_n\delta\hat{\theta}$. This result allows to rewrite Eqs. (5.10b) and (5.10c) as

$$\delta\hat{\Omega}_n = \boldsymbol{\Lambda}^T(\delta\hat{\omega}_n + \widetilde{\boldsymbol{\omega}}_n\delta\hat{\theta}) \tag{5.11a}$$

$$\delta[\overset{\triangledown}{\hat{\omega}_n}] = \delta\hat{\theta}_{,S} = \delta\hat{\omega}_n + \widetilde{\boldsymbol{\omega}}_n\delta\hat{\theta}, \tag{5.11b}$$

respectively. If $\delta\hat{\theta}$ ($\delta\hat{\Theta}$) is parameterized in terms of other kind of pseudo–vectors as those described in §A.2.6 and summarized in Table A.1, the deduction of the admissible variations of the strain vectors and tensors is more complicated and it will be omitted here.
Summarizing the above results in matrix form, we can rewrite Eqs. (5.8a) to (5.11b) as

$$\begin{bmatrix} \delta\hat{\gamma}_n \\ \delta\hat{\omega}_n \end{bmatrix} = \underbrace{\begin{bmatrix} [\frac{\mathrm{d}}{\mathrm{d}S}\mathbf{I}] & \widetilde{\boldsymbol{t}}_1 \\ 0 & ([\frac{\mathrm{d}}{\mathrm{d}S}\mathbf{I}] - \widetilde{\boldsymbol{\omega}}_n) \end{bmatrix}}_{\boldsymbol{B}^{\mathrm{s}}(\hat{\varphi},\boldsymbol{\Lambda})} \begin{bmatrix} \delta\hat{\varphi} \\ \delta\hat{\theta} \end{bmatrix} = \boldsymbol{B}^{\mathrm{s}}(\hat{\varphi},\Lambda)\hat{\eta}^{\mathrm{s}} \tag{5.12a}$$

$$\begin{bmatrix} \delta\hat{\Gamma}_n \\ \delta\hat{\Omega}_n \end{bmatrix} = \underbrace{\begin{bmatrix} \boldsymbol{\Lambda}^T[\frac{\mathrm{d}}{\mathrm{d}S}\mathbf{I}] & \boldsymbol{\Lambda}^T\boldsymbol{\Pi}[\hat{\varphi}_{,S}\,] \\ 0 & \boldsymbol{\Lambda}^T[\frac{\mathrm{d}}{\mathrm{d}S}\mathbf{I}] \end{bmatrix}}_{\bar{\boldsymbol{B}}^{\mathrm{s}}(\hat{\varphi},\boldsymbol{\Lambda})} \begin{bmatrix} \delta\hat{\varphi} \\ \delta\hat{\theta} \end{bmatrix} = \bar{\boldsymbol{B}}^{\mathrm{s}}(\hat{\varphi},\Lambda)\hat{\eta}^{\mathrm{s}} \tag{5.12b}$$

for the admissible variations of the spatial and material descriptions of the strain vectors, respectively. The operator $[\frac{\mathrm{d}}{\mathrm{d}S}\mathbf{I}]$ is defined as $[\frac{\mathrm{d}}{\mathrm{d}S}\mathbf{I}](\bullet) = \mathbf{I}\cdot(\bullet)_{,S}$. The corresponding expressions for the co–rotated variations are rearranged as

$$\begin{bmatrix} \overset{\triangledown}{\delta[\hat{\gamma}_n]} \\ \overset{\triangledown}{\delta[\hat{\omega}_n]} \end{bmatrix} = \underbrace{\begin{bmatrix} [\frac{\mathrm{d}}{\mathrm{d}S}\mathbf{I}] & \boldsymbol{\Pi}[\hat{\varphi}_{,S}\,] \\ 0 & [\frac{\mathrm{d}}{\mathrm{d}S}\mathbf{I}] \end{bmatrix}}_{\boldsymbol{B}(\hat{\varphi})} \begin{bmatrix} \delta\hat{\varphi} \\ \delta\hat{\theta} \end{bmatrix} = \boldsymbol{B}(\hat{\varphi})\cdot\hat{\eta}^{\mathrm{s}} = (\mathbf{I}_{\boldsymbol{\Lambda}}\bar{\boldsymbol{B}}^{\mathrm{s}})\hat{\eta}^{\mathrm{s}} \tag{5.12c}$$

where $\mathbf{I}_{\boldsymbol{\Lambda}}$ is a (6×6) matrix formed by four (3×3) blocks. The blocks located on and above the diagonal are equal to $\boldsymbol{\Lambda}$ and the another one is zero. This matrix perform the push–forward operation on $\bar{\boldsymbol{B}}(\hat{\varphi},\boldsymbol{\Lambda})$.

5.1.2.c Material updating of the rotational field

Alternatively, if the material updating procedure is chosen for the rotational field *i.e.* $\hat{\eta}^{\mathrm{m}} = (\delta\hat{\varphi}, \delta\hat{\Theta})$, we obtain the following expressions for the spatial, material and co–rotated versions

of the translational strain vector:

$$\begin{aligned} D\hat{\gamma}_n \cdot \hat{\eta}^{\mathrm{m}} = \delta\hat{\gamma}_n &= \delta\hat{\varphi}_{,S} - \delta\boldsymbol{\Lambda}\hat{E}_1 = \delta\hat{\varphi}_{,S} - \boldsymbol{\Lambda}\delta\widetilde{\boldsymbol{\Theta}}\hat{E}_1 \\ &= \delta\hat{\varphi}_{,S} + \boldsymbol{\Lambda}\widetilde{\boldsymbol{E}}_1\delta\hat{\Theta} \qquad (5.13a) \\ D\hat{\Gamma}_n \cdot \hat{\eta}^{\mathrm{m}} \equiv \delta\hat{\Gamma}_n &= \delta[\boldsymbol{\Lambda}^T\hat{\gamma}_n] = \delta\boldsymbol{\Lambda}^T\hat{\gamma}_n + \boldsymbol{\Lambda}^T\delta\hat{\gamma}_n \\ &= -\delta\widetilde{\boldsymbol{\Theta}}\boldsymbol{\Lambda}^T\hat{\varphi}_{,S} + \boldsymbol{\Lambda}^T\delta\hat{\varphi}_{,S} \\ &= \boldsymbol{\Pi}[\boldsymbol{\Lambda}^T\hat{\varphi}_{,S}]\delta\hat{\Theta} + \boldsymbol{\Lambda}^T\delta\hat{\varphi}_{,S} \qquad (5.13b) \\ \delta_{\boldsymbol{\Lambda}}[\hat{\gamma}_n] = \delta[\overset{\triangledown}{\hat{\gamma}_n}] &= \boldsymbol{\Lambda}\delta\hat{\Gamma}_n = \delta\hat{\varphi}_{,S} + \boldsymbol{\Lambda}\boldsymbol{\Pi}[\boldsymbol{\Lambda}^T\hat{\varphi}_{,S}]\delta\hat{\Theta} \\ &= \delta\hat{\varphi}_{,S} + \boldsymbol{\Pi}[\hat{\varphi}_{,S}]\delta\hat{\theta}. \qquad (5.13c) \end{aligned}$$

Eqs. (5.13a), (5.13b) and (5.13c) are completely equivalent to those given in Eqs. (5.8a), (5.8b) and (5.8c) provided that $\delta\widetilde{\boldsymbol{\Theta}} = \boldsymbol{\Lambda}^T\delta\widetilde{\boldsymbol{\theta}}\boldsymbol{\Lambda}$.
For the case of the spatial, material and co–rotated version of curvature tensors, we have

$$\begin{aligned} D\widetilde{\boldsymbol{\omega}}_n \cdot \delta\widetilde{\boldsymbol{\Theta}} = \delta\widetilde{\boldsymbol{\omega}}_n &= \underset{\rightarrow}{\boldsymbol{\Lambda}_n}(\delta\widetilde{\boldsymbol{\Theta}}_{,S}) = (\delta\boldsymbol{\Lambda}_n)_{,S}\,\boldsymbol{\Lambda}_n^T + \boldsymbol{\Lambda}_{n,S}\,(\delta\boldsymbol{\Lambda}_n)^T \\ &= (\boldsymbol{\Lambda}_{n,S}\,\delta\widetilde{\boldsymbol{\Theta}} + \boldsymbol{\Lambda}_n\delta\widetilde{\boldsymbol{\Theta}}_{,S})\boldsymbol{\Lambda}_n^T - \boldsymbol{\Lambda}_{n,S}\,\delta\widetilde{\boldsymbol{\Theta}}\boldsymbol{\Lambda}_n^T \\ &= \boldsymbol{\Lambda}_n\delta\widetilde{\boldsymbol{\Theta}}_{,S}\,\boldsymbol{\Lambda}_n^T \qquad (5.14a) \\ D\widetilde{\boldsymbol{\Omega}}_n \cdot \delta\widetilde{\boldsymbol{\Theta}} = \delta\widetilde{\boldsymbol{\Omega}}_n &= \delta(\boldsymbol{\Lambda}^T\widetilde{\boldsymbol{\omega}}_n\boldsymbol{\Lambda}) = (\delta\boldsymbol{\Lambda})^T\widetilde{\boldsymbol{\omega}}_n\boldsymbol{\Lambda} + \boldsymbol{\Lambda}^T\delta\widetilde{\boldsymbol{\omega}}_n\boldsymbol{\Lambda} + \boldsymbol{\Lambda}^T\widetilde{\boldsymbol{\omega}}_n\delta\boldsymbol{\Lambda} \\ &= -\delta\widetilde{\boldsymbol{\Theta}}\boldsymbol{\Lambda}^T\widetilde{\boldsymbol{\omega}}_n\boldsymbol{\Lambda} + \delta\widetilde{\boldsymbol{\Theta}}_{,S} + \boldsymbol{\Lambda}^T\widetilde{\boldsymbol{\omega}}_n\boldsymbol{\Lambda}\delta\widetilde{\boldsymbol{\Theta}} \\ &= \delta\widetilde{\boldsymbol{\Theta}}_{,S} + \widetilde{\boldsymbol{\Omega}}_n\delta\widetilde{\boldsymbol{\Theta}} - \delta\widetilde{\boldsymbol{\Theta}}\widetilde{\boldsymbol{\Omega}}_n \\ &= \delta\widetilde{\boldsymbol{\Theta}}_{,S} + [\widetilde{\boldsymbol{\Omega}}_n, \delta\widetilde{\boldsymbol{\Theta}}] \qquad (5.14b) \\ \delta[\overset{\triangledown}{\widetilde{\boldsymbol{\omega}}_n}] &= \boldsymbol{\Lambda}\delta\widetilde{\boldsymbol{\Omega}}_n\boldsymbol{\Lambda}^T = \boldsymbol{\Lambda}[\delta\widetilde{\boldsymbol{\Theta}}_{,S} + \widetilde{\boldsymbol{\Omega}}_n\delta\widetilde{\boldsymbol{\Theta}} - \delta\widetilde{\boldsymbol{\Theta}}\widetilde{\boldsymbol{\Omega}}_n]\boldsymbol{\Lambda}^T \\ &= \underset{\rightarrow}{\boldsymbol{\Lambda}}(\delta\widetilde{\boldsymbol{\Theta}}_{,S} + [\widetilde{\boldsymbol{\Omega}}_n, \delta\widetilde{\boldsymbol{\Theta}}]) = \delta\widetilde{\boldsymbol{\theta}}_{,S} \qquad (5.14c) \end{aligned}$$

with the following relations for the associated axial vectors:

$$\begin{aligned} D\hat{\omega}_n \cdot \delta\hat{\Theta} = \delta\hat{\omega}_n &= \boldsymbol{\Lambda}_n\delta\hat{\Theta}_{,S} \qquad (5.15a) \\ D\hat{\Omega}_n \cdot \delta\hat{\Theta} = \delta\hat{\Omega}_n &= \delta\hat{\Theta}_{,S} + \widetilde{\boldsymbol{\Omega}}_n\delta\hat{\Theta} \qquad (5.15b) \\ \delta[\overset{\triangledown}{\hat{\omega}_n}] &= \boldsymbol{\Lambda}\delta\hat{\Omega}_n = \boldsymbol{\Lambda}\delta\hat{\Theta}_{,S} + \widetilde{\boldsymbol{\omega}}_n\boldsymbol{\Lambda}\delta\hat{\Theta}. \qquad (5.15c) \end{aligned}$$

Summarizing the above results in matrix form, we can rewrite Eqs. (5.13a) to (5.15c) as

$$\begin{bmatrix} \delta\hat{\gamma}_n \\ \delta\hat{\omega}_n \end{bmatrix} = \underbrace{\begin{bmatrix} [\frac{\mathrm{d}}{\mathrm{d}S}\mathbf{I}] & \boldsymbol{\Lambda}\widetilde{\boldsymbol{E}}_1 \\ 0 & \boldsymbol{\Lambda}_n[\frac{\mathrm{d}}{\mathrm{d}S}\mathbf{I}] \end{bmatrix}}_{\boldsymbol{B}^{\mathrm{m}}(\hat{\varphi},\boldsymbol{\Lambda})} \begin{bmatrix} \delta\hat{\varphi} \\ \delta\hat{\Theta} \end{bmatrix} = \boldsymbol{B}^{\mathrm{m}}(\hat{\varphi},\boldsymbol{\Lambda})\hat{\eta}^{\mathrm{m}} \qquad (5.16a)$$

$$\begin{bmatrix} \delta\hat{\Gamma}_n \\ \delta\hat{\Omega}_n \end{bmatrix} = \underbrace{\begin{bmatrix} \boldsymbol{\Lambda}^T[\frac{\mathrm{d}}{\mathrm{d}S}\mathbf{I}] & \boldsymbol{\Pi}[\boldsymbol{\Lambda}^T\hat{\varphi}_{,S}] \\ 0 & \big([\frac{\mathrm{d}}{\mathrm{d}S}\mathbf{I}] + \widetilde{\boldsymbol{\Omega}}_n\big) \end{bmatrix}}_{\bar{\boldsymbol{B}}^{\mathrm{m}}(\hat{\varphi},\boldsymbol{\Lambda})} \begin{bmatrix} \delta\hat{\varphi} \\ \delta\hat{\Theta} \end{bmatrix} = \bar{\boldsymbol{B}}^{\mathrm{m}}(\hat{\varphi},\boldsymbol{\Lambda})\hat{\eta}^{\mathrm{m}} \qquad (5.16b)$$

for the admissible variations of the spatial and material descriptions of the strain vectors, respectively; the co–rotated admissible variations is written in matrix form as

$$\begin{bmatrix} \overset{\triangledown}{\delta[\hat{\gamma}_n]} \\ \overset{\triangledown}{\delta[\hat{\omega}_n]} \end{bmatrix} = \underbrace{\begin{bmatrix} [\frac{\mathrm{d}}{\mathrm{d}S}\mathbf{I}] & \boldsymbol{\Lambda}\boldsymbol{\Pi}[\boldsymbol{\Lambda}^T\hat{\varphi}_{,S}\,] \\ 0 & \boldsymbol{\Lambda}[\frac{\mathrm{d}}{\mathrm{d}S}\mathbf{I} + \widetilde{\boldsymbol{\Omega}}_n] \end{bmatrix}}_{\bar{\boldsymbol{B}}(\hat{\varphi},\boldsymbol{\Lambda})} \begin{bmatrix} \delta\hat{\varphi} \\ \delta\hat{\Theta} \end{bmatrix} = \bar{\boldsymbol{B}}(\hat{\varphi},\boldsymbol{\Lambda})\hat{\eta}^{\mathrm{m}}. \tag{5.16c}$$

Additionally, a summarization of the linearized forms of the spatial and material versions of reduced strain measures considering the spatial and material updating rule for the rotational part is presented in Tables 5.1 and 5.2.

Table 5.1: Linearized forms of the translational strains.

	$\delta\hat{\gamma}_n$	$\delta\hat{\Gamma}_n$	$\overset{\triangledown}{\delta[\hat{\gamma}_n]}$
$\hat{\eta}^{\mathrm{s}}$	$\delta\hat{\varphi}_{,S} + \widetilde{\boldsymbol{t}}_1\delta\hat{\theta}$	$\boldsymbol{\Lambda}^T(\delta\hat{\varphi}_{,S} + \boldsymbol{\Pi}[\hat{\varphi}_{,S}\,]\delta\hat{\theta})$	$\delta\hat{\varphi}_{,S} + \boldsymbol{\Pi}[\hat{\varphi}_{,S}\,]\delta\hat{\theta}$
$\hat{\eta}^{\mathrm{m}}$	$\delta\hat{\varphi}_{,S} + \boldsymbol{\Lambda}\widetilde{\boldsymbol{E}}_1\delta\hat{\Theta}$	$\boldsymbol{\Pi}[\boldsymbol{\Lambda}^T\hat{\varphi}_{,S}\,]\delta\hat{\Theta} + \boldsymbol{\Lambda}^T\delta\hat{\varphi}_{,S}$	$\delta\hat{\varphi}_{,S} + \boldsymbol{\Pi}[\hat{\varphi}_{,S}\,]\boldsymbol{\Lambda}\delta\hat{\Theta}$

Table 5.2: Linearized forms of the rotational strains.

	$\delta\widetilde{\boldsymbol{\omega}}_n$	$\delta\widetilde{\boldsymbol{\Omega}}_n$	$\overset{\triangledown}{\delta[\widetilde{\boldsymbol{\omega}}_n]}$	$\delta\hat{\omega}_n$	$\delta\hat{\Omega}_n$	$\overset{\triangledown}{\delta[\hat{\omega}_n]}$
$\hat{\eta}^{\mathrm{s}}$	$\delta\widetilde{\boldsymbol{\theta}}_{,S} + [\delta\widetilde{\boldsymbol{\theta}}, \widetilde{\boldsymbol{\omega}}_n]$	$\boldsymbol{\Lambda}^T\delta\widetilde{\boldsymbol{\theta}}_{,S}\,\boldsymbol{\Lambda}$	$\delta\widetilde{\boldsymbol{\theta}}_{,S}$	$\delta\hat{\theta}_{,S} - \widetilde{\boldsymbol{\omega}}_n\delta\hat{\theta}$	$\boldsymbol{\Lambda}^T\delta\hat{\theta}_{,S}$	$\delta\hat{\theta}_{,S}$
$\hat{\eta}^{\mathrm{m}}$	$\boldsymbol{\Lambda}_n\delta\widetilde{\boldsymbol{\Theta}}_{,S}\,\boldsymbol{\Lambda}_n^T$	$\delta\widetilde{\boldsymbol{\Theta}}_{,S} + [\widetilde{\boldsymbol{\Omega}}_n, \delta\widetilde{\boldsymbol{\Theta}}]$	$\delta\widetilde{\boldsymbol{\theta}}_{,S}$	$\boldsymbol{\Lambda}_n\delta\hat{\Theta}_{,S}$	$\delta\hat{\Theta}_{,S} + \widetilde{\boldsymbol{\Omega}}_n\delta\hat{\Theta}$	$\delta\hat{\theta}_{,S}$

5.1.3 Linearization of the spin variables

Considering the spatial description of the admissible variation of the current rod configuration $\hat{\eta}^{\mathrm{s}} \approx (\delta\hat{\varphi}, \delta\widetilde{\boldsymbol{\theta}})$, and the spatial form of the angular velocity tensor $\widetilde{\boldsymbol{v}}_n = \dot{\boldsymbol{\Lambda}}_n\boldsymbol{\Lambda}_n^T \in T^{\mathrm{spa}}_{\boldsymbol{\Lambda}}SO(3)$ of the current rod relative to the curved reference rod, Eq. (3.31b), one obtains the following linearized form

$$\begin{aligned} D\widetilde{\boldsymbol{v}}_n \cdot \delta\widetilde{\boldsymbol{\theta}} = \delta\widetilde{\boldsymbol{v}}_n &\triangleq \delta\big(\dot{\boldsymbol{\Lambda}}_n\boldsymbol{\Lambda}_n^T\big) = (\delta\dot{\boldsymbol{\Lambda}}_n)\boldsymbol{\Lambda}_n^T + \dot{\boldsymbol{\Lambda}}_n(\delta\boldsymbol{\Lambda}_n^T) \\ &= (\delta\dot{\widetilde{\boldsymbol{\theta}}}\boldsymbol{\Lambda}_n + \delta\widetilde{\boldsymbol{\theta}}\dot{\boldsymbol{\Lambda}}_n)\boldsymbol{\Lambda}_n^T + \dot{\boldsymbol{\Lambda}}_n(-\boldsymbol{\Lambda}_n^T\delta\widetilde{\boldsymbol{\theta}}) \\ &= \delta\dot{\widetilde{\boldsymbol{\theta}}}\boldsymbol{\Lambda}_n\boldsymbol{\Lambda}_n^T + \delta\widetilde{\boldsymbol{\theta}}\dot{\boldsymbol{\Lambda}}_n\boldsymbol{\Lambda}_n^T - \dot{\boldsymbol{\Lambda}}_n\boldsymbol{\Lambda}_n^T\delta\widetilde{\boldsymbol{\theta}} \\ &= \delta\dot{\widetilde{\boldsymbol{\theta}}} + \delta\widetilde{\boldsymbol{\theta}}\widetilde{\boldsymbol{v}}_n - \widetilde{\boldsymbol{v}}_n\delta\widetilde{\boldsymbol{\theta}} \\ &= \delta\dot{\widetilde{\boldsymbol{\theta}}} + [\delta\widetilde{\boldsymbol{\theta}}, \widetilde{\boldsymbol{v}}_n]. \end{aligned} \tag{5.17a}$$

The admissible variation of the axial vector of $\widetilde{\boldsymbol{v}}_n$, the angular velocity vector, $\hat{v}_n \in T^{\mathrm{spa}}_{\boldsymbol{\Lambda}}$, is

$$D\hat{v}_n \cdot \delta\hat{\theta} = \delta\hat{v}_n = \delta\dot{\hat{\theta}} - \widetilde{\boldsymbol{v}}_n\delta\hat{\theta}. \tag{5.17b}$$

By the other hand, considering the spatial form of the angular acceleration tensor of the current rod referred to the curved reference rod $\dot{\widetilde{\boldsymbol{v}}}_n = \dot{\boldsymbol{\Lambda}}_n\dot{\boldsymbol{\Lambda}}_n^T + \ddot{\boldsymbol{\Lambda}}_n\boldsymbol{\Lambda}_n^T \in T^{\mathrm{spa}}_{\boldsymbol{\Lambda}}SO(3)$, Eq. (A.121), we

obtain that its admissible variation can be expressed as

$$D\dot{\widetilde{\boldsymbol{v}}}_n \cdot \delta\widetilde{\boldsymbol{\theta}} = \delta\widetilde{\boldsymbol{\alpha}}_n = (\delta\dot{\boldsymbol{\Lambda}}_n)\dot{\boldsymbol{\Lambda}}_n^T + \dot{\boldsymbol{\Lambda}}_n(\delta\dot{\boldsymbol{\Lambda}}_n^T) + (\delta\ddot{\boldsymbol{\Lambda}}_n)\boldsymbol{\Lambda}_n^T + \ddot{\boldsymbol{\Lambda}}_n\delta\boldsymbol{\Lambda}_n^T.$$

Prior to obtain an explicit expression for the linear form, we have to consider the following results:

$$\begin{aligned}
\delta(\dot{\boldsymbol{\Lambda}}_n^T) &= (\delta(\dot{\boldsymbol{\Lambda}}_n^T)) = ((\delta\widetilde{\boldsymbol{\theta}}\dot{\boldsymbol{\Lambda}}_n)^T) = -\dot{\boldsymbol{\Lambda}}_n^T\delta\widetilde{\boldsymbol{\theta}} - \boldsymbol{\Lambda}_n^T\delta\dot{\widetilde{\boldsymbol{\theta}}} \\
\delta(\dot{\boldsymbol{\Lambda}}_n) &= (\delta\widetilde{\boldsymbol{\theta}}\dot{\boldsymbol{\Lambda}}_n) = \delta\dot{\widetilde{\boldsymbol{\theta}}}\boldsymbol{\Lambda}_n + \delta\widetilde{\boldsymbol{\theta}}\dot{\boldsymbol{\Lambda}}_n \\
\delta(\ddot{\boldsymbol{\Lambda}}_n) &= (\delta\dot{\dot{\boldsymbol{\Lambda}}}_n) = (\delta\dot{\widetilde{\boldsymbol{\theta}}}\boldsymbol{\Lambda}_n) = \delta\ddot{\widetilde{\boldsymbol{\theta}}}\boldsymbol{\Lambda}_n + 2\delta\dot{\widetilde{\boldsymbol{\theta}}}\dot{\boldsymbol{\Lambda}}_n + \delta\widetilde{\boldsymbol{\theta}}\ddot{\boldsymbol{\Lambda}}_n
\end{aligned}$$

which after several algebraic manipulations allow to obtain

$$D\dot{\widetilde{\boldsymbol{v}}}_n \cdot \delta\widetilde{\boldsymbol{\theta}} = \delta\widetilde{\boldsymbol{\alpha}}_n = \delta\ddot{\widetilde{\boldsymbol{\theta}}} + \delta\dot{\widetilde{\boldsymbol{\theta}}}\widetilde{\boldsymbol{v}}_n - \widetilde{\boldsymbol{v}}_n\delta\dot{\widetilde{\boldsymbol{\theta}}} + \delta\widetilde{\boldsymbol{\theta}}\widetilde{\boldsymbol{\alpha}}_n - \widetilde{\boldsymbol{\alpha}}_n\delta\widetilde{\boldsymbol{\theta}} = \delta\ddot{\widetilde{\boldsymbol{\theta}}} + [\delta\dot{\widetilde{\boldsymbol{\theta}}}, \widetilde{\boldsymbol{v}}_n] + [\delta\widetilde{\boldsymbol{\theta}}, \widetilde{\boldsymbol{\alpha}}_n] \tag{5.17c}$$

with the associated admissible variation of the axial vector $\dot{\hat{v}}_n \in T_{\boldsymbol{\Lambda}}^{\text{spa}}$ given by

$$D\dot{\hat{v}}_n \cdot \delta\hat{\theta} = \delta\hat{\alpha}_n = \delta\ddot{\hat{\theta}} - \widetilde{\boldsymbol{v}}_n\delta\dot{\hat{\theta}} - \widetilde{\boldsymbol{\alpha}}_n\delta\hat{\theta}. \tag{5.17d}$$

Employing analogous procedures as those followed through Eqs. (5.17a) to (5.17d), the admissible variations of the material forms of the angular velocity and acceleration tensors $\widetilde{\boldsymbol{V}} \in T_{\boldsymbol{\Lambda}}^{\text{mat}}SO(3)$ and $\dot{\widetilde{\boldsymbol{V}}} \in T_{\boldsymbol{\Lambda}}^{\text{mat}}SO(3)$ are

$$\begin{aligned}
D\widetilde{\boldsymbol{V}} \cdot \delta\widetilde{\boldsymbol{\theta}} = \delta\widetilde{\boldsymbol{V}} &= \boldsymbol{\Lambda}_0^T\delta\widetilde{\boldsymbol{V}}_n\boldsymbol{\Lambda}_0 = \boldsymbol{\Lambda}_0^T[(\delta\boldsymbol{\Lambda}_n)^T\dot{\boldsymbol{\Lambda}}_n + \boldsymbol{\Lambda}_n^T(\delta\dot{\boldsymbol{\Lambda}}_n)]\boldsymbol{\Lambda}_0 \\
&= \boldsymbol{\Lambda}_0^T[-\boldsymbol{\Lambda}_n^T\delta\widetilde{\boldsymbol{\theta}}\dot{\boldsymbol{\Lambda}}_n + \boldsymbol{\Lambda}_n^T(\delta\dot{\widetilde{\boldsymbol{\theta}}}\boldsymbol{\Lambda}_n + \delta\widetilde{\boldsymbol{\theta}}\dot{\boldsymbol{\Lambda}}_n)]\boldsymbol{\Lambda}_0 \\
&= -\boldsymbol{\Lambda}^T\delta\widetilde{\boldsymbol{\theta}}\widetilde{\boldsymbol{v}}_n\boldsymbol{\Lambda} + \boldsymbol{\Lambda}^T\delta\dot{\widetilde{\boldsymbol{\theta}}}\boldsymbol{\Lambda} + \boldsymbol{\Lambda}^T\delta\widetilde{\boldsymbol{\theta}}\widetilde{\boldsymbol{v}}_n\boldsymbol{\Lambda} \\
&= \boldsymbol{\Lambda}^T\delta\dot{\widetilde{\boldsymbol{\theta}}}\boldsymbol{\Lambda} \qquad (5.18a) \\
D\dot{\widetilde{\boldsymbol{V}}} \cdot \delta\widetilde{\boldsymbol{\theta}} \equiv \delta\widetilde{\boldsymbol{A}} &= ((\delta\dot{\boldsymbol{\Lambda}})^T)\delta\dot{\boldsymbol{\Lambda}} + (\dot{\boldsymbol{\Lambda}^T})\delta\dot{\boldsymbol{\Lambda}} + \delta\boldsymbol{\Lambda}^T\ddot{\boldsymbol{\Lambda}} + \boldsymbol{\Lambda}^T(\delta\ddot{\boldsymbol{\Lambda}}) \\
&= (-\dot{\boldsymbol{\Lambda}^T}\delta\widetilde{\boldsymbol{\theta}})\dot{\boldsymbol{\Lambda}} + (\dot{\boldsymbol{\Lambda}^T})(\delta\dot{\widetilde{\boldsymbol{\theta}}}\boldsymbol{\Lambda} + \delta\widetilde{\boldsymbol{\theta}}\dot{\boldsymbol{\Lambda}}) - \boldsymbol{\Lambda}^T\delta\widetilde{\boldsymbol{\theta}}\ddot{\boldsymbol{\Lambda}} + \boldsymbol{\Lambda}^T(\dot{\delta\dot{\widetilde{\boldsymbol{\theta}}}\boldsymbol{\Lambda}} + \delta\widetilde{\boldsymbol{\theta}}\dot{\boldsymbol{\Lambda}}) \\
&= \boldsymbol{\Lambda}^T\Big[\delta\ddot{\widetilde{\boldsymbol{\theta}}} + \delta\dot{\widetilde{\boldsymbol{\theta}}}\widetilde{\boldsymbol{v}} - \widetilde{\boldsymbol{v}}\delta\dot{\widetilde{\boldsymbol{\theta}}}\Big]\boldsymbol{\Lambda} \\
&= \boldsymbol{\Lambda}^T\Big[\delta\ddot{\widetilde{\boldsymbol{\theta}}} + [\delta\dot{\widetilde{\boldsymbol{\theta}}}, \widetilde{\boldsymbol{v}}]\Big]\boldsymbol{\Lambda}. \qquad (5.18b)
\end{aligned}$$

Additionally, the linearized form of the axial vectors $\hat{V}_n$, $\dot{\hat{V}}_n \in T_{\boldsymbol{\Lambda}}^{\text{mat}}$ are

$$\begin{aligned}
D\hat{V}_n \cdot \delta\hat{\theta} &= \delta\hat{V}_n = \boldsymbol{\Lambda}^T\delta\dot{\hat{\theta}} \qquad (5.19a) \\
D\dot{\hat{V}}_n \cdot \delta\hat{\theta} &= \delta\hat{A}_n = \boldsymbol{\Lambda}^T(\delta\ddot{\hat{\theta}} - \widetilde{\boldsymbol{v}}_n\delta\dot{\hat{\theta}}) \qquad (5.19b)
\end{aligned}$$

5.1.3.a Material updating of the rotational field

If we chose the material description of the admissible variation of the current rod configuration $\hat{\eta}^{\text{m}} \cong (\delta\hat{\varphi}, \delta\widetilde{\boldsymbol{\Theta}})$, then, the admissible variations of the spatial and material forms of the angular velocity and acceleration tensors can be calculated employing the same procedures as described

above. The resulting expressions are summarized as follows:

$$\begin{aligned}
D\widetilde{\boldsymbol{v}}\cdot\delta\widetilde{\boldsymbol{\Theta}}=\delta\widetilde{\boldsymbol{v}} &= \delta(\dot{\boldsymbol{\Lambda}}\boldsymbol{\Lambda}^T)=(\delta\dot{\boldsymbol{\Lambda}})\boldsymbol{\Lambda}^T+\dot{\boldsymbol{\Lambda}}(\delta\boldsymbol{\Lambda})^T\\
&= (\dot{\boldsymbol{\Lambda}}\delta\widetilde{\boldsymbol{\Theta}}+\boldsymbol{\Lambda}\delta\dot{\widetilde{\boldsymbol{\Theta}}})\boldsymbol{\Lambda}^T+\dot{\boldsymbol{\Lambda}}(-\delta\widetilde{\boldsymbol{\Theta}}\boldsymbol{\Lambda}^T)\\
&= \boldsymbol{\Lambda}\delta\dot{\widetilde{\boldsymbol{\Theta}}}\boldsymbol{\Lambda}^T \qquad (5.20a)\\
D\widetilde{\boldsymbol{V}}\cdot\delta\widetilde{\boldsymbol{\Theta}}=\delta\widetilde{\boldsymbol{V}} &= \delta(\boldsymbol{\Lambda}^T\dot{\boldsymbol{\Lambda}})=(\delta\boldsymbol{\Lambda})^T\dot{\boldsymbol{\Lambda}}+\boldsymbol{\Lambda}^T(\delta\dot{\boldsymbol{\Lambda}})\\
&= -\delta\widetilde{\boldsymbol{\Theta}}\boldsymbol{\Lambda}^T\dot{\boldsymbol{\Lambda}}+\boldsymbol{\Lambda}^T(\dot{\boldsymbol{\Lambda}}\delta\widetilde{\boldsymbol{\Theta}}+\boldsymbol{\Lambda}\delta\dot{\widetilde{\boldsymbol{\Theta}}})\\
&= \delta\dot{\widetilde{\boldsymbol{\Theta}}}-\delta\widetilde{\boldsymbol{\Theta}}\widetilde{\boldsymbol{V}}+\widetilde{\boldsymbol{V}}\delta\widetilde{\boldsymbol{\Theta}}=\delta\dot{\widetilde{\boldsymbol{\Theta}}}+[\widetilde{\boldsymbol{V}},\delta\widetilde{\boldsymbol{\Theta}}] \qquad (5.20b)\\
D\dot{\widetilde{\boldsymbol{v}}}\cdot\delta\widetilde{\boldsymbol{\Theta}}=\delta\widetilde{\boldsymbol{\alpha}} &= (\delta\dot{\boldsymbol{\Lambda}})\boldsymbol{\Lambda}^T+\ddot{\boldsymbol{\Lambda}}(\delta\boldsymbol{\Lambda})^T+(\delta\dot{\boldsymbol{\Lambda}})(\dot{\boldsymbol{\Lambda}}^T)+\dot{\boldsymbol{\Lambda}}((\delta\dot{\boldsymbol{\Lambda}})^T)\\
&= (\dot{\boldsymbol{\Lambda}}\delta\widetilde{\boldsymbol{\Theta}}+\boldsymbol{\Lambda}\delta\dot{\widetilde{\boldsymbol{\Theta}}})\dot{\boldsymbol{\Lambda}}^T-\ddot{\boldsymbol{\Lambda}}(\delta\widetilde{\boldsymbol{\Theta}}\boldsymbol{\Lambda}^T)+(\dot{\boldsymbol{\Lambda}}\delta\widetilde{\boldsymbol{\Theta}}+\boldsymbol{\Lambda}\delta\dot{\widetilde{\boldsymbol{\Theta}}})(\dot{\boldsymbol{\Lambda}}^T)-\dot{\boldsymbol{\Lambda}}(\delta\dot{\widetilde{\boldsymbol{\Theta}}}\boldsymbol{\Lambda}^T)\\
&= \boldsymbol{\Lambda}\big[\delta\ddot{\widetilde{\boldsymbol{\Theta}}}+\widetilde{\boldsymbol{V}}\delta\dot{\widetilde{\boldsymbol{\Theta}}}-\delta\dot{\widetilde{\boldsymbol{\Theta}}}\widetilde{\boldsymbol{V}}\big]\boldsymbol{\Lambda}^T\\
&= \boldsymbol{\Lambda}\big[\delta\ddot{\widetilde{\boldsymbol{\Theta}}}+[\widetilde{\boldsymbol{V}},\delta\dot{\widetilde{\boldsymbol{\Theta}}}]\big]\boldsymbol{\Lambda}^T \qquad (5.20c)\\
D\dot{\widetilde{\boldsymbol{V}}}\cdot\delta\widetilde{\boldsymbol{\Theta}}=\delta\widetilde{\boldsymbol{A}} &= ((\boldsymbol{\Lambda}\delta\dot{\widetilde{\boldsymbol{\Theta}}})^T)\dot{\boldsymbol{\Lambda}}+(\dot{\boldsymbol{\Lambda}}^T)(\boldsymbol{\Lambda}\delta\dot{\widetilde{\boldsymbol{\Theta}}})+(\boldsymbol{\Lambda}\delta\widetilde{\boldsymbol{\Theta}})^T\ddot{\boldsymbol{\Lambda}}+\boldsymbol{\Lambda}^T(\dot{\boldsymbol{\Lambda}}\delta\dot{\widetilde{\boldsymbol{\Theta}}})\\
&= \delta\ddot{\widetilde{\boldsymbol{\Theta}}}+\delta\widetilde{\boldsymbol{\Theta}}(\boldsymbol{\Lambda}^T\ddot{\boldsymbol{\Lambda}}-\widetilde{\boldsymbol{V}}\widetilde{\boldsymbol{V}})+(\boldsymbol{\Lambda}^T\ddot{\boldsymbol{\Lambda}}-\widetilde{\boldsymbol{V}}\widetilde{\boldsymbol{V}})\delta\widetilde{\boldsymbol{\Theta}}-(\delta\dot{\widetilde{\boldsymbol{\Theta}}}\widetilde{\boldsymbol{V}}+\widetilde{\boldsymbol{V}}\delta\dot{\widetilde{\boldsymbol{\Theta}}})\\
&= \delta\ddot{\widetilde{\boldsymbol{\Theta}}}+\widetilde{\boldsymbol{A}}\delta\widetilde{\boldsymbol{\Theta}}-\delta\widetilde{\boldsymbol{\Theta}}\widetilde{\boldsymbol{A}}+\widetilde{\boldsymbol{V}}\delta\dot{\widetilde{\boldsymbol{\Theta}}}-\delta\dot{\widetilde{\boldsymbol{\Theta}}}\widetilde{\boldsymbol{V}}\\
&= \delta\ddot{\widetilde{\boldsymbol{\Theta}}}+[\widetilde{\boldsymbol{V}},\delta\dot{\widetilde{\boldsymbol{\Theta}}}]+[\widetilde{\boldsymbol{A}},\delta\widetilde{\boldsymbol{\Theta}}] \qquad (5.20d)
\end{aligned}$$

with the corresponding axial vectors given by

$$\begin{aligned}
D\hat{v}\cdot\delta\hat{\Theta}=\delta\hat{v} &= \boldsymbol{\Lambda}\delta\dot{\hat{\Theta}} \qquad (5.21a)\\
D\hat{V}\cdot\delta\hat{\Theta}=\delta\hat{V} &= \delta\dot{\hat{\Theta}}+\widetilde{\boldsymbol{V}}\delta\hat{\Theta} \qquad (5.21b)\\
D\dot{\hat{v}}\cdot\delta\hat{\Theta}=\delta\hat{\alpha} &= \boldsymbol{\Lambda}\big[\delta\ddot{\hat{\Theta}}+\widetilde{\boldsymbol{V}}\delta\hat{\Theta}\big] \qquad (5.21c)\\
D\dot{\hat{V}}\cdot\delta\hat{\Theta}=\delta\hat{A} &= \delta\ddot{\hat{\Theta}}+\widetilde{\boldsymbol{A}}\delta\hat{\Theta}+\widetilde{\boldsymbol{V}}\delta\dot{\hat{\Theta}}. \qquad (5.21d)
\end{aligned}$$

A summary of the results for the linearized forms of the spin variables using the spatial and material updating rules for the rotational field is presented in Table 5.3.

5.1.4 Linearization of the strain rates

By one hand, considering the spatial rule for updating the rotational part of the motion, we have that the linearized form of the spatial description of the translational strain rate vector given in Eq. (3.79a) can be obtained considering that $\delta\widetilde{\boldsymbol{v}}_n=(\delta\dot{\widetilde{\boldsymbol{\theta}}}+\delta\widetilde{\boldsymbol{\theta}}\widetilde{\boldsymbol{v}}_n-\widetilde{\boldsymbol{v}}_n\delta\widetilde{\boldsymbol{\theta}})$ and $\delta\hat{t}_1=\delta\widetilde{\boldsymbol{\theta}}\hat{t}_1$ in the following way:

$$\begin{aligned}
D\dot{\hat{\gamma}}_n\cdot\hat{\eta}^{\mathrm{s}}=\delta\dot{\hat{\gamma}}_n &= \delta\big[\dot{\hat{\varphi}}_{,S}-\widetilde{\boldsymbol{v}}_n\hat{t}_1\big]\\
&= \delta\dot{\hat{\varphi}}_{,S}-\delta\widetilde{\boldsymbol{v}}_n\hat{t}_1+\widetilde{\boldsymbol{v}}_n\delta\hat{t}_1\\
&= \delta\dot{\hat{\varphi}}_{,S}-(\delta\dot{\widetilde{\boldsymbol{\theta}}}+\delta\widetilde{\boldsymbol{\theta}}\widetilde{\boldsymbol{v}}_n-\widetilde{\boldsymbol{v}}_n\delta\widetilde{\boldsymbol{\theta}})\hat{t}_1+\widetilde{\boldsymbol{v}}_n\delta\widetilde{\boldsymbol{\theta}}\hat{t}_1\\
&= \delta\dot{\hat{\varphi}}_{,S}-\delta\dot{\widetilde{\boldsymbol{\theta}}}\hat{t}_1-\delta\widetilde{\boldsymbol{\theta}}\widetilde{\boldsymbol{v}}_n\hat{t}_1\\
&= \delta\dot{\hat{\varphi}}_{,S}-\widetilde{\boldsymbol{t}}_1\delta\dot{\hat{\theta}}-\widetilde{\boldsymbol{v}}_n\widetilde{\boldsymbol{t}}_1\delta\hat{\theta} \qquad (5.22a)
\end{aligned}$$

Table 5.3: Linearized forms of the spin variables.

	$\hat{\eta}^{\mathrm{s}}$ (Spatial updating)	$\hat{\eta}^{\mathrm{m}}$ (Material updating)
$\delta\widetilde{\boldsymbol{v}}_n$	$\delta\dot{\widetilde{\boldsymbol{\theta}}} + [\delta\widetilde{\boldsymbol{\theta}}, \widetilde{\boldsymbol{v}}_n]$	$\boldsymbol{\Lambda}\delta\dot{\widetilde{\boldsymbol{\Theta}}}\boldsymbol{\Lambda}^T$
$\delta\dot{\widetilde{\boldsymbol{v}}}_n$	$\delta\ddot{\widetilde{\boldsymbol{\theta}}} + [\delta\dot{\widetilde{\boldsymbol{\theta}}}, \widetilde{\boldsymbol{v}}_n] + [\delta\widetilde{\boldsymbol{\theta}}, \widetilde{\boldsymbol{\alpha}}_n]$	$\boldsymbol{\Lambda}\big(\delta\ddot{\widetilde{\boldsymbol{\Theta}}} + [\widetilde{\boldsymbol{V}}, \delta\dot{\widetilde{\boldsymbol{\Theta}}}]\big)\boldsymbol{\Lambda}^T$
$\delta\widetilde{\boldsymbol{V}}$	$\boldsymbol{\Lambda}^T\delta\dot{\widetilde{\boldsymbol{\theta}}}\boldsymbol{\Lambda}$	$\delta\dot{\widetilde{\boldsymbol{\Theta}}} + [\widetilde{\boldsymbol{V}}, \delta\widetilde{\boldsymbol{\Theta}}]$
$\delta\dot{\widetilde{\boldsymbol{V}}}$	$\boldsymbol{\Lambda}^T\big(\delta\ddot{\widetilde{\boldsymbol{\theta}}} + [\delta\dot{\widetilde{\boldsymbol{\theta}}}, \widetilde{\boldsymbol{v}}]\big)\boldsymbol{\Lambda}$	$\delta\ddot{\widetilde{\boldsymbol{\Theta}}} + [\widetilde{\boldsymbol{V}}, \delta\dot{\widetilde{\boldsymbol{\Theta}}}] + [\widetilde{\boldsymbol{A}}, \delta\widetilde{\boldsymbol{\Theta}}]$
$\delta\hat{v}_n$	$\delta\dot{\hat{\theta}} - \widetilde{\boldsymbol{v}}_n\delta\hat{\theta}$	$\boldsymbol{\Lambda}\delta\dot{\hat{\Theta}}$
$\delta\dot{\hat{v}}_n$	$\delta\ddot{\hat{\theta}} - \widetilde{\boldsymbol{v}}_n\delta\dot{\hat{\theta}} - \widetilde{\boldsymbol{\alpha}}_n\delta\hat{\theta}$	$\boldsymbol{\Lambda}\big(\delta\ddot{\hat{\Theta}} + \widetilde{\boldsymbol{V}}\delta\hat{\Theta}\big)$
$\delta\hat{V}_n$	$\boldsymbol{\Lambda}^T\delta\dot{\hat{\theta}}$	$\delta\dot{\hat{\Theta}} + \widetilde{\boldsymbol{V}}\delta\hat{\Theta}$
$\delta\dot{\hat{V}}_n$	$\boldsymbol{\Lambda}^T(\delta\ddot{\hat{\theta}} - \widetilde{\boldsymbol{v}}_n\delta\dot{\hat{\theta}})$	$\delta\ddot{\hat{\Theta}} + \widetilde{\boldsymbol{A}}\delta\hat{\Theta} + \widetilde{\boldsymbol{V}}\delta\dot{\hat{\Theta}}$

and the linearized form of the material description of the translational strain rate vector given in Eq. (3.79b) can be obtained considering that $\delta\boldsymbol{\Lambda}^T = -\boldsymbol{\Lambda}^T\delta\widetilde{\boldsymbol{\theta}}$ as

$$\begin{aligned} D\dot{\hat{\Gamma}}_n\cdot\hat{\eta}^{\mathrm{s}} = \delta\dot{\hat{\Gamma}}_n &= \delta\big[\boldsymbol{\Lambda}^T(\dot{\hat{\varphi}}_{,S} - \widetilde{\boldsymbol{v}}_n\hat{\varphi}_{,S})\big] \\ &= -\boldsymbol{\Lambda}^T\delta\widetilde{\boldsymbol{\theta}}(\dot{\hat{\varphi}}_{,S} - \widetilde{\boldsymbol{v}}_n\hat{\varphi}_{,S}) + \boldsymbol{\Lambda}^T\delta(\dot{\hat{\varphi}}_{,S} - \widetilde{\boldsymbol{v}}_n\hat{\varphi}_{,S}) \\ &= \boldsymbol{\Lambda}^T(\boldsymbol{\Pi}[\dot{\hat{\varphi}}_{,S}]\delta\hat{\theta} + \widetilde{\boldsymbol{v}}_n\boldsymbol{\Pi}[\hat{\varphi}_{,S}]\delta\hat{\theta} + \delta\dot{\hat{\varphi}}_{,S} - \delta\widetilde{\boldsymbol{v}}_n\hat{\varphi}_{,S} - \widetilde{\boldsymbol{v}}_n\delta\hat{\varphi}_{,S}) \\ &= \boldsymbol{\Lambda}^T\big((\boldsymbol{\Pi}[\dot{\hat{\varphi}}_{,S}] - \widetilde{\boldsymbol{v}}_n\boldsymbol{\Pi}[\hat{\varphi}_{,S}])\delta\hat{\theta} + \boldsymbol{\Pi}[\hat{\varphi}_{,S}]\delta\dot{\hat{\theta}} + \delta\dot{\hat{\varphi}}_{,S} - \widetilde{\boldsymbol{v}}_n\Delta\hat{\varphi}_{,S}\big). \end{aligned} \tag{5.22b}$$

REMARK 5.1. Note that the strain rate vectors $\dot{\hat{\gamma}}_n$ and $\dot{\hat{\Gamma}}_n$ depend on time derivatives of the configuration variables, therefore, formally the linearization process is carried out as $D(\bullet)\cdot\hat{\eta}^{\mathrm{s}} + D(\bullet)\cdot\dot{\hat{\eta}}^{\mathrm{s}}$; considering perturbations onto $\hat{\eta}^{\mathrm{s}}$ and its time derivative, however, the same notation as before is used for avoiding a excesive proliferation of symbols ■

By the other hand, the linearized form of the spatial and material descriptions of the rotational strain rate vectors, given in Eqs. (3.80a) and (3.80b), can be obtained considering that $\delta\hat{\omega}_n = \delta\hat{\theta}_{,S} - \widetilde{\boldsymbol{\omega}}_n\delta\hat{\theta}$ and $\delta\hat{v}_n = \delta\dot{\hat{\theta}} - \widetilde{\boldsymbol{v}}_n\delta\hat{\theta}$ in the following way:

$$\begin{aligned} D\dot{\hat{\omega}}_n\cdot\hat{\eta}^{\mathrm{s}} = \delta\dot{\hat{\omega}}_n &= \delta\big[\hat{v}_{n,S} + \widetilde{\boldsymbol{v}}_n\hat{\omega}_n\big] \\ &= (\delta\hat{v}_n)_{,S} + (\delta\widetilde{\boldsymbol{v}}_n)\hat{\omega}_n + \widetilde{\boldsymbol{v}}_n(\delta\hat{\omega}_n) \\ &= \delta\dot{\hat{\theta}}_{,S} - \widetilde{\boldsymbol{\omega}}_n\delta\dot{\hat{\theta}} - (\widetilde{\boldsymbol{v}}_{n,S} - \widetilde{\boldsymbol{v}}_n\widetilde{\boldsymbol{\omega}}_n)\delta\hat{\theta} \\ &= \delta\dot{\hat{\theta}}_{,S} - \widetilde{\boldsymbol{\omega}}_n\delta\dot{\hat{\theta}} - \dot{\hat{\omega}}_n\delta\hat{\theta} \end{aligned} \tag{5.23a}$$

$$\begin{aligned} D\dot{\hat{\Omega}}_n\cdot\hat{\eta}^{\mathrm{s}} = \delta\dot{\hat{\Omega}}_n &= \delta\big[\boldsymbol{\Lambda}^T\hat{v}_{n,S}\big] \\ &= -\boldsymbol{\Lambda}^T\delta\widetilde{\boldsymbol{\theta}}\hat{v}_{n,S} + \boldsymbol{\Lambda}^T(\delta\hat{v}_{n,S}) \\ &= \boldsymbol{\Lambda}^T\boldsymbol{\Pi}[\hat{v}_{n,S}]\delta\hat{\theta} + \boldsymbol{\Lambda}^T\big(\delta\dot{\hat{\theta}} - \widetilde{\boldsymbol{v}}_n\delta\hat{\theta}\big)_{,S} \\ &= \boldsymbol{\Lambda}^T\boldsymbol{\Pi}[\hat{v}_{n,S}]\delta\hat{\theta} + \boldsymbol{\Lambda}^T\big(\delta\dot{\hat{\theta}}_{,S} - \widetilde{\boldsymbol{v}}_{n,S}\,\delta\hat{\theta} - \widetilde{\boldsymbol{v}}_n\delta\hat{\theta}_{,S}\big) \\ &= \boldsymbol{\Lambda}^T\big[\delta\dot{\hat{\theta}}_{,S} - \widetilde{\boldsymbol{v}}_n\delta\hat{\theta}_{,S}\big]. \end{aligned} \tag{5.23b}$$

The co–rotated variation of the translational and rotational strain rates can be calculated considering the definition of the Lie's variation (see Appendix A) *i.e.* $\delta\,[\overset{\triangledown}{\dot{\hat{\omega}}}_n]= \boldsymbol{\Lambda}\big[\delta\dot{\hat{\Omega}}_n\big]$ and $\delta[\overset{\triangledown}{\dot{\hat{\gamma}}}_n]= \boldsymbol{\Lambda}\big[\delta\dot{\hat{\Gamma}}_m\big]$, respectively [258]; which explicitly are given by

$$\delta[\overset{\triangledown}{\dot{\hat{\gamma}}}_n] = (\dot{\widetilde{\boldsymbol{\varphi}}}_{,S} - \widetilde{\boldsymbol{v}}_n\widetilde{\boldsymbol{\varphi}}_{,S})\delta\hat{\theta} + \widetilde{\boldsymbol{\varphi}}_{,S}\,\delta\dot{\hat{\theta}} + \delta\dot{\hat{\varphi}}_{,S} - \widetilde{\boldsymbol{v}}_n\delta\hat{\varphi}_{,S} \tag{5.23c}$$

$$\delta[\overset{\triangledown}{\dot{\hat{\omega}}}_n] = \delta\dot{\hat{\theta}}_{,S} - \widetilde{\boldsymbol{v}}_n\delta\hat{\theta}_{,S}\,. \tag{5.23d}$$

Following analogous procedures it is possible to show that the linearized forms of the corresponding spatial and material descriptions and the co-rotated strain rate tensors can be expressed as

$$\begin{aligned} D\dot{\widetilde{\boldsymbol{\omega}}}_n\cdot\hat{\eta}^{\mathrm{s}} = \delta\dot{\widetilde{\boldsymbol{\omega}}}_n &= \delta\dot{\widetilde{\boldsymbol{\theta}}}_{,S} + \delta\dot{\widetilde{\boldsymbol{\theta}}}\widetilde{\boldsymbol{\omega}}_n - \widetilde{\boldsymbol{\omega}}_n\delta\dot{\widetilde{\boldsymbol{\theta}}} + \delta\widetilde{\boldsymbol{\theta}}\dot{\widetilde{\boldsymbol{\omega}}}_n - \dot{\widetilde{\boldsymbol{\omega}}}_n\delta\widetilde{\boldsymbol{\theta}} \\ &= \delta\dot{\widetilde{\boldsymbol{\theta}}}_{,S} + [\delta\dot{\widetilde{\boldsymbol{\theta}}}, \widetilde{\boldsymbol{\omega}}_n] + [\delta\widetilde{\boldsymbol{\theta}}, \dot{\widetilde{\boldsymbol{\omega}}}_n] \qquad (5.24a) \\ D\dot{\widetilde{\boldsymbol{\Omega}}}_n\cdot\hat{\eta}^{\mathrm{s}} = \delta\dot{\widetilde{\boldsymbol{\Omega}}}_n &= \boldsymbol{\Lambda}^T(\delta\dot{\widetilde{\boldsymbol{\theta}}}_{,S} + \delta\widetilde{\boldsymbol{\theta}}_{,S}\,\widetilde{\boldsymbol{v}}_n - \widetilde{\boldsymbol{v}}_n\delta\widetilde{\boldsymbol{\theta}}_{,S})\boldsymbol{\Lambda} \\ &= \boldsymbol{\Lambda}^T(\delta\dot{\widetilde{\boldsymbol{\theta}}}_{,S}\,[\delta\widetilde{\boldsymbol{\theta}}_{,S}\,, \widetilde{\boldsymbol{v}}_n])\boldsymbol{\Lambda} \qquad (5.24b) \\ \delta[\overset{\triangledown}{\dot{\widetilde{\boldsymbol{\omega}}}}_n] &= \boldsymbol{\Lambda}(\delta\dot{\widetilde{\boldsymbol{\Omega}}}_n)\boldsymbol{\Lambda}^T = \delta\dot{\widetilde{\boldsymbol{\theta}}}_{,S} + \delta\widetilde{\boldsymbol{\theta}}_{,S}\,\widetilde{\boldsymbol{v}}_n - \widetilde{\boldsymbol{v}}_n\delta\widetilde{\boldsymbol{\theta}}_{,S} \\ &= \delta\dot{\widetilde{\boldsymbol{\theta}}}_{,S} + [\delta\widetilde{\boldsymbol{\theta}}_{,S}\,, \widetilde{\boldsymbol{v}}_n]. \qquad (5.24c) \end{aligned}$$

Finally, the material and co-rotated descriptions of the linearized increment of the strain rate at material point level is calculated as

$$D\hat{\mathcal{S}}_n\cdot\hat{\eta}^{\mathrm{s}} = \delta\hat{\mathcal{S}}_n = \delta\dot{\hat{\mathcal{E}}}_n = \delta\dot{\hat{\Gamma}}_n + \delta\dot{\hat{\Omega}}_n\times\hat{\mathscr{E}} \tag{5.25}$$

$$\delta[\overset{\triangledown}{\dot{\hat{\epsilon}}}_n] = \delta\hat{s}_n = \delta[\overset{\triangledown}{\dot{\hat{\varepsilon}}}_n] = \boldsymbol{\Lambda}\delta\dot{\hat{\mathcal{E}}}_n = \delta[\overset{\triangledown}{\dot{\hat{\gamma}}}_n] + \delta[\overset{\triangledown}{\dot{\hat{\omega}}}_n]\times\hat{\mathscr{T}} \tag{5.26}$$

where it has been considered the fact that $\hat{\mathscr{T}} = \boldsymbol{\Lambda}\hat{\mathscr{E}}$.
The terms $\delta\dot{\hat{\varphi}}$, $\delta\dot{\hat{\varphi}}_{,S}$, $\delta\dot{\hat{\theta}}$ and $\delta\dot{\hat{\theta}}_{,S}$ of Eqs. (5.23c) and (5.23d) do not allow to express directly the co-rotated variations of the strain rate vectors in terms of $\delta\hat{\varphi}$ and $\delta\hat{\theta}$. To this end, the specific time–stepping scheme used in the numerical integration of the equations of motion provides the needed relations [365]. This aspect will be explained in detail in §6.
For the present developments, lets suppose that there exist two linear operators $\boldsymbol{\mathscr{H}}_a \in \mathcal{L}(\mathbb{R}^3, \mathbb{R}^{3*})$ and $\boldsymbol{\mathscr{H}}_b(\hat{\theta}) \in \mathcal{L}(T^{\mathrm{spa}}_{\boldsymbol{\Lambda}}, T^{\mathrm{spa}*}_{\boldsymbol{\Lambda}})$ such that

$$\delta\dot{\hat{\varphi}} = \boldsymbol{\mathscr{H}}_a\delta\hat{\varphi}, \qquad \delta\dot{\hat{\varphi}}_{,S} = \boldsymbol{\mathscr{H}}_a\delta\hat{\varphi}_{,S} + \boldsymbol{\mathscr{H}}_{a,S}\,\delta\hat{\varphi} \tag{5.27a}$$

$$\delta\dot{\hat{\theta}} = \boldsymbol{\mathscr{H}}_b\delta\hat{\theta}, \qquad \delta\dot{\hat{\theta}}_{,S} = \boldsymbol{\mathscr{H}}_b\delta\hat{\theta}_{,S} + \boldsymbol{\mathscr{H}}_{b,S}\,\delta\hat{\theta} \tag{5.27b}$$

Therefore, Eqs. (5.23c) and (5.23d) can be rearranged as

$$\begin{bmatrix} \delta[\overset{\triangledown}{\dot{\hat{\gamma}}}_n] \\ \delta[\overset{\triangledown}{\dot{\hat{\omega}}}_n] \end{bmatrix} = \underbrace{\begin{bmatrix} \boldsymbol{\mathscr{H}}_a[\frac{\mathrm{d}}{\mathrm{d}S}\mathbf{I}] + \boldsymbol{\mathscr{H}}_{a,S} - \widetilde{\boldsymbol{v}}_n[\frac{\mathrm{d}}{\mathrm{d}S}\mathbf{I}] & \dot{\widetilde{\boldsymbol{\varphi}}}_{,S} + \widetilde{\boldsymbol{\varphi}}_{,S}\,\boldsymbol{\mathscr{H}}_b - \widetilde{\boldsymbol{v}}_n\widetilde{\boldsymbol{\varphi}}_{,S} \\ 0 & (\boldsymbol{\mathscr{H}}_b - \widetilde{\boldsymbol{v}}_n)[\frac{\mathrm{d}}{\mathrm{d}S}\mathbf{I}] + \boldsymbol{\mathscr{H}}_{b,S} \end{bmatrix}}_{[\boldsymbol{\mathcal{V}}(\hat{\varphi},\hat{\theta})]} \begin{bmatrix} \delta\hat{\varphi} \\ \delta\hat{\theta} \end{bmatrix} = \boldsymbol{\mathcal{V}}\hat{\eta}^{\mathrm{s}} \tag{5.28}$$

where $\dot{\widetilde{\boldsymbol{\varphi}}}_{,S} = \boldsymbol{\Pi}[\dot{\hat{\varphi}}_{,S}]$, $\widetilde{\boldsymbol{\varphi}}_{,S} = \boldsymbol{\Pi}[\hat{\varphi}_{,S}]$, $\mathbf{I}$ is the 3×3 identity matrix and the operator $[\frac{\mathrm{d}}{\mathrm{d}S}\mathbf{I}]$ is defined

as $[\frac{\mathrm{d}}{\mathrm{d}S}](\bullet) = \mathbf{I}\frac{\mathrm{d}}{\mathrm{d}S}(\bullet)$. It is worth to note that the tensor $\boldsymbol{\mathcal{V}}$ is configuration dependent and it couples the rotational and translational parts of the motion.

5.1.4.a Material updating of the rotational field

If we chose the material description of the admissible variation of the current rod configuration $\hat{\eta}^{\mathrm{m}} \cong (\delta\hat{\varphi}, \delta\widetilde{\boldsymbol{\Theta}})$, then, the admissible variations of the spatial form of the translational strain rate vector can be calculated considering $\delta\hat{t}_1 = \boldsymbol{\Lambda}\widetilde{\boldsymbol{E}}_1\delta\hat{\Theta}$ and the result of Eq. (5.20a) as

$$\begin{aligned} D\dot{\hat{\gamma}}_n \cdot \hat{\eta}^{\mathrm{m}} = \delta\dot{\hat{\gamma}}_n &= \delta\dot{\hat{\varphi}}_{,S} - \delta\widetilde{\boldsymbol{v}}_n\hat{t}_1 - \widetilde{\boldsymbol{v}}_n\delta\hat{t}_1 \\ &= \delta\dot{\hat{\varphi}}_{,S} - \boldsymbol{\Lambda}\delta\dot{\widetilde{\boldsymbol{\Theta}}}\boldsymbol{\Lambda}^T\hat{t}_1 - \widetilde{\boldsymbol{v}}_n\boldsymbol{\Lambda}\widetilde{\boldsymbol{E}}_1\delta\hat{\Theta} \\ &= \delta\dot{\hat{\varphi}}_{,S} - \boldsymbol{\Lambda}\widetilde{\boldsymbol{E}}_1\delta\dot{\hat{\Theta}} - \boldsymbol{\Lambda}\widetilde{\boldsymbol{V}}_n\widetilde{\boldsymbol{E}}_1\delta\hat{\Theta} \\ &= \delta\dot{\hat{\varphi}}_{,S} - \widetilde{\boldsymbol{t}}_1\big(\delta\dot{\hat{\Theta}} - \widetilde{\boldsymbol{V}}_n\delta\hat{\Theta}\big) \end{aligned} \tag{5.29a}$$

for the case of the material form of the translational strain rate vector, we have

$$\begin{aligned} D\dot{\hat{\Gamma}}_n \cdot \hat{\eta}^{\mathrm{m}} = \delta\dot{\hat{\Gamma}}_n &= \delta\big[\boldsymbol{\Lambda}^T(\dot{\hat{\varphi}}_{,S} - \widetilde{\boldsymbol{v}}_n\hat{\varphi}_{,S})\big] \\ &= (\delta\boldsymbol{\Lambda})^T(\dot{\hat{\varphi}}_{,S} - \widetilde{\boldsymbol{v}}_n\hat{\varphi}_{,S}) + \boldsymbol{\Lambda}^T(\delta\dot{\hat{\varphi}}_{,S} - \delta\widetilde{\boldsymbol{v}}_n\hat{\varphi}_{,S} - \delta\widetilde{\boldsymbol{v}}_n\delta\hat{\varphi}_{,S}) \\ &= -\delta\widetilde{\boldsymbol{\Theta}}\boldsymbol{\Lambda}^T(\dot{\hat{\varphi}}_{,S} - \widetilde{\boldsymbol{v}}_n\hat{\varphi}_{,S}) + \boldsymbol{\Lambda}^T\delta\dot{\hat{\varphi}}_{,S} - \delta\dot{\widetilde{\boldsymbol{\Theta}}}\boldsymbol{\Lambda}^T\hat{\varphi}_{,S} - \widetilde{\boldsymbol{V}}_n\boldsymbol{\Lambda}^T\delta\hat{\varphi}_{,S} \\ &= \dot{\widetilde{\boldsymbol{\Gamma}}}_n\delta\hat{\Theta} + \boldsymbol{\Pi}[\boldsymbol{\Lambda}^T\hat{\varphi}_{,S}]\delta\dot{\hat{\Theta}} + \boldsymbol{\Lambda}^T\delta\dot{\hat{\varphi}}_{,S} - \widetilde{\boldsymbol{V}}_n\boldsymbol{\Lambda}^T\delta\hat{\varphi}_{,S} \end{aligned} \tag{5.29b}$$

where $\dot{\widetilde{\boldsymbol{\Gamma}}}_n$ is the skew–symmetric tensor obtained from $\dot{\hat{\Gamma}}_n$. Finally, the co–rotated variation is obtained as

$$\delta[\overset{\triangledown}{\dot{\hat{\gamma}}}_n] = \boldsymbol{\Lambda}\delta\dot{\hat{\Gamma}}_n = [\overset{\triangledown}{\dot{\widetilde{\boldsymbol{\gamma}}}}_n]\,\boldsymbol{\Lambda}\delta\hat{\Theta} + \boldsymbol{\Lambda}\boldsymbol{\Pi}[\boldsymbol{\Lambda}^T\hat{\varphi}_{,S}]\delta\dot{\hat{\Theta}} + \delta\dot{\hat{\varphi}}_{,S} - \widetilde{\boldsymbol{v}}_n\delta\hat{\varphi}_{,S} \tag{5.29c}$$

where $[\overset{\triangledown}{\dot{\widetilde{\boldsymbol{\gamma}}}}_n] = \boldsymbol{\Pi}[[\overset{\triangledown}{\dot{\hat{\gamma}}}_n]] \in so(3)$. In the case of the spatial form of rotational strain rate tensor and considering the results of Eqs. (5.13c) and (5.20a), we have

$$\begin{aligned} D\dot{\widetilde{\boldsymbol{\omega}}}_n \cdot \delta\hat{\Theta} = \delta\dot{\widetilde{\boldsymbol{\omega}}}_n = &\ \delta(\widetilde{\boldsymbol{v}}_{n,S} + \widetilde{\boldsymbol{v}}_n\widetilde{\boldsymbol{\omega}}_n - \widetilde{\boldsymbol{\omega}}_n\widetilde{\boldsymbol{v}}_n) \\ = &\ (\boldsymbol{\Lambda}\delta\dot{\widetilde{\boldsymbol{\Theta}}}\boldsymbol{\Lambda}^T)_{,S} + \boldsymbol{\Lambda}\delta\dot{\widetilde{\boldsymbol{\Theta}}}\widetilde{\boldsymbol{\Omega}}_n\boldsymbol{\Lambda}^T + \boldsymbol{\Lambda}\widetilde{\boldsymbol{V}}_n\delta\widetilde{\boldsymbol{\Theta}}_{,S}\,\boldsymbol{\Lambda}^T - \boldsymbol{\Lambda}\delta\widetilde{\boldsymbol{\Theta}}_{,S}\,\widetilde{\boldsymbol{V}}_n\boldsymbol{\Lambda}^T - \boldsymbol{\Lambda}\widetilde{\boldsymbol{\Omega}}_n\dot{\widetilde{\boldsymbol{\Theta}}}\boldsymbol{\Lambda}^T \\ = &\ \boldsymbol{\Lambda}\big\{\delta\dot{\widetilde{\boldsymbol{\Theta}}}_{,S} + \widetilde{\boldsymbol{V}}_n\delta\widetilde{\boldsymbol{\Theta}}_{,S} - \delta\widetilde{\boldsymbol{\Theta}}_{,S}\,\widetilde{\boldsymbol{V}}_n\big\}\boldsymbol{\Lambda}^T \\ = &\ \boldsymbol{\Lambda}\big\{\delta\dot{\widetilde{\boldsymbol{\Theta}}}_{,S} + [\widetilde{\boldsymbol{V}}_n, \delta\widetilde{\boldsymbol{\Theta}}_{,S}]\big\}\boldsymbol{\Lambda}^T. \end{aligned} \tag{5.30a}$$

For the case of the material form of the strain rate tensor, considering Eqs. (3.80b) and (5.20a), we obtain

$$\begin{aligned} D\dot{\widetilde{\boldsymbol{\Omega}}}_n \cdot \delta\hat{\Theta} = \delta\dot{\widetilde{\boldsymbol{\Omega}}}_n = &\ \delta(\boldsymbol{\Lambda}^T\widetilde{\boldsymbol{v}}_{n,S}\,\boldsymbol{\Lambda}) \\ = &\ (\delta\boldsymbol{\Lambda})^T\widetilde{\boldsymbol{v}}_{n,S}\,\boldsymbol{\Lambda} + \boldsymbol{\Lambda})^T(\delta\widetilde{\boldsymbol{v}}_n)_{,S}\,\boldsymbol{\Lambda} + \boldsymbol{\Lambda})^T\widetilde{\boldsymbol{v}}_{n,S}\,\delta\boldsymbol{\Lambda} \\ = &\ \dot{\widetilde{\boldsymbol{\Omega}}}_n\delta\widetilde{\boldsymbol{\Theta}} - \delta\widetilde{\boldsymbol{\Theta}}\dot{\widetilde{\boldsymbol{\Omega}}}_n + \boldsymbol{\Lambda}^T(\boldsymbol{\Lambda}_{,S}\,\delta\dot{\widetilde{\boldsymbol{\Theta}}}\boldsymbol{\Lambda}^T + \boldsymbol{\Lambda}\delta\dot{\widetilde{\boldsymbol{\Theta}}}_{,S}\,\boldsymbol{\Lambda}^T + \boldsymbol{\Lambda}\delta\dot{\widetilde{\boldsymbol{\Theta}}}(\boldsymbol{\Lambda}^T)_{,S})\boldsymbol{\Lambda} \\ = &\ \delta\dot{\widetilde{\boldsymbol{\Theta}}}_{,S} + \dot{\widetilde{\boldsymbol{\Omega}}}_n\delta\widetilde{\boldsymbol{\Theta}} - \delta\widetilde{\boldsymbol{\Theta}}\dot{\widetilde{\boldsymbol{\Omega}}}_n + \widetilde{\boldsymbol{\Omega}}_n\delta\dot{\widetilde{\boldsymbol{\Theta}}} - \delta\dot{\widetilde{\boldsymbol{\Theta}}}\widetilde{\boldsymbol{\Omega}}_n \\ = &\ \delta\dot{\widetilde{\boldsymbol{\Theta}}}_{,S} + [\dot{\widetilde{\boldsymbol{\Omega}}}_n, \delta\widetilde{\boldsymbol{\Theta}}] + [\widetilde{\boldsymbol{\Omega}}_n, \delta\dot{\widetilde{\boldsymbol{\Theta}}}]. \end{aligned} \tag{5.30b}$$

Taking into account the previous result we have that the co–rotated form of the strain rate tensor is given by

$$\delta[\overset{\triangledown}{\dot{\widetilde{\boldsymbol{\omega}}}}_n]= \boldsymbol{\Lambda}[\delta\dot{\widetilde{\boldsymbol{\Theta}}}_{,S} +[\dot{\widetilde{\boldsymbol{\Omega}}}_n, \delta\widetilde{\boldsymbol{\Theta}}] + [\widetilde{\boldsymbol{\Omega}}_n, \delta\dot{\widetilde{\boldsymbol{\Theta}}}]]\boldsymbol{\Lambda}^T. \tag{5.30c}$$

The axial vectors of the strain rate tensor of Eqs. (5.30a) to (5.30a) are then given by

$$D\dot{\hat{\omega}}_n \cdot \delta\hat{\Theta} = \delta\dot{\hat{\omega}}_n = \boldsymbol{\Lambda}\big\{\delta\dot{\hat{\Theta}}_{,S} +\widetilde{\boldsymbol{V}}_n\delta\hat{\Theta}_{,S}\,\big\} \tag{5.31a}$$

$$D\dot{\hat{\Omega}}_n \cdot \delta\hat{\Theta} = \delta\dot{\hat{\Omega}}_n = \delta\dot{\hat{\Theta}}_{,S} +\dot{\widetilde{\boldsymbol{\Omega}}}_n\delta\hat{\Theta} + \widetilde{\boldsymbol{\Omega}}_n, \delta\dot{\hat{\Theta}} \tag{5.31b}$$

$$\delta[\overset{\triangledown}{\dot{\hat{\omega}}}_n] = \boldsymbol{\Lambda}\delta\dot{\hat{\Omega}}_n = \boldsymbol{\Lambda}[\delta\dot{\hat{\Theta}}_{,S} +\dot{\widetilde{\boldsymbol{\Omega}}}_n\delta\hat{\Theta} + \widetilde{\boldsymbol{\Omega}}_n, \delta\dot{\hat{\Theta}}]. \tag{5.31c}$$

It is worth note that $\delta\,[\overset{\triangledown}{\dot{\hat{\omega}}}_n] \neq D\,[\overset{\triangledown}{\dot{\hat{\omega}}}_n]\cdot\hat{\eta}^{\mathrm{m}}$, where on the right hand side the linearization of the co–rotated curvature strain rate vector is performed on the tangent space where it belongs *i.e.* $T^{\mathrm{mat}}_{\boldsymbol{\Lambda}}$.

Analogously as for the case of the spatial updating of the rotational field, one obtains that the material and co-rotated descriptions of the linearized increment of the strain rate at material point level are calculated as

$$\delta\hat{\mathcal{S}}_n = \delta\dot{\hat{\mathcal{E}}}_n = \delta\dot{\hat{\Gamma}}_n + \delta\dot{\hat{\Omega}}_n \times \hat{\mathscr{E}} \tag{5.32}$$

$$\delta\hat{s}_n = \delta[\overset{\triangledown}{\dot{\hat{\varepsilon}}}_n]= \boldsymbol{\Lambda}\delta\dot{\hat{\mathcal{E}}}_n = \delta[\overset{\triangledown}{\dot{\hat{\gamma}}}_n] +\delta[\overset{\triangledown}{\dot{\hat{\omega}}}_n] \times\hat{\mathscr{T}}. \tag{5.33}$$

The terms $\delta\dot{\hat{\varphi}}$, $\delta\dot{\hat{\varphi}}_{,S}$, $\delta\dot{\hat{\Theta}}$ and $\delta\dot{\hat{\Theta}}_{,S}$ of Eqs. (5.29c) and (5.31c) do not allow to express directly the co-rotated variations of the strain rate vectors in terms of $\hat{\eta}^{\mathrm{m}}$. The specific time–stepping scheme used in the numerical integration of the equations of motion provides the needed relations [365]. This aspect will be explained in detail in §6.

Analogously as for the case of the spatial updating of the rotations, lets suppose that there exist an additional linear operator $\boldsymbol{\mathscr{H}}^{\mathrm{m}}_{b}(\hat{\Theta}) \in \mathcal{L}(T^{\mathrm{mat}}_{\boldsymbol{\Lambda}}, T^{\mathrm{mat}}_{\boldsymbol{\Lambda}})$ such that

$$\delta\dot{\hat{\Theta}} = \boldsymbol{\mathscr{H}}^{\mathrm{m}}_{b}\delta\hat{\Theta}, \qquad \delta\dot{\hat{\Theta}}_{,S} = \boldsymbol{\mathscr{H}}^{\mathrm{m}}_{b}\delta\hat{\Theta}_{,S} +\boldsymbol{\mathscr{H}}^{\mathrm{m}}_{b},_S\,\delta\hat{\Theta} \tag{5.34}$$

Therefore, Eqs. (5.29c) and (5.31c) can be rearranged as

$$\begin{bmatrix} \overset{\triangledown}{\delta[\dot{\hat{\gamma}}_n]} \\ \overset{\triangledown}{\delta[\dot{\hat{\omega}}_n]} \end{bmatrix} = \underbrace{\begin{bmatrix} (\boldsymbol{\mathscr{H}}_a - \widetilde{\boldsymbol{v}}_n)[\frac{\mathrm{d}}{\mathrm{d}S}\mathbf{I}] + \boldsymbol{\mathscr{H}}_a,_S & [\overset{\triangledown}{\dot{\widetilde{\boldsymbol{\gamma}}}_n]}\,\boldsymbol{\Lambda} + \boldsymbol{\Lambda}\boldsymbol{\Pi}[\boldsymbol{\Lambda}^T\hat{\varphi},_S\,]\boldsymbol{\mathscr{H}}^{\mathrm{m}}_{b} \\ 0 & \boldsymbol{\Lambda}(\boldsymbol{\mathscr{H}}^{\mathrm{m}}_{b}[\frac{\mathrm{d}}{\mathrm{d}S}\mathbf{I}] + \boldsymbol{\mathscr{H}}^{\mathrm{m}}_{b},_S +\dot{\widetilde{\boldsymbol{\Omega}}}_n + \widetilde{\boldsymbol{\Omega}}_n\boldsymbol{\mathscr{H}}^{\mathrm{m}}_{b}) \end{bmatrix}}_{[\bar{\boldsymbol{\mathcal{V}}}(\hat{\varphi},\hat{\Theta})]} \begin{bmatrix} \delta\hat{\varphi} \\ \delta\hat{\Theta} \end{bmatrix} = \bar{\boldsymbol{\mathcal{V}}}\hat{\eta}^{\mathrm{m}}. \tag{5.35}$$

It is worth to note that the tensor $\bar{\boldsymbol{\mathcal{V}}}$ is configuration dependent and it couples the rotational and translational parts of the motion.

5.2 Linearization of the stress resultants and stress couples

5.2.1 Elastic case

Considering the variation of strains, Eqs. (5.8a) trough (5.11b), the constitutive relations for stress resultant and couples in material form given in §3.7 for the linear case and denoting

$\mathbf{C}^{\mathrm{me}}_n = \mathbf{C}^{\mathrm{me}}_{nn}$ and $\mathbf{C}^{\mathrm{me}}_m = \mathbf{C}^{\mathrm{me}}_{mm}$, one obtains that

$$\begin{aligned} D\hat{n}^{\mathrm{m}} \cdot \hat{\eta}^{\mathrm{s}} = \delta\hat{n}^{\mathrm{m}} &= \bar{\mathbf{C}}^{\mathrm{me}}_{nn}\delta\hat{\Gamma}_n + \bar{\mathbf{C}}^{\mathrm{me}}_{nm}\delta\hat{\Omega}_n \\ &= \bar{\mathbf{C}}^{\mathrm{me}}_{nn}\boldsymbol{\Lambda}^T(\delta\hat{\varphi}_{,S} + \boldsymbol{\Pi}[\hat{\varphi}_{,S}]\delta\hat{\theta}) + \bar{\mathbf{C}}^{\mathrm{me}}_{nm}\boldsymbol{\Lambda}^T\delta\hat{\theta}_{,S} \end{aligned} \tag{5.36}$$

where $\bar{\mathbf{C}}^{\mathrm{me}}_{ij}$, $(i,j \in \{n,m\})$ are the material forms of the elastic constitutive tensors obtained according to the mixing rule as explained in §4.3. Hence, employing the pullback and push–forward operations we obtain the Lie variation (or co–rotated variation) as

$$\begin{aligned} \delta\overset{\triangledown}{[\hat{n}]} &= \boldsymbol{\Lambda}\delta(\boldsymbol{\Lambda}^T\hat{n}) = \boldsymbol{\Lambda}\delta\hat{n}^{\mathrm{m}} \\ &= \underbrace{\boldsymbol{\Lambda}\bar{\mathbf{C}}^{\mathrm{me}}_{nn}\boldsymbol{\Lambda}^T}_{\bar{\mathbf{C}}^{\mathrm{se}}_{nn}}(\delta\hat{\varphi}_{,S} + \boldsymbol{\Pi}[\hat{\varphi}_{,S}]\delta\hat{\theta}) + \underbrace{\boldsymbol{\Lambda}\bar{\mathbf{C}}^{\mathrm{me}}_{nm}\boldsymbol{\Lambda}^T}_{\bar{\mathbf{C}}^{\mathrm{se}}_{nm}}\delta\hat{\theta}_{,S} \\ &= \bar{\mathbf{C}}^{\mathrm{se}}_{nn}(\delta\hat{\varphi}_{,S} + \boldsymbol{\Pi}[\hat{\varphi}_{,S}]\delta\hat{\theta}) + \bar{\mathbf{C}}^{\mathrm{se}}_{nm}\delta\hat{\theta}_{,S} \end{aligned} \tag{5.37}$$

where $\bar{\mathbf{C}}^{\mathrm{se}}_{ij}$, $(i,j \in \{n,m\})$ are the spatial forms of the elastic constitutive tensors. Similarly, one obtain for the case of the stress couples

$$D\hat{m}^{\mathrm{m}} \cdot \hat{\eta}^{\mathrm{s}} = \delta\hat{m}^{\mathrm{m}} = \bar{\mathbf{C}}^{\mathrm{me}}_{mn}\boldsymbol{\Lambda}^T(\delta\hat{\varphi}_{,S} + \boldsymbol{\Pi}[\hat{\varphi}_{,S}]\delta\hat{\theta}) + \bar{\mathbf{C}}^{\mathrm{me}}_{mm}\boldsymbol{\Lambda}^T\delta\hat{\theta}_{,S} \tag{5.38}$$

$$\delta\overset{\triangledown}{[\hat{m}]} = \bar{\mathbf{C}}^{\mathrm{se}}_{mn}(\delta\hat{\varphi}_{,S} + \boldsymbol{\Pi}[\hat{\varphi}_{,S}]\delta\hat{\theta}) + \bar{\mathbf{C}}^{\mathrm{se}}_{mm}\delta\hat{\theta}_{,S}\,. \tag{5.39}$$

The linear form of the spatial stress resultant is calculated noticing the following relation for the co–rotated variation: $\delta\overset{\triangledown}{[\hat{n}]} = \delta\hat{n} - \delta\widetilde{\boldsymbol{\theta}}\hat{n} = \delta\hat{n} + \widetilde{\boldsymbol{n}}\delta\hat{\theta}$, (where $\widetilde{\boldsymbol{n}} = \boldsymbol{\Pi}[\hat{n}]$) as

$$\begin{aligned} D\hat{n} \cdot \hat{\eta}^{\mathrm{s}} = \delta\hat{n} &= \delta\overset{\triangledown}{[\hat{n}]} + \delta\widetilde{\boldsymbol{\theta}}\hat{n} = \delta\overset{\triangledown}{[\hat{n}]} - \widetilde{\boldsymbol{n}}\delta\hat{\theta} \\ &= \bar{\mathbf{C}}^{\mathrm{se}}_{nn}(\delta\hat{\varphi}_{,S} + \boldsymbol{\Pi}[\hat{\varphi}_{,S}]\delta\hat{\theta}) + \bar{\mathbf{C}}^{\mathrm{se}}_{nm}\delta\hat{\theta}_{,S} - \widetilde{\boldsymbol{n}}\delta\hat{\theta} \\ &= \bar{\mathbf{C}}^{\mathrm{se}}_{nn}\delta\hat{\varphi}_{,S} + (\bar{\mathbf{C}}^{\mathrm{se}}_{n}\boldsymbol{\Pi}[\hat{\varphi}_{,S}] - \widetilde{\boldsymbol{n}})\delta\hat{\theta} + \bar{\mathbf{C}}^{\mathrm{se}}_{nm}\delta\hat{\theta}_{,S} \end{aligned} \tag{5.40}$$

and analogously for the variation of the spatial form of the stress couple

$$D\hat{m} \cdot \hat{\eta}^{\mathrm{s}} = \delta\hat{m} = \bar{\mathbf{C}}^{\mathrm{se}}_{mn}\delta\hat{\varphi}_{,S} + (\bar{\mathbf{C}}^{\mathrm{se}}_{mn}\boldsymbol{\Pi}[\hat{\varphi}_{,S}] - \widetilde{\boldsymbol{m}})\delta\hat{\theta} + \bar{\mathbf{C}}^{\mathrm{se}}_{m}\delta\hat{\theta}_{,S}\,. \tag{5.41}$$

The derivation of expressions for the admissible variations of the stress resultants and couples for a general parametrization of the rotational field are omitted here.
The results obtained for the admissible variation of the stress resultant and couples given in Eqs. (5.36) to (5.41) can be summarized and written in matrix form as

$$\begin{bmatrix} \delta\hat{n}^{\mathrm{m}} \\ \delta\hat{m}^{\mathrm{m}} \end{bmatrix} = \underbrace{\begin{bmatrix} \bar{\mathbf{C}}^{\mathrm{me}}_{nn} & \bar{\mathbf{C}}^{\mathrm{me}}_{nm} \\ \bar{\mathbf{C}}^{\mathrm{me}}_{mn} & \bar{\mathbf{C}}^{\mathrm{me}}_{mm} \end{bmatrix}}_{\bar{\mathbf{C}}^{\mathrm{me}}} \underbrace{\begin{bmatrix} \boldsymbol{\Lambda}^T[\frac{\mathrm{d}}{\mathrm{d}S}\mathbf{I}] & \boldsymbol{\Lambda}^T\boldsymbol{\Pi}[\hat{\varphi}_{,S}] \\ 0 & \boldsymbol{\Lambda}^T[\frac{\mathrm{d}}{\mathrm{d}S}\mathbf{I}] \end{bmatrix}}_{\bar{\boldsymbol{B}}^{\mathrm{s}}(\hat{\varphi},\boldsymbol{\Lambda})} \begin{bmatrix} \delta\hat{\varphi} \\ \delta\hat{\theta} \end{bmatrix} = [\bar{\mathbf{C}}^{\mathrm{me}}\bar{\boldsymbol{B}}^{\mathrm{s}}]\hat{\eta}^{\mathrm{s}} \tag{5.42}$$

where the material form of the constitutive tensor $\bar{\mathbf{C}}^{\mathrm{me}}$ has been given in Eqs. (3.164a) to (3.164d). By other hand, the co–rotated admissible variation of the stress resultant and couples

is

$$\begin{bmatrix} \overset{\triangledown}{\delta[\hat{n}]} \\ \overset{\triangledown}{\delta[\hat{m}]} \end{bmatrix} = \underbrace{\begin{bmatrix} \bar{\mathbf{C}}^{\mathrm{se}}_{nn} & \bar{\mathbf{C}}^{\mathrm{se}}_{nm} \\ \bar{\mathbf{C}}^{\mathrm{se}}_{mn} & \bar{\mathbf{C}}^{\mathrm{se}}_{mm} \end{bmatrix}}_{\bar{\mathbf{C}}^{\mathrm{se}}} \underbrace{\begin{bmatrix} [\frac{\mathrm{d}}{\mathrm{d}S}\mathbf{I}] & \mathbf{\Pi}[\hat{\varphi},_S\,] \\ 0 & [\frac{\mathrm{d}}{\mathrm{d}S}\mathbf{I}] \end{bmatrix}}_{\boldsymbol{B}(\hat{\varphi})} \begin{bmatrix} \delta\hat{\varphi} \\ \delta\hat{\theta} \end{bmatrix} = [\bar{\mathbf{C}}^{\mathrm{se}}\boldsymbol{B}]\hat{\eta}^{\mathrm{s}} \tag{5.43}$$

it is worth noting the relations $\mathbf{I}_{\mathbf{\Lambda}}\bar{\mathbf{C}}^{\mathrm{me}}\mathbf{I}^T_{\mathbf{\Lambda}} = \bar{\mathbf{C}}^{\mathrm{se}}$ and $\mathbf{I}_{\mathbf{\Lambda}}\bar{\boldsymbol{B}}^{\mathrm{s}} = \boldsymbol{B}$ where the push–forward operation by $\mathbf{\Lambda}$ has been used to carry the material form of the constitutive tensor to the spatial form, *i.e.* $\mathbf{C}^{\mathrm{se}} = \mathbf{\Lambda}\mathbf{C}^{\mathrm{me}}_{ij}\mathbf{\Lambda}^T$ $(i,j \in \{n,m\})$.
Finally, the spatial form of the admissible variation of the stress resultant and couples can be expressed in matrix form as

$$\begin{bmatrix} \delta\hat{n} \\ \delta\hat{m} \end{bmatrix} = \Bigg\{ \underbrace{\begin{bmatrix} \bar{\mathbf{C}}^{\mathrm{se}}_{nn} & \bar{\mathbf{C}}^{\mathrm{se}}_{nm} \\ \bar{\mathbf{C}}^{\mathrm{se}}_{mn} & \bar{\mathbf{C}}^{\mathrm{se}}_{mm} \end{bmatrix}}_{\bar{\mathbf{C}}^{\mathrm{se}}} \underbrace{\begin{bmatrix} [\frac{\mathrm{d}}{\mathrm{d}S}\mathbf{I}] & \mathbf{\Pi}[\hat{\varphi},_S\,] \\ 0 & [\frac{\mathrm{d}}{\mathrm{d}S}\mathbf{I}] \end{bmatrix}}_{\boldsymbol{B}(\hat{\varphi})} + \underbrace{\begin{bmatrix} 0 & -\widetilde{\boldsymbol{n}} \\ 0 & -\widetilde{\boldsymbol{m}} \end{bmatrix}}_{\mathscr{N}} \Bigg\} \begin{bmatrix} \delta\hat{\varphi} \\ \delta\hat{\theta} \end{bmatrix} = \big\{ \bar{\mathbf{C}}^{\mathrm{se}}\boldsymbol{B} + \mathscr{N} \big\} \hat{\eta}^{\mathrm{s}} \tag{5.44}$$

where the tensor $\mathscr{N}$ takes into account for the stress state existing in the current rod configuration.

5.2.1.a Material updating of the rotational field

Considering the variation of strains, Eqs. (5.8a) trough (5.11b), the constitutive relations for stress resultant and couples in material form given in §3.7 for the linear case, one obtains that

$$D\hat{n}^{\mathrm{m}} \cdot \hat{\eta}^{\mathrm{m}} = \delta\hat{n}^{\mathrm{m}} = \bar{\mathbf{C}}^{\mathrm{me}}_{nn}\delta\hat{\Gamma}_n + \bar{\mathbf{C}}^{\mathrm{me}}_{nm}\delta\hat{\Omega}_n = \bar{\mathbf{C}}^{\mathrm{me}}_{nn}(\mathbf{\Pi}[\mathbf{\Lambda}^T\hat{\varphi},_S\,]\delta\hat{\Theta} + \mathbf{\Lambda}^T\delta\hat{\varphi},_S\,) + \bar{\mathbf{C}}^{\mathrm{me}}_{nm}(\delta\hat{\Theta},_S + \widetilde{\mathbf{\Omega}}_n\delta\hat{\Theta}). \tag{5.45}$$

Additionally, employing the pullback and push–forward operations we obtain the Lie variation, (or co–rotated variation), as

$$\overset{\triangledown}{\delta[\hat{n}]} = \mathbf{\Lambda}\delta(\mathbf{\Lambda}^T\hat{n}) = \mathbf{\Lambda}\delta\hat{n}^{\mathrm{m}} = \bar{\mathbf{C}}^{\mathrm{se}}_{nn}(\mathbf{\Lambda}\mathbf{\Pi}[\mathbf{\Lambda}^T\hat{\varphi},_S\,]\delta\hat{\Theta} + \delta\hat{\varphi},_S\,) + \bar{\mathbf{C}}^{\mathrm{se}}_{nm}(\mathbf{\Lambda}\delta\hat{\Theta},_S + \widetilde{\boldsymbol{\omega}}_n\mathbf{\Lambda}\delta\hat{\Theta}) \tag{5.46}$$

where $\bar{\mathbf{C}}^{\mathrm{se}}_{ij}$, $(i,j \in \{n,m\})$ are the spatial forms of the elastic constitutive tensors. Similarly, one obtain for the case of the stress couples

$$\begin{aligned} D\hat{m}^{\mathrm{m}} \cdot \hat{\eta}^{\mathrm{m}} = \delta\hat{m}^{\mathrm{m}} &= \bar{\mathbf{C}}^{\mathrm{me}}_{mn}(\mathbf{\Pi}[\mathbf{\Lambda}^T\hat{\varphi},_S\,]\delta\hat{\Theta} + \mathbf{\Lambda}^T\delta\hat{\varphi},_S\,) + \bar{\mathbf{C}}^{\mathrm{me}}_{mm}(\delta\hat{\Theta},_S + \widetilde{\mathbf{\Omega}}_n\delta\hat{\Theta}) && (5.47) \\ \overset{\triangledown}{\delta[\hat{m}]} &= \bar{\mathbf{C}}^{\mathrm{se}}_{mn}(\mathbf{\Lambda}\mathbf{\Pi}[\mathbf{\Lambda}^T\hat{\varphi},_S\,]\delta\hat{\Theta} + \delta\hat{\varphi},_S\,) + \bar{\mathbf{C}}^{\mathrm{se}}_{mm}(\mathbf{\Lambda}\delta\hat{\Theta},_S + \widetilde{\boldsymbol{\omega}}_n\mathbf{\Lambda}\delta\hat{\Theta}). && (5.48) \end{aligned}$$

The linear form of the spatial stress resultant is calculated noticing the following relation for the co–rotated variation: $\overset{\triangledown}{\delta[\hat{n}]} = \delta\hat{n} - \delta\widetilde{\mathbf{\Theta}}\hat{n} = \delta\hat{n} + \widetilde{\boldsymbol{n}}\delta\hat{\Theta}$ as

$$\begin{aligned} D\hat{n} \cdot \hat{\eta}^{\mathrm{m}} = \delta\hat{n} &= \overset{\triangledown}{\delta[\hat{n}]} + \delta\widetilde{\boldsymbol{\theta}}\hat{n} = \overset{\triangledown}{\delta[\hat{n}]} - \widetilde{\boldsymbol{n}}\delta\hat{\theta} \\ &= \bar{\mathbf{C}}^{\mathrm{se}}_{nn}(\mathbf{\Lambda}\mathbf{\Pi}[\mathbf{\Lambda}^T\hat{\varphi},_S\,]\delta\hat{\Theta} + \delta\hat{\varphi},_S\,) + \bar{\mathbf{C}}^{\mathrm{se}}_{nm}(\mathbf{\Lambda}\delta\hat{\Theta},_S + \widetilde{\boldsymbol{\omega}}_n\mathbf{\Lambda}\delta\hat{\Theta}) - \widetilde{\boldsymbol{n}}\delta\hat{\Theta} \\ &= \bar{\mathbf{C}}^{\mathrm{se}}_{nn}\delta\hat{\varphi},_S + (\bar{\mathbf{C}}^{\mathrm{se}}_{nn}\mathbf{\Lambda}\mathbf{\Pi}[\mathbf{\Lambda}^T\hat{\varphi},_S\,] + \bar{\mathbf{C}}^{\mathrm{se}}_{nm}\widetilde{\boldsymbol{\omega}}_n\mathbf{\Lambda} - \widetilde{\boldsymbol{n}})\delta\hat{\Theta} + \bar{\mathbf{C}}^{\mathrm{se}}_{nm}\mathbf{\Lambda}\delta\hat{\Theta},_S \end{aligned} \tag{5.49}$$

and analogously for the variation of the spatial form of the stress couple

$$D\hat{m} \cdot \hat{\eta}^{\mathrm{m}} = \delta\hat{m} = \bar{\mathbf{C}}^{\mathrm{se}}_{mn}\delta\hat{\varphi},_S + (\bar{\mathbf{C}}^{\mathrm{se}}_{mn}\mathbf{\Lambda}\mathbf{\Pi}[\mathbf{\Lambda}^T\hat{\varphi},_S\,] + \bar{\mathbf{C}}^{\mathrm{se}}_{mm}\widetilde{\boldsymbol{\omega}}_n\mathbf{\Lambda} - \widetilde{\boldsymbol{m}})\delta\hat{\Theta} + \bar{\mathbf{C}}^{\mathrm{se}}_{mm}\mathbf{\Lambda}\delta\hat{\Theta},_S\,. \tag{5.50}$$

The results obtained for the admissible variation of the stress resultant and couples given in Eqs. (5.36) to (5.41) can be summarized and written in matrix form as

$$\begin{bmatrix} \delta\hat{n}^{\mathrm{m}} \\ \delta\hat{m}^{\mathrm{m}} \end{bmatrix} = \underbrace{\begin{bmatrix} \bar{\mathbf{C}}^{\mathrm{me}}_{nn} & \bar{\mathbf{C}}^{\mathrm{me}}_{nm} \\ \bar{\mathbf{C}}^{\mathrm{me}}_{mn} & \bar{\mathbf{C}}^{\mathrm{me}}_{mm} \end{bmatrix}}_{\bar{\mathbf{C}}^{\mathrm{me}}} \underbrace{\begin{bmatrix} \boldsymbol{\Lambda}^T[\frac{\mathrm{d}}{\mathrm{d}S}\mathbf{I}] & \boldsymbol{\Pi}[\boldsymbol{\Lambda}^T\hat{\varphi}_{,S}\,] \\ 0 & ([\frac{\mathrm{d}}{\mathrm{d}S}\mathbf{I}] + \widetilde{\boldsymbol{\Omega}}_n) \end{bmatrix}}_{\bar{\boldsymbol{B}}^{\mathrm{m}}(\hat{\varphi},\boldsymbol{\Lambda})} \begin{bmatrix} \delta\hat{\varphi} \\ \delta\hat{\Theta} \end{bmatrix} = [\bar{\mathbf{C}}^{\mathrm{me}}\bar{\boldsymbol{B}}^{\mathrm{m}}]\hat{\eta}^{\mathrm{m}} \tag{5.51}$$

where the material form of the constitutive tensor $\bar{\mathbf{C}}^{\mathrm{me}}$ has been given in Eqs. (3.164a) to (3.164d). By other hand, the co–rotated admissible variation of the stress resultant and couples is

$$\begin{bmatrix} \delta[\overset{\triangledown}{\hat{n}}] \\ \delta[\overset{\triangledown}{\hat{m}}] \end{bmatrix} = \underbrace{\begin{bmatrix} \bar{\mathbf{C}}^{\mathrm{se}}_{nn} & \bar{\mathbf{C}}^{\mathrm{se}}_{nm} \\ \bar{\mathbf{C}}^{\mathrm{se}}_{mn} & \bar{\mathbf{C}}^{\mathrm{se}}_{mm} \end{bmatrix}}_{\bar{\mathbf{C}}^{\mathrm{se}}} \underbrace{\begin{bmatrix} [\frac{\mathrm{d}}{\mathrm{d}S}\mathbf{I}] & \boldsymbol{\Lambda}\boldsymbol{\Pi}[\boldsymbol{\Lambda}^T\hat{\varphi}_{,S}\,] \\ 0 & (\boldsymbol{\Lambda}[\frac{\mathrm{d}}{\mathrm{d}S}\mathbf{I}] + \widetilde{\boldsymbol{\omega}}_n\boldsymbol{\Lambda}) \end{bmatrix}}_{\bar{\boldsymbol{B}}(\hat{\varphi})} \begin{bmatrix} \delta\hat{\varphi} \\ \delta\hat{\Theta} \end{bmatrix} = [\bar{\mathbf{C}}^{\mathrm{se}}\bar{\boldsymbol{B}}]\hat{\eta}^{\mathrm{m}} \tag{5.52}$$

Finally, the spatial form of the admissible variation of the stress resultant and couples can be expressed in matrix form as

$$\begin{bmatrix} \delta\hat{n} \\ \delta\hat{m} \end{bmatrix} = \left[\underbrace{\begin{bmatrix} \bar{\mathbf{C}}^{\mathrm{se}}_{nn} & \bar{\mathbf{C}}^{\mathrm{se}}_{nm} \\ \bar{\mathbf{C}}^{\mathrm{se}}_{mn} & \bar{\mathbf{C}}^{\mathrm{se}}_{mm} \end{bmatrix}}_{\bar{\mathbf{C}}^{\mathrm{se}}} \underbrace{\begin{bmatrix} [\frac{\mathrm{d}}{\mathrm{d}S}\mathbf{I}] & \boldsymbol{\Lambda}\boldsymbol{\Pi}[\boldsymbol{\Lambda}^T\hat{\varphi}_{,S}\,] \\ 0 & (\boldsymbol{\Lambda}[\frac{\mathrm{d}}{\mathrm{d}S}\mathbf{I}] + \widetilde{\boldsymbol{\omega}}_n\boldsymbol{\Lambda}) \end{bmatrix}}_{\bar{\boldsymbol{B}}(\hat{\varphi})} + \underbrace{\begin{bmatrix} 0 & -\widetilde{\boldsymbol{n}} \\ 0 & -\widetilde{\boldsymbol{m}} \end{bmatrix}}_{\mathscr{N}} \right] \begin{bmatrix} \delta\hat{\varphi} \\ \delta\hat{\Theta} \end{bmatrix} = \{\bar{\mathbf{C}}^{\mathrm{se}}\bar{\boldsymbol{B}} + \mathscr{N}\}\hat{\eta}^{\mathrm{m}} \tag{5.53}$$

where the tensor $\mathscr{N}$ takes into account for the stress state existing in the current rod configuration.

5.2.2 Inelastic case

In Chapter 4 (§4.2.2) it has been shown that the linearized form of the material version of the total (possibly rate dependent) FPK stress vector can be expressed as

$$\delta\hat{P}^{\mathrm{mt}}_1 = \delta\hat{P}^{\mathrm{m}}_1 + \delta\hat{P}^{\mathrm{mv}}_1 = \bar{\boldsymbol{\mathcal{C}}}^{\mathrm{mv}}\delta\hat{\mathcal{E}}_n + \bar{\boldsymbol{\eta}}^{\mathrm{ms}}\delta\hat{\mathcal{S}}_n \tag{5.54}$$

where $\bar{\boldsymbol{\mathcal{C}}}^{\mathrm{mv}}$ and $\bar{\boldsymbol{\eta}}^{ms}$ are the material form of the rate dependent[4] and viscous tangent constitutive tensors, calculated using the mixing rule for composites as explained in Section 4.3. The term $\delta\hat{\mathcal{S}}_n$ is the linearized increment of the material description of the strain rate vector, Eq. (5.25) or (5.32).

The co–rotated form of Eq. (5.54) is obtained by means of applying the push–forward by the rotation tensor $\boldsymbol{\Lambda}$ as

$$\delta[\overset{\triangledown}{\hat{P}^{\mathrm{t}}_1}] = \boldsymbol{\Lambda}\delta\hat{P}^{\mathrm{mt}}_1 = \boldsymbol{\Lambda}\delta\hat{P}^{\mathrm{m}}_1 + \boldsymbol{\Lambda}\delta\hat{P}^{\mathrm{mv}}_1 = \bar{\boldsymbol{\mathcal{C}}}^{\mathrm{sv}}\delta[\overset{\triangledown}{\hat{\varepsilon}_n}] + \bar{\boldsymbol{\eta}}^{\mathrm{ss}}\delta[\overset{\triangledown}{\hat{s}_n}] \tag{5.55}$$

where $\bar{\boldsymbol{\mathcal{C}}}^{\mathrm{sv}} = \boldsymbol{\Lambda}\bar{\boldsymbol{\mathcal{C}}}^{\mathrm{mv}}\boldsymbol{\Lambda}^T$ and $\bar{\boldsymbol{\eta}}^{\mathrm{ss}} = \boldsymbol{\Lambda}\bar{\boldsymbol{\eta}}^{\mathrm{sv}}\boldsymbol{\Lambda}^T$ are the spatial form of the corresponding constitutive tensors.

By other hand, the components of the spatial version of the total FPK stress vector can be expressed in the local (time varying) frame $\{\hat{t}_i\}$ as $\hat{P}^{\mathrm{t}}_1 = P^{\mathrm{t}}_{1i}\hat{t}_i$ and in the case of its material

[4]Here it has been used the denomination *rate dependent* tangent tensor for the general case of a material presenting viscosity, however it is replaced by the rate independent version when corresponds without altering the formulation.

form $\hat{P}_1^{\rm mt} = P_{1i}^{\rm mt}\hat{E}_i$; taking an admissible variation in both cases, one obtains

$$\begin{aligned} \delta\hat{P}_1^{\rm mt} &= \delta P_{1i}^{\rm mt}\hat{E}_i & (5.56a)\\ \delta\hat{P}_1^{\rm t} &= \delta P_{1i}^{\rm t}\hat{t}_i + \delta\widetilde{\boldsymbol{\theta}}P_{1i}^{\rm t}\hat{t}_i = \delta P_{1i}^{\rm t}\hat{t}_i + \delta\widetilde{\boldsymbol{\theta}}\hat{P}_1^{\rm t}. & (5.56b)\end{aligned}$$

The co-rotated version of the linearized increment of the FPK stress vector is obtained by means of applying the push–forward to $\delta\hat{P}_1^{\rm mt}$ according to

$$\overset{\triangledown}{\delta[\hat{P}_1^{\rm t}]} = \boldsymbol{\Lambda}\delta\hat{\mathbf{P}}_1^{\rm mt} = \delta P_{1i}^{\rm t}\hat{t}_i \tag{5.57a}$$

where it is possible to deduce, taking into account Eqs. (5.55) and (5.55), that

$$\delta\hat{P}_1^{\rm t} = \overset{\triangledown}{\delta[\hat{P}_1^{\rm t}]} + \delta\widetilde{\boldsymbol{\theta}}\hat{P}_1^{\rm t} = \boldsymbol{\mathcal{C}}^{\rm sv}\overset{\triangledown}{\delta[\hat{\varepsilon}_n]} + \boldsymbol{\eta}^{\rm ss}\overset{\triangledown}{\delta[\hat{s}_n]} + \delta\widetilde{\boldsymbol{\theta}}\hat{P}_1^{\rm t} \tag{5.57b}$$

where it is possible to replace $\delta\widetilde{\boldsymbol{\theta}} \in so(3)$ by $\delta\widetilde{\boldsymbol{\Theta}} \in so(3)$ if the material updating rule is preferred. As it has been detailed in §3.3.4, Eqs. (3.95b) and (3.97b), one has explicit expressions for $\hat{n}$ and $\hat{m}$ and the corresponding linearized forms can be estimated starting from the result provided in Eq. (5.57b) and integrating over the cross sectional area as

$$\begin{bmatrix} \delta\hat{n} \\ \delta\hat{m} \end{bmatrix} = \underbrace{\begin{bmatrix} \bar{\mathbf{C}}_{nn}^{\rm sv} & \bar{\mathbf{C}}_{nm}^{\rm sv} \\ \bar{\mathbf{C}}_{mn}^{\rm sv} & \bar{\mathbf{C}}_{mm}^{\rm sv} \end{bmatrix}}_{\bar{\mathbf{C}}^{\rm sv}} \begin{bmatrix} \overset{\triangledown}{\delta[\hat{\gamma}_n]} \\ \overset{\triangledown}{\delta[\hat{\omega}_n]} \end{bmatrix} + \underbrace{\begin{bmatrix} \bar{\boldsymbol{\Upsilon}}_{nn}^{\rm ss} & \bar{\boldsymbol{\Upsilon}}_{nm}^{\rm ss} \\ \bar{\boldsymbol{\Upsilon}}_{mn}^{\rm ss} & \bar{\boldsymbol{\Upsilon}}_{mm}^{\rm ss} \end{bmatrix}}_{\boldsymbol{\Upsilon}^{\rm ss}} \begin{bmatrix} \overset{\triangledown}{\delta[\hat{\gamma}_n]} \\ \overset{\triangledown}{\delta[\hat{\omega}_n]} \end{bmatrix} + \underbrace{\begin{bmatrix} 0 & -\widetilde{\boldsymbol{n}} \\ 0 & -\widetilde{\boldsymbol{m}} \end{bmatrix}}_{\mathscr{N}} \begin{bmatrix} \delta\hat{\varphi} \\ \delta\hat{\theta} \end{bmatrix} \tag{5.58}$$

where $\bar{\mathbf{C}}_{ij}^{\rm sv}$ and $\bar{\boldsymbol{\Upsilon}}_{ij}^{\rm ss}$, $(i,j = n,m)$ are the spatial forms of the *reduced tangential* and *reduced viscous tangential* constitutive tensors, which are calculated simply replacing $\bar{\boldsymbol{\mathcal{C}}}^{\rm se}$ in each material point on the cross section by the tangential $\bar{\boldsymbol{\mathcal{C}}}^{\rm sv}$ and viscous $\bar{\boldsymbol{\eta}}^{\rm se}$ constitutive tensors in spatial description, and integrating over the cross section according the procedure described in §4.4 for the elastic case. It is interesting to note that in the present formulation the reduced tangential and viscous constitutive tensors are rate dependent. The corresponding material forms are obtained as $\bar{\mathbf{C}}_{ij}^{\rm mv} = \boldsymbol{\Lambda}^T\bar{\mathbf{C}}_{ij}^{sv}\boldsymbol{\Lambda}$ and $\bar{\boldsymbol{\Upsilon}}_{ij}^{\rm mv} = \boldsymbol{\Lambda}^T\bar{\boldsymbol{\Upsilon}}_{ij}^{ss}\boldsymbol{\Lambda}$.
If the spatial rule for the the updating procedure of the rotational field is used, Eq. (5.58) can be rewritten, along with expressions for the linearized form of the material and co–rotated versions of the stress resultant and couples, as

$$\begin{aligned} \overset{\triangledown}{\delta[\hat{\Phi}]} &= (\bar{\mathbf{C}}^{\rm sv}\boldsymbol{B} + \bar{\boldsymbol{\Upsilon}}^{\rm ss}\boldsymbol{\mathcal{V}})\hat{\eta}^{\rm s} & (5.59a)\\ \delta\hat{\Phi}^{\rm m} &= (\bar{\mathbf{C}}^{\rm mv}\bar{\boldsymbol{B}}^{\rm s} + \bar{\boldsymbol{\Upsilon}}^{\rm ms}\bar{\boldsymbol{\mathcal{V}}}^{\rm s})\hat{\eta}^{\rm s} & (5.59b)\\ \delta\hat{\Phi} &= (\bar{\mathbf{C}}^{\rm sv}\boldsymbol{B} + \bar{\boldsymbol{\Upsilon}}^{\rm ss}\boldsymbol{\mathcal{V}} + \mathscr{N})\hat{\eta}^{\rm s} & (5.59c)\end{aligned}$$

where the notation $\delta\hat{\Phi} = [\delta\hat{n}, \delta\hat{m}]$, $\overset{\triangledown}{\delta[\hat{\Phi}]} = [\overset{\triangledown}{\delta[\hat{n}]}, \overset{\triangledown}{\delta[\hat{m}]}]$ and $\delta\hat{\Phi}^{\rm m} = [\delta\hat{n}^{\rm m}, \delta\hat{m}^{\rm m}]$ has been used. In the deduction of Eqs. (5.59a) to (5.59a) it also has been used the results of Eqs. (5.12a), (5.16a), (5.12c) and (7.47).

If the material updating rule is preferred Eqs. (5.59a) to (5.59c) take the following form:

$$\begin{aligned}
\delta[\overset{\triangledown}{\hat{\Phi}}] &= (\bar{\mathbf{C}}^{\mathrm{sv}}\bar{\boldsymbol{B}} + \bar{\boldsymbol{\Upsilon}}^{\mathrm{ss}}\bar{\boldsymbol{\mathcal{V}}})\hat{\eta}^{\mathrm{m}} && (5.60a)\\
\delta\hat{\Phi}^{\mathrm{m}} &= (\bar{\mathbf{C}}^{\mathrm{mv}}\bar{\boldsymbol{B}} + \bar{\boldsymbol{\Upsilon}}^{\mathrm{ms}}\bar{\boldsymbol{\mathcal{V}}}^{\mathrm{m}})\hat{\eta}^{\mathrm{m}} && (5.60b)\\
\delta\hat{\Phi} &= (\bar{\mathbf{C}}^{\mathrm{sv}}\bar{\boldsymbol{B}} + \bar{\boldsymbol{\Upsilon}}^{\mathrm{ss}}\bar{\boldsymbol{\mathcal{V}}} + \boldsymbol{\mathscr{N}})\hat{\eta}^{\mathrm{m}} && (5.60c)
\end{aligned}$$

where it has been taken into account the results of Sections 5.1.4 and 5.2.1.

5.2.3 Equivalence between G^{m} and G^{s}

Prior to carry out formally the linearization of the virtual work functional, Eq. (3.145), we will show the equivalence between the material, G^{m}, and spatial, G^{s}, phrasing of this scalar quantity as it has been noted in Remark 3.6.
Consider again any admissible variation in spatial description $\hat{\eta}^{\mathrm{s}} \in T_{\Phi}\mathcal{C}_{t_*}$ superposed onto the configuration $(\hat{\varphi}_*, \boldsymbol{\Lambda}_*) \in \mathcal{C}_t$ at time t_*. Substituting Eqs. (5.8b), (5.8c), (5.10b) and (5.10c) into Eq. (3.147) one obtains the internal part of the material description of the *weak form of the momentum balance* equations [363, 365], $G^{\mathrm{m}}(\hat{\varphi}_*, \boldsymbol{\Lambda}_*, \hat{\eta}^{\mathrm{s}})$, or virtual work; taking the internal contribution of this expression one has that

$$\begin{aligned}
G^{\mathrm{m}}_{\mathrm{int}}(\hat{\varphi}_*, \boldsymbol{\Lambda}_*, \hat{\eta}^{\mathrm{s}}) &= \int_0^L (\delta\hat{\Gamma}_{n*}\cdot\hat{n}^{\mathrm{m}}_* + \delta\hat{\Omega}_{n*}\cdot\hat{m}^{\mathrm{m}}_*)\mathrm{d}S\\
&= \int_0^L \Big\{\big[\boldsymbol{\Lambda}_*^T(\delta\hat{\varphi}_{,S} + \boldsymbol{\Pi}[\hat{\varphi}_{*,S}]\delta\hat{\theta})\big]\cdot\hat{n}^{\mathrm{m}}_* + (\boldsymbol{\Lambda}_*^T\delta\hat{\theta}_{,S})\cdot\hat{m}^{\mathrm{m}}_*\Big\}\mathrm{d}S\\
&= \int_0^L \big\{(\delta\hat{\varphi}_{,S} + \boldsymbol{\Pi}[\hat{\varphi}_{*,S}]\delta\hat{\theta})\cdot(\boldsymbol{\Lambda}_*\hat{n}^{\mathrm{m}}_*) + \delta\hat{\theta}_{,S}\cdot(\boldsymbol{\Lambda}_*\hat{m}^{\mathrm{m}}_*)\big\}\mathrm{d}S\\
&= \int_0^L \big\{(\delta\hat{\varphi}_{,S} + \boldsymbol{\Pi}[\hat{\varphi}_{*,S}]\delta\hat{\theta})\cdot\hat{n}_* + \delta\hat{\theta}_{,S}\cdot\hat{m}_*\big\}\mathrm{d}S\\
&= \int_0^L \big\{\delta\big[\overset{\triangledown}{\hat{\gamma}_n}\big]_*\cdot\hat{n}_* + \delta\big[\overset{\triangledown}{\hat{\omega}_n}\big]_*\cdot\hat{m}_*\big\}\mathrm{d}S\\
&= G^{\mathrm{s}}_{\mathrm{int}}(\hat{\varphi}_*, \boldsymbol{\Lambda}_*, \hat{\eta}^{\mathrm{s}}). && (5.61)
\end{aligned}$$

Considering the external contribution contribution, G^{s}_{ext}, we obtain

$$\begin{aligned}
G^{\mathrm{s}}_{\mathrm{ext}}(\hat{\varphi}_*, \boldsymbol{\Lambda}_*, \hat{\eta}^{\mathrm{s}}) &= \int_0^L \Big\{\delta\hat{\varphi}\cdot\hat{\mathcal{N}}^{\mathrm{s}}_* + \delta\hat{\theta}\cdot\hat{\mathcal{M}}^{\mathrm{s}}_*\Big\}\mathrm{d}S = \int_{[0,L]} \Big\{\delta\hat{\varphi}\cdot\boldsymbol{\Lambda}_*\hat{\mathcal{N}}^{\mathrm{m}}_* + \delta\hat{\theta}\cdot\boldsymbol{\Lambda}_*\hat{\mathcal{M}}^{\mathrm{m}}_*\Big\}\mathrm{d}S\\
&= \int_0^L \Big\{\boldsymbol{\Lambda}_*^T\delta\hat{\varphi}\cdot\hat{\mathcal{N}}^{\mathrm{m}}_* + \boldsymbol{\Lambda}_*^T\delta\hat{\theta}\cdot\hat{\mathcal{M}}^{\mathrm{m}}_*\Big\}\mathrm{d}S = \int_0^L \Big\{\boldsymbol{\Lambda}_*^T\delta\hat{\varphi}\cdot\hat{\mathcal{N}}^{\mathrm{m}}_* + \delta\hat{\Theta}\cdot\hat{\mathcal{M}}^{\mathrm{m}}_*\Big\}\mathrm{d}S\\
&= G^{\mathrm{m}}_{\mathrm{ext}}(\hat{\varphi}_*, \boldsymbol{\Lambda}_*, \hat{\eta}^{\mathrm{s}}). && (5.62)
\end{aligned}$$

where $\boldsymbol{\Lambda}_*^T\delta\hat{\varphi}$ can be seen as the materialization of the spatial quantity $\delta\hat{\varphi}$.

$$\begin{aligned}
G^{\mathrm{s}}_{\mathrm{ine}}(\hat{\varphi}, \boldsymbol{\Lambda}, \hat{\eta}^{\mathrm{s}}) &= \int_0^L \Big\{\delta\hat{\varphi}\cdot\mathcal{A}_{\rho_0}\ddot{\hat{\varphi}}_* + \delta\hat{\theta}\cdot\Big[\boldsymbol{\mathcal{I}}_{\rho_0 *}\hat{\alpha}_* + \widetilde{\boldsymbol{v}}_*(\boldsymbol{\mathcal{I}}_{\rho_0 *}\hat{v}_*)\Big]\Big\}\mathrm{d}S\\
&= \int_0^L \Big\{\delta\hat{\varphi}\cdot\mathcal{A}_{\rho_0}\ddot{\hat{\varphi}}_* + \delta\hat{\Theta}\cdot\Big[\mathbf{I}_{\rho_0 *}\hat{A}_{n*} + \widetilde{\boldsymbol{V}}_{n*}(\mathbf{I}_{\rho_0 *}\hat{V}_{n*})\Big]\Big\}\mathrm{d}S\\
&= G^{\mathrm{m}}_{\mathrm{ine}}(\hat{\varphi}_*, \boldsymbol{\Lambda}_*, \hat{\eta}^{\mathrm{s}}). && (5.63)
\end{aligned}$$

In Eqs. (5.62) to (5.63) the relation between spatial and material descriptions for the angular velocity and acceleration, via the pullback operator by the rotation tensor $\boldsymbol{\Lambda}$, $\hat{V}_n = \boldsymbol{\Lambda}^T \hat{v}_n$ and $\hat{A}_n = \boldsymbol{\Lambda}^T \hat{\alpha}_n$, have been used. The material form of the inertia tensor, (rotational mass), given in Eq. (3.134) in spatial form is obtained by means of the pullback operator for second order tensors $\mathbf{I}_{\rho_0} = \boldsymbol{\Lambda}^T \boldsymbol{\mathcal{I}}_{\rho_0} \boldsymbol{\Lambda}$. In the same way the material forms of the external applied forces and moments $\hat{\mathcal{N}}$ and $\hat{\mathcal{M}}$ are obtained as $\hat{\mathcal{N}}^{\mathrm{m}} = \boldsymbol{\Lambda}^T \hat{\mathcal{N}}$, $\hat{\mathcal{M}}^{\mathrm{m}} = \boldsymbol{\Lambda}^T \hat{\mathcal{M}}$ respectively. Note that independently if the material or spatial form is selected for linearization, always the admissible variation $\hat{\eta}^{\mathrm{s}}$ is given in spatial form.

5.3 Linearization of the virtual work functional

In order to obtain numerical solution procedures of Newton type one need the linearized equilibrium or state equation, which can be achieved through the linearization of the principle of virtual work in its continuum form. The main objective of this section is to obtained the linearized form of the virtual work functional in the form more convenient to a C^1 continuous finite element formulation, thought a C^0 continuous curved rod element[5]. In this section advantages of the results obtained in the previous sections is taken.
Considering the spatial form for the admissible variation $\hat{\eta}^{\mathrm{s}}$ and denoting by $\mathscr{L}[G(\hat{\varphi}_*, \boldsymbol{\Lambda}_*, \hat{\eta}^{\mathrm{s}})]$ the linear part of the functional $G(\hat{\varphi}, \boldsymbol{\Lambda}, \hat{\eta}^{\mathrm{s}})$ at the configuration defined by $(\hat{\varphi}, \boldsymbol{\Lambda}) \equiv (\hat{\varphi}_*, \boldsymbol{\Lambda}_*) \in \mathcal{C}_t$; by definition we have

$$\mathscr{L}[G(\hat{\varphi}_*, \boldsymbol{\Lambda}_*, \hat{\eta}^{\mathrm{s}})] \triangleq G(\hat{\varphi}_*, \boldsymbol{\Lambda}_*, \hat{\eta}^{\mathrm{s}}) + DG(\hat{\varphi}_*, \boldsymbol{\Lambda}_*, \hat{\eta}^{\mathrm{s}}) \cdot \hat{p}^{\mathrm{s}} \tag{5.64}$$

where the Frêchet differential $DG(\hat{\varphi}_*, \boldsymbol{\Lambda}_*, \hat{\eta}^{\mathrm{s}}) \cdot \hat{p}^{\mathrm{s}}$ is obtained through the directional derivative formula (see Defs. A.21 and A.22 of §A.5)

$$DG(\hat{\varphi}_*, \boldsymbol{\Lambda}_*, \hat{\eta}^{\mathrm{s}}) \cdot \hat{p}^{\mathrm{s}} = \frac{\mathrm{d}}{\mathrm{d}\beta}\Big|_{\beta=0} G(\hat{\varphi}_*, \boldsymbol{\Lambda}_*, \hat{\eta}^{\mathrm{s}}, \beta \hat{p}^{\mathrm{s}})$$

and $\hat{p}^{\mathrm{s}} \equiv (\Delta\hat{\varphi}, \Delta\hat{\theta}) \in T_\Phi \mathcal{C}_t$ is an admissible variation as described in §5.1. The physical interpretation of Eq. (5.64) is standard [363, 186]. The term $G(\hat{\varphi}_*, \boldsymbol{\Lambda}_*, \hat{\eta}^{\mathrm{s}})$ supplies the *unbalanced force* at the configuration $(\hat{\varphi}_*, \boldsymbol{\Lambda}_*) \in \mathcal{C}_t$ and the term $DG(\hat{\varphi}_*, \boldsymbol{\Lambda}_*, \hat{\eta}^{\mathrm{s}}) \cdot \hat{p}^{\mathrm{s}}$, linear in $\hat{p}^{\mathrm{s}}$, yields the so called *tangential stiffness*. If $(\hat{\varphi}_*, \boldsymbol{\Lambda}_*)$ is an equilibrium configuration, we must have $G(\hat{\varphi}_*, \boldsymbol{\Lambda}_*, \hat{\eta}^{\mathrm{s}}) = 0$ for any $\hat{\eta}^{\mathrm{s}} \equiv (\delta\hat{\varphi}, \delta\hat{\theta})$.

5.3.1 Linearization of $G_{\mathbf{int}}$

Before to develop the linearization of the internal force term, Eq. (3.143), it is necessary to obtain the linear part of the co–rotated variations of the reduced strain vectors, $\delta[\overset{\triangledown}{\hat{\Phi}}]$, given in matrix form in Eq. (5.12c) *i.e.*

$$\begin{aligned}
D\delta[\overset{\triangledown}{\hat{\Psi}}_*] \cdot \hat{p}^{\mathrm{s}} &= D(\boldsymbol{B}_* \hat{\eta}^{\mathrm{s}}) \cdot \hat{p}^{\mathrm{s}} \\
&= \begin{bmatrix} D(\delta\hat{\varphi}_{,S} + \boldsymbol{\Pi}[\hat{\varphi}_{*,S}]\delta\hat{\theta}) \cdot \hat{p}^{\mathrm{s}} \\ D(\delta\hat{\theta}_{,S}) \cdot \hat{p}^{\mathrm{s}} \end{bmatrix} \\
&= \begin{bmatrix} \Delta\delta\hat{\varphi}_{,S} + \boldsymbol{\Pi}[\Delta\hat{\varphi}_{,S}]\delta\hat{\theta} \\ \Delta\delta\hat{\theta}_{,S} \end{bmatrix} = \begin{bmatrix} 0 & \boldsymbol{\Pi}[\Delta\hat{\varphi}_{,S}] \\ 0 & 0 \end{bmatrix} \begin{bmatrix} \delta\hat{\varphi} \\ \delta\hat{\theta} \end{bmatrix} = \boldsymbol{\Psi}(\hat{p}^{\mathrm{s}})^T \hat{\eta}^{\mathrm{s}}
\end{aligned} \tag{5.65}$$

[5] A rigorous mathematical foundation of the linearization procedures can be found in [251].

where $\delta[\overset{\triangledown}{\hat{\Psi}}]_* = [\delta[\overset{\triangledown}{\hat{\gamma}}]_n, \delta[\overset{\triangledown}{\hat{\omega}}]_n]^T$ and it has been neglected the terms of order $\Delta\delta(\bullet) \approx 0$. The matrix denoted by $\boldsymbol{\Psi}$ has been given in the transposed form by convenience.
Moreover, considering the previous result, employing Eqs. (5.59a) and (5.59c) for the linearized increment of the internal cross sectional force and moment vectors and Eq. (5.12c) for the co–rotated variations of the reduced strain vectors it is possible to express in matrix form the linearization of the internal term of the virtual work as

$$\begin{aligned} DG_{\text{int}*} \cdot \hat{p}^{\text{s}} &= \int_0^L D(\delta[\overset{\triangledown}{\hat{\Psi}}]_* \cdot \hat{\Phi}_*) \cdot \hat{p}^{\text{s}} \mathrm{d}S \\ &= \int_0^L \big((D\delta[\overset{\triangledown}{\hat{\Psi}}]_* \cdot \hat{p}^{\text{s}}) \cdot \hat{\Phi}_* + \delta[\overset{\triangledown}{\hat{\Psi}}]_* \cdot (D\hat{\Phi}_* \cdot \hat{p}^{\text{s}}) \big) \mathrm{d}S \\ &= \int_0^L \big(\hat{\eta}^{\text{s}T} \boldsymbol{\Psi}(\hat{p}^{\text{s}}) \hat{\Phi}_* + \hat{\eta}^{\text{s}T} \boldsymbol{B}_*^T (\bar{\mathbf{C}}_*^{\text{sv}} \boldsymbol{B}_* + \bar{\boldsymbol{\Upsilon}}_*^{\text{ss}} \boldsymbol{\mathcal{V}}_* + \boldsymbol{\mathcal{N}}_*) \hat{p}^{\text{s}} \big) \mathrm{d}S. \end{aligned} \tag{5.66}$$

By other hand, it is necessary to note that

$$\boldsymbol{\Psi}(\hat{p}^{\text{s}}) \hat{\Phi}_* = \begin{bmatrix} 0 & 0 \\ -\boldsymbol{\Pi}[\Delta\hat{\varphi}, _S] & 0 \end{bmatrix} \begin{bmatrix} \hat{n}_* \\ \hat{m}_* \end{bmatrix} = \begin{bmatrix} 0 & 0 \\ \widetilde{\boldsymbol{n}}_* [\frac{\mathrm{d}}{\mathrm{d}S} \mathbf{I}] & 0 \end{bmatrix} \begin{bmatrix} \Delta\hat{\varphi} \\ \Delta\hat{\theta} \end{bmatrix} = \boldsymbol{\mathcal{F}}_* \hat{p}^{\text{s}} \tag{5.67}$$

which allows to rewrite Eq. (5.66) as

$$\begin{aligned} DG_{\text{int}*} \cdot \hat{p}^{\text{s}} &= \int_0^L \hat{\eta}^{\text{s}T} \big(\boldsymbol{\mathcal{F}}_* + \boldsymbol{B}_*^T \bar{\mathbf{C}}_*^{\text{sv}} \boldsymbol{B}_* + \boldsymbol{B}_*^T \bar{\boldsymbol{\Upsilon}}_*^{\text{ss}} \boldsymbol{\mathcal{V}}_* + \boldsymbol{B}_*^T \boldsymbol{\mathcal{N}}_* \big) \hat{p}^{\text{s}} \mathrm{d}S \\ &= \underbrace{\int_0^L \hat{\eta}^{\text{s}T} \big(\boldsymbol{B}_*^T \bar{\mathbf{C}}_*^{\text{sv}} \boldsymbol{B}_* \big) \hat{p}^{\text{s}} \mathrm{d}S}_{K_{M*}} + \underbrace{\int_{[0,L]} \hat{\eta}^{\text{s}T} \big(\boldsymbol{\mathcal{F}}_* + \boldsymbol{B}_*^T \boldsymbol{\mathcal{N}}_* \big) \hat{p}^{\text{s}} \mathrm{d}S}_{K_{G*}} \\ &+ \underbrace{\int_0^L \hat{\eta}^{\text{s}T} \big(\boldsymbol{B}_*^T \bar{\boldsymbol{\Upsilon}}_*^{\text{ss}} \boldsymbol{\mathcal{V}}_* \big) \hat{p}^{\text{s}} \mathrm{d}S}_{K_{V*}} \\ &= K_{M*} + K_{G*} + K_{V*} \end{aligned} \tag{5.68}$$

where the scalars K_{M*} K_{G*} and K_{V*} correspond to the *material* (constitutive), *geometric* (stress dependant) and *viscous* tangential stiffness.

REMARK 5.2. Several observations can be made in Eq. (5.68):

(i) The linear part $DG_{\text{int}}(\hat{\varphi}_*, \boldsymbol{\Lambda}_*, \hat{\eta}^{\text{s}}) \cdot \hat{p}^{\text{s}}$ constitutes a bilinear form (operator) on $T_{\hat{x}}\mathcal{C}_{t_*}$.

(ii) The matrix $[\boldsymbol{B}^T \bar{\mathbf{C}}^{\text{sv}} \boldsymbol{B}]_*$ of K_{M*} is always symmetric although configuration dependent; in contrast with the matrices $[\boldsymbol{\mathcal{F}} + \boldsymbol{B}^T \boldsymbol{\mathcal{N}}]_*$ and $[\boldsymbol{B}^T \bar{\boldsymbol{\Upsilon}}^{\text{ss}} \boldsymbol{\mathcal{V}}]_*$ of K_{G*} K_{V*} respectively; which are always nonsymmetric away from equilibrium ■

5.3.2 Linearization of G_{ine}

Considering the spatial form of the kinematically admissible variation $\hat{\eta}^{\text{s}} \in T_\Phi \mathcal{C}_t$, the inertial term of the virtual work functional, Eq. (3.144), can be expressed as

$$G_{\text{ine}}(\hat{\varphi}_*, \boldsymbol{\Lambda}_*, \hat{\eta}^{\text{s}}) = \int_0^L \hat{\eta}^{\text{s}T} \begin{bmatrix} \mathcal{A}_{\rho_0} \ddot{\hat{\varphi}}_* \\ \boldsymbol{\mathcal{I}}_{\rho_0} \hat{\alpha}_{n*} + \widetilde{\boldsymbol{v}}_{n*} \boldsymbol{\mathcal{I}}_{\rho_0} \hat{v}_{n*} \end{bmatrix} \mathrm{d}S = \int_0^L \hat{\eta}^{\text{s}T} \begin{bmatrix} \mathcal{A}_{\rho_0} \ddot{\hat{\varphi}}_* \\ \boldsymbol{\Lambda} (\mathbf{I}_{\rho_0} \hat{A}_{n*} + \widetilde{\boldsymbol{V}}_{n*} \mathbf{I}_{\rho_0} \hat{V}_{n*}) \end{bmatrix} \mathrm{d}S \tag{5.69}$$

where the spatial form of the rotational terms is phrased in terms of the material angular acceleration and velocity of the current rod relative to the curved reference rod, by means of the push-forward operation by $\boldsymbol{\Lambda}$, by convenience. Employing the same procedure as for the internal virtual work, we have that the linearized increment of the acceleration term G_{ine} is

$$\begin{aligned} & DG_{\text{ine}}(\hat{\varphi}_*, \boldsymbol{\Lambda}_*, \hat{\eta}^{\text{s}}) \cdot \hat{p}^{\text{s}} = \\ = & \int_0^L \hat{\eta}^{\text{s}T} \begin{bmatrix} D[\mathcal{A}_{\rho_0} \ddot{\hat{\varphi}}_*] \cdot \hat{p}^{\text{s}} \\ D[\boldsymbol{\Lambda}_* \{ \mathbf{I}_{\rho_0} \hat{A}_{n*} + \widetilde{\boldsymbol{V}}_{n*} \mathbf{I}_{\rho_0} \hat{V}_{n*} \}] \cdot \hat{p}^{\text{s}} \end{bmatrix} \mathrm{d}S \\ = & \int_0^L \hat{\eta}^{\text{s}T} \begin{bmatrix} \mathcal{A}_{\rho_0} \Delta \ddot{\hat{\varphi}}_* \\ \underbrace{(\Delta \boldsymbol{\Lambda}_*)[\mathbf{I}_{\rho_0} \hat{A}_{n*} + \widetilde{\boldsymbol{V}}_{n*} \mathbf{I}_{\rho_0} \hat{V}_{n*}]}_{\hat{\Xi}_{\theta_1}} + \underbrace{\boldsymbol{\Lambda}_* [\Delta (\mathbf{I}_{\rho_0} \hat{A}_{n*} + \widetilde{\boldsymbol{V}}_{n*} \mathbf{I}_{\rho_0} \hat{V}_{n*})]}_{\hat{\Xi}_{\theta_2}} \end{bmatrix} \mathrm{d}S. \end{aligned} \tag{5.70}$$

Considering that $\Delta \boldsymbol{\Lambda} = \Delta \widetilde{\boldsymbol{\theta}} \boldsymbol{\Lambda}$ and $\boldsymbol{\Pi}[\hat{v}_a]\hat{v}_b = -\boldsymbol{\Pi}[\hat{v}_b]\hat{v}_a$, $\forall \hat{v}_a, \hat{v}_b \in \mathbb{R}^3$, it is possible to give the following expressions for the terms $\hat{\Xi}_{\theta_1}$ and $\hat{\Xi}_{\theta_2}$ in Eq. (5.70) as

$$\hat{\Xi}_{\theta_1} = -\boldsymbol{\Pi}[\boldsymbol{\Lambda}_* (\mathbf{I}_{\rho_0} \hat{A}_{n*} + \widetilde{\boldsymbol{V}}_{n*} \mathbf{I}_{\rho_0} \hat{V}_{n*})] \Delta \hat{\theta} \tag{5.71a}$$

$$\begin{aligned} \hat{\Xi}_{\theta_2} &= \boldsymbol{\Lambda}_* \mathbf{I}_{\rho_0} (\Delta \hat{A}_{n*}) + \boldsymbol{\Lambda}_* \boldsymbol{\Pi}[\Delta \hat{V}_{n*}](\mathbf{I}_{\rho_0} \hat{V}_{n*}) + \boldsymbol{\Lambda}_* \widetilde{\boldsymbol{V}}_{n*} \mathbf{I}_{\rho_0} (\Delta \hat{V}_{n*}) \\ &= \boldsymbol{\Lambda}_* \mathbf{I}_{\rho_0} \Delta \hat{A}_{n*} + (\boldsymbol{\Lambda}_* \widetilde{\boldsymbol{V}}_{n*} \mathbf{I}_{\rho_0} - \boldsymbol{\Lambda}_* \boldsymbol{\Pi}[\mathbf{I}_{\rho_0} \hat{V}_{n*}]) \Delta \hat{V}_{n*} \end{aligned} \tag{5.71b}$$

Noticing that from Eqs. (5.19a) and (5.19b) that $\Delta \hat{V}_n = \boldsymbol{\Lambda}^T \Delta \dot{\hat{\theta}}$ and $\Delta \hat{A}_n = \boldsymbol{\Lambda}^T (\Delta \ddot{\hat{\theta}} - \widetilde{\boldsymbol{v}}_n \Delta \dot{\hat{\theta}})$; it is possible to rewrite Eqs. (5.71a) and (5.71b) as

$$\hat{\Xi}_{\theta_1} = -\boldsymbol{\Pi}[\boldsymbol{\mathcal{I}}_{\rho_0 *} \hat{\alpha}_{n*} + \widetilde{\boldsymbol{v}}_{n*} \boldsymbol{\mathcal{I}}_{\rho_0 *} \hat{v}_{n*}] \Delta \hat{\theta} \tag{5.72a}$$

$$\begin{aligned} \hat{\Xi}_{\theta_2} &= (\boldsymbol{\Lambda}_* \mathbf{I}_{\rho_0} \boldsymbol{\Lambda}_*^T) \Delta \ddot{\hat{\theta}} + \boldsymbol{\Lambda}_* (\widetilde{\boldsymbol{V}}_{n*} \mathbf{I}_{\rho_0} - \mathbf{I}_{\rho_0} \widetilde{\boldsymbol{V}}_{n*} - \boldsymbol{\Pi}[\mathbf{I}_{\rho_0} \hat{V}_{n*}]) \boldsymbol{\Lambda}_*^T \Delta \dot{\hat{\theta}} \\ &= \boldsymbol{\mathcal{I}}_{\rho_0 *} \Delta \ddot{\hat{\theta}} + (\widetilde{\boldsymbol{v}}_{n*} \boldsymbol{\mathcal{I}}_{\rho_0 *} - \boldsymbol{\mathcal{I}}_{\rho_0 *} \widetilde{\boldsymbol{v}}_{n*} - \boldsymbol{\Pi}[\boldsymbol{\mathcal{I}}_{\rho_0 *} \hat{v}_{n*}]) \Delta \dot{\hat{\theta}}. \end{aligned} \tag{5.72b}$$

This last results alow to rewrite the linear part of the acceleration term G_{ine} as

$$\begin{aligned} DG_{\text{ine}}(\hat{\varphi}_*, \boldsymbol{\Lambda}_*, \hat{\eta}^{\text{s}}) \cdot \hat{p}^{\text{s}} &= \int_0^L \hat{\eta}^{\text{s}T} \Big[\boldsymbol{M}_* \begin{bmatrix} \Delta \ddot{\hat{\varphi}} \\ \Delta \ddot{\hat{\theta}} \end{bmatrix} + \boldsymbol{C}_{\text{gyr}*} \begin{bmatrix} \Delta \dot{\hat{\varphi}} \\ \Delta \dot{\hat{\theta}} \end{bmatrix} + \boldsymbol{K}_{\text{cent}*} \begin{bmatrix} \Delta \hat{\varphi} \\ \Delta \hat{\theta} \end{bmatrix} \Big] \mathrm{d}S \\ &= M_* + K_{\text{gyr}*} + K_{\text{cent}*} \end{aligned} \tag{5.73}$$

where the *mass*, *gyroscopic* and *centrifugal* stiffness matrices are defined as follows [88]

$$\big[\boldsymbol{M}\big] = \begin{bmatrix} \mathcal{A}_{\rho_0} \mathbf{I} & 0 \\ 0 & \boldsymbol{\mathcal{I}}_{\rho_0} \end{bmatrix} \tag{5.74a}$$

$$\big[\boldsymbol{C}_{\text{gyr}}\big] = \begin{bmatrix} 0 & 0 \\ 0 & \{\widetilde{\boldsymbol{v}}_n \boldsymbol{\mathcal{I}}_{\rho_0} - \boldsymbol{\mathcal{I}}_{\rho_0} \widetilde{\boldsymbol{v}}_n - \boldsymbol{\Pi}[\boldsymbol{\mathcal{I}}_{\rho_0} \hat{v}_n]\} \end{bmatrix} \tag{5.74b}$$

$$\big[\boldsymbol{K}_{\text{cent}}\big] = \begin{bmatrix} 0 & 0 \\ 0 & -\boldsymbol{\Pi}[\{\boldsymbol{\mathcal{I}}_{\rho_0} \hat{\alpha}_n + \widetilde{\boldsymbol{v}}_n (\boldsymbol{\mathcal{I}}_{\rho_0} \hat{v}_n)\}] \end{bmatrix} \tag{5.74c}$$

and M_*, $K_{\text{gyr}*}$ and $K_{\text{cent}*}$ are the corresponding *translational*, *gyroscopic* and *centrifugal* terms of the tangential stiffness, respectively.
From the previous equations it is possible to appreciate the mass matrix $\boldsymbol{M}$ is always symmetric; the gyroscopic matrix depends linearly on angular velocities and the centrifugal stiffness matrix

depends linearly on angular acceleration and quadratically on angular velocity.

5.3.3 Linearization of $G_{\mathbf{ext}}$

Following the same procedure as for the internal and inertial terms of the virtual work, the external contribution to the virtual work, Eq. (3.146), can be written as

$$G_{\text{ext}}(\hat{\varphi}_*, \mathbf{\Lambda}_*, \hat{\eta}^{\text{s}}) = \int_0^L \hat{\eta}^{\text{s}T} \begin{bmatrix} \hat{\mathcal{N}}^* \\ \hat{\mathcal{M}}^* \end{bmatrix} \mathrm{d}S + \sum_{k=1}^{Np} \hat{\eta}_k^{\text{s}T} \begin{bmatrix} \hat{P}_g^k + \mathbf{\Lambda}_* \hat{\bar{P}}_p^k \\ \hat{M}_g^k \end{bmatrix} \tag{5.75}$$

where the terms $\mathcal{N}^*$ and $\mathcal{M}^*$ consider the contribution of distributed and body external loadings. The summation term consider the contribution of all concentrated forces and moments. Np is the number of points where external loads are applied. Recalling Eqs. (3.169) through (3.173b), Eq. (5.75) can be rewritten as

$$\begin{aligned} G_{\text{ext}}(\hat{\varphi}_*, \mathbf{\Lambda}_*, \hat{\eta}^{\text{s}}) &= \int_0^L \hat{\eta}^{\text{s}T} \Big(\begin{bmatrix} \mathrm{d}\hat{f}_g + \mathrm{d}\hat{f}_{d*} + \mathrm{d}\hat{f}_{p*} \\ \mathrm{d}\hat{m}_g + \mathrm{d}\hat{m}_{d*} + \mathrm{d}\hat{m}_{p*} \end{bmatrix} + \begin{bmatrix} \hat{\mathscr{R}}_\varphi \\ \hat{\mathscr{R}}_\theta \end{bmatrix} \Big) \mathrm{d}S + \sum_{k=1}^{Np} \hat{\eta}_k^{\text{s}T} \begin{bmatrix} \hat{P}_g^k + \hat{P}_{p*}^k \\ \hat{M}_g^k \end{bmatrix} \\ &= \lambda \Big(\int_0^L \hat{\eta}^{\text{s}T} \Big(\begin{bmatrix} \hat{\mathcal{N}}_g + c_{N*} \hat{\mathcal{N}}_d + \mathbf{\Lambda}_* \hat{\bar{\mathcal{N}}}_p \\ \hat{\mathcal{M}}_g + c_{M*} \hat{\mathcal{M}}_d + \mathbf{\Lambda}_* \hat{\bar{\mathcal{M}}}_p \end{bmatrix} + \underbrace{\begin{bmatrix} \int_{\mathcal{A}_0} g_0 \rho_0 (\hat{b} + \ddot{\hat{a}}) \mathrm{d}\mathcal{A}_0 \\ \int_{\mathcal{A}_0} g_0 \widetilde{\boldsymbol{\mathcal{J}}} (\hat{b} + \ddot{\hat{a}}) \mathrm{d}\mathcal{A}_0 \end{bmatrix}}_{\hat{\mathscr{D}}_{\text{bd}}} \Big) \mathrm{d}S \\ &\quad + \sum_{k=1}^{Np} \hat{\eta}_k^{\text{s}T} \begin{bmatrix} \hat{P}_g^k + \mathbf{\Lambda}_* \hat{\bar{P}}_p^k \\ \hat{M}_g^k \end{bmatrix} \Big) \end{aligned} \tag{5.76}$$

which give rise to the external loading. In many practical engineering application the body load contribution arranged in the term $\hat{\mathscr{D}}_{\text{bd}} = [\hat{\mathscr{R}}_\varphi \hat{\mathscr{R}}_\theta]$, which considers the earthquake loading, can be reduced to the form of distributed forces and moments and therefore, no additional considerations will be made about it. In the case of earthquake loading the external body moment contribution can be neglected remaining only the force body loads due to the base acceleration $\ddot{\hat{a}}$ which is configuration independent and it vanish in the linearization process for obtaining the tangential stiffness tensor. The corresponding linearization is given by

$$\begin{aligned} D G_{\text{ext}}(\hat{\varphi}_*, \mathbf{\Lambda}_*, \hat{\eta}^{\text{s}}) \cdot \hat{p}^{\text{s}} &= \lambda \Big(\int_0^L \hat{\eta}^{\text{s}T} \Delta \begin{bmatrix} \hat{\mathcal{N}}_g + c_{N*} \hat{\mathcal{N}}_d + \mathbf{\Lambda}_* \hat{\bar{\mathcal{N}}}_p \\ \hat{\mathcal{M}}_g + c_{M*} \hat{\mathcal{M}}_d + \mathbf{\Lambda}_* \hat{\bar{\mathcal{M}}}_p \end{bmatrix} \mathrm{d}S + \sum_{k=1}^{Np} \hat{\eta}_k^{\text{s}T} \begin{bmatrix} \hat{P}_g^k + \mathbf{\Lambda}_* \hat{\bar{P}}_p^k \\ \hat{M}_g^k \end{bmatrix} \Big) \\ &= \lambda \Big(\int_0^L \hat{\eta}^{\text{s}T} \begin{bmatrix} \hat{\mathcal{N}}_d \Delta c_{N*} + \Delta \mathbf{\Lambda}_* \hat{\bar{\mathcal{N}}}_p \\ \hat{\mathcal{M}}_d \Delta c_{M*} + \Delta \mathbf{\Lambda}_* \hat{\bar{\mathcal{M}}}_p \end{bmatrix} \mathrm{d}S + \sum_{k=1}^{Np} \hat{\eta}_k^{\text{s}T} \begin{bmatrix} \Delta \mathbf{\Lambda}_* \hat{\bar{P}}_p^k \\ 0 \end{bmatrix} \Big) \\ &= \lambda \Big(\int_0^L \hat{\eta}^{\text{s}T} \begin{bmatrix} -\hat{\mathcal{N}}_d (\hat{\mathscr{C}}_{N*} \cdot \Delta\hat{\varphi}_{,S}) + \Delta \widetilde{\boldsymbol{\theta}} \hat{\mathcal{N}}_p \\ -\hat{\mathcal{M}}_d (\hat{\mathscr{C}}_{M*} \cdot \Delta\hat{\varphi}_{,S}) + \Delta \widetilde{\boldsymbol{\theta}} \hat{\mathcal{M}}_p \end{bmatrix} \mathrm{d}S + \sum_{k=1}^{Np} \hat{\eta}_k^{\text{s}T} \begin{bmatrix} \Delta \widetilde{\boldsymbol{\theta}} \hat{P}_{p*}^k \\ 0 \end{bmatrix} \Big) \\ &= \lambda \Big(\int_0^L \hat{\eta}^{\text{s}T} \begin{bmatrix} -(\hat{\mathcal{N}}_d \otimes \hat{\mathscr{C}}_{N*}) \Delta\hat{\varphi}_{,S} - \widetilde{\boldsymbol{\mathcal{N}}}_p \Delta\hat{\theta} \\ -(\hat{\mathcal{M}}_d \otimes \hat{\mathscr{C}}_{M*}) \Delta\hat{\varphi}_{,S} - \widetilde{\boldsymbol{\mathcal{M}}}_p \Delta\hat{\theta} \end{bmatrix} \mathrm{d}S - \sum_{k=1}^{Np} \hat{\eta}_k^{\text{s}T} \begin{bmatrix} \widetilde{\boldsymbol{P}}_{p*}^k \Delta\hat{\theta} \\ 0 \end{bmatrix} \Big) \\ &= -\lambda \Big(\int_0^L \hat{\eta}^{\text{s}T} \Big(\begin{bmatrix} (\hat{\mathcal{N}}_d \otimes \hat{\mathscr{C}}_{N*}) [\frac{\mathrm{d}}{\mathrm{d}S} \mathbf{I}] + \widetilde{\boldsymbol{\mathcal{N}}}_p \\ (\hat{\mathcal{M}}_d \otimes \hat{\mathscr{C}}_{M*}) [\frac{\mathrm{d}}{\mathrm{d}S} \mathbf{I}] + \widetilde{\boldsymbol{\mathcal{M}}}_p \end{bmatrix} \hat{p}^{\text{s}} \mathrm{d}S + \sum_{k=1}^{Np} \hat{\eta}_k^{\text{s}T} \begin{bmatrix} \widetilde{\boldsymbol{P}}_{p*}^k \\ 0 \end{bmatrix} \hat{p}_k^{\text{s}} \Big) \end{aligned} \tag{5.77}$$

where the vectors $\hat{\mathscr{C}}_{N*}$ and $\hat{\mathscr{C}}_{M*}$ are defined as

$$\hat{\mathscr{C}}_{N*} = \frac{2}{\lambda}\int_0^\lambda (\widetilde{\mathbf{d}}_N)^2\hat{\varphi}_{,S}\,\mathrm{d}\lambda; \qquad \hat{\mathscr{C}}_{M*} = \frac{2}{\lambda}\int_0^\lambda (\widetilde{\mathbf{d}}_M)^2\hat{\varphi}_{,S}\,\mathrm{d}\lambda, \tag{5.78}$$

respectively. Therefore, it is possible to write

$$\Delta c_{N*} = -\hat{\mathscr{C}}_{N*}\cdot\Delta\hat{\varphi}_{,S}\,; \qquad \Delta c_{M*} = -\hat{\mathscr{C}}_{M*}\cdot\Delta\hat{\varphi}_{,S}\,, \tag{5.79}$$

for the *deformation-dependent* loading of type **II** or $\hat{\mathscr{C}}_{N*} = 0$ and $\hat{\mathscr{C}}_{M*} = 0$ for *deformation-independent* loading of type **I**.
The term $DG_{\mathrm{ext}}(\hat{\varphi}_*, \mathbf{\Lambda}_*, \hat{\eta}^{\mathrm{s}})\cdot\hat{p}^{\mathrm{s}} = K_{P*}$ corresponds to the *loading* dependent part of the tangential stiffness.
Finally, Eq. (5.64) can be rewritten as

$$\mathscr{L}[G(\hat{\varphi}_*, \mathbf{\Lambda}_*, \hat{\eta}^{\mathrm{s}}, \hat{p}^{\mathrm{s}})] = G_* + K_{M*} + K_{V*} + K_{G*} + K_{P*} + M_* + K_{\mathrm{gyr}*} + K_{\mathrm{cent}*}. \tag{5.80}$$

The discretization of Eq. (5.80) by using the FEM will be explained in detail in Chapter 7.

5.4 Material updating rule of the rotational field

Analogously as for the case of the spatial updating of the rotation field, it is possible to chose the material form of the admissible variation $\hat{p}^{\mathrm{m}} \in T_\Phi\mathcal{C}_t$ yielding to the result that are presented in the next sections.

5.4.1 Linearization of $G_{\mathbf{int}}$

In this case, the linear part of the co–rotated variations of the reduced strain vectors, Eq. (5.12c), is given by

$$\begin{aligned}
D\delta[\overset{\triangledown}{\hat{\Psi}}_*]\cdot\hat{p}^{\mathrm{m}} &= D(\bar{\boldsymbol{B}}_*\hat{\eta}^{\mathrm{m}})\cdot\hat{p}^{\mathrm{m}} \\
&= \begin{bmatrix} D(\delta\hat{\varphi}_{,S} + \mathbf{\Lambda}_*\mathbf{\Pi}[\mathbf{\Lambda}_*^T\hat{\varphi}_{*,S}]\delta\hat{\Theta})\cdot\hat{p}^{\mathrm{m}} \\ D(\mathbf{\Lambda}_*\delta\hat{\Theta}_{,S} + \mathbf{\Lambda}_*\widetilde{\mathbf{\Omega}}_{n*}\delta\hat{\Theta})\cdot\hat{p}^{\mathrm{m}} \end{bmatrix} \\
&= \begin{bmatrix} \mathbf{\Lambda}_*[\delta\widetilde{\mathbf{\Theta}}\Delta\widetilde{\mathbf{\Theta}} - \Delta\widetilde{\mathbf{\Theta}}\delta\widetilde{\mathbf{\Theta}}]\mathbf{\Lambda}_*^T\hat{\varphi}_{*,S} + \mathbf{\Lambda}_*\mathbf{\Pi}[\mathbf{\Lambda}_*^T\Delta\hat{\varphi}_{,S}]\delta\hat{\Theta} \\ \mathbf{\Lambda}_*\Delta\widetilde{\mathbf{\Theta}}\delta\hat{\Theta}_{,S} + \mathbf{\Lambda}_*\Delta\widetilde{\mathbf{\Theta}}\widetilde{\mathbf{\Omega}}_{n*}\delta\hat{\Theta} + \mathbf{\Lambda}_*(\Delta\widetilde{\mathbf{\Theta}}_{,S} + [\widetilde{\mathbf{\Omega}}_{n*}, \Delta\widetilde{\mathbf{\Theta}}])\delta\hat{\Theta} \end{bmatrix} \\
&= \begin{bmatrix} 0 & \mathbf{\Lambda}_*\Big[\mathbf{\Pi}[\mathbf{\Lambda}_*^T\hat{\varphi}_{*,S}]\Delta\widetilde{\mathbf{\Theta}} + \mathbf{\Pi}[\mathbf{\Lambda}_*^T\Delta\hat{\varphi}_{,S}]\Big] \\ 0 & \mathbf{\Lambda}_*\Big[\Delta\widetilde{\mathbf{\Theta}}[\tfrac{\mathrm{d}}{\mathrm{d}S}\mathbf{I}] + \Delta\widetilde{\mathbf{\Theta}}\widetilde{\mathbf{\Omega}}_{n*} + \Delta\widetilde{\mathbf{\Theta}}_{,S} + \mathbf{\Pi}[\widetilde{\mathbf{\Omega}}_{n*}\Delta\hat{\Theta}]\Big] \end{bmatrix}\begin{bmatrix} \delta\hat{\varphi} \\ \delta\hat{\Theta} \end{bmatrix} \\
&= \bar{\mathbf{\Psi}}^T(\hat{p}^{\mathrm{m}})\hat{\eta}^{\mathrm{m}}
\end{aligned} \tag{5.81}$$

where $\delta\overset{\triangledown}{[\hat{\Psi}]}_* = [\delta\overset{\triangledown}{[\hat{\gamma}]}_n, \delta\overset{\triangledown}{[\hat{\omega}]}_n]^T$ and it has been neglected the terms of order $\Delta\delta(\bullet) \approx 0$. The matrix $\bar{\mathbf{\Psi}}$ has been given in the transposed for by convenience. Then, employing Eqs. (5.60a) and (5.60c) for the linearized increment of the internal cross sectional force and moment vectors, it is possible to express in matrix form the linearization of the internal term of the virtual work

as

$$
\begin{aligned}
D G_{\mathrm{int}*}\cdot\hat{p}^{\mathrm{m}} &= \int_0^L D(\delta[\overset{\triangledown}{\hat{\Psi}}]_*\cdot\hat{\Phi}_*)\cdot\hat{p}^{\mathrm{m}}\mathrm{d}S = \int_0^L \big((D\delta[\overset{\triangledown}{\hat{\Psi}}]_*\cdot\hat{p}^{\mathrm{m}})\cdot\hat{\Phi}_* + \delta[\overset{\triangledown}{\hat{\Psi}}]_*\cdot(D\hat{\Phi}_*\cdot\hat{p}^{\mathrm{m}})\big)\mathrm{d}S \\
&= \int_0^L \big(\hat{\eta}^{\mathrm{m}T}\bar{\boldsymbol{\Psi}}(\hat{p}^{\mathrm{m}})\hat{\Phi}_* + \hat{\eta}^{\mathrm{m}T}\bar{\boldsymbol{B}}_*^T(\bar{\mathbf{C}}_*^{\mathrm{sv}}\bar{\boldsymbol{B}}_* + \bar{\boldsymbol{\Upsilon}}_*^{\mathrm{ss}}\bar{\boldsymbol{\mathcal{V}}}_* + \boldsymbol{\mathscr{N}}_*)\hat{p}^{\mathrm{m}}\big)\mathrm{d}S. \qquad (5.82)
\end{aligned}
$$

By other hand, it is necessary to note that

$$
\begin{aligned}
\bar{\boldsymbol{\Psi}}(\hat{p}^{\mathrm{m}})\hat{\Phi}_* &= \left[\begin{array}{c|c} 0 & 0 \\ \hline \Big[\Delta\widetilde{\boldsymbol{\Theta}}\boldsymbol{\Pi}[\boldsymbol{\Lambda}_*^T\hat{\varphi}_{*,S}]- \\ -\boldsymbol{\Pi}[\boldsymbol{\Lambda}_*^T\Delta\hat{\varphi}_{,S}]\Big]\boldsymbol{\Lambda}_*^T & \Big[\widetilde{\boldsymbol{\Omega}}_{n*}\Delta\widetilde{\boldsymbol{\Theta}} - \Delta\widetilde{\boldsymbol{\Theta}}[\frac{\mathrm{d}}{\mathrm{d}S}\mathbf{I}]- \\ -\Delta\widetilde{\boldsymbol{\Theta}}_{,S} - \boldsymbol{\Pi}[\widetilde{\boldsymbol{\Omega}}_{n*}\Delta\hat{\Theta}]\Big]\boldsymbol{\Lambda}_*^T \end{array}\right]\begin{bmatrix}\hat{n}_* \\ \hat{m}_*\end{bmatrix} \\
&= \left[\begin{array}{c|c} 0 & 0 \\ \hline \widetilde{\boldsymbol{n}}^{\mathrm{m}}\boldsymbol{\Lambda}_*^T[\frac{\mathrm{d}}{\mathrm{d}S}\mathbf{I}] & \Big[\boldsymbol{\Pi}[\boldsymbol{\Lambda}_*^T\hat{\varphi}_{*,S}]\widetilde{\boldsymbol{n}}^{\mathrm{m}}+ \\ & +\widetilde{\boldsymbol{m}}_{,S}^{\mathrm{m}}+\widetilde{\boldsymbol{m}}^{\mathrm{m}}[\frac{\mathrm{d}}{\mathrm{d}S}\mathbf{I}] \\ & +\{\widetilde{\boldsymbol{m}}^{\mathrm{m}}\widetilde{\boldsymbol{\Omega}}_{n*} - \widetilde{\boldsymbol{\Omega}}_{n*}\widetilde{\boldsymbol{m}}^{\mathrm{m}}\}\Big] \end{array}\right]\begin{bmatrix}\Delta\hat{\varphi} \\ \Delta\hat{\Theta}\end{bmatrix} = \bar{\boldsymbol{\mathscr{F}}}_*\hat{p}^{\mathrm{m}} \qquad (5.83)
\end{aligned}
$$

which allows to rewrite Eq. (5.82) as

$$
\begin{aligned}
D G_{\mathrm{int}*}\cdot\hat{p}^{\mathrm{m}} &= \int_0^L \hat{\eta}^{\mathrm{m}T}\big(\bar{\boldsymbol{\mathscr{F}}}_* + \bar{\boldsymbol{B}}_*^T\bar{\mathbf{C}}_*^{\mathrm{sv}}\bar{\boldsymbol{B}}_* + \bar{\boldsymbol{B}}_*^T\bar{\boldsymbol{\Upsilon}}_*^{\mathrm{ss}}\bar{\boldsymbol{\mathcal{V}}}_* + \bar{\boldsymbol{B}}_*^T\boldsymbol{\mathscr{N}}_*\big)\hat{p}^{\mathrm{m}}\mathrm{d}S \\
&= \underbrace{\int_0^L \hat{\eta}^{\mathrm{m}T}\big(\bar{\boldsymbol{B}}_*^T\bar{\mathbf{C}}_*^{\mathrm{sv}}\bar{\boldsymbol{B}}_*\big)\hat{p}^{\mathrm{m}}\mathrm{d}S}_{K_{M*}^{\mathrm{m}}} + \underbrace{\int_{[0,L]} \hat{\eta}^{\mathrm{m}T}\big(\bar{\boldsymbol{\mathscr{F}}}_* + \bar{\boldsymbol{B}}_*^T\boldsymbol{\mathscr{N}}_*\big)\hat{p}^{\mathrm{m}}\mathrm{d}S}_{K_{G*}^{\mathrm{m}}} \\
&+ \underbrace{\int_0^L \hat{\eta}^{\mathrm{m}T}\big(\bar{\boldsymbol{B}}_*^T\bar{\boldsymbol{\Upsilon}}_*^{\mathrm{ss}}\bar{\boldsymbol{\mathcal{V}}}_*\big)\hat{p}^{\mathrm{m}}\mathrm{d}S}_{K_{V*}^{\mathrm{m}}} \\
&= K_{M*}^{\mathrm{m}} + K_{G*}^{\mathrm{m}} + K_{V*}^{\mathrm{m}} \qquad (5.84)
\end{aligned}
$$

where the scalars K_{M*}^{m} K_{G*}^{m} and K_{V*}^{m} correspond to the material (constitutive), geometric (stress dependant) and viscous tangential stiffness. The same observations made in Remark 5.2 hold when using the material updating rule for the rotations.

5.4.2 Linearization of G_{ine}

Considering the material updating rule for rotations, $\hat{\eta}^{\mathrm{m}} \in T_{\hat{x}}\mathcal{C}_t$, the inertial term of the virtual work functional can be expressed as

$$
G_{\mathrm{ine}}(\hat{\varphi}_*, \boldsymbol{\Lambda}_*, \hat{\eta}^{\mathrm{m}}) = \int_{[0,L]} \hat{\eta}^{\mathrm{m}T}\begin{bmatrix}\mathcal{A}_{\rho_0}\ddot{\hat{\varphi}}_* \\ \mathbf{I}_{\rho_0}\hat{A}_{n*} + \widetilde{\boldsymbol{V}}_{n*}\mathbf{I}_{\rho_0}\hat{V}_{n*}\end{bmatrix}\mathrm{d}S \qquad (5.85)
$$

Employing the same procedure as for the internal virtual work, we have that the linearized increment of the acceleration term G_{ine} is

$$
D G_{\mathrm{ine}}(\hat{\varphi}_*, \boldsymbol{\Lambda}_*, \hat{\eta}^{\mathrm{m}})\cdot\hat{p}^{\mathrm{m}} = \int_0^L \hat{\eta}^{\mathrm{m}T}\begin{bmatrix} D[\mathcal{A}_{\rho_0}\ddot{\hat{\varphi}}_*]\cdot\hat{p}^{\mathrm{s}} \\ D[\mathbf{I}_{\rho_0}\hat{A}_{n*} + \widetilde{\boldsymbol{V}}_{n*}\mathbf{I}_{\rho_0}\hat{V}_{n*}]\cdot\hat{p}^{\mathrm{m}}\end{bmatrix}\mathrm{d}S
$$

$$= \int_0^L \hat{\eta}^{\mathrm{m}T} \begin{bmatrix} \mathcal{A}_{\rho_0} \Delta\ddot{\hat{\varphi}}_* \\ \underbrace{\mathbf{I}_{\rho_0}\Delta\hat{A}_{n*} + \Delta\widetilde{\boldsymbol{V}}_{n*}\mathbf{I}_{\rho_0}\hat{V}_{n*} + \widetilde{\boldsymbol{V}}_{n*}\mathbf{I}_{\rho_0}\Delta\hat{V}_{n*}}_{\hat{\Xi}^{\mathrm{m}}_{\Theta}} \end{bmatrix} \mathrm{d}S \tag{5.86}$$

considering Eqs. (5.21b) and (5.21d), it is possible to give the following expression for the terms $\hat{\Xi}^{\mathrm{m}}$ in Eq. (5.86) as

$$\begin{aligned} \hat{\Xi}^{\mathrm{m}}_{\Theta} &= \mathbf{I}_{\rho_0}\Delta\hat{A}_{n*} + (\widetilde{\boldsymbol{V}}_{n*}\mathbf{I}_{\rho_0} - \boldsymbol{\Pi}[\mathbf{I}_{\rho_0}\hat{V}_{n*}])\Delta\hat{V}_{n*} \\ &= \mathbf{I}_{\rho_0}(\Delta\ddot{\hat{\Theta}} + \widetilde{\boldsymbol{A}}_{n*}\Delta\hat{\Theta} + \widetilde{\boldsymbol{V}}_{n*}\Delta\dot{\hat{\Theta}}) + (\widetilde{\boldsymbol{V}}_{n*}\mathbf{I}_{\rho_0} - \boldsymbol{\Pi}[\mathbf{I}_{\rho_0}\hat{V}_{n*}])(\Delta\dot{\hat{\Theta}} + \widetilde{\boldsymbol{V}}_{n*}\Delta\hat{\Theta}) \\ &= \mathbf{I}_{\rho_0}\Delta\ddot{\hat{\Theta}} + (\mathbf{I}_{\rho_0}\widetilde{\boldsymbol{V}}_{n*} - \boldsymbol{\Pi}[\mathbf{I}_{\rho_0}\hat{V}_{n*}] + \widetilde{\boldsymbol{V}}_{n*}\mathbf{I}_{\rho_0})\Delta\dot{\hat{\Theta}} \\ &\quad + (\mathbf{I}_{\rho_0}\widetilde{\boldsymbol{A}}_{n*} - \boldsymbol{\Pi}[\mathbf{I}_{\rho_0}\hat{V}_{n*}]\widetilde{\boldsymbol{V}}_{n*} + \widetilde{\boldsymbol{V}}_{n*}\mathbf{I}_{\rho_0}\widetilde{\boldsymbol{V}}_{n*})\Delta\hat{\Theta} \end{aligned} \tag{5.87}$$

This last results alow to rewrite the linear part of the acceleration term G_{ine} as

$$\begin{aligned} DG_{\mathrm{ine}}(\hat{\varphi}_*, \boldsymbol{\Lambda}_*, \hat{\eta}^{\mathrm{m}}) \cdot \hat{p}^{\mathrm{m}} &= \int_0^L \hat{\eta}^{\mathrm{m}T} [\boldsymbol{M}^{\mathrm{m}}_* \begin{bmatrix} \Delta\ddot{\hat{\varphi}} \\ \Delta\ddot{\hat{\Theta}} \end{bmatrix} + \boldsymbol{C}^{\mathrm{m}}_{\mathrm{gyr}*} \begin{bmatrix} \Delta\dot{\hat{\varphi}} \\ \Delta\dot{\hat{\Theta}} \end{bmatrix} + \boldsymbol{K}^{\mathrm{m}}_{\mathrm{cent}*} \begin{bmatrix} \Delta\hat{\varphi} \\ \Delta\hat{\Theta} \end{bmatrix}] \mathrm{d}S \\ &= M^{\mathrm{m}}_* + K^{\mathrm{m}}_{\mathrm{gyr}*} + K^{\mathrm{m}}_{\mathrm{cent}*} \end{aligned} \tag{5.88}$$

where the *mass*, *gyroscopic* and *centrifugal* stiffness matrices are defined as follows

$$\left[\boldsymbol{M}^{\mathrm{m}}\right] = \begin{bmatrix} \mathcal{A}_{\rho_0}\mathbf{I} & 0 \\ 0 & \mathbf{I}_{\rho_0} \end{bmatrix} \tag{5.89a}$$

$$\left[\boldsymbol{C}^{\mathrm{m}}_{\mathrm{gyr}}\right] = \begin{bmatrix} 0 & 0 \\ 0 & (\mathbf{I}_{\rho_0}\widetilde{\boldsymbol{V}}_n - \boldsymbol{\Pi}[\mathbf{I}_{\rho_0}\hat{V}_n] + \widetilde{\boldsymbol{V}}_n\mathbf{I}_{\rho_0}) \end{bmatrix} \tag{5.89b}$$

$$\left[\boldsymbol{K}^{\mathrm{m}}_{\mathrm{cent}}\right] = \begin{bmatrix} 0 & 0 \\ 0 & (\mathbf{I}_{\rho_0}\widetilde{\boldsymbol{A}}_n - \boldsymbol{\Pi}[\mathbf{I}_{\rho_0}\hat{V}_n]\widetilde{\boldsymbol{V}}_n + \widetilde{\boldsymbol{V}}_n\mathbf{I}_{\rho_0}\widetilde{\boldsymbol{V}}_n) \end{bmatrix} \tag{5.89c}$$

and M_*, $K_{\mathrm{gyr}*}$ and $K_{\mathrm{cent}*}$ are the corresponding *translational*, *gyroscopic* and *centrifugal* terms of the tangential stiffness, respectively.
From the above equations it is possible to appreciate the mass matrix $\boldsymbol{M}^{\mathrm{m}}$ is always symmetric and constant; the gyroscopic and centrifugal stiffness matrices depend on the angular velocities and accelerations.

5.4.3 Linearization of $G_{\mathbf{ext}}$

Considering the material updating rule for the rotational field and taking admissible variation $\hat{p}^{\mathrm{m}} \in \eta^{\mathrm{m}}$, Eq. (3.146), can be written as

$$\begin{aligned} G_{\mathrm{ext}}(\hat{\varphi}_*, \boldsymbol{\Lambda}_*, \hat{\eta}^{\mathrm{m}}) &= \int_0^L \hat{\eta}^{\mathrm{m}T} (\begin{bmatrix} \mathrm{d}\hat{f}_g + \mathrm{d}\hat{f}_{d*} + \mathrm{d}\hat{f}_{p*} \\ \mathrm{d}\hat{m}_g + \mathrm{d}\hat{m}_{d*} + \mathrm{d}\hat{m}_{p*} \end{bmatrix} + \begin{bmatrix} \hat{\mathscr{R}}_{\varphi} \\ \hat{\mathscr{R}}_{\theta} \end{bmatrix}) \mathrm{d}S + \sum_{k=1}^{Np} \hat{\eta}^{\mathrm{m}T}_k \begin{bmatrix} \hat{P}^k_g + \hat{P}^k_{p*} \\ \hat{M}^k_g \end{bmatrix} \\ &= \lambda (\int_0^L \hat{\eta}^{\mathrm{m}T} (\begin{bmatrix} \hat{\mathcal{N}}_g + \hat{\mathscr{R}}_{\varphi} + c_{N*}\hat{\mathcal{N}}_d + \boldsymbol{\Lambda}_*\hat{\tilde{\mathcal{N}}}_p \\ \hat{\mathcal{M}}_g + \hat{\mathscr{R}}_{\theta} + c_{M*}\hat{\mathcal{M}}_d + \boldsymbol{\Lambda}_*\hat{\tilde{\mathcal{M}}}_p \end{bmatrix}) \mathrm{d}S + \sum_{k=1}^{Np} \hat{\eta}^{\mathrm{m}T}_k \begin{bmatrix} \hat{P}^k_g + \boldsymbol{\Lambda}_*\hat{\tilde{P}}^k_p \\ \hat{M}^k_g \end{bmatrix}) \end{aligned} \tag{5.90}$$

where $\hat{\mathscr{R}}_{\varphi} = \int_{\mathcal{A}_0} g_0\rho_0(\hat{b} + \ddot{\hat{a}})\mathrm{d}\mathcal{A}_0$ and $\hat{\mathscr{R}}_{\theta} = \int_{\mathcal{A}_0} g_0\widetilde{\boldsymbol{\mathcal{J}}}(\hat{b} + \ddot{\hat{a}})\mathrm{d}\mathcal{A}_0$ consider the earthquake loading and, along with $\hat{\mathcal{N}}_g$ and $\hat{\mathcal{M}}_g$, vanish in the linearization process. The corresponding linear part

is given by

$$
\begin{aligned}
DG_{\mathrm{ext}*}(\hat{\eta}^{\mathrm{m}})\cdot\hat{p}^{\mathrm{m}} &= \lambda(\int_0^L \hat{\eta}^{\mathrm{m}T}\Delta\begin{bmatrix}\hat{\mathcal{N}}_g + c_{N*}\hat{\mathcal{N}}_d + \boldsymbol{\Lambda}_*\hat{\tilde{\mathcal{N}}}_p\\ \hat{\mathcal{M}}_g + c_{M*}\hat{\mathcal{M}}_d + \boldsymbol{\Lambda}_*\hat{\tilde{\mathcal{M}}}_p\end{bmatrix}\mathrm{d}S + \sum_{k=1}^{Np}\hat{\eta}_k^{\mathrm{m}T}\begin{bmatrix}\hat{P}_g^k + \boldsymbol{\Lambda}_*\hat{\tilde{P}}_p^k\\ \hat{M}_g^k\end{bmatrix})\\
&= \lambda(\int_0^L \hat{\eta}^{\mathrm{m}T}\begin{bmatrix}\hat{\mathcal{N}}_d\Delta c_{N*} + \Delta\boldsymbol{\Lambda}_*\hat{\tilde{\mathcal{N}}}_p\\ \hat{\mathcal{M}}_d\Delta c_{M*} + \Delta\boldsymbol{\Lambda}_*\hat{\tilde{\mathcal{M}}}_p\end{bmatrix}\mathrm{d}S + \sum_{k=1}^{Np}\hat{\eta}_k^{\mathrm{m}T}\begin{bmatrix}\Delta\boldsymbol{\Lambda}_*\hat{\tilde{P}}_p^k\\ 0\end{bmatrix})\\
&= \lambda(\int_0^L \hat{\eta}^{\mathrm{m}T}\begin{bmatrix}-\hat{\mathcal{N}}_d(\hat{\mathscr{C}}_{N*}\cdot\Delta\hat{\varphi}_{,S}) + \Delta\widetilde{\boldsymbol{\Theta}}\hat{\mathcal{N}}_p\\ -\hat{\mathcal{M}}_d(\hat{\mathscr{C}}_{M*}\cdot\Delta\hat{\varphi}_{,S}) + \Delta\widetilde{\boldsymbol{\Theta}}\hat{\mathcal{M}}_p\end{bmatrix}\mathrm{d}S + \sum_{k=1}^{Np}\hat{\eta}_k^{\mathrm{m}T}\begin{bmatrix}\Delta\widetilde{\boldsymbol{\Theta}}\hat{P}_{p*}^k\\ 0\end{bmatrix})\\
&= \lambda(\int_0^L \hat{\eta}^{\mathrm{m}T}\begin{bmatrix}-(\hat{\mathcal{N}}_d\otimes\hat{\mathscr{C}}_{N*})\Delta\hat{\varphi}_{,S} - \widetilde{\boldsymbol{\mathcal{N}}}_p\Delta\hat{\Theta}\\ -(\hat{\mathcal{M}}_d\otimes\hat{\mathscr{C}}_{M*})\Delta\hat{\varphi}_{,S} - \widetilde{\boldsymbol{\mathcal{M}}}_p\Delta\hat{\Theta}\end{bmatrix}\mathrm{d}S - \sum_{k=1}^{Np}\hat{\eta}_k^{\mathrm{m}T}\begin{bmatrix}\widetilde{\boldsymbol{P}}_{p*}^k\Delta\hat{\Theta}\\ 0\end{bmatrix})\\
&= -\lambda(\int_0^L \hat{\eta}^{\mathrm{m}T}(\begin{bmatrix}(\hat{\mathcal{N}}_d\otimes\hat{\mathscr{C}}_{N*})[\frac{\mathrm{d}}{\mathrm{d}S}\mathbf{I}] + \widetilde{\boldsymbol{\mathcal{N}}}_p\\ (\hat{\mathcal{M}}_d\otimes\hat{\mathscr{C}}_{M*})[\frac{\mathrm{d}}{\mathrm{d}S}\mathbf{I}] + \widetilde{\boldsymbol{\mathcal{M}}}_p\end{bmatrix}\hat{p}^{\mathrm{m}}\mathrm{d}S + \sum_{k=1}^{Np}\hat{\eta}_k^{\mathrm{m}T}\begin{bmatrix}\widetilde{\boldsymbol{P}}_{p*}^k\\ 0\end{bmatrix}\hat{p}_k^{\mathrm{m}})\\
&= K_{P*}^{\mathrm{m}}
\end{aligned}
\tag{5.91}
$$

where the vectors $\hat{\mathscr{C}}_{N*}$, $\hat{\mathscr{C}}_{M*}$, c_{N*} and c_{M*} have been defined in Eqs. (5.78) and (5.79).

Finally, Eq. (5.64) can be rewritten as

$$
\mathscr{L}[G(\hat{\varphi}_*, \boldsymbol{\Lambda}_*, \hat{\eta}^{\mathrm{s}}, \hat{p}^{\mathrm{s}})] = G_* + K_{M*}^{\mathrm{m}} + K_{V*}^{\mathrm{m}} + K_{G*}^{\mathrm{m}} + K_{P*}^{\mathrm{m}} + M_*^{\mathrm{m}} + K_{\mathrm{gyr}*}^{\mathrm{m}} + K_{\mathrm{cent}*}^{\mathrm{m}}. \tag{5.92}
$$

The discretization of Eq. (5.92) by using the FEM will be explained in detail in Chapter 7.

5.4.4 Symmetry of the tangent stiffness

The symmetry of the material part $\boldsymbol{K}_{\mathrm{M}}$ is obvious, while the geometric part $\boldsymbol{K}_{\mathrm{G}}$ is not symmetric in general. The symmetry of the tangent stiffness, or more precisely the second variation of the internal virtual power, is in general a rather involved issue. A detailed derivation and analysis can be found in the work of Simo [371]. In this work only a simple explanation following Ref. [245] is presented.
Consider a unrestricted finite dimensional manifold $\mathcal{M}$. Let us introduce a r-parametrized curve on this manifold such that

$$
\begin{aligned}
\hat{\alpha} : \mathbb{R} &\rightarrow \mathcal{M}\\
r &\mapsto \hat{\alpha}(r), \qquad \hat{q} = \hat{\alpha}(0), \quad \delta\hat{q} = \hat{\alpha}_{,r}(0)
\end{aligned}
$$

where $\delta\hat{q}$ is the tangent to the curve α at the point q on the manifold $\mathcal{M}$, see Fig. 5.1.
Let $W \in \mathbb{R}$ be a (scalar) work function on the manifold *i.e.*

$$
\begin{aligned}
W : \mathcal{M} &\rightarrow \mathbb{R}\\
\hat{q} &\mapsto W(\hat{q}).
\end{aligned}
$$

The first variation of the work function at the point $\hat{q} \in \mathcal{M}$ in the direction $\delta\hat{q} \in T_{\hat{q}}\mathcal{M}$ reads

$$
\delta W(\hat{q}, \delta\hat{q}) := \frac{\mathrm{d}W(\hat{\alpha}(r))}{\mathrm{d}r}\Big|_{r=0} = D_{\hat{\alpha}}W(\hat{\alpha}(0))\cdot\delta\hat{q}. \tag{5.93}
$$

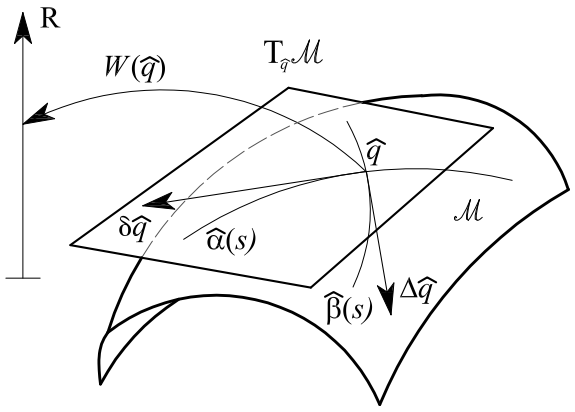

Figure 5.1: A geometric representation of the parameterized curve $\hat{\alpha}(r)$ and the work function $W(\hat{q})$ on the manifold $\mathcal{M}$.

The first variation depends linearly on the direction $\delta\hat{q}$, hence we may write $\delta W = \hat{f}^* \cdot \delta\hat{q}$, where the *pseudo-force* vector $\hat{f}^*(\hat{q})$ belongs at $T^*_{\hat{q}}\mathcal{M}$.
By other hand, we call the point $\hat{q}_0 \in \mathcal{M}$ a *critical point* of W, *i.e.* an equilibrium, if $\delta W(\hat{q}_0, \delta\hat{q})$ vanishes for arbitrary $\delta\hat{q} \in T_{\hat{q}}\mathcal{M}$. At the critical point the corresponding force vector $\hat{f}^*(\hat{q}_0)$ vanishes.
In order to give the second variation of W on $\mathcal{M}$, we introduce another curve with the following properties:

$$\begin{aligned} \hat{\beta} : \mathbb{R} &\rightarrow \mathcal{M} \\ s &\mapsto \hat{\beta}(s), \qquad \hat{q} = \hat{\beta}(0), \quad \delta\hat{q} = \hat{\beta}_{,s}\,(0) \end{aligned}$$

where $\Delta\hat{q} \in T_{\hat{q}}\mathcal{M}$ is the tangent to the curve $\hat{\beta}$. Note that the virtual displacement $\delta\hat{q}(s) \in T_{\hat{\beta}(s)}\mathcal{M}$ depends on the curve $\hat{\beta}$ if the base point varies according to the curve $\hat{\beta}$, see Fig. 5.1.
It is possible to write the second variation of W on $\mathcal{M}$ as

$$\begin{aligned} \delta^2 W(\hat{q}; \delta\hat{q}; \Delta\hat{q}) &:= \frac{\mathrm{d}\delta W(\hat{\beta}(s))}{\mathrm{d}s}\Big|_{s=0} = \frac{\mathrm{d}\big(\hat{f}^*(\hat{\beta}(s))\big) \cdot \delta\hat{q}(\hat{\beta}(s))}{\mathrm{d}s}\Big|_{s=0} \\ &= [D_{\hat{\beta}}\hat{f}^*(\hat{\beta}(0)) \cdot \Delta\hat{q}] \cdot \delta\hat{q}(\hat{\beta}(0)) + \hat{f}^*(\hat{\beta}(0)) \cdot [D_{\hat{\beta}}\delta\hat{q}(\hat{\beta}(0)) \cdot \Delta\hat{q}] \end{aligned} \tag{5.94}$$

where the first term is often denoted by $\mathbf{H}(\hat{q}, \delta\hat{q}, \Delta\hat{q})$ that is the *Hessian* of the function W, which could be denoted by

$$\mathbf{H}(\hat{q}, \delta\hat{q}, \Delta\hat{q}) := D_{\hat{\alpha}\hat{\beta}} W(\hat{\alpha}(0), \hat{\beta}(0)) : (\delta\hat{q} \otimes \Delta\hat{q}),$$

that is a *symmetric form* on $\mathcal{M}$ *i.e.* $\mathbf{H}(\hat{q}, \delta\hat{q}, \Delta\hat{q}) = \mathbf{H}(\hat{q}; \Delta\hat{q}; \delta\hat{q})$ since the Fréchet partial derivatives commute $D_{\hat{\alpha}\hat{\beta}}W = D_{\hat{\beta}\hat{\alpha}}W$ for the smooth function W.
However, the second term in Eq. (5.94), $\hat{f}^*(\hat{\beta}(0)) \cdot (D_{\hat{\beta}}\delta\hat{q}(\hat{\beta}(0)) \cdot \Delta\hat{q})$, is generally nonsymmetric, unless $\hat{q}_0 = \hat{q}(\hat{\beta}(0))$ is a critical point. At the critical point we have the force vector $\hat{f}^*(\hat{q}_0) = 0$, recovering the symmetry to the second variation of the function W.
An important result is that the nonsymmetric term vanishes also if $\mathcal{M}$ is flat as in the case of the general problems of solid mechanics parameterized in terms of Euclidean coordinates, then we get $D_{\hat{\beta}}\delta\hat{q}(\hat{\beta}(0)) \equiv 0$.

As it has been explained in previous sections the current rod placement $\mathcal{C}_t$, Eq. (3.23), is a nonlinear manifold. Independently if we use the spatial or the material updating rule for rotations, we obtain a nonsymmetric geometric stiffness, K_{G}, after linearizing the virtual work functional, Eq. (5.68) or Eq. (5.84). Therefore, we have a nonsymmetric tangent stiffness tensor away from the equilibrium of the system. However, at an equilibrium point we recover the symmetry for conservative loadings [178, 363].

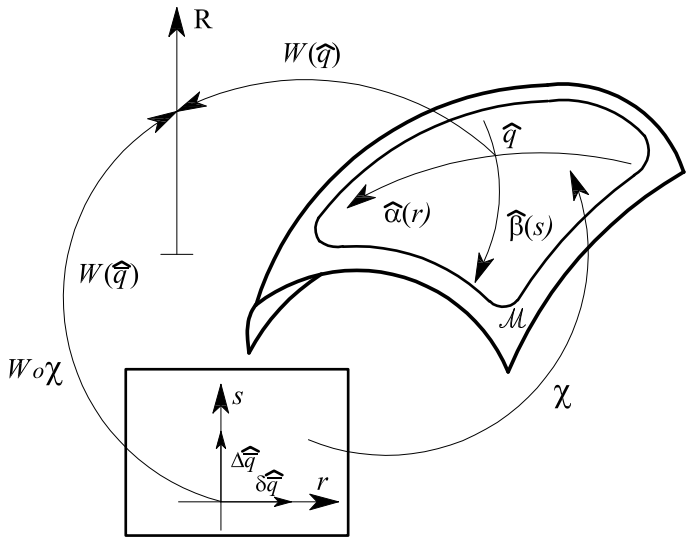

Figure 5.2: Geometric representation for the parametrization of the two-manifold $\mathcal{M}$. χ is the parametrization mapping and $W \circ \chi$ the decomposition mapping.

Mäkinen [246, 245] suggest a way to obtain symmetric stiffness tensor for rods even away from the equilibrium points employing an appropriated parametrization of the manifold $\mathcal{C}_t$. The chosen parametrization χ maps from a open set in an Euclidean space into a open set of the manifold $\mathcal{M}$ (see Fig. 5.2).
The parameterized work function $W \circ \chi : \mathcal{U} \subset \mathbb{R} \rightarrow \mathbb{R}$ is mapping from an Euclidean set into a set of real numbers $\mathbb{R}$. Since the set of an Euclidean space is a flat manifold, the nonsymmetric term of Eq. (5.94) will always vanish. Specifically, the rotation manifold $SO(3)$ could be parameterized by the material rotation vector $\hat{\Psi} \in T_I^{\mathrm{mat}} = \mathbb{R}^3$ (see §A.4 of Chapter A), however in this case the linearization process become considerably more involved (see *e.g.* Cardona and Gerardin [88]).

Chapter 6

Time-steeping schemes and configuration update

This chapter concerns with the presentation of a time–stepping scheme consistent with the kinematic assumptions made for the rod model (see §3) *i.e.* able to manage variables belonging to $SO(3)$ and its tangent space [92]. The time–stepping scheme chosen for the updating procedure corresponds to the *classical Newmark* algorithm for the translational part of the motion and it can be consulted, for example in Refs. [42, 107, 170] among others. In the case of the rotational part, explanations and new developments follow the procedures originally proposed by Simo and Vu-Quoc[1] [365], which has been also applied in a large set of posterior works (see §2).
The crucial difficulty rely on the development of a version of the Newmark scheme consistent with the nonlinear nature of rotations. To this end, time is considered as a set of discrete instants. The problem consists in determining values of points in the configuration manifold (and their related kinematical objects) at these instants, which fulfils the equilibrium equations. As usual, at each time step the linearized problem is solved by means of an iterative scheme until convergency is achieved. Therefore, consistent updating procedures for strains, strain rates, stresses, etc, have to be developed. In the present work, an *iterative* updating procedure is performed *i.e.* the kinematics variables are updated with respect to the last iterative configuration attained in a given time step. In this sense, the present approach corresponds to an *Eulerian* updating procedure. Other works prefers to carry out the updating, as well as the consistent linearization, on the last converged configuration [183] yielding to an *updated Lagrangian* procedure or work directly on the initial configuration yielding to a *total Lagrangian* formulation [88, 247]. Even when both, the updated lagrangian and the total one, can present some advantages such as symmetric stiffness tensors, in the author opinion, the algebraic processes required for obtaining consistent updating procedures as well as tangential stiffness tensors are much more involved. Each section of the present work covers both possibilities: the spatial and the material updating rule for the rotational part of the motion.
Some discussions about the validness of more refined formulations of the Newmark's method, [246, 244, 247], are also addressed. On other hand, more refined *energy–momentum* conserving algorithms [19, 186, 340, 372] are also presented by completeness and with the objective of developing an energy conserving–decaying scheme based on constitutive damping. Finally, and in the category of a proposal, some results are presented about the possibility of deducing consistent time–stepping schemes based on the use of variational integrators which inherit in the discrete case some conserving properties arising from Hamiltonian structure of the problem.

[1] Other authors have developed specific time–stepping schemes for the co–rotational approach [169].

6.1 Formulation of the problem

An iterative step-by-step integration scheme, which considers finite rotations, is here presented following the work of Ref. [365]. The proposed method employs the discrete counterparts of the exponential map, summarized in Table A.1, and the *parallel transport*[2] in $SO(3)$ as it will be explained in the next sections. The algorithm and the associated configuration update procedure can be formulated in either the material or the spatial descriptions.
Let the subscript n to denote the temporal discrete approximation of a given time–varying quantity at time $t_n \in \mathbb{R}^+$. Thus, for the field corresponding to the translational part of the motion one has,

$$\hat{\varphi}_n(S) \triangleq \hat{\varphi}(S, t_n) \tag{6.1a}$$
$$\dot{\hat{\varphi}}_n(S) \triangleq \dot{\hat{\varphi}}(S, t_n) \tag{6.1b}$$
$$\ddot{\hat{\varphi}}_n(S) \triangleq \ddot{\hat{\varphi}}(S, t_n) \tag{6.1c}$$

and for the rotational field and its associated kinetics variables

$$\mathbf{\Lambda}_n(S) \triangleq \mathbf{\Lambda}(S, t_n) \in SO(3) \tag{6.2a}$$
$$\hat{v}_n(S) \triangleq \hat{v}(S, t_n), \qquad \hat{\alpha}_n(S) \triangleq \hat{\alpha}(S, t_n) \in T^{\text{spa}}_{\mathbf{\Lambda}} \tag{6.2b}$$
$$\hat{V}_n(S) \triangleq \hat{V}(S, t_n), \qquad \hat{A}_n(S) \triangleq \hat{A}(S, t_n) \in T^{\text{mat}}_{\mathbf{\Lambda}} \tag{6.2c}$$

where the subscript n in Eqs. (6.2a) to (6.2c) denotes time and do not refers to the incremental quantity from the curved reference rod to the current one. The corresponding angular velocity and angular acceleration tensors can be obtained as usual suing the $\mathbf{\Pi}[\bullet] = \widetilde{\bullet}$ operator.
The basic problem consists in:

(i) Given a configuration $(\hat{\varphi}_n, \mathbf{\Lambda}_n) \in \mathcal{C}_{t_n}$, its associated linear and angular velocity vectors, $(\dot{\hat{\varphi}}_n, \hat{v}_n) \in \mathbb{R}^3 \times T^{\text{spa}}_{\mathbf{\Lambda}_n}$, and linear and angular acceleration vectors $(\ddot{\hat{\varphi}}_n, \hat{\alpha}_n) \in \mathbb{R}^3 \times T^{\text{spa}}_{\mathbf{\Lambda}_n}$,

(ii) obtain the *updated* configuration $(\hat{\varphi}_{n+1}, \mathbf{\Lambda}_{n+1}) \in \mathcal{C}_{t_{n+1}}$ and the corresponding associated linear and angular velocity vectors $(\dot{\hat{\varphi}}_{n+1}, \hat{v}_{n+1}) \in \mathbb{R}^3 \times T^{\text{spa}}_{\mathbf{\Lambda}_{n+1}}$, and the updated linear and angular acceleration vectors $(\ddot{\hat{\varphi}}_{n+1}, \hat{\alpha}_{n+1}) \in \mathbb{R}^3 \times T^{\text{spa}}_{\mathbf{\Lambda}_{n+1}}$, in a manner that is consistent with the virtual work principle.

The material forms of the angular velocity and acceleration vectors can be obtained by using the discrete version of the pullback and push-forward relations between material and spatial descriptions at times t_n and t_{n+1}. These relations have been summarized in Table 6.1.

Table 6.1: Discrete push–forward relations between angular velocity and acceleration vectors at times t_n and t_{n+1}.

Material		Spatial	
t_n	t_{n+1}	t_n	t_{n+1}
$\hat{V}_n$	$\hat{V}_{n+1}$	$\hat{v}_n = \mathbf{\Lambda}_n \hat{V}_n$	$\hat{v}_{n+1} = \mathbf{\Lambda}_{n+1} \hat{V}_{n+1}$
$\hat{A}_n$	$\hat{A}_{n+1}$	$\hat{\alpha}_n = \mathbf{\Lambda}_n \hat{A}_n$	$\hat{\alpha}_{n+1} = \mathbf{\Lambda}_{n+1} \hat{A}_{n+1}$

[2]For a formal definition of the *parallel transport* see *e.g.* [119, 251].

REMARK 6.1. It is worth to note that $\widetilde{\boldsymbol{v}}_n \in T^{\text{spa}}_{\boldsymbol{\Lambda}_n} SO(3)$ and $\widetilde{\boldsymbol{v}}_{n+1} \in T^{\text{spa}}_{\boldsymbol{\Lambda}_{n+1}} SO(3)$ *i.e.* they belong to different tangent spaces on the rotational manifold *i.e.* with different base points, therefore they should not be added directly. The same applies for $\widetilde{\boldsymbol{\alpha}}_n$, $\widetilde{\boldsymbol{\alpha}}_{n+1}$; $\widetilde{\boldsymbol{V}}_n$, $\widetilde{\boldsymbol{V}}_{n+1}$; and $\widetilde{\boldsymbol{A}}_n$, $\widetilde{\boldsymbol{A}}_{n+1}$ and the corresponding associated skew–symmetric tensors ■

6.1.1 Newmark algorithm on the rotational manifold

In this work the classical Newmark algorithm for nonlinear elastodynamics [365] is employed to update the translational part of the configuration and its associated dynamic variables, $(\hat{\varphi}_n, \dot{\hat{\varphi}}_n, \ddot{\hat{\varphi}}_n)$ and, therefore, no explicit details are given in this section[3].
In the case of the rotational part, Simo and Vu-Quoc [365] purpose the Newmark time–stepping algorithm formulated in material form and given in Table 6.2, where $\beta \in [0, \frac{1}{2}]$, $\gamma \in [0, 1]$ are the classical (scalar) parameters of the algorithm and Δt is the time step length.

Table 6.2: Newmark algorithm on $\mathbb{R}^3 \times SO(3)$.

Translation	Rotation
$\hat{\varphi}_{n+1} = \hat{\varphi}_n + \hat{u}_n$	$\boldsymbol{\Lambda}_{n+1} = \boldsymbol{\Lambda}_n \exp\big[\widetilde{\boldsymbol{\Theta}}_n\big] \equiv \exp\big[\widetilde{\boldsymbol{\theta}}_n\big]\boldsymbol{\Lambda}_n$
$\hat{u}_n = \Delta t\dot{\hat{\varphi}}_n + (\Delta t)^2\big[(\frac{1}{2}-\beta)\ddot{\hat{\varphi}}_n + \beta\ddot{\hat{\varphi}}_{n+1}\big]$	$\hat{\Theta}_n = \Delta t\hat{V}_n + (\Delta t)^2\big[(\frac{1}{2}-\beta)\hat{A}_n + \beta\hat{A}_{n+1}\big]$
$\dot{\hat{\varphi}}_{n+1} = \dot{\hat{\varphi}}_n + \Delta t\big[(1-\gamma)\ddot{\hat{\varphi}}_n + \gamma\ddot{\hat{\varphi}}_{n+1}\big]$	$\hat{V}_{n+1} = \hat{V}_n + \Delta t\big[(1-\gamma)\hat{A}_n + \gamma\hat{A}_{n+1}\big]$

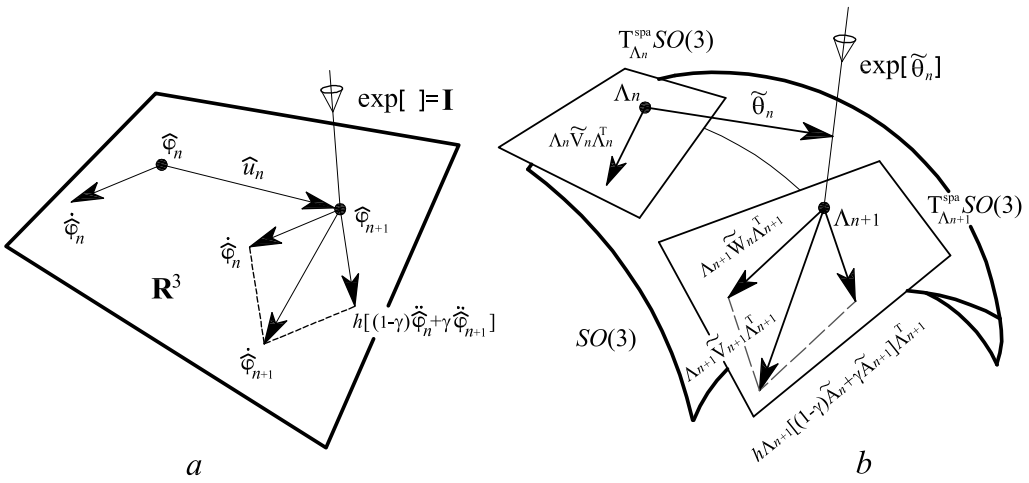

Figure 6.1: Discrete configuration updating in spatial form. (a): Translational part in $\mathbb{R}^3$. (b): Rotational part in $SO(3)$.

The geometric interpretation of the algorithm is shown in Fig. 6.1. For the translational part the time–stepping procedure takes place in $\mathbb{R}^3$ and, therefore, the exponential map reduces to the identity and the parallel transport is simply a shift in the base point. For the rotation part the time–stepping procedure takes place in $SO(3)$. A given configuration $\boldsymbol{\Lambda}_n \in SO(3)$ is updated forward in time by means of exponentiating the incremental rotation $\hat{\theta}_n \in \mathbb{R}^3$ to obtain $\boldsymbol{\Lambda}_{n+1} = \exp[\widetilde{\boldsymbol{\theta}}_n]\boldsymbol{\Lambda}_n$ (or in material description $\boldsymbol{\Lambda}_{n+1} = \boldsymbol{\Lambda}_n \exp[\widetilde{\boldsymbol{\Theta}}_n]$). This procedure ensure $\boldsymbol{\Lambda}_{n+1}$

[3] A formal presentation of time–stepping algorithms can be reviewed in [42, 107, 108, 170, 307].

remains in $SO(3)$ by making use of the discrete form of the exponential map. Note that in Fig. 6.1*b* the step forward in time is performed in material description by employing

$$\widetilde{\boldsymbol{v}}_{n+1} = \boldsymbol{\Lambda}_{n+1}\widetilde{\boldsymbol{V}}_{n+1}\boldsymbol{\Lambda}_{n+1}^{T} \qquad \text{and} \qquad \widetilde{\boldsymbol{\alpha}}_{n+1} = \boldsymbol{\Lambda}_{n+1}\widetilde{\boldsymbol{A}}_{n+1}\boldsymbol{\Lambda}_{n+1}^{T}.$$

This makes sense since $\hat{V}_{n+1}$ and $\hat{A}_{n+1}$ belongs in the same vector space $T^{\text{mat}}_{\boldsymbol{\Lambda}_{n+1}} \approx \mathbb{R}^3$.

REMARK 6.2. Mäkinen in Ref. [244] notes that the scheme presented for the rotational part by Simo and Vu-Quoc is only an approximated version to the correct one, due to the fact that the second and third formulas in Table 6.2 make no sense because the angular velocity vector $\hat{V}_n$ and the angular acceleration $\hat{A}_n$ belongs to different tangent space than the angular velocity and acceleration, $\hat{\Omega}_{n+1}$ and $\hat{A}_{n+1}$ *i.e.* $\hat{\Theta}_n$, $\hat{V}_n$, $\hat{A}_n \in T^{\text{mat}}_n$ and $\hat{\Theta}_{n+1}$, $\hat{V}_{n+1}$, $\hat{A}_{n+1} \in T^{\text{mat}}_{n+1}$. However, that is not necessarily correct due to the fact that the material (respectively spatial) spin vectors by itself belongs to $T^{\text{m}}_{\mathbf{I}}$ (respectively $T^{\text{s}}_{\mathbf{I}}$) and therefore, they should be additive. The nonadditive case has been explained above ■

If material form of the angular velocity and acceleration vectors are considered as independent variables using the Newmark scheme of Table 6.2, the obtained solution procedure yields to the case where the rotational and translational parts are integrated in similar way. However, this would be in contradiction with the fact that the rotation group $SO(3)$ is a non-trivial manifold and not a linear space.
Mäkinen [244] purpose a remedy for this contradiction employing the tangential transformation defined in Eq. A.74 to obtain a linearized and additive approximation between two consecutive rotation vectors which define the rotational part of the configuration of the system.
In this work only the approximated version of the Newmark algorithm on rotational manifold, as originally proposed in [365], will be employed, due to the fact that the present study is concerned with structures which dissipate most of the energy throughout inelastic mechanisms and therefore, no great advantages are obtained by means of using more sophisticated formulations for time–stepping algorithms[4].

6.1.2 Configuration update

The linearized form of Eq. (3.146) (see §5.3 and §5.4 of Chapter 5) is solved in a Newton–Raphson scheme for each time step t_{n+1}. Usually, each time step require several iterations to converge; lets denote generically by (i) to the i$^{\text{th}}$ iteration. Assuming that the configuration $(\hat{\varphi}^{(i)}_{n+1}, \boldsymbol{\Lambda}^{(i)}_{n+1}) \in \mathcal{C}_{t_{n+1}}$ is known, by solving the linearized system it is possible to obtain a *incremental field* $\hat{p}^{\text{s}}_{n+1} = (\Delta\hat{\varphi}^{(i)}_{n+1}, \Delta\hat{\theta}^{(i)}_{n+1})$ such as

$$\mathscr{L}[G(\hat{\varphi}^{(i)}_{n+1}, \boldsymbol{\Lambda}^{(i)}_{n+1}, \hat{\eta}^{\text{s}})] = G(\hat{\varphi}^{(i)}_{n+1}, \boldsymbol{\Lambda}^{(i)}_{n+1}, \hat{\eta}^{\text{s}}) + DG(\hat{\varphi}^{(i)}_{n+1}, \boldsymbol{\Lambda}^{(i)}_{n+1}, \hat{\eta}^{\text{s}}) \cdot \hat{p}^{\text{s}(i)}_{n+1} \approx 0 \qquad (6.3)$$

which is approximately zero for a new family of configuration variables in equilibrium (see §5.4.4). Then, the basic setup [365] is:

□ Given $(\hat{\varphi}^{(i)}_{n+1}, \boldsymbol{\Lambda}^{(i)}_{n+1}) \in \mathcal{C}_{t_{n+1}}$ and the incremental field $(\Delta\hat{\varphi}^{(i)}_{n+1}, \Delta\hat{\theta}^{(i)}_{n+1}) \in T\mathcal{C}_{t_{n+1}}$.

[4]See Mäkinen [244, 247] for an improved Newmark scheme, Betsch and Steinmann [62] for a constrained version of the problem of determining a precise dynamics of rods; Energy/momentum schemes can be consulted in the works of Simo *et al.* [373], Armero and Romero [19, 20, 21, 340] or Ibrahimbegović [189].

- ☐ Update $(\hat{\varphi}_{n+1}^{(i)}, \mathbf{\Lambda}_{n+1}^{(i)}) \in \mathcal{C}_{t_{n+1}}$ to $(\hat{\varphi}_{n+1}^{(i+1)}, \mathbf{\Lambda}_{n+1}^{(i+1)}) \in \mathcal{C}_{t_{n+1}}$ in a manner consistent with the time–stepping algorithm given in Table 6.2.

The translational part is updated as usual in $\mathbb{R}^3$, in this case the exponential map reduces to the identity and parallel transport reduces to *shift* the base point (see Fig. 6.2*a*). The central issue concerns the update of incremental rotation.

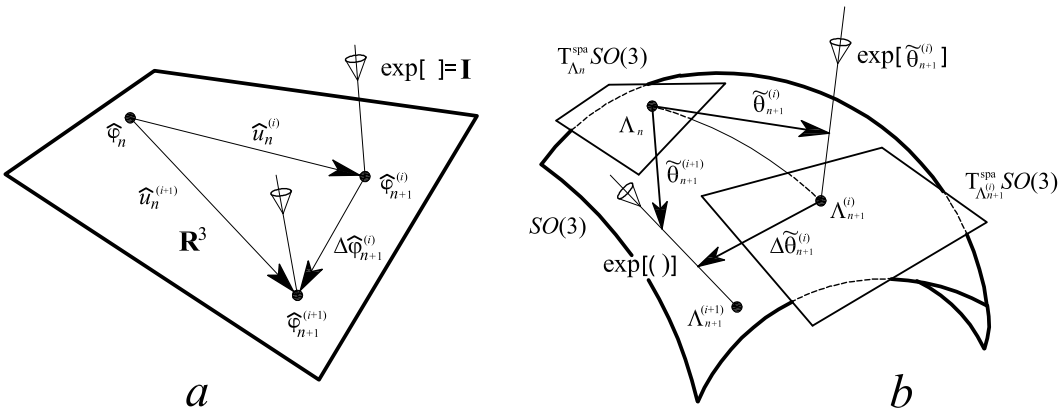

Figure 6.2: Iterative configuration updating in spatial form. (*a*): Translational part in $\mathbb{R}^3$. (*b*): Rotational part in $SO(3)$.

Taking into account the results of Appendix A and using the exponential map, one has

$$\mathbf{\Lambda}_{n+1}^{(i)} = \exp[\widetilde{\boldsymbol{\theta}}_n^{(i)}]\mathbf{\Lambda}_n \tag{6.4a}$$

$$\mathbf{\Lambda}_{n+1}^{(i+1)} = \exp[\widetilde{\boldsymbol{\theta}}_n^{(i+1)}]\mathbf{\Lambda}_n \tag{6.4b}$$

where $\widetilde{\boldsymbol{\theta}}_n^{(i)}$ and $\widetilde{\boldsymbol{\theta}}_n^{(i+1)}$ are the skew–symmetric tensors associated to the spatial form of the rotation vectors which parameterize the rotation from $\mathbf{\Lambda}_n$ to $\mathbf{\Lambda}_{n+1}^{(i)}$ and $\mathbf{\Lambda}_{n+1}^{(i+1)}$ corresponding to the iterations (i) and $(i+1)$, respectively. Note that the incremental rotation $\Delta\hat{\theta}_{n+1}^{(i)}$ is *non-additive* to $\hat{\theta}_{n+1}^{(i)}$ but

$$\mathbf{\Lambda}_{n+1}^{(i+1)} = \exp[\Delta\widetilde{\boldsymbol{\theta}}_{n+1}^{(i)}]\mathbf{\Lambda}_{n+1}^{(i)}. \tag{6.5}$$

By other hand, it is interesting to note the fact that both $\widetilde{\boldsymbol{\theta}}_n^{(i)}\mathbf{\Lambda}_n$ and $\widetilde{\boldsymbol{\theta}}_n^{(i+1)}\mathbf{\Lambda}_n$ are elements of the same tangent space $\in T^{\text{spa}}_{\mathbf{\Lambda}_n}SO(3)$ and $\Delta\widetilde{\boldsymbol{\theta}}_{n+1}^{(i)}\mathbf{\Lambda}_n^{(i)} \in T^{\text{spa}}_{\mathbf{\Lambda}_{n+1}}SO(3)$, therefore, the updating procedure described in Eqs. (6.4a) to (6.5) makes perfect sense (see Fig. 6.2*b*).
The second formula in Eq. (6.4a) requires the obtention of $\hat{\theta}_n^{(i+1)}$ from $\hat{\theta}_n^{(i)}$ and $\Delta\hat{\theta}_{n+1}^{(i)}$; this procedure can be carried out with the aid of Eq. (A.76) as

$$\hat{\theta}_n^{(i+1)} = \hat{\theta}_n^{(i)} + \mathbf{T}(\hat{\theta}_n^{(i)})\Delta\hat{\theta}_{n+1}^{(i)}. \tag{6.6}$$

REMARK 6.3. In Ref. [365] the procedure defined in Eq. (6.5) is preferred for updating the rotation tensor in each iteration of a time-step. Other authors [178, 182] prefer to use Eqs. (6.4a) and (6.6) *i.e.* the total incremental rotation vector is the main independent variable selected for describing rotations. This last choice of parametrization for rotations produce symmetric tangential stiffness matrices but the deduction and implementation of the resulting numerical problem become much more complicated and time consuming during calculations ■

6.1.3 Updating procedure for the angular velocity and acceleration

As it has been described translational velocities $\dot{\hat{\varphi}}^{(i)}_{n+1}$ and accelerations $\ddot{\hat{\varphi}}^{(i+1)}_{n+1}$ in each point of the current rod can be obtained by means of employing the formulas of Table 6.2 as usual in elastodynamics. The iterative version of the time–stepping algorithm is presented in Table 6.3. The updated angular velocity $\hat{V}^{(i+1)}_{n+1}$ and acceleration $\hat{A}^{(i+1)}_{n+1}$ vectors in material form[5] are obtained assuming the following *approximation* for the time-step t_{n+1} iterations (i) and $(i+1)$:

$$\begin{aligned}\hat{\Theta}^{(i+1)}_{n} &= \Delta t\hat{V}_n + (\Delta t)^2\big[(\frac{1}{2}-\beta)\hat{A}_n + \beta\hat{A}^{(i+1)}_{n+1}\big]\\ \hat{\Theta}^{(i)}_{n} &= \Delta t\hat{V}_n + (\Delta t)^2\big[(\frac{1}{2}-\beta)\hat{A}_n + \beta\hat{A}^{(i)}_{n+1}\big]\end{aligned} \tag{6.7}$$

where $\hat{\Theta}^{(i)}_n = \mathbf{\Lambda}^T_n\hat{\theta}^{(i)}_n$ and $\hat{\Theta}^{(i+1)}_n = \mathbf{\Lambda}^T_n\hat{\theta}^{(i+1)}_n$. Subtracting the two expressions of Eq. (6.7) one obtains

$$\hat{A}^{(i+1)}_{n+1} = \hat{A}^{(i)}_{n+1} + \frac{1}{(\Delta t)^2\beta}\big[\hat{\Theta}^{(i+1)}_n - \hat{\Theta}^{(i)}_n\big]. \tag{6.8}$$

Similarly, in the case of the material angular velocities one has,

$$\begin{aligned}\hat{V}^{(i+1)}_{n} &= \hat{V}_n + \Delta t\big[(1-\gamma)\hat{A}_n + \gamma\hat{A}^{(i+1)}_{n+1}\big]\\ \hat{V}^{(i)}_{n} &= \hat{V}_n + \Delta t\big[(1-\gamma)\hat{A}_n + \gamma\hat{A}^{(i)}_{n+1}\big]\end{aligned} \tag{6.9}$$

subtracting the two expressions of Eqs. (6.9) and employing Eq. (6.8) one obtains

$$\hat{V}^{(i+1)}_{n+1} = \hat{V}^{(i)}_{n+1} + \frac{\gamma}{\Delta t\beta}\big[\hat{\Theta}^{(i+1)}_n - \hat{\Theta}^{(i)}_n\big]. \tag{6.10}$$

The complete iterative updating procedure for the dynamic variables employing the Newmark algorithm has been summarized in Table 6.3.

Table 6.3: Discrete Newmark algorithm.

Translation	Rotation
$\hat{\varphi}^{(i+1)}_{n+1} = \hat{\varphi}^{(i)}_{n+1} + \hat{u}^{(i)}_{n+1}$ $\dot{\hat{\varphi}}^{(i+1)}_{n+1} = \dot{\hat{\varphi}}^{(i)}_{n+1} + \frac{\gamma}{\Delta t\beta}\Delta\hat{\varphi}^{(i)}_{n+1}$ $\ddot{\hat{\varphi}}^{(i+1)}_{n+1} = \ddot{\hat{\varphi}}^{(i)}_{n+1} + \frac{1}{(\Delta t)^2\beta}\Delta\hat{\varphi}^{(i)}_{n+1}$	$\mathbf{\Lambda}^{(i+1)}_{n+1} = \exp\big[\Delta\widetilde{\boldsymbol{\theta}}^{(i)}_{n+1}\big]\mathbf{\Lambda}^{(i)}_{n+1}$ $\exp\big[\widetilde{\boldsymbol{\theta}}^{(i+1)}_{n}\big] = \exp\big[\Delta\widetilde{\boldsymbol{\theta}}^{(i)}_{n+1}\big]\exp\big[\widetilde{\boldsymbol{\theta}}^{(i)}_{n}\big]$ $\hat{V}^{(i+1)}_{n+1} = \hat{V}^{(i)}_{n+1} + \frac{\gamma}{\Delta t\beta}\big[\hat{\Theta}^{(i+1)}_n - \hat{\Theta}^{(i)}_n\big]$ $\hat{A}^{(i+1)}_{n+1} = \hat{A}^{(i)}_{n+1} + \frac{1}{(\Delta t)^2\beta}\big[\hat{\Theta}^{(i+1)}_n - \hat{\Theta}^{(i)}_n\big]$

In each iteration the angular velocity and acceleration are updated in the material description, their spatial counterparts are obtained throughout the push-forward relations:

$$\hat{v}^{(i+1)}_{n+1} = \mathbf{\Lambda}^{(i+1)}_{n+1}\hat{V}^{(i+1)}_{n+1}; \qquad \text{and} \qquad \hat{\alpha}^{(i+1)}_{n+1} = \mathbf{\Lambda}^{(i+1)}_{n+1}\hat{A}^{(i+1)}_{n+1}.$$

[5] As it has been highlighted in [365] the material description is more advantageous for writing time–stepping algorithms in $SO(3)$ due to the inertia tensor has constant components.

A geometric interpretation of the procedure summarized in Table 6.3 is given in spatial description taking into account that

$$\hat{v}_{n+1}^{(i+1)} = \mathbf{\Lambda}_{n+1}^{(i+1)}\mathbf{\Lambda}_{n+1}^{(i)T}\hat{v}_{n+1}^{(i)} + \frac{\gamma}{(\Delta t)^2\beta}\mathbf{\Lambda}_{n+1}^{(i+1)}\mathbf{\Lambda}_{n}^{T}\big[\hat{\theta}_{n}^{(i+1)} - \hat{\theta}_{n}^{(i)}\big] \tag{6.11}$$

Since $\mathbf{\Lambda}_{n+1}^{(i+1)}\mathbf{\Lambda}_{n+1}^{(i)T} : T^{\text{spa}}_{\mathbf{\Lambda}_{n+1}^{(i)}}SO(3) \to T^{\text{spa}}_{\mathbf{\Lambda}_{n+1}^{(i+1)}}SO(3)$ and $\mathbf{\Lambda}_{n+1}^{(i+1)}\mathbf{\Lambda}_{n}^{T} : T^{\text{spa}}_{\mathbf{\Lambda}_{n}}SO(3) \to T^{\text{spa}}_{\mathbf{\Lambda}_{n+1}^{(i+1)}}SO(3)$, the first term in Eq. (6.11) may be interpreted as the *parallel transport* of $\hat{v}_{n+1}^{(i)}$ from $T^{\text{spa}}_{\mathbf{\Lambda}_{n+1}^{(i)}}SO(3)$ to $T^{\text{spa}}_{\mathbf{\Lambda}_{n+1}^{(i+1)}}SO(3)$; whereas the second term is the parallel transport of $\big[\hat{\theta}_{n}^{(i+1)} - \hat{\theta}_{n}^{(i)}\big]$ from $T^{\text{spa}}_{\mathbf{\Lambda}_{n}}SO(3)$ to $T^{\text{spa}}_{\mathbf{\Lambda}_{n+1}^{(i+1)}}SO(3)$ (see Figure 6.1).
The update procedure summarized in Table 6.3 applies for $i \geq 1$. For $i = 0$, the *initial guess* in the Newton process, one sets:

$$\hat{\varphi}_{n+1}^{(0)} = \hat{\varphi}_n, \qquad \mathbf{\Lambda}_{n+1}^{(0)} = \mathbf{\Lambda}_n. \tag{6.12}$$

With this assumption $(\dot{\hat{\varphi}}_{n+1}^{(0)}, \hat{v}_{n+1}^{(0)})$ and $(\ddot{\hat{\varphi}}_{n+1}^{(0)}, \hat{\alpha}_{n+1}^{(0)})$ are computed by the Newmark formulae of Table 6.2 giving

$$\hat{A}_{n+1}^{(0)} = \big[1 - \frac{1}{2\beta}\big]\hat{A}_n - \frac{\hat{V}_n}{\beta\Delta t} \tag{6.13}$$

$$\hat{V}_{n+1}^{(0)} = \hat{V}_n + \Delta t\big[(1-\gamma)\hat{A}_n + \gamma\hat{A}_{n+1}^{(0)}\big]. \tag{6.14}$$

6.1.3.a Corrected Newmark scheme

As it has been explained in Section 6.1.1 (see Remarks 6.1 and 6.2) the Newmark scheme on the rotation manifold presented in Table 6.2 or equivalently in Eqs. (6.7) and (6.9) is only an approximated formulation (see Mäkinen [244]).
This scheme can not be corrected directly with the aid of the tangential transformation $\mathbf{T}$ given in Eq. (A.76), because it is a linearized operator and the incremental rotation vector $\hat{\theta}_n$ is not necessarily a small quantity. However, the iterative form of the Newmark scheme (see Table 6.3) may be adjusted with the aid of $\mathbf{T}$ obtaining

$$\hat{\Theta}_{n}^{(i+1)} = \hat{\Theta}_{n}^{(i)} + \Delta\hat{\Theta}_{n}^{(i)} \quad \in T_{\Lambda_n}^{\text{mat}} \tag{6.15a}$$

$$\hat{V}_{n+1}^{(i+1)} = \hat{V}_{n+1}^{(i)} + \frac{\gamma}{\Delta t\beta}\mathbf{T}(\hat{\Theta}_{n}^{(i+1)})\Delta\hat{\Theta}_{n}^{(i)} \tag{6.15b}$$

$$\hat{A}_{n+1}^{(i+1)} = \hat{A}_{n+1}^{(i)} + \frac{1}{(\Delta t)^2\beta}\mathbf{T}(\hat{\Theta}_{n}^{(i+1)})\Delta\hat{\Theta}_{n}^{(i)} + \frac{\gamma}{\Delta t\beta}\dot{\mathbf{T}}(\hat{\Theta}_{n}^{(i+1)})\Delta\hat{\Theta}_{n}^{(i)} \tag{6.15c}$$

$$\mathbf{\Lambda}_{n+1} = \mathbf{\Lambda}_n\exp[\hat{\Theta}_{n}^{m}] = \exp[\hat{\theta}_{n}^{m}]\mathbf{\Lambda}_n; \quad \text{for convergent solution } \hat{\Theta}_{n}^{m}. \tag{6.15d}$$

In this case, the tangential transformation is a map $\mathbf{T} : T_n^{\text{mat}} \to T_{n+1}^{\text{mat}}$ so the scheme defined in Eqs. (6.15a) to (6.15d) makes sense due to all the vectors belongs to the same vector space on the rotation manifold. During iteration, they occupy on a linear space, (a fixed tangential vector space), which changes with time-step. The last term in Eq. (6.15c) arise from the existence of the non-constant tangential transformation $\mathbf{T}$ in Eq. (6.15b). This Newmark time–stepping algorithm can be called *exact updated Lagrangian formulation*, where unknown rotational vectors belongs to the tangential space of previously converged configuration, (see [246, 245, 244] for

more details).

6.1.4 Iterative strain and strain rate updating procedure

The discrete form, about the configuration $(\hat{\varphi}^{(i)}_{n+1}, \mathbf{\Lambda}^{(i)}_{n+1}) \in \mathcal{C}_{t_{n+1}}$ of the spatial form of the translational and rotational strains, existing in each point $S \in L$ of the mid-curve of the current rod configuration relative to the curved reference configuration (summarized in Table 3.1 of §3.4.1), can be written as

$$\{\hat{\gamma}_n\}^{(i)}_{n+1} = \{\hat{\varphi}_{,S}\}^{(i)}_{n+1} - \{\hat{t}_1\}^{(i)}_{n+1} \tag{6.16a}$$

$$\{\hat{\omega}_n\}^{(i)}_{n+1} = \operatorname{axial}\big[(\mathbf{\Lambda}_{n,S})^{(i)}_{n+1}(\mathbf{\Lambda}^T_n)^{(i)}_{n+1}\big] \tag{6.16b}$$

where the material description is obtained employing the pullback operation as

$$\{\hat{\Gamma}_n\}^{(i)}_{n+1} = \mathbf{\Lambda}^{(i)T}_{n+1}\{\hat{\gamma}_n\}^{(i)}_{n+1} \tag{6.17a}$$

$$\{\hat{\Omega}_n\}^{(i)}_{n+1} = \mathbf{\Lambda}^{(i)T}_{n+1}\{\hat{\omega}_n\}^{(i)}_{n+1}. \tag{6.17b}$$

Given an incremental field $(\Delta\hat{\varphi}^{(i)}_{n+1}, \Delta\hat{\theta}^{(i)}_{n+1})$, it is possible to construct an update algorithm as it is described in the next subsections.

6.1.4.a Translational strains

Displacements are updated as described in Table 6.3, the vector normal to the cross section $\hat{t}_1$ is updated by means of the application of the incremental (iterative) rotation tensor, obtained from the exponentiation of the iterative rotation increment $\exp\big[\Delta\hat{\theta}^{(i)}_{n+1}\big]$, on the previous iterative rotation tensor to obtain the updated orientation triad $\{\hat{t}_j\}^{(i)}_{n+1}$ at time t_{n+1}, iteration $(i+1)$. Therefore, the spatial form of the updated translational strains vector is computed as

$$\begin{aligned}\{\hat{\gamma}_n\}^{(i+1)}_{n+1} &= \{\hat{\varphi}_{,S}\}^{(i)}_{n+1} + \{\Delta\hat{\varphi}_{,S}\}^{(i)}_{n+1} - \exp\big[\Delta\hat{\theta}^{(i)}_{n+1}\big]\{\hat{t}_1\}^{(i)}_{n+1} \\ &= \{\hat{\varphi}_{,S}\}^{(i+1)}_{n+1} - \{\hat{t}_1\}^{(i+1)}_{n+1}\end{aligned} \tag{6.18a}$$

and

$$\{\hat{\Gamma}_n\}^{(i+1)}_{n+1} = \exp\big[\Delta\hat{\theta}^{(i)}_{n+1}\big]\mathbf{\Lambda}^{(i)T}_{n+1}\{\hat{\gamma}_n\}^{(i+1)}_{n+1} = \mathbf{\Lambda}^{(i+1)T}_{n+1}\{\hat{\gamma}_n\}^{(i+1)}_{n+1} \tag{6.18b}$$

for the material description.

6.1.4.b Rotational strains

An additive updating rule for the spatial form of the rotational strain tensor (curvature tensor) can be constructed based on Eq. (3.37a) of Section 3.1.6 as follows

$$\begin{aligned}\{\widetilde{\boldsymbol{\omega}}_n\}^{(i+1)}_{n+1} &= \Delta\{\widetilde{\boldsymbol{\omega}}_n\}^{(i)}_{n+1} + \exp[\Delta\widetilde{\boldsymbol{\theta}}^{(i)}_{n+1}]\{\widetilde{\boldsymbol{\omega}}_n\}^{(i)}_{n+1}\exp[\Delta\widetilde{\boldsymbol{\theta}}^{(i)}_{n+1}]^T \quad \in T^{\text{spa}}_{\mathbf{\Lambda}^{(i+1)}_{n+1}}SO(3) \\ &= \frac{\mathrm{d}(\exp[\Delta\widetilde{\boldsymbol{\theta}}^{(i)}_{n+1}])}{\mathrm{d}S}\exp[-\Delta\widetilde{\boldsymbol{\theta}}^{(i)}_{n+1}] + \exp[\Delta\widetilde{\boldsymbol{\theta}}^{(i)}_{n+1}]\{\widetilde{\boldsymbol{\omega}}_n\}^{(i)}_{n+1}\exp[\Delta\widetilde{\boldsymbol{\theta}}^{(i)}_{n+1}]^T\end{aligned} \tag{6.19a}$$

and for the material description one obtains

$$\{\widetilde{\mathbf{\Omega}}_n\}_{n+1}^{(i+1)} = \mathbf{\Lambda}_{n+1}^{(i)T}\exp\big[\Delta\widetilde{\boldsymbol{\theta}}_{n+1}^{(i)}\big]^T\{\widetilde{\boldsymbol{\omega}}_n\}_{n+1}^{(i+1)} = \mathbf{\Lambda}_{n+1}^{(i+1)T}\{\widetilde{\boldsymbol{\omega}}_n\}_{n+1}^{(i+1)} \quad \in T^{\text{mat}}_{\mathbf{\Lambda}_{n+1}^{(i+1)}}SO(3). \tag{6.19b}$$

Finally, the updated rotational strain vectors are obtained as

$$\{\hat{\omega}_n\}_{n+1}^{(i+1)} = \text{axial}[\{\widetilde{\boldsymbol{\omega}}_n\}_{n+1}^{(i+1)}] \tag{6.19c}$$

$$\{\hat{\Omega}_n\}_{n+1}^{(i+1)} = \text{axial}[\{\widetilde{\mathbf{\Omega}}_n\}_{n+1}^{(i+1)}]. \tag{6.19d}$$

In Eq. (6.19a) it is necessary to compute the term $(\mathrm{d}(\exp[\Delta\hat{\theta}_{n+1}^{(i)}])/\mathrm{d}S)\exp[-\Delta\hat{\theta}_{n+1}^{(i)}]$ which can be done according to the methods described in Ref. [363] or [199]. The first method due to Simo and Vu-Quoc is described in §B.2 of Appendix B but details will be omitted in this section by briefly.

6.1.4.c Strain vector at material point level

The spatial form of the iterative strain vector at given material point on the current cross section, Eq. (3.59), is obtained from the results of Eqs. (6.18a) and (6.19a) as

$$\{\hat{\varepsilon}_n\}_{n+1}^{(i+1)} = \frac{1}{|\mathbf{F}_0|}\Big[\{\hat{\gamma}_n\}_{n+1}^{(i+1)} + \{\widetilde{\boldsymbol{\omega}}_n\}_{n+1}^{(i+1)}\{\hat{\mathscr{T}}\}_{n+1}^{(i+1)}\Big]. \tag{6.20}$$

The material form of $\{\hat{\varepsilon}_n\}_{n+1}^{(i+1)}$, which is used for integrating the constitutive equations, is obtained by means of the pullback operation with the updated rotation tensor $\mathbf{\Lambda}_{n+1}^{(i+1)}$ as

$$\{\hat{\mathcal{E}}_n\}_{n+1}^{(i+1)} = \mathbf{\Lambda}_{n+1}^{(i+1)T}\{\hat{\varepsilon}_n\}_{n+1}^{(i+1)} = \frac{1}{|\mathbf{F}_0|}\Big[\{\Gamma_n\}_{m}^{(i+1)} + \{\widetilde{\mathbf{\Omega}}_n\}_{n+1}^{(i+1)}\hat{\mathscr{E}}\Big] \tag{6.21}$$

with $|\mathbf{F}_0|^{-1} = (\mathbf{\Lambda}_0^T\hat{\varphi}_{0,S}\cdot\hat{E}_1 + \xi_3\hat{\Omega}_{02} - \xi_2\hat{\Omega}_{03})$ [207], which is a initial geometric parameter.

6.1.4.d Strain rate vector

An objective measure [300] of the strain rate vector on each material point of the cross section of the current rod is obtained from Eq. (3.81c). Having estimated $\hat{\varphi}_{n+1}^{(i+1)}$, $\dot{\hat{\varphi}}_{n+1}^{(i+1)}$ and $\hat{v}_{n+1}^{(i+1)}$ from Newmark's algorithm, it is possible to construct the discrete form of the co–rotated strain rate vector as

$$\{\hat{s}_n\}_{m+1}^{(i+1)} = \{\dot{\widetilde{\varphi}}_{,S}\}_{n+1}^{(i+1)} - \{\widetilde{\boldsymbol{v}}_{n+1}\}_{n+1}^{(i+1)}\{\widetilde{\varphi}_{,S}\}_{n+1}^{(i+1)} + \{\widetilde{\boldsymbol{v}}_{n,S}\}_{n+1}^{(i+1)}\hat{\mathscr{E}}_{n+1}^{(i+1)} \tag{6.22a}$$

$$\{\hat{\mathcal{S}}\}_{n+1}^{(i+1)} = \mathbf{\Lambda}_{n+1}^{(i+1)T}\{\hat{s}_n\}_{n+1}^{(i+1)}. \tag{6.22b}$$

In Eq. (6.22a) it has been supposed that $\hat{\varphi}_{n+1}^{(i+1)}$, $\dot{\hat{\varphi}}_{n+1}^{(i+1)}$ and $\{\widetilde{\boldsymbol{v}}_n\}_{n+1}^{(i+1)} = \mathbf{\Pi}[\{\hat{v}_n\}_{n+1}^{(i+1)}]$ are known functions of the coordinate $S \in [0, L]$; this assumption will be explicitly explained in Section 7 about finite element implementation.

REMARK 6.4. In Eq. (6.22a) it has been supposed that the angular velocity tensor is interpolated at the integration point bye means of using an *isoparametric* [170] approximation *i.e.* $\{\widetilde{\boldsymbol{v}}_n\}_{n+1}^{(i+1)}(S) = \sum_I^{N_\mathrm{d}} N_I(S)\{\widetilde{\boldsymbol{v}}_n^I\}_{n+1}^{(i+1)}$ and, therefore, the term $\{\widetilde{v}_{,S}\}_m^{(i+1)}$ is calculated as $\sum_I^{N_\mathrm{d}} N_I(S)_{,S}\{\widetilde{\boldsymbol{v}}_n^I\}_m^{(i+1)}$, where N_d is the number of nodal points on a beam element ■

Another possibility for estimating the discrete form of the strain rate vector is by means of applying the finite difference method as follows:

$$\{\hat{s}_n\}_{n+1}^{(i+1)} = \mathbf{\Lambda}_{n+1}^{(i+1)}\Big[\frac{\{\hat{\mathcal{E}}_n\}_{n+1}^{(i+1)} - \{\hat{\mathcal{E}}_n\}_n}{\Delta t}\Big] \tag{6.23}$$

where Δt is the length of the time-step between the current configuration and the previous one at t_n.

6.2 Discrete form of the linearized functional

In order to give an explicit expression for the term $DG(\hat{\varphi}_{n+1}^{(i)}, \mathbf{\Lambda}_{n+1}^{(i)}, \hat{\eta}^{\mathrm{s}})$, Eq. (6.3), entering in the iterative Newton–Raphson scheme, one has to be able to write the discrete version of the linear forms of §5 in terms of the spatial form of the incremental (iterative) field $(\Delta\hat{\varphi}_{n+1}^{(i)}, \Delta\hat{\theta}_{n+1}^{(i)}) \in T\mathcal{C}_{t_{n+1}}$.
First, in analogous manner as in §5.1.1, it is necessary to calculate the discrete counterpart of a *curve of perturbed configurations* in $\mathcal{C}_{t_{n+1}}$, that is, a map

$$\begin{array}{rcl} \mathbb{R} & \to & \mathcal{C}_{t_{n+1}} \\ \varepsilon & \mapsto & (\hat{\varphi}_{\varepsilon(n+1)}^{(i)}, \mathbf{\Lambda}_{\varepsilon(n+1)}^{(i)}) \end{array} \tag{6.24}$$

by setting

$$\hat{\varphi}_{\varepsilon(n+1)}^{(i)} \triangleq \hat{\varphi}_{n+1}^{(i)} + \varepsilon\Delta\hat{\varphi}_{n+1}^{(i)} \tag{6.25a}$$

$$\mathbf{\Lambda}_{\varepsilon(n+1)}^{(i)} \triangleq \exp[\varepsilon\Delta\widetilde{\boldsymbol{\theta}}_{n+1}^{(i)}]\exp[\widetilde{\boldsymbol{\theta}}_{n+1}^{(i)}]\mathbf{\Lambda}_n. \tag{6.25b}$$

Then one defines the linearized quantities $(\Delta\hat{\varphi}_{\varepsilon(n+1)}^{(i)}, \Delta\mathbf{\Lambda}_{\varepsilon(n+1)}^{(i)})$ as the objects in the tangent space $T\mathcal{C}_{n+1}$ given in terms of the directional derivative by the following expressions:

$$\Delta\hat{\varphi}_{n+1}^{(i)} \triangleq \frac{\mathrm{d}}{\mathrm{d}\varepsilon}\Big|_{\varepsilon=0}\hat{\varphi}_{\varepsilon(n+1)}^{(i)} = \Delta\hat{\varphi}_{n+1}^{(i)} \tag{6.26a}$$

$$\delta\mathbf{\Lambda}_{n+1}^{(i)} \triangleq \frac{\mathrm{d}}{\mathrm{d}\varepsilon}\Big|_{\varepsilon=0}\mathbf{\Lambda}_{\varepsilon(n+1)}^{(i)} = \Delta\widetilde{\boldsymbol{\theta}}_{n+1}^{(i)}\mathbf{\Lambda}_n^{(i)}. \tag{6.26b}$$

To proceed further with the linearization of the incremental rotational vector, we make use of representations for $\mathbf{\Lambda}_{\varepsilon(n+1)}^{(i)}$ and $\mathbf{\Lambda}_{n+1}^{(i)}$ in terms of exponential maps starting at $\mathbf{\Lambda}_n$.
By one hand, one has that $\mathbf{\Lambda}_{\varepsilon(n+1)}^{(i)} = \exp[\widetilde{\boldsymbol{\theta}}_{\varepsilon(n)}^{(i)}]\mathbf{\Lambda}_n$ and, $\widetilde{\boldsymbol{\theta}}_{\varepsilon(n)}^{(i)}\mathbf{\Lambda}_n$ and $\widetilde{\boldsymbol{\theta}}_n^{(i)}\Lambda_n$ belong to $T_{\mathbf{\Lambda}_n}^{\mathrm{spa}}SO(3)$.
We have to note that [365] $\Delta\widetilde{\boldsymbol{\theta}}_{n+1}^{(i)}\mathbf{\Lambda}_{n+1}^{(i)}$ belongs to the tangent space $T_{\mathbf{\Lambda}_{n+1}^{(i)}}^{\mathrm{spa}}SO(3)$ at $\mathbf{\Lambda}_{n+1}^{(i)}$ and hence,

$$\exp\big[\widetilde{\boldsymbol{\theta}}_{\varepsilon(n)}^{(i)}\big] = \exp\big[\varepsilon\Delta\widetilde{\boldsymbol{\theta}}_{n+1}^{(i)}\big]\exp\big[\widetilde{\boldsymbol{\theta}}_n^{(i)}\big] \tag{6.27}$$

with this relation in mind, we obtain the linearization of the *discrete incremental rotation* $\hat{\theta}_{\varepsilon(n)}^{(i)}$, which is the axial vector of $\widetilde{\boldsymbol{\theta}}_{\varepsilon(n)}^{(i)}$ in Eq. (6.27), as

$$D\hat{\theta}_n^{(i)} \cdot \Delta\hat{\theta}_{n+1}^{(i)} \triangleq \delta\hat{\theta}_n^{(i)} = \frac{\mathrm{d}}{\mathrm{d}\varepsilon}\Big|_{\varepsilon=0}\hat{\theta}_{\varepsilon(n)}^{(i)} = \mathbf{T}(\hat{\theta}_n^{(i)})\Delta\hat{\theta}_{n+1}^{(i)} \tag{6.28}$$

where $\mathbf{T} : T^{\text{spa}}_{\mathbf{\Lambda}^{(i)}_{n+1}} SO(3) \to T^{\text{spa}}_{\mathbf{\Lambda}_n} SO(3)$ is the linear tangential map defined in Eq. (A.76) of §A.4.4. From Eq. (6.28) and the time–stepping algorithm of Table 6.3 it is possible to write the linearized forms of the angular velocity and acceleration in material form about the configuration $(\hat{\varphi}^{(i)}_{n+1}, \mathbf{\Lambda}^{(i)}_{n+1})$ as

$$\delta\hat{V}^{(i)}_{n+1} = \frac{\gamma}{\Delta t\beta}\mathbf{\Lambda}^T_n\mathbf{T}(\hat{\theta}^{(i)}_n)\Delta\hat{\theta}^{(i)}_{n+1} \tag{6.29a}$$

$$\delta\hat{A}^{(i)}_{n+1} = \frac{1}{(\Delta t)^2\beta}\mathbf{\Lambda}^T_n\mathbf{T}(\hat{\theta}^{(i)}_n)\Delta\hat{\theta}^{(i)}_{n+1} \tag{6.29b}$$

If the material form of the incremental (iterative) field $(\Delta\hat{\varphi}^{(i)}_{n+1}, \Delta\hat{\Theta}^{(i)}_{n+1}) \in T\mathcal{C}_{t_{n+1}}$ is preferred a set of equivalent iterative rules are obtained. First, it is necessary to calculate the discrete counterpart of a *curve of perturbed configurations* $(\hat{\varphi}^{(i)}_{\varepsilon(n+1)}, \mathbf{\Lambda}^{(i)}_{\varepsilon(n+1)}) \in \mathcal{C}_{t_{n+1}}$. Here we only will concentrate on the rotational field because the translational part is the same as for the spatial incremental field. Then we have

$$\mathbf{\Lambda}^{(i)}_{\varepsilon(n+1)} := \mathbf{\Lambda}_n \exp[\widetilde{\mathbf{\Theta}}^{(i)}_{n+1}]\exp[\varepsilon\Delta\widetilde{\mathbf{\Theta}}^{(i)}_{n+1}]. \tag{6.30}$$

and

$$\delta\mathbf{\Lambda}^{(i)}_{n+1} := \frac{\mathrm{d}}{\mathrm{d}\varepsilon}\Big|_{\varepsilon=0}\mathbf{\Lambda}^{(i)}_{\varepsilon(n+1)} = \mathbf{\Lambda}^{(i)}_n\Delta\widetilde{\mathbf{\Theta}}^{(i)}_{n+1}. \tag{6.31}$$

By one hand, one has that $\mathbf{\Lambda}^{(i)}_{\varepsilon(n+1)} = \mathbf{\Lambda}_n\exp[\widetilde{\mathbf{\Theta}}^{(i)}_{\varepsilon(n)}]$, $\mathbf{\Lambda}_n\widetilde{\mathbf{\Theta}}^{(i)}_{\varepsilon(n)}$ and $\Lambda_n\widetilde{\mathbf{\Theta}}^{(i)}_n \in T^{\text{spa}}_{\mathbf{\Lambda}_n}SO(3)$, in the same manner, $\mathbf{\Lambda}^{(i)}_{n+1}\Delta\widetilde{\mathbf{\Theta}}^{(i)}_{n+1} \in T^{\text{mat}}_{\Lambda^{(i)}_{n+1}} SO(3)$ which allow to write

$$\exp\big[\widetilde{\mathbf{\Theta}}^{(i)}_{\varepsilon(n)}\big] = \exp\big[\widetilde{\mathbf{\Theta}}^{(i)}_n\big]\exp\big[\varepsilon\Delta\widetilde{\mathbf{\Theta}}^{(i)}_{n+1}\big]. \tag{6.32}$$

Then, the linearization of the material form of the *discrete incremental rotation* $\hat{\Theta}^{(i)}_{\varepsilon(n)}$, which is the axial vector of $\widetilde{\mathbf{\Theta}}^{(i)}_{\varepsilon(n)}$ is obtained as

$$D\hat{\Theta}^{(i)}_n \cdot \Delta\hat{\Theta}^{(i)}_{n+1} = \delta\hat{\Theta}^{(i)}_n = \frac{\mathrm{d}}{\mathrm{d}\varepsilon}\Big|_{\varepsilon=0}\hat{\Theta}^{(i)}_{\varepsilon(n)} = \mathbf{T}^T(\hat{\Theta}^{(i)}_n)\Delta\hat{\Theta}^{(i)}_{n+1} \tag{6.33}$$

where $\mathbf{T}$ is the same tensor as in Eq. (6.28) but written in terms of $\hat{\Theta}^{(i)}_n$ and $\mathbf{T}^T : T^{\text{mat}}_{\mathbf{\Lambda}^{(i)}_{n+1}} SO(3) \to T^{\text{mat}}_{\mathbf{\Lambda}_n}SO(3)$ (see §A.4.4). In this case, the linearized forms of the angular velocity and acceleration in material form about the configuration $(\hat{\varphi}^{(i)}_{n+1}, \mathbf{\Lambda}^{(i)}_{n+1})$ reads

$$\delta\hat{V}^{(i)}_{n+1} = \frac{\gamma}{\Delta t\beta}\mathbf{T}^T(\hat{\Theta}^{(i)}_n)\Delta\hat{\Theta}^{(i)}_{n+1} \tag{6.34a}$$

$$\delta\hat{A}^{(i)}_{n+1} = \frac{1}{(\Delta t)^2\beta}\mathbf{T}^T(\hat{\Theta}^{(i)}_n)\Delta\hat{\Theta}^{(i)}_{n+1} \tag{6.34b}$$

6.2.1 Discrete form of the out of balance forces

The discrete form of the *out-of-balance force* term of Eq. (6.3), $G(\hat{\varphi}^{(i)}_{n+1}, \mathbf{\Lambda}^{(i)}_{n+1}, \eta) \cong G^{(i)}_{n+1}$, is obtained from the contribution of the *internal, external* and *inertial* terms as follows

6.2.1.a Internal component

The discrete contribution of the internal component to the residual force vector is obtained as

$$\begin{aligned} G^{(i)}_{\text{int}(n+1)} &= \int_0^L \hat{\eta}^{\text{s}T} \boldsymbol{B}(\hat{\varphi}^{(i)}_{n+1})^T \hat{\Phi}^{(i)}_{n+1} \text{d}S \\ &= \int_0^L \hat{\eta}^{\text{m}T} \bar{\boldsymbol{B}}(\hat{\varphi}^{(i)}_{n+1}, \boldsymbol{\Lambda}^{(i)}_{n+1})^T \hat{\Phi}^{(i)}_{n+1} \text{d}S \end{aligned} \tag{6.35}$$

where the discrete forms of the operators $\boldsymbol{B}^{(i)}_{n+1}$ and $\bar{\boldsymbol{B}}^{(i)}_{n+1}$ are obtained evaluating the expressions of Eqs. (5.12c) and (5.16c) at the configuration $(\hat{\varphi}^{(i)}_{n+1}, \boldsymbol{\Lambda}^{(i)}_{n+1})$. Observe that the internal force and moment vector $\hat{\Phi}^{(i)}_{n+1}$ corresponds to those calculated at the time step t_{n+1} iteration (i).

6.2.1.b Inertial component

The discrete contribution of the inertial forces to the out of balance force vector is obtained as

$$\begin{aligned} G^{(i)}_{\text{ine}(n+1)} &= \int_0^L \hat{\eta}^{\text{s}T} \left[\begin{array}{c} \mathcal{A}_{\rho_0} \ddot{\hat{\varphi}}^{(i)}_{n+1} \\ \boldsymbol{\mathcal{I}}^{(i)}_{\rho_0(n+1)} \{\hat{\alpha}_n\}^{(i)}_{n+1} + \{\widetilde{\boldsymbol{v}}_n\}^{(i)}_{n+1} (\boldsymbol{\mathcal{I}}^{(i)}_{\rho_0(n+1)} \{\hat{v}_n\}^{(i)}_{n+1}) \end{array} \right] \text{d}S \\ &= \int_0^L \hat{\eta}^{\text{m}T} \left[\begin{array}{c} \mathcal{A}_{\rho_0} \ddot{\hat{\varphi}}^{(i)}_{n+1} \\ \mathbf{I}_{\rho_0} \{\hat{A}_n\}^{(i)}_{n+1} + \{\widetilde{\boldsymbol{V}}_n\}^{(i)}_{n+1} (\mathbf{I}_{\rho_0} \{\hat{V}_n\}^{(i)}_{n+1}) \end{array} \right] \text{d}S \end{aligned} \tag{6.36a}$$

where the discrete form of the spatial inertial tensor $\boldsymbol{\mathcal{I}}_{\rho_0}$ is obtained bey means of the push–forward operation by the rotation tensor $\boldsymbol{\Lambda}^{(i)}_{n+1}$ acting on the material form of the inertial tensor $\mathbf{I}_{\rho_0}$, according to $\mathcal{I}^{(i)}_{\rho_0(n+1)} = \boldsymbol{\Lambda}^{(i)}_{n+1}(\mathbf{I}_{\rho_0}) = \boldsymbol{\Lambda}^{(i)}_{n+1} \mathbf{I}_{\rho_0} \boldsymbol{\Lambda}^{T(i)}_{n+1}$.
Additionally, considering the time–stepping algorithm of Table 6.3 it is possible to construct an iterative updating for the inertial component of the out of balance force vector as

$$G^{(i+1)}_{\text{ine}(n+1)} = G^{(i)}_{\text{ine}(n+1)} + \frac{1}{(\Delta t)^2 \beta} \int_0^L \hat{\eta}^{\text{m}T} \left[\begin{array}{c} \mathcal{A}_{\rho_0} \Delta \hat{\varphi}^{(i)}_{n+1} \\ \hat{\mho}^{(i+1)}_n + (\gamma \Delta t)^2 \widetilde{\boldsymbol{\mho}}^{(i+1)}_n (\mathbf{I}_{\rho_0} \hat{\mho}^{(i+1)}_n) \end{array} \right] \text{d}S \tag{6.36b}$$

where $\hat{\mho}^{(i+1)}_n = [\hat{\Theta}^{(i+1)}_n - \hat{\Theta}^{(i)}_n]$.

6.2.1.c External component

By the other hand, the discrete contribution of the external loading to the out of balance force vector is obtained as

$$G^{(i)}_{\text{ext}(n+1)} = \lambda \Big(\int_0^L \hat{\eta}^{\text{s}T} \Big(\begin{bmatrix} \hat{\mathcal{N}}_g + \hat{\mathscr{R}}_\varphi + c^{(i)}_{N(n+1)} \hat{\mathcal{N}}_d + \boldsymbol{\Lambda}^{(i)}_{(n+1)} \hat{\bar{\mathcal{N}}}_p \\ \hat{\mathcal{M}}_g + \hat{\mathscr{R}}_\theta + c^{(i)}_{M(n+1)} \hat{\mathcal{M}}_d + \boldsymbol{\Lambda}^{(i)}_{(n+1)} \hat{\bar{\mathcal{M}}}_p \end{bmatrix} \Big) \text{d}S + \sum_{k=1}^{Np} \hat{\eta}^{\text{s}T}_k \begin{bmatrix} \hat{P}^k_g + \boldsymbol{\Lambda}^{(i)}_{(n+1)} \hat{\bar{P}}^k_p \\ \hat{M}^k_g \end{bmatrix} \Big) \tag{6.37}$$

which is obtained evaluating the configuration dependent terms of the different types of applied forces and moments (see §3.8) at the configuration $(\hat{\varphi}^{(i)}_{n+1}, \boldsymbol{\Lambda}^{(i)}_{n+1})$.

6.2.2 Discrete tangential stiffness

Of course, if the configuration $(\hat{\varphi}^{(i)}_{n+1}, \mathbf{\Lambda}^{(i)}_{n+1}) \in \mathcal{C}_{t_{n+1}}$ is an equilibrium configuration, it follows that $G^{(i)}_{n+1} \approx 0 \ \forall \hat{\eta} \in T\mathcal{C}_{n+1}$. On the contrary a next iteration has to be performed using the discrete form of the tangential stiffness $DG^{(i)}_{n+1} \cdot \hat{p}^{\mathrm{s}(i)}_{n+1}$, Eq. (6.3), which is obtained as the sum of the three contributions *i.e.* the internal, external and inertial terms as

$$\begin{aligned} DG^{(i)}_{n+1} \cdot \hat{p}^{\mathrm{s}(i)}_{n+1} &= \left[DG^{(i)}_{\mathrm{int}(n+1)} + DG^{(i)}_{\mathrm{ine}(n+1)} + DG^{(i)}_{\mathrm{ext}(n+1)}\right] \cdot \hat{p}^{\mathrm{s}(i)}_{n+1} \\ &= \left[K_M + K_V + K_G + K_P + M + K_{\mathrm{gyr}} + K_{\mathrm{cent}}\right]^{(i)}_{n+1} \\ &= \left[K^{\mathrm{m}}_M + K^{\mathrm{m}}_V + K^{\mathrm{m}}_G + K^{\mathrm{m}}_P + M^{\mathrm{m}} + K^{\mathrm{m}}_{\mathrm{gyr}} + K^{\mathrm{m}}_{\mathrm{cent}}\right]^{(i)}_{n+1} \\ &= DG^{(i)}_{n+1} \cdot \hat{p}^{\mathrm{m}(i)}_{n+1}. \end{aligned} \tag{6.38}$$

In this section, explicit expressions for the different terms which contributes to the discrete tangent stiffness are given according to Section 5.3.

6.2.2.a Internal tangential stiffness

According to Eq. (5.68) we have that the discrete version of the tangential stiffness due to the contribution of the internal forces, $[K_M + K_G + K_V]^{(i)}_{n+1}$, is obtained as

$$\begin{aligned} K^{(i)}_{M(n+1)} &= \int_0^L \hat{\eta}^{\mathrm{s}} [\boldsymbol{B}(\hat{\varphi}^{(i)}_{n+1})]^T \begin{bmatrix} \bar{\mathbf{C}}^{\mathrm{sv}}_{nn} & \bar{\mathbf{C}}^{\mathrm{sv}}_{nm} \\ \bar{\mathbf{C}}^{\mathrm{sv}}_{mn} & \bar{\mathbf{C}}^{\mathrm{sv}}_{mn} \end{bmatrix}^{(i)}_{n+1} [\mathbf{B}(\hat{\varphi}^{(i)}_{n+1})] \hat{p}^{\mathrm{s}(i)}_{n+1} \mathrm{d}S \\ &= \int_0^L \hat{\eta}^{\mathrm{s}} \boldsymbol{B}^{(i)T}_{n+1} \bar{\mathbf{C}}^{\mathrm{sv}}(\mathbf{\Lambda}^{(i)}_{n+1}) \boldsymbol{B}^{(i)}_{n+1} \hat{p}^{\mathrm{s}(i)}_{n+1} \mathrm{d}S \end{aligned} \tag{6.39a}$$

where $\bar{\mathbf{C}}^{\mathrm{sv}}_{ij}(\mathbf{\Lambda}^{(i)}_{n+1}) = \mathbf{\Lambda}^{(i)}_{n+1} \bar{\mathbf{C}}^{\mathrm{mv}}_{ij} \mathbf{\Lambda}^{(i)T}_{n+1}$ $i, j \in \{n, m\}$ and $\boldsymbol{B}^{(i)}_{n+1}$ is obtained from Eq. (5.12c) evaluating at $\hat{\varphi}^{(i)}_{,S(n+1)}$. By the other hand, the geometric part given by

$$K^{(i)}_{G(n+1)} = \int_0^L \hat{\eta}^{\mathrm{s}} [\boldsymbol{B}^{(i)T}_{n+1} \boldsymbol{\mathcal{N}}^{(i)}_{n+1} + \boldsymbol{\mathscr{F}}^{(i)}_{n+1}] \hat{p}^{\mathrm{s}(i)}_{n+1} \mathrm{d}S \tag{6.39b}$$

where the stress dependent tensors $\boldsymbol{\mathcal{N}}$ and $\boldsymbol{\mathscr{F}}$ are calculated according to Eqs. (5.58) and (5.67) but the associated values of the stress resultant and couples are those corresponding to $\hat{\mathbf{\Phi}}^{(i)}_{n+1} \in T^*\mathcal{C}_{n+1}$.
The viscous dependent part is obtained as

$$K^{(i)}_{G(n+1)} = \int_0^L \hat{\eta}^{\mathrm{s}} [\boldsymbol{B}^{(i)T}_{n+1} \bar{\mathbf{\Upsilon}}^{\mathrm{ss}(i)}_{n+1} \boldsymbol{\mathcal{V}}^{(i)}_{n+1}] \hat{p}^{\mathrm{s}(i)}_{n+1} \mathrm{d}S \tag{6.39c}$$

where $\bar{\mathbf{\Upsilon}}^{\mathrm{ss}(i)}_{ij(n+1)}(\mathbf{\Lambda}^{(i)}_{n+1}) = \mathbf{\Lambda}^{(i)}_{n+1} \bar{\mathbf{\Upsilon}}^{\mathrm{ss}}_{ij} \mathbf{\Lambda}^{T(i)}_{n+1}$ $i, j \in \{n, m\}$ are calculated according to Eqs. (4.53a) and (4.53b). The strain rate dependent tensor $\boldsymbol{\mathcal{V}}^{(i)}_{n+1}$ can be calculated considering the fact that Newmark's time stepping scheme, Eq. (6.29a), along with the discrete form of the result of Eq.

(5.19a), which allow to establish the following equivalences:

$$\begin{aligned}\Delta\dot{\hat{\varphi}}^{(i)}_{n+1} &= [\gamma/(\Delta t\beta)]\mathbf{I}\Delta\hat{\varphi}^{(i)}_{n+1}\\ \Delta\hat{V}^{(i)}_{n+1} &= [\gamma/(\Delta t\beta)]\boldsymbol{\Lambda}^T_n\mathbf{T}(\hat{\theta}^{(i)}_n)\Delta\hat{\theta}^{(i)}_{n+1} = \boldsymbol{\Lambda}^T_n\Delta\dot{\hat{\theta}}^{(i)}_n\end{aligned}$$

identifying the tensors $[\gamma/(\Delta t\beta)]\mathbf{I}$ and $[\gamma/(\Delta t\beta)]\mathbf{T}(\hat{\theta}^{(i)}_n)$ with $\boldsymbol{\mathscr{H}}_a$ and $\boldsymbol{\mathscr{H}}_b$ of Eqs. (5.27a) and (5.27b), respectively; Therefore, the following expressions are obtained:

$$\Delta\dot{\hat{\theta}}^{(i)}_n = \frac{\gamma}{\Delta t\beta}\mathbf{T}(\hat{\theta}^{(i)}_n)\Delta\hat{\theta}^{(i)}_{n+1} \tag{6.40a}$$

$$\Delta\dot{\hat{\theta}}^{(i)}_{,S(n)} = \frac{\gamma}{\Delta t\beta}\big[\mathbf{T}(\hat{\theta}^{(i)}_n)\Delta\hat{\theta}^{(i)}_{,S(n+1)} + \mathbf{T}(\hat{\theta}^{(i)}_n)_{,S}\,\Delta\hat{\theta}^{(i)}_{n+1}\big] \tag{6.40b}$$

and $\delta\dot{\hat{\varphi}}^{(i)}_{n+1} = [\gamma/(\Delta t\beta)]\mathbf{I}\Delta\hat{\varphi}^{(i)}_{,S(n+1)}$. In Eqs. (6.40a) and (6.40b) the explicit expression for $\mathbf{T}(\hat{\theta})_{,S}$ can be consulted in Ref. [88]. Finally, the discrete form of Eqs. (5.23c) and (5.23d) can be rearranged as

$$\overset{\triangledown}{\delta[\hat{\Phi}]} = \begin{bmatrix}\gamma_{t\beta}\mathbf{I}[\frac{\mathrm{d}}{\mathrm{d}S}\mathbf{I}] - \widetilde{\boldsymbol{v}}^{(i)}_{n+1}[\frac{\mathrm{d}}{\mathrm{d}S}\mathbf{I}] & \dot{\widetilde{\boldsymbol{\varphi}}}^{(i)}_{,S(n+1)} + \widetilde{\boldsymbol{\varphi}}^{(i)}_{,S(n+1)}\,\gamma_{t\beta}\mathbf{T}^{(i)}_n - \widetilde{\boldsymbol{v}}^{(i)}_{n+1}\widetilde{\boldsymbol{\varphi}}^{(i)}_{,S(n+1)}\\ 0 & (\gamma_{t\beta}\mathbf{T}^{(i)}_n - \widetilde{\boldsymbol{v}}_n)[\frac{\mathrm{d}}{\mathrm{d}S}\mathbf{I}] + \gamma_{t\beta}[\mathbf{T}^{(i)}_n[\frac{\mathrm{d}}{\mathrm{d}S}\mathbf{I}] + \mathbf{T}^{(i)}_{n,S}]\end{bmatrix}\begin{bmatrix}\delta\hat{\varphi}\\ \Delta\hat{\theta}\end{bmatrix} = \boldsymbol{\mathcal{V}}^{(i)}_{n+1}\hat{p}^{\mathrm{s}(i)}_{n+1} \tag{6.41}$$

where the scalar $\gamma_{t\beta} = \frac{\gamma}{\Delta t\beta}$ and $\mathbf{T}^{(i)}_n = \mathbf{T}(\hat{\theta}^{(i)}_n)$.
On the other hand, if the material updating rule is preferred for the rotational part and according to Eq. (5.84) we have that the discrete version of the tangential stiffness due to the contribution of the internal forces, $[K^{\mathrm{m}}_M + K^{\mathrm{m}}_G + K^{\mathrm{m}}_V]^{(i)}_{n+1}$, is obtained as

$$K^{\mathrm{m}(i)}_{M(n+1)} = \int_0^L \hat{\eta}^{\mathrm{m}}\bar{\boldsymbol{B}}^{(i)T}_{n+1}\bar{\mathbf{C}}^{\mathrm{sv}}(\boldsymbol{\Lambda}^{(i)}_{n+1})\bar{\boldsymbol{B}}^{(i)}_{n+1}\hat{p}^{\mathrm{m}(i)}_{n+1}\mathrm{d}S \tag{6.42a}$$

where the sub-matrices $\bar{\mathbf{C}}^{\mathrm{sv}}_{ij}(\boldsymbol{\Lambda}^{(i)}_{n+1})$ $i,j\in\{n,m\}$ of the reduced constitutive tensor $\bar{\mathbf{C}}^{\mathrm{sv}}$ are as in Eq. (6.39a) and $\bar{\boldsymbol{B}}^{(i)}_{n+1} = \bar{\boldsymbol{B}}(\hat{\varphi}^{(i)}_{n+1}, \boldsymbol{\Lambda}^{(i)}_{n+1})$ is obtained from Eq. (5.16c) evaluating at $(\hat{\varphi}^{(i)}_{n+1}, \boldsymbol{\Lambda}^{(i)}_{n+1})$ and its derivatives with respect to the arch–length $S\in[0,L]$. The geometric part given by

$$K^{\mathrm{m}(i)}_{G(n+1)} = \int_0^L \hat{\eta}^{\mathrm{m}}\big[\bar{\boldsymbol{B}}^{(i)T}_{n+1}\boldsymbol{\mathcal{N}}^{(i)}_{n+1} + \bar{\boldsymbol{\mathscr{F}}}^{(i)}_{n+1}\big]\hat{p}^{\mathrm{m}(i)}_{n+1}\mathrm{d}S \tag{6.42b}$$

where the stress dependent tensor $\bar{\boldsymbol{\mathscr{F}}}((\hat{\varphi},\boldsymbol{\Lambda})^{(i)}_{n+1}, \hat{\Phi}^{(i)}_{n+1})$ is calculated according to Eq. (5.83). The viscous dependent part is obtained as

$$K^{\mathrm{m}(i)}_{G(n+1)} = \int_0^L \hat{\eta}^{\mathrm{m}}\big[\bar{\boldsymbol{B}}^{(i)T}_{n+1}\bar{\boldsymbol{\Upsilon}}^{\mathrm{ss}(i)}_{n+1}\bar{\boldsymbol{\mathcal{V}}}^{(i)}_{n+1}\big]\hat{p}^{\mathrm{m}(i)}_{n+1}\mathrm{d}S. \tag{6.42c}$$

In this case, the material strain rate dependent tensor $\bar{\boldsymbol{\mathcal{V}}}^{(i)}_{n+1}$ can be calculated considering Eqs. (6.29a) and (5.21b), being established the following equivalences:

$$\Delta\hat{V}^{(i)}_{n+1} = [\gamma/(\Delta t\beta)]\mathbf{T}^T(\hat{\Theta}^{(i)}_n)\Delta\hat{\Theta}^{(i)}_{n+1} = \Delta\dot{\hat{\Theta}}^{(i)}_{n+1} + \widetilde{\boldsymbol{V}}^{(i)}_{n+1}\Delta\hat{\Theta}^{(i)}_{n+1} \tag{6.42d}$$

which allows to deduce the following expressions for the tensor $\boldsymbol{\mathscr{H}}^{\mathrm{m}}_{b}$ of Eq. (7.47) and its derivative $\boldsymbol{\mathscr{H}}^{\mathrm{m}}_{b},_{S}$ as follows:

$$\begin{aligned}
\Delta\dot{\hat{\Theta}}^{(i)}_{n+1} &= \big[\gamma_{t\beta}\mathbf{T}^{T(i)}_{n} - \widetilde{\boldsymbol{V}}^{(i)}_{n+1}\big]\Delta\hat{\Theta}^{(i)}_{n+1} && \text{(6.43a)}\\
\Delta\dot{\hat{\Theta}},_{S}{}^{(i)}_{n} &= \big[\gamma_{t\beta}\mathbf{T}^{T(i)}_{n} - \widetilde{\boldsymbol{V}}^{(i)}_{n+1}\big]\Delta\hat{\Theta},^{(i)}_{S(n+1)} + \big[\gamma_{t\beta}\mathbf{T},^{T(i)}_{S(n)} - \widetilde{\boldsymbol{V}},^{(i)}_{S(n+1)}\big]\Delta\hat{\Theta}^{(i)}_{n+1}\\
&= \boldsymbol{\mathscr{H}}^{\mathrm{m}(i)}_{b(n+1)}\Delta\hat{\Theta},^{(i)}_{S(n+1)} + \boldsymbol{\mathscr{H}}^{\mathrm{m}}_{b},^{(i)}_{S(n+1)}\Delta\hat{\Theta}^{(i)}_{n+1} && \text{(6.43b)}
\end{aligned}$$

where $\mathbf{T}^{T(i)}_{n} = \mathbf{T}^{T}(\hat{\Theta}^{(i)}_{n})$, $\mathbf{T},^{T(i)}_{S(n)} = \mathbf{T},^{T}_{S}(\hat{\Theta}^{(i)}_{n})$ and the explicit expression for $\mathbf{T},^{T}_{S}$ can be consulted in Ref. [88]. Finally, the discrete form of Eq. (7.47) can be expressed as

$$\overset{\triangledown}{\delta}[\hat{\Phi}] = \left[\begin{array}{c|c} \gamma_{t\beta}\mathbf{I}[\frac{\mathrm{d}}{\mathrm{d}S}\mathbf{I}] - \widetilde{\boldsymbol{v}}^{(i)}_{n+1}[\frac{\mathrm{d}}{\mathrm{d}S}\mathbf{I}] & \begin{array}{c}\overset{\triangledown}{[\dot{\tilde{\boldsymbol{\gamma}}}_{n}]}{}^{(i)}_{n+1}\boldsymbol{\Lambda}^{(i)}_{n+1} + \\ \boldsymbol{\Lambda}^{(i)}_{n+1}\boldsymbol{\Pi}[\boldsymbol{\Lambda}^{T(i)}_{n+1}\hat{\varphi},^{(i)}_{S(n+1)}]\boldsymbol{\mathscr{H}}^{\mathrm{m}(i)}_{b(n+1)}\end{array} \\ \hline 0 & \begin{array}{c}\boldsymbol{\Lambda}^{(i)}_{n+1}(\boldsymbol{\mathscr{H}}^{\mathrm{m}(i)}_{b(n+1)}[\frac{\mathrm{d}}{\mathrm{d}S}\mathbf{I}] + \\ \boldsymbol{\mathscr{H}}^{\mathrm{m}}_{b},^{(i)}_{S(n+1)} + \dot{\widetilde{\boldsymbol{\Omega}}}^{(i)}_{n+1} + \widetilde{\boldsymbol{\Omega}}^{(i)}_{n+1}\boldsymbol{\mathscr{H}}^{\mathrm{m}(i)}_{b(n+1)})\end{array} \end{array}\right]\begin{bmatrix}\delta\hat{\varphi}\\ \delta\hat{\Theta}\end{bmatrix} = \bar{\boldsymbol{\mathcal{V}}}^{(i)}_{n+1}\hat{p}^{\mathrm{m}(i)}_{n+1}. \tag{6.44}$$

It is worth to note that, in general, $\bar{\boldsymbol{\mathcal{V}}}$ is configuration dependent and it couples the rotational and translational parts of the motion.

6.2.2.b Inertial tangent stiffness

Considering the iterative Newmark time–stepping scheme of Table 6.3, it is possible to rewrite the discrete form of the term $\mathcal{A}_{\rho_0}\ddot{\hat{\varphi}}$ in Eq. (5.70) as

$$\mathcal{A}_{\rho_0}\Delta\ddot{\hat{\varphi}}^{(i)}_{n+1} = \frac{1}{h^2\beta}\mathcal{A}_{\rho_0}\mathbf{I}\Delta\hat{\varphi}^{(i)}_{n+1} = \boldsymbol{\Xi}_{\varphi}\Delta\hat{\varphi}^{(i)}_{n+1} \tag{6.45}$$

where it is possible to see that $\boldsymbol{\Xi}_{\varphi}$ is a constant (configuration independent) tensor. Employing the results of Eqs. (6.29a) and (6.29b), it is possible to rewrite the terms $\hat{\Xi}_{\theta_1}$ and $\hat{\Xi}_{\theta_2}$ of Eqs. (5.71a) and (5.71a) in discrete form as

$$\begin{aligned}
\hat{\Xi}^{(i)}_{\theta_1(n+1)} &= -\boldsymbol{\Pi}\Big[\boldsymbol{\Lambda}^{(i)}_{n+1}\{\mathbf{I}_{\rho_0}\{\hat{A}_{n}\}^{(i)}_{n+1} + \{\widetilde{\boldsymbol{V}}_{n}\}^{(i)}_{n+1}(\mathbf{I}_{\rho_0}\{\hat{V}_{n}\}^{(i)}_{n+1})\}\Big]\Delta\hat{\theta}^{(i)}_{n+1} && \text{(6.46a)}\\
\hat{\Xi}^{(i)}_{\theta_2(n+1)} &= \frac{1}{(\Delta t)^2\beta}\boldsymbol{\Lambda}^{(i)}_{n+1}\Big\{\mathbf{I}_{\rho_0} + \Delta t\gamma\Big(\{\widetilde{\boldsymbol{V}}_{n}\}^{(i)}_{n+1}\mathbf{I}_{\rho_0} - \boldsymbol{\Pi}[\mathbf{I}_{\rho_0}\{\hat{V}_{n}\}^{(i)}_{n+1}]\Big)\Big\}\boldsymbol{\Lambda}^{T}_{n}\mathbf{T}(\hat{\theta}^{(i)}_{n})\Delta\hat{\theta}^{(i)}_{n+1} && \text{(6.46b)}
\end{aligned}$$

then, the following result is obtained:

$$\hat{\Xi}^{(i)}_{\theta_1(n+1)} + \hat{\Xi}^{(i)}_{\theta_2(n+1)} = \boldsymbol{\Xi}^{(i)}_{\theta(n+1)}\Delta\hat{\theta}^{(i)}_{n+1} \tag{6.47}$$

where the $\boldsymbol{\Xi}^{(i)}_{\theta(n+1)}$ is a *nonsymmetric* and *configuration dependent* tensor. This last result allows to obtain the discrete form of the inertial contribution to the tangential stiffness as

$$\begin{aligned}
D\mathbf{G}^{(i)}_{\mathrm{ine}(n+1)}\cdot\hat{p}^{\mathrm{s}(i)}_{n+1} &= [M + K_{\mathrm{gyr}} + K_{\mathrm{cent}}]^{(i)}_{n+1} = K^{(i)}_{\mathrm{ine}(n+1)}\\
&= \int_{0}^{L}\hat{\eta}^{\mathrm{s}T}\begin{bmatrix}\boldsymbol{\Xi}_{\varphi} & 0\\ 0 & \boldsymbol{\Xi}^{(i)}_{\theta(n+1)}\end{bmatrix}\hat{p}^{\mathrm{s}(i)}_{n+1}\mathrm{d}S = \int_{0}^{L}\hat{\eta}^{\mathrm{s}T}\mathbf{M}^{(i)}_{\varphi\theta(n+1)}\hat{p}^{\mathrm{s}(i)}_{n+1}\mathrm{d}S
\end{aligned} \tag{6.48}$$

where the explicit expression (in matrix form) of the inertial stiffness tensor $\mathbf{M}^{(i)}_{\varphi\theta(n+1)}$ is

$$\mathbf{M}^{(i)}_{\varphi\theta(n+1)} = \left[\begin{array}{c|c} \frac{1}{(\Delta t)^2\beta}\mathcal{A}_{\rho_0}\mathbf{I} & 0 \\ \hline 0 & \begin{array}{l} -\mathbf{\Pi}\Big[\mathbf{\Lambda}^{(i)}_{n+1}\{\mathbf{I}_{\rho_0}\{\hat{A}_n\}^{(i)}_{n+1} + \{\widetilde{\boldsymbol{V}}_n\}^{(i)}_{n+1}(\mathbf{I}_{\rho_0}\{\hat{V}_n\}^{(i)}_{n+1})\}\Big] + \\ \frac{1}{(\Delta t)^2\beta}\mathbf{\Lambda}^{(i)}_{n+1}\Big\{\mathbf{I}_{\rho_0} + \Delta t\gamma\Big(\{\widetilde{\boldsymbol{V}}_n\}^{(i)}_{n+1}\mathbf{I}_{\rho_0} - \mathbf{\Pi}[\mathbf{I}_{\rho_0}\{\hat{V}_n\}^{(i)}_{n+1}]\Big)\Big\}\mathbf{\Lambda}^T_n\mathbf{T}^{(i)}_n \end{array} \end{array}\right] \quad (6.49)$$

By the other hand, if the material updating rule for rotations is preferred one has, from Eqs. (6.34a) and (6.34b), that

$$\begin{aligned} \hat{\Xi}^{\mathrm{m}(i)}_{\Theta(n+1)} &= \mathbf{I}_{\rho_0}\Delta\hat{A}^{(i)}_{n(n+1)} + (\widetilde{\boldsymbol{V}}^{(i)}_{n(n+1)}\mathbf{I}_{\rho_0} - \mathbf{\Pi}[\mathbf{I}_{\rho_0}\hat{V}^{(i)}_{n(n+1)}])\Delta\hat{V}^{(i)}_{n(n+1)} \\ &= \Big[\frac{1}{(\Delta t)^2\beta}\mathbf{I}_{\rho_0} + \frac{\gamma}{\Delta t\beta}(\widetilde{\boldsymbol{V}}^{(i)}_{n(n+1)}\mathbf{I}_{\rho_0} - \mathbf{\Pi}[\mathbf{I}_{\rho_0}\hat{V}^{(i)}_{n(n+1)}])\Big]\mathbf{T}^{T(i)}_n\Delta\hat{\Theta}^{(i)}_{n+1} = \mathbf{\Xi}^{\mathrm{m}(i)}_{\Theta(n+1)}\Delta\hat{\Theta}^{(i)}_{n+1} \end{aligned} \quad (6.50)$$

where $\mathbf{T}^{T(i)}_n = \mathbf{T}^T(\hat{\Theta}^{(i)}_n)$ and $\mathbf{\Xi}^{\mathrm{m}(i)}_{\Theta(n+1)}$ is also a nonsymmetric and configuration dependent tensor, which considers the contributions of the centripetal and centrifugal effects. Eq. (6.51) allows to rewrite the discrete form of the inertial contribution to the tangential stiffness as

$$\begin{aligned} D\mathbf{G}^{(i)}_{\mathrm{ine}(n+1)}\cdot\hat{p}^{\mathrm{m}(i)}_{n+1} &= [M^{\mathrm{m}} + K^{\mathrm{m}}_{\mathrm{gyr}} + K^{\mathrm{m}}_{\mathrm{cent}}]^{(i)}_{n+1} = K^{\mathrm{m}(i)}_{\mathrm{ine}(n+1)} \\ &= \int_0^L \hat{\eta}^{\mathrm{m}T}\begin{bmatrix}\mathbf{\Xi}_\varphi & 0\\ 0 & \mathbf{\Xi}^{\mathrm{m}(i)}_{\Theta(n+1)}\end{bmatrix}\hat{p}^{\mathrm{m}(i)}_{n+1}\mathrm{d}S = \int_0^L \hat{\eta}^{\mathrm{s}T}\mathbf{M}^{\mathrm{m}(i)}_{\varphi\Theta(n+1)}\hat{p}^{\mathrm{m}(i)}_{n+1}\mathrm{d}S \end{aligned} \quad (6.51)$$

where the explicit expression (in matrix form) of the inertial stiffness tensor $\mathbf{M}^{\mathrm{m}(i)}_{\varphi\Theta(n+1)}$ is

$$\mathbf{M}^{\mathrm{m}(i)}_{\varphi\Theta(n+1)} = \left[\begin{array}{c|c} \frac{1}{(\Delta t)^2\beta}\mathcal{A}_{\rho_0}\mathbf{I} & 0 \\ \hline 0 & \Big[\frac{1}{(\Delta t)^2\beta}\mathbf{I}_{\rho_0} + \frac{\gamma}{\Delta t\beta}(\widetilde{\boldsymbol{V}}^{(i)}_{n(n+1)}\mathbf{I}_{\rho_0} - \mathbf{\Pi}[\mathbf{I}_{\rho_0}\hat{V}^{(i)}_{n(n+1)}])\Big]\mathbf{T}^{T(i)}_n \end{array}\right]. \quad (6.52)$$

6.2.2.c External load tangential stiffness

The discrete form of the contribution to the tangential stiffness due to external loading K_L is obtained directly from Eq. (5.77) as

$$\begin{aligned} D\mathbf{G}^{(i)}_{\mathrm{ext}(n+1)}\cdot\hat{p}^{\mathrm{m}(i)}_{n+1} &= -\lambda\Big(\int_0^L \hat{\eta}^{\mathrm{s}T}\Big(\begin{bmatrix}(\hat{\mathcal{N}}^{(i)}_{d(n+1)}\otimes\hat{\mathscr{C}}^{(i)}_{N(n+1)})[\frac{\mathrm{d}}{\mathrm{d}S}\mathbf{I}] + \widetilde{\boldsymbol{\mathcal{N}}}^{(i)}_{p(n+1)}\\ (\hat{\mathcal{M}}^{(i)}_{d(n+1)}\otimes\hat{\mathscr{C}}^{(i)}_{M(n+1)})[\frac{\mathrm{d}}{\mathrm{d}S}\mathbf{I}] + \widetilde{\boldsymbol{\mathcal{M}}}^{(i)}_{p(n+1)}\end{bmatrix}\hat{p}^{\mathrm{s}(i)}_{n+1}\mathrm{d}S \\ &\quad + \sum_{k=1}^{Np}\hat{\eta}^{\mathrm{s}T}_k\begin{bmatrix}\widetilde{\boldsymbol{P}}^{k(i)}_{p(n+1)}\\ 0\end{bmatrix}\hat{p}^{\mathrm{s}(i)}_{k(n+1)}\Big) \end{aligned} \quad (6.53)$$

where the involved loading quantities as well as the vectors $\hat{\mathscr{C}}_N$ and $\hat{\mathscr{C}}_M$ have to be evaluated at the configuration $(\hat{\varphi}^{(i)}_{n+1}, \mathbf{\Lambda}^{(i)}_{n+1}) \in \mathcal{C}_{t_{n+1}}$.

6.3 Lagrangian and Hamiltonian formulation of the problem

6.3.1 Lagrangian formulation

Preliminaries. The *Lagrangian* formulation of mechanics can be based on the variational principles behind *Newton*'s fundamental laws of force balance. One chooses a configuration space manifold $\mathcal{C}_t$ with generic coordinates denoted by $\hat{q}_\Phi = (\hat{\varphi}, \mathbf{\Lambda})$ that describe the configuration of the system under study.
The velocity phase space $\overline{T}\mathcal{C}_t$ corresponds to the tangent bundle of $\mathcal{C}_t$ (see §3.1.2). Coordinates on $\overline{T}\mathcal{C}_t$ are denoted by $(\hat{q}_\Phi, \dot{\hat{q}}_\Phi) \equiv (\hat{\varphi}, \mathbf{\Lambda}, \dot{\hat{\varphi}}, \dot{\mathbf{\Lambda}})$. The *Lagrangian* is regarded as a function

$$\begin{array}{rcl} \mathfrak{L}_g : T\mathcal{C}_t & \rightarrow & \mathbb{R} \\ (\hat{q}_\Phi, \dot{\hat{q}}_\Phi) & \mapsto & \mathfrak{L}_g(\hat{q}_\Phi, \dot{\hat{q}}_\Phi, t) \end{array} \tag{6.54}$$

or equivalently, $\mathfrak{L}_g(\hat{q}_\Phi, \dot{\hat{q}}_\Phi, t) \equiv \mathfrak{L}_g(\hat{\varphi}, \mathbf{\Lambda}, \dot{\hat{\varphi}}, \dot{\mathbf{\Lambda}}, t)$. Usually, $\mathfrak{L}_g$ is the kinetic minus the potential energy of the system and the following relations hold $\dot{\hat{q}}_\Phi = \mathrm{d}\hat{q}_\Phi/\mathrm{d}t$ for the variables characterizing the system's velocity. The *variational principle* of *Hamilton* states that the variation of the action is stationary at a solution [252]:

$$\delta\mathfrak{S} = \delta \int_a^b \mathfrak{L}_g(\hat{q}_\Phi, \dot{\hat{q}}_\Phi, t)\mathrm{d}t = 0. \tag{6.55}$$

where the limits of the integral dotes the initial a final time, $a \approx t_a$ and $b \approx t_b$, respectively. In this principle, one chooses curves $\hat{q}_\Phi(t)$ joining two fixed points in $\mathcal{C}_t$ over a fixed time interval $[a, b]$, and calculates the action $\mathfrak{S}$, which is the time integral of the Lagrangian, regarded as a function of this curve. *Hamiltons principle* states that the action has a critical point at a solution in the space of curves, which is equivalent to the *Euler-Lagrange* equations:

$$\frac{\mathrm{d}}{\mathrm{d}t}\frac{\partial \mathfrak{L}_g}{\partial \dot{\hat{q}}_\Phi} - \frac{\mathrm{d}\mathfrak{L}_g}{\mathrm{d}\hat{q}_\Phi} = 0. \tag{6.56}$$

If external forces are applied on the system, they have to be added to the right side of Eq. (6.56).
Lagrangian formulation of the rod theory. By one hand, the kinetic energy of the rod model is calculated as

$$\begin{aligned} K(\hat{q}_\Phi, \dot{\hat{q}}_\Phi, t) &= \frac{1}{2}\int_{\mathcal{B}_t} \rho_0 \langle \dot{\hat{x}}, \dot{\hat{x}} \rangle \mathrm{d}V = \frac{1}{2}\int_0^L (\mathcal{A}_{\rho_0} |\dot{\hat{\varphi}}|^2 \mathrm{d}S + \hat{v}_n \cdot \boldsymbol{\mathcal{I}}_{\rho_0} \hat{v}_n)\mathrm{d}S \\ &= \frac{1}{2}\int_0^L (\mathcal{A}_{\rho_0} |\dot{\hat{\varphi}}|^2 \mathrm{d}S + \hat{V}_n \cdot \mathbf{I}_{\rho_0} \hat{V}_n)\mathrm{d}S. \end{aligned} \tag{6.57}$$

By the other hand, the remaining term is the potential energy. The following consideration is the case in which the external loading is conservative, which implies the existence of a potential function $W_{\mathrm{ext}} : \mathcal{C}_t \rightarrow \mathbb{R}$ such that the potential energy of the system is obtained as

$$V(\hat{\varphi}, \mathbf{\Lambda}) = V_{\mathrm{int}}(\hat{\varphi}, \mathbf{\Lambda}) + V_{\mathrm{ext}}(\hat{\varphi}, \mathbf{\Lambda}) \tag{6.58a}$$

$$V_{\mathrm{int}}(\hat{\varphi}, \mathbf{\Lambda}) = \int_0^L W_{\mathrm{str}}(\hat{\Gamma}_n, \hat{\Omega}_n)\mathrm{d}S \tag{6.58b}$$

$$V_{\mathrm{ext}}(\hat{\varphi}, \mathbf{\Lambda}) = \int_0^L W_{\mathrm{ext}}(\hat{\varphi}, \mathbf{\Lambda})\mathrm{d}S \tag{6.58c}$$

where $W_{\rm str}$ is the strain energy function per unit of volume defined in §3.7 and the potential $V_{\rm int}(\hat{q}_\Phi)$ is *left* $SO(3)$ *invariant i.e.* $V_{\rm int}(\mathbf{Q}\hat{q}_\Phi) = V_{\rm ext}(\hat{q}_\Phi), \forall \mathbf{Q} \in SO(3)$. Simo *et al.* demonstrated in [373] that if this is the case, then

$$V_{\rm ext} = V_{\rm ext}(\mathbf{\Lambda}^T\hat{\varphi})$$

with a particular case given by $V_{\rm ext}(\|\hat{\varphi}\|)$ (central forces).
In this manner, the Lagrangian for a rod subjected to a conservative system of loads is obtained as $\mathfrak{L}_g(\hat{q}_\Phi) = K(\hat{q}_\Phi, \dot{\hat{q}}_\Phi) - V_{\rm int}(\hat{q}_\Phi) - V_{\rm ext}(\hat{q}_\Phi)$ and the Hamilton principle reads

$$\delta\mathfrak{S} = \delta\int_a^b \mathfrak{L}_g(\hat{q}_\Phi, \dot{\hat{q}}_\Phi, t)\mathrm{d}t = \int_a^b (\delta K(\hat{q}_\Phi, \dot{\hat{q}}_\Phi) - \delta V_{\rm int}(\hat{q}_\Phi) - \delta V_{\rm ext}(\hat{q}_\Phi))\mathrm{d}t = 0. \tag{6.59}$$

Prior to the linearization of the action the linearization of the kinetic energy, considering the spatial updating rule for rotations and Eqs. (6.57) and (5.19a), is obtained:

$$\begin{aligned} DK\cdot\hat{\eta}^{\rm s} = \delta K &= \frac{1}{2}\Big[\int_0^L 2\mathcal{A}_{\rho_0}\dot{\hat{\varphi}}\cdot\delta\dot{\hat{\varphi}}\mathrm{d}S + \int_0^L(\delta\hat{V}_n\cdot\mathbf{I}_{\rho_0}\hat{V}_n + \hat{V}_m\cdot\mathbf{I}_{\rho_0}\delta\hat{V}_n)\mathrm{d}S\Big] \\ &= \int_0^L \mathcal{A}_{\rho_0}\dot{\hat{\varphi}}\cdot\delta\dot{\hat{\varphi}}\mathrm{d}S + \frac{1}{2}\Big[\int_0^L(\delta\dot{\hat{\theta}}\cdot\mathbf{\Lambda}\mathbf{I}_{\rho_0}\hat{V}_n + \hat{V}_n\cdot\mathbf{I}_{\rho_0}\mathbf{\Lambda}^T\delta\dot{\hat{\theta}})\mathrm{d}S\Big] \\ &= \int_0^L \mathcal{A}_{\rho_0}\dot{\hat{\varphi}}\cdot\delta\dot{\hat{\varphi}}\mathrm{d}S + \frac{1}{2}\Big[\int_0^L(\delta\dot{\hat{\theta}}\cdot\boldsymbol{\mathcal{I}}_{\rho_0}\hat{v}_n + \hat{v}_n\cdot\boldsymbol{\mathcal{I}}_{\rho_0}\delta\dot{\hat{\theta}})\mathrm{d}S\Big] \\ &= \int_0^L(\mathcal{A}_{\rho_0}\dot{\hat{\varphi}}\cdot\delta\dot{\hat{\varphi}} + \boldsymbol{\mathcal{I}}_{\rho_0}\hat{v}_n\cdot\delta\dot{\hat{\theta}})\mathrm{d}S. \end{aligned} \tag{6.60}$$

The linearization of Eq. (6.72b) is obtained considering the results of Eqs. (5.16a) and (5.61) as

$$\begin{aligned} DV_{\rm int}\cdot\hat{\eta}^{\rm s} = \delta V_{\rm int} &= \int_0^L(\partial_{\hat{\Gamma}_n}W_{\rm str}\cdot\delta\hat{\Gamma}_n + \partial_{\hat{\Omega}_n}W_{\rm str}\cdot\hat{\Omega}_n)\mathrm{d}S \\ &= \int_0^L(\hat{n}^{\rm m}\cdot\delta\hat{\Gamma}_n + \hat{m}^{\rm m}\cdot\delta\hat{\Omega}_n)\mathrm{d}S \\ &= \int_0^L(\hat{\Phi}\cdot\boldsymbol{B}\hat{\eta}^{\rm s})\mathrm{d}S = G_{\rm int}(\hat{q}_\Phi, \hat{\eta}^{\rm s}) \end{aligned} \tag{6.61}$$

where the notations $\partial_{\hat{\Gamma}_n}W_{\rm str}\cdot\delta\hat{\Gamma}_n = \hat{n}^{\rm m}$ and$\partial_{\hat{\Omega}_n}W_{\rm str}\cdot\hat{\Omega}_n = \hat{m}^{\rm m}$ for the hyperelastic constitutive relations have been used.
Denoting $\mathbf{\Lambda}^T\hat{\varphi} \equiv \hat{\varphi}^{\rm m}$, considering $\delta\hat{\varphi}^{\rm m} = \mathbf{\Lambda}^T(\delta\hat{\varphi} + \widetilde{\boldsymbol{\varphi}}\delta\hat{\theta})$ one obtains that the linear part of Eq. (6.58c) is given by

$$\begin{aligned} DV_{\rm ext}\cdot\hat{\eta}^{\rm s} = \delta V_{\rm ext} &= \int_0^L \delta W_{\rm ext}(\mathbf{\Lambda}^T\hat{\varphi})\mathrm{d}S = \int_0^L(\partial_{\hat{\varphi}^{\rm m}}W_{\rm ext}\cdot[\mathbf{\Lambda}^T(\delta\hat{\varphi} + \widetilde{\boldsymbol{\varphi}}\delta\hat{\theta})]\mathrm{d}S \\ &= \int_0^L(\mathbf{\Lambda}\partial_{\hat{\varphi}^{\rm m}}W_{\rm ext}\cdot\delta\hat{\varphi} - \hat{\varphi}\times\mathbf{\Lambda}\partial_{\hat{\varphi}^{\rm m}}W_{\rm ext}\cdot\delta\hat{\theta})\mathrm{d}S \\ &= \int_0^L(\hat{\mathcal{N}}\cdot\delta\hat{\varphi} - \hat{\varphi}\times\hat{\mathcal{N}}\cdot\delta\hat{\theta})\mathrm{d}S \\ &= \int_0^L(\hat{\mathcal{N}}\cdot\delta\hat{\varphi} + \hat{\mathcal{M}}\cdot\delta\hat{\theta})\mathrm{d}S = G_{\rm ext}(\hat{q}_\Phi, \hat{\eta}^{\rm s}). \end{aligned} \tag{6.62}$$

From the above equation it is possible to see that in the conservative case, the external loads per unit of arch–length are $\hat{\mathcal{N}} = -\boldsymbol{\Lambda}\partial_{\hat{\varphi}^{\mathrm{m}}} W_{\mathrm{ext}}$ and $\hat{\mathcal{M}} = -\hat{\varphi} \times \hat{\mathcal{N}}$ recovering a result of [373]. Then, the Hamilton principle, Eq. 6.59, can be rewritten as

$$\delta\mathfrak{S} = \int_a^b \Big[\int_0^L (\mathcal{A}_{\rho_0} \dot{\hat{\varphi}} \cdot \delta\dot{\hat{\varphi}} + \boldsymbol{\mathcal{I}}_{\rho_0} \hat{v}_n \cdot \delta\dot{\hat{\theta}}) \mathrm{d}S - G_{\mathrm{int}}(\hat{q}_\Phi, \hat{\eta}^{\mathrm{s}}) - G_{\mathrm{ext}}(\hat{q}_\Phi, \hat{\eta}^{\mathrm{s}}) \Big] \mathrm{d}t = 0. \tag{6.63}$$

By one hand,

$$\int_a^b \int_0^L \mathcal{A}_{\rho_0} \dot{\hat{\varphi}} \cdot \delta\dot{\hat{\varphi}} \mathrm{d}S\mathrm{d}t = \int_0^L [\mathcal{A}_{\rho_0} \dot{\hat{\varphi}} \cdot \delta\hat{\varphi}] \Big|_a^b \mathrm{d}S - \int_a^b \int_0^L \mathcal{A}_{\rho_0} \ddot{\hat{\varphi}} \cdot \delta\hat{\varphi} \mathrm{d}S\mathrm{d}t \tag{6.64a}$$

$$\int_a^b \int_0^L \boldsymbol{\mathcal{I}}_{\rho_0} \hat{v}_n \cdot \delta\dot{\hat{\theta}} \mathrm{d}S\mathrm{d}t = \int_0^L [\boldsymbol{\mathcal{I}}_{\rho_0} \hat{v}_n \cdot \delta\hat{\theta}] \Big|_a^b \mathrm{d}S - \int_a^b \int_0^L (\dot{\boldsymbol{\mathcal{I}}}_{\rho_0} \hat{v}_n) \cdot \delta\hat{\theta} \mathrm{d}S\mathrm{d}t \tag{6.64b}$$

and, therefore, δK becomes

$$\delta K = \int_a^b \int_0^L \big[\mathcal{A}_{\rho_0} \ddot{\hat{\varphi}} \cdot \delta\hat{\varphi} + (\dot{\boldsymbol{\mathcal{I}}}_{\rho_0} \hat{v}_n) \cdot \delta\hat{\theta} \big] \mathrm{d}S\mathrm{d}t \tag{6.65}$$

where it has been used the fact that the admissible variations of the configuration variables are zero in the initial and final times *i.e.* $\hat{\eta}^{\mathrm{s}}|_a = 0$ and $\hat{\eta}^{\mathrm{s}}|_b = 0$.
By the other hand,

$$\begin{aligned} G_{\mathrm{int}} &= \int_a^b \int_0^L (\hat{n} \cdot \delta\hat{\varphi}_{,S} - \widetilde{\boldsymbol{\varphi}}_{,S} \hat{n} \cdot \delta\hat{\theta} + \hat{m} \cdot \delta\hat{\theta}_{,S}) \mathrm{d}S\mathrm{d}t \\ &= \int_a^b (\hat{n} \cdot \delta\hat{\varphi} + \hat{m} \cdot \delta\hat{\theta}) \Big|_0^L \mathrm{d}t - \int_a^b \int_0^L (\hat{n}_{,S} \cdot \delta\hat{\varphi} + \hat{\varphi}_{,S} \times \hat{n} \cdot \delta\hat{\theta} + \hat{m}_{,S} \cdot \delta\hat{\theta}) \mathrm{d}S\mathrm{d}t \\ &= \int_a^b (\hat{\Phi} \cdot \delta\hat{q}_\Phi) \Big|_{\partial_\Phi \hat{\varphi}} \mathrm{d}t - \int_a^b \Big(\int_0^L \hat{n}_{,S} \cdot \delta\hat{\varphi} \mathrm{d}S + \int_0^L (\hat{m}_{,S} + \hat{\varphi}_{,S} \times \hat{n}) \cdot \delta\hat{\theta} \mathrm{d}S \Big) \mathrm{d}t. \end{aligned} \tag{6.66}$$

Considering *Neumann* boundary conditions of the type $\partial_\Phi \hat{\varphi} = \emptyset$; $\forall t$, one obtains

$$\begin{aligned} \delta\mathfrak{S} &= \int_a^b \int_0^L \big[\mathcal{A}_{\rho_0} \ddot{\hat{\varphi}} - (\hat{n}_{,S} + \hat{\mathcal{N}}) \big] \cdot \delta\hat{\varphi} \mathrm{d}S\mathrm{d}t \\ &\quad + \int_a^b \int_0^L \big[(\dot{\boldsymbol{\mathcal{I}}}_{\rho_0} \hat{v}_n) - (\hat{m}_{,S} + \hat{\varphi}_{,S} \times \hat{n} + \hat{\mathcal{M}}) \big] \cdot \delta\hat{\theta} \mathrm{d}S\mathrm{d}t = 0 \end{aligned} \tag{6.67}$$

Taking into account that $\hat{\eta}^{\mathrm{s}}$ is arbitrary, the reduced equilibrium equations of Eqs. (3.121) and (3.133) are recovered. Analogously, in the general cases those equations have to be supplemented with the boundary conditions (3.137a) to (3.137d).

6.3.2 Hamiltonian formulation

The *Hamiltonian* formulation of the mechanics[6] provides an alternative framework for the treatment of the dynamic response of geometrically exact rod theories [116]. In this section a brief review of the main consequences of exploiting the Hamiltonian structure of the present rod theory will be summarized. One of the most attractive aspect of the formulation of the mechanical

[6] A theoretical treatment of the Lagrangian and Hamiltonian formulations of mechanics can be found in Marsden and Ratiu [255]

problem staring from the construction of the *Hamiltonian functional* rather that a weak form of the equilibrium equations, as in §3.6, is the possibility of the development of time–stepping algorithms which inherit in the discrete case the conservation properties, that is *momentum maps*, of the continuum problem and exhibit good energy conservation in the long term (see the works of Simo and Simo *et al.* [372, 373]. More details about some works devoted to the development of the so called *energy-momentum* conserving time–stepping schemes, highlighting their advantages, will be addressed in next sections.
Considering the Eqs. (3.122) and (3.134) the following definitions can be constructed:

$$\hat{p} := \mathcal{A}_{\rho_0}\dot{\hat{\varphi}} \in \mathbb{R}^3 \tag{6.68a}$$

$$\hat{\pi} := \boldsymbol{\mathcal{I}}_{\rho_0}\hat{v}_n = \boldsymbol{\Lambda}\mathbf{I}_{\rho_0}\hat{V}_n \in T^{\text{spa}}_{\boldsymbol{\Lambda}} \tag{6.68b}$$

which provide the definition for the spatial field $\hat{\Pi}_\Phi(\hat{p},\hat{\pi})$ of *generalized momenta* via the *Legendre* transformations (see [372, 373, 255]).
Further, $\hat{Z} = (\hat{\varphi}, \boldsymbol{\Lambda}, \hat{\Pi}_\Phi)$ designates an arbitrary point in the infinite dimensional phase space $P\mathcal{C}_t = T^*\mathcal{C}_t$ *i.e.* the co–tangent space to the configuration manifold of Def. 3.7 and §A.
The *linear* and *angular* momentum associated to $\hat{Z} \in P\mathcal{C}_t$ are

$$\hat{L}(\hat{Z}) = \int_0^L \hat{p}\mathrm{d}S = \int_0^L \mathcal{A}_{\rho_0}\dot{\hat{\varphi}}\mathrm{d}S \tag{6.69a}$$

$$\hat{J}(\hat{Z}) = \int_0^L (\hat{\varphi}\times\hat{p}+\hat{\pi})\mathrm{d}S = \int_0^L (\hat{\varphi}\times\dot{\hat{\varphi}} + \boldsymbol{\Lambda}\mathbf{I}_{\rho_0}\hat{V}_n)\mathrm{d}S \tag{6.69b}$$

and the total force and total torque acting on the rod are

$$\hat{F}_{\text{ext}} = \int_0^L \hat{\mathcal{N}}\mathrm{d}S + [\hat{n}_\Sigma]_{\partial_\Sigma\hat{\varphi}_0} \tag{6.70a}$$

$$\hat{T}_{\text{ext}} = \int_0^L [\hat{\varphi}\times\hat{\mathcal{N}} + \hat{\mathcal{M}}]\mathrm{d}S + [\hat{\varphi}\times\hat{n}_\Sigma + \hat{m}_\Sigma]_{\partial_\Sigma\hat{\varphi}_0} \tag{6.70b}$$

which constitute the *external loading*. As stated by Simo *et al.* in [373] if: (i) the external loading is equilibrated *i.e.* $\hat{F}_{\text{ext}} = 0$ and $\hat{T}_{\text{ext}} = 0\ \forall t \in [0,T]$ and (ii) the prescribed boundary conditions are of the *Neumann* type *i.e.* $\partial_\Phi\hat{\varphi}_0 = \emptyset$, then

$$\frac{\mathrm{d}\hat{L}}{\mathrm{d}t} = 0 \quad \text{and} \quad \frac{\mathrm{d}\hat{J}}{\mathrm{d}t} = 0 \tag{6.71}$$

which is a consequence of the Euler laws of motion which implies that if total force and torque on a mechanical system are zero then the time rate of change in the linear and angular momentum is also zero, therefore the quantities $\hat{L}$ and $\hat{J}$ of Eq. (6.70a) and (6.70b) are conserved.
A demonstration of the preceding result can be deduced taking into account Eq. (6.67) as

$$\begin{aligned}\frac{\mathrm{d}\hat{L}}{\mathrm{d}t} &= \int_0^L \dot{\hat{p}}\mathrm{d}S = \int_0^L (\hat{n}_{,S} + \hat{\mathcal{N}})\mathrm{d}S \\ &= \int_0^L \hat{\mathcal{N}}\mathrm{d}S + \hat{n}\big|_{\partial_\Sigma\hat{\varphi}_0} = \hat{F}_{\text{ext}}\end{aligned} \tag{6.72a}$$

$$\begin{aligned}\frac{\mathrm{d}\hat{J}}{\mathrm{d}t} &= \int_0^L (\hat{\varphi}\times\dot{\hat{p}}+\dot{\hat{\pi}})\mathrm{d}S \\ &= \int_0^L (\hat{\varphi}\times(\hat{n}_{,S}+\hat{\mathcal{N}})+\hat{m}_{,S}+\hat{\varphi}_{,S}\times\hat{n}+\hat{\mathcal{M}})\mathrm{d}S \\ &= \int_0^L \big[(\hat{\varphi}\times\hat{n})_{,S}+\hat{m}_{,S}\big]\mathrm{d}S+\int_0^L(\hat{\varphi}\times\hat{\mathcal{N}}+\hat{\mathcal{M}})\mathrm{d}S \\ &= \int_0^L(\hat{\varphi}\times\hat{\mathcal{N}}+\hat{\mathcal{M}})\mathrm{d}S+(\hat{\varphi}\times\hat{n}+\hat{m})\big|_{\partial_\Sigma\hat{\varphi}_0} = \hat{T}_{\mathrm{ext}} \end{aligned} \tag{6.72b}$$

where it has been used $\dot{\hat{\varphi}}\times\hat{\dot{p}}=0$.
Additionally, the *total energy* of the system is the *Hamiltonian* $H_g := K+V_{\mathrm{int}}+V_{\mathrm{ext}}$, ($H_g : P\mathcal{C}_t\to\mathbb{R}$). It is worth to note that

$$K(\hat{Z},t)=\frac{1}{2}\int_0^L(\dot{\hat{\varphi}}\cdot\hat{p}\mathrm{d}S+\hat{v}_n\cdot\hat{\pi}_n)\mathrm{d}S. \tag{6.73}$$

The following property holds: The Hamiltonian H_g is conserved by the dynamics in the sense that

$$\frac{\mathrm{d}H_g}{\mathrm{d}t}=0 \quad \text{in} \quad [0,T]. \tag{6.74}$$

A length but straightforward manipulation shows, considering $\dot{W}_{\mathrm{int}}=\partial_{\hat{\Gamma}_n}W_{\mathrm{int}}\cdot\dot{\hat{\Gamma}}_n+\partial_{\hat{\Omega}_n}\cdot W_{\mathrm{int}}\dot{\hat{\Omega}}_n$, the Lie definition of co–rotated derivative of §3.2.4, Eqs. (3.79c) and (3.81c) and integration by parts, that

$$\dot{K} = \frac{1}{2}\int_0^L(\ddot{\hat{\varphi}}\cdot\hat{p}+\dot{\hat{\varphi}}\cdot\dot{\hat{p}}+\dot{\hat{v}}\cdot\hat{\pi}+\hat{v}\cdot\dot{\hat{\pi}})\mathrm{d}S=\int_0^L(\dot{\hat{\varphi}}\cdot\dot{\hat{p}}+\hat{v}\cdot\dot{\hat{\pi}})\mathrm{d}S \tag{6.75a}$$

$$\begin{aligned}\dot{V}_{\mathrm{int}} &= \int_0^L(\partial_{\hat{\Gamma}_n}W_{\mathrm{int}}\cdot\dot{\hat{\Gamma}}_n+\partial_{\hat{\Omega}_n}W_{\mathrm{int}}\cdot\dot{\hat{\Omega}}_n)\mathrm{d}S=\int_0^L(\hat{n}\cdot\overset{\triangledown}{[\hat{\gamma}]}_n+\hat{m}\cdot\overset{\triangledown}{[\hat{\omega}]}_n)\mathrm{d}S \\ &= \int_0^L\hat{n}\cdot\dot{\hat{\varphi}}_{,S}\,\mathrm{d}S-\int_0^L\hat{n}\cdot\widetilde{\boldsymbol{v}}_n\hat{\varphi}_{,S}\,\mathrm{d}S+\int_0^L\hat{m}\cdot\hat{v}_{,S}\,\mathrm{d}S \\ &= (\hat{\Phi}\cdot\dot{\hat{q}}_\Phi)\big|_0^L-(\int_0^L\hat{n}_{,S}\cdot\dot{\hat{\varphi}}\mathrm{d}S-\int_0^L(\hat{\varphi}\times\hat{n})\cdot\hat{v}\mathrm{d}S+\int_0^L\hat{m}_{,S}\cdot\hat{v}\mathrm{d}S) \end{aligned} \tag{6.75b}$$

$$\dot{V}_{\mathrm{ext}} = \int_0^L(\hat{N}\cdot\dot{\hat{\varphi}}+\hat{M}\cdot\hat{v})\mathrm{d}S. \tag{6.75c}$$

Then, considering the fact that $\dot{\hat{q}}_\Phi$ also belongs in the space of admissible variations, $\dot{H}_g=\dot{K}+\dot{V}_{\mathrm{int}}+\dot{V}_{\mathrm{ext}}$ and after replacing Eqs. (6.75a) to (6.75c) and regrouping terms, one yields $\dot{H}_g=0$.

6.4 Energy–momentum conserving schemes

The main motivation for the development of numerical algorithms which inherit the conservation properties of the Hamiltonian dynamical systems are [373]: (i) Conserved quantities often capture important characteristics of the long–term dynamics. (ii) Conservation of energy usually leads to algorithmic stability. In this section and by completeness, the description of the most representatives results in this area is performed.

In the case of the rod models, probably the pioneering work in the development of such algorithms were carried out by Simo *et al.* [372, 373]. In that case, the *design* of the algorithm is carried out in two steps: (i) Construction of a family of algorithms which conserve the linear and angular momentum under equilibrated external loadings. (ii) The construction of an algorithmic counterpart of the elastic constitutive equations, in a manner that ensures energy conservation. To this end, the weak form of the problem is written as

$$G(\hat{Z},\hat{\eta}^{\mathrm{s}}) = \int_0^L (\hat{\Pi}_\Phi \cdot \hat{\eta}^{\mathrm{s}})\mathrm{d}S + G_{\mathrm{int}}(\hat{q}_\Phi,\hat{\eta}^{\mathrm{s}}) - G_{\mathrm{ext}}(\hat{q}_\Phi,\hat{\eta}^{\mathrm{s}}) \tag{6.76}$$

with G_{int} and G_{ext} as given in Eqs. (6.62) and (6.67), respectively and the spatial updating rule for the rotational field is preferred.

6.4.1 Momentum conserving time–stepping algorithm

Let $[t_n, t_{n+1}]$ $(t_{n+1} - t_n = \Delta t)$ be the time interval, then a midpoint approximation to the time evolution of the configuration variables is given by

$$\frac{(\hat{\varphi}_{n+1} - \hat{\varphi}_n)}{\Delta t} = \frac{1}{2}[\dot{\hat{\varphi}}_{n+1} + \dot{\hat{\varphi}}_n] = \mathcal{A}_{\rho_0}^{-1}\hat{p}_{n+1/2} = \hat{\mathtt{u}}_m \tag{6.77a}$$

$$\frac{(\boldsymbol{\Lambda}_{n+1} - \boldsymbol{\Lambda}_n)}{\Delta t} = \frac{1}{2}(\boldsymbol{\Lambda}_{n+1} + \boldsymbol{\Lambda}_n)\frac{1}{2}(\widetilde{\boldsymbol{V}}_{n+1} + \widetilde{\boldsymbol{V}}_n) \tag{6.77b}$$

where both the rotation tensor and the material form of the angular velocity are simultaneously approximated. Denoting $\widetilde{\boldsymbol{V}}_m = \Delta t 1/2(\widetilde{\boldsymbol{V}}_{n+1} + \widetilde{\boldsymbol{V}}_n)$ it is possible to develop an updating rule for the rotation tensor, using the *Cayley transform*, $\mathrm{cay}[\bullet]$, as

$$\boldsymbol{\Lambda}_{n+1} = \boldsymbol{\Lambda}_n \mathrm{cay}[\widetilde{\boldsymbol{V}}_m] = \mathrm{cay}[\widetilde{\boldsymbol{v}}_m]\boldsymbol{\Lambda}_n \tag{6.78}$$

$$\mathrm{cay}[\widetilde{\boldsymbol{V}}_m] = \mathbf{I} + \frac{2}{1 + \frac{1}{2}|V_m|^2}[\frac{1}{2}\widetilde{\boldsymbol{V}}_m + \frac{1}{4}\widetilde{\boldsymbol{V}}_m^2], \quad \hat{v}_m = \boldsymbol{\Lambda}_n \hat{V}_m. \tag{6.79}$$

The algorithmic approximation of Eq. (6.76) is then provided by

$$\frac{1}{\Delta t}\int_0^L (\delta\hat{\varphi}\cdot[\hat{p}_{n+1} - \hat{p}_n] + \delta\hat{\theta}\cdot[\hat{\pi}_{n+1} - \hat{\pi}_n])\mathrm{d}S + \int_0^L (\hat{n}\cdot[\delta\hat{\varphi}_{,S} - \delta\hat{\theta}\times\hat{\varphi}_{,S(n+1/2)}] + \hat{m}\cdot\delta\hat{\theta}_{,S})\mathrm{d}S = G_{\mathrm{ext}}(\hat{\Psi},\hat{q}_\Phi,\hat{\eta}^{\mathrm{s}}) \tag{6.80}$$

where $\hat{\varphi}_{n+1/2} := 1/2(\hat{\varphi}_{n+1} + \hat{\varphi}_n)$, $\boldsymbol{\Lambda}_{n+1/2} := 1/2(\boldsymbol{\Lambda}_{n+1} + \boldsymbol{\Lambda}_n)$; $\hat{\Psi} := [\hat{n}^T, \hat{m}^T]$ are arbitrary and the contribution of the external loading G_{ext} is assumed conservative. Note that the algorithmic approximation of Eq. (6.80) avoids the inclusion of terms depending on the acceleration. Assuming Neumann boundary conditions and equilibrated loading ($G_{\mathrm{ext}}(\hat{\Psi},\hat{\zeta},\hat{\eta}^{\mathrm{s}}) = 0$, $G_{\mathrm{ext}}(\hat{\Psi},\hat{\zeta}\times\hat{\varphi}_{n+1/2},\hat{\eta}^{\mathrm{s}}) = 0$, $\forall\hat{\zeta}\in\mathbb{R}^3$), then the total linear and angular momentum is conserved *i.e.* (i) $\hat{L}_{n+1} = \hat{L}_n$ and (ii) $\hat{J}_{n+1} = \hat{J}_n$); independently of $\hat{\Psi}$.
The demonstration is based on [373]:

(i) Taking $\delta\hat{\varphi} = \hat{\zeta}$=constant $\in\mathbb{R}^3$, $\delta\hat{\theta} = 0$ and replacing in Eq. (6.80) one obtains

$$\frac{1}{\Delta t}\int_0^L \hat{\zeta}\cdot[\hat{p}_{n+1} - \hat{p}_n]\mathrm{d}S = \hat{\zeta}\cdot[\hat{L}_{n+1} - \hat{L}_n] = 0 \rightarrow \hat{L}_{n+1} = \hat{L}_n \tag{6.81}$$

(ii) For the conservation of angular momentum one choose $\delta\hat{\varphi} = \hat{\zeta} \times \hat{\varphi}_{n+1/2}$ and $\delta\hat{\theta} = \hat{\zeta}$=constant (but arbitrary). After replacing in Eq. (6.80) the term depending on $\hat{\Psi}$ vanish ($\hat{\zeta}_{,S} = 0$) yielding to

$$\frac{1}{\Delta t}\int_0^L (\hat{\zeta} \times \hat{\varphi}_{n+1/2}) \cdot [\hat{p}_{n+1} - \hat{p}_n] + \hat{\zeta} \cdot [\hat{\pi}_{n+1} - \hat{\pi}_n] \mathrm{d}S \tag{6.82}$$

using the identities

$$(\hat{\zeta} \times \hat{\varphi}_{n+1/2}) \cdot [\hat{p}_{n+1} - \hat{p}_n] = \hat{\zeta} \cdot (\hat{\varphi}_{n+1/2} \times [\hat{p}_{n+1} - \hat{p}_n]) \tag{6.83a}$$

$$\hat{\varphi}_{n+1/2} \times (\hat{p}_{n+1} - \hat{p}_n) = \hat{\varphi}_{n+1} \times \hat{p}_{n+1} - \hat{\varphi}_n \times \hat{p}_n - (\hat{\varphi}_{n+1} - \hat{\varphi}_n) \times \hat{p}_{n+1/2} \tag{6.83b}$$

with the fact that $(\hat{\varphi}_{n+1} - \hat{\varphi}_n) = \mathcal{A}_{\rho_0}^{-1} \Delta t \hat{p}_{n+1/2}$ and replacing in Eq. (6.82) one obtains

$$\hat{\zeta} \cdot [\hat{J}_{n+1} - \hat{J}_n] = 0 \rightarrow \hat{J}_{n+1} = \hat{J}_n \tag{6.84}$$

REMARK 6.5. It is worth to note that the algorithm proposed in Eq. (6.80) conserves the linear and angular momentum with independence of the stress field $\hat{\Psi}$ ■

6.4.2 Conservation of Energy

The second step in the design of an energy conserving time stepping scheme is to specify the algorithmic constitutive equations consistent with §3.7 and enforcing energy conservation.
The updating rule defined in Eqs. (6.77a) and (6.77b) determine the following incremental relations for the strain fields:

$$\hat{\Gamma}_{n+1} - \hat{\Gamma}_n = \mathbf{\Lambda}_{n+1/2}^T (\hat{\mathrm{u}}_{m,S} - \hat{v}_m \times \hat{\varphi}_{,S(n+1/2)}) \tag{6.85a}$$

$$\hat{\Omega}_{n+1} - \hat{\Omega}_n = \mathbf{\Lambda}_{n+1/2}^{*T} \hat{v}_{n,S}\,, \qquad \mathbf{\Lambda}_{n+1/2}^{*} = \mathrm{Det}[\mathbf{\Lambda}_{n+1/2}] \mathbf{\Lambda}_{n+1/2}^{-T} \tag{6.85b}$$

The demonstration of the fact that the updating procedure defined in Eqs. (**??**) and (6.86) is deduced from the midpoint approximation to the time evolution of the configuration variables can be consulted in [373].
Following restrictions on the law of conservation of energy have to be imposed. To this end, it is sufficient to show that Eqs. (6.77a), (6.77b) and (6.80) (under the assumption of conservation of dead loading) exactly conserve the energy conservation of the Hamiltonian system ($H_g(\hat{Z}_{n+1}) = H_g(\hat{Z}_n)$) if the algorithmic constitutive equations hod the following relation:

$$W_{\mathrm{int}}(\hat{\Gamma}_{n+1}, \hat{\Omega}_{n+1}) - W_{\mathrm{int}}(\hat{\Gamma}_n \hat{\Omega}_n) = \hat{n}^{\mathrm{m}} \cdot (\hat{\Gamma}_{n+1} - \hat{\Gamma}_n) + \hat{m}^{\mathrm{m}} \cdot (\hat{\Omega}_{n+1} - \hat{\Omega}_n) \tag{6.86}$$

where $\hat{n} = \mathbf{\Lambda}_{n+1/2} \hat{n}^{\mathrm{m}}$ and $\hat{m}^{\mathrm{m}} = \mathbf{\Lambda}_{n+1/2}^{*} \hat{n}^{\mathrm{m}}$.
The proof is constructed considering as admissible variations $\delta\hat{\varphi} = \hat{\mathrm{u}}_m$ and $\delta\hat{\theta} = \hat{v}_m$ and the fact that $\mathbf{\Lambda}_{n+1}^T \hat{v}_m = \mathbf{\Lambda}_n^T \hat{v}_m = \hat{V}_m$. Then,

$$\begin{aligned} \frac{1}{\Delta t} \hat{v}_m \cdot (\hat{\pi}_{n+1} - \hat{\pi}_n) &= \frac{1}{\Delta t} [\mathbf{\Lambda}_{n+1}^T \hat{v}_m \cdot \mathbf{I}_{\rho_0} \hat{V}_{n+1} - \mathbf{\Lambda}_n^T \hat{v}_m \cdot \mathbf{I}_{\rho_0} \hat{V}_n] \\ &= \frac{1}{2} [\hat{V}_{n+1} \cdot \mathbf{I}_{\rho_0} \hat{V}_{n+1} - \hat{V}_n \cdot \mathbf{I}_{\rho_0} \hat{V}_n]. \end{aligned} \tag{6.87}$$

Considering $\hat{\mathtt{u}}_m = \Delta t \hat{\varphi}_{n+1/2}$ it is obtained that

$$\frac{1}{\Delta t}\hat{\mathtt{u}}_m \cdot (\hat{p}_{n+1} - \hat{p}_n) = \hat{\varphi}_{n+1/2} \cdot \mathcal{A}_{\rho_0}(\hat{\varphi}_{n+1} - \hat{\varphi}_n) = \frac{1}{2}\mathcal{A}_{\rho_0}[|\hat{\varphi}_{n+1}|^2 - |\hat{\varphi}_n|^2] \tag{6.88}$$

Therefore, considering the form chosen for the admissible variations, one has

$$K(\hat{\Pi}_{\Phi(n+1)}) - K(\hat{\Pi}_{\Phi(n)}) = G_{\text{ext}} - G_{\text{int}} \tag{6.89}$$

and additionally, considering the updating rule for strains given in Eqs. (6.85a) and (6.85b) one has that

$$\hat{n} \cdot (\hat{\mathtt{u}}_{m,S} - \hat{v}_m \times \hat{\varphi}_{,S(n+1/2)}) + \hat{m} \cdot \hat{v}_{n,S} = \hat{n}^{\mathrm{m}} \cdot (\hat{\Gamma}_{n+1} - \hat{\Gamma}_n) + \hat{m}^{\mathrm{m}} \cdot (\hat{\Omega}_{n+1} - \hat{\Omega}_n) \tag{6.90}$$

Taking into account that the external loading is assumed conservative and inserting the previous equation int Eq. (6.89) the following result is obtained:

$$\int_0^L (W_{\text{int}}(\hat{\Gamma}_{n+1}, \hat{\Omega}_{n+1}) - W_{\text{int}}(\hat{\Gamma}_n \hat{\Omega}_n) - \hat{n}^{\mathrm{m}} \cdot (\hat{\Gamma}_{n+1} - \hat{\Gamma}_n) + \hat{m}^{\mathrm{m}} \cdot (\hat{\Omega}_{n+1} - \hat{\Omega}_n))\mathrm{d}S = 0 \tag{6.91}$$

which hods if conservation of energy holds yielding the desired result. Then, the algorithmic constitutive equations in its simplest form are given by

$$\hat{n}^{\mathrm{m}} = \mathcal{C}^{\mathrm{me}}_{nn}\frac{1}{2}[\hat{\Gamma}_{n+1} - \hat{\Gamma}_n] \tag{6.92a}$$

$$\hat{m}^{\mathrm{m}} = \mathcal{C}^{\mathrm{me}}_{mm}\frac{1}{2}[\hat{\Omega}_{n+1} - \hat{\Omega}_n] \tag{6.92b}$$

which fulfill Eq. (6.86).

The spatial discretization (using a Galerkin approximation) and the finite element implementation of the present time discrete algorithms which fulfill the conservation of momentum maps and energy is carried out in detail in [373]; additionally, the corresponding linearization of Eq. (6.80) and its implementation in a iterative scheme is deduced and supplemented by a set of numerical examples. Those results are omitted here and can be consulted in the mentioned reference.

Posteriorly, several works have contributed to improve the formulation presented in [373]: For example, in [340] Romero and Armero present new FE formulation for the dynamics 3D (elastic) geometrically exact rods which leads to an objective[7] approximation of the strain measures (avoiding path-dependence in the numerical results). They employ a direct FE interpolation of the vector directors of the cross section. The proposed formulation includes a energy-momentum (by construction) conserving time-stepping algorithm which provides a improved approach to the dynamics of the underlined Hamiltonian system (see also [19, 20, 23, 21] and references there in). Betsch and Steinmann [57, 62] propose a new beam FE formulation based upon the geometrically exact beam theory which also retains the frame-indifference of the underlying beam theory. (see also [58, 59, 60, 61]). To this end, they introduces a re-parametrization of the weak form corresponding to the equations of motion of rod. Ibrahimbegović and Mamouri in [189] an extension of a time-integration energy conserving scheme for geometrically exact rods which includes properties of controllable energy decay, as well as numerical dissipation of high-frequency contribution to total response (see also [182, 186, 183, 191]). The list of works

[7] Objective in the sense of frame-indifferent under superposed rigid body motions.

is large, additional contributions can be reviewed in §2.1.3.

6.5 Variational integration

The variational method for deriving integrators means that the resulting algorithms automatically have a number of properties. In particular, they are *symplectic* methods, they exactly preserve momenta associated to symmetries of the system, and they have excellent longtime energy stability (see §2.1.3 for a more complete review of relevant references). Variational methods preserve the geometry of the geometric structure of the continuum system. In the present case it corresponds to the nonlinear nature of the configuration manifold. We are primarily interested in discrete Lagrangian mechanics for deriving integrators for mechanical systems. In this section a proposal for the development a variational integrator for the present rod theory is presented.

6.5.1 Summary of the method

In following a brief review of the method for deriving variational integrators is presented following the developments of [222, 253, 254] and references therein. When deriving a variational integrator, the velocity phase space $\hat{Z} \in P\mathcal{C}_t$ of the continuous Lagrangian is replaced by $(\hat{q}_{\Phi(n)}, \hat{q}_{\Phi(n+1)}) \in \mathcal{C}_t \times \mathcal{C}_t$ and the discrete Lagrangian $\mathfrak{L}_D$ is chosen such that it approximates a segment of the action integral

$$\mathfrak{L}_D(\hat{q}_{\Phi(n)}, \hat{q}_{\Phi(n+1)}) \approx \int_0^{\Delta t} \mathfrak{L}_g(\hat{q}_{\Phi(n,n+1)}, \dot{\hat{q}}_{\Phi(n,n+1)})\mathrm{d}t$$

where $\hat{q}_{\Phi(n,n+1)}$ is the solution of the Euler-Lagrange equation satisfying boundary conditions $\hat{q}_{\Phi(n,n+1)}(0) = \hat{q}_{\Phi(n)}$ and $\hat{q}_{\Phi(n,n+1)}(\Delta t) = \hat{q}_{\Phi(n+1)}$. Then, the discrete action sum $\mathfrak{G}_D = \sum \mathfrak{L}_D(\hat{q}_{\Phi(n)}, \hat{q}_{\Phi(n+1)})$ approximates the action integral $\mathfrak{G}$. Taking the variations of the action sum, we obtain the discrete Euler-Lagrange equation

$$D_{\hat{q}_{\Phi(n)}}\mathfrak{L}_D(\hat{q}_{\Phi(n-1)}, \hat{q}_{\Phi(n)}) + D_{\hat{q}_{\Phi(n)}}\mathfrak{L}_D(\hat{q}_{\Phi(n)}, \hat{q}_{\Phi(n+1)})$$

where $D_{\hat{q}_{\Phi(n)}}\mathfrak{L}_D$ denotes the partial derivative of $\mathfrak{L}_D$ with respect to $\hat{q}_{\Phi(n)}$. This yields a discrete Lagrangian map $F_{\mathfrak{L}_D} : (\hat{q}_{\Phi(n-1)}, \hat{q}_{\Phi(n)}) \to (\hat{q}_{\Phi(n)}, \hat{q}_{\Phi(n+1)})$. Using a discrete analogue of the Legendre transformation, referred to as a discrete fiber derivative $\mathbb{F}\mathfrak{L}_D : \mathcal{C}_t \times \mathcal{C}_t \to T^*\mathcal{C}_t$, variational integrators can be expressed in Hamiltonian form as

$$\hat{p}_{\Phi(n)} = -D_{\hat{q}_{\Phi(n)}}\mathfrak{L}_D(\hat{q}_{\Phi(n)}, \hat{q}_{\Phi(n+1)}) \tag{6.93a}$$

$$\hat{p}_{\Phi(n)} = D_{\hat{q}_{\Phi(n+1)}}\mathfrak{L}_D(\hat{q}_{\Phi(n)}, \hat{q}_{\Phi(n+1)}). \tag{6.93b}$$

This yields a discrete Hamiltonian map $\bar{F}_{\mathfrak{L}_D} : (\hat{q}_{\Phi(n)}, \hat{p}_{\Phi(n)}) \mapsto (\hat{q}_{\Phi(n+1)}, \hat{p}_{\Phi(n)})$ which constitutes the integrator of the equation of motion and inherit the previous mentioned advantages (see §2.1.3. The method consist in implicitly Eq. (6.93a) for $\hat{q}_{\Phi(n+1)}$ then introduce it into Eq. (6.93b) to obtain $\hat{q}_{\Phi(n+1)}$. Therefore, Any integrator which is the discrete *Euler-Lagrange* equation for some discrete Lagrangian is called a variational integrator.

6.5.2 Variation integrator for the rod model

Given two time steps t_n and t_{n+1} the updating procedure for the configurational variables is

$$\hat{\varphi}_{n+1} = \hat{\varphi}_n + \hat{\varphi}_{in} \tag{6.94a}$$
$$\boldsymbol{\Lambda}_{n+1} = \boldsymbol{\Lambda}_{in}\boldsymbol{\Lambda}_n \tag{6.94b}$$

where $\hat{\varphi}_{in} \in \mathbb{R}^3$ and $\boldsymbol{\Lambda}_{in} \in SO(3)$ are the incremental (between two time steps) displacement and rotation. Therefore, $\boldsymbol{\Lambda}_{n+1} \in SO(3)$.
Considering that $\dot{\boldsymbol{\Lambda}} = \widetilde{\boldsymbol{v}}\boldsymbol{\Lambda}^T$, $\widetilde{\boldsymbol{v}} \in T^{\text{spa}}_{\boldsymbol{\Lambda}}SO(3)$ on has that the translational velocity $\dot{\hat{\varphi}}$ and the skew–symmetric tensors $\widetilde{\boldsymbol{v}}$ and $\widetilde{\boldsymbol{V}}$ (angular velocities) can be approximated by

$$\dot{\hat{\varphi}}_n = \frac{\hat{\varphi}_{n+1} - \hat{\varphi}_n}{\Delta t} = \frac{\hat{\varphi}_{in}}{\Delta t} \tag{6.95a}$$
$$\widetilde{\boldsymbol{v}}_n = \frac{\boldsymbol{\Lambda}_{n+1} - \boldsymbol{\Lambda}_n}{\Delta t}\boldsymbol{\Lambda}_n^T = \frac{1}{\Delta t}(\boldsymbol{\Lambda}_{in} - \mathbf{I}) \tag{6.95b}$$
$$\widetilde{\boldsymbol{V}}_n = \boldsymbol{\Lambda}_n^T\frac{\boldsymbol{\Lambda}_{n+1} - \boldsymbol{\Lambda}_n}{\Delta t} = \frac{1}{\Delta t}(\boldsymbol{\Lambda}_n^T\boldsymbol{\Lambda}_{in}\boldsymbol{\Lambda}_n - \mathbf{I}), \tag{6.95c}$$

with $\widetilde{\boldsymbol{V}}_n = \boldsymbol{\Lambda}_n^T\widetilde{\boldsymbol{v}}_n\boldsymbol{\Lambda}_n$ and the corresponding axial vectors obtained as

$$\hat{V}_n = \text{axial}[\widetilde{\boldsymbol{V}}_n] \quad \text{and} \quad \hat{v}_n = \text{axial}[\widetilde{\boldsymbol{v}}_n].$$

REMARK 6.6. Note that due to the nature approximation used for $\widetilde{\boldsymbol{v}}_n$ and $\widetilde{\boldsymbol{V}}_n$, both are not skew–symmetric and

$$\widetilde{\boldsymbol{v}}_n + \widetilde{\boldsymbol{v}}_n^T = (\Delta t)^{-1}(\boldsymbol{\Lambda}_{in} + \boldsymbol{\Lambda}_{in}^T - 2\mathbf{I}) \neq 0 \tag{6.96a}$$
$$\widetilde{\boldsymbol{V}}_n + \widetilde{\boldsymbol{V}}_n^T = (\Delta t)^{-1}(\boldsymbol{\Lambda}_n^T\boldsymbol{\Lambda}_{n+1} + \boldsymbol{\Lambda}_{n+1}^T\boldsymbol{\Lambda}_n - 2\mathbf{I}) \neq 0 \tag{6.96b}$$

therefore, in the algebraic manipulations it has to considered that $\widetilde{\boldsymbol{v}}_n\hat{a}\cdot\hat{b} = \hat{a}\cdot\widetilde{\boldsymbol{v}}_n^T\hat{b} \neq -\hat{a}\cdot\widetilde{\boldsymbol{v}}_n\hat{b}$, $\forall\hat{a}, \hat{b} \in \mathbb{R}^3$ (the same applies for $\widetilde{\boldsymbol{V}}_n$) ■

Then the kinetic energy, Eq. (6.57), is approximated by

$$K_n = \frac{1}{2(\Delta t)^2}\int_0^L (\mathcal{A}_{\rho_0}|\hat{\varphi}_{in}|^2 \mathrm{d}S + \text{axial}[\boldsymbol{\Lambda}_n^T\boldsymbol{\Lambda}_{n+1} - \mathbf{I}]\cdot\mathbf{I}_{\rho_0}\text{axial}[\boldsymbol{\Lambda}_n^T\boldsymbol{\Lambda}_{n+1} - \mathbf{I}])\mathrm{d}S \tag{6.97a}$$

considering that

$$|\widetilde{\boldsymbol{V}}_n\hat{\mathscr{E}}|^2 = |[\boldsymbol{\Lambda}_n^T\boldsymbol{\Lambda}_{n+1} - \mathbf{I}]\hat{\mathscr{E}}|^2 = \frac{[\boldsymbol{\Lambda}_{n+1}^T\boldsymbol{\Lambda}_n - \mathbf{I}][\boldsymbol{\Lambda}_n^T\boldsymbol{\Lambda}_{n+1} - \mathbf{I}]\hat{\mathscr{E}}\cdot\hat{\mathscr{E}}}{(\Delta t)^2} = \frac{\text{Tr}([\boldsymbol{\Lambda}_{n+1}^T\boldsymbol{\Lambda}_n - \boldsymbol{\Lambda}_n^T\boldsymbol{\Lambda}_{n+1}]\boldsymbol{\mathscr{E}}_d)}{(\Delta t)^2}.$$

where $\boldsymbol{\mathscr{E}}_d = \hat{\mathscr{E}}\otimes\hat{\mathscr{E}}$ and considering $\boldsymbol{\mathscr{E}} = \int_{\mathcal{A}_0}\boldsymbol{\mathscr{E}}_d\mathrm{d}\mathcal{A}_0$ Eq. (6.97a) can be rewritten as

$$K_n = \frac{1}{2(\Delta t)^2}\int_0^L (\mathcal{A}_{\rho_0}|\hat{\varphi}_{in}|^2 + \text{Tr}([\boldsymbol{\Lambda}_{n+1}^T\boldsymbol{\Lambda}_n - \boldsymbol{\Lambda}_n^T\boldsymbol{\Lambda}_{n+1}]\boldsymbol{\mathscr{E}}))\mathrm{d}S \tag{6.97b}$$

The potential energy is at time t_n (equivalently for t_{n+1}) is obtained from Eqs. (6.72a) to (6.58c) as

$$V_n = V_{\text{int}(n)} + V_{\text{ext}(n)} = \int_0^L W_{\text{str}}(\hat{\Gamma}_{n(n)}, \hat{\Omega}_{n(n)})\mathrm{d}S + \int_0^L W_{\text{ext}}(\hat{\varphi}_{nn}, \boldsymbol{\Lambda}_n)\mathrm{d}S \tag{6.98}$$

A discrete version of the Lagrangian of the system in the time interval $[t_n, t_{n+1}]$ is constructed as an approximation of the action integral $\mathfrak{A}$ as

$$\begin{aligned}\mathfrak{L}_D(\hat{q}_{\Phi(n)}, \hat{q}_{\Phi(n+1)}) &= \frac{\Delta t}{2}\Big[\mathfrak{L}_g(\hat{\varphi}_n, \frac{\hat{\varphi}_{in}}{\Delta t}, \mathbf{\Lambda}_n, \frac{[\mathbf{\Lambda}_n^T\mathbf{\Lambda}_{n+1} - \mathbf{I}]}{\Delta t}) \\ &\quad +\mathfrak{L}_g(\hat{\varphi}_{n+1}, \frac{\hat{\varphi}_{in}}{\Delta t}, \mathbf{\Lambda}_{n+1}, \frac{[\mathbf{\Lambda}_n^T\mathbf{\Lambda}_{n+1} - \mathbf{I}]}{\Delta t})\Big] \\ &= \frac{\Delta t}{2}\Big[2K_n - (V_{\text{int}(n)} + V_{\text{ext}(n)}) - (V_{\text{int}(n+1)} + V_{\text{ext}(n+1)})\Big] \qquad (6.99)\end{aligned}$$

The corresponding linear forms, using the spatial updating rule for rotations, are

$$\delta\dot{\hat{\varphi}}_n = \frac{\delta\hat{\varphi}_{n+1} - \delta\hat{\varphi}_n}{\Delta t} = \frac{\delta\hat{\varphi}_{in}}{\Delta t} \qquad (6.100a)$$

$$\delta\mathbf{\Lambda}_{in} = \delta\widetilde{\boldsymbol{\theta}}_{n+1}\mathbf{\Lambda}_{n+1}\mathbf{\Lambda}_n^T + \mathbf{\Lambda}_{n+1}(\delta\mathbf{\Lambda}_n)^T = \delta\widetilde{\boldsymbol{\theta}}_{n+1}\mathbf{\Lambda}_{in} - \mathbf{\Lambda}_{in}\delta\widetilde{\boldsymbol{\theta}}_n \qquad (6.100b)$$

$$\begin{aligned}\delta\widetilde{\boldsymbol{v}}_n &= \frac{\delta(\mathbf{\Lambda}_{n+1} - \mathbf{\Lambda}_n)}{\Delta t}\mathbf{\Lambda}_n^T + \frac{\mathbf{\Lambda}_{n+1} - \mathbf{\Lambda}_n}{\Delta t}(\delta\mathbf{\Lambda}_n)^T \\ &= \frac{\delta\widetilde{\boldsymbol{\theta}}_{n+1}\mathbf{\Lambda}_{in}}{\Delta t} - \frac{\mathbf{\Lambda}_{in}\delta\widetilde{\boldsymbol{\theta}}_n}{\Delta t} = \delta\widetilde{\boldsymbol{\theta}}_{n+1}\widetilde{\boldsymbol{v}}_n - \widetilde{\boldsymbol{v}}_n\delta\widetilde{\boldsymbol{\theta}}_{n+1} + (\delta\widetilde{\boldsymbol{\theta}}_{n+1} - \delta\widetilde{\boldsymbol{\theta}}_n)(\Delta t)^{-1} \\ &= \delta\widetilde{\boldsymbol{\theta}}_{n+1}\widetilde{\boldsymbol{v}}_n - \widetilde{\boldsymbol{v}}_n\delta\widetilde{\boldsymbol{\theta}}_{n+1} + \delta\dot{\widetilde{\boldsymbol{\theta}}}_n \qquad (6.100c)\end{aligned}$$

$$\begin{aligned}\delta\widetilde{\boldsymbol{V}}_n &= (\delta\mathbf{\Lambda}_n)^T\frac{\mathbf{\Lambda}_{n+1} - \mathbf{\Lambda}_n}{\Delta t} + \mathbf{\Lambda}_n^T\frac{\delta(\mathbf{\Lambda}_{n+1} - \mathbf{\Lambda}_n)}{\Delta t} = \mathbf{\Lambda}_n^T(\delta\widetilde{\boldsymbol{\theta}}_{n+1} - \delta\widetilde{\boldsymbol{\theta}}_n)(\Delta t)^{-1}\mathbf{\Lambda}_{n+1} \\ &= \mathbf{\Lambda}_n^T\delta\dot{\widetilde{\boldsymbol{\theta}}}_n\mathbf{\Lambda}_{n+1}. \qquad (6.100d)\end{aligned}$$

Considering the previous results one obtains that linearization of the discrete form of the kinetic and potential energy are

$$\begin{aligned}\delta K_n &= \frac{1}{2(\Delta t)^2}\int_0^L (2\mathcal{A}_{\rho_0}(\delta\dot{\hat{\varphi}}_{n+1}\cdot[\dot{\hat{\varphi}}_{n+1} - \dot{\hat{\varphi}}_n] - \delta\dot{\hat{\varphi}}_n\cdot[\dot{\hat{\varphi}}_{n+1} - \dot{\hat{\varphi}}_n]) \\ &\quad +\text{Tr}([\mathbf{\Lambda}_n^T(\mathbf{\Lambda}_{in}\delta\widetilde{\boldsymbol{\theta}}_n + \delta\widetilde{\boldsymbol{\theta}}_n\mathbf{\Lambda}_{in})\mathbf{\Lambda}_n - \mathbf{\Lambda}_n^T(\mathbf{\Lambda}_{in}\delta\widetilde{\boldsymbol{\theta}}_{n+1} + \delta\widetilde{\boldsymbol{\theta}}_n\mathbf{\Lambda}_{in})\mathbf{\Lambda}_n]\boldsymbol{\mathscr{E}}))\text{d}S \qquad (6.101)\end{aligned}$$

$$\begin{aligned}\delta V_{\text{int}(n)} &= \int_0^L (\hat{n}_n^{\text{m}}\cdot\mathbf{\Lambda}_n^T[\delta\hat{\varphi}_{,S(n)} - \delta\widetilde{\boldsymbol{\theta}}_n\hat{\varphi}_{,S}] + \hat{m}_n^{\text{m}}\cdot\mathbf{\Lambda}_n^T\delta\hat{\theta}_{n,S})\text{d}S \\ &= \int_0^L (\hat{n}_n\cdot[\delta\hat{\varphi}_{,S(n)} - \delta\widetilde{\boldsymbol{\theta}}_n\hat{\varphi}_{,S}] + \hat{m}_n\cdot\delta\hat{\theta}_{n,S})\text{d}S \qquad (6.102)\end{aligned}$$

$$\delta V_{\text{ext}(n)} = \int_0^L (\hat{\mathcal{N}}\cdot\delta\hat{\varphi}_n + \hat{\mathcal{M}}\cdot\delta\hat{\theta}_n)\text{d}S \qquad (6.103)$$

Then, considering $N = (t_b - t_a)/(\Delta t)$ one obtains that the discrete variation of the action integral over two times t_a, t_b is

$$\delta\mathfrak{G}_D = \sum_{k=0}^{(N\Delta t-1)}\delta\mathfrak{L}_D(\hat{q}_{\Phi(k)}, \hat{q}_{\Phi(k+1)}) = \sum_{k=0}^{(N\Delta t-1)}\frac{\Delta t}{2}\Big[2\delta K_n - \delta V_n) - \delta V_{n+1}\Big]. \qquad (6.104)$$

Replacing the results of Eqs. (6.101) to (6.103), rearranging the index of the summation and grouping terms should provide a set of equations equivalent to those of Eqs. (6.93a) and (6.93a), which are the variational integrator.

Chapter 7

Finite element implementation

This chapter describes the spatial discretization used in the *Galerkin* [170] finite element approximation of the time discretization presented in §6 for the (weak) variational equations described in §5.3.3. As usual in the FEM the applied procedure yields to a system of nonlinear algebraic equations well suited for the application of the Newton iterative method. Then, the main purpose of this part of the work is to develop a Galerkin discretization of the linearized form of the virtual work functional consistent with the time discretization previously discussed.
As in the case of the formulation of a time-discrete version of the problem, the main difficulty arises in the fact that the spatial interpolation of the configuration variables should be consistent with the nonlinear nature of the configuration manifold $\mathbb{R}^3 \times SO(3)$. The developed elements are based on isoparametric interpolations of both the incremental displacement and the incremental rotation vectors.
It should be addressed again that, the material or spatial updating rule for the rotations are equivalent and, therefore, their corresponding interpolated (iterative or incremental) rotation vectors can be used to parameterize and update the rotational variables. In this manner and by completeness, both schemes are presented yielding to the corresponding tangential stiffness matrices and unbalanced force vectors. However, the numerical procedures based on the spatial form of the iterative incremental rotation vector are preferred to others[1], due to the fact that it makes the expressions for the internal, external and inertial vectors and the tangential matrices concise and explicit, as opposed to the case when using the incremental rotation vector. This choice seems to be more efficient and robust for computations and more convenient for programming. The obtained inertial and viscous tangential matrices are consistent with the Newmark updating procedure described in §6.
Finally, a section devoted to the cross sectional analysis is included, explaining the numerical obtention of the iterative cross sectional forces and moments as well as the cross sectional tangential tensors required in the full Newton–Raphson scheme.

7.1 Finite element discretization

In following we consider a FE discretization of a generic one–dimensional domain $[0, L]$:

$$[0, L] = \bigcup_{e=1}^{\mathrm{N}_e} \mathrm{I}_e^h; \qquad (\mathrm{I}_i^h \cap \mathrm{I}_j^h = \emptyset;\ \forall\, i, j \in \{1 \cdots \mathrm{N}_e\}) \tag{7.1}$$

[1] See *e.g.* Ibrahimbegović Ref. [178] for the employment of an updated *additive* rotation vector or Cardona *et al.* Ref. [88] for the total Lagrangian formulation

where $\mathrm{I}_e^h \subset [0, L]$ denotes a typical element with length $h > 0$, and N_e is the total number of elements. The space of admissible variations $T\mathcal{C}_t$ is approximated by a finite dimensional subspace $V^h \subset T\mathcal{C}_t$.
As usual, the calculations are performed on an element basis [365]. Accordingly, let $\hat{\eta}^{sh}$ be the restriction to a typical element I_e^h of the incremental displacement field/rotation field (using the spatial updating rule for rotations) $\hat{\eta}^{sh} \equiv (\Delta\hat{\varphi}^h, \Delta\hat{\theta}^h) \in V^h$ superposed onto the configuration $(\hat{\varphi}_*, \mathbf{\Lambda}_*) \in \hat{C}_{t^*}$ (at $t = t_*$).
The conventional *Lagrangian interpolation* [42] is used for describing the initially curved/twisted reference rod configuration $\hat{\varphi}_{0(e)}$, the current rod position vector $\hat{\varphi}_{(e)}$, the displacement vector, $\hat{u}_{(e)}$ and the linearized increments $\Delta\hat{\varphi}_{(e)}$ and $\Delta\hat{\theta}_{(e)}$ of any rod element[2] *i.e.*

$$s \in [-1,1] \;\; \mapsto \;\; \left\{ \begin{array}{r} \hat{\varphi}_{0(e)}(s) = \sum_{I=1}^{\mathrm{N}_d} N_I(s)\hat{\varphi}_{0I(e)} \\ \hat{\varphi}_{(e)}(s) = \sum_{I=1}^{\mathrm{N}_d} N_I(s)\hat{\varphi}_{I(e)} \\ \Delta\hat{\theta}_{(e)}(s) = \sum_{I=1}^{\mathrm{N}_d} N_I(s)\Delta\hat{\theta}_{I(e)} \\ \Delta\hat{\varphi}_{(e)}(s) = \sum_{I=1}^{\mathrm{N}_d} N_I(s)\delta\hat{\varphi}_{I(e)}; \end{array} \right. \tag{7.2}$$

where N_d is the number of nodes on a given element and $N_I(s)$ $I = 1 \cdots \mathrm{N}_d$ are the local (elemental) shape functions. Note that in Eq. (7.2) the symbol Δ denoting the linearized increment can be replaced by δ denoting the admissible variation. Therefore, the value at $s \in [-1, 1]$ of any vectorial quantity, denoted generically by $\hat{\mathrm{H}}(s)^{(e)}$, is obtained from the values at the nodes as

$$\begin{aligned} \hat{\mathrm{H}}_{(e)}(s) = & \left[\begin{array}{ccc|c|ccc|c|ccc} N_{11} & \cdots & 0 & & N_{I1} & \cdots & 0 & & N_{\mathrm{N}_d 1} & \cdots & 0 \\ \vdots & \ddots & \vdots & \cdots & \vdots & \ddots & \vdots & \cdots & \vdots & \ddots & \vdots \\ 0 & \cdots & N_{16} & & 0 & \cdots & N_{I6} & & 0 & \cdots & N_{\mathrm{N}_d 6} \end{array}\right] \left[\begin{array}{c} \hat{\mathrm{H}}_1 \\ \vdots \\ \hat{\mathrm{H}}_I \\ \vdots \\ \hat{\mathrm{H}}_{\mathrm{N}_d 1} \end{array}\right]_{(e)} \\ & \underbrace{\qquad\qquad}_{[\mathbf{N}_I(S)]} \\ = & \left[\mathbf{N}_1 | \cdots | \mathbf{N}_I | \cdots | \mathbf{N}_{\mathrm{N}_d 1}\right] \hat{\mathrm{H}}^{(e)} = [\mathbf{N}]\hat{\mathrm{H}}_{(e)} \end{aligned} \tag{7.3}$$

where $\hat{\mathrm{H}}_{(e)I}$ is the value of the vectorial quantity $\hat{\mathrm{H}}_{(e)}$ at the node I; $[\mathbf{N}(s)_I] = \mathrm{Diag}[N(s)_{Ii}]$, $(i = 1, \ldots, 6)$ is the diagonal matrix with the values of the shape function corresponding to the node I evaluated at s. With this notation in mind, for example, the value of the admissible variation in the third degree of freedom of displacement at s in the element (e) is obtained as $\delta\varphi_{e3}(s) = [\mathbf{N}]_{3\bullet} \cdot \delta\hat{\mathrm{H}}_e$, with $\delta\hat{\mathrm{H}}_e = [\delta\hat{\varphi}_1^T \cdots \delta\hat{\theta}_1, \cdots, \delta\hat{\varphi}_{\mathrm{N}_d} \cdots \delta\hat{\theta}_{\mathrm{N}_d}^T]_{(e)}$ and $[\mathbf{N}]_{3\bullet}$ the third row of the matrix $\mathbf{N}$. The same holds for the components of $\delta\hat{\theta}_{(e)}$, $\delta\hat{\Theta}_{(e)}$, etc. Recovering the expressions given in Eqs. (7.2).
The updating procedure for the rotations can be carried out in either *material* or *spatial* representations [245] due to the fact that both representations are equivalents and the denominations material or spatial are employed only to indicate the way in which rotations are handled. A comparison between both formulations can be found in [88].

REMARK 7.1. A possibility for calculating the interpolated values of the skew–symmetric tensor $\widetilde{\boldsymbol{\theta}}(s)_{(e)}$ (or $\widetilde{\boldsymbol{\Theta}}(s)_{(e)}$) is given by calculating $\hat{\theta}(s)_{(e)}$ ($\hat{\Theta}(s)_{(e)}$ respectively) using Eq. (7.3) and then applying the operator $\mathbf{\Pi}[\bullet]$ (see §A.2.1 of Appendix A). Other possibility is the direct

[2]The superscript (e) is used in reference to the e^{th} element in the mesh.

interpolation using the matrix $\mathbf{N}$ of the values of the skew–symmetric tensors $\widetilde{\mathbf{\Theta}}(s)_{(e)I}$ at the nodes, taking advantages of the linearity of $so(3)$. ■

By contrast with the result of the preceding Remark, if the rotation tensor $\mathbf{\Lambda}(S)$ has to be determined we have

$$\mathbf{\Lambda}(s)_{(e)} = \exp[\widetilde{\boldsymbol{\theta}}(s)_{(e)}] \neq [\mathbf{N}]_{(4-6)\bullet}\exp[\widetilde{\boldsymbol{\theta}}_{I(e)}] = \overline{\mathbf{\Lambda}} \tag{7.4}$$

where $[\mathbf{N}]_{(4-6)\bullet}$ is the matrix corresponding to the rows 4 to 6 of the matrix $\mathbf{N}$. Therefore, the rotation tensor obtained from the interpolated values of the rotation tensor is a rotation tensor; however, in general we have that $\overline{\mathbf{\Lambda}\mathbf{\Lambda}}^T \neq \mathbf{I}$ and in this way the interpolation by the shape forms of the nodal values of the rotation tensor do not produce a rotation tensor due to the fact that $SO(3)$ is not a linear space.

7.1.1 Spatial derivatives

The derivative with respect to the parameter $S \in [0, L]$ of the quantities defined by in Eqs. (7.2) can be calculated starting from Eq. (7.3) as

$$\hat{\mathrm{H}}(s)_{(e),S} = \left[\mathbf{N}_{1,S}|\cdots|\mathbf{N}_{I,S}|\cdots|\mathbf{N}_{\mathrm{N}_d,S}\right]\hat{\mathrm{H}}^{(e)} = [\mathbf{N},_S]\hat{\mathrm{H}}^{(e)} \tag{7.5}$$

where it has been used the generic notation $\hat{\mathrm{H}}(s)_{(e)}$ and $[\mathbf{N}_{I,S}] = \mathrm{Diag}[N(S)_{Ii,S}]$, $(i = 1, \ldots, 6)$ corresponds to the diagonal matrix constructed from the derivatives with respect to S of the shape functions N_I corresponding to the node I of the element.
As usual in FE implementations shape functions normalized with respect to a curvilinear coordinate[3] $s \in [-1, 1]$ are used; and in this case Eq. (7.5) is rewritten as

$$\hat{\mathrm{H}}(s)_{(e),S} = J_s^{-1}[\mathbf{N},_s]\hat{\mathrm{H}}^{(e)} \tag{7.6}$$

with $J_s = \sqrt{\hat{\varphi}_{0,S}\cdot\hat{\varphi}_{0,S}}$ being the Jacobian of the transformation between S and s.

7.2 FE approximation of the out of balance force vector

Following standard procedures for nonlinear finite element analysis [310], the element contribution to the residual force vector is obtained from the discrete approximation to the weak form of momentum balance.

7.2.1 Internal force vector

The finite element approximation of the internal component of the virtual work principle, given in Eq. (3.147), $G^h_{\mathrm{int}}(\hat{\varphi}, \mathbf{\Lambda}, \hat{\eta}^{\mathrm{s}h})_{(e)}$, with $\hat{\eta}^{\mathrm{s}h} = [\hat{\eta}^{\mathrm{s}}_1 \cdots \hat{\eta}^{\mathrm{s}}_I \cdots \hat{\eta}^{\mathrm{s}}_{\mathrm{N}_d}]^T = [(\delta\hat{\varphi}_1, \delta\hat{\theta}_1)\cdots(\delta\hat{\varphi}_{\mathrm{N}_d}, \delta\hat{\theta}_{\mathrm{N}_d})]^T \in V^h$ the vector containing nodal values of the admissible variation of the configuration variables

[3] Usually called it natural coordinates.

$(\hat{\varphi}, \mathbf{\Lambda})_{(e)}$ is

$$\begin{aligned} G^h_{\text{int}}(\hat{\varphi}, \mathbf{\Lambda}, \hat{\eta}^{\text{s}h})_{(e)} &= \int_{[0,L_e]} (\begin{bmatrix} \delta[\overset{\triangledown}{\hat{\gamma}}_n] \\ \delta[\overset{\triangledown}{\hat{\omega}}_n] \end{bmatrix} \cdot \begin{bmatrix} \hat{n} \\ \hat{m} \end{bmatrix}) \mathrm{d}S = \int_{[0,L]} (\big[[\boldsymbol{B}][\mathbf{N}]\hat{\eta}^{\text{s}h}\big]^T \begin{bmatrix} \hat{n} \\ \hat{m} \end{bmatrix}) \mathrm{d}S \\ &= \int_{[0,L_e]} ([\hat{\eta}^{\text{s}}_1 \cdots \hat{\eta}^{\text{s}}_I \cdots \hat{\eta}^{\text{s}}_{\text{N}_d}][\mathbf{N}_1 \cdots \mathbf{N}_I \cdots \mathbf{N}_{\text{N}_d}]^T [\boldsymbol{B}]^T \begin{bmatrix} \hat{n} \\ \hat{m} \end{bmatrix}) \mathrm{d}S \end{aligned} \tag{7.7}$$

where it has been considered Eq. (5.12c) and the following expression is obtained for the generic term $\mathbf{N}_I^T \boldsymbol{B}^T$:

$$\mathbf{N}_I^T \boldsymbol{B}^T = \begin{bmatrix} N_{I,S}\,\mathbf{I} & 0 \\ -N_I \widetilde{\boldsymbol{\varphi}}_{,S} & N_{I,S}\,\mathbf{I} \end{bmatrix} \tag{7.8}$$

with $\widetilde{\boldsymbol{\varphi}}_{,S} = J_s^{-1} \mathbf{\Pi} \big[[\mathbf{N}_{(1-3)\bullet,s}]\hat{\varphi}_{(e)}\big]$ according to Eq. (7.5). In this way , it is possible to rewrite Eq. (7.7) as

$$\begin{aligned} G^h_{\text{int}}(\hat{\varphi}, \mathbf{\Lambda}, \hat{\eta}^{\text{s}h})_{(e)} &= \begin{bmatrix} \hat{\eta}^{\text{s}}_1 \\ \vdots \\ \hat{\eta}^{\text{s}}_I \\ \vdots \\ \hat{\eta}^{\text{s}}_{\text{N}_d} \end{bmatrix} \cdot \int_{[0,L_e]} (J_s^{-1} \begin{bmatrix} N_{1,s}\,\mathbf{I} & 0 \\ -N_1 \widetilde{\boldsymbol{\varphi}}_{,s} & N_{1,s}\,\mathbf{I} \\ & \vdots \\ N_{I,s}\,\mathbf{I} & 0 \\ -N_I \widetilde{\boldsymbol{\varphi}}_{,s} & N_{I,s}\,\mathbf{I} \\ & \vdots \\ N_{\text{N}_d,s}\,\mathbf{I} & 0 \\ -N_{\text{N}_d} \widetilde{\boldsymbol{\varphi}}_{,s} & N_{\text{N}_d,s}\,\mathbf{I} \end{bmatrix} \begin{bmatrix} \hat{n} \\ \hat{m} \end{bmatrix}) \mathrm{d}S \\ &= \sum_{I=1}^{\text{N}_d} \begin{bmatrix} \delta\hat{\varphi}_I \\ \delta\hat{\theta}_I \end{bmatrix} \cdot \int_{[0,L_{(e)}]} (J_s^{-1} \begin{bmatrix} N_{I,s}\,\hat{n} \\ N_{I,s}\,\hat{m} - N_I \widetilde{\boldsymbol{\varphi}}_{,s}\,\hat{n} \end{bmatrix}) \mathrm{d}S \\ &= \hat{\eta}^{\text{s}hT} \sum_{I=1}^{\text{N}_d} \hat{q}^h_{\text{int}(e)I}. \end{aligned} \tag{7.9}$$

Here, $\hat{q}^h_{\text{int}(e)I}$ denotes the internal force vector related to the node I in a typical element I^h_e. The integral appearing in this equation can be calculated using a standard numerical procedure selecting a set of N_{ip} integration points on the element and using the corresponding weighting factors W_J $(J = 1, \ldots, N_{ip})$ (*e.g.* Gauss, Lobbato etc. [170]). Therefore, the term $\hat{q}^h_{\text{int}(e)I}$ is obtained as

$$\hat{q}^h_{\text{int}(e)I} = \begin{bmatrix} \int_0^{L_e} (J_s^{-1} N_{I,s}\,\hat{n}) \mathrm{d}S \\ \int_0^{L_e} J_s^{-1} (N_{I,s}\,\hat{m} - N_I \widetilde{\boldsymbol{\varphi}}_{,s}\,\hat{n}) \mathrm{d}S \end{bmatrix} = \sum_{J=1}^{N_{ip}} \begin{bmatrix} J_s^{-1} N_{I,s}\,\hat{n} \\ J_s^{-1} (N_{I,s}\,\hat{m} - N_I \widetilde{\boldsymbol{\varphi}}_{,s}\,\hat{n}) \end{bmatrix} \Big|_J J_s W_J \tag{7.10}$$

where $(\bullet)|_J$ denotes the evaluation of the given quantity at the integration point number J. The evaluation of the spatial form of the cross sectional forces and moments, $\hat{n}$ and $\hat{m}$, at the integration points is carried out by means of and appropriated cross sectional analysis as it will be explained in the next sections.

7.2.2 External force vector

In the same way as for the internal force vector, the finite element approximation of the external component of the virtual work principle, given in Eq. (3.142), $G^h_{\text{ext}}(\hat{\varphi}, \mathbf{\Lambda}, \hat{\eta}^{sh})_{(e)} = G^h_{\text{ext}(e)}$ is

$$\begin{aligned} G^h_{\text{ext}(e)} &= \hat{\eta}^{sh}_{(e)} \cdot \int_{[0,L_e]} ([\mathbf{N}]^T \begin{bmatrix} \hat{\mathcal{N}} \\ \hat{\mathcal{M}} \end{bmatrix})_{(e)} \mathrm{d}S \\ &= \sum_{I=1}^{\mathrm{N}_d} \begin{bmatrix} \Delta\hat{\varphi}_I \\ \Delta\hat{\theta}_I \end{bmatrix} \cdot \int_{[0,L_e]} N_I \begin{bmatrix} \hat{\mathcal{N}}_g + c_N \hat{\mathcal{N}}_d + \mathbf{\Lambda}\hat{\tilde{\mathcal{N}}}_p \\ N_I[\hat{\mathcal{M}}_g + c_M \hat{\mathcal{M}}_d + \mathbf{\Lambda}\hat{\tilde{\mathcal{M}}}_p] \end{bmatrix} \mathrm{d}S \\ &= \sum_{I=1}^{\mathrm{N}_d} \begin{bmatrix} \Delta\hat{\varphi}_I \\ \Delta\hat{\theta}_I \end{bmatrix} \cdot \sum_{J=1}^{N_{ip}} \begin{bmatrix} N_I[\hat{\mathcal{N}}_g + c_N \hat{\mathcal{N}}_d + \mathbf{\Lambda}\hat{\tilde{\mathcal{N}}}_p] \\ N_I[\hat{\mathcal{M}}_g + c_M \hat{\mathcal{M}}_d + \mathbf{\Lambda}\hat{\tilde{\mathcal{M}}}_p] \end{bmatrix} \Bigg|_J J_s W_J = \hat{\eta}^{shT} \sum_{I=1}^{\mathrm{N}_d} \hat{q}^h_{\text{ext}(e)I} \end{aligned} \tag{7.11}$$

where $\hat{q}^h_{\text{ext}(e)I}$ is the external load vector at the node I.

7.2.3 Inertial force vector

The internal nodal forces in the dynamic case correspond to those of the static case but adding the inertial contribution, which can be calculated starting from Eq. (3.144), $G^h_{\text{ine}}(\hat{\varphi}, \mathbf{\Lambda}, \hat{\eta}^{sh})_{(e)}$ as

$$\begin{aligned} G^h_{\text{int}}(\hat{\varphi}, \mathbf{\Lambda}, \hat{\eta}^{sh})_{(e)} &= \hat{\eta}^{sh}_{(e)} \cdot \int_{[0,L_{(e)}]} ([\mathbf{N}]^T \begin{bmatrix} A_{\rho_0} \ddot{\hat{\varphi}} \\ \boldsymbol{\mathcal{I}}_{\rho_0} \hat{\alpha}_n + \widetilde{\hat{\boldsymbol{v}}}_n \boldsymbol{\mathcal{I}}_{\rho_0} \hat{v}_n \end{bmatrix}_{(e)}) \mathrm{d}S \\ &= \sum_{I=1}^{\mathrm{N}_d} \begin{bmatrix} \Delta\hat{\varphi}_I \\ \Delta\hat{\theta}_I \end{bmatrix} \cdot \int_{[0,L_e]} N_I \begin{bmatrix} A_{\rho_0} \ddot{\hat{\varphi}} \\ \boldsymbol{\mathcal{I}}_{\rho_0} \hat{\alpha}_n + \widetilde{\hat{\boldsymbol{v}}}_n \boldsymbol{\mathcal{I}}_{\rho_0} \hat{v}_n \end{bmatrix}_{(e)} \mathrm{d}S \\ &= \sum_{I=1}^{\mathrm{N}_d} \begin{bmatrix} \Delta\hat{\varphi}_I \\ \Delta\hat{\theta}_I \end{bmatrix} \cdot \sum_{J=1}^{N_{ip}} \begin{bmatrix} N_I A_{\rho_0} \ddot{\hat{\varphi}} \\ N_I[\boldsymbol{\mathcal{I}}_{\rho_0} \hat{\alpha}_n + \widetilde{\hat{\boldsymbol{v}}}_n \boldsymbol{\mathcal{I}}_{\rho_0} \hat{v}_n] \end{bmatrix} \Bigg|_J J_s W_J \end{aligned} \tag{7.12}$$

$$= \hat{\eta}^{shT} \sum_{I=1}^{\mathrm{N}_d} \hat{q}^h_{\text{ine}(e)I} \tag{7.13}$$

where $\hat{q}^h_{\text{ext}(e)I}$ is the inertial force load vector at the node I.
Finally, considering the results of Eqs. (7.10), (7.11) and (7.13), the *unbalanced force* term is written as

$$G^h_{(e)}(\hat{\varphi}, \mathbf{\Lambda}, \hat{\eta}^{sh}) = \hat{\eta}^{sh} \cdot \hat{q}^h_{(e)} = \hat{\eta}^{shT} \sum_{I=1}^{\mathrm{N}_d} (\hat{q}^h_{\text{int}(e)I} + \hat{q}^h_{\text{ine}(e)I} - \hat{q}^h_{\text{ext}(e)I}) \tag{7.14}$$

7.3 FE approximation of the tangential stiffness

The FE discretization of the tangent stiffness matrix is obtained from the linearized form of the virtual work principle as given in Section 6.2.1 [178, 228, 207, 363], or equivalently by means of the linearization of the nodal unbalanced load vector as

$$\Delta\hat{q}^h_{(e)I} = [\mathbf{K}^h_e]_{IJ} \cdot [\Delta\hat{\varphi}, \Delta\hat{\theta}]^e_J. \tag{7.15}$$

Here $[\mathbf{K}_{IJ}]_e^h$ is the tangential stiffness matrix, relating the nodes I and J at a given configuration, in the element e. In the same manner as it was done for the unbalance load vector, the static and dynamic cases will be treated separately.

7.3.1 Internal contribution to the tangential stiffness

Considering $\hat{\eta}^{\mathrm{sh}}(S) = \mathbf{N}\hat{\eta}^{\mathrm{sh}}_{(e)}$ and $\hat{p}^{\mathrm{sh}}(S) = \mathbf{N}\hat{p}^{\mathrm{sh}}_{(e)}$ (see Eq. (7.3)), it is possible to consider the FE approximation of the linearized form of the internal contribution to the virtual work principle, Eq. (5.68), relative to the element I_e^h at a given configuration, which can be expressed as

$$\begin{aligned} DG^h_{\mathrm{int}(e)} \cdot \hat{p}^{\mathrm{sh}} &= \hat{\eta}^{\mathrm{sh}T} \underbrace{\Big[\int_0^{L_e} (\mathbf{N}^T \boldsymbol{B}^T \bar{\mathbf{C}}^{\mathrm{sv}} \boldsymbol{B}\mathbf{N}) \mathrm{d}S\Big]}_{\mathbf{K}_{M(e)}} \hat{p}^{\mathrm{sh}} \\ &+ \hat{\eta}^{\mathrm{sh}T} \underbrace{\Big[\int_0^{L_e} (\mathbf{N}^T (\boldsymbol{\mathscr{F}} + \boldsymbol{B}^T \boldsymbol{\mathscr{N}}) \mathbf{N}) \mathrm{d}S\Big]}_{\mathbf{K}_{G(e)}} \hat{p}^{\mathrm{sh}} + \hat{\eta}^{\mathrm{sh}T} \underbrace{\Big[\int_0^{L_e} (\mathbf{N}^T (\boldsymbol{B}^T \bar{\boldsymbol{\Upsilon}}^{\mathrm{ss}} \boldsymbol{\mathcal{V}}) \mathbf{N}) \mathrm{d}S\Big]}_{\mathbf{K}_{V(e)}} \hat{p}^{\mathrm{sh}} \\ &= \hat{\eta}^{\mathrm{sh}T} (\mathbf{K}_{M(e)} + \mathbf{K}_{G(e)} + \mathbf{K}_{V(e)}) \hat{p}^{\mathrm{sh}} \end{aligned} \tag{7.16}$$

where $[\mathbf{K}_{M(e)}]$, $[\mathbf{K}_{G(e)}]$ and $[\mathbf{K}_{V(e)}]$ are the *material* (constitutive), *geometric* and *viscous* components of the element stiffness matrix at the current configuration.
Then we have that the material stiffness matrix can be written as

$$[\mathbf{K}_{M(e)}] = \sum_{I,J}^{\mathrm{N}_d} \int_{[0,L]} \mathbf{N}_I^T \boldsymbol{B}^T \bar{\mathbf{C}}^{\mathrm{sv}} \boldsymbol{B} \mathbf{N}_J \mathrm{d}S = \sum_{I,J}^{\mathrm{N}_d} [\mathbf{K}_{M(e)}]_{IJ} \tag{7.17}$$

where $[\mathbf{K}_{M(e)}]_{IJ}$ denote the sub-matrix coupling the nodes I and J of the finite element with explicit expression, after the numerical integration procedure, given by

$$[\mathbf{K}_{M(e)}]_{IJ} = \sum_K^{N_{ip}} J_s^{-1} \left[\begin{array}{c|c} N_{I,s} N_{J,s} \mathbf{C}^{\mathrm{sv}}_{nn} & N_{I,s} (\mathbf{C}^{\mathrm{sv}}_{nn} \widetilde{\boldsymbol{\varphi}}_{,s} + \mathbf{C}^{\mathrm{sv}}_{nm} N_{J,s}) \\ \hline \mathbf{C}^{\mathrm{sv}}_{mn} N_{I,s} N_{J,s} & N_{I,s} (\mathbf{C}^{\mathrm{sv}}_{mn} \widetilde{\boldsymbol{\varphi}}_{,s} N_J + \mathbf{C}^{\mathrm{sv}}_{mm} N_{J,s}) \\ -N_I N_{J,s} \mathbf{C}^{\mathrm{sv}}_{nn} \widetilde{\boldsymbol{\varphi}}_{,s} & -N_I \widetilde{\boldsymbol{\varphi}}_{,s} (\mathbf{C}^{\mathrm{sv}}_{nn} \widetilde{\boldsymbol{\varphi}}_{,s} N_J + \mathbf{C}^{\mathrm{sv}}_{nm} N_{J,s}) \end{array} \right] \Bigg|_K W_K \tag{7.18}$$

which is always symmetric.
In an analogous manner for the term $[\mathbf{K}_{G(e)}]_{IJ}$, taking into account Eq. (7.8) one has

$$\begin{aligned} [\mathbf{K}_{G(e)}]_{IJ} &= \sum_K^{N_{ip}} \Big(\underbrace{\left[\begin{array}{cc} 0 & 0 \\ N_I \widetilde{\boldsymbol{n}} N_{J,s} & 0 \end{array} \right]}_{\mathbf{N}_I \boldsymbol{\mathscr{F}} \mathbf{N}_J} + \underbrace{\left[\begin{array}{cc} 0 & -N_{I,s} \widetilde{\boldsymbol{n}} N_J \\ 0 & (N_I \widetilde{\boldsymbol{\varphi}}_{,s} \widetilde{\boldsymbol{n}} N_J - N_{I,s} \widetilde{\boldsymbol{m}} N_J) \end{array} \right]}_{\mathbf{N}_I^T \boldsymbol{B}^T \boldsymbol{\mathcal{N}} \mathbf{N}_J} \Big) \Big|_K W_K \\ &= \sum_K^{N_{ip}} \Big(\left[\begin{array}{cc} 0 & -N_{I,s} \widetilde{\boldsymbol{n}} N_J \\ N_I \widetilde{\boldsymbol{n}} N_{J,s} & (N_I (\hat{n} \otimes \hat{\varphi}_{,s} - \hat{n} \cdot \hat{\varphi}_{,s} \mathbf{I}) + N_{I,s} \widetilde{\boldsymbol{m}}) N_J \end{array} \right] \Big|_K W_K \end{aligned} \tag{7.19}$$

which is not necessarily symmetric and it has been used the identity of Eq. (A.21b) of §A.
Analogously, the FE discretization of the viscous component off the tangential stiffness is com-

puted as

$$[\mathbf{K}_{V(e)}] = \sum_{IJ}^{\mathrm{N}_d} \int_{[0,L]} \mathbf{N}_I^T (\boldsymbol{B}^T \bar{\boldsymbol{\Upsilon}}^{\mathrm{ss}} \boldsymbol{\mathcal{V}}) \mathbf{N}_J \mathrm{d}S = \sum_{IJ}^{\mathrm{N}_d} [\mathbf{K}_{V(e)}]_{IJ} \tag{7.20}$$

where the sub-matrix I–J of the viscous component of the tangential stiffness matrix is given by

$$[\mathbf{K}_{V(e)}]_{IJ} = J_s^{-1} \sum_{K}^{N_{ip}} \left[\begin{array}{c|c} N_{I,s}\, \bar{\boldsymbol{\Upsilon}}^{\mathrm{ss}}_{nn} N_{J,s}\, (\gamma_{t\beta}\mathbf{I} - \widetilde{\boldsymbol{v}}) & \begin{array}{l} N_{I,s} \{ \bar{\boldsymbol{\Upsilon}}^{\mathrm{ss}}_{nn} N_J (\dot{\widetilde{\boldsymbol{\varphi}}}_{,s} + \widetilde{\boldsymbol{\varphi}}_{,s}\, \gamma_{t\beta}\mathbf{T} - \\ \quad - \widetilde{\boldsymbol{v}}\widetilde{\boldsymbol{\varphi}}_{,s}\,) + \bar{\boldsymbol{\Upsilon}}^{\mathrm{ss}}_{nm} ((2\gamma_{t\beta}\mathbf{T} - \\ \quad + \widetilde{\boldsymbol{v}}_n) N_{J,s} + \gamma_{t\beta}\mathbf{T}_{,s}\, N_J) \} \end{array} \\ \hline N_{J,s}\, (\gamma_{t\beta}\mathbf{I} - \widetilde{\boldsymbol{v}}) (N_{I,s}\, \bar{\boldsymbol{\Upsilon}}^{\mathrm{ss}}_{mn} - N_I \widetilde{\boldsymbol{\varphi}}_{,s}\, \bar{\boldsymbol{\Upsilon}}^{\mathrm{ss}}_{nn}) & \begin{array}{l} (N_{I,s}\, \bar{\boldsymbol{\Upsilon}}^{\mathrm{ss}}_{mm} - N_I \widetilde{\boldsymbol{\varphi}}_{,s}\, \bar{\boldsymbol{\Upsilon}}^{\mathrm{ss}}_{nn}) N_J (\dot{\widetilde{\boldsymbol{\varphi}}}_{,s} + \\ \quad + \widetilde{\boldsymbol{\varphi}}_{,s}\, \gamma_{t\beta}\mathbf{T} - \widetilde{\boldsymbol{v}}\widetilde{\boldsymbol{\varphi}}_{,s}\,) + \\ \quad + (N_{I,s}\, \bar{\boldsymbol{\Upsilon}}^{\mathrm{ss}}_{nm} - \\ \quad\quad - N_I \widetilde{\boldsymbol{\varphi}}_{,s}\, \bar{\boldsymbol{\Upsilon}}^{\mathrm{ss}}_{nn}) ((\gamma_{t\beta} 2\mathbf{T} - \\ \quad\quad - \widetilde{\boldsymbol{v}}_n) N_{J,s} + \gamma_{t\beta}\mathbf{T}_{,s}\, N_J) \end{array} \end{array} \right]_K W_K \tag{7.21}$$

7.3.2 Inertial contribution to the tangential stiffness

The finite element discretization of the inertial contribution to the elemental tangent stiffness $K_{\mathrm{ine}(e)}$, Eq. (6.48), is obtained as

$$K_{\mathrm{ine}(e)} = \hat{\eta}^{shT} \Big[\int_0^{L_{(e)}} \mathbf{N}^T \mathbf{M}_{\varphi\theta} \mathbf{N} \mathrm{d}S \Big] \hat{p}^{sh} = \hat{\eta}^{shT} [\mathbf{K}_{\mathrm{ine}(e)}] \hat{p}^{sh} \tag{7.22}$$

where the elemental inertial stiffness matrix $[\mathbf{K}_{\mathrm{ine}(e)}]$ is calculated as

$$[\mathbf{K}_{\mathrm{ine}(e)}] = \sum_{IJ}^{\mathrm{N}_d} \int_0^{L_{(e)}} \mathbf{N}_I^T \mathbf{M}_{\varphi\theta} \mathbf{N}_J \mathrm{d}S = \sum_{IJ}^{\mathrm{N}_d} [\mathbf{K}_{\mathrm{ine}(e)}]_{IJ} \tag{7.23}$$

where $[\mathbf{K}_{\mathrm{ine}(e)}]_{IJ}$, coupling the degree of freedom of node I and of node J, is the sum of the operators $\{[\mathbf{K}_M]_e^h + [\mathbf{K}_G]_e^h + [\mathbf{K}_L]_e^h\}_{IJ}$ of Eq. (7.16). The explicit expression for $[\mathbf{K}_{\mathrm{ine}(e)}]_{IJ}$ Eq. (6.49) is the following:

$$\begin{aligned} [\mathbf{K}_{\mathrm{ine}(e)}]_{IJ} &= \int_0^{L_{(e)}} \mathbf{N}_I^T \begin{bmatrix} \boldsymbol{\Xi}_\varphi & 0 \\ 0 & \boldsymbol{\Xi}_\theta \end{bmatrix} \mathbf{N}_J \mathrm{d}S \quad \in \mathbb{R}^{6\times 6} \\ &= \sum_{k}^{N_{ip}} \left[\begin{array}{c|c} \frac{1}{(\Delta t)^2 \beta} \mathcal{A}_{\rho_0} N_I N_J & 0 \\ \hline 0 & \begin{array}{l} \Big[- \boldsymbol{\Lambda}\boldsymbol{\Pi}[\mathbf{I}_{\rho_0} \hat{A}_n + \hat{V}_n \times \mathbf{I}_{\rho_0} \hat{V}_n] \\ \quad + \frac{1}{(\Delta t)^2 \beta} \boldsymbol{\Lambda} (\mathbf{I}_{\rho_0} - \Delta t \gamma \boldsymbol{\Pi}[\mathbf{I}_{\rho_0} \hat{V}_n] \\ \quad \Delta t \gamma \boldsymbol{\Pi}[\hat{V}_n \mathbf{I}_{\rho_0}]) \Big] \boldsymbol{\Lambda}^{*T} \mathbf{T} N_I N_J \end{array} \end{array} \right]_K J_s W_K \end{aligned} \tag{7.24a}$$

where $\boldsymbol{\Lambda}^{*T}$ corresponds to the last converged configuration and the remaining $\boldsymbol{\Lambda}$'s are the iterative ones as described in §6.2. Both $\boldsymbol{\Xi}_\varphi$ and $\boldsymbol{\Xi}_\theta$ are elements of $\mathbb{R}^{3\times 3}$. As noted in Section 6.2.2.b, the tangent inertia matrix is *nonsymmetric* and *configuration dependent*. This property concerns only the rotational degrees of freedom. The sub-matrix $\boldsymbol{\Xi}_\varphi$ corresponds to the translational degrees of freedom and is constant, as usually found in the expression for the consistent matrix when the deformation map takes values in a linear space.

7.3.3 External contribution to the tangential stiffness

By the linearization of the external load vector, (see Eq. (5.77)), one obtains the discrete form of the tangential stiffness matrix due to the applied loadings.

$$\begin{aligned} K_{P(e)} &= \hat{\eta}^{shT}\left[\int_0^{L_e}\mathbf{N}^T\begin{bmatrix}(\hat{\mathcal{N}}_d\otimes\hat{\mathscr{C}}_N)[\frac{\mathrm{d}}{\mathrm{d}S}\mathbf{I}]+\widetilde{\boldsymbol{\mathcal{N}}}_p\\(\hat{\mathcal{M}}_d\otimes\hat{\mathscr{C}}_M)[\frac{\mathrm{d}}{\mathrm{d}S}\mathbf{I}]+\widetilde{\boldsymbol{\mathcal{M}}}_p\end{bmatrix}\mathbf{N}\mathrm{d}S\right]\hat{p}^{sh}\\ &= \hat{\eta}^{shT}([\mathbf{K}_{P(e)}]\hat{p}^{sh}=\hat{\eta}^{shT}([\mathbf{K}_{P1(e)}]+[\mathbf{K}_{P1(e)}])\hat{p}^{sh} \end{aligned} \tag{7.25}$$

where

$$\begin{aligned} [\mathbf{K}_{P1(e)}] &= \sum_{IJ}^{\mathrm{N}_d}\int_0^{L_e}\mathbf{N}_I^T\begin{bmatrix}(\hat{\mathcal{N}}_d\otimes\hat{\mathscr{C}}_N)[\frac{\mathrm{d}}{\mathrm{d}S}\mathbf{I}]\\(\hat{\mathcal{M}}_d\otimes\hat{\mathscr{C}}_M)[\frac{\mathrm{d}}{\mathrm{d}S}\mathbf{I}]\end{bmatrix}\mathbf{N}_J\mathrm{d}S=\sum_{IJ}^{\mathrm{N}_d}[\mathbf{K}_{P1(e)}]_{IJ}\\ [\mathbf{K}_{P2(e)}] &= \sum_{IJ}^{\mathrm{N}_d}\int_0^{L_e}\mathbf{N}_I^T\begin{bmatrix}\widetilde{\boldsymbol{\mathcal{N}}}_p\\\widetilde{\boldsymbol{\mathcal{M}}}_p\end{bmatrix}\mathbf{N}_J\mathrm{d}S=\sum_{IJ}^{\mathrm{N}_d}[\mathbf{K}_{P2(e)}]_{IJ}. \end{aligned}$$

The two components of the tangent stiffness matrix due to external loading coupling the nodes I and J are explicitly given by

$$[\mathbf{K}_{P1(e)}]_{IJ}=\sum_{k}^{N_{ip}}\left[\begin{array}{c}N_IN_{J,s}\,\hat{\mathcal{N}}_d\otimes\hat{\mathscr{C}}_N\\N_IN_{J,s}\,\hat{\mathcal{M}}_d\otimes\hat{\mathscr{C}}_M\end{array}\right]\Bigg|_K W_K \tag{7.26a}$$

the second part is known as the *pressure* stiffness matrix and is given by

$$[\mathbf{K}_{P2(e)}]_{IJ}=\sum_{k=1}^{N_{ip}}\left[\begin{array}{c}N_IN_J\widetilde{\boldsymbol{\mathcal{N}}}_p\\N_IN_J\widetilde{\boldsymbol{\mathcal{M}}}_p\end{array}\right]\Bigg|_K J_sW_K. \tag{7.26b}$$

REMARK 7.2. According to Li [228] both $[\mathbf{K}_{P1}]_e$ and $[\mathbf{K}_{P2}]_e$ can be neglected for small displacements/rotations but not for large displacements/rotations, especially when an exact bifurcation analysis is needed [180, 89, 187] ■

Finally, the tangent stiffness matrix of Eq. (7.15), relating the nodes I and J, is given by

$$[\mathbf{K}^h_{(e)}]_{IJ}=\Big[[\mathbf{K}_{M(e)}]+[\mathbf{K}_{G(e)}]+[\mathbf{K}_{V(e)}]+[\mathbf{K}_{\mathrm{ine}(e)}]+[\mathbf{K}_{P1(e)}]+[\mathbf{K}_{P2(e)}]\Big]_{IJ}. \tag{7.27}$$

7.4 Material updating of the rotational field

In the case of the material updating rule of the rotational field we have that the space of admissible variations $T\mathcal{C}_t$ is approximated by a finite dimensional subspace $V^{\mathrm{m}h}\subset T\mathcal{C}_t$. Accordingly, an element in $V^{\mathrm{m}h}$ is given by $\hat{\eta}^{\mathrm{m}h}_e\equiv(\Delta\hat{\varphi}^h,\Delta\hat{\Theta}^h)$ superposed onto the configuration $(\hat{\varphi}_*,\boldsymbol{\Lambda}_*)\in\hat{C}_{t^*}$. The conventional *Lagrangian interpolation* [42] is used for describing the incremental rotation $\hat{\Theta}_{(e)}$ and its linearized (iterative) increment $\Delta\hat{\Theta}_{(e)}$ of any rod element *i.e.*

$$\hat{\Theta}_{(e)}(s)=\sum_{I=1}^{\mathrm{N}_d}N_{\mathrm{I}}(s)\hat{\Theta}_{\mathrm{I}(e)}\qquad\Delta\hat{\Theta}_{(e)}(S)=\sum_{I=1}^{\mathrm{N}_d}N_{\mathrm{I}}(s)\Delta\hat{\Theta}_{\mathrm{I}(e)}. \tag{7.28}$$

Note that in Eq. (7.28) the symbol Δ denoting the linearized increment can be replaced by δ denoting the admissible variation. Therefore, the value at $s \in [-1,1]$ of any (material) vectorial quantity, denoted generically by $\hat{\mathrm{H}}^{\mathrm{m}(e)}$, is obtained from the values at nodes as

$$\hat{\mathrm{H}}(S)^{\mathrm{m}}_{e} = \left[\mathbf{N}_1|\cdots|\mathbf{N}_I|\cdots|\mathbf{N}_{\mathrm{N}_d}\right]\hat{\mathrm{H}}^{\mathrm{m}}_{e} = [\mathbf{N}]\hat{\mathrm{H}}^{\mathrm{m}}_{e} \tag{7.29}$$

where $\hat{\mathrm{H}}^{\mathrm{m}}_{e} = [\hat{\mathrm{H}}^{\mathrm{m}}_{1e}\cdots\hat{\mathrm{H}}^{\mathrm{m}}_{\mathrm{N}_d e}]$ with $\hat{\mathrm{H}}^{\mathrm{m}}_{Ie}$ is the value of the material form of the vectorial quantity $\hat{\mathrm{H}}^{\mathrm{m}}$ at the node I. For example, the value of the admissible variation in the third degree of freedom of rotation at s in the element (e) is obtained as $\delta\Theta_{e3}(S) = (\delta\mathbf{N}_{6\bullet})\cdot\delta\hat{\mathrm{H}}^{\mathrm{m}}_{e}$, with $\delta\hat{\mathrm{H}}^{\mathrm{m}}_{e} = [\delta\hat{\varphi}^T_1\cdots\delta\hat{\Theta}_1,\cdots,\delta\hat{\varphi}_{\mathrm{N}_d}\cdots\delta\hat{\Theta}^T_{\mathrm{N}_d}]_e$ and $\mathbf{N}_{6\bullet}$ the six$^{\mathrm{th}}$ row of the matrix $\mathbf{N}$.
The derivative with respect to the parameter $S \in [0,L]$ of the quantities defined in Eq. (7.29) can be calculated in analogous manner as in Eq. (7.5) *i.e.*

$$\hat{\mathrm{H}}(s)^{\mathrm{m}}_{(e)},_S = \left[\mathbf{N}_{1,S}|\cdots|\mathbf{N}_{I,S}|\cdots|\mathbf{N}_{\mathrm{N}_d,S}\right]\hat{\mathrm{H}}^{\mathrm{m}}_{e} = [\mathbf{N},_S]\hat{\mathrm{H}}^{\mathrm{m}}_{e} \tag{7.30}$$

where it has been used the generic notation $\hat{\mathrm{H}}(S)^{\mathrm{m}}_{e}$ and Eq. (7.5) can be rewritten as

$$\hat{\mathrm{H}}(S)^{\mathrm{m}}_{(e)},_S = J_s^{-1}[\mathbf{N},_s]\hat{\mathrm{H}}^{\mathrm{m}}_{e} \tag{7.31}$$

with $J_s = \sqrt{\hat{\varphi}_{0,S}\cdot\hat{\varphi}_{0,S}}$ being the Jacobian of the transformation between S and s (see §7.1.1).

7.5 FE approximation of the out of balance force vector

Following standard procedures for nonlinear finite element analysis [310], the element contribution to the residual force vector is obtained from the discrete approximation to the weak form of momentum balance.

7.5.1 Internal force vector

The FE approximation of the internal component of the virtual work principle, given in Eq. (3.147), $G^h_{\mathrm{int}}(\hat{\varphi},\mathbf{\Lambda},\hat{\eta}^{\mathrm{m}h})_{(e)}$, with $\hat{\eta}^{\mathrm{m}h}=[\hat{\eta}^{\mathrm{m}}_1\cdots\hat{\eta}^{\mathrm{m}}_I\cdots\hat{\eta}^{\mathrm{m}}_{\mathrm{N}_d}]^T=[(\delta\hat{\varphi}_1,\delta\hat{\Theta}_1)\cdots(\delta\hat{\varphi}_{\mathrm{N}_d},\delta\hat{\Theta}_{\mathrm{N}_d})]^T \in V^{\mathrm{m}h}$ the vector containing nodal values of the admissible variation of the configuration variables $(\hat{\varphi},\mathbf{\Lambda})_{(e)}$ is

$$G^h_{\mathrm{int}}(\hat{\varphi},\mathbf{\Lambda},\hat{\eta}^h)_{(e)} = \int_0^{L_e}([\hat{\eta}^{\mathrm{m}}_1\cdots\hat{\eta}^{\mathrm{m}}_I\cdots\hat{\eta}^{\mathrm{m}}_{\mathrm{N}_d}][\mathbf{N}_1\cdots\mathbf{N}_I\cdots\mathbf{N}_{\mathrm{N}_d}]^T[\bar{\boldsymbol{B}}]^T\begin{bmatrix}\hat{n}\\ \hat{m}\end{bmatrix})\mathrm{d}S \tag{7.32}$$

where it has been considered Eq. (5.12c) and the following expression is obtained for the generic term $\mathbf{N}^T_I\bar{\boldsymbol{B}}^T$:

$$\mathbf{N}^T_I\bar{\boldsymbol{B}}^T = \begin{bmatrix} N_{I,S}\,\mathbf{I} & 0\\ -N_I\mathbf{\Lambda}^T\widetilde{\boldsymbol{\varphi}}_{,S} & [N_{I,S}\,\mathbf{I} - N_I\widetilde{\mathbf{\Omega}}_n]\mathbf{\Lambda}^T\end{bmatrix} \tag{7.33}$$

with $\widetilde{\boldsymbol{\varphi}}_{,S} = J_s^{-1}\mathbf{\Pi}\big[[\mathbf{N}_{(1-3)\bullet,s}]\hat{\varphi}_{(e)}\big]$ according to Eq. (7.5). In this way , it is possible to rewrite Eq. (7.32) as

$$
\begin{aligned}
G^h_{\text{int}}(\hat{\varphi},\mathbf{\Lambda},\hat{\eta}^{\text{m}h})_{(e)} &= \hat{\eta}^{\text{m}h}\cdot\int_0^{L_e}(J_s^{-1}\begin{bmatrix} N_{1,s}\,\mathbf{I} & 0 \\ -N_1\mathbf{\Lambda}^T\widetilde{\boldsymbol{\varphi}}_{,S} & [N_{1,s}\,\mathbf{I}-N_1\widetilde{\mathbf{\Omega}}_n]\mathbf{\Lambda}^T \\ & \vdots \\ N_{\text{N}_d,s}\,\mathbf{I} & 0 \\ -N_{\text{N}_d}\mathbf{\Lambda}^T\widetilde{\boldsymbol{\varphi}}_{,S} & [N_{\text{N}_d,s}\,\mathbf{I}-N_{\text{N}_d}\widetilde{\mathbf{\Omega}}_n]\mathbf{\Lambda}^T \end{bmatrix}\begin{bmatrix}\hat{n}\\ \hat{m}\end{bmatrix})\text{d}S \\
&= \sum_{I=1}^{\text{N}_d}\begin{bmatrix}\delta\hat{\varphi}_I\\ \delta\hat{\Theta}_I\end{bmatrix}\cdot\int_0^{L_e}(J_s^{-1}\begin{bmatrix} N_{I,s}\,\hat{n} \\ -N_I\widetilde{\boldsymbol{\varphi}}_{,s}\,\hat{n}^{\text{m}}+[N_{I,s}\,\mathbf{I}-N_I\widetilde{\mathbf{\Omega}}_n]\hat{m}^{\text{m}}\end{bmatrix})\text{d}S \\
&= \sum_{I=1}^{\text{N}_d}\hat{\eta}^{\text{m}}_I\cdot\hat{q}^h_{\text{int}(e)I}.
\end{aligned}
\tag{7.34}
$$

Here, $\hat{q}^h_{\text{int}(e)I}$ denotes the internal force vector related to the node I in a typical element I^h_e. Numerically, the term $\hat{q}^h_{\text{int}(e)I}$ is obtained as

$$
\hat{q}^h_{\text{int}(e)I} = \sum_{J=1}^{N_{ip}}\begin{bmatrix} N_{I,s}\,\hat{n} \\ -N_I\widetilde{\boldsymbol{\varphi}}_{,s}\,\hat{n}^{\text{m}}+[N_{I,s}\,\mathbf{I}-N_I\widetilde{\mathbf{\Omega}}_n]\hat{m}^{\text{m}}\end{bmatrix}\Big|_J W_J. \tag{7.35}
$$

As in Section 7.5.1, the evaluation of the spatial form of the cross sectional forces and moments, $\hat{n}$ and $\hat{m}$ is carried out by means of and appropriated cross sectional analysis.

7.5.2 External force vector

The FE approximation of the external component of the virtual work principle, given in Eq. (3.142), $G^h_{\text{ext}}(\hat{\varphi},\mathbf{\Lambda},\hat{\eta}^{\text{m}h})_e = G^{\text{m}h}_{\text{ext}(e)}$ is

$$
\begin{aligned}
G^{\text{m}h}_{\text{ext}(e)} &= \hat{\eta}^{\text{m}h}_{(e)}\cdot\int_{[0,L_e]}([\mathbf{N}]^T\begin{bmatrix}\hat{\mathcal{N}}\\ \hat{\mathcal{M}}\end{bmatrix}_{(e)})\text{d}S \\
&= \sum_{I=1}^{\text{N}_d}\begin{bmatrix}\Delta\hat{\varphi}_I\\ \Delta\hat{\Theta}_I\end{bmatrix}\cdot\int_{[0,L_e]}N_I\begin{bmatrix}\hat{\mathcal{N}}_g+c_N\hat{\mathcal{N}}_d+\mathbf{\Lambda}\hat{\tilde{\mathcal{N}}}_p \\ N_I[\hat{\mathcal{M}}_g+c_M\hat{\mathcal{M}}_d+\mathbf{\Lambda}\hat{\tilde{\mathcal{M}}}_p]\end{bmatrix}\text{d}S \\
&= \sum_{I=1}^{\text{N}_d}\begin{bmatrix}\Delta\hat{\varphi}_I\\ \Delta\hat{\Theta}_I\end{bmatrix}\cdot\sum_{J=1}^{N_{ip}}\begin{bmatrix}N_I[\hat{\mathcal{N}}_g+c_N\hat{\mathcal{N}}_d+\mathbf{\Lambda}\hat{\tilde{\mathcal{N}}}_p] \\ N_I[\hat{\mathcal{M}}_g+c_M\hat{\mathcal{M}}_d+\mathbf{\Lambda}\hat{\tilde{\mathcal{M}}}_p]\end{bmatrix}\Big|_J J_s W_J \\
&= \sum_{I=1}^{\text{N}_d}\hat{\eta}^{\text{m}}_I\cdot\hat{q}^h_{\text{ext}(e)I}
\end{aligned}
\tag{7.36a}
$$

where $\hat{q}^h_{\text{ext}(e)I}$ is the external load vector at the node I.

7.5.3 Inertial force vector

The FE discretization of the inertial contribution to the out of balance force vector can be calculated starting from Eq. (3.144), $G^h_{\text{ine}}(\hat{\varphi}, \mathbf{\Lambda}, \hat{\eta}^{\text{m}h})_{(e)}$ as

$$\begin{aligned} G^h_{\text{int}}(\hat{\varphi}, \mathbf{\Lambda}, \hat{\eta}^{\text{m}h})_{(e)} &= \hat{\eta}^{\text{m}h}_{(e)} \cdot \int_{[0,L_e]} ([\mathbf{N}]^T \begin{bmatrix} A_{\rho_0}\ddot{\hat{\varphi}} \\ \mathbf{I}_{\rho_0}\hat{A}_n + \widetilde{\hat{\boldsymbol{V}}}_n \mathbf{I}_{\rho_0}\hat{V}_n \end{bmatrix}_{(e)}) \text{d}S \\ &= \sum_{I=1}^{\text{N}_d} \begin{bmatrix} \Delta\hat{\varphi}_I \\ \Delta\hat{\Theta}_I \end{bmatrix} \cdot \sum_{J=1}^{N_{ip}} \begin{bmatrix} N_I A_{\rho_0}\ddot{\hat{\varphi}} \\ N_I[\mathbf{I}_{\rho_0}\hat{A}_n + \widetilde{\hat{\boldsymbol{V}}}_n \mathbf{I}_{\rho_0}\hat{V}_n] \end{bmatrix} \Bigg|_J J_s W_J \qquad (7.37) \\ &= \sum_{I=1}^{\text{N}_d} \hat{\eta}_I \cdot \hat{q}^{\text{m}h}_{\text{ine}(e)I} \qquad (7.38) \end{aligned}$$

where $\hat{q}^{\text{m}h}_{\text{ext}(e)I}$ is the inertial force load vector at the node I. Finally, considering the results of Eqs. (7.34), (7.36a) and (7.37), the *unbalanced force* term is written as

$$G^h_{(e)}(\hat{\varphi}, \mathbf{\Lambda}, \hat{\eta}^{\text{m}h}) = \hat{\eta}^h \cdot \hat{q}^{\text{m}h}_{(e)} = \sum_{I=1}^{\text{N}_d} \hat{\eta}^h_{(e)I} \cdot (\hat{q}^{\text{m}h}_{\text{int}(e)I} + \hat{q}^{\text{m}h}_{\text{ine}(e)I} - \hat{q}^{\text{m}h}_{\text{ext}(e)I}) \qquad (7.39)$$

7.6 FE approximation of the tangential stiffness

In this section the FE discretization of the tangent stiffness deduced considering the material updating rule for rotations is presented, according with the results of Section 6.2.2.

7.6.1 Internal contribution to the tangential stiffness

Considering $\hat{\eta}^{\text{m}h}(S) = \mathbf{N}\hat{\eta}^{\text{m}(e)}$ and $\hat{p}^{\text{m}h}(S) = \mathbf{N}\hat{p}^{\text{m}(e)}$, one obtains that the FE approximation of the linearized form of the internal contribution to the virtual work principle, Eq. (5.84) can be expressed as

$$\begin{aligned} D G^h_{\text{int}(e)} \cdot \hat{p}^{\text{m}h} &= \hat{\eta}^{\text{m}hT} (\underbrace{\Big[\int_0^{L_e} (\mathbf{N}^T \bar{\boldsymbol{B}}^T \bar{\mathbf{C}}^{\text{sv}} \bar{\boldsymbol{B}} \mathbf{N}) \text{d}S \Big]}_{\mathbf{K}^{\text{m}}_{M(e)}} \\ &\quad + \underbrace{\Big[\int_0^{L_e} (\mathbf{N}^T (\bar{\boldsymbol{\mathscr{F}}} + \bar{\boldsymbol{B}}^T \boldsymbol{\mathscr{N}}) \mathbf{N}) \text{d}S \Big]}_{\mathbf{K}^{\text{m}}_{G(e)}} \hat{p}^{\text{m}h} + \underbrace{\Big[\int_0^{L_e} (\mathbf{N}^T (\bar{\boldsymbol{B}}^T \bar{\boldsymbol{\Upsilon}}^{\text{ss}} \bar{\boldsymbol{\mathscr{V}}}) \mathbf{N}) \text{d}S \Big]}_{\mathbf{K}^{\text{m}}_{V(e)}}) \hat{p}^{\text{m}h} \\ &= \hat{\eta}^{\text{m}hT} (\mathbf{K}^{\text{m}}_{M(e)} + \mathbf{K}^{\text{m}}_{G(e)} + \mathbf{K}^{\text{m}}_{V(e)}) \hat{p}^{\text{m}h} \qquad (7.40) \end{aligned}$$

where $[\mathbf{K}^{\text{m}}_{M(e)}]$, $[\mathbf{K}^{\text{m}}_{G(e)}]$ and $[\mathbf{K}^{\text{m}}_{V(e)}]$ are the *material* (constitutive), *geometric* and *viscous* components of the element stiffness matrix at the current configuration consistent with a material updating of the rotational field. Then, we have

$$[\mathbf{K}^{\text{m}}_{M(e)}] = \sum_{I,J}^{\text{N}_d} \int_0^{L_e} \mathbf{N}_I^T \bar{\boldsymbol{B}}^T \bar{\mathbf{C}}^{\text{sv}} \bar{\boldsymbol{B}} \mathbf{N}_J \text{d}S = \sum_{I,J}^{\text{N}_d} [\mathbf{K}^{\text{m}}_{M(e)}]_{IJ} \qquad (7.41)$$

with $[\mathbf{K}^{\mathrm{m}}_{M(e)}]_{IJ}$ given by

$$[\mathbf{K}^{\mathrm{m}}_{M(e)}]_{IJ} = \sum_{K}^{N_{ip}} J_s^{-1} \left[\begin{array}{c|c} N_{I,s}\, N_{J,s}\, \mathbf{C}^{\mathrm{sv}}_{nn} & N_{I,s}\left[\mathbf{C}^{\mathrm{sv}}_{nn}\widetilde{\boldsymbol{\varphi}}_{,s}\,\boldsymbol{\Lambda} N_J + \right. \\ & \left. + \mathbf{C}^{\mathrm{sv}}_{nm}\boldsymbol{\Lambda}[N_{J,s}\,\mathbf{I} + \widetilde{\boldsymbol{\Omega}}_n N_J]\right] \\ \hline [N_{I,s}\,\mathbf{I} - N_I\widetilde{\boldsymbol{\Omega}}_n]\boldsymbol{\Lambda}^T\mathbf{C}^{\mathrm{sv}}_{mn}N_{J,s} & -N_I\boldsymbol{\Lambda}^T\widetilde{\boldsymbol{\varphi}}_{,s}\left[\mathbf{C}^{\mathrm{sv}}_{nn}\widetilde{\boldsymbol{\varphi}}_{,s}\,\boldsymbol{\Lambda} N_J + \right. \\ -N_I\boldsymbol{\Lambda}^T\widetilde{\boldsymbol{\varphi}}_{,s}\,\mathbf{C}^{\mathrm{sv}}_{nn}N_{J,s} & \left. \mathbf{C}^{\mathrm{sv}}_{nm}\boldsymbol{\Lambda}[N_{J,s}\,\mathbf{I} + \widetilde{\boldsymbol{\Omega}}_n N_J]\right] + \\ & [N_{I,s}\,\mathbf{I} - N_I\widetilde{\boldsymbol{\Omega}}_n]\boldsymbol{\Lambda}^T\left[\mathbf{C}^{\mathrm{sv}}_{mn}\widetilde{\boldsymbol{\varphi}}_{,s}\,\boldsymbol{\Lambda} N_J \right. \\ & \left. + \mathbf{C}^{\mathrm{sv}}_{mm}\boldsymbol{\Lambda}[N_{J,s} + \widetilde{\boldsymbol{\Omega}}_n N_J]\right] \end{array} \right]\Bigg|_K W_K \tag{7.42}$$

which is always symmetric. In an analogous manner for the term $[\mathbf{K}_{G(e)}]_{IJ}$, taking into account Eq. (7.8) one has

$$\begin{aligned} [\mathbf{K}_{G(e)}]_{IJ} &= \sum_{K}^{N_{ip}} (\mathbf{N}_I \bar{\boldsymbol{\mathscr{F}}} \mathbf{N}_J + \mathbf{N}_I^T \bar{\boldsymbol{B}}^T \boldsymbol{\mathcal{N}} \mathbf{N}_J)\Big|_K J_s W_K \\ &= \sum_{K}^{N_{ip}} ([\mathbf{K}_{G1(e)}]_{IJ} + [\mathbf{K}_{G2(e)}]_{IJ})\Big|_K W_K \end{aligned} \tag{7.43}$$

where

$$[\mathbf{K}_{G1(e)}]_{IJ} = \left[\begin{array}{c|c} 0 & 0 \\ \hline N_I\widetilde{\boldsymbol{n}}^{\mathrm{m}}\boldsymbol{\Lambda}^T N_{J,s} & N_I\Big[(\boldsymbol{\Pi}[\boldsymbol{\Lambda}^T\hat{\varphi}_{,s}]\widetilde{\boldsymbol{n}}^{\mathrm{m}} + \widetilde{\boldsymbol{m}}^{\mathrm{m}}_{,s})N_J + \\ & \widetilde{\boldsymbol{m}}^{\mathrm{m}} N_{J,s} + J_s\{\widetilde{\boldsymbol{m}}^{\mathrm{m}}\widetilde{\boldsymbol{\Omega}}_n - \widetilde{\boldsymbol{\Omega}}_n\widetilde{\boldsymbol{m}}^{\mathrm{m}}\}N_J\Big] \end{array} \right] \tag{7.44a}$$

$$[\mathbf{K}_{G2(e)}]_{IJ} = \left[\begin{array}{cc} 0 & -N_{I,s}\,\widetilde{\boldsymbol{n}} N_J \\ 0 & N_I\widetilde{\boldsymbol{\varphi}}_{,s}\,\widetilde{\boldsymbol{n}}^{\mathrm{m}} N_J - ([N_{I,s}\,\mathbf{I} - N_I J_s\widetilde{\boldsymbol{\Omega}}_n]\widetilde{\boldsymbol{m}}^{\mathrm{m}} N_J \end{array} \right] \tag{7.44b}$$

which, inserting Eqs. (7.45) and (7.44b) in (7.43) yields to

$$[\mathbf{K}_{G(e)}]_{IJ} = \sum_{K}^{N_{ip}} \Bigg(\left[\begin{array}{c|c} 0 & -N_{I,s}\,\widetilde{\boldsymbol{n}} N_J \\ \hline N_I\widetilde{\boldsymbol{n}}^{\mathrm{m}}\boldsymbol{\Lambda}^T N_{J,s} & N_I\Big[\boldsymbol{\Pi}[\boldsymbol{\Lambda}^T\hat{\varphi}_{,s}]\widetilde{\boldsymbol{n}}^{\mathrm{m}} + \widetilde{\boldsymbol{m}}^{\mathrm{m}}_{,s} + \\ & J_s\boldsymbol{\Pi}[\widetilde{\boldsymbol{m}}^{\mathrm{m}}\hat{\Omega}_n] + \widetilde{\boldsymbol{\varphi}}_{,s}\,\widetilde{\boldsymbol{n}}^{\mathrm{m}}\Big] N_J \\ & N_I\widetilde{\boldsymbol{m}}^{\mathrm{m}} N_{J,s} - [N_{I,s}\,\mathbf{I} - N_I J_s\widetilde{\boldsymbol{\Omega}}_n]\widetilde{\boldsymbol{m}}^{\mathrm{m}} N_J \end{array} \right] \Bigg) \Bigg|_K W_K \tag{7.45}$$

which is not necessarily symmetric and it has been used the identity of Eq. (A.21b) of §A. The FE discretization of the viscous component off the tangential stiffness is computed as

$$[\mathbf{K}_{V(e)}] = \sum_{IJ}^{\mathrm{N}_d} \int_{[0,L]} \mathbf{N}_I^T(\bar{\boldsymbol{B}}^T\bar{\boldsymbol{\Upsilon}}^{\mathrm{ss}}\bar{\boldsymbol{\mathcal{V}}})\mathbf{N}_J \mathrm{d}S = \sum_{IJ}^{\mathrm{N}_d} [\mathbf{K}^{\mathrm{m}}_{V(e)}]_{IJ}. \tag{7.46}$$

Considering the results of Eqs. (4.55), (7.33) and (7.47) one obtains that the sub-matrix I–J of the viscous component of the tangential stiffness matrix is given by

$$[\mathbf{K}_{V(e)}]_{IJ} = J_s^{-1}\sum_{K}^{N_{ip}} \left[\begin{array}{c|c} N_{I,s}\,\bar{\boldsymbol{\Upsilon}}^{\mathrm{ss}}_{nn}(\gamma_{t\beta}\mathbf{I} - \widetilde{\boldsymbol{v}}_n)N_{J,s} & \begin{array}{l} N_{I,s}\,(\bar{\boldsymbol{\Upsilon}}^{\mathrm{ss}}_{nn}(\overset{\triangledown}{[\dot{\widetilde{\boldsymbol{\gamma}}}_n]}\boldsymbol{\Lambda} + \widetilde{\boldsymbol{\varphi}}_{,S}\,\boldsymbol{\Lambda}\boldsymbol{\mathscr{H}}^{\mathrm{m}}_b)N_J + \\ \bar{\boldsymbol{\Upsilon}}^{\mathrm{ss}}_{nm}\boldsymbol{\Lambda}(\boldsymbol{\mathscr{H}}^{\mathrm{m}}_b N_{J,s} + [\boldsymbol{\mathscr{H}}^{\mathrm{m}}_{b,s} + \\ \dot{\widetilde{\boldsymbol{\Omega}}}_n + \widetilde{\boldsymbol{\Omega}}_n\boldsymbol{\mathscr{H}}^{\mathrm{m}}_b]N_J)) \end{array} \\ \hline \begin{array}{l} -N_I\boldsymbol{\Lambda}^T\widetilde{\boldsymbol{\varphi}}_{,S}\,\bar{\boldsymbol{\Upsilon}}^{\mathrm{ss}}_{nn}(\gamma_{t\beta}\mathbf{I} \\ -\widetilde{\boldsymbol{v}}_n)N_{J,s} + [N_{I,S}\,\mathbf{I} - \\ N_I\widetilde{\boldsymbol{\Omega}}_n]\boldsymbol{\Lambda}^T\bar{\boldsymbol{\Upsilon}}^{\mathrm{ss}}_{mn}(\gamma_{t\beta}\mathbf{I} \\ -\widetilde{\boldsymbol{v}}_n)N_{J,s} \end{array} & \begin{array}{l} -N_I\boldsymbol{\Lambda}^T\widetilde{\boldsymbol{\varphi}}_{,S}\left[\bar{\boldsymbol{\Upsilon}}^{\mathrm{ss}}_{nn}(\overset{\triangledown}{[\dot{\widetilde{\boldsymbol{\gamma}}}_n]}\boldsymbol{\Lambda} + \right. \\ \widetilde{\boldsymbol{\varphi}}_{,S}\,\boldsymbol{\Lambda}\boldsymbol{\mathscr{H}}^{\mathrm{m}}_b)N_J + \\ \left.\bar{\boldsymbol{\Upsilon}}^{\mathrm{ss}}_{nm}\boldsymbol{\Lambda}(\boldsymbol{\mathscr{H}}^{\mathrm{m}}_b N_{J,s} + [\boldsymbol{\mathscr{H}}^{\mathrm{m}}_{b,s} + \dot{\widetilde{\boldsymbol{\Omega}}}_n + \widetilde{\boldsymbol{\Omega}}_n\boldsymbol{\mathscr{H}}^{\mathrm{m}}_b]N_J)\right] + \\ [N_{I,S}\,\mathbf{I} - N_I\widetilde{\boldsymbol{\Omega}}_n]\boldsymbol{\Lambda}^T\left[\bar{\boldsymbol{\Upsilon}}^{\mathrm{ss}}_{mn}(\overset{\triangledown}{[\dot{\widetilde{\boldsymbol{\gamma}}}_n]}\boldsymbol{\Lambda} + \right. \\ \widetilde{\boldsymbol{\varphi}}_{,S}\,\boldsymbol{\Lambda}\boldsymbol{\mathscr{H}}^{\mathrm{m}}_b)N_J + \\ \left.\bar{\boldsymbol{\Upsilon}}^{\mathrm{ss}}_{mm}\boldsymbol{\Lambda}(\boldsymbol{\mathscr{H}}^{\mathrm{m}}_b N_{J,s} + [\boldsymbol{\mathscr{H}}^{\mathrm{m}}_{b,s} + \dot{\widetilde{\boldsymbol{\Omega}}}_n + \widetilde{\boldsymbol{\Omega}}_n\boldsymbol{\mathscr{H}}^{\mathrm{m}}_b]N_J)\right] \end{array} \end{array}\right]\Bigg|_K W_K. \tag{7.47}$$

7.6.2 Inertial contribution of the tangential stiffness

The FE discretization of the inertial contribution to the elemental tangent stiffness $K^{\mathrm{m}}_{\mathrm{ine}(e)}$, Eq. (6.51) is obtained as

$$K^{\mathrm{m}}_{\mathrm{ine}(e)} = \hat{\eta}^{h\mathrm{m}T}\Big[\int_0^{L_e}\mathbf{N}^T\mathbf{M}_{\varphi\Theta}\mathbf{N}\mathrm{d}S\Big]\hat{p}^{h\mathrm{m}T} = \hat{\eta}^{h\mathrm{m}T}[\mathbf{K}^{\mathrm{m}}_{\mathrm{ine}(e)}]\hat{p}^{h\mathrm{m}T} \tag{7.48}$$

where the elemental inertial stiffness matrix $[\mathbf{K}_{\mathrm{ine}(e)}]$ is calculated as

$$[\mathbf{K}^{\mathrm{m}}_{\mathrm{ine}(e)}] = \sum_{IJ}^{\mathrm{N}_d}\int_0^{L_e}\mathbf{N}_I^T\mathbf{M}_{\varphi\Theta}\mathbf{N}_J\mathrm{d}S = \sum_{IJ}^{\mathrm{N}_d}[\mathbf{K}^{\mathrm{m}}_{\mathrm{ine}(e)}]_{IJ} \tag{7.49}$$

where the explicit expression for $[\mathbf{K}^{\mathrm{m}}_{\mathrm{ine}(e)}]_{IJ}$ is the following:

$$\begin{aligned}[\mathbf{K}_{\mathrm{ine}(e)}]_{IJ} &= \int_0^{L_{(e)}}\mathbf{N}_I^T\begin{bmatrix}\boldsymbol{\Xi}_\varphi & 0\\ 0 & \boldsymbol{\Xi}_\theta\end{bmatrix}\mathbf{N}_J\mathrm{d}S \quad \in\mathbb{R}^{6\times 6}\\ &= \sum_K^{N_{ip}}\left[\begin{array}{c|c}\frac{1}{(\Delta t)^2\beta}\mathcal{A}_{\rho_0}N_IN_J & 0\\ \hline 0 & \begin{array}{l}\Big[\frac{1}{(\Delta t)^2\beta}\mathbf{I}_{\rho_0} + \\ \frac{\gamma}{\Delta t\beta}(\widetilde{\boldsymbol{V}}_n\mathbf{I}_{\rho_0} - \boldsymbol{\Pi}[\mathbf{I}_{\rho_0}\hat{V}_n])\Big]\mathbf{T}^TN_IN_J\end{array}\end{array}\right]\Bigg|_K J_sW_K.\end{aligned} \tag{7.50}$$

As noted in Section 6.2.2.b, the tangent inertia matrix is *nonsymmetric* and *configuration dependent*. This property concerns only the rotational degrees of freedom. The sub-matrix $\boldsymbol{\Xi}_\varphi$ corresponds to the translational degrees of freedom and is constant.

7.6.3 External contribution of the tangential stiffness

By the linearization of the external load vector, (see Eq. (5.91)), one obtains

$$\begin{aligned} K^{\mathrm{m}}_{P(e)} &= \hat{\eta}^{\mathrm{m}hT}\left[\int_0^{L_e}\mathbf{N}^T\begin{bmatrix}(\hat{\mathcal{N}}_d\otimes\hat{\mathscr{C}}_N)[\frac{\mathrm{d}}{\mathrm{d}S}\mathbf{I}]+\widetilde{\boldsymbol{\mathcal{N}}}_p\\(\hat{\mathcal{M}}_d\otimes\hat{\mathscr{C}}_M)[\frac{\mathrm{d}}{\mathrm{d}S}\mathbf{I}]+\widetilde{\boldsymbol{\mathcal{M}}}_p\end{bmatrix}\mathbf{N}\mathrm{d}S\right]\hat{p}^{\mathrm{m}h}\\ &= \hat{\eta}^{\mathrm{m}hT}\left[\sum_{IJ}^{\mathrm{N}_d}\int_0^{L_e}\mathbf{N}_I^T\begin{bmatrix}(\hat{\mathcal{N}}_d\otimes\hat{\mathscr{C}}_N)[\frac{\mathrm{d}}{\mathrm{d}S}\mathbf{I}]\\(\hat{\mathcal{M}}_d\otimes\hat{\mathscr{C}}_M)[\frac{\mathrm{d}}{\mathrm{d}S}\mathbf{I}]\end{bmatrix}\mathbf{N}_J\mathrm{d}S+\sum_{IJ}^{\mathrm{N}_d}\int_0^{L_e}\mathbf{N}_I^T\begin{bmatrix}\widetilde{\boldsymbol{\mathcal{N}}}_p\\\widetilde{\boldsymbol{\mathcal{M}}}_p\end{bmatrix}\mathbf{N}_J\mathrm{d}S\right]\hat{p}^{\mathrm{m}h}\\ &= \hat{\eta}^{\mathrm{m}hT}\Big[\sum_{IJ}^{\mathrm{N}_d}[\mathbf{K}^{\mathrm{m}}_{P1(e)}]_{IJ}+\sum_{IJ}^{\mathrm{N}_d}[\mathbf{K}^{\mathrm{m}}_{P2(e)}]_{IJ}\Big]\hat{p}^{\mathrm{m}h}\\ &= \hat{\eta}^{\mathrm{m}hT}\Big[[\mathbf{K}^{\mathrm{m}}_{P1(e)}]+[\mathbf{K}^{\mathrm{m}}_{P2(e)}]\Big]\hat{p}^{\mathrm{m}h} \end{aligned} \tag{7.51}$$

The two components of the tangent stiffness matrix due to external loading coupling the nodes I and J are explicitly given by

$$[\mathbf{K}^{\mathrm{m}}_{P1(e)}]_{IJ} = \sum_k^{N_{ip}}\left[\begin{array}{c}N_IN_{J,s}\hat{\mathcal{N}}_d\otimes\hat{\mathscr{C}}_N\\N_IN_{J,s}\hat{\mathcal{M}}_d\otimes\hat{\mathscr{C}}_M\end{array}\right]\Bigg|_K W_K \tag{7.52a}$$

$$[\mathbf{K}^{\mathrm{m}}_{P2(e)}]_{IJ} = \sum_{k=1}^{N_{ip}}\left[\begin{array}{c}N_IN_J\widetilde{\boldsymbol{\mathcal{N}}}_p\\N_IN_J\widetilde{\boldsymbol{\mathcal{M}}}_p\end{array}\right]\Bigg|_K J_sW_K. \tag{7.52b}$$

Finally, the tangent stiffness matrix of Eq. (7.15), relating the nodes I and J, is given by

$$[\mathbf{K}^{\mathrm{m}h}_{(e)}]_{IJ} = \Big[[\mathbf{K}^{\mathrm{m}}_{M(e)}]+[\mathbf{K}^{\mathrm{m}}_{G(e)}]+[\mathbf{K}^{\mathrm{m}}_{V(e)}]+[\mathbf{K}^{\mathrm{m}}_{\mathrm{ine}(e)}]+[\mathbf{K}^{\mathrm{m}}_{P1(e)}]+[\mathbf{K}^{\mathrm{m}}_{P2(e)}]\Big]_{IJ}. \tag{7.53}$$

7.7 Iterative Newton–Raphson scheme

As it has been previously mentioned, an iterative form of the Newton–Raphson scheme, Eq. (6.3), (see §6.1.2) is used for solving the discrete (in space and time) version of the linearized form of the virtual work functional.

The standard procedures for the FEM holds, then, one has (for more details it is possible to consult classical textbooks such as those of Refs. [42, 107, 108, 170]) that the *global unbalanced force vector*, the *global stiffness matrix* and the *incremental configuration field* as

$$\hat{q} = \mathop{\mathbf{A}}_{e,I}^{N_e\times N_d}\hat{q}^h_{(e)I};\quad [\mathbf{K}] = \mathop{\mathbf{A}}_{e,I,J}^{N_e\times N_d}[\mathbf{K}^h_{(e)}]_{IJ};\quad \hat{p} = \mathop{\mathbf{A}}_{e,I}^{N_e\times N_d}\hat{p}^h_{(e)I}; \tag{7.54}$$

respectively; where $\mathbf{A}$ denotes the usual assembly procedure which runs over the number of elements N_e and their corresponding nodal points N_d. Then, by means of using the FEM the solution of the nonlinear system of differential equations of the rod is reduced to to solving the following linear systems of equations for obtaining the iterative increments of the configuration variables

$$\hat{\eta}^{\mathrm{s}}\cdot\Big[\hat{q}^{\mathrm{s}}+[\mathbf{K}]\hat{p}^{\mathrm{s}}\Big]^{(i)}_{n+1}\approx 0\quad\rightarrow\quad \hat{p}^{\mathrm{s}(i)}_{n+1} = (-[\mathbf{K}]^{-1}\hat{q}^{\mathrm{s}})^{(i)}_{n+1} \tag{7.55}$$

where the super and sub-scripts (i) and $n+1$ corresponds to the iteration and time, respectively; as described in Chapter 6. If the material updating rule is preferred one simply obtains

$$\hat{p}^{\mathrm{m}(i)}_{n+1} = (-[\mathbf{K}^{\mathrm{m}}]^{-1}\hat{q}^{\mathrm{m}})^{(i)}_{n+1}. \tag{7.56}$$

Note that Eq. (7.55) is valid for both the static or dynamic cases. If the mechanical problem consists of a sequence of imposed/displacement steps or inertial terms are considered it is necessary to maintain fixed the value of the load amplification parameter λ of the external force term. Normally, the parameter λ is considered as other variable when control techniques are employed, *e.g.* arch–length methods. However, details are omitted here and it can be consulted in [107, 108].

Having obtained an iterative field $\hat{p}^{(i)}_{n+1}$, the results of Chapter 6 are used for updating the configuration variables $(\hat{\varphi}, \mathbf{\Lambda}) \in T\mathcal{C}_t$, the related linear and angular velocity and acceleration, the strain and strain rate fields existing on each integration point (see Fig. 7.1). The present formulation makes use of uniformly reduced integration on the pure displacement and rotation weak form to avoid shear locking [178, 363], however, the inertial terms are integrated in exact manner. It remains to determine the stress field existing on each material point in the cross sections associated to integration points, this is done by means of an appropriated cross sectional analysis that will be explained in following.

7.7.1 Cross sectional analysis

The cross sectional analysis is carried out expanding each integration point on the beam axis in a set of integration points located on each fiber on cross section. In order to perform this operation, the beam cross section is meshed into a grid of quadrilaterals, each of them corresponding to a fiber oriented along the beam axis (see Fig. 7.2).

The estimation of the average stress level existing on each quadrilateral is carried out by integrating the constitutive equations of the compounding materials of the composite associated to the corresponding quadrilateral and applying the mixing rule as explained in §4.3. The geometry of each quadrilateral is described by means of normalized bi-dimensional shapes functions and several integration points can be specified in order to estimate more precisely the value of a given function according to a selected integration rule. In the case of the average value of the material form of the FPK stress vector acting on a quadrilateral we have

$$\hat{P}^{\mathrm{m}}_1 = \frac{1}{A_c}\int_{A_c} \hat{P}^{\mathrm{m}}_1 \mathrm{d}A_c = \frac{1}{A_c}\sum_{p=1}^{N_p}\sum_{q=1}^{N_q} \hat{P}^{\mathrm{m}}_1(y_p, z_q) J_{pq} W_{pq} \tag{7.57}$$

where A_c is the area of the quadrilateral, N_p and N_q are the number of integration points in the two directions of the normalized geometry of the quadrilateral, $\hat{P}^{\mathrm{m}}_1(y_p, z_q)$ is the value of the FPK stress vector existing on a integration point with coordinates (y_p, z_q) with respect to the reference beam axis, which is obtained from the corresponding material strain vector $\hat{\mathcal{E}}_n$ using the constitutive laws and the mixing rule, J_{pq} is the Jacobian of the transformation between normalized coordinates and cross sectional coordinates and W_{pq} are the weighting factors.

The coefficients of the tangent constitutive tensors can be estimated in an analogous manner as in Eq. (7.57) but replacing $\hat{P}^{\mathrm{m}}_1(y_p, z_q)$ by $\bar{\boldsymbol{\mathcal{C}}}^{\mathrm{mt}}(y_p, z_q)$ *i.e.*

$$\bar{\boldsymbol{\mathcal{C}}}^{\mathrm{mt}} = \frac{1}{A_c}\int_{A_c} \bar{\boldsymbol{\mathcal{C}}}^{\mathrm{mt}} \mathrm{d}A_c = \frac{1}{A_c}\sum_{p=1}^{N_p}\sum_{q=1}^{N_q} \bar{\boldsymbol{\mathcal{C}}}^{\mathrm{mt}}(y_p, z_q) J_{pq} W_{pq}. \tag{7.58}$$

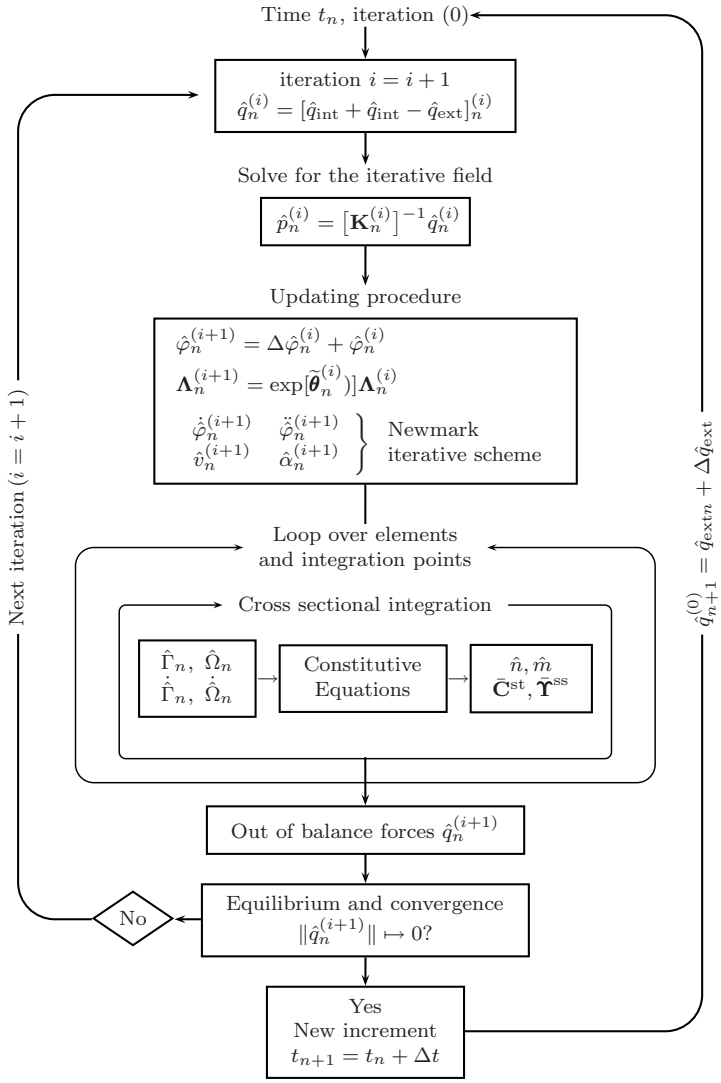

Figure 7.1: Iterative Newton–Raphson scheme (spatial form).

Finally, having obtained the stress level on each quadrilateral, the cross sectional forces and moments are obtained by means of the discrete form of Eqs. (3.94a) and (3.94b) as

$$\hat{n}^{\rm m} = \sum_{k=1}^{N_{\rm fiber}} (A_c)_k (\hat{P}_1^{\rm m})_k \tag{7.59a}$$

$$\hat{m}^{\rm m} = \sum_{k=1}^{N_{\rm fiber}} (A_c)_k \hat{\ell}_k \times (\hat{P}_1^{\rm m})_k \tag{7.59b}$$

were $N_{\rm fiber}$ is the number of quadrilaterals of the beam cross section, $(A_c)_k$ is the area of the k quadrilateral, $(\hat{P}_1^{\rm m})_k$ is the average value of the material form of the FPK stress vector and $\hat{\ell}_k = (0, y_k, z_k)$ are the coordinates of the gravity center of the k^{th} quadrilateral with respect to the local beam reference frame.
By applying the same procedure as in Eqs. (7.59a) and (7.59b), we have that the material form

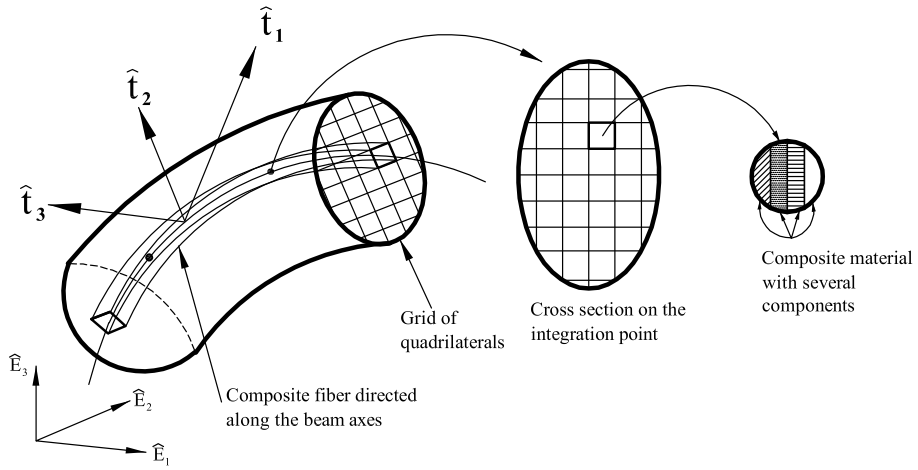

Figure 7.2: Discrete fiber like model of the beam element.

of the reduced tangential tensors of Eqs. (4.53a) and (4.53b) are numerically estimated as

$$\bar{\mathbf{C}}^{\mathrm{mt}}_{nn} = \sum_{k=1}^{N_{\mathrm{fiber}}} (A_c)_k (\bar{\boldsymbol{\mathcal{C}}}^{\mathrm{mt}})_k \tag{7.60a}$$

$$\bar{\mathbf{C}}^{\mathrm{mt}}_{nm} = -\sum_{k=1}^{N_{\mathrm{fiber}}} (A_c)_k (\bar{\boldsymbol{\mathcal{C}}}^{\mathrm{mt}})_k (y_k \widetilde{\boldsymbol{E}}_2 + z_k \widetilde{\boldsymbol{E}}_3) \tag{7.60b}$$

$$\bar{\mathbf{C}}^{\mathrm{mt}}_{mn} = \sum_{k=1}^{N_{\mathrm{fiber}}} (A_c)_k \widetilde{\boldsymbol{\ell}}_k (\bar{\boldsymbol{\mathcal{C}}}^{\mathrm{mt}})_k \tag{7.60c}$$

$$\bar{\mathbf{C}}^{\mathrm{mt}}_{mm} = -\sum_{k=1}^{N_{\mathrm{fiber}}} (A_c)_k \widetilde{\boldsymbol{\ell}}_k (\bar{\boldsymbol{\mathcal{C}}}^{\mathrm{mt}})_k (y_k \widetilde{\boldsymbol{E}}_2 + z_k \widetilde{\boldsymbol{E}}_3) \tag{7.60d}$$

where $\widetilde{\boldsymbol{\ell}}_k$ is the skew–symmetric tensor obtained from $\hat{\ell}_k$ and $(\bar{\boldsymbol{\mathcal{C}}}^{\mathrm{mt}})_k$ is the material form of the tangent constitutive tensor for the composite material of the k^{th} quadrilateral.
Analogously, having obtained the values of the viscous tangent constitutive tensors $\bar{\boldsymbol{\eta}}^{\mathrm{ss}}$, at each fiber, the reduced constitutive tensor $[\bar{\boldsymbol{\Upsilon}}^{\mathrm{ss}}]$ is obtained as [258]

$$\bar{\boldsymbol{\Upsilon}}^{\mathrm{ss}}_{nn} = \sum_{k=1}^{Nfiber} (A_c)_k (\bar{\boldsymbol{\eta}}^{\mathrm{ss}})_k \tag{7.61a}$$

$$\bar{\boldsymbol{\Upsilon}}^{\mathrm{ss}}_{nm} = -\sum_{k=1}^{Nfiber} (A_c)_k (\bar{\boldsymbol{\eta}}^{\mathrm{ss}})_k (y_k \widetilde{\boldsymbol{E}}_2 + z_k \widetilde{\boldsymbol{E}}_3) \tag{7.61b}$$

$$\bar{\boldsymbol{\Upsilon}}^{\mathrm{ss}}_{mn} = \sum_{k=1}^{Nfiber} (A_c)_k \widetilde{\boldsymbol{\ell}}_k (\bar{\boldsymbol{\eta}}^{\mathrm{ss}})_k \tag{7.61c}$$

$$\bar{\boldsymbol{\Upsilon}}^{\mathrm{ss}}_{mm} = -\sum_{k=1}^{Nfiber} (A_c)_k \widetilde{\boldsymbol{\ell}}_k (\bar{\boldsymbol{\eta}}^{\mathrm{ss}})_k (y_k \widetilde{\boldsymbol{E}}_2 + z_k \widetilde{\boldsymbol{E}}_3) \tag{7.61d}$$

From the point of view of the numerical implementations, in a given loading step and iteration of the global Newton–Raphson scheme, two additional integration loops are required for the *cross sectional analysis*:

(i) The first one is a loop over the quadrilaterals (or equivalently fibers). In this loop, having obtained the material form of the reduced strain measures $\hat{\Gamma}_n$ and $\hat{\Omega}_n$ (or equivalently $\widetilde{\boldsymbol{\Omega}}_n$) and their time derivatives $\dot{\hat{\Gamma}}_n$ and $\dot{\hat{\Omega}}_n$, the strain measure $\hat{\mathcal{E}}_n$ and the strain rate measure $\hat{\mathcal{S}}_n$ are calculated according to the updating procedure of §6.1.4 and they are imposed for each simple material associated to the composite of a given fiber.

(ii) The second loop runs over each simple material associated to the composite of the quadrilateral. In this case, the FPK stress vector, $\hat{P}_1^{\mathrm{m}}$, and the tangent constitutive relations, $\bar{\boldsymbol{\mathcal{C}}}^{\mathrm{mt}}$ and $\bar{\boldsymbol{\eta}}^{\mathrm{ms}}$, are calculated for each component according to their specific constitutive equations; the behavior of the composite is recovered with the help of the mixing theory, summarized in Eqs. (4.48) to (4.46b).

(iii) The integration procedure carried out over the fibers allows to obtain the cross sectional forces and moments and the reduced tangential tensors.

Fig. 7.3 shows the flow chart of the cross sectional analysis procedure for a cross section with N_{fiber} fibers and k simple components associated to each fiber. Finally, the discrete version of the spatial form of the reduced forces and moments, $\hat{n} = \boldsymbol{\Lambda}\hat{m}^{\mathrm{m}}$ and $\hat{m} = \boldsymbol{\Lambda}\hat{m}^{\mathrm{m}}$, and sectional tangent stiffness tensors $\bar{\mathbf{C}}_{ij}^{\mathrm{st}} = \boldsymbol{\Lambda}\bar{\mathbf{C}}_{ij}^{\mathrm{mt}}\boldsymbol{\Lambda}^T$ and $\bar{\boldsymbol{\Upsilon}}_{ij}^{\mathrm{st}} = \boldsymbol{\Lambda}\bar{\boldsymbol{\Upsilon}}_{ij}^{\mathrm{mt}}\boldsymbol{\Lambda}^T$ $(i,j \in \{n,m\})$ are calculated [258, 260].

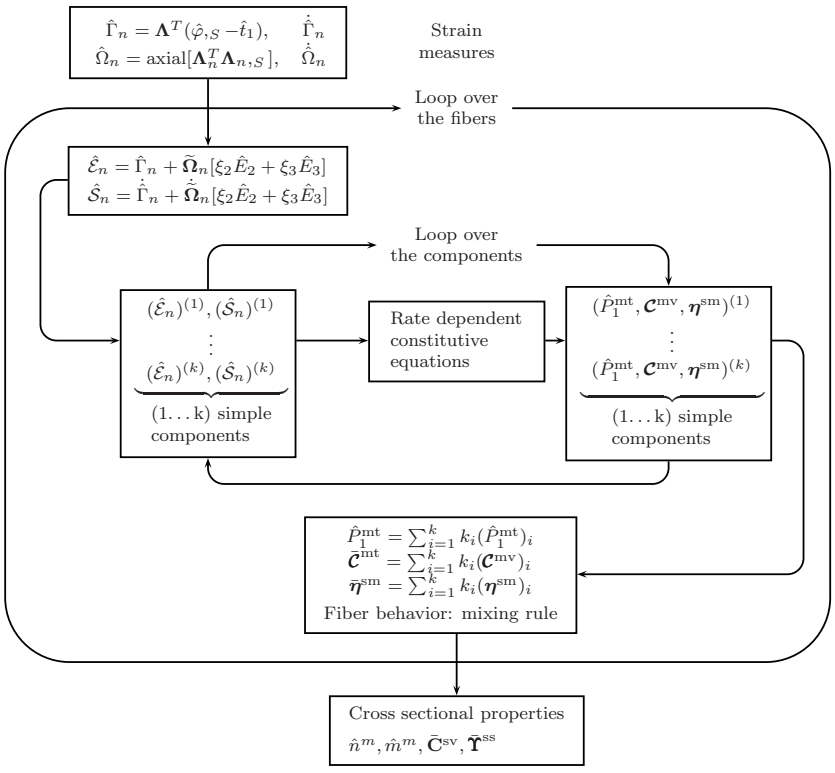

Figure 7.3: Flow chart of the cross sectional integration.

This method avoids the formulation of constitutive laws at cross sectional level. As it has been

previously explained, the sectional behavior is obtained as the weighted sum of the contribution of the fibers, conversely to other works which develop global sectional integration methods [411, 431]. Material nonlinearity, such as degradation or plasticity, is captured by means of the constitutive laws of the simple materials at each quadrilateral. The nonlinear relation between the reduced strain measures and cross sectional forces and moments are obtained from Eq. (7.59b). Each section is associated to the volume of a part of the beam and, therefore, constitutive nonlinearity at beam element level is captured through the sectional analysis.
General shapes for cross sections can be analyzed by means of the proposed integration method. However, two limitations have to be considered:

(i) Mechanical problems involving large deformations out of the cross sectional plane can not be reproduced due to the planarity of the cross sections assumed in the kinematical assumptions.

(ii) Mechanical equilibrium at element level does not implies mechanical equilibrium among fibers in the inelastic range due to the fact that the present beam model solves the constitutive equations for each fiber independently of the behavior of the contiguous ones.

If materials presenting *softening* are associated to the fibers, the strain localization phenomenon can occur on specific integration points on the beam for certain loading levels [24, 26, 301, 303]. Softening behavior of fibers imply the induction of a softer response at cross sectional level and, in this manner, the strain localization induced at material point level is translated to the cross sectional force-displacement relationships. In general, the structural response becomes dependent on the mesh size. In this work, the mesh independent response of the structure is obtained regularizating the energy dissipated on each fiber and limiting this value to the specific fracture energy of the material. Details about the regularization process can be consulted in §4. However, other alternative procedures based on considering *strong discontinuities* on the generalized displacement field of the beam can be consulted in [25, 24, 26].

7.7.1.a Shear correction factors

As it has been above highlighted, the kinematics assumptions limit the quality of the description obtained for the cross sectional strain field mainly due to the fact that the shears strains are estimated in an average sense. Other limitations derived from the kinematic assumptions are related to the estimation of out of plane components of the strain field at material point level *i.e.* $\mathcal{E}_{n22}$, $\mathcal{E}_{n33}$, $\mathcal{E}_{n23}$ which are equal to zero [310]; Therefore, the their stress counterparts are also equal to zero, even in the nonlinear range.
In this work some additional hypothesis are made to improve the strain field at cross sectional level. Having obtained the mean shear strains at material point level $\bar{\mathcal{E}}^m_{n12}(S,\xi_\beta)$ and $\bar{\mathcal{E}}^m_{n13}(S,\xi_\beta)$, where the over-head bar symbol is used to empathize that we are referring to the average shear strains, then we proceed to correct them using the *Jourawsky*'s stress distribution [36] according to

$$\mathcal{E}_{n12}(S,\xi_\beta) = \bar{\mathcal{E}}_{n12}(S,\xi_\beta)\mathcal{A}^*_2\left(\frac{\mathscr{S}_{\mathcal{A}3}(\xi_2)}{\mathrm{I}_{33}b(\xi_2)}\right) \tag{7.62a}$$

$$\mathcal{E}_{n13}(S,\xi_\beta) = \bar{\mathcal{E}}_{n13}(S,\xi_\beta)\mathcal{A}^*_3\left(\frac{\mathscr{S}_{\mathcal{A}2}(\xi_3)}{\mathrm{I}_{22}b(\xi_3)}\right) \tag{7.62b}$$

where $\mathcal{A}^*_2 = \chi_2\mathcal{A}_{00}$ and $\mathcal{A}^*_3 = \chi_3\mathcal{A}_{00}$ are the reduced cross sections of $\mathcal{A}$, χ_2 and χ_3 are the shear stress distribution factors [159], $b(\xi_2)$ and $\mathrm{b}(\xi_3)$ are width and thickness of the cross section, I_{22}

and I_{ξ_3} are the inertia moments and $\mathscr{S}_{\mathcal{A}2}(\xi_3)$ and $\mathscr{S}_{\mathcal{A}3}(\xi_2)$ are the statical moments with respect to the neutral axis of the upper portion and left portion of the cross section, respectively.
The proposed procedure does not provide an exact solution for the shear components of the strain tensor but assures an important improvement with respect to the mean values. It is worth to note that Jourawsky correction works well fundamentally for the case of close solid sections and in the linear elastic range, what is exactly the opposite case to what happen in large nonlinear incursion of the material or in the case of thin walled sections.
Additional improvements can be done in determining a more exact shear strain distribution at cross sectional level, *e.g.* in Refs. [370, 151, 149] coupled torsional warping functions have been included in the large strain/displacement kinematics of the rods allowing to obtain the complete large strain tensor but with the cost of adding degrees of freedom in the formulation and a secondary finite element problem have to be solved to verify sectional equilibrium. Some works have been dedicated to specific sectional shapes deducing warping functions and shear correction factors, *e.g.* for thin walled sections see Ref. [284]. Other authors [411] have concentrated in developing efficient procedures for analyzing curved and twisted rods with general cross sectional shapes based on the derivation of a general equations for three-dimensional solids with appropriated boundary conditions for deducing enhanced warping functions and shear correction factors.

Chapter 8

Local irregularities

The term *local irregularity* is used for referring to parts of framed structures where the basic hypothesis of: (a) slenderness and/or (b) the presence of smooth variations of the geometric or material properties along the rod axis; are not fulfilled. In those cases, conventional models for the nonlinear analysis of rod–like structures can fail in predicting the mechanical response [96, 158]. A detailed presentation about local irregularities and the numerical approaches followed to include them in reduced models can be reviewed in §2.3.1 and §2.3.2.
In this work, two types of local irregularities are considered:

(i) *Energy dissipating devices.* In this case, devices are strategically added to the structures with the purpose of changing their dynamic characteristics, providing extra energy dissipation, controlling lateral displacements, preventing second order effects among other benefits. In abstract terms, these devices can be seen as a *dissipative nucleus* connecting two degree of freedom of the structure.

(ii) *Geometric irregularities.* This case is referred to small parts of the structure which need to be described with a full 3D geometric model because the typical hypothesis for rod elements are not fulfilled. Typical geometric irregularities are precast connecting joints or poorly detailed monolithic joints of RC structures. In a great number of occasions the global mechanical response of the structure is determined by the inelastic incursions suffered in the geometric irregularity (see §2.3.2).

The following two sections are devoted to the development of numerical methods for the consistent inclusion and the numerical treatment of local irregularities in the developed full constitutive and geometric nonlinear rod theory. Section 8.1 is devoted to the development of a special FE for energy dissipating devices and §8.2 covers the development of a *two–scale* (global and local) approach for the numerical treatment of geometric irregularities. In the second case, the resulting step-by-step iterative algorithm is implemented in a multiprocessor scheme taking advantage of the different nature of the problems to be solved in each scale. In both cases, advantages and limitations of the proposed approaches are discussed.

8.1 Energy dissipating devices

The finite deformation model for EDDs is obtained from the beam model releasing the rotational degrees of freedom and supposing that all the mechanical behavior of the device is described in terms of the evolution of a unique material point in the middle of the resulting bar.
The current position of a point in the EDD bar is obtained from Eq. (3.22) and considering that

$\xi_\beta = 0$ as $\hat{x} = \hat{\varphi}(S,t)$. Supposing that the current orientation of the EDD bar of initial length L^* is given by the tensor $\mathbf{\Lambda}^*(t)$, ($\mathbf{\Lambda}^*{}_{,S} = 0$, $\dot{\mathbf{\Lambda}}^* \neq 0$), the spatial position of the *dissipative point* in the EDD is obtained as $\hat{\varphi}(L^*/2,t)$ where $L^*/2$ is the arch–length coordinate of the middle point in the bar element and the axial strain and strain rate in the dissipative point are obtained from Eqs. (3.70) and (3.82) as

$$\mathcal{E}_{d_1}(t) = \left\{(\mathbf{\Lambda}^{*T}\hat{\varphi}_{,S}) \cdot \hat{E}_1\right\}\Big|_{(L^*/2,t)} - 1 \tag{8.1a}$$

$$\dot{\mathcal{E}}_{d_1}(t) = \left\{(\mathbf{\Lambda}^{*T}(\dot{\hat{\varphi}}_{,S} - \widetilde{\boldsymbol{v}}_n\hat{\varphi}_{,S})) \cdot \hat{E}_1\right\}\Big|_{(L^*/2,t)} \approx \frac{\mathrm{d}}{\mathrm{d}t}\hat{\Gamma}_1(t)\Big|_{(L^*/2,t)} \tag{8.1b}$$

Finally, the contribution of the EDD bar to the functional of Eq. (3.145), written in the material description, is given by

$$\mathbf{G}_{\mathrm{EDD}} = \int_{L^*} P_d^{\mathrm{m}}\delta\mathcal{E}_{d_1}dS + \left\{(\delta\hat{\varphi})^T[\mathbf{M}]_d(\ddot{\hat{\varphi}})\right\}\Big|_{(L^*/2,t)} \tag{8.2}$$

where it was assumed that $\boldsymbol{\mathcal{I}}_{\rho_0} \approx 0$, *i.e.* the contribution of the EDDs to the rotational mass of the system is negligible and $[\mathbf{M}]_d$ is the EDD's *translational inertia* matrix, *i.e.* the mass of the control system is supposed to be concentrated on the middle point of the bar. The term $\delta\mathcal{E}_{d_1}$ is given by

$$\delta\mathcal{E}_{d_1} = (\mathbf{\Lambda}^{*T}(\delta\hat{\varphi}_{,S} - \delta\widetilde{\boldsymbol{\theta}}\hat{\varphi}_{,S}))\cdot\hat{E}_1 \tag{8.3}$$

which corresponds to the linearized form (variation) of the material form of the axial strain in the EDD.

8.1.1 Constitutive relations for EDDs

The constitutive law proposed for EDDs is based on a previous work of the authors [259] which provides a versatile strain-stress relationship with the following general form:

$$P_d^{\mathrm{m}}(\mathcal{E}_{d_1}, \dot{\mathcal{E}}_{d_1}, t) = P_{d_1}^{\mathrm{m}}(\mathcal{E}_{d_1}, t) + P_{d_2}^{\mathrm{m}}(\dot{\mathcal{E}}_{d_1}, t) \tag{8.4}$$

where P_d^{m} is the average stress in the EDD, $\mathcal{E}_{d_1}$ the strain level, t the time, $\dot{\mathcal{E}}_{d_1}$ the strain rate, $P_{d_1}^{\mathrm{m}}$ and $P_{d_2}^{\mathrm{m}}$ are the strain dependent and rate dependent parts of the stress, respectively. The model uncouples the total stress in viscous and non–viscous components, which correspond to a viscous dashpot device acting in parallel with a nonlinear hysteretic spring. The purely viscous component does not requires to be a linear function of the strain rate. From the experimental results carried out on a large variety of different types of devices (see §2.3.1.a), it is possible to deduce that the function $P_{d_1}^{\mathrm{m}}$ should have the following characteristics:

(i) Axial hardening for strains over 150%.

(ii) Variable shear modulus for fitting the strain-stress curves obtained during the tests.

(iii) The initial slope of a loading or unloading branch is only a function of the point in the strain-stress space where the velocity changes of sign, allowing to obtain complex hysteretic cycles as in the case of elastomers (see [259]).

Therefore, *hardening* and variable elastic modulus can be reproduced as it will be explained in following.

8.1.1.a Rate dependent part.

The viscous component of the stress has the following general form:

$$P_{d_2}^{\mathrm{m}}(\dot{\mathcal{E}}_{d_1}, t) = c_d(\dot{\mathcal{E}}_{d_1})\dot{\mathcal{E}}_{d_1} \tag{8.5}$$

where c_d is the (nonlinear) viscous coefficient of the device which is obtained fitting a polynomial to the experimental data [259]. In following a method for the case of elastomers is proposed:
Let to suppose that it has been performed a set of N_t cyclic sinusoidal tests on a EDD device at different maximum displacements u_j $(j = 1, \ldots, \mathrm{N}_t)$, each of them repeated at different frequencies ϖ_i $(i = 1, \ldots, \mathrm{N}_f)$, obtaining a total of $\mathrm{N}_t \times \mathrm{N}_f$ tests.
Let ΔE be the dissipated energy increment[1], corresponding to two cyclic tests carried out at the same maximum displacement, u, but for different consecutive frequencies ϖ_{i+1} and ϖ_i, (in this case, i is the frequency index), which is given by

$$\begin{aligned} \Delta E &= A_t h_t \Big(\oint (P_{d_1}^{\mathrm{m}} + P_{d_2}^{\mathrm{m}(i+1)}) \mathrm{d}\mathcal{E}_{d_1} - \oint (P_{d_1}^{\mathrm{m}} + P_{d_2}^{\mathrm{m}(i)}) \mathrm{d}\mathcal{E}_{d_1} \Big) \\ &= A_t h_t \oint (P_{d_2}^{\mathrm{m}(i+1)} - P_{d_2}^{\mathrm{m}(i)}) \mathrm{d}\mathcal{E}_{d_1} \end{aligned} \tag{8.6}$$

where A_t and h_t are the average area and the average thickness of the test specimen and the term $(P_{d_1}^{\mathrm{m}} + P_{d_2}^{\mathrm{m}})$ is the average shear stress according to Eq. (8.5). $P_{d_2}^{\mathrm{m}(i)})$ is the viscous component of the average stress for the cycles applied with loading frequency ϖ_i. An additional working hypothesis is the following expression for the viscous component of the force:

$$A_t P_{d_2}^{\mathrm{m}} = h_t c_d(\varpi)\dot{\mathcal{E}}_{d_1} = h_t c_d(\dot{\mathcal{E}}_{d_1})\dot{\mathcal{E}}_{d_1}. \tag{8.7}$$

To obtain a numerical estimation for the function $P_{d_2}^{\mathrm{m}}$, it is possible to suppose that, for a test carried out with a loading frequency wi and maximum displacement u_j, dissipation is related to velocity through the damping coefficient, c_{dij}. Considering only symmetric tests, Eq. (8.6) can be rewritten as

$$\begin{aligned} \dot{\mathcal{E}}_{d_1}(u_j, \varpi_i) &= \frac{u_j}{h_t} \varpi_i \cos(\varpi_i t) \\ \Delta E &= u_j^2 \varpi_{i+1}^2 \int_0^{T_{i+1}} c_{d(i+1)j} \cos(\varpi_{i+1} t) \mathrm{d}t - u_j^2 \varpi_i^2 \int_0^{T_i} c_{dij} \cos(\varpi_i t) \mathrm{d}t. \end{aligned} \tag{8.8}$$

If the values of the two loading frequencies are close, we can suppose that the coefficients c_{dij} are approximately the same, *i.e.* $c_{d(i+1)j} = c_{dij}$, and calculate them as follows:

$$c_{dij} = \frac{\Delta E}{u_j^2 \left[\varpi_{i+1}^2 \int_0^{T_{i+1}} \cos^2(\varpi_{i+1} t) \mathrm{d}t - \varpi_i^2 \int_0^{T_i} \cos^2(\varpi_i t) \mathrm{d}t \right]} \tag{8.9}$$

It is possible to fit a polynomial to the values of all the coefficient c_{dij} obtained from sinusoidal tests for two different consecutive frequencies and fixed displacement level. This polynomial is a function of the frequency and describes the *damping coefficient* of Eq. (8.8). For example, for the case of elastomers with high content of *black fumes*[2], the bigger dispersion is obtained for values

[1] The dissipated energy is calculated as the area of the hysteretic cycles obtained from sinusoidal test as explained by Mata *et al.* in [259].

[2] Black fumes are some chemical components with high content of carbon which are added to the rubber's mixture for increasing the damping capacity of the material [215].

of the damping coefficient in the range 0.0-0.5 Hz, because in this set of tests a non viscous part of the dissipated energy is involved. For higher frequency values, this effect disappears according to Eq. (8.6). If the values for the first range of the tests are omitted, it is possible to consider that Eq. (8.5) is approximately equivalent to

$$P_d^{\mathrm{m}} = P_{d_1}^{\mathrm{m}} + \frac{h_t}{A_t}\bar{c}_d\dot{\mathcal{E}}_{d_1} \tag{8.10}$$

where $\bar{c}_d$ is an experimental constant.

8.1.1.b Rate independent part

Strain hardening. The capacity of the model for simulating hardening for strain levels over 150% is given by an appropriated nonlinear elastic backbone added to the non viscous hysteretic cycles, as it can be seen in the scheme of Fig. 8.1. The proposed backbone is defined numerically by means of a polynomial, whose coefficients are fitted to experimental data.

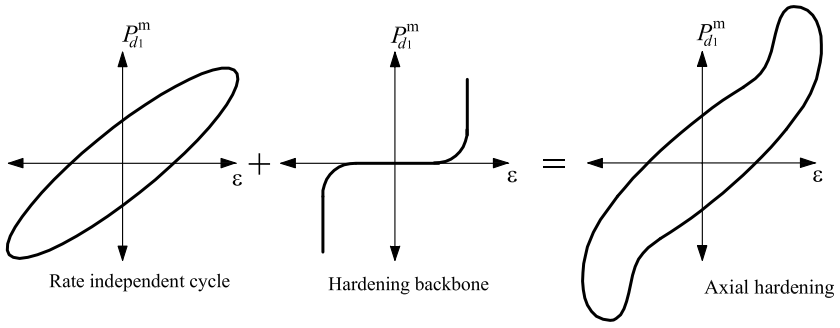

Figure 8.1: Nonlinear elastic backbone added to the rate independent part of the constitutive relation.

The explicit expression for the nonlinear elastic spring representing the hardening backbone depends on the specific device to be modeled; for example for the case of the high damping elastomer of Ref. [259] the following formula is obtained:

$$P_{d_1}^{\mathrm{m}h} = \mathrm{sgn}[\dot{\mathcal{E}}_{d_1}]A_0(\langle|\mathcal{E}_{d_1}| - A_1\rangle)^{A_2}; \tag{8.11}$$

where A_0, A_1 and A_2 are scalar obtained from the experimental tests.

Hysteretic spring. The response of the nonlinear hysteretic spring is obtained solving the following system of nonlinear differential equations [259]:

$$P_{d_1}^{\mathrm{m}}(\mathcal{E}_{d_1}, t) = K_y(\mathcal{E}_{d_1}^{\flat}, P_d^{\mathrm{m}\flat})\mathcal{E}_{d_1} + [K_e(\mathcal{E}_{d_1}^{\flat}, P_d^{\mathrm{m}\flat}) - K_y(\mathcal{E}_{d_1}^{\flat}, P_d^{\mathrm{m}\flat})]e \tag{8.12a}$$

$$\begin{aligned} &\text{if} \quad \dot{\mathcal{E}}_{d_1}e \geqslant 0 \quad \rightarrow \quad \dot{e} = \left[1 - \left|\frac{e}{d_y(\mathcal{E}_{d_1}^{\flat}, P_d^{\mathrm{m}\flat})}\right|^{n(\mathcal{E}_{d_1}^{\flat}, P_d^{\mathrm{m}\flat})}\right]\dot{\mathcal{E}}_{d_1} \\ &\text{else} \quad \rightarrow \quad \dot{e} = \dot{\mathcal{E}}_{d_1} \end{aligned} \tag{8.12b}$$

where K_y is the post yielding stiffness, K_e the elastic stiffness, d_y is the yielding strain of the material, and e represents an internal variable of plastic (hysteretic) strain, which takes a values in the range $[-d_y, d_y]$. The parameter n in the associated flow rule of Eq. (8.12b) describes the degree of smoothness exhibited by the transition zone between the pre and the post yielding

branches of the hysteretic cycle. The model solves the system of equations taking into account that K_e, K_y, d_y, and n are function of the point in the strain-stress space where the last change of sign of the strain rate has occurred, which is denoted as $(\mathcal{E}_{d_1}^{\flat}, P_d^{\mathrm{m}\flat})$ in Eqs. (8.12a) and (8.12b). Therefore, the proposed algorithm updates the parameters of the model for each change of sign of the strain rate. If there is no change in the sign of the strain rate the parameters of the model are maintained constants. Axial hardening can be incorporated by means of adding the nonlinear elastic backbone $P_{d_1}^{\mathrm{m}h}$ to Eq. (8.12a).
The parameters K_e, K_y, d_y, n are nonlinear functions of $(\mathcal{E}_{d_1}^{\flat}, P_d^{\mathrm{m}\flat})$ *i.e.*

$$K_e = \wp_1(\mathcal{E}_{d_1}^{\flat}, P_d^{\mathrm{m}\flat}); \quad K_y = \wp_2(\mathcal{E}_{d_1}^{\flat}, P_d^{\mathrm{m}\flat}); \quad d_y = \wp_3(\mathcal{E}_{d_1}^{\flat}, P_d^{\mathrm{m}\flat}); \quad n = \wp_4(\mathcal{E}_{d_1}^{\flat}, P_d^{\mathrm{m}\flat}). \tag{8.13}$$

Explicit expression for $\wp_k$ $(k = 1, \ldots, 4)$ (in function of $(\mathcal{E}_{d_1}^{\flat}, P_d^{\mathrm{m}\flat})$) are determined from experimental data. In any case with the present model it is possible to simulate the mechanical behavior of a wide variety of devices *e.g.*

- $c_d = 0$, $\wp_1 = \wp_2 =$ constant, $\wp_3 \sim \infty$ and $\wp_4 = 1$ an elastic spring is obtained. This case corresponds to devices designed as re-centering[3] elements in structures.

- $c_d =$ constant, $\wp_1 = \wp_2 = 0$, $\wp_3 \sim \infty$ and $\wp_4 = 1$ a viscous dashpot is obtained. This case can be found in devices applied to control the effects of wind loads.

- $c_d =$ constant, $\wp_1 = \wp_2 =$ constant, $\wp_3 \sim \infty$ and $\wp_4 = 1$ the Maxwell's model is obtained. This case corresponds to a typical viscous device with a re-centering mechanism included.

- $c_d =$ constant, $\wp_1 \geqslant \wp_2 > 0$, $n \in [1, 100]$ and $\mathcal{E}_y > 0$ a visco-plastic device can be simulated (Assuming uncoupled Maxwell's viscosity). Particularly, if $c_d = \wp_2 = 0$ and $n = 1$ a bilinear perfectly-plastic model is obtained. This type of models are the most used manner of simulating displacement dependent EDDs in buildings.

- $c_d = (\dot{\mathcal{E}}_{d_1})^{K_c}$ $(0 < K_c < 1)$, $\wp_1 = \wp_2 = 0$,$\wp_3 \sim \infty$ and $\wp_4 = 1$ a nonlinear viscous dashpot is obtained. Some modern viscous devices employ complex valves's systems which produce a nonlinear grow (with a saturation level) in the curve force-velocity curve of the damper (see *e.g.* [382] Ch. 6).

- In the case of high damping elastomers such as those considered in Ref. [259]) it is possible to obtain: $c_d = 0.12$ Ns/m, $\wp_1 = -0.14 + 0.95\mathcal{E}_{d_1}^{\flat} - 2.45(\mathcal{E}_{d_1}^{\flat})^2 + 3.19(\mathcal{E}_{d_1}^{\flat})^3 - 2.25(\mathcal{E}_{d_1}^{\flat})^4 + +0.89(\mathcal{E}_{d_1}^{\flat})^5 - 0.20(\mathcal{E}_{d_1}^{\flat})^6 + 0.04(\mathcal{E}_{d_1}^{\flat})^7$, the post-yielding stiffness function is maintained constant and equal to the value of the slope of the tangent to the enveloping curve of the test carried out for a strain level of 200%, due to the fact that the tests show that all the loading or unloading branches finally converges to the enveloping curve $\wp_2 = 3.3$. The yield strain function $\wp_3$ is obtained intersecting the line with slope $\wp_2$ and the enveloping line with slope $\wp_2$. The yield strain is measured from the point where changes of sign to the intersecting point. The analytical expression for $\wp_3$ is

$$\wp_3 = \frac{|P_d^{\mathrm{m}\flat}| - |P_0^{\mathrm{m}\flat} - P_d^{\mathrm{m}\flat}|}{\wp_2 - \wp_1}$$

[3]The re-centering forces are considered to be of importance in structures subjected to strong earthquakes which possibly will suffer a great level of damage and permanent deformation due to inelastic incursions in the structural elements. The presence of re-centering mechanism help to recover the original configuration of the structure after the seismic action.

where $P_0^{\mathrm{m}\flat}$ is a parameter calculated evaluating the line with slope $\wp_2$ at zero strain level. The function $\wp_4$ has to take values within the range $[1, \infty]$. By means of appropriated simulations and using a minimization procedure it is possible to see that can be taken $\wp_4 \approx 1$. Several visco elastic devices are based on high damping elastomers.

- If deformation over 150% are applied on the previously described model it is necessary to include the corresponding axial hardening effect which can bee added with the formula for $P_{d_1}^{\mathrm{m}h}$ in Eq. 8.11 considering $A_0 = 5.0$, and $A_1 = A_2 = 1.5$ (for more details see [259]).

More complex material behaviors, such as those of other types of rubber or smart based devices, can be simulated by means of appropriated expressions for the parameters of the model.

Tangent stiffness. The tangent relation for the EDDs is obtained numerically using the *perturbation* method described in Ref. [91]. It consists in applying a small increment[4] to the strain $\mathcal{E}_{d_1}$, denoted by $\delta\mathcal{E}_{d_1}$, after solving the system of Eq. (8.12b) for the total strain $(\mathcal{E}_{d_1} + \delta\mathcal{E}_{d_1})$, the new stress level $P_{d_1}^{\mathrm{m}}$ is determined. Further, the hardening and viscous contributions have to added to obtain the new total stress $P_d^{\mathrm{m}}(\mathcal{E}_{d_1} + \delta\mathcal{E}_{d_1})$. The tangential stiffness of the device, K^t, is then calculated as

$$K^t = \frac{\delta P_d^{\mathrm{m}}}{\delta\mathcal{E}_{d_1}} = \frac{P_d^{\mathrm{m}}(\mathcal{E}_{d_1} + \delta\mathcal{E}_{d_1}) - P_d^{\mathrm{m}}(\mathcal{E}_{d_1})}{\delta\mathcal{E}_{d_1}}. \tag{8.14}$$

It is important to note that the sign of the perturbation have to be the same as $\dot{\mathcal{E}}_{d_1}$ to obtain a tangential stiffness consistent with the sign of the loading process in the device when cyclic actions are considered.

8.1.2 Integration algorithm

The flow chart of the algorithm that integrates the system of Eqs. (8.12b) is shown in Fig. 8.2. The algorithm starts by assigning initial values to the parameters of the model. For each strain level $\mathcal{E}_{d_1}^i$ the algorithm verifies if the strain rate, changes of sign. If this is the case, an updating procedure for the parameters $\wp_k$ $(k = 1, \ldots, 4)$ is carried out. On the contrary, the parameters are maintained. Then plastic strain and stress are then estimated. The same algorithm is used for calculating the tangential stiffness as it was previously explained.

8.1.3 Linearization

The linearization of the contribution of the EDDs to the total virtual work is obtained working on Eq. (8.2) as[5]

$$\begin{aligned} D[\mathbf{G}_{\mathrm{EDD}}] \cdot \hat{\eta}^{\mathrm{s}} &= \int_{L^*} \delta P_d^{\mathrm{m}} \delta\mathcal{E}_{d_1} dS + \int_{L^*} P_d^{\mathrm{m}} \delta(\delta\mathcal{E}_{d_1}) dS + \left\{(\delta\hat{\varphi})^T [\mathbf{M}]_d (\delta\ddot{\hat{\varphi}})\right\}\Big|_{(L^*/2,t)} \\ &= \int_{L^*} K^t (\delta\mathcal{E}_{d_1})^2 dS + \int_{L^*} P_d^{\mathrm{m}} \delta(\delta\mathcal{E}_{d_1}) dS + \left\{(\delta\hat{\varphi})^T [\mathbf{M}]_d (\delta\ddot{\hat{\varphi}})\right\}\Big|_{(L^*/2,t)} \end{aligned} \tag{8.15}$$

$$\delta\mathcal{E}_{d_1} = (\mathbf{\Lambda}^{*T}(\delta\hat{\varphi}_{,S} - \delta\widetilde{\boldsymbol{\theta}}\hat{\varphi}_{,S})) \cdot \hat{E}_1 \tag{8.16}$$

[4] Here the notion of smallness corresponds to the precision of the machine used in the numerical simulations.
[5] By briefly only the case when spatial updating rule for rotation is used is given.

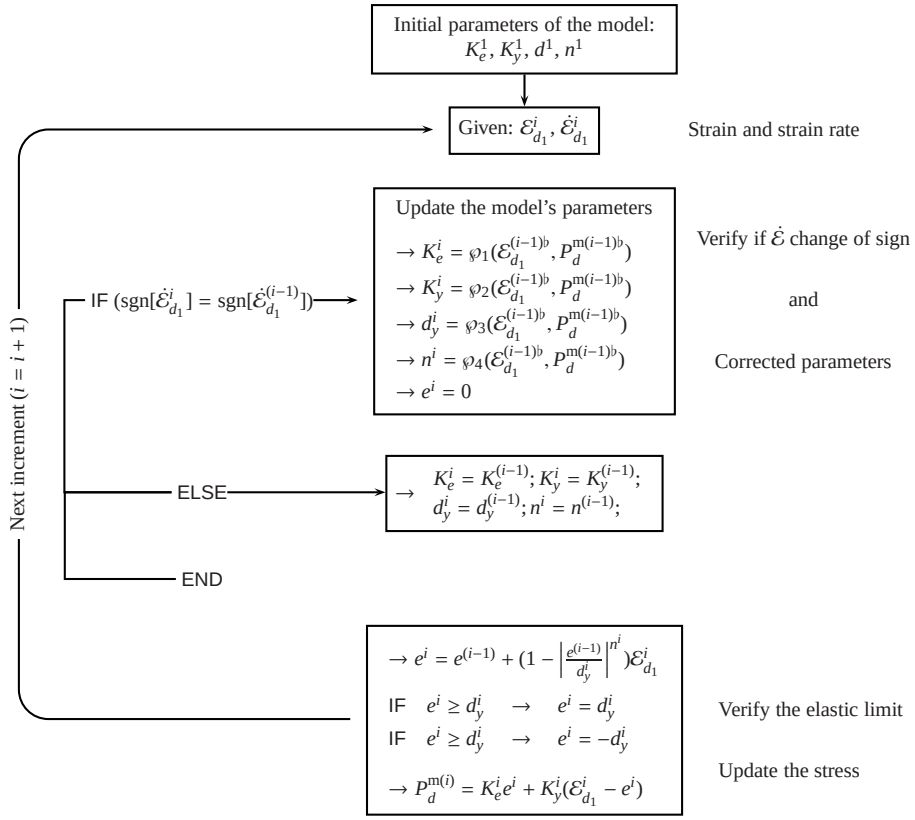

Figure 8.2: Flowchart of the constitutive relation for EDDs.

8.2 Geometric irregularities

As it has been explained in §2.3.2, most of the refined nonlinear models for rod structures are subjected to the following limitations:

(i) The structures present either fully monolithic connections among elements or some of their degree of freedoms are released. Therefore, structural failures due to damage inside of the nodes, often are not properly considered.

(ii) The shape and the mechanical properties of the cross sections are considered constants in an element, therefore, the beam models show serious difficulties in reproducing structural behaviors dominated by *local changes* in the geometry.

Additionally, in Chapter 2 several types of attempts carried out for modeling the effects of local irregularities or local complex stress concentrations in framed structures have been described and abundant references can be there reviewed. They cover from the so called plastic hinge models with appropriated moment-curvature relations to specific solid-to-beam transition elements. Moreover, an alternative approach, combining precision, generality and computational efficiency consists of coupling reduced 1D and full 3D numerical models for different parts of the structure. In this case, most of the elements are prismatic rods and local irregularities or zones corresponding to the connecting joints receive a more detailed geometric description. The connection between models of different dimensions is done through *interface–surfaces*.
The present section is concerned to the development of a *two–scale* (global and local) approach for the fully nonlinear (geometric and constitutive) analysis of framed structures with local geometric irregularities. At *global* scale level, all the elements of the FE model are rods; however, if

(locally) geometric irregularities appear, a *zoom view* of the corresponding element is performed, consisting in a fully 3D model which constitutes the *local* scale level. The dimensional–coupling between scales is performed through *surface–interfaces* imposing the kinematic hypothesis assumed for the beam model. This method avoids the use of multi-points constraints or Lagrange multipliers. Starting from the full 3D stress state existing in the local model, cross sectional forces and moments, required at global level, are recovered by integrating at the surface–interface in an analogous manner as for the cross sectional analysis of beams [258]. An iterative Newton–Raphson scheme based on the displacement method, which considers the interaction between scales is developed to obtain the response at the global level even in the nonlinear dynamic range. Force and displacement equilibrium is checked at both, local and global levels, ensuring that compatible configurations are reached for the whole problem. The tangential stiffness of the local model is obtained numerically applying small perturbations on the current configuration and obtaining the corresponding reaction forces reduced to the degree of freedom of the global level.

8.2.1 Description of the proposed model

The whole body of the framed structure can be seen as divided in two different sets:

(i) By one hand, $\mathcal{B}$ corresponds to the part of the body[6] which is susceptible to be described by means of an assembly of reduced 1D models which are connected each to the others by means of monolithic joints.

(ii) By the another hand, one can consider the set

$$\boldsymbol{\Omega}_s := \{ \bigcup_{p=1}^{N_\Omega} \boldsymbol{\Omega}_{ps} \} \tag{8.17}$$

composed by $p = 1 \dots N_\Omega$ parts of the structure which present geometric irregularities.

The set $\mathcal{B}$ constitutes the *global* scale of the problem, where the advantages of the dimensional–reduction of the problem are taken into account, including geometric nonlinearities. Beam cross sections can be meshed into a grid of fibers with appropriated constitutive laws if desired as described in §3 and §4.
The geometry and the distribution of materials of each element of the set $\boldsymbol{\Omega}_s$ is described carefully by means of a full 3D approach, therefore, elements of this set are treated at more reduced scale, the *local* scale, (in terms of the degree of detailing considered).
The connection between $\mathcal{B}$ and one part $\boldsymbol{\Omega}_{ps} \in \boldsymbol{\Omega}_s$ is obtained through the set

$$\partial\boldsymbol{\Omega}_{ps} := \{ \bigcup_{k=1}^{N_{p\Omega}} \partial\boldsymbol{\Omega}_{kps} \} \tag{8.18}$$

where $k = 1 \dots N_{p\Omega}$ is an index running over the number of *interface–surfaces*, $\partial\boldsymbol{\Omega}_{kps} \in \mathbb{R}^2$. Each element of $\partial\boldsymbol{\Omega}_{ps}$ has one-to-one correspondence with the end cross section of a beam element connecting to $\boldsymbol{\Omega}_{ps}$. See Fig. 8.3.
Therefore, for example if one have a beam element, generically denoted by $\mathcal{B}_i$, connected to the

[6] By simplicity, in this work a part of a body is identified with all the material points which occupy a region on the 3D space and can be conveniently described using a coordinate system. For a more elaborate definition see §A.3.

geometric irregularity $\mathbf{\Omega}_{ps}$ through the cross section $\mathcal{A}_i$, then necessarily there exist a $\partial\mathbf{\Omega}_{kps}$ (for some $k \in [1 \dots N_{p\Omega}]$ such that

$$\mathcal{A}_i \equiv \partial\mathbf{\Omega}_{kps} \tag{8.19}$$

and both abstract elements are subjected to the same motion.

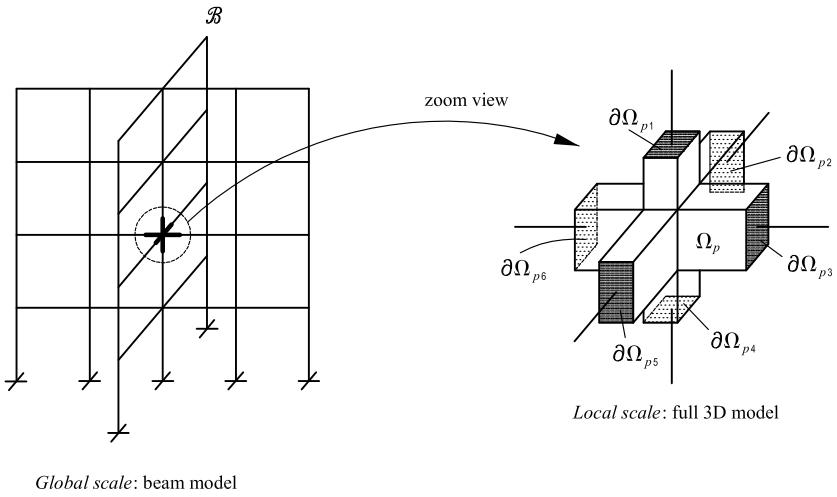

Figure 8.3: Schematic representation of the two–scale model.

At global scale level, the so called *dimensional-coupling* [280, 292] is obtained enforcing at local level, *i.e.* on each $\partial\mathbf{\Omega}_{kps}$ of a given $\mathbf{\Omega}_{ps}$, the fulfillment of the kinematic hypothesis assumed for the 1D model.
In the present work, planarity of the cross section is assumed during the motion and, therefore, the surface–interfaces of the local model displace and rotate as a rigid body and, in this sense, warping or cross sectional distortion is not included. Reduced forces and moments from the local models are obtained though integration of the reaction forces in the interfaces in an analogous manner as for the cross sectional analysis of beams [258].
The local model constitutes a *zoom view* made on a part of the structure, $\mathbf{\Omega}_{ps}$, which is treated at global level as an additional 1D element. Fig. 8.4 presents a illustrative example: a structure consisting of a 1D model and a 2D model deforms due to the motion $\phi(t)$ (t time). It is possible to see that the cross section of the end of the beam corresponds to the surface–interface of the 3D model, which moves as a 2D rigid body.
In other words, given a motion of the structure, the global scale only treats with reduced quantities as usual in beam's theories but the required quantities originating from elements of the set $\mathbf{\Omega}_s$ are obtained solving a 3D problem subjected to the beam kinematics's assumptions as boundary conditions on the displacements of $\partial\mathbf{\Omega}_{ps}$. In the following sections, a presentation of both, the local and the global models, as well as the step-by-step numerical algorithm for solving the two–scale problem is presented.

REMARK 8.1. The proposed formulation can be seen as an *ad-hoc* numerical *homogenization* by means of an appropriated micro description of the domain corresponding to the local scale using the FEM. A similar approach has been used for the treatment of structures made of composite materials [308] ■

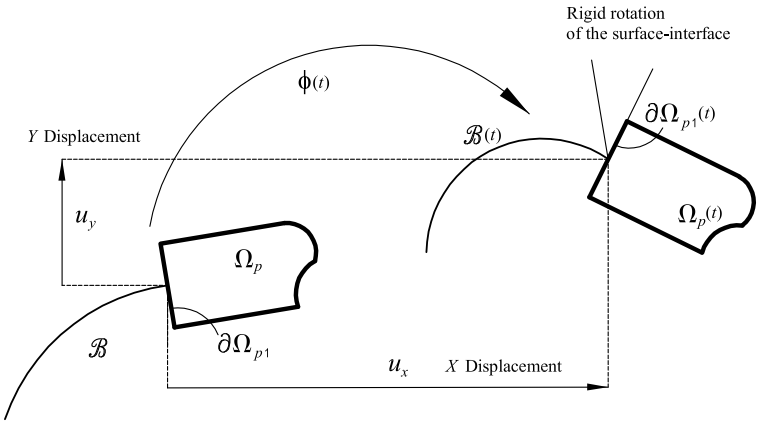

Figure 8.4: Imposition of the kinematic hypothesis of the 1D model on the surface–interface $\partial\mathbf{\Omega}_{p1}$.

8.3 Global scale: rod model

At global level, all the elements are rods, therefore, the Reissner–Simo formulation for beams that can undergo large deformations in space, considering a free of stress curved reference configuration and expanded for considering an inhomogeneous distribution of composite materials on arbitrarily shaped cross sections is considered. A detailed presentation of the theory can be reviewed in Chapters 3 and 4.

8.3.1 Kinematics and balance laws

As it has been explained in §3.1.3 the deformation moves $\hat{\varphi}_0(S)$ to $\hat{\varphi}(S,t)$ at time t adding a translational displacement. Simultaneously, $\mathbf{\Lambda}_0(S)$ is rotated together with the cross section to $\mathbf{\Lambda}(S,t) = \mathbf{\Lambda}_n\mathbf{\Lambda}_0$ by means of the *incremental rotation tensor* $\mathbf{\Lambda}_n(S,t)$ for the spatial updating of the new compound rotation. Then, the position vector of any material point with coordinates (S,ξ_β) on the reference beam configuration, $\hat{x}_0$, and on the current beam configuration, $\hat{x}$, are given by

$$\hat{x}_0 = \hat{\varphi}_0(S) + \mathbf{\Lambda}_0(S)\xi_\beta\hat{E}_\beta \tag{8.20a}$$

$$\hat{x} = \hat{\varphi}(S,t) + \mathbf{\Lambda}(S,t)\xi_\beta\hat{E}_\beta \tag{8.20b}$$

respectively. Therefore, the displacement field on each material point on a cross section $\mathcal{A}(S)$, at time t, is obtained as

$$\hat{u}(S,\xi_\beta,t) = \hat{x} - \hat{x}_0. \tag{8.21}$$

The associated strain vectors in spatial, $\hat{\epsilon}_n$, or material, $\hat{\mathcal{E}}_n$, forms acting on a material point on the current beam cross section are given in Eqs. (3.68a), (3.68b) and (3.70). An objective measure of the strain rate vector $\hat{s}_n$ can be deduced by taking the material time derivative of $\hat{\mathcal{E}}_n$ and using the Lie derivative operator as given in Eqs. (3.78a), (3.78b) and (3.82).
The material form of the FPK stress vector $\hat{P}_1^{\mathrm{m}}$, referred to the curved reference beam is energetically conjugated to $\hat{\mathcal{E}}_n$, as it can be confirmed from §3.4. Integrating over the cross section, it is possible to obtain the spatial form of the stress resultant $\hat{n}^{\mathrm{m}}$ and the stress couple $\hat{m}^{\mathrm{m}}$ according Eqs. (3.94a) and (3.94b). With the corresponding spatial forms obtained through the push–forward operator (see §3.3.4).

The spatial form of the *reduced balance equations* of the current beam, referred to the curved reference beam, have been deduced in §3.5. Particularly, in Eqs. (3.121) and (3.133). Starting from these equations it is possible to deduce the spatial description of the nonlinear functional corresponding to the *virtual work principle*, Eqs. (3.142) to (3.145), which is recalled here in compact form:

$$\mathrm{G_G}(\hat{\varphi}, \boldsymbol{\Lambda}, \hat{\eta}^{\mathrm{s}}) = \mathrm{G_{Gint}}(\hat{\varphi}, \boldsymbol{\Lambda}, \hat{\eta}^{\mathrm{s}}) + \mathrm{G_{Gine}}(\hat{\varphi}, \boldsymbol{\Lambda}, \hat{\eta}^{\mathrm{s}}) - \mathrm{G_{Gext}}(\hat{\varphi}, \boldsymbol{\Lambda}, \hat{\eta}^{\mathrm{s}}) - \hat{\eta}^{\mathrm{s}} \cdot \hat{\Phi}\Big|_0^L = 0 \tag{8.22}$$

where the subscript G has been added to the internal, inertial and external components of the scalar $G(\bullet)$ for referring to the global scale. It also corresponds to the weak form of the balance equations [178, 363].

8.3.2 Constitutive laws

Points on the cross sections are assumed to have associated a composite material as explained in §4. The composite is formed by several simple constituents which can have associated any of the following constitutive models: linear elasticity, rate independent plasticity and damage or visco damage. All these models have been developed considering a suitable form compatible with the kinematics described in Eqs. (8.20a) and (8.20a) and the details can be consulted in §4.2.2 to §4.2.3. For the purpose of explaining the present two–scale formulation it is enough to say that each compounding substance on a given material point has associated a constitutive law in the following way:

$$\hat{P}_1^{\mathrm{m}} = f(\hat{\mathcal{E}}_n, \hat{s}_n, \bar{\boldsymbol{\alpha}}) \tag{8.23}$$

where $\hat{P}_1^{\mathrm{m}}$ and $\hat{\mathcal{E}}_n$ are the material form of the FPK stress and strain vectors, respectively, $f(\bullet)$ is the function describing the constitutive relation depending on the set $\bar{\boldsymbol{\alpha}} = \{\bar{\alpha}_1, \ldots, \bar{\alpha}_n\}$ composed by n internal variables. Additionally, a tangent consecutive relation between linearized increments of strain and stress exist and it is expressed as

$$\delta\hat{P}_1^{\mathrm{m}} = \boldsymbol{\mathcal{C}}^{\mathrm{mt}}\delta\hat{\mathcal{E}}_n. \tag{8.24}$$

The mixing rule for composites is used to obtain the resulting stress and tangential tensor at material point level according to the explanations of §4.3 and §4.4. On another hand, a mesh independent response of the structure is obtained regularizing the dissipated energy at constitutive level as explained in §4.1.

8.4 Local model: 3D connecting joint

Once a local irregularity has been detected on a given rod, a zoom view, corresponding to the local 3D scale, is opened. This section is devoted to explain the mechanical problem which has to be solved at local level. Firstly, it is worth to recall that the *dimensional–coupling* between scales is obtained throughout imposing the plane cross section assumption for beams on the surface–interfaces in the 3D model (see Fig. 8.4).

8.4.1 Equilibrium equations and boundary conditions

Assuming a massless local model ($\rho_0 = 0$), we obtain that points on the (plane) surface–interfaces are subjected to the same motion as the corresponding cross sections of the beams connected to them. At local level, the momentum balance equations of the body $\boldsymbol{\Omega}_{ps}$, with $\partial\boldsymbol{\Omega}_{ps} = \bigcup_k \partial\boldsymbol{\Omega}_{psk}$

$(k = 1, \ldots, N_{p\Omega})$ surface–interfaces, are described by

$$\left.\begin{array}{l} \nabla \cdot \mathbf{S} = 0 \\ \mathbf{S} = \mathbf{S}^T \end{array}\right\} \qquad \text{in} \quad \boldsymbol{\Omega}_{ps} \in \mathbb{R}^3 \tag{8.25a}$$

$$\hat{x} = \phi_k(\hat{\varphi}_k, \boldsymbol{\Lambda}_k) \qquad \text{in} \quad \partial\boldsymbol{\Omega}_{psk} \in \mathbb{R}^2 \quad k = 1, \ldots, N_{p\Omega} \tag{8.25b}$$

where $\mathbf{S}$ is the *second Piola–Kirchhoff* (SPK) stress tensor, no external body forces are applied *i.e.* $\hat{b}_0 = 0$ as well as prescribed traction on the boundaries ($\mathbf{S} \cdot \hat{N} = 0$). The functions ϕ_k of Eq. (8.25b), defining the natural boundary conditions of the problem, are prescribed in accordance with Eq. (8.20b) and they read[7] as

$$\hat{x}_L = \hat{\varphi}_k - \hat{\varphi}_{0k} + (\boldsymbol{\Lambda}_k - \boldsymbol{\Lambda}_{0k})\hat{\chi} = \hat{u}_k; \quad \forall \hat{x}_L \in \partial\boldsymbol{\Omega}_{psk} \tag{8.26}$$

where $\hat{\varphi}_k$, $\hat{\varphi}_{0k}$, $\boldsymbol{\Lambda}_k$, $\boldsymbol{\Lambda}_{0k}$ are the current and reference displacement fields and rotation tensors associated to the beam connecting to the k^{th} surface–interface, $\hat{u}_k$ is the corresponding displacement, $\hat{\chi}$ is the local position vector of the material point $\hat{x}_L$ lying on the surface–interface $\partial\boldsymbol{\Omega}_{psk}$. In an analogous manner as for the finite strain beam theory $\hat{\chi}$ is defined considering the movable local axis $\hat{t}_{k(\beta)} = \boldsymbol{\Lambda}_k \hat{E}_\beta$ *i.e.* $\hat{\chi} = \xi_\beta \hat{t}_{k(\beta)}$ (see Fig. 8.5).

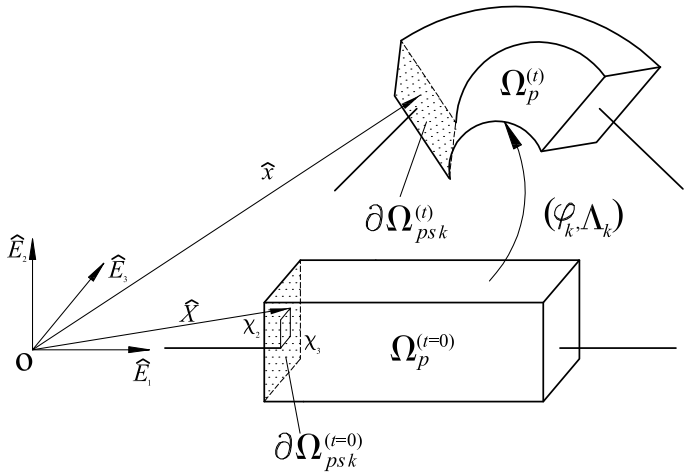

Figure 8.5: Time evolution of the material points lying on the surface–interfaces.

Following standard arguments in continuum mechanics [251] we have that the weak statement of Eqs. (8.25a) and (8.25b) is given by

$$G_L(\hat{x}, \delta\hat{x}) = \int_{\boldsymbol{\Omega}_{ps}(t=0)} \mathbf{S} : \delta\mathbf{E} \mathrm{d}V = 0 \tag{8.27}$$

where $\mathbf{E}$ is the Green–Lagrange (GL) strain tensor energetically conjugated to $\mathbf{S}$ and t the time. It is worth to note that all strain-stress field developed in the body $\boldsymbol{\Omega}_{ps}$ during the motion, is derived from the imposition of the displacement field of Eq. (8.25b).

[7] The subscript L has been introduced to highlight that the respective quantity is referred to the local model.

8.4.2 Constitutive equations

In an analogous manner, as explained in section 8.3.2 for the case of the beams, material points on $\mathbf{\Omega}_{ps}$ are assumed to have associated a composite material [90, 306]. The composite can be formed by several simple constituents with their own constitutive models. In this case, the GL deformation tensor $\mathbf{E}$ is complete in the sense that all the 9 components can be determined from a given displacement field; in contrast with the case of beam where the kinematics hypothesis limits the number of accessible components (see Eqs. 8.20b and 8.23) to those acting on the face of the cross section. Therefore, rate dependent and independent constitutive models for plastic and degrading materials can be formulated based on a solid thermodynamic basis. Additionally, the mixing rule is used to treat the resulting composite [90]. In following, a brief review of the main characteristics of the employed models is given; however, for a more detailed description of the respective formulations or their numerical implementations, it is necessary to consult the references to previous works of the authors [90, 238, 301, 305, 306].
Particularly, brittle materials such as concrete are treated by means of a isotropic damage model, where the degrading behavior of a material point is conducted by the evolution of a scalar parameter d which range over $[0, 1]$ (0 for the undamaged elastic behavior and 1 for a completely damaged point). The model is able to differentiate between tensile and compressive properties of the material. The mesh independent response of structures presenting softening behavior is obtained by means of regularizing the dissipated energy at integration point level according to the specific fracture energy obtained in simple tension or compression tests. A detailed description of this model can be found in [238, 301]. Alternatively, a more refined coupled plastic damage model can be used to simulate the behavior of concrete [240]. This model can develop plastic deformations simultaneously with the degradation of the mechanical properties. Specific yield criteria and potential functions for concrete, such as Mohr–Coulomb, can be included in this model [305].
Some structures present an intrinsic orthotropic behavior due to the presence and distribution of steel reinforcements. By one hand, the *longitudinal reinforcement* can be seen as a material which has elastic plastic behavior directed along the line of the reinforcing bars. By the other hand, the *transversal reinforcements*, such as the usual stirrups, contribute to confine the concrete and help to resist shear forces. A plastic model for orthotropic materials is used to simulate the mechanical behavior of steel reinforcements [90]. Imposing the mechanical properties of the concrete in the direction perpendicular to the axis of the reinforcing bar and orienting the plastic flow in the direction of the reinforcement, it is possible to simulate the typical behavior of the steel bars.

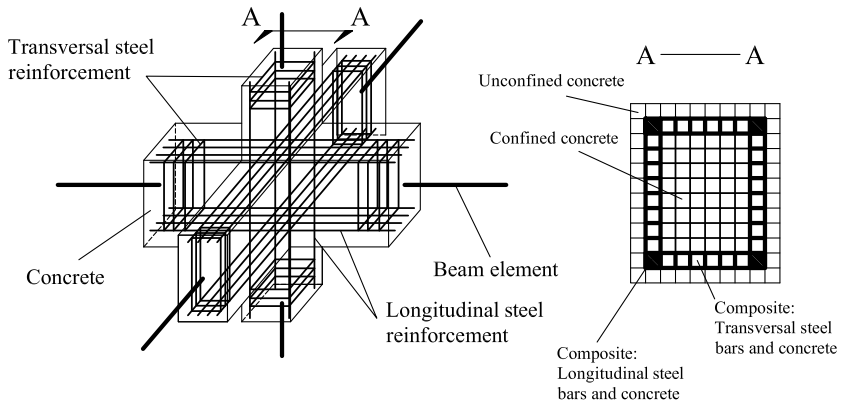

Figure 8.6: FE model of the local scale including directional reinforcements.

From the point of view of the construction of a FE model of the local irregularity, one proceed meshing the geometry as usual; then the material associated to elements located in places where longitudinal reinforcements are present, is considered as a composite material according to the mixing rule. The composite material is made of two phases:

(i) A phase described by means of a degrading material or a plastic damage model and

(ii) a phase corresponding to the content of reinforcements (longitudinal and/or transversal). The mechanical properties of the reinforcing phase (anisotropic elastic constitutive tensor and stress threshold) are defined in a manner such that the directionality of the reinforcement is considered.

Fig. 8.6 shows the 3D joint of a typical RC structure with a rather complex distribution of steel reinforcements. In the same figure, the view A–A shows a typical FE discretization of one of its cross sections where three kinds of materials are used:

(i) a purely damaging model for the elements of the unconfined zone.

(ii) A coupled plastic damage model for the confined zone of the concrete.

(iii) A composite material with three phases for the zone where longitudinal and transversal steel reinforcements appear altogether with the concrete. Each phase of the mixture contributes according to its volumetric fraction [257].

The proposed approach for considering arbitrary distribution of materials in the local scale model has the advantage of avoiding the usage of highly refined FE meshes which try to describe the geometry of each reinforcing bar appearing in the model.

8.4.3 Cross sectional and boundary surface analysis

From the point of view of the numerical implementation, an arbitrarily shaped beam cross section is meshed into a grid of quadrilaterals, each of them corresponding to a fiber oriented along the beam axis. An appropriated cross sectional analysis for fiber beam models in finite deformation has been presented in references [258, 260]. The estimation of the value of a given function on a quadrilateral is carried out by performing the numerical integration of the values calculated at specific points according to a selected integration rule and then dividing by the quadrilateral's area. In those works, an integration of the constitutive equation of each simple material existing on each fiber level is followed by the application of the mixing rule and a posterior integration on the cross sectional surface. The same procedure allows to determine the cross sectional tangential stiffness.
In the case of the dimensional–coupling between scales, after a displacement field in the local scale problem fulfilling Eqs. (8.25a) and (8.25b) has been determined, it remains opened the question about how to determine the reduced forces and moments which should equilibrate the system of Eqs. (3.121) and (3.133). The solution to the problem is provided by the fact that numerically the restriction of Eq. (8.25b) is forced on a discrete set of points

$$X_{psk} = \bigcup_i \hat{x}^i_{psk} \tag{8.28}$$

corresponding to nodes of a FE mesh, on each surface–interface $\partial\mathbf{\Omega}_{psk}$ $(k = 1, \ldots, N_{p\Omega})$. After the numerical solution of the discrete problem has been carried out, a set of reaction forces

$$R_{psk} = \bigcup_i \hat{r}^i_{psk} \tag{8.29}$$

corresponding to the nodal reactions, appears on each of the $\partial\mathbf{\Omega}_{psk}$. The reduced forces and moments acting on the k^{th} surface–interface are then calculated as

$$\hat{N}_G = \sum_i \hat{r}^i_{psk} \tag{8.30a}$$

$$\hat{M}_G = \sum_i \widetilde{\boldsymbol{l}}_i \hat{r}^i_{psk} \tag{8.30b}$$

where $\hat{N}_G$, $\hat{M}_G$ are the reduced force and moment vector obtained from the full 3D problem of the local scale, $\widetilde{\boldsymbol{l}}_i$ is the skew–symmetric tensor obtained from $\hat{l}_i = (\chi_2, \chi_3)_i$, the vector of coordinates of the i^{th} restricted point on the k^{th} surface–interface.

REMARK 8.2. It is worth to note that in order to get achieve equilibrium at global level, the reduced forces and moments obtained from the global and local scales have to self-equilibrate. Considering that the displacement and rotation field is the same for both scales due to the kinematics assumption, one obtains that this condition enforces that the work done by both models is the same at the surface–interfaces ■

8.5 Numerical procedure

In this section a Newton type numerical solution procedure based on the linearized form of the weak form of Eq. (8.22) is presented. A complete survey about the linearization can be reviewed in §5. The interaction between scales is explained as well as the method used for the obtention of the reduced tangential tensor of the local scale problem.

8.5.1 Global scale: consistent linearization for beams

At global scale level each element behaves as a rod, therefore, the numerical solution for most of the elements is based on obtaining the linear part of the functional of Eq. (8.22) which can be written as

$$\mathscr{L}[\mathrm{G}_{G*}(\hat{\varphi}_*, \mathbf{\Lambda}_*, \hat{\eta}^{\mathrm{s}})] = \mathrm{G}_{G*}(\hat{\eta}^{\mathrm{s}}) + D\mathrm{G}_{G*}(\hat{\eta}^{\mathrm{s}}) \cdot \hat{p}^{\mathrm{s}} \tag{8.31}$$

where $\mathscr{L}[\mathrm{G}_{G*}(\hat{\eta}^{\mathrm{s}})]$ is the linear part of the functional $\mathrm{G}_G(\hat{\varphi}, \mathbf{\Lambda}, \hat{\eta}^{\mathrm{s}})$ at the configuration defined by $(\hat{\varphi}_*, \mathbf{\Lambda}_*)$ and $\hat{p}^{\mathrm{s}} \in \eta^{\mathrm{s}}$ is an admissible variation considering the spatial updating rule for rotations. The term $\mathrm{G}_{G*}(\hat{\eta}^{\mathrm{s}})$ supplies the unbalanced force and it is expressed as the sum of three terms corresponding to the contribution of internal, external and inertial terms, $\mathrm{G}_{G*\mathrm{int}}$, $\mathrm{G}_{G*\mathrm{ext}}$, $\mathrm{G}_{G*\mathrm{ine}}$, respectively. The part $D\mathrm{G}_{G*}(\hat{\eta}^{\mathrm{s}}) \cdot \hat{p}^{\mathrm{s}}$ (linear in $\hat{p}^{\mathrm{s}}$) gives the tangential stiffness, as explained in §5.3.
Details about the linearization of the internal and external terms and its numerical implementation has been already presented in §5, §6 and §7, including the material updating rule for the rotational field and an arbitrary distribution of inelastic materials. In any case, the linearization

procedure finally yields to

$$\mathscr{L}[\mathrm{G}_{G*}] = \mathrm{G}_{G*} + [\mathrm{K}_M + \mathrm{K}_G + \mathrm{K}_V + \mathrm{K}_P + \mathrm{K}_{\mathrm{ine}}]_*. \tag{8.32}$$

The spatial and temporal discretization of the problem of Eq. (8.32) and the numerical implementation in a FE code follows the procedures described in previous chapters for the case of an appropriated version of the Newmark's implicit time stepping algorithm and an iterative procedure for updating the pertaining variables in the context of the Newton–Raphson scheme.

8.5.2 Local scale: FE model and reduced tangential stiffness

At global scale level a iterative step-by-step Newton–Raphson scheme is used to solve the discrete version of the linearized form of the functional, G_L, given in Eq. (8.27) considering the boundary conditions of Eq. (8.25b). The usual FE procedure is applied as described for example in [42], therefore, details are omitted here. After convergency is achieved the reduced forces and moments corresponding to the surface–interfaces are estimated from the reaction forces as explained in Section 8.4.3.

The another ingredient required in the global scale is the *reduced tangential tensor i.e.* the tangential stiffness obtained from the 3D model but reduced to the beams degree of freedom connected to the surface–interfaces. This tensor is obtained by means of applying the *perturbation* method [90] as follows:

(i) Supposing a local scale model used to describe the solid $\boldsymbol{\Omega}_{ps}$, with $\partial\boldsymbol{\Omega}_{ps} = \bigcup_k \partial\boldsymbol{\Omega}_{psk}$ ($k = 1, \ldots, N_{p\Omega}$) surface–interfaces, we have[8] ($6 \times N_{p\Omega}$) degrees of freedom (DOFs) corresponding to the beams connected to the solid. After a displacement field fulfilling Eqs. (8.25a)–(8.25b) (in the nonlinear range) has been determined, a set of perturbations on each one of the ($6 \times N_{p\Omega}$) DOFs is performed. In this case a perturbation in the p^{th} DOF consist in imposing of a displacement field with a magnitude close to the numerical precision of the computer machine on the nodes of the corresponding surface–interface[9]. Let denote one of such perturbations by δU_G^p.

(ii) For the new boundary condition corresponding to each δU_G^p, the problem defined by Eqs. (8.25a)–(8.25b) is solved and then the corresponding increments in the reaction forces of the restricted nodes of the body are calculated.

(iii) By means of using the formulas of Eqs. (8.30a)–(8.30b) the increment of the reduced forces and moments are calculated. Let denote them by $\delta\hat{N}_G^{pq}$ and $\delta\hat{M}_G^{pq}$ ($q = 1, \ldots, N_{p\Omega}$), which physically correspond to the stiffness in the q^{th} DOF due to a infinitesimal displacement (correspondingly rotation) in the p^{th} DOF.

Therefore, the numerical estimation tangential stiffness of the local scale model reduced to the global DOFs in the global scale is given by

$$[\mathscr{K}]_L^{\mathrm{t}} = \begin{bmatrix} \delta\hat{N}_G^{11} & \cdots & \delta\hat{N}_G^{1q} \\ \vdots & \ddots & \vdots \\ \delta\hat{M}_G^{q1} & \cdots & \delta\hat{N}_G^{qq} \end{bmatrix}. \tag{8.33}$$

[8] They correspond to 3 displacements and 3 rotation on each surface–interface connected to the solid.

[9] Perturbations on translational DOFs impose translational displacement fields on the nodes of the surface–interface and perturbations on rotational DOFs impose infinitesimal (additive) rigid body rotations.

It is worth noting that initially the tangent stiffness of Eq. (8.33) corresponds to the elastic one, $[\mathscr{K}]^0_L$, and in this case, the applied perturbation can have any magnitude.

8.5.3 Two–scale Newton–Raphson integration procedure

As it has been explained, the two scales are dimensionally–coupled through the reduced forces and moments and the tangential tensors. From the numerical point of view, at global scale level once a loading step is applied the corresponding displacement and rotation fields are obtained on the nodal DOFs. After that, the following sequence of steps is carried out:

(i) If the element corresponds to a free of irregularity rod, the strain fields are calculated on each fiber of the cross sections corresponding to an integration point and the reduced forces, moments and tangential matrices are determined as described in [258, 260]. If the element presents a geometric singularity, the full 3D problem at local scale level is solved using an iterative Newton–Raphson scheme in the FEM and imposing the rod's kinematics assumptions on the surface interfaces. It is worth to note that, in the nonlinear range, several iterations can be needed at local scale level to obtain the converged field which provides the *not necessarily convergent* reduced forces and moments at global scale level.

(ii) After convergency is achieved at local scale level the obtained reduced forces, moments and tangential tensor are sent to the global iterative scheme to the check convergency. If this is the case, the algorithm proceed to apply a next load increment. If not, a new iteration is performed at global level.

The flow chart of the two–scale Newton–Raphson iterative is shown in Fig. 8.7.

8.5.4 Computational aspects

From the point of view of the implementation in a numerical code, the problem is managed by means of a *master–slave* approach, where the global scale problem acts as the master, sending a *trial* displacement field to the local scale models (slaves) and then receives the corresponding internal forces, moments and tangential tensors estimated by means of integration on the surface interfaces. The iterative process is finished when the global convergence is achieved. Computationally, the proposed approach is well suited to be implemented in a *parallelized algorithm*, where the mater and slave problems are solved independently by different programs. The communication between processes (and processors) is carried out by mean of an appropriated library of communication. In this way, minimal intervention on existing codes (specific for beams and solids), allow obtaining the response of the whole structure in the nonlinear static and dynamic analysis. Finally, numerical examples are included showing the capabilities of the proposed formulation.
The proposed two–scale formulation for beam structures with local irregularities is very well suited to be computationally implemented using the advantages of the parallel computation. The *message passing interface* (MPI) system [381] is used to pass information among different process (or processors) which can correspond to programs of different nature that share information during execution. In the present case, a *master–slave* approach is followed using the MPI library coupled with two Fortran codes; one of them, the master, is specific for the structural analysis of beams and the other one, corresponding to the slave, specific for structural analysis of solids. See Fig. 8.8.
The following steps summarize the basic features of the computational implementation of the Newton–Raphson iterative scheme described in §8.5.3:

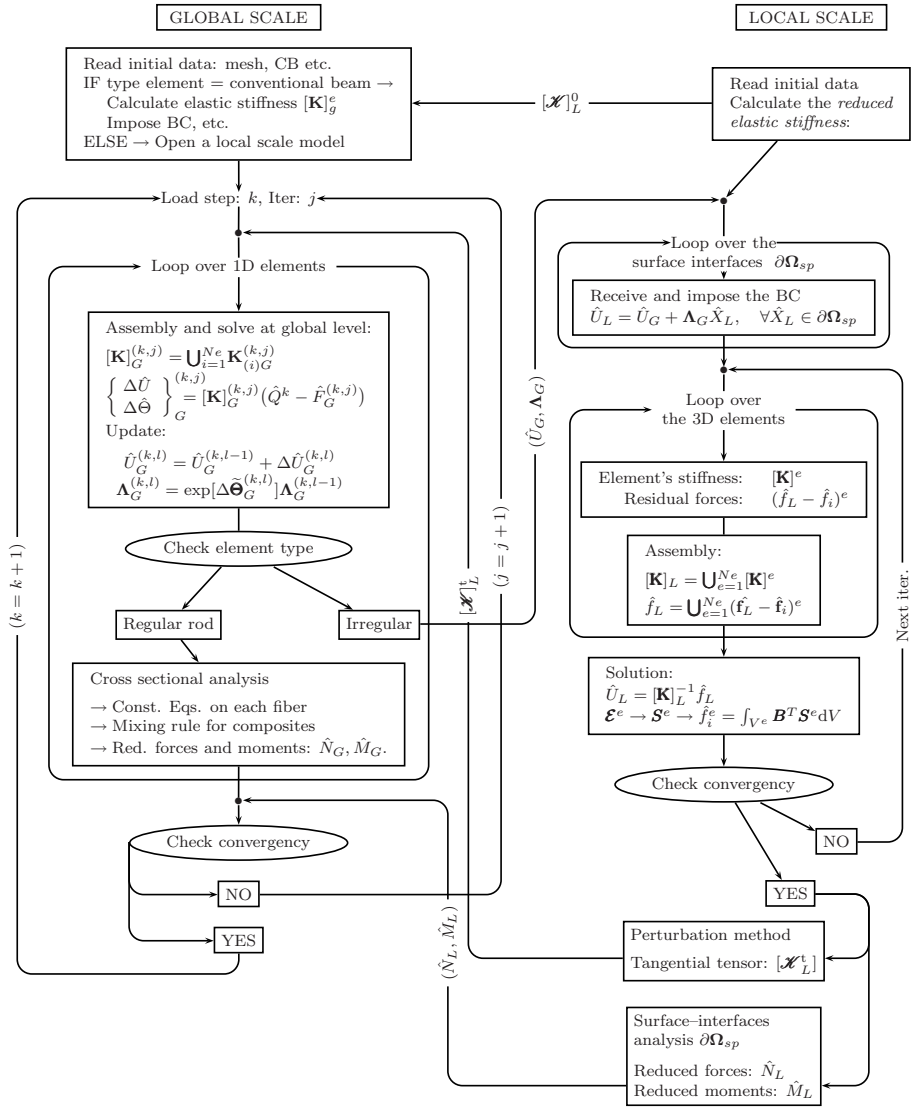

Figure 8.7: Flow chart of the two–scale Newton–Raphson iterative scheme.

(i) The program which solves the global scale problem acts as the master and initially send the order for run in independent processes, as many slave programs as local irregularities appears in the structure.

(ii) Each one of the slaves is an independent process corresponding to the execution of a specific program for the analysis of solids, which is in charge of solving the local scale problem. It is worth to note that each slave process can be executed on the same processor of the computer machine as the master or in a different one if a multiprocessor machine is being used. In the first case, the time required for the calculations increase linearly[10] with the number of slaves because the processor only can work on a program per time. In the second case, the time required decreases because the structural response from several

[10]Here the word 'linearly' is used to indicate that the time required for calculations is function of the number of slaves, since it would not be possible to maintain a strict linearity in the consumption of time when inelasticity has place in the models.

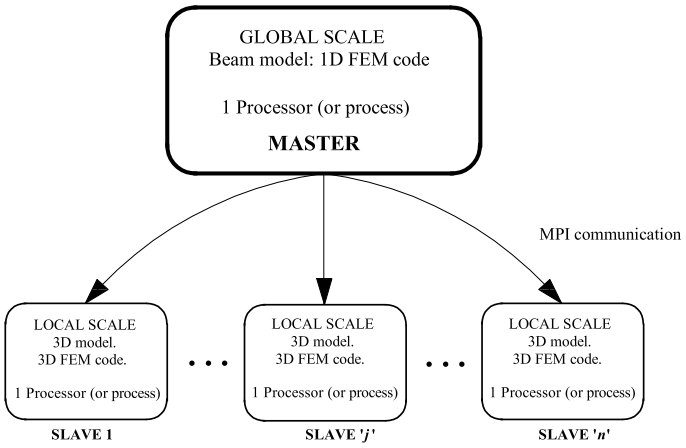

Figure 8.8: Schematic representation of the master–slave approach.

slaves can be obtained simultaneously. In any case, the use of the MPI system helps to perform a minimal intervention on existing codes specific for the analysis of 1D or 3D structures. The main advantage of using the MPI standard lie in the fact that the changes to be implemented in existing codes are limited to include the `SEND` and `RECEIVE` calls corresponding to the synchronized *message passing* through the master and its slaves.

(iii) The message passing among processes corresponds to the *sending* from the master of the rotation and displacement fields of the surface–interfaces of each slave and the *receiving* from the slaves to the master of the reduced forces, moments and tangential tensors on each iteration according to the flow chart of Fig. 8.7. Other information, typical of iterative schemes, such as global convergency in a time step or warnings are also passed for the opportune updating the data base in the slave processes.

8.5.5 Limitations of the present formulation

From the computational point of view, in spite of the mentioned advantages obtained from using the MPI system some difficulties can be mentioned:

(i) It is rather difficult to debug the execution of the coupled problem using the standard debugging tools of the modern developer environments which are in most cases developed for the construction of individual programs.

(ii) For the moment, there is not control over the order in which the synchronized messages are passed from different slaves to the master, which resemble complicated for studying the execution of the programs by mean of witting texts to the user–screen.

From the point of view of the formulation and its numerical implementation, several limitations where observed during the numerical simulation of the response of structures:

(i) At local level, if a great part of the 3D body suffer inelastic incursions the stress distributions on the surface–interfaces can become very complex and enormous difficulties in obtaining global convergency can be observed. The main reason for this behavior can be related with the fact that in the nonlinear range, plane sections do not remain plane[11],

[11] Mainly, when degrading materials are used.

and therefore, the resulting reduced forces and moments have values that are far from the one obtained on the cross sections of the connecting beams. A possible solution for this problem consist into consider local models representing a larger part of the structure, in a way such that the local inelastic effects are concentrated in a zone that remains far from the surface interfaces, confining the inelasticity. By other hand, if the proposed remedy is employed, the massless assumption for the local scale model can introduce larger errors in dynamic analysis and a new formulation considering inertial forces appear as necessary.

(ii) The imposition of the restrictions given in Eqs. (8.25b) enforces to maintain the size and shape of the $\partial\mathbf{\Omega}_{psk}$'s, therefore, reaction forces contained in the plane of the surface–interfaces derived from the Poisson coefficient, ν, of the materials became in plane reduced forces (shear forces and torsion moment) 'ν–dependent'. To overcome the difficulties encountered in the numerical simulations an additional assumption has been done, it corresponds to assume $\nu = 0$ for the materials of the FEs lying on the surface–interfaces. In this way the plane and undeformed hypothesis assumed for beam elements is enforced in the local scale.

Chapter 9

Numerical Examples

The previously described geometric and constitutive nonlinear formulation for beams has been implemented in a FEM computer code. In this section several numerical examples illustrating the capacities of the model and the versatility of the proposed damage index are presented.

9.1 Validation examples: elastic case

9.1.1 Unrolling and rerolling of a circular beam

This validation example considers the unrolling and rerolling of the elastic circular cantilever beam shown in Fig. 9.1. This example has been reported by Kapania and Li in Ref. [207] where four node initially curved FE elements are used. The case of an initially straight cantilever beam has been also reproduced in [178]. The initially circular beam has a radio $R = 5/\pi$, unitary square cross sectional area and the following properties for the material: elastic modulus E =1200 and Poisson coefficient ν =0.0. The FE mesh consist of ten equally spaced, quadratic, initially curved elements. An unitary bending moment M is applied at the free end. Four loading steps are applied, each of them with a moment increment $\Delta M = 10\pi$. The convergence tolerance is 1×10^{-7}. The deformed configurations of the beam are shown in Fig. 9.1. The displacements of the free end for an applied moment of 10π are 6.365 in the vertical direction and -0.001 in the horizontal direction. For an applied moment of 20π, the mentioned values are 0.003 and 9.998, respectively, and are very close to those given in [207]. The number of iterations to reach the convergence in the first and second loading steps are 18 and 22, respectively.

9.1.2 Flexible beam in helicoidal motion

The example corresponds to the validation of the proposed formulation for the elastic case. For comparative purposes, an example of Ref. [183] has been reproduced here. It corresponds to the helicoidal motion of a straight beam constrained to slide and rotate along the vertical axil Z of Figure 9.2. A constant vertical load and torque is applied during 2.5 s as indicated in the same Figure. Due to the fact that it is a purely elastic example, no cross sectional integration is required and the mechanical properties are taken from [183] as: $E\mathcal{A}= G\mathcal{A}= 10^4$, $E\mathbf{I}= G\boldsymbol{J}= 10^3$, $\mathcal{A}_\rho = 1.0$ and $\boldsymbol{J}_\rho = \text{Diag}[20, 10, 10]$, where E and G are the Young and shear elastic modulus and $\mathcal{A}$,$\mathbf{I}$,$\boldsymbol{J}$,$\mathcal{A}_\rho$ and $\boldsymbol{J}_\rho$ are the cross sectional area, the second moment of inertia, the torsional inertia, the beam mass and the inertial dyadic per unit of length, respectively. Ten linear beam elements and a time–step size Δt=0.5 s were used in the numerical simulations. The results

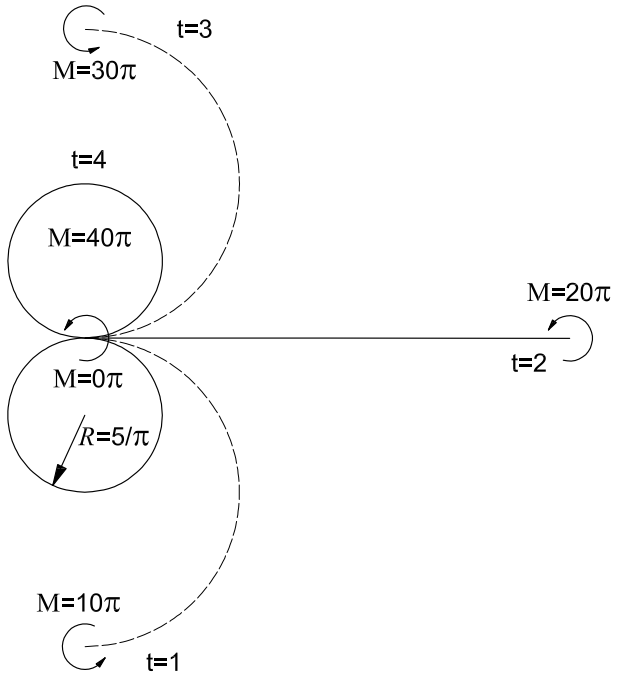

Figure 9.1: Deformed configurations of the circular beam.

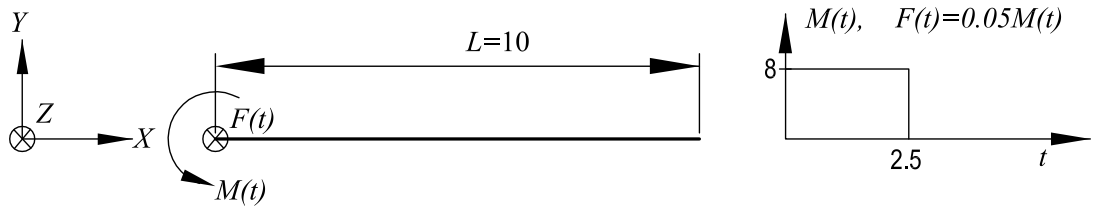

Figure 9.2: Flexible beam in helicoidal motion

of the numerical simulations are presented in Fig. 9.3 which are in good agreement with those given in [183] for the three components of the displacement of the free end of the beam.

9.2 Nonlinear static examples

9.2.1 Mesh independent response of a composite cantilever beam

The RC cantilever beam shown in Fig. 9.16 is used to study if, regularizing the dissipated energy at constitutive level, it is possible to obtain a mesh independent response when including softening materials. Forty increments of imposed displacements were applied in the Y direction to obtain the capacity curve of the beam. Four meshes of 10, 20 40 and 80 quadratic elements with the Gauss integration rule where considered in the simulations. The beam cross section was meshed into 20 equally spaced layers. The steel bars were included as a part of the composite material with a volumetric fraction corresponding to their contributing area to the total area of the layer where they are located. The mechanical properties of the concrete and steel are summarized in Table 9.2, where E and ν are the elastic modulus and Poisson coefficient, respectively; G_f is the fracture energy, f_c is the ultimate compression limit and n is the ratio of the compression to the tension yielding limits, according to Eq. (4.11c). Fig. 9.17 shows the capacity curve relating the vertical reaction with the displacement of the free end. It is

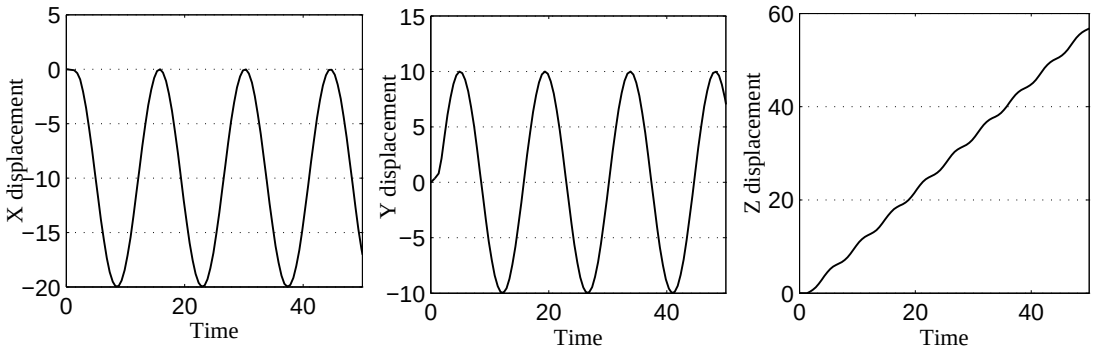

Figure 9.3: Displacements time history response of the free end of the beam.

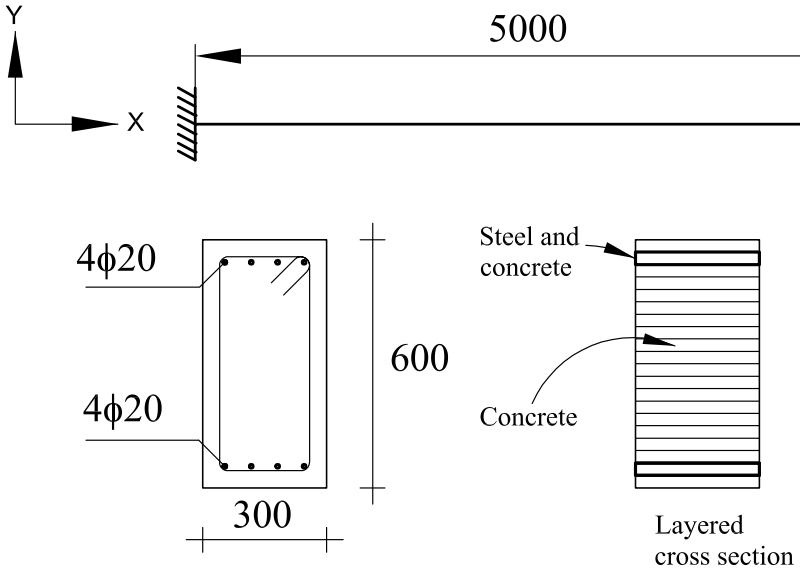

Figure 9.4: RC cantilever beam.

possible to see that the numerical responses converge to that corresponding to the model with the greater number of elements. Further information can be obtained from the evolution of the local damage index at cross sectional level, which is shown in Fig. 9.6 for the 4 meshes and the loading steps 10, 25 and 40. In all the cases, strain localization occurs in the first element but, in the case of the mesh with 10 elements, localization occurs before than in the other cases and a worse redistribution of the damage is obtained, what can explain the differences observed in Fig. 9.17. Finally, Fig. 9.18 shows the evolution of the global damage index which allows to appreciate the mesh independent response of the structure.

9.2.2 Framed dome

The elastic and plastic mechanical behavior of framed domes has been studied in several works. For example, in Ref. [118] domes formed by trusses are studied; in [318] initially straight beam elements are used to study the elastic plastic behavior of domes including isotropic and kinematic hardening; in [284] a co–rotational formulation for beam elements with lumped plasticity is presented; and in [396] a plastic hinge formulation assuming small strains and the Euler–Bernoulli hypothesis is employed for studying the nonlinear behavior of domes including the mechanical buckling and post critical loading paths.

Table 9.1: Mechanical properties

	E Mpa	ν Mpa	f_c Mpa	n	G_f Nmm^{-2}
Concrete	21000	0.20	25	8	1
Steel	200000	0.15	500	1	500

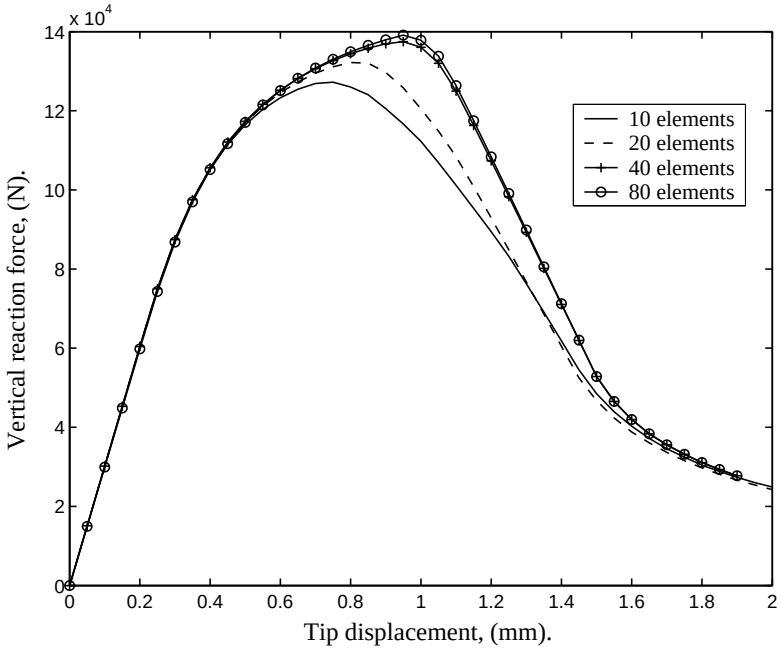

Figure 9.5: Vertical reaction versus tip displacement.

In this example, the nonlinear mechanical behavior of the framed dome shown in Fig. 9.8 is studied with the objective of validating the proposed formulation in the inelastic range. The linear elastic properties of the material are: elastic modulus 20700 MNm^{-2} and Poisson's coefficient 0.17. Three constitutive relations are employed: (1) Linear elastic; (2) Perfect plasticity ($G_f = 1 \times 10^{10}$ Nm^{-2}) with associated Von Mises yield criterion and an elastic limit of $f_c = 80\,\mathrm{Nm}^{-2}$; and (3) Damage model with equal tensile and compression limits, $n = 1$, a fracture energy of $G_{f,c} = 50\,\mathrm{Nm}^{-2}$ and the same elastic limit as in case (2). Three elements with two Gauss integration points are used for each structural member. A vertical point load of $P_0 = 123.8$ N acting on the apex of the dome is applied and the displacement control technique is used in the simulations. Fig. 9.9 shows the deflection of the vertical apex in function of the loading factor $\lambda = P_t/P_0$ (P_t is the current applied load) for the three constitutive relations. It is possible to see in Figure 9.9 a good agreement with the results given by Park and Lee in Ref. [318] for the stable branch of the elastic loading factor–displacement responses. When comparing both results for the elastic plastic case, it is possible to see a good agreement for the elastic limit of the structure; however, when deformation grows, the differences can reach 30% for the predicted value of the load carrying capacity of the dome. Moreover, the curve corresponding to the damage model has been added to Fig. 9.9. In both cases, when inelastic constitutive relations are employed, the curve of the global structural response shows a snap–through which couples constitutive and geometric effects.

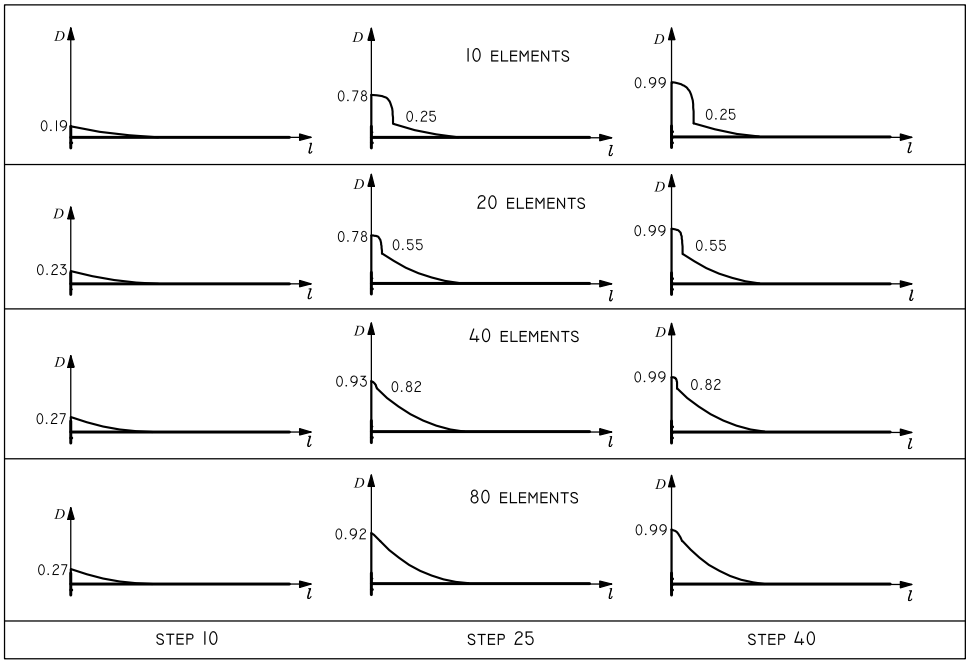

Figure 9.6: Evolution of the local cross sectional damage index: Strain localization. The symbols D and l are the damage index and the length of the beam, respectively.

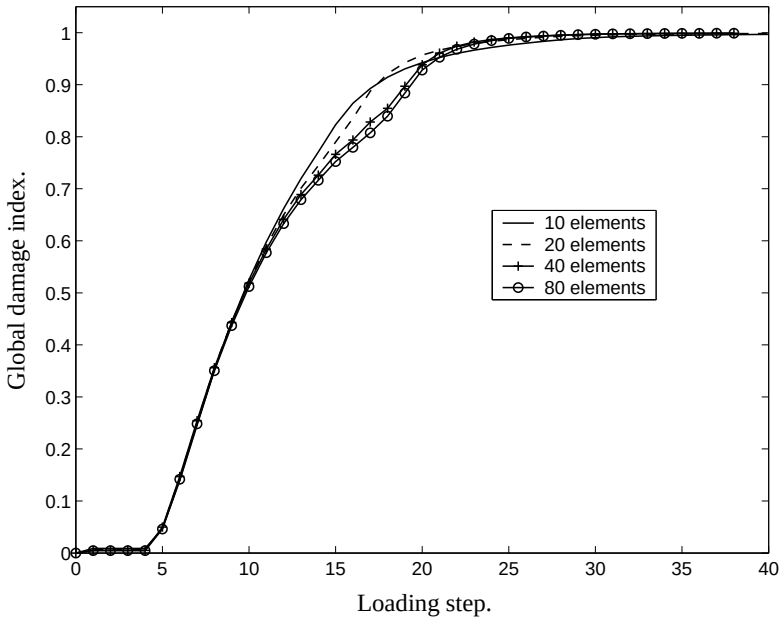

Figure 9.7: Global damage index.

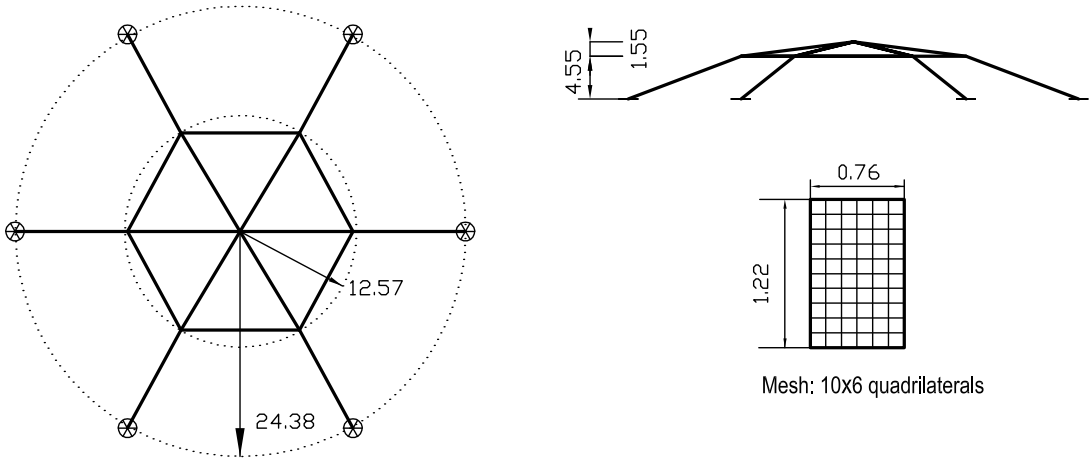

Figure 9.8: Framed dome and detail of the cross sectional mesh.

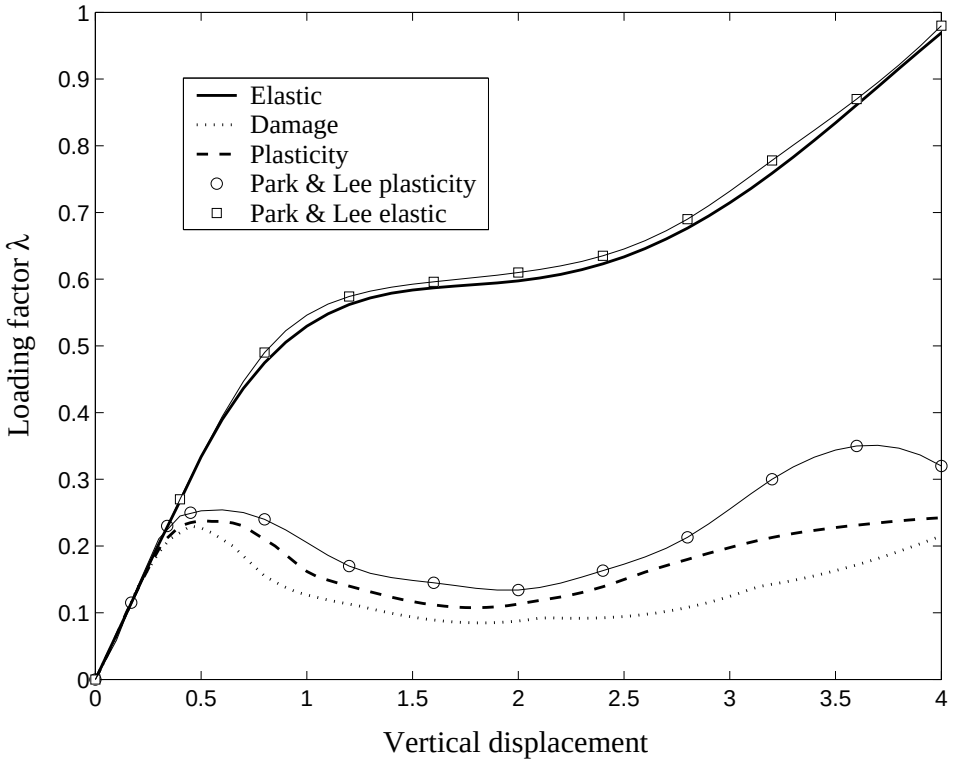

Figure 9.9: Loading factor-displacement curve of the vertical apex of the dome.

9.2.3 Nonlinear response of a forty–five degree cantilever bend

This example performs the coupled geometrically and constitutive nonlinear analysis of a cantilever bend placed in the horizontal X-Y plane, with a vertical load F applied at the free end, as shown in Fig. 9.10. The radius of the bend has 100 mm with unitary cross section. The linear elastic case of this example involves large 3D rotations and an initially curved geometry; therefore, it has been considered in several works as a good validation test [178, 207, 363]. The mechanical properties for the elastic case are an elastic modulus of 1×10^7 Nmm^{-2} and a shear modulus of 5×10^6 Nmm^{-2}. Four quadratic initially curved elements are used in the FE

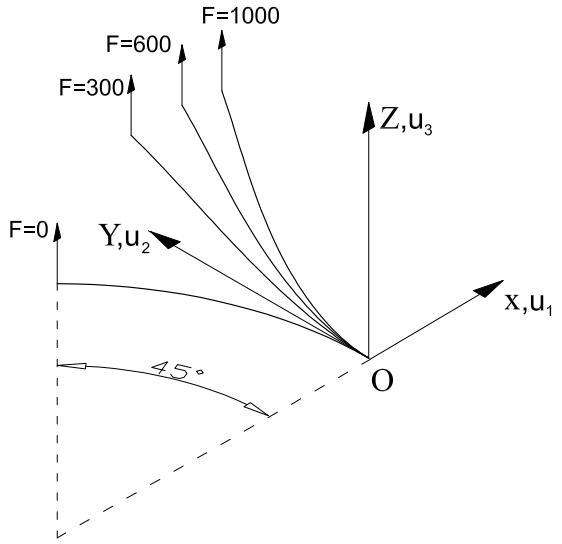

Figure 9.10: Initial geometry and some examples of the deformed configurations for the linear elastic case of the 45^o cantilever bend.

discretization with two Gauss integration points per element. Solutions are obtained by using thirty equal load increments of 100 N. The history of the tip displacements is shown in Fig. 9.11. The tip displacements for an applied load of 600 N are: U_1=13.56 mm. U_2=-23.81 mm and U_3=53.51 mm (see Fig. 9.10) which are values close to those obtained by other authors [207]. The coupled geometric and constitutive nonlinear response of the structure was obtained

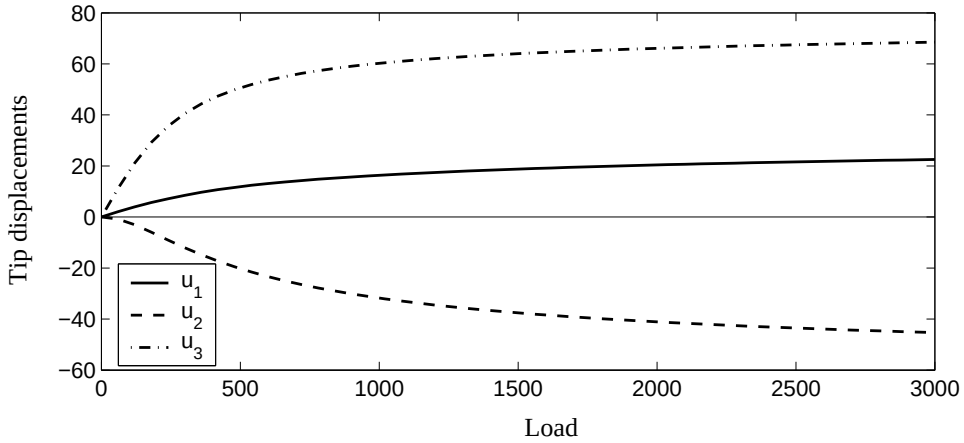

Figure 9.11: Different components of the tip displacement (linear case).

for three materials:

(i) Elastic plastic with Von Mises yield criterion, associated flow rule, a fracture energy of $G_f = 1 \times 10^{10}$ Nmm^{-2}, and a tension to compression ratio $n = 1$.
(ii) Degrading material with $n = 1$ and $G_f = 5 \times 10^4$ Nmm^{-2}.
(iii) A composite formed by equal parts of the materials (i) and (ii). In all the cases, the elastic limit is taken $f_c = 7 \times 10^4$ Nmm^{-2}.

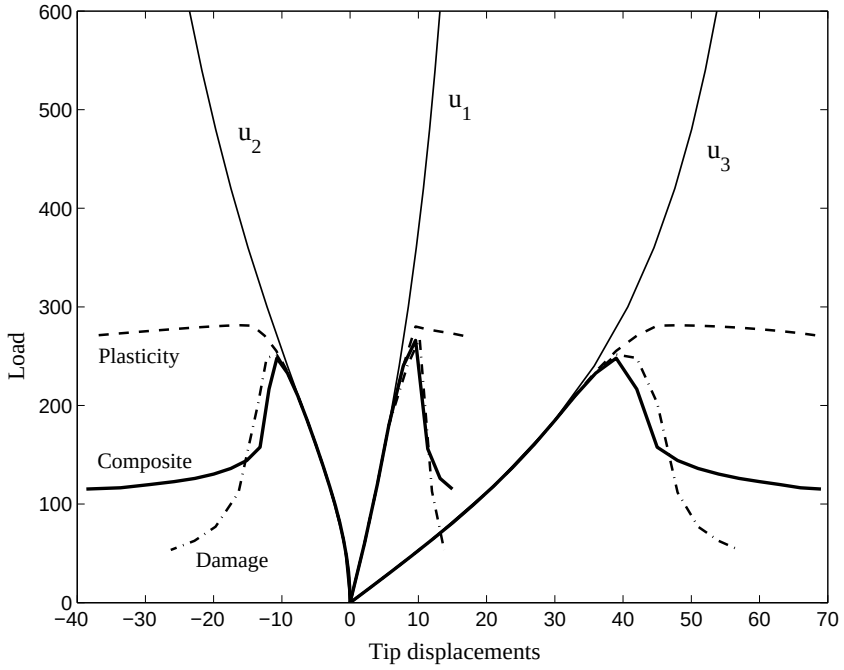

Figure 9.12: Different components of the tip displacement (nonlinear case).

The beam cross section was meshed into a grid of 10×10 quadrilaterals with one integration point per fiber. A set of 35 imposed displacements of 2 mm was applied. The convergence tolerance was taken equal to 10^{-4} for residual forces and displacements. Fig. 9.12 shows the results obtained from the numerical simulations for tip displacements superposed to the elastic response. It is possible to observe in this figure that:

(1) The elastic plastic case converges to a fixed value of 274 N for the vertical reaction after the redistribution of the damage has occurred along the beam length, which can be considered the final stage in the formation of a plastic hinge in the structure.
(2) In the case of the degrading material, the analyze were stopped in the loading step 29 due to lack of convergency with an evident loss in the load carrying capacity.
(3) The response of the composite materials show two phases: the first one corresponds to the degradation of the damaging phase; during the second one the vertical reaction is stabilized in a value equal to 112 N, which is due to the mechanical response of the plastic phase.

In all the cases, a great amount of iterations were required to obtain convergence (>50 in the softening phase). However, in the case of the material (ii) the analyze were finalized after 300 iterations due to the fact that the development of axial forces in the deformed configuration literally cuts the beam for vertical displacements beyond 57 mm.

9.2.4 Nonlinear analysis of a right angle frame

The right angle frame of Fig. 9.13 is subjected to a concentrated out of plane load $P = 0.3$ N acting on the middle of the span of one of the two members of length $L = 100$ mm. Forty equally sized loading steps have been used. Each member is modeled using four quadratic elements with two Gauss integration points. The square beam cross sections with a side length $a = 3$ mm are meshed into a grid of 4×4 quadrilaterals with four integration points per fiber. The convergence tolerance is taken as 1×10^{-4}.

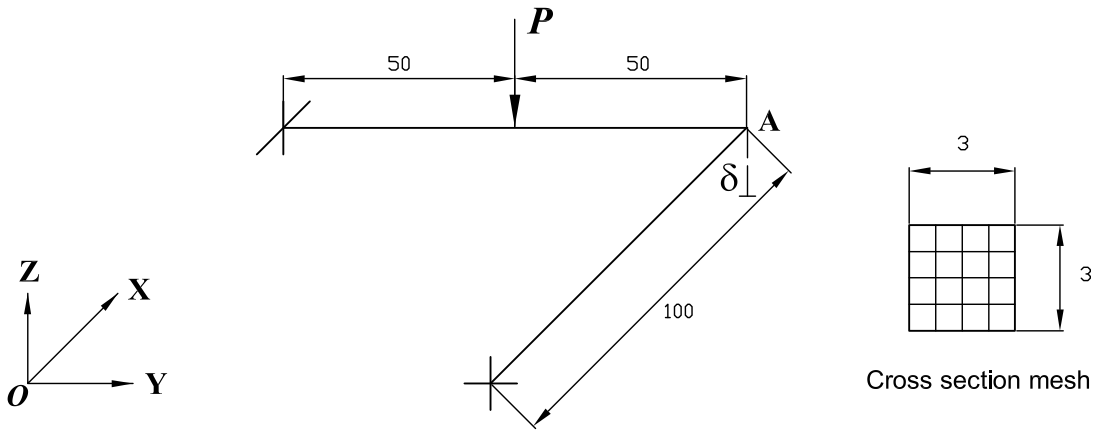

Figure 9.13: Right bent description.

The constitutive and geometric nonlinear response of the frame is computed for four different materials with the same elastic modulus $E = 720$ Nmm^{-2}, Poisson coefficient $\nu = 0.3$ and yielding threshold $f_c = 1$ Nmm^{-2}. The other characteristics of the materials are:

(i) Associated Von Mises plasticity with a compression to tension ratio $n = 1$ and fracture energy $G_f = 1 \times 10^5$ Nmm^{-2}.

(ii) Damage model with $n = 2$, $G_f = 0.1$ Nmm^{-2}.

(iii) Composite with a 20% of (i) and 80% of (ii).

(iv) a composite with a 10% of (i) a 80% of (ii) and a 10% of a material having only linear elastic properties.

Fig. 9.14 shows a comparison between the results obtained for the applied force versus the vertical deflection of the point A (see Figure 9.13) for the material (i) and the results given in Refs. [318, 357]. The results shown in Fig. 9.14 are normalized considering that I is the inertia of the square cross section and $M_0 = a^3 f_c/6$. A good agreement with the results obtained in the mentioned references is obtained.

Fig. 9.15*a* shows the load deflection curve of the point A for the four considered materials. It is possible to appreciate that in the case of the material (iii), after the damaging phase of the composite has been degraded, the response of the structure is purely plastic. In the case of the material (iv), in the large displacements range of the response, the elastic phase dominates the mechanical behavior. Fig. 9.15*b* shows the evolution of the global damage index for the four materials. It is worth to note that the damage index corresponding to material (iii) grows faster than the others, but, when the plastic phase dominates the the response (approx. loading step 32), the highest damage index is associated to the material (ii). In the large displacements range, the smallest values of global damage index corresponds to the material (iv) due to the effect of the elastic component.

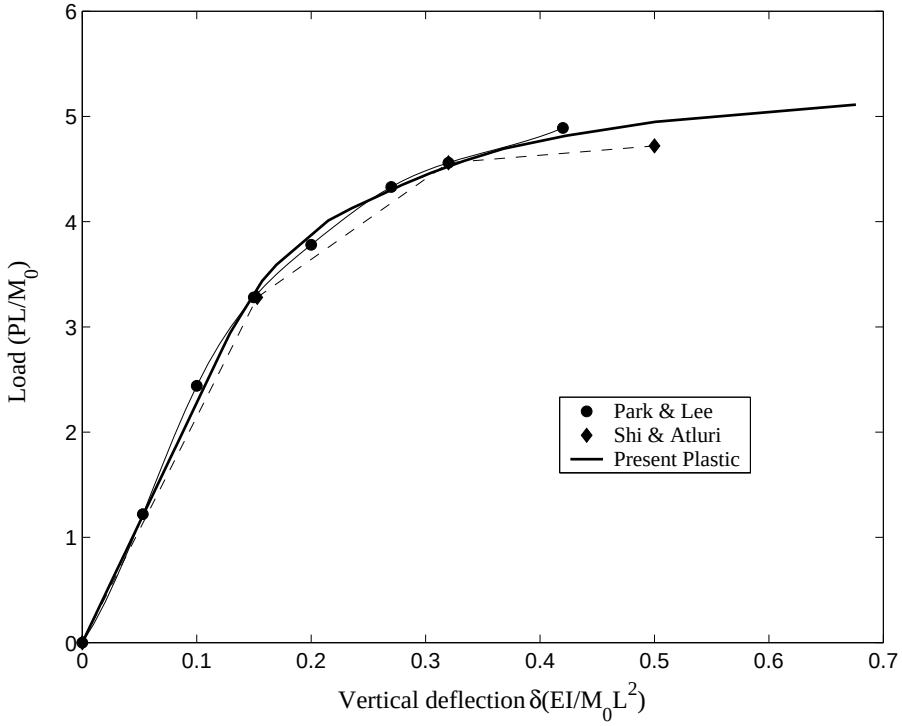

Figure 9.14: Load–deflection curve.

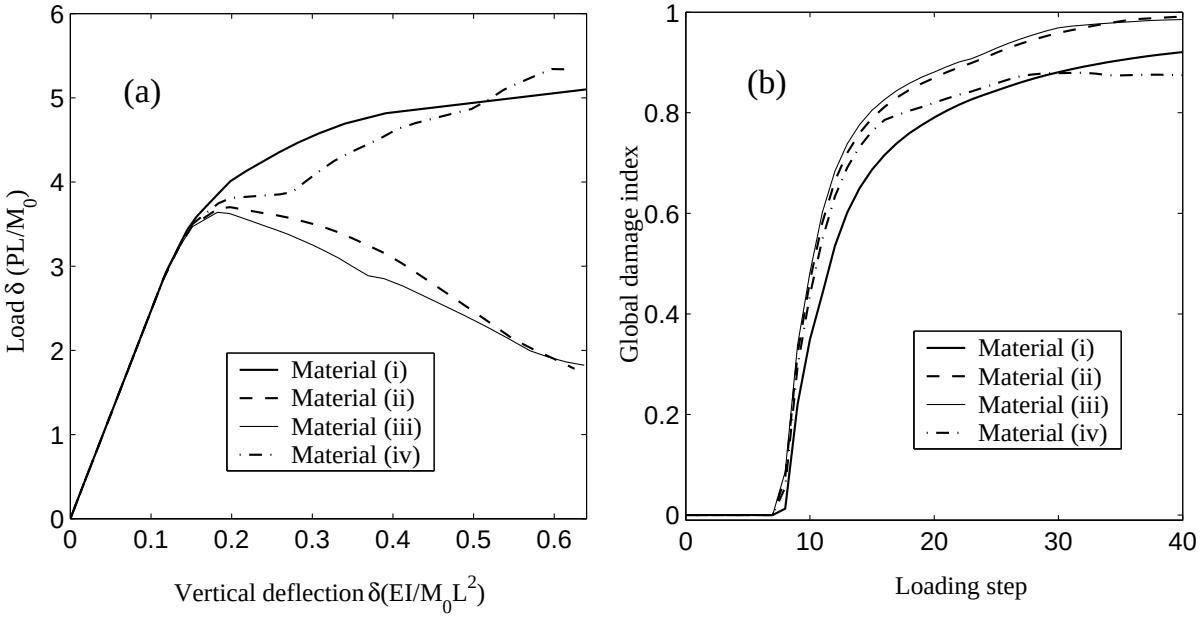

Figure 9.15: (a): Load deflection curves. (b): Global damage indices.

9.3 Nonlinear dynamic examples

9.3.1 Visco elastic right angle cantilever beam

The right angle cantilever beam shown in Fig. 9.16a is dynamically loaded by an out of plane concentrated force of 250 N at the elbow. The shape and duration of the applied load is show in the same figure. The total duration of the analysis is 4.5 s, which includes the period of time when the load is being applied and the following free vibration of the system. The time step is 0.03 s. The mechanical properties are: an elastic modulus of 5.0×10^4 Nmm^{-2}, a Poisson coefficient of 0.2 and a mass density of 0.1 Kgmm^{-3}. Three quadratic elements with two Gauss integration points have been used for each structural member. The cross section is meshed into a equally spaced 8×8 quadrilaterals equipped with one integration point. Several deformed shapes of the system are show in Figure 9.16b for the undamped elastic case. It is interesting to note that the motion of the system involves large torsion and bending and the magnitude of the displacements is of the same order as the dimensions of the initial geometry. Three values

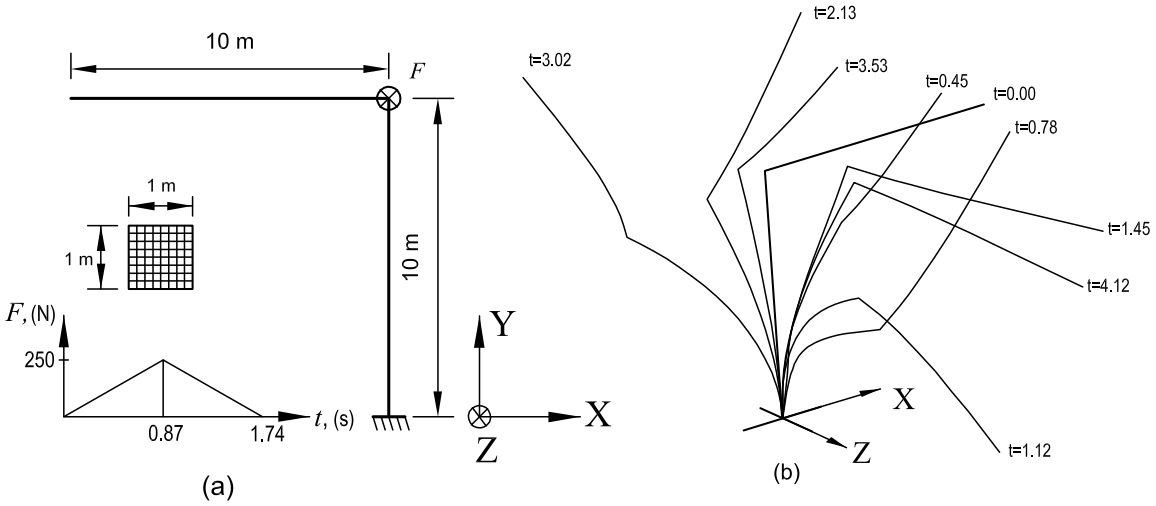

Figure 9.16: Right angle frame. (a): A concentrated out of plane load is applied on the elbow node. (b): Deformed configurations for different time steps for the case of the undamped system.

for the viscosity η =0.01, 0.03 and 0.04 s are used in the numerical simulations, along with the visco elastic constitutive law, in order to highlight the effects of the damping on the behavior of the system. Figs. 9.17a and 9.17b show the time history of the displacement of the tip and the elbow in Y direction for the undamped system and for the three values of the viscosity. It is possible to see from these figures that increasing values of the viscosity contributes to decrease the maximum displacements of the system during the nonlinear oscillations.
Viscosity also contributes to dissipate the high frequency content in the response, what can be seen due to the fact that increasing values of the parameter η imply smoother time history responses. Finally, a more significative appreciation of the effects of viscosity can be obtained from Fig. 9.18, where the time history of the displacements of the tip in the $Y-Z$ plane is shown. It is possible to see in this figure, that the increment of the value of η diminishes the amplitude of the motion of the mechanical system.

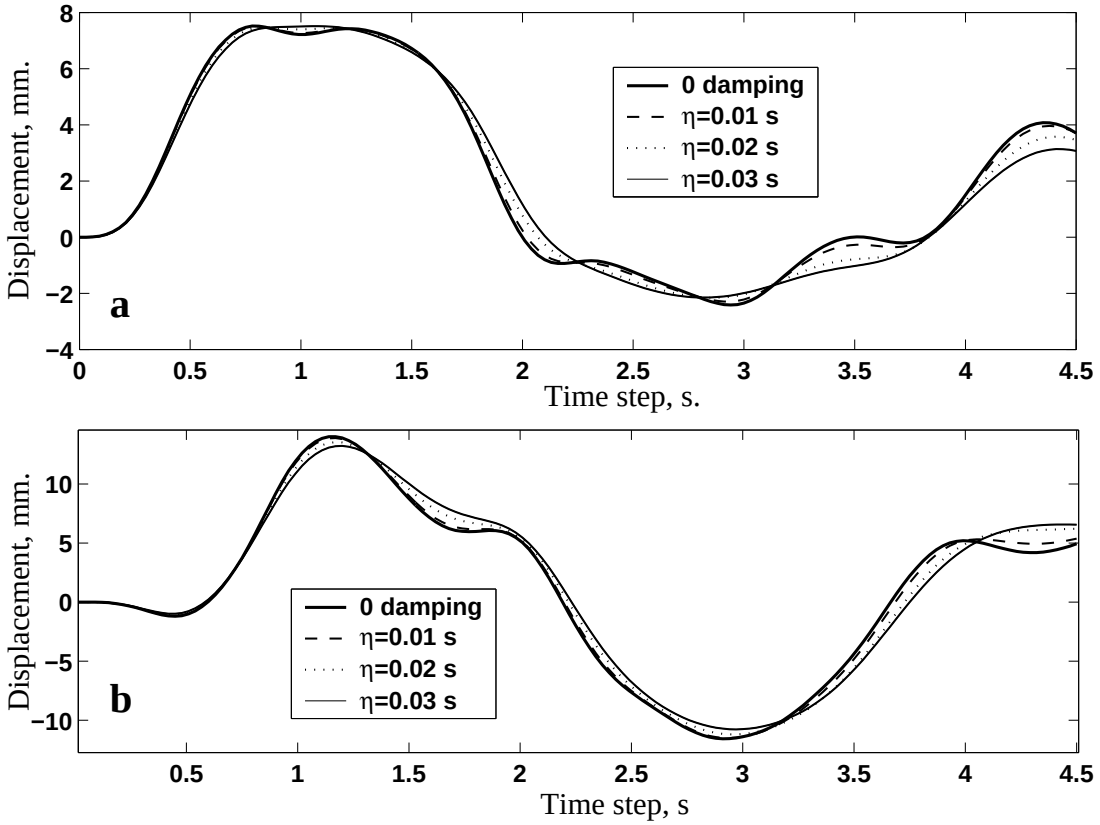

Figure 9.17: Displacement time history responses in the Y direction. (a): Tip. (b): Elbow.

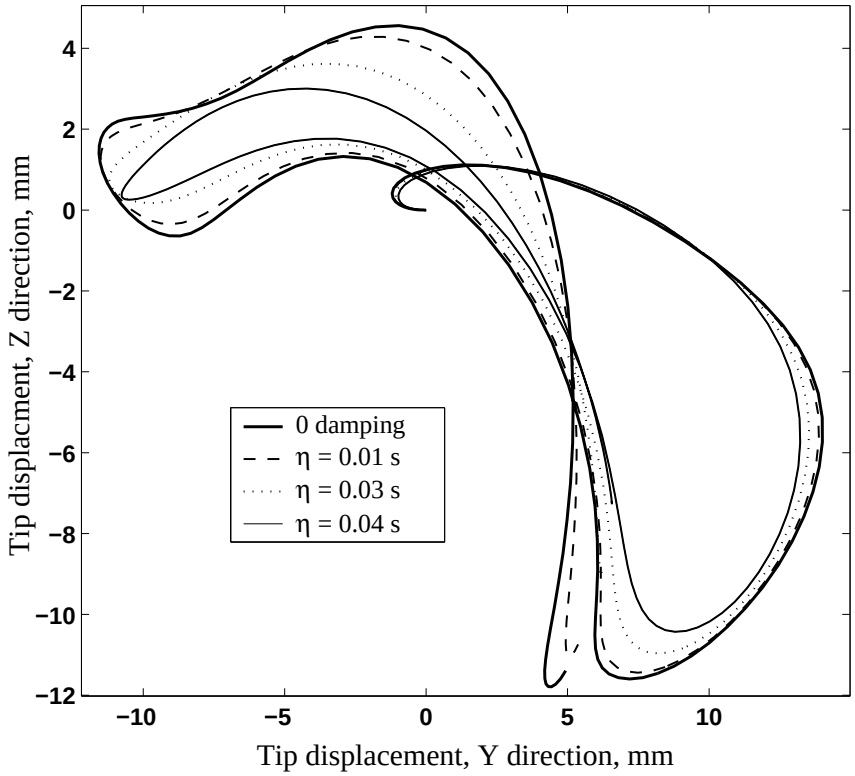

Figure 9.18: Tip displacements time history response in the Y-Z plane.

9.3.2 Near resonance response of a composite cantilever beam

This example studies the cantilever beam subjected to a sinusoidal base acceleration shown in Fig. 9.19. Different constitutive behaviors for the material are considered:

(i) Visco elastic with different viscosity values.
(ii) Visco damage model.
(iii) Composite material with two simple constituents: a visco damage phase and a rate independent plastic phase, both of them with a volumetric fraction of 50%.

The elastic properties of the three materials are the same, excepting the fracture energy (see Table 9.2). The beam has been modeled using 20 quadratic elements and a reduced integration scheme is used in order to avoid shear locking [370]; the beam cross section has been meshed into a grid of 8×8 quadrilaterals with four integration points in each of them. A linear modal analysis of the beam model gives a fundamental period of 1.77 s and the second and third modes have periods of 0.27 and 0.099 s, respectively. The dynamic nonlinear response of the beam is

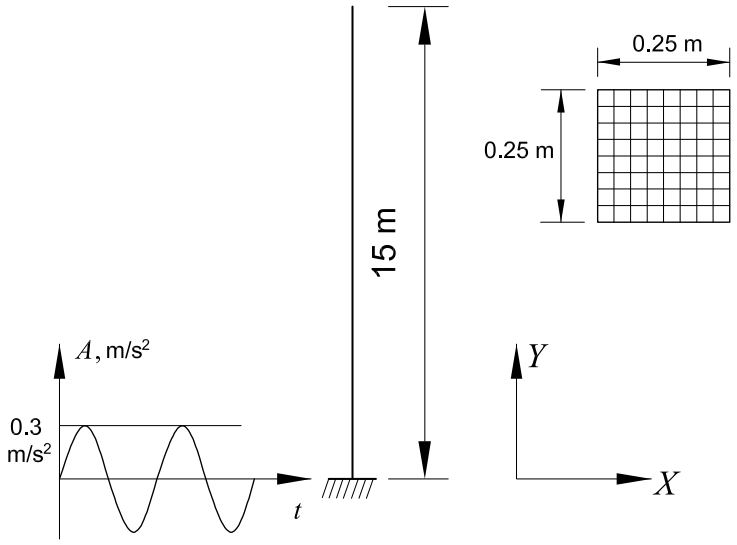

Figure 9.19: Vertical cantilever beam subjected to a sinusoidal base acceleration.

Table 9.2: Mechanical properties.

	E Mpa	ν	f_c Mpa	n	G_f Nmm^{-2}	ρ_0 Kgmm^{-3}
Rate dependent	2.5×10^4	0.20	25	1	25	2.4×10^{-9}
Rate independent	2.5×10^4	0.15	500	1	5000	2.4×10^{-9}

obtained for a sinusoidal excitation with a frequency of 1.75 s aimed to induce near–resonance effects in the first elastic mode. The time step is 0.03 s. Three values for viscosity have been considered: 0.0, 0.01, 0.025 s. Fig. 9.20 shows the displacement time history of the top node in the horizontal and vertical directions. Important reductions in the amplitude of the oscillations are obtained as the viscosity is increased. For the value of $\eta = 0.025$ s almost all the second order effects are suppressed due to reductions of the dynamic amplification of the response. Vertical displacements are reduced from 400 mm for the undamped case to 12 mm.
As it has been mentioned, due to the change of configuration of the structure near the resonance,

the displacements in the vertical direction are amplified and, therefore, axial forces with high frequency content appear in the response.
As stated in Ref. [182], the suppression of high frequency content becomes a desirable feature of a nonlinear time stepping scheme. In the present formulation, the reduction of the contribution of the higher modes to the response is obtained by adding viscous mechanisms to the constitutive laws. In Figure 9.21, the beam structure is subjected to a sinusoidal base acceleration record with a period of 0.1 s acting during 2.5 s followed by a free vibration of 2.5 s. The time step is 0.005 s. The horizontal displacement response of the top node of the system is depicted in Fig. 9.21a where it is possible to see that the a coupled response corresponding to the first and third modes dominates the structural behavior. Amplification of the the third mode is observed. It is also possible to appreciate in this figure that increments in the values of the viscosity ($\eta = 0.000, 0.001, 0.005$ s) have the effect of reducing mainly the vibration associated to the higher modes. This result is in good agreement with the solution proposed in [182] in the sense that dissipative mechanisms, for time stepping schemes, based on the strain rate or velocity contributes to eliminate the high frequency content in the response. Fig. 9.21*b* shows the temporal evolution of the energy dissipation which is a scalar quantity calculated from Eq. (4.29) at constitutive level and then integrating over the volume of the structure. It is possible to see that higher values of η implies higher dissipation rates and the stabilization of the response is achieved before. Finally, the cantilever beam is subjected to a sinusoidal base acceleration

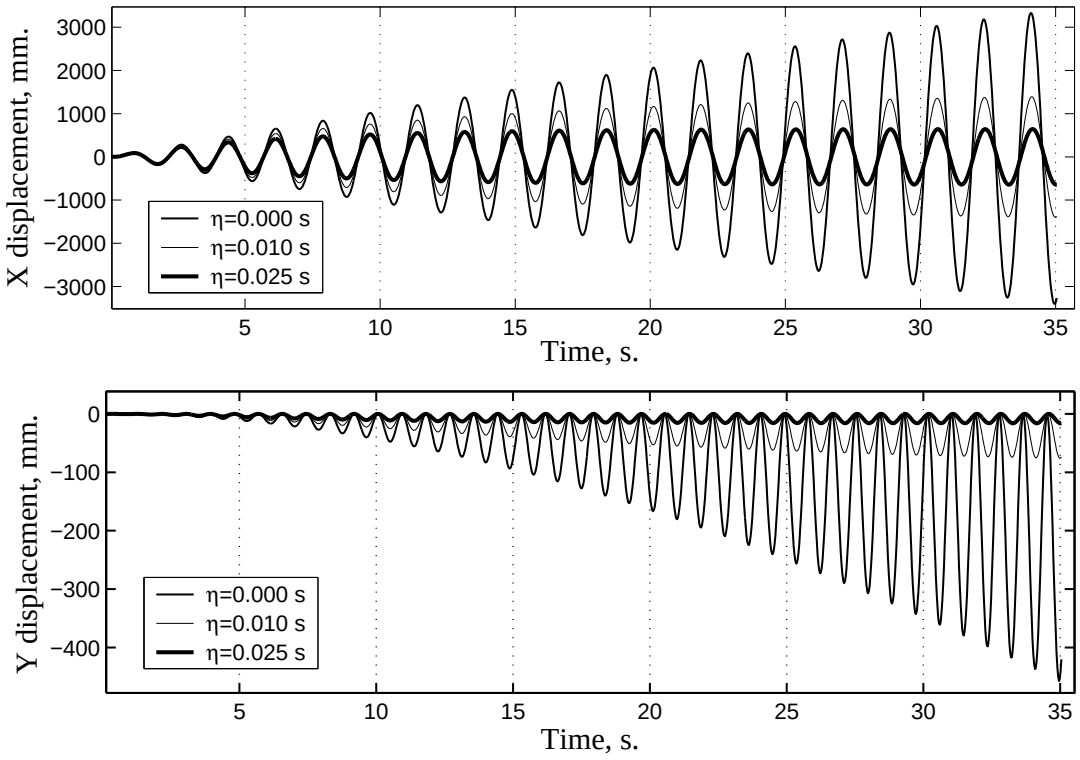

Figure 9.20: Horizontal and vertical displacement at the top.

with a period of 1.75 s and a duration of 35 s in order to induce near–resonance response. The time step is 0.03 s. The dynamic response was obtained for three constitutive options: the first one corresponds to the visco damage model with $\eta = 0.001$ s, the second one is the elastic plastic model, where the energy dissipation is obtained by displacement dependent (no viscous) mechanisms and the third one is a composite material with a 50 % of the first material and a 50%

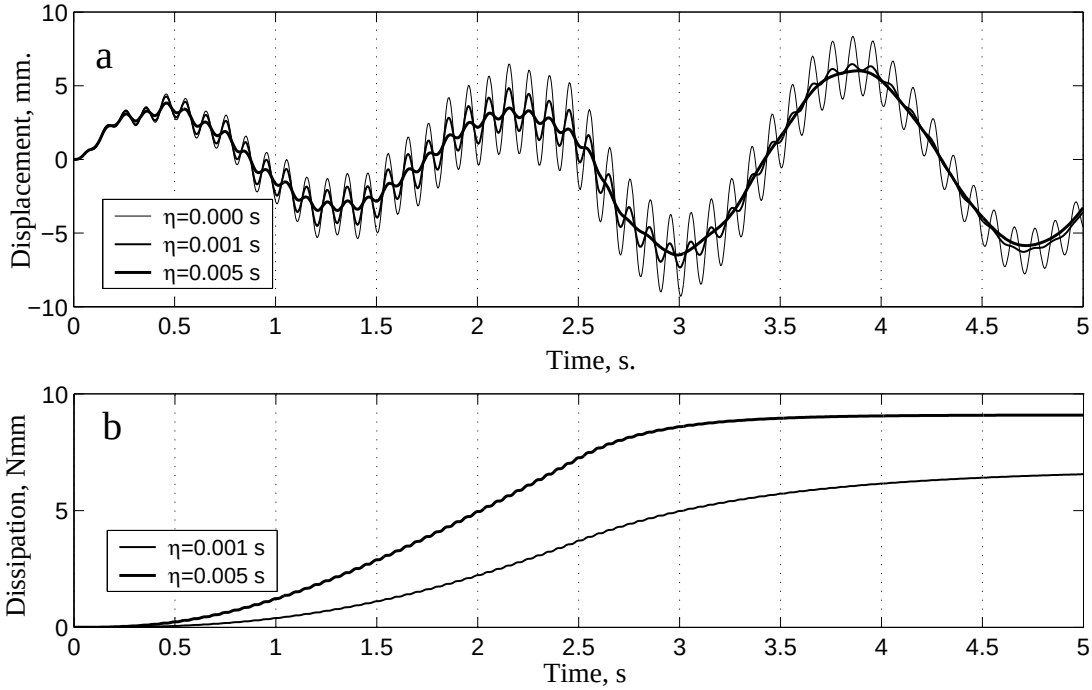

Figure 9.21: (a): High frequency content suppression. (b): Energy dissipation.

of the second one. Fig. 9.22a compares the response for the viscous damage model with the undamped elastic case. It is possible to see that the change of the mechanical properties of the material due to the progressive damage induces stiffness degradation, changing the instantaneous dynamical properties of the structure. In this case, the period of the structure is increased due to the fact that the damage auto decouples the structural response from resonance. Dissipation due to damage is added to the viscous one and, therefore, extra energy dissipation contributes to reduce the dynamic response.

Fig. 9.22b shows comparative results for the time history of the three constitutive behaviors. It is worth noting that, in the case of the composite material, when most of the material corresponding to the visco damage model has been degraded in the softening zone [258], the response of the structure is controlled by the plastic behavior. After a degrading phase between the 3 and 13 s the response of the composite coincides with that corresponding to the purely plastic model. Finally, Figs. 9.23a and 9.23b show the evolution of the global damage indices and dissipated energy for the three different constitutive options.

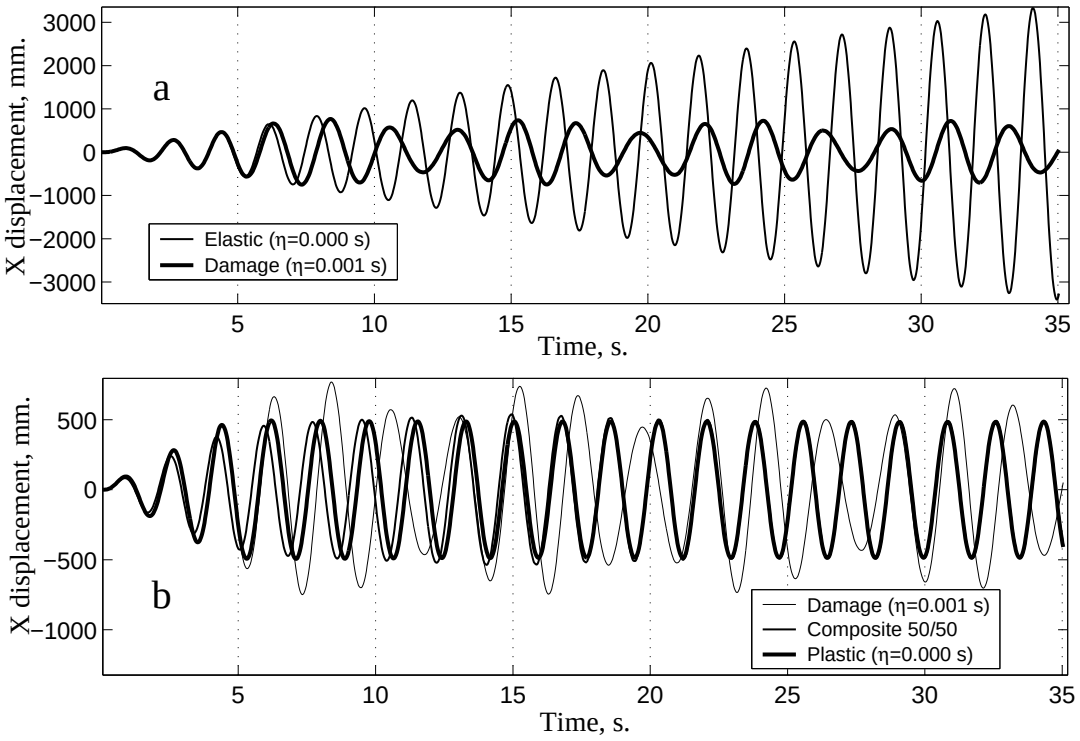

Figure 9.22: Coupled geometric and constitutive nonlinear dynamic responses. (a): Undamped elastic response compared with a visco damage constitutive model. (b): Visco damage, plastic and composite responses.

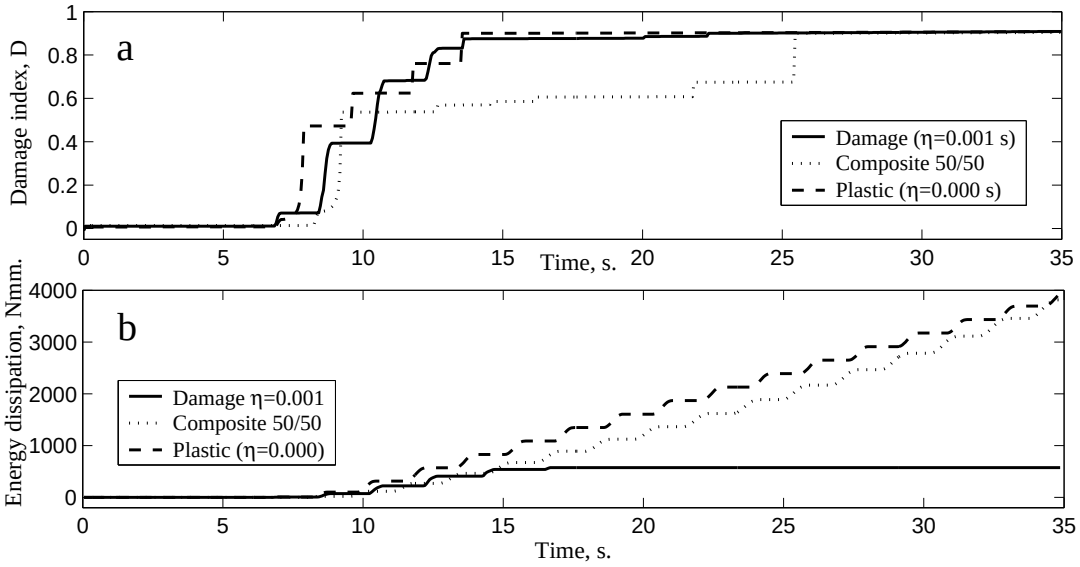

Figure 9.23: (a): Evolution of the global damage index during the dynamic response. (b): Evolution of the energy dissipation.

9.3.3 Nonlinear vibration of a spatially curved structure

The 3D structure shown in Fig. 9.24 is an open ring located in the X–Y plane, which has a fixed end and the another one is connected to a straight column lying on the X–Z plane. Two loads are applied on the points A and B in the X and Z directions respectively. The shape and duration of the loading is given in the same figure. The loading step is 0.01 s. The mechanical properties of the materials are: $E = 5 \times 10^4$ Nmm^{-2}, $\nu = 0.0$, $G_f = 1000$ Nmm^{-2}, $n = 1$, $\rho_0 = 1 \times 10^{-8}$ Kgmm^{-3} and $f_c = 8$ Mpa. Three cases are studied:

(i) Elastic case.
(ii) Visco damage model with η=0.004 s.
(iii) Rate independent plasticity with $G_f = 1 \times 10^7$ Nmm^{-2}.

The same threshold limit is used for the models (ii) and (iii). Twenty quadratic, initially

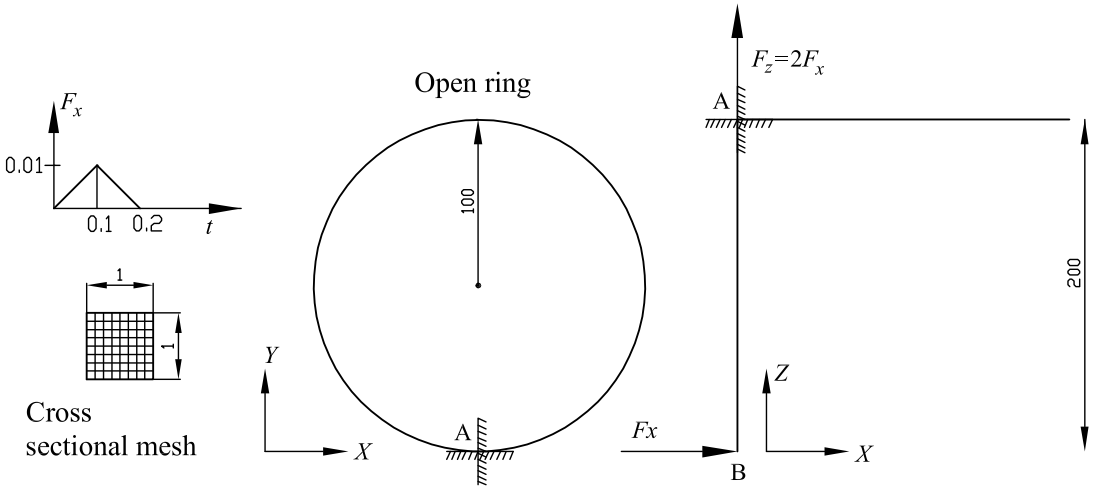

Figure 9.24: Three–dimensional curved beam structure.

curved elements are used for the ring and ten quadratic elements for the column considering two Gauss integration points. The beam cross section is meshed into a 8×8 grid of equally spaced quadrilaterals with one integration point per fiber. Due to the directions of the applied loads and the development of inertial forces, each member of the structure is subjected to a complex state of internal stresses including torsion, flexion extension and shearing. Figs. 9.25 and 9.26 show the nonlinear time history responses for the three components of the displacement of the points A and B of Fig. 9.24. It is worth to note that the displacements of the systems with inelastic behavior are greater than the elastic case due to the fact that the initial loading induces degradation and plasticity and the structure needs to develop more displacement for finding a configuration stable with the new loading state. In the plastic case the structure finally vibrates about a configuration which includes permanent deformation as it can be evidenced from the Z component of both figures.

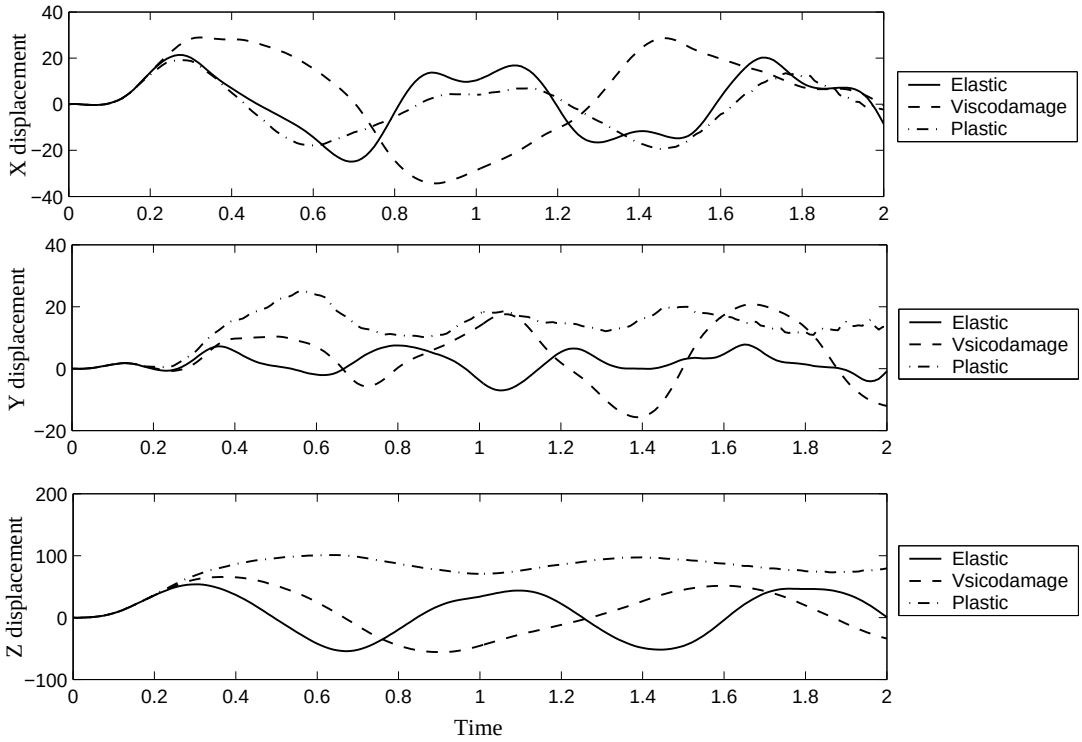

Figure 9.25: Displacement time history response of the node A.

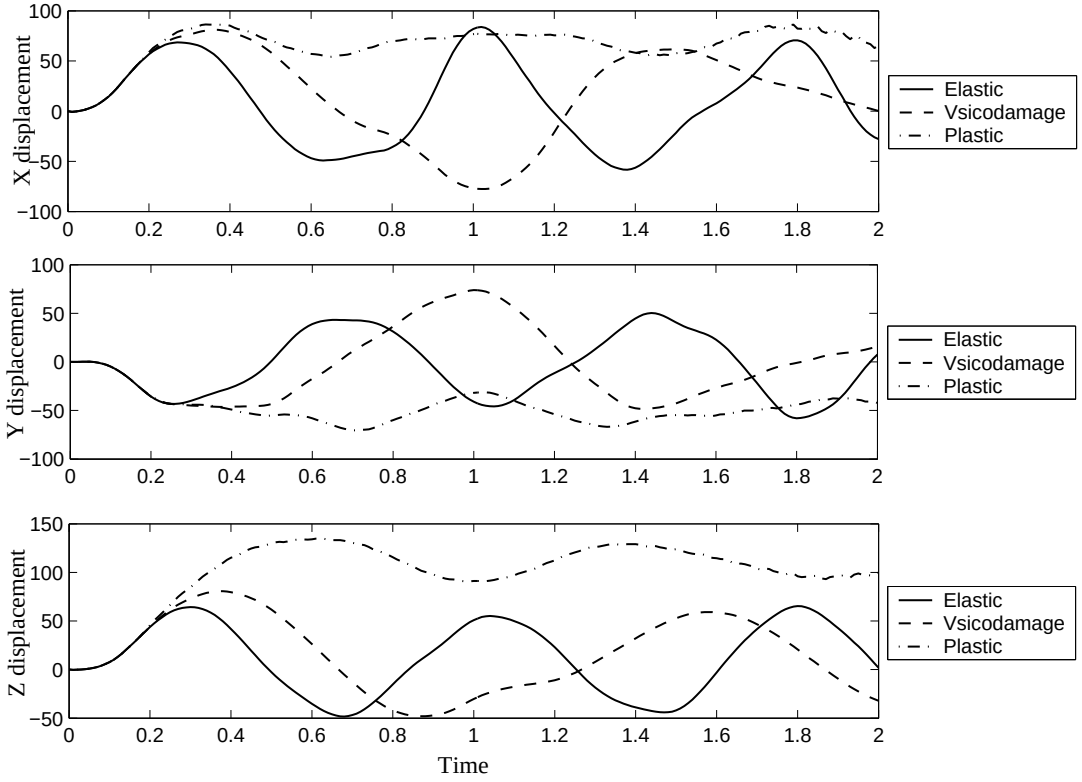

Figure 9.26: Displacement time history response of the node B.

9.4 Reinforced concrete structures

9.4.1 Experimental–numerical comparative study of a scaled RC building model

The first example corresponds to the comparison between the numerical simulation obtained by means of the proposed formulation and the experimental data obtained by Lu and reported in reference [235] for the seismic analysis of a scaled model (1:5.5) of a benchmark regular bare frame (BFR). The structure was designed for a ductility class *medium* in accordance with the Eurocode 8 [120] with a peak ground acceleration of $0.3g$ and a soil profile A. Details about loads, geometry, material properties and distribution of steel reinforcements can be consulted in the same publication. In the experimental program, the structure was subjected to several scaled versions of the N–S component of the El Centro 1940 earthquake record.
Four quadratic elements with two Gauss integration points were used for each beam and column. Cross sections where meshed into a grid of 20 equally spaced layers. Longitudinal steel reinforcements were included in the external layers as part of a composite material. The fracture energy of the damage model used for concrete was modified to take into account the confining effect of transversal stirrups [258]. A tension to compression ration of 10 was used for concrete and 1 for steel. In the numerical simulations, the model is subjected to a push–over analysis. Static forces derived from the inertial contribution of the masses are applied at the floor levels considering an inverted triangular distribution.
A relationship between the measured base shear and the top lateral displacement is given in Ref. [235] for each seismic record. This curve is compared in Fig. 9.27 with the capacity curve obtained by using the numerical push–over analysis. It is possible to see that the push–over anal-

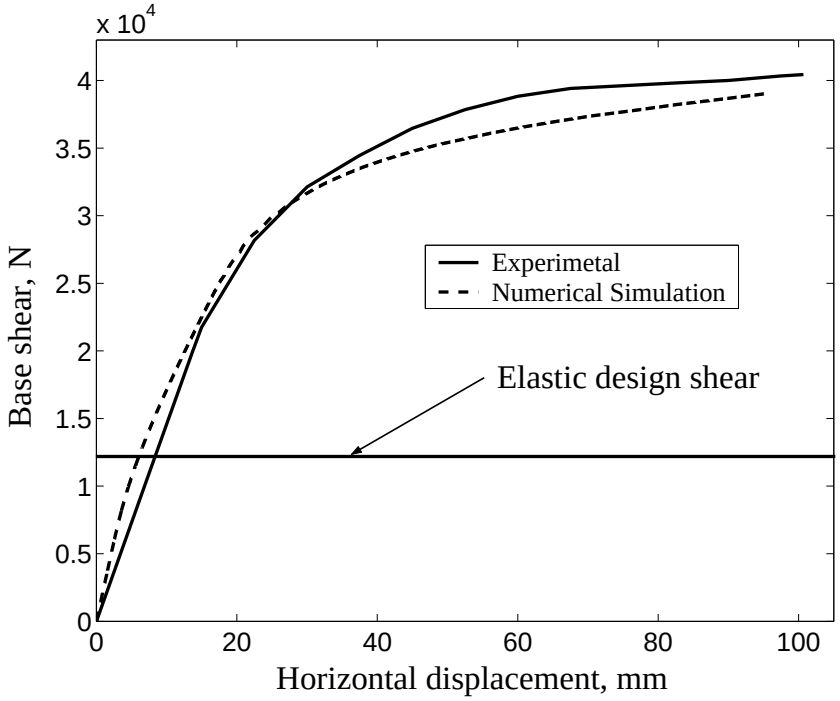

Figure 9.27: Comparison between numerical and experimental push–over analyze: Capacity curves.

ysis gives a good approximation for the global maximum response and, therefore, it constitutes

a suitable numerical procedure for estimating the expected nonlinear properties of structures subjected lo seismic actions. In the same figure, it is possible to appreciate that in both, the numerical simulation and the experimental cases, the characteristic values of the structure; that is, global ductility level, elastic limit and over–strength, are similar. Fig. 9.28 shows a comparison

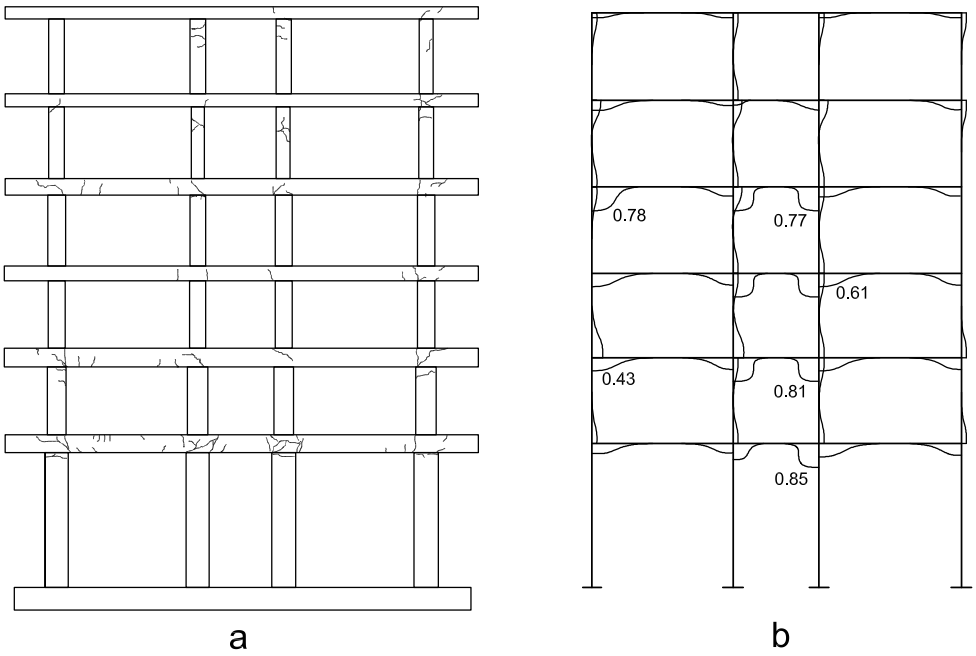

Figure 9.28: Damage. (a): Experimental: Map of fissures. (b): Numerical: Cross sectional damage index.

between the distribution of cross sectional damage predicted numerically and the map of fissures obtained after the application of several shaking table tests. In this case, the proposed damage index along with the geometric and constitutive formulation used for beams is able to reproduce the general failure mechanism of the structure where dissipation is mainly concentrated in the beam elements.

9.4.2 Study of a RC plane frame

The precise characterization of the nonlinear behavior of RC framed structures has important applications in earthquake engineering. A great amount of effort has been focused on studying the *capacity* of structures, frequently defined in terms of a set of applied horizontal forces and the corresponding lateral displacements. These curves allow to estimate several global parameters such as ductility, over-strength, yielding and collapse loads, inter story drifts and other derived damage characteristics [123, 209]. A static characterization of the response in preferred due to the fact that a nonlinear time history analysis is more expensive in computational time. In spite that capacity curves are widely accepted as valid substitutes of time history analysis, the question about if cyclic or increasing loads paths are more convenient to obtain the curves, stays still opened [123].
In this work the capacity curve of the RC structure described in Fig. 9.29 is obtained for two loading conditions: An increasing load and a cyclic load, both of them applied on the top floor. The RC frame is typical for an urban building, with a first floor higher than the others. The building was seismically designed according to the Eurocode 8, for firm soil, a base acceleration

of $0.3g$ and a ductility reduction factor of 4 [120]. Both geometric and constitutive nonlinear

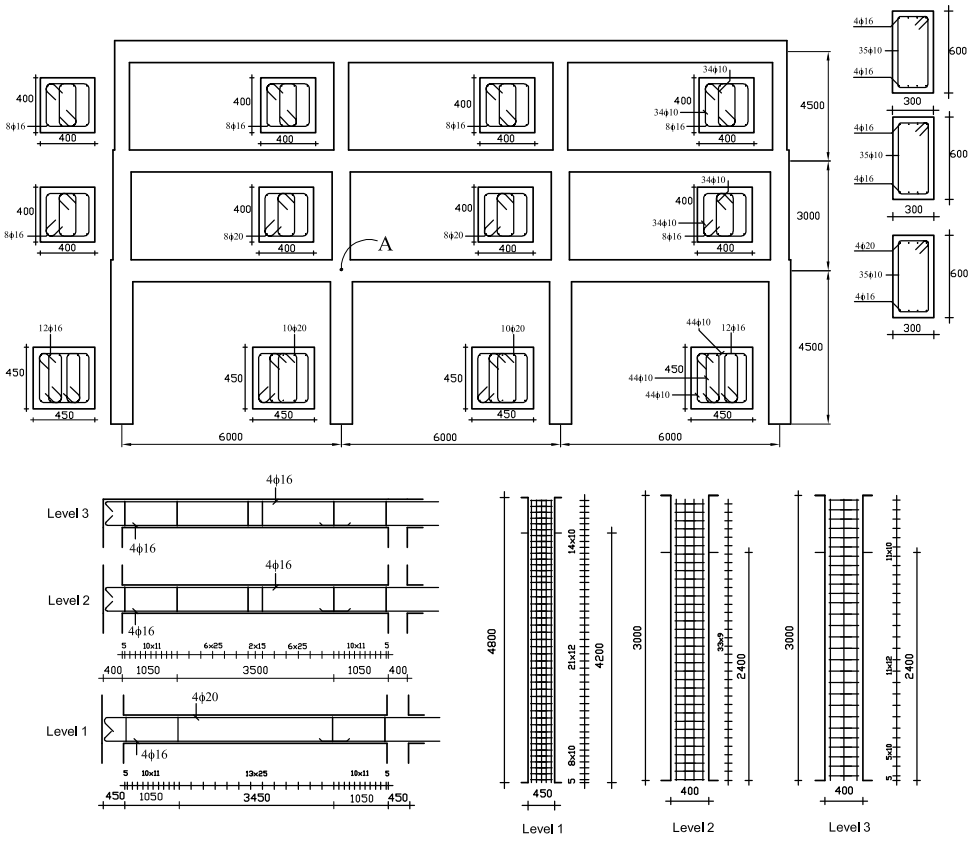

Figure 9.29: RC planar frame details.

behaviors are considered in the model, which is defined using 4 quadratic elements with two Gauss integration points for each beam or column. The mechanical properties of the materials are the same as those given in the Table 9.2 but the tensile fracture energy of the concrete takes values between 1.5 and 3.0 N-mm, corresponding to different steel ratios of the stirrups.

The capacity curve is obtained by means of numerical simulations with load control on the horizontal displacement of the right top node of the structure. This method allows to advance beyond the conventional collapse point, on the softening branch of the capacity curve. The results are shown in Fig. 9.30, where it is possible to see that the curve defined by the increasing load test is the envelop of the maximum values of the results of the cyclic test.

The global damage indices for both simulations are shown in Fig. 9.31. It is possible from this figure that, for the case of a cyclic action, the structure maintains low values of the damage index during more time than in the case of an increasing load. This result is in a good agreement with the well know result that pulse like actions are much more destructive than cyclic actions.

Finally, Fig. 9.32 shows the moment-curvature relationship for the elements converging to the joint A OF Figure 9.29, for both increasing and cyclic loads. It is possible to see that most part of the energy dissipates in the beams during the cyclic loading. This observation is in agreement with the expected behavior of well designed frames, with weak beams and strong columns. The results for the increasing and cyclic load simulations of Fig. 9.32 allow to see the formation of a plastic hinge: the moment-curvature curve presents a highly nonlinear hysteretic behavior. The large incursion in the nonlinear range for the case of the increasing load can help to explain why the global damage index grows faster than for cyclic loads.

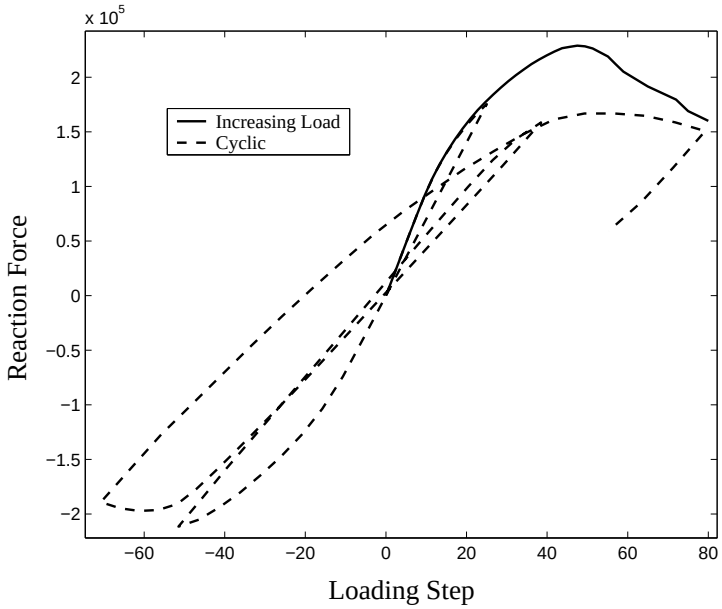

Figure 9.30: Increasing loading versus cyclic loading.

The previously described geometric and constitutive nonlinear dynamic formulation for beams has been implemented in a FEM computer code. In this section several numerical examples illustrating the capacities of the model for predicting the dynamic behavior of beam structures including rate dependent effects are presented.

9.4.3 Dynamic study of a RC beam structure

This example studies of the fully geometric and constitutive static and dynamic behavior of the RC beam structure shown in Fig. 9.33. The structure was seismically designed according to the Euro-code 8, for firm soil, a base acceleration of $0.4g$ and a ductility reduction factor of 6. The distribution of steel reinforcements are given in the same figure and Table 9.3. The precise analysis of the response allows to carry out a safer determination of the seismic design parameters, such as: damage, ductility, overstrength, collapse load, inter story drifts, energy dissipation capacity, etc. [123, 209]. The study of the time evolution of the local damage index throughout the structural elements provides relevant information about the structural zones where ductility demand and energy dissipation are concentrated. These results allow validating and improving the engineering design of buildings located in high seismic areas.
The model is developed using four quadratic elements with two Gauss integration points in each structural element. Most of the mechanical properties of the materials are given in Table 9.4. Each cross section is meshed into a grid of 8×8 quadrilaterals with one integration point by fiber. The tensile fracture energy of the concrete takes values between 3 and 6.0 Nmm^{-2}, corresponding to different steel ratios of the stirrups. The mass density of the concrete of the beams is modified in order to consider the mass contribution of the dead and live loads acting at the corresponding floor level. A viscosity value of $\eta = 0.001$ s has been supposed for the concrete. A linear modal analysis reveals that the periods of the first four modal shapes are: 1.20, 0.36, 0.19 and 0.12 s, respectively.
Firstly, a static *pushover* test using the inverted triangular loading path is performed in order to obtain the characteristic *capacity curve* of the structure expressed in terms of the horizontal

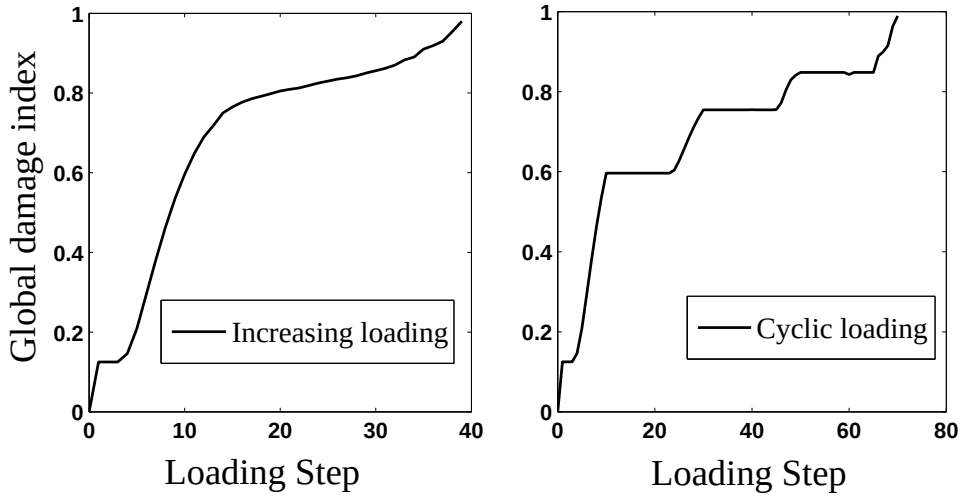

Figure 9.31: Global damage indices.

Table 9.3: Steel reinforcement details of the different zones of the building.

Zone	1	2	3	4	5	6
Section type	C1	C1	C2	C2	C3	C3
Stirrup	ϕ12@12	ϕ12@15	ϕ12@12	ϕ12@15	ϕ12@12	ϕ12@15
Zone	7	8	9	10	11	12
Section type	C4	C4	C5	C5	C6	C6
Stirrup	ϕ12@12	ϕ12@15	ϕ10@12	ϕ10@15	ϕ10@12	ϕ10@15
Zone	13	14	15	16	17	18
Section type	B1	B1	B2	B2	B3	B3
Stirrup	ϕ12@12	ϕ12@20	ϕ12@12	ϕ12@20	ϕ10@12	ϕ10@20

displacement of the left top corner node and the horizontal reaction on the supports. Even if capacity curves are widely accepted as valid substitutes of time history analysis, the question about if dynamic or increasing load paths are more convenient to obtain capacity curves, stays still opened [123]. Secondly, the structure is subjected to an increasing sinusoidal base acceleration of period 1.2 s for inducing a near to resonance response, with minimum and maximum values of acceleration of 50 and 200 mms^{-2}, respectively. The time step is 0.04 s.
The capacity curve obtained by means of the pushover analysis and the hysteretic cycles in the dynamic case are superposed in Fig. 9.34, where it is possible to see that the capacity curve underestimate the real response of the the structure for the low amplitude hysteretic cycles. After an important degradation of the concrete has occurred, the hysteretic cycles are enclosed by the capacity curve. This fact justifies the employment of push-over response curves for predicting the seismic response of regular buildings, due to the fact that frequently, during a seismic action, the first movements contribute to the initial cracking of the concrete and, when the strongest vibrations have place, the response of the structure should be limited by the capacity curve case. The global ductility value, estimated from the capacity curve is about 6, in good agreement with the hypothesis of design.
The evolution of the local damage indices provides more precise information about the ductility demand and energy dissipation demand for the principal structural members. Fig. 9.35*a* shows the evolution of the local damage index for the static case. It is possible to see that the nonlinear

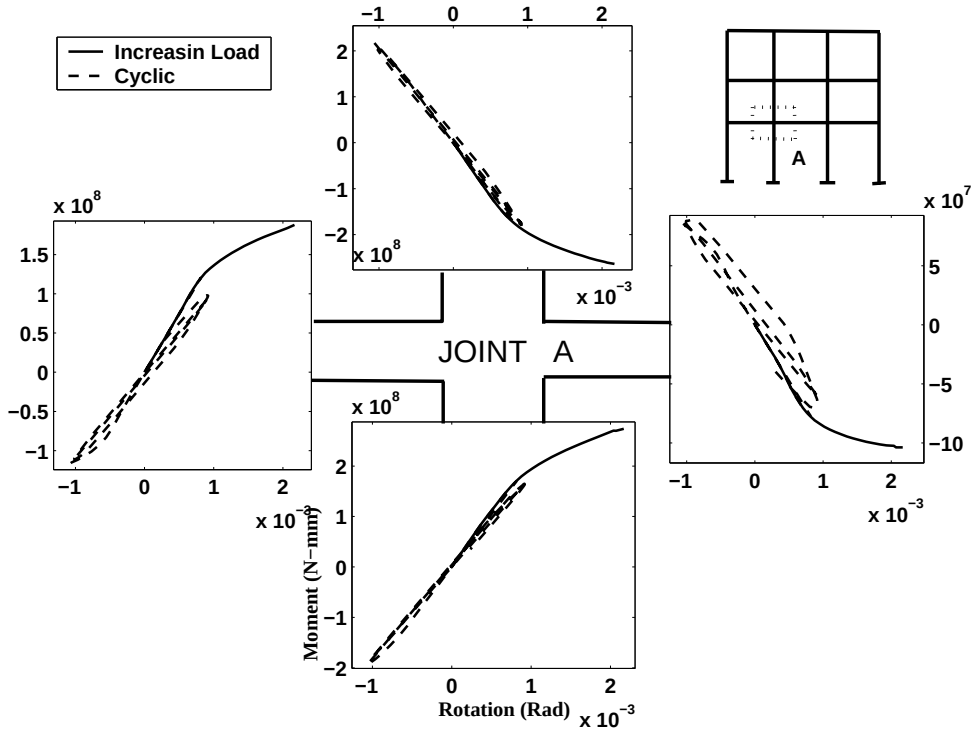

Figure 9.32: Plastic hinge.

Table 9.4: Mechanical Properties of the materials.

	E Mpa	ν	f_c Mpa	n	G_f Nmm^{-2}
Concrete	21000	0.20	25	8	1
Steel	200000	0.15	500	1	500

behavior is concentrated mainly in the beam elements of the first three floors and in the base columns. This result is in good agreement with the design guidelines included in most of the modern seismic codes, that is, the building was designed with weak–beams and strong–columns aiming to dissipate the energy without affecting the global stability of the structure. Moreover, the concentration of damage at the base of the columns indicate that these members should be provided with extra reinforcements in order to obtain large inelastic incursions without brittle failures. The diagram of Fig. 9.35*a* shows the evolution of the damage index corresponding to the static case while Fig. 9.35*b* shows the the corresponding to the dynamic case. It is possible to see that the failure mechanisms are similar with energy dissipation concentrated in the beams and in the base of the columns.

It is worth to note that even although the fiber model allows to predict complex nonlinear structural responses in both, static and dynamic cases, the numerical cost of the cross sectional analysis can be significants when compared with the lumped nonlinear models. In this case, a typical cross section meshed into a grid of 8×8 quadrilaterals with 3 materials requires solving 3×8×8 constitutive equations. After that, a cross sectional integration procedure is required in order to obtain the reduced forces and tangential tensors. In contrast, only one integration procedure is carried out for lumped models.

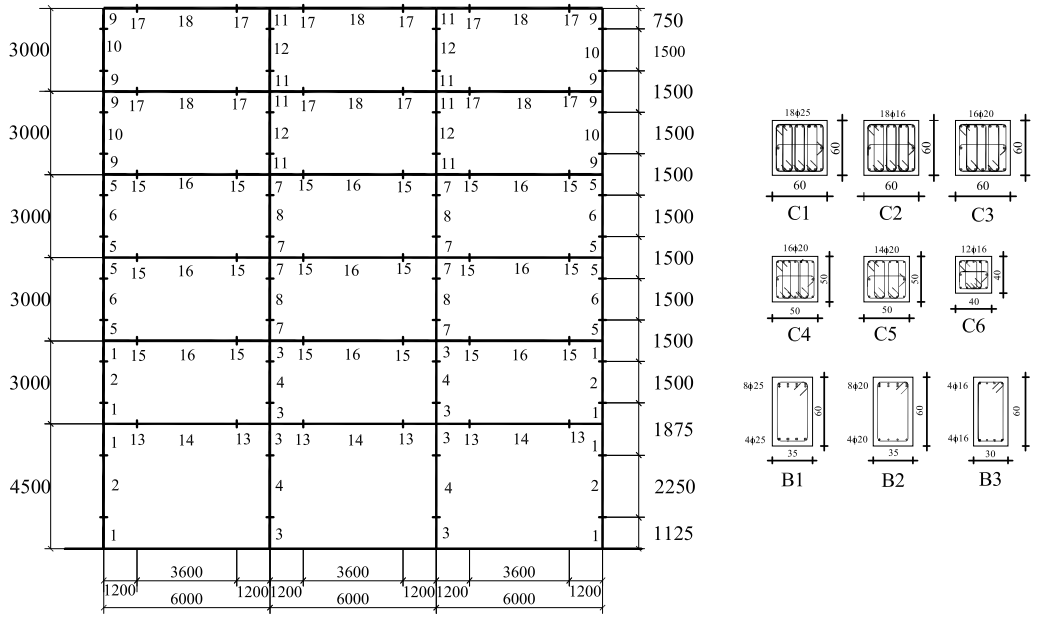

Figure 9.33: Structural model of the RC planar frame.

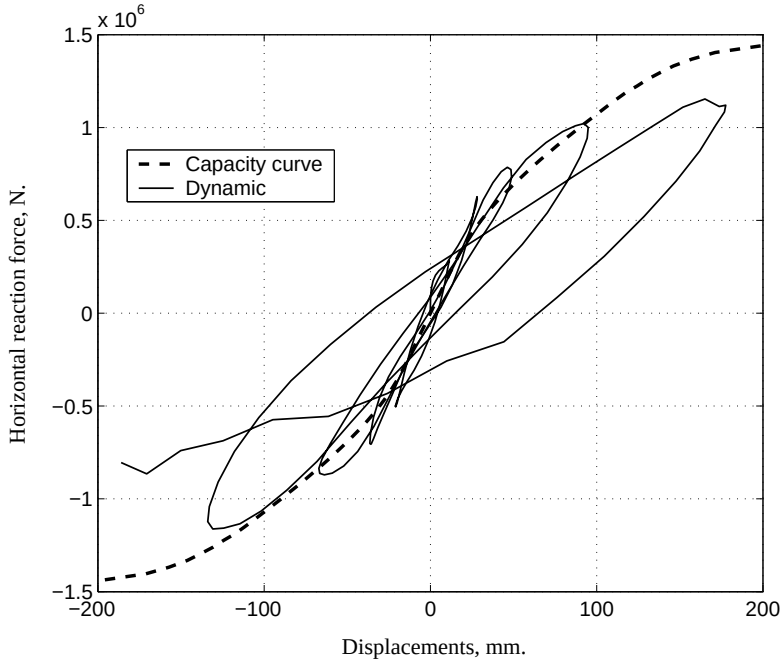

Figure 9.34: Horizontal displacements versus base reaction for the static pushover and the dynamic analysis.

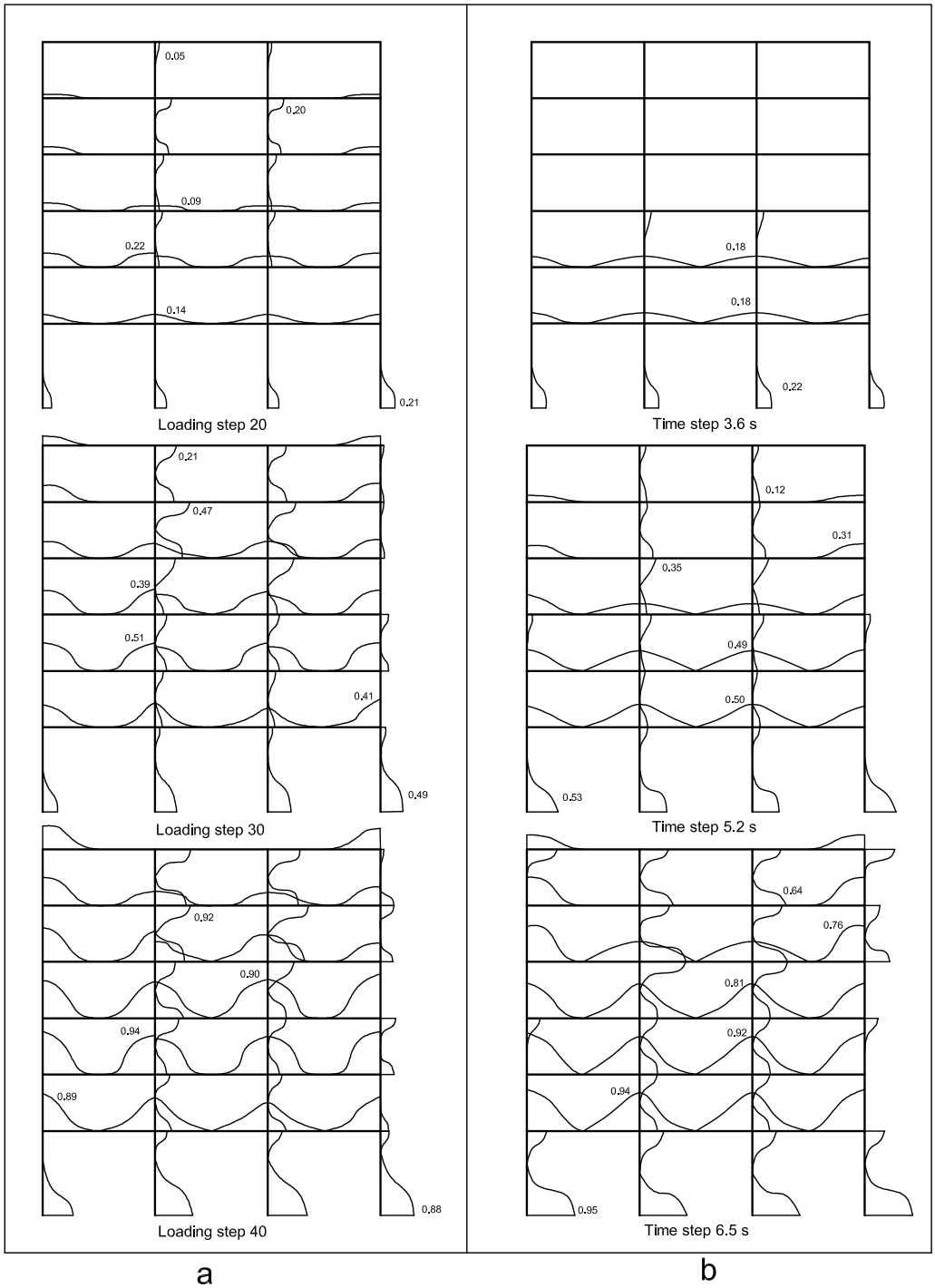

Figure 9.35: Evolution of the local damage indices. (a): Pushover analysis. (b): Dynamic case.

9.5 Precast concrete structures

9.5.1 Seismic response of a precast RC building with EDDs

The nonlinear seismic response of a typical precast RC industrial building shown in Fig. 9.36 is studied. The building has a bay width of 24 m and 12 m of inter–axes length. The story hight is 12 m. The concrete of the structure is H-35, (35 MPa, ultimate compression), with an elastic modulus of 290.000 MPa. It has been assumed a Poisson coefficient of $\nu = 0.2$, a tension/compression relation of 10 and a fracture energy of g_f =1 N/mm^{-2}. The ultimate tensile stress for the steel is 510 MPa with $\nu = 0.15$, $g_f = 500$ N/mm^{-2} and elastic modulus of 200000 MPa. This figure also shows some details of the steel reinforcement of the cross sections. The dimensions of the columns are 60x60 cm^2. The beam has an initial high of 40 cm on the supports and 140 cm in the middle of the span. The permanent loads considered are 1000 N/m^2 and the weight of upper half of the closing walls with 225.000 N. The input acceleration is the same as in the example of §9.4.1.

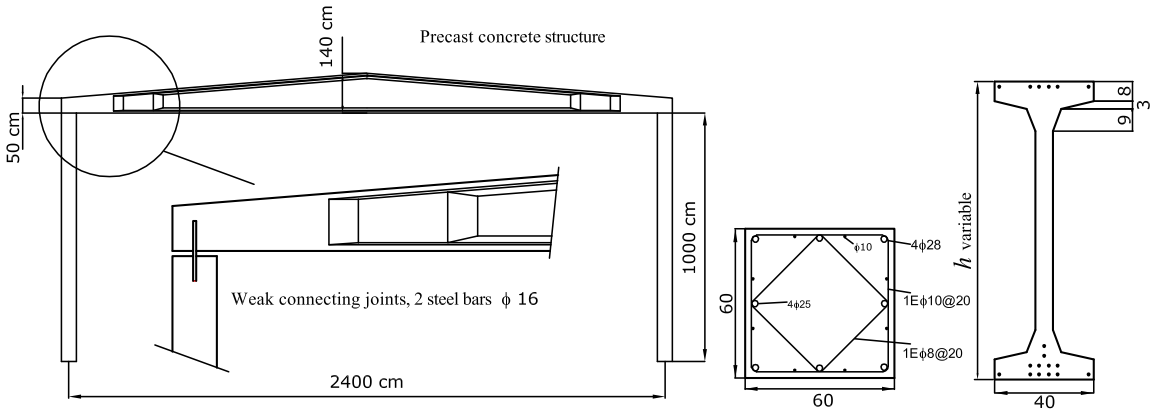

Figure 9.36: Description of the structure.

The building is meshed using 8 quadratic elements with two Gauss integration points for the resulting beam and column. The cross sectional grid of fibers is shown in Fig. 9.48. One integration point is used for each quadrilateral. The EDD was simulated by means of employing the previously described model reproducing a purely plastic dissipative mechanism. The properties of the device were designed for yielding with an axial force of 200.000 N and for a relative displacement between the two ending nodes of 1.2 mm. Hardening or viscous effects were not considered. The length of the devices was of 3.1 m. First, a set of numerical static pushover analysis are performed considering the following cases:

(i) The bare frame under small displacements assumption.
(ii) The bare frame in finite deformation.
(iii) The frame with EDDs and small deformation.
(iv) Idem as (iii) but with finite deformation.

The purpose is to establish clearly the importance of considering second order effect coupled with inelasticity in the study of flexible structures.

Figure 9.49*a* shows the capacity curves obtained for the four mentioned cases. In this figure it is possible to see that for both, the controlled and uncontrolled cases, the small strain assumption overestimate the real load carrying capacity of the structure, due to the fact that the vertical load derived from the weight comprise the columns contributing to control the cracking and

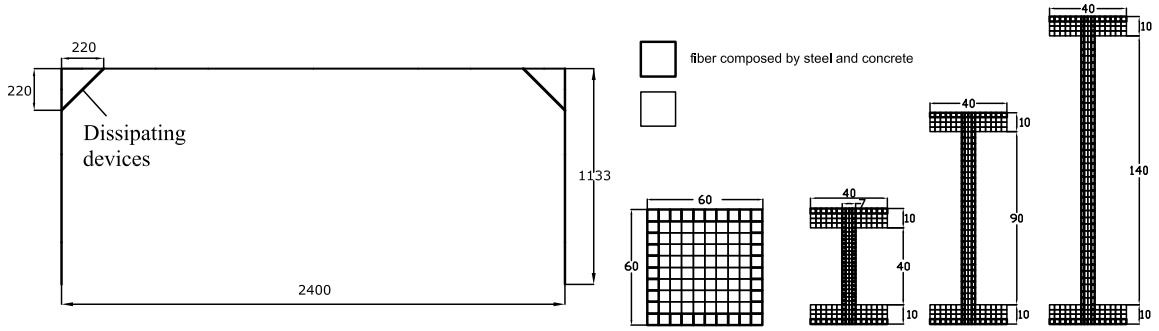

Figure 9.37: Model of the precast industrial frame with energy dissipating devices and meshes of the beam cross sections.

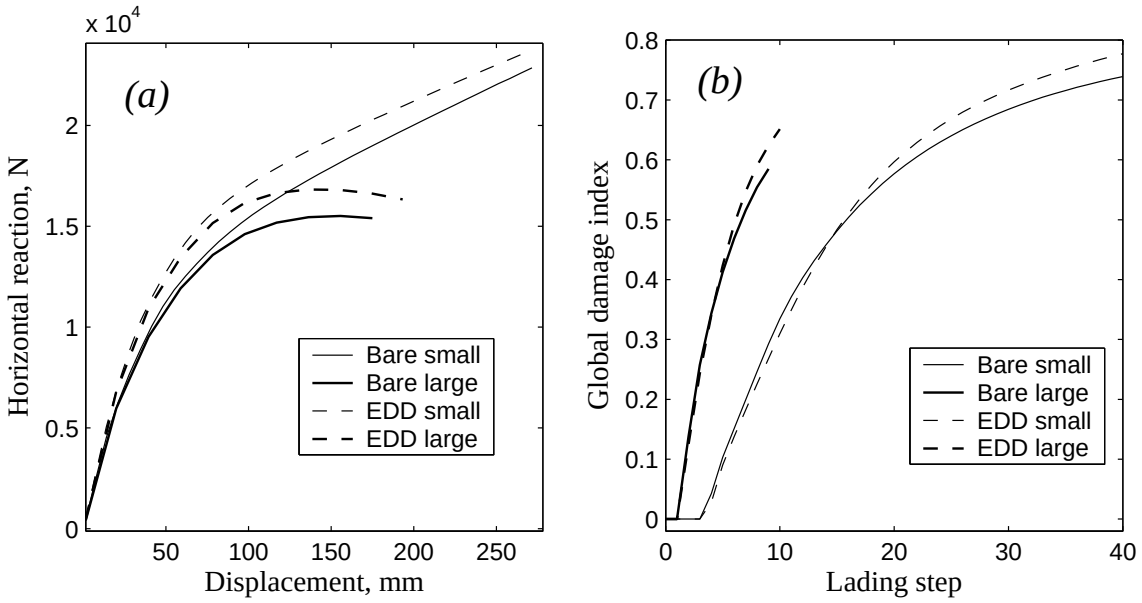

Figure 9.38: (a): Capacity curves. (b): Evolution of the global damage index.

degradation due to the lateral loading. In the case of finite deformation, the so called P–Δ [403] (second order) effects are taken into account and an anticipated strength degradation is observed for displacements over 60 mm which is a lateral displacement level expectable under strong seismic excitations. Additionally, the incorporation of EDDs increases the stiffness and the yielding point (at global level) of the structure without affecting the global ductility. Is is worth to note that the softening behavior observed for the finite deformation model is not captured in the cases (i) and (iii).

Figure 9.49b presents the evolution of the global damage index for the cases (i)–(iv). Here it is possible to appreciate that the global damage index grows quickly for the cases when finite deformation is considered and the benefits of adding EDDs are not visible due to the fact that the pushover analysis does not takes into account energy dissipation criteria.

On another hand, the results of the numerical simulations in the dynamic range allow seeing that the employment of plastic EDDs contributes to improve the seismic behavior of the structure for the case of the employed acceleration record. Figure 9.50a shows the hysteretic cycles obtained from the lateral displacement of the upper beam–column joint and the horizontal reaction (base shear) in the columns for the structure with and without devices. It is possible to appreciate

that the non–controlled structure (bare frame) presents greater lateral displacements and more structural damage, (greater hysteretic area than for the controlled case). Figure 9.50*b* shows the hysteretic cycles obtained in the EDD, evidencing that part of the dissipated energy is concentrated in the controlling devices, as expected. Figure 9.6.3 shows the time history response

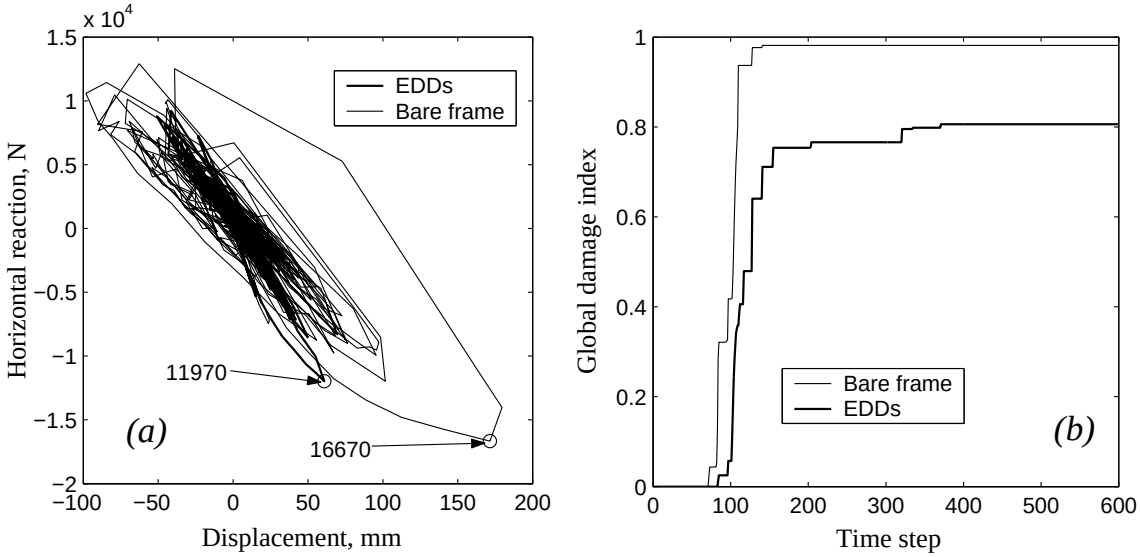

Figure 9.39: (*a*): Base shear–displacement relationship. (*b*): Evolution of the global damage index.

of the horizontal displacement, velocity and acceleration of the upper beam–column joint for the uncontrolled and the controlled case. A reduction of approximately 65.5 % is obtained for the maximum lateral displacement when compared with the bare frame. Acceleration and velocity are controlled in the same way, but only 37.9 and 26.9 % of reduction is obtained. A possible explanation for the limited effectiveness of the EDD is that the devices only contribute to increase the ductility of the beam–column joint without alleviating the base shear demand on the columns due to the dimensions of the device and its location in the structure. By other hand, joints are critical points in precast structures and therefore, the employment of EDDs combined with a careful design of the columns can help to improve their seismic behavior.

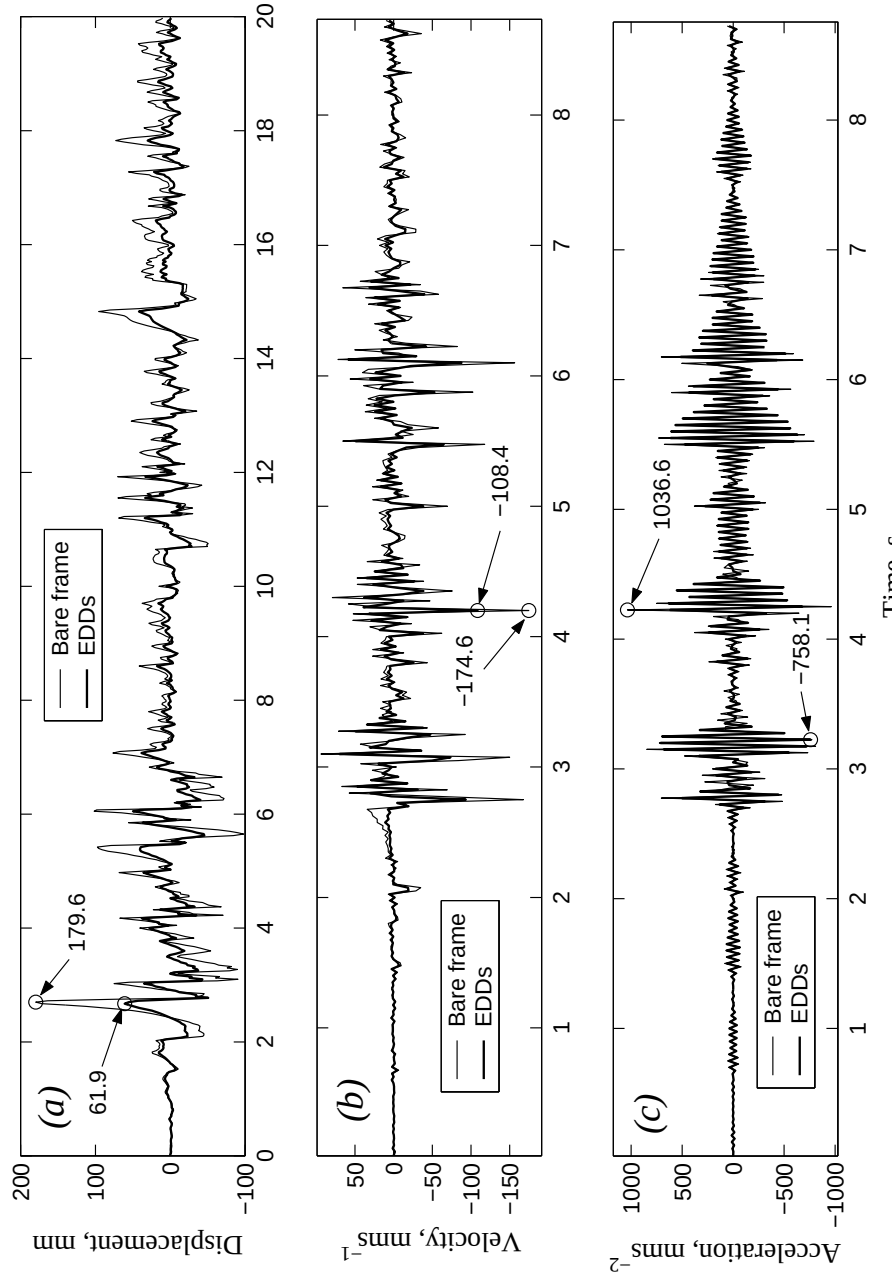

Figure 9.40: Time history responses of the top beam–column joint. (a): Horizontal displacement. (b): Velocity. (c): Acceleration.

9.5.2 Seismic response of a 3D urban building with EDDs

This example corresponds to the study of the seismic nonlinear response a 3-storey urban building designed according to the Eurocode 8 [120] for a ductility class medium, a soil profile A with a peak ground acceleration of $0.2g$, see Fig. 9.41*a*. The main purpose of this example consist into show the ability of the proposed formulation for simulating the geometric and constitutive nonlinear behavior of a 3D structure with and without EDDs, highlighting some complex phenomenon such as the torsional response coupled with P–Δ effects for the case of a nonuniform distribution of mass. The building is subjected to an scaled version of the N–S component of the El Centro earthquake record to obtain a peak acceleration of $0.3g$ greater than the maximum horizontal load allowed by design. The loading is applied according to the axis A–B og Fig. 9.41*a*. The mechanical properties for steel and concrete are the same as in example 9.5.1.

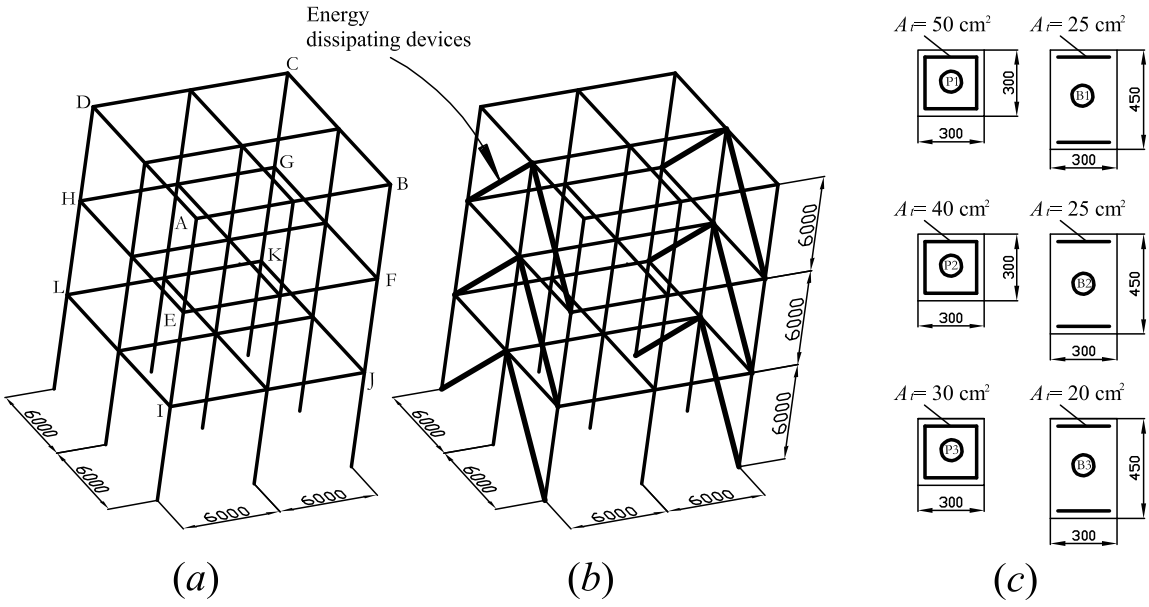

Figure 9.41: 3–storey urban building. (*a*): Bare frame. (*b*): Structure with EDDs incorporated. (*c*): RC detailing.

Inertial forces are considered as those derived from the contribution of the mass corresponding to a concrete floor of 130 mm thickness along with the sum of dead and live loads of 2500 N/mm^2 (uniformly distributed on the floors). Structural torsion is induced adding two point masses on the top corners of the right face of the building with values corresponding to the 10% of the total floor's mass. Therefore, even when the seismic record is applied in one direction, coupled displacement will appear in the another one due to inhomogeneous distribution of masses.
Several practical aspects of the performance of a engineering structure can be considered: structural torsion, distribution of the damage, over-strength and ductility. This situation is particulary important for seismic loading due to the fact that modern design takes into account the capacity of the structure to resist loads with an adequate combination of strength, ductility and flexibility. In this case, realistic studies involve material nonlinearities as well as geometric effects. Three cases are considered:

(i) Bare building (full nonlinear model).
(ii) Elastic bare equipped with viscous EDDs. The location of the viscous devices is shown in Fig Fig. 9.41*b* and their mechanical properties are: (i) A linear viscous coefficient of

$c_d = 10.000$ Ns^{-1} with (ii) an exponent of $n = 0.5$ (see §8.1.1).

(iii) Full nonlinear model of the building equipped with viscous EDDs (idem mechanical properties as in (ii)).

The purpose of including the case (ii) is to investigate what is the influence on the structural response of the widely used (*a priori*) assumption that considers the building's structure remaining elastic as consequence of the benefits obtained from EDDs.

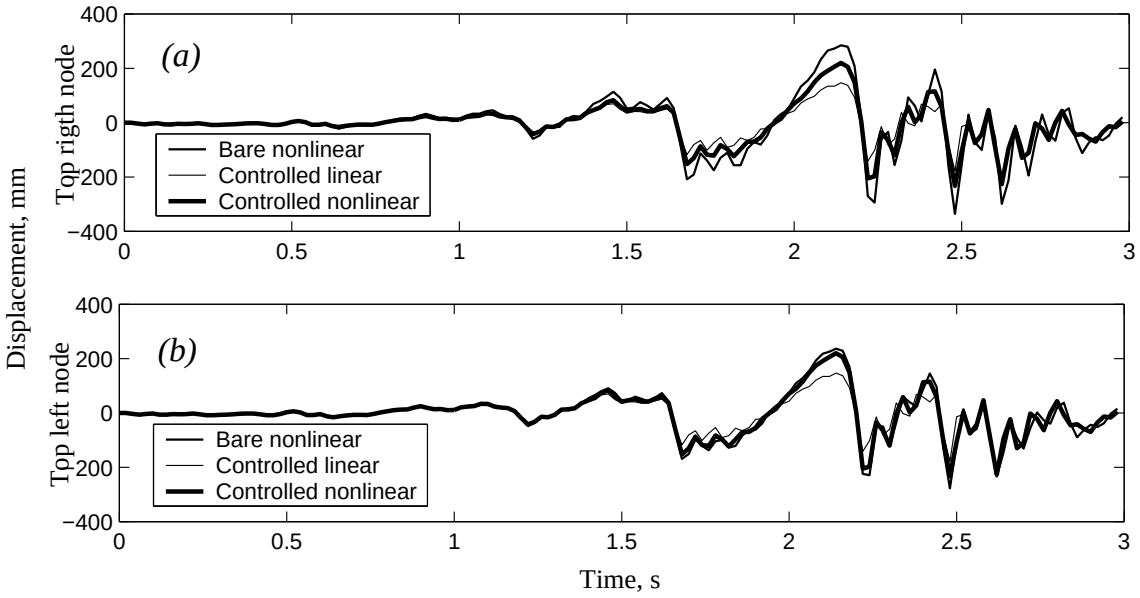

Figure 9.42: Displacement time history response in the direction of the applied record. (a): Node B. (b): Node C.

The displacement time history responses of the nodes B and C of the building in the direction of the applied record are shown in Fig. 9.42a and 9.42b, respectively. The difference observed in these figures is due to the fact that the torsional effect due to the inhomogeneous distribution of masses induces a rotational motion about the inertial center of the floors. Additionally, it is possible to appreciate that the use of the proposed viscous dampers contributes to alleviate the maximum global displacement demand decreasing the response about a 25%. However, another important result is given by the fact that clearly the *a priori* consideration that the main structure remains elastic underestimates the displacement demand and therefore, the ductility demand on the structural elements.

By the other hand, Fig. 9.43a and 9.43b shows the displacement time history response of the nodes C and D in the direction perpendicular to the application of the loading. Therefore, they are produced due to the torsion. The main two aspect that have to be highlighted in this case are: (i) Again the assumption of a linear bare structure is not able to capture appropriately the torsional components of the motion and (ii) The inclusion of viscous EDDs can alleviate significatively the torsional response in the nonlinear range. It has to be noted, however, that the masses added in the present example are rather small compared with the total one.

It is worth noting that damage appears on column elements due to the poor seismic considerations taken into account in the design (weak column-strong beams). Evolution of the global damage index is presented for the full nonlinear controlled and uncontrolled cases in Fig. 9.44. In the same manner as before, the benefits obtained from the application of EDDs are clearly evidenced.

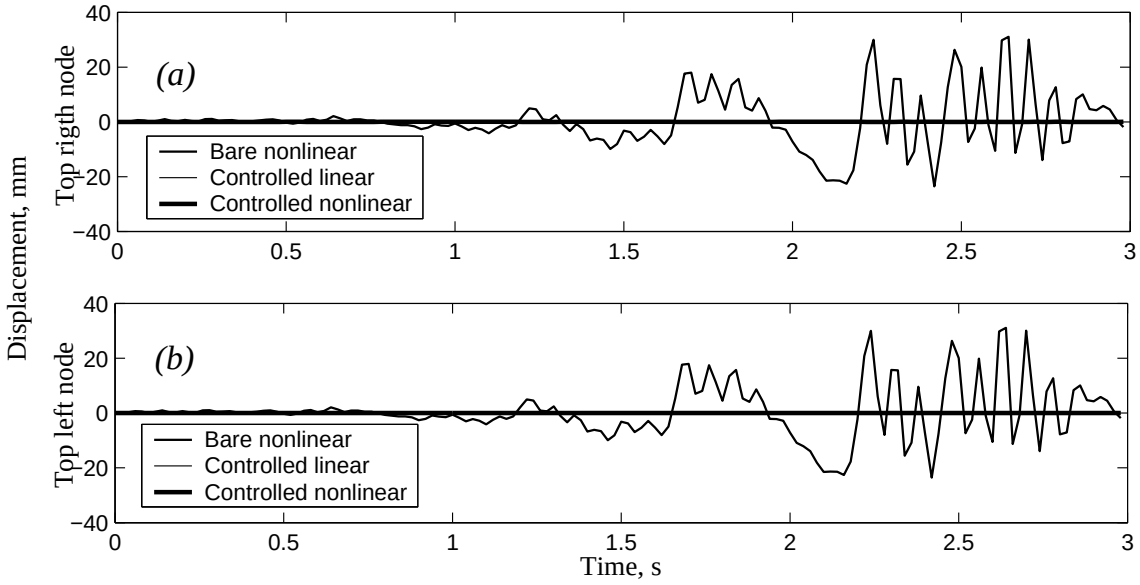

Figure 9.43: Displacement time history response in the direction of the applied record. (a): Node C. (b): Node D.

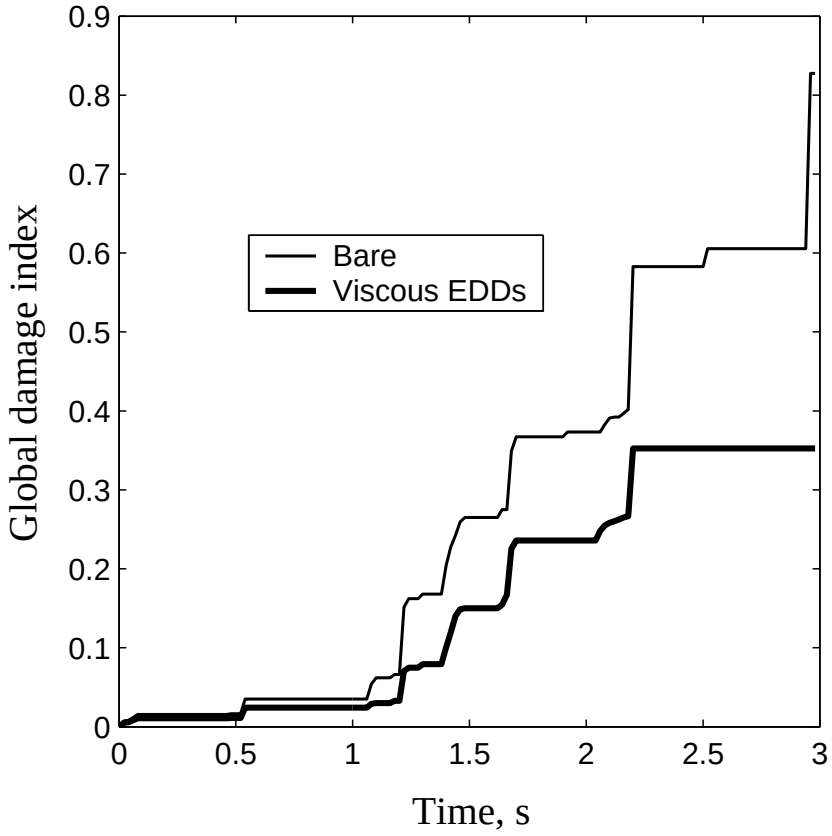

Figure 9.44: Time history response of the global damage index.

9.6 Two–scale model: Numerical simulations

9.6.1 Elastic example

The fist example corresponds to the 3D loading of the cantilever beam of Fig. 9.45. The beam is simulated using 5 quadratic beam elements for each of the segments located on the right and left sides of the central one. The central segment is simulated using a two–scale approach. Ten linear hexahedra are used in the direction X and a mesh of 4×4 hexahedra are used for the surface–interface, giving a total of 192 elements in the local model. One Gauss integration point is used in each FE of the local model. The applied loadings as well as the material properties are given in the same figure.

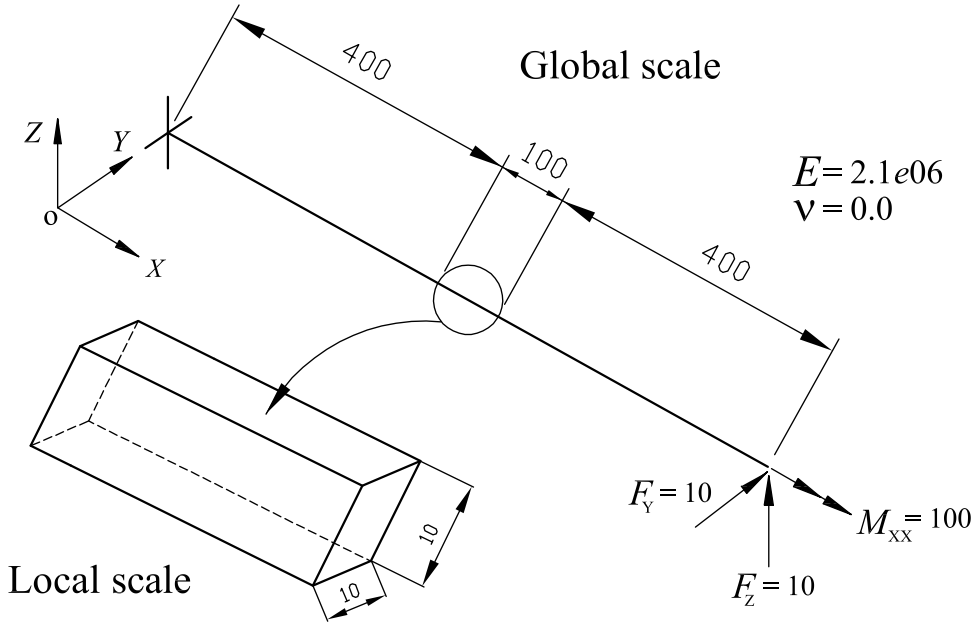

Figure 9.45: Elastic cantilever beam subjected to 3D loading.

Figure 9.46 shows a comparison between the displacement response in the Y and Z directions obtained from the two–scale model and the ones obtained using a simple elastic FE beam model. Its is possible to see a good agreement between both results.
Figure 9.47 shows the distribution of the reaction forces on the surface–interface of the local model. It is worth noting that complex force distributions are well reproduced in the local model due to its capacity for representing the full 3D geometry of the beam, in contrast with that obtained in the beam model, due to the limitations of the kinematics assumptions. Moreover, as it has been explained before, reduced forces and moments are then calculated using Eqs. (8.30a) and (8.30b).

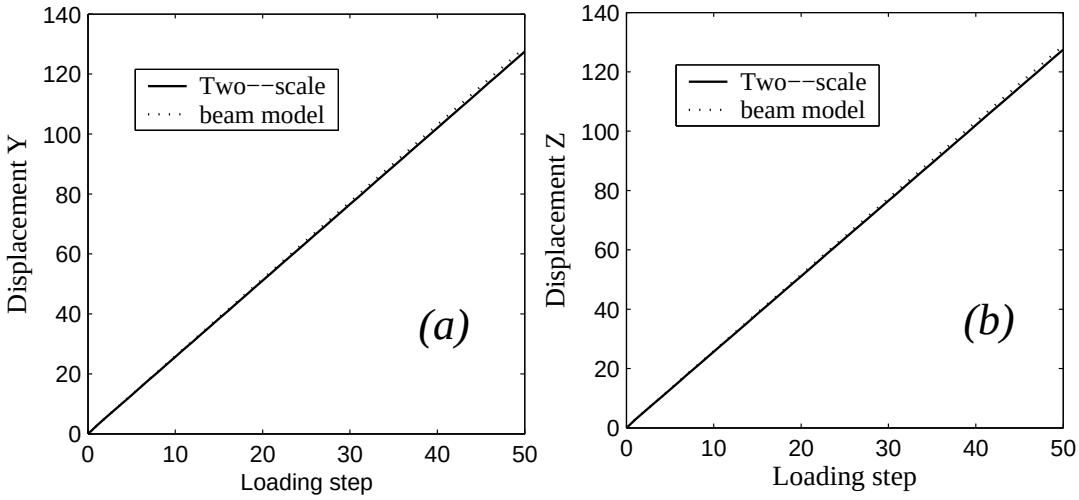

Figure 9.46: Comparison between the displacement response obtained from the beam and the two–scale models. (a, b): Displacements in Y and Z directions, respectively.

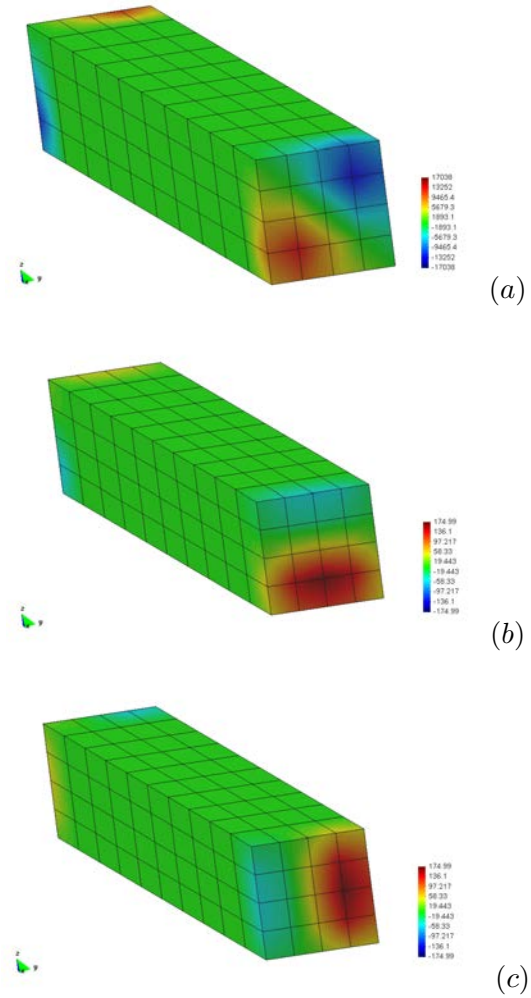

Figure 9.47: Reaction force distributions on the surface–interfaces. (a): Force in X direction. (b): Force in Y direction. (c): Force in Z direction.

9.6.2 Nonlinear static example

The seismic response of the precast RC industrial building of Fig. 9.36 has been studied by the authors in reference [261] considering monolithic joints. The building has a bay width of 24 m and 12 m of inter–axes length. The story hight is 12 m. The concrete has a ultimate compression of 35 MPa, with $E = 290.000$ MPa, $\nu = 0.2$ and a tension/compression relation of 10. The ultimate tensile stress for the steel is 510 MPa with $\nu = 0.15$, $E = 200000$ Mpa and $\nu = 0.15$. The dimensions of the columns are 60x60 cm^2. The beam has an initial high of 40 cm on the supports and 140 cm in the middle of the span. The permanent loads are 1000 N/m^2 and the weight of upper half part of the closing walls with 225.000 N.

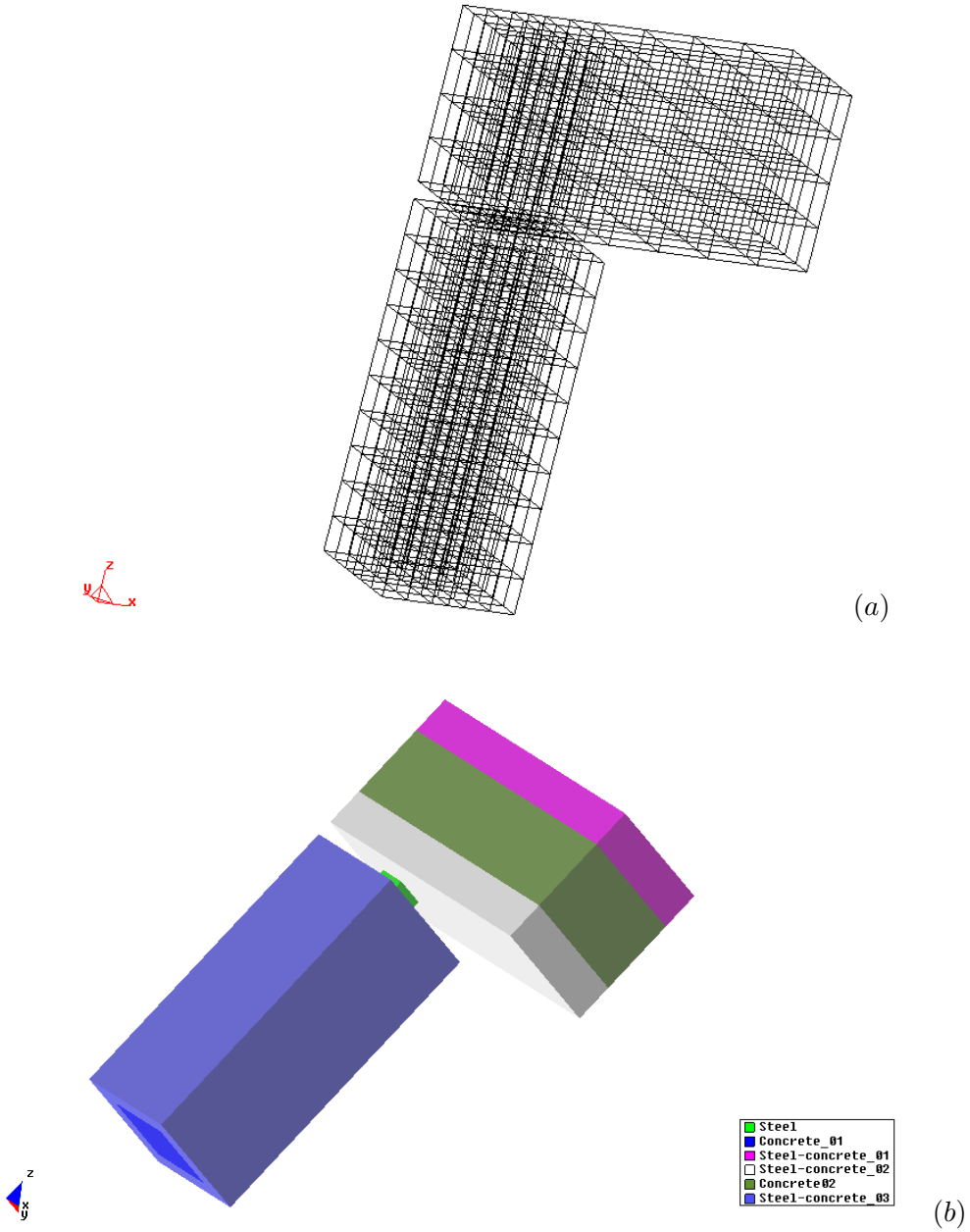

Figure 9.48: FE model of the local scale problem. (a): Mesh. (b): Distribution of materials.

The building is meshed using 8 quadratic beam elements with two Gauss integration points for the resulting beams and column. Details about the steel reinforcement and the grid of quadrilateral of the cross sections can be consulted in the same reference. Additionally, we consider a local scale model corresponding to the precast connecting joint which is clearly a local irregularity in the structure, see Fig. 9.36. The FE model used for the local scale is shown in Fig. 9.48 and it corresponds to a segment of the column and beam of 60 cm measured along their respective axis, which allows to cover completely the connecting zone where two steel bars with 16 mm diameter are used to transmit forces and moments among vertical and horizontal elements.
A total of 608 hexahedral FE are used with one Gauss integration point. Considering that the mixing rule is used in the local 3D model, several zones (see Figure 9.48*b*) with different volumetric fractions of steel and concrete are defined, representing the longitudinal and transversal reinforcements in the structure.
A static pushover analysis is performed considering: (i) the frame with monolithic joints in finite deformation. (ii) The two–scale model in finite deformation. The purpose is to establish clearly the importance of considering an appropriated description of the local irregularities in the structures as well as the second order effect coupled with inelasticity in the study of flexible structures. Figure 9.49*a* shows the capacity curves obtained for the two mentioned cases. It

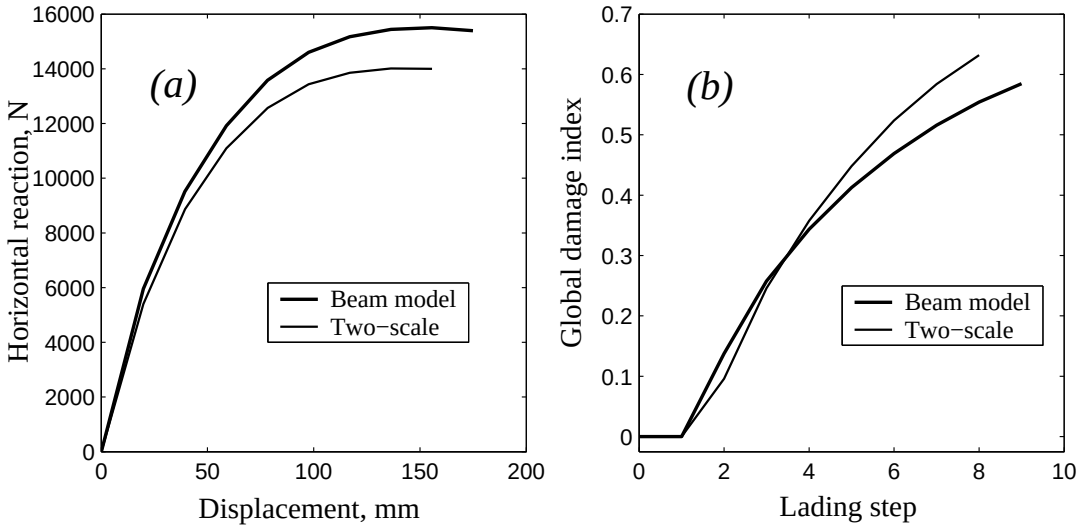

Figure 9.49: (*a*): Capacity curves. (*b*): Evolution of the global damage index.

is possible to see in this figure that the stiffness and ductility levels are overestimated in the case when the monolithic joints are employed. The use of finite deformation allows to take into account the so called effect P–Δ [261] and an anticipated strength degradation is observed for displacements over 60 mm which is a lateral displacement level expectable under strong seismic excitations. Softening behavior is observed for both models. Figure 9.49*b* shows the evolution of the global damage index for both models. This index grows quickly for the two–scale model due to the fact that the greater part of the degradation and energy dissipation take place inside of the connecting joint.

9.6.3 Nonlinear dynamic example

In this example, the nonlinear seismic response of the structure of Example 9.6.2 is simulated by means of the two–scale model. The input acceleration is the N–S component of the El Centro 1940 earthquake record. The response obtained from the two–scale model is compared with that obtained from the nonlinear dynamic response of a beam model. Figure 9.50 shows the hysteretic cycles obtained from the lateral displacement of the upper beam–column joint and the horizontal reaction (base shear) in the columns for both models. Again it is possible to appreciate the influence of the local irregularity in the dynamic response: more energy dissipation and lateral displacements are obtained in the two–scale model. Figure 9.6.3 shows the time history

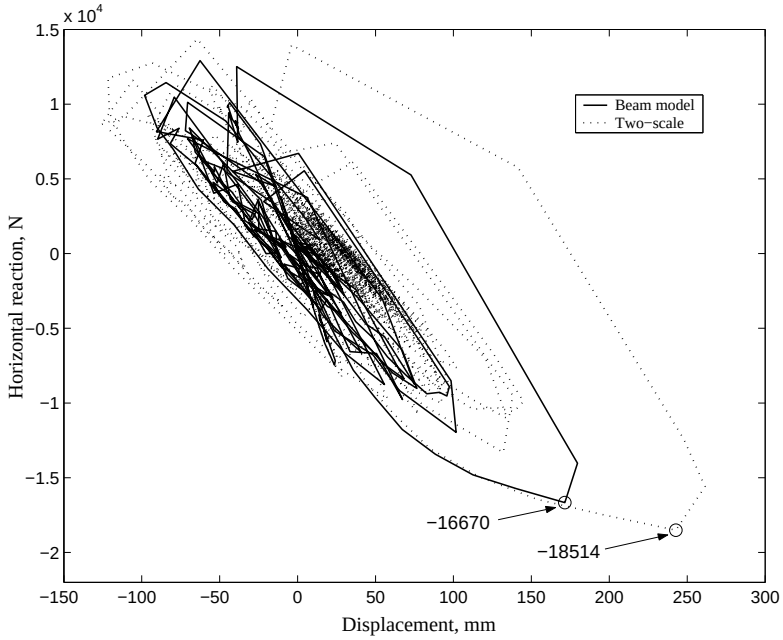

Figure 9.50: Base shear–displacement relationship.

response of the horizontal displacement and acceleration of the upper beam–column joint for both models. Displacements and accelerations are greater (∼45% and ∼14%, respectively) when the two–scale model is used in the numerical simulations, revealing that the nonlinear seismic response of precast and of other RC structures with local irregularities can be dominated by the mechanical behavior of the joints.
Finally, Figure 9.52 shows several stages of the nonlinear inclusions experienced by the local model.

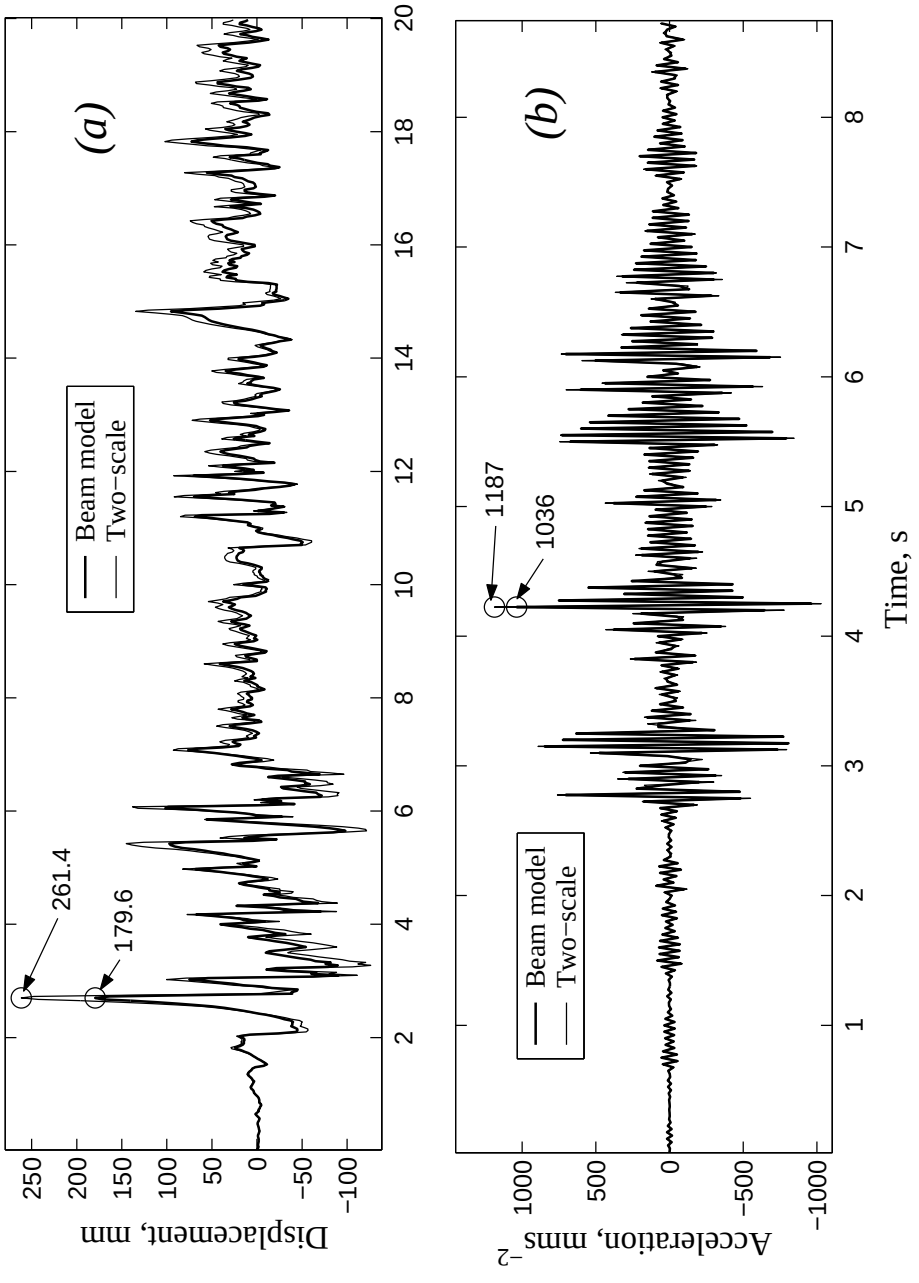

Figure 9.51: Time history responses of the top beam–column joint. (a): Horizontal displacement. (b): Acceleration.

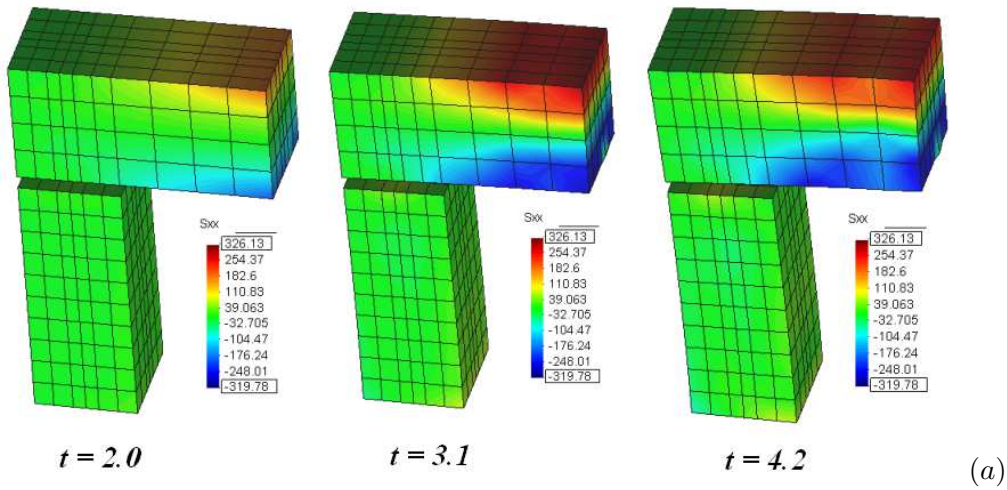

(a)

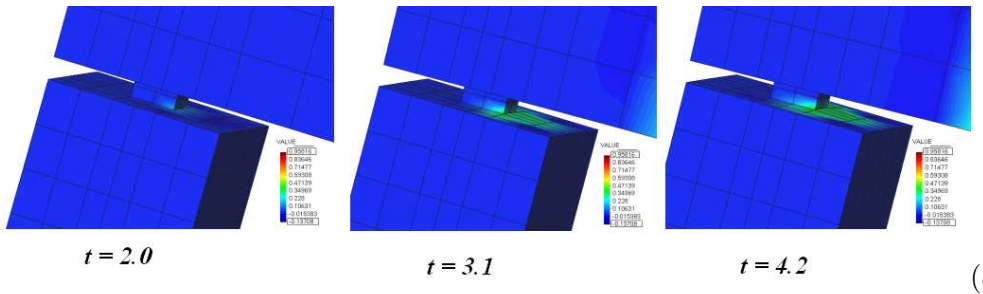

(b)

Figure 9.52: Nonlinear response in the local model at times $t = 2.0, 3.1, 4.2$ s. (a): Stress in the Y direction. (b): Damage concentration around the connecting bar in the joint.

Chapter 10

Conclusions and further research

In this chapter conclusions about the results obtained in the formulation and the numerical implementation of a rod model able to consider the fully geometric and constitutive nonlinearity as well as the local irregularities described in §8 are described and discussed in section §10.1; section §10.2 is dedicated to the statement of new lines of research related to the different topics covered in this thesis.

10.1 Conclusions

In this section a detailed response to the partial objectives declared in the list of §1.2 is given. Particularly, is possible to see that in what regard to

(I) **The theoretical objectives**

(I.1) In §3 a deep study and a theoretical analysis of the continuum based theory of rods capable of undergoing large displacements and rotations under the Reissner–Simo hypothesis has been performed. In the present case, an initially curved and unstressed rod is considered as the reference configuration. A detailed description of the kinematic assumptions is carried out in the framework of the configurational description of the mechanics. The equations of the motion are deduced from the local form of the linear and angular balance conditions and integrating over the rod's volume. An appropriated (weak) form for the numerical implementations is deduced for the nonlinear functional corresponding to virtual work principle. A discussion about the deduction of reduced constitutive relations considering hyperelastic materials. Therefore, the objective (i.1) is widely covered in this chapter.

(I.2) After defining translational and rotational strain vectors and calculating the deformation gradient tensor, in §3.2 explicit expressions for the material, spatial and co–rotational versions strain measure and for the objective measure of the strain rate acting on each material point of the cross section, in terms of the variables defining the deformation map, its derivatives and the geometry of the beam cross section are given. The conjugated stress measures existing at material point level are developed and power balance condition is used to deduce the stress measure energetically conjugated to the cross sectional strain measures. In this case, the objective (i.2) is fulfilled.

(I.3) The objective (i.3) of §1.2 is fulfilled in Chapter 4 which has been devoted to the development of rate dependent and independent inelastic constitutive laws for simple

material associated to points on the cross sections, in terms of the First Piola Kirchhoff stress tensor and the corresponding energetically conjugated strain measure. Two types of nonlinear constitutive models for simple materials are included: the damage and plasticity models are considered in a manner consistent with the kinematics of the rod model and the laws thermodynamics for adiabatic processes. Rate dependent behavior and viscosity is included by means of a Maxwell model.

(I.4) In the same chapter, it has been highlighted the fact that material points on the cross section are considered as formed by a composite material *i.e.* a homogeneous mixture of different components, each of them with its own constitutive law. The composite's behavior is obtained by means of an appropriated version of mixing theory which considers the kinematic assumptions of the present rod theory. The mechanical response of the composite is obtained supposing a rheological model where all the components work in parallel. Those results provide a response to the objectives declared in (i.4).

(I.5) Additionally, in §4.4 a continuum version of the cross sectional analysis has been developed including explicit expressions for the stress resultant and stress couples assuming planarity of the cross sections. Warping variables or iterative procedures for obtaining corrected strain fields are avoided in the present formulation. Consistent cross sectional tangential constitutive tensors are deduced including rate dependent inelasticity in composite materials which fulfills the objective (i.5).

(I.6) Objective (i.6) is covered in §4.5 where a continuum version of local and global damage indices able to describe the evolution of the remaining load carrying capacity of complex structures is developed. The proposed indices are based on the ratio existing between the inelastic stresses and their elastic counterparts.

(I.7) The correct (in a manner consistent with the geometry of the configurational manifold) linearization of the weak form of the nonlinear balance equations is carried out in §5 including the effects of the rate dependent inelasticity existing at material point level which leads to the consistent deduction of the mass and viscous tangent stiffness. The fact that the rotational part of the displacement field can be updated using two alternatively rules, the material and the spatial one, implies that two sets of linearized kinetics and kinematics quantities can be obtained, according to the updating rule chosen. By completeness, both set of linearized expressions are obtained in the sections of that chapter. The corresponding rate dependent and independent parts of the tangential stiffness were deduced and added to the loading and geometric terms. Therefore, objective (i.7) of the list of section §1.2 is fulfilled.

(I.8) In (i.8) it has been declared the need of disposing of an specific rod element for EDDs. The development of a specific rod element well suited for modeling the mechanical behavior of energy dissipating devices to be incorporated to the present full geometric and constitutive rod theory is described extensively in §8.1 of Chapter 8.

(I.9) The development of appropriated one–dimensional force-displacement and/or moment-curvature relations for the description of the nonlinear hysteretic behavior of different types of energy dissipators is covered in §8.1.1.

(I.10) The appropriated theoretical framework for the development of a two–scale model of rod structures with local geometric irregularities is considered in §8.2. Sections 8.2.1 to 8.4 includes the formulation of the general problem in the both scales as well as their interaction. Kinematical hypothesis as well as other simplifications are explained in detail. In this manner, objective (i.10) (see §1.2) is fulfilled.

(II) **Numerical objectives**

(II.1) Objective (ii.1) claims about the need of disposing of numerical algorithms for the integration of the constitutive laws for simple materials developed in §4, as well as for the obtention of the mechanical behavior of composites. In the same chapter, sections 4.2.2, 4.2.3 and 4.3 it is possible to find the corresponding algorithms.

(II.2) In Chapter 6 the time discretization of the linearized version of the virtual work principle is performed according to the Newmark's method following the procedures originally proposed in [365]. A time–stepping scheme consistent with the kinematic assumptions made for the rod model *i.e.* able to manage variables belonging to $SO(3)$ and its tangent space is presented in §6.1.1. At each time step the linearized problem is solved by means of an iterative scheme until convergency is achieved. In §6.1.2 to §6.1.4 the corresponding (Eulerian) updating iterative procedure for the kinetics and kinematics variables as well as for the strain and strain rate measures is developed. The spatial and the material updating rule for the rotational part of the motion are considered. Taking into account the previous results it is possible to see that objective (ii.2) is fulfilled. It is worth to note that even though using small time steps the numerical dissipation can be reduced, additional benefits in the numerical performance could be obtained employing energy-momentum conserving schemes, at least in the conservative limit of the problems.

(II.3) The purpose declared in (ii.3) is accomplished in §6.5 of §6. In that section some theoretical development about the application of variational integrators for the time discretization of the action integral of Hamiltonian system is discussed extensively. The analysis includes a brief presentation of the Hamiltonian version of the rod's problem and a summary of the main aspects of energy-momentum conserving algorithms.

(II.4) The development of an appropriated cross sectional analysis, consistent with the kinematical hypothesis and based on the fiber discretization of the cross section, is carried out in §7.7.1 as declared in (ii.4). Each fiber should have associated a composite material. The developed procedure performs the calculation of reduced cross sectional forces and moments, the tangential stiffness tensors and the damage indices at material point and cross sectional level. The proposed method, even when inexact from the point of view of the elasticity theory, gives a computationally convenient way of approximating the strain-stress distribution in the section. Two additional integration loops, running on the number of fibers and the number of simple components, are required (see Fig. 7.3).

(II.5) Chapter 7 describes the spatial discretization used in the Galerkin finite element approximation of the time discretization presented in §6 for the linearized form of the virtual work equations. The resulting FE approach yields to a system of nonlinear algebraic equations well suited for the application of the Newton iterative method. Again, the main difficulty arises in the fact that the spatial interpolation of the configuration variables should be consistent with the nonlinear nature of $\mathcal{C}_t$ (see §3.1). The developed elements are based on isoparametric interpolations of both the displacement and the incremental rotation parameters. Considering that the material or spatial updating rule for the rotations are equivalent, their corresponding interpolated iterative incremental rotation vectors can be used to parameterize the rotational variables. By completeness, both schemes are presented yielding to the corresponding tangential matrices and unbalanced force vectors. In the practice, the numerical procedures based on the spatial form of the iterative incremental rotation vector are preferred because it makes the expressions for the internal, external and inertial

vectors and the tangential matrices more concise and explicit. The obtained inertial and viscous tangential matrices are consistent with the Newmark updating procedure described in §6.

(II.6) Explicit expressions for the iterative Newton–Raphson scheme consistent with the Newmark's updating scheme for the dynamic variables described in §6.1 is developed in §7.7 (see Fig. 7.1), therefore, objective (ii.6) is fulfilled.

(II.7) An integration algorithm for the constitutive relation assigned to the energy dissipating devices is developed in §8.1.2 along with a method for obtaining the forces or moment in the devices for a given strain field.

(II.8) The two–scale model developed and described in detail in §8.2 for studying the nonlinear response of framed structures with local geometric irregularities is numerically implemented using a FE approach in §8.5. The numerical coupling between scales is developed starting from the full 3D stress state existing in the local model, cross sectional forces and moments, required at global level, are recovered by integrating at the surface–interface in an analogous manner as for the cross sectional analysis of beams as it is explained in §8.5.3. In this manner, objective (ii.8) is fulfilled.

(II.9) The iterative Newton–Raphson scheme based on the displacement method, which considers the interaction between scales is developed in §8.5.3 (see Fig. 8.7). It allows to obtain the response at the global level even in the nonlinear dynamic range. Equilibrium is checked at both, local and global levels, ensuring that compatible configurations are reached for the whole problem. The tangential stiffness of the local model is obtained numerically applying the perturbation method on the current configuration and obtaining the corresponding reaction forces reduced to the degree of freedom of the rod model as explained in §8.4.3; in the same section the corresponding reaction forces reduced to the degree of freedom of the global level are used for estimating the reduced forces and moments in the local model.

(II.10) The numerical implementation of the two–scale model for framed structures with local irregularities is implemented computationally in a parallelized version of the *master–slave* approach for managing the multi–scale problems. The global scale problem acts as the master, sending a trial displacement fields to the local scale models (slaves) and then receives the corresponding internal forces and tangential tensors. The iterative process is finished when the global convergence is achieved. The communication between processes is carried out by mean of an appropriated library of communication (MPI library; see [381]). The developed approach facilitates a minimal intervention on existing codes specific for beams and solids. Those results contribute to fulfil objective (ii.10).

(III) **Practical objectives**

(III.1) The numerical validation of the proposed formulation, in the static and dynamic cases, is performed throughout a set of examples considering linear elastic constitutive laws with initially straight and curved beams. See §9.1 were it is possible to appreciate a good agreement with results of existing literature.

(III.2) Additionally, the proposed formulation is validated throughout an extensive set of numerical examples (statics and dynamics) covering inelastic constitutive equations in §9.2. The results are compared with those provided in existing literature when possible (for the case of plasticity). In other cases new examples are presented, mainly in what regard to the study of the response of degrading composite structures in both the static and dynamic cases.

(III.3) The verification of the obtention of a mesh independent response for structures presenting softening materials is carried out in the example of §9.2.1. Mesh independency is obtained by means of the regularization of the energy dissipated at constitutive level considering the characteristic length of the volume associated to a specific integration point and the fracture energy of the materials. The same example includes details pertaining to the evolution of global and local damage indices. It is also possible to see that the proposed damage indices allow to identify the global load carrying capacity of the structure and the damage state of the different members. Considering (III.1) to (III.3), it is clear that objectives (iii.1) to (iii.3) are fulfilled.

(III.4) The ability of the proposed model for predicting the ultimate load, ductility and other relevant engineering parameters of real structures is verified in §9.4.1. In this example the response predicted numerically is compared with experimental results of experimental push–over analysis performed on a scaled model. It is possible to see the good approximation for the global maximum response and for the characteristic values of the structure; *i.e.* global ductility level, elastic limit and over–strength. Also, the comparison between the distribution of cross sectional damage predicted numerically and the map of fissures obtained after the application of several shaking table tests gives reasonably good results.

(III.5) The ability of the proposed damage indices for predicting the load carrying capacity of structures is verified from the conclusions given in (III.1) to (III.3), however, the most convincing results can be obtained from §9.4.1 to §9.5.2.

(III.6) To study of the static and dynamic (even seismic) response of real two and three-dimensional precast and cast in place reinforced concrete structures is presented in the detailed examples of §9.4.2 to §9.5.2 comparing the results obtained when full nonlinearity is not considered in the numerical simulations. The presented results include the obtention of capacity curves (including the effects of cyclic static actions), the evolution of local and global damage indices, time history response of relevant degrees of freedom, the hysteretic cycles obtained from the action of dynamic loads, the seismic responses and localization and characterization of nonlinearities in framed elements (see Fig. 9.32).

(III.7) The study the possibility of improve the dynamic (seismic) response of real civil engineering structures by means of using energy dissipating devices is extensively considered in §9.4.3 to §9.5.2.

(III.8) To study of the nonlinear static and dynamic response of precast concrete structures including EDDs is carried out extensively in §9.5.1 and §9.5.2. Controlled and uncontrolled cases, the small and large strain assumptions are compared showing that the infinitesimal deformation hypothesis overestimate the real load carrying capacity of the structure, due to the fact that self-weight loads comprise the columns contributing to control the degradation due to the lateral loading. In the case of finite deformation, the so called P–Δ effects are taken into account and an anticipated strength degradation is observed due to lateral displacement levels expectable under strong seismic motions. Additionally, the incorporation of EDDs increases the stiffness and the yielding point (at global level) of the structure without affecting the global ductility. Again, studies are focused on the evolution of the damage indices confirming the mentioned effects. Moreover, the results of the numerical simulations in the dynamic range allow seeing that the employment of plastic EDDs contributes to improve the seismic behavior of the structures for the case of the employed acceleration record. It is possible to appreciate that the non–controlled structure presents

greater lateral displacements and larger structural damage. Reductions are observed for the displacement, velocity and acceleration time history responses when appropriated EDDs are included. More details can be reviewed in the mentioned sections. Conclusion (III.5) to (III.9) fulfil the objectives declared in (iii.5) to (iii.9)

(III.9) Several numerical examples in §9.6 validates the proposed two–scale approach for the study of the nonlinear static and dynamic response of structures (even precast ones with non ductile connecting joints) with local geometric irregularities. The linear elastic case is validated in §9.6.1. In the practical case of a precast concrete structure the advantages of using the proposed approach is verified in the static and dynamic cases of examples §9.6.2 and §9.6.3, respectively. Therefore, the objective (iii.9) is fulfilled.

10.1.1 Summary of conclusions

In summary, after reviewing the content of the chapters of this work, it is possible to confirm that it has been developed a formulation for rod structures able to consider in a coupled manner geometric and constitutive sources of nonlinearity in both the static and the dynamic ranges. Additionally, the same formulation has bee extended for allowing the inclusion of passive energy dissipating elements as an special case of rods and geometric irregularities as a full three-dimensional body connected to the framed structure by means of a two–scale model.

The proposed formulation is based on the geometrically exact 3D formulation for rods due to Reissner and Simo considering an initially curved reference configuration, which has been extended to include arbitrary distribution of composite materials in the cross sections. Each material point of the cross section is assumed to be composed of several simple materials with their own constitutive laws. Constitutive laws for the simple materials are based on thermodynamically consistent formulations allowing to obtain more realistic estimations of the energy dissipation in the nonlinear range. The simple mixing rule for composites is used for modeling complex material behaviors at material point level. Viscosity is included at the constitutive level by means of a thermodynamically consistent visco damage model developed in terms of the material description of the material form of the FPK stress vector.

A detailed cross sectional analysis, consistent with the kinematic hypothesis is also presented. From the numerical point of view, the cross sections are meshed into a grid of quadrilaterals, each of them corresponding to fibers directed along the axis of the beam. An additional integration loop, running on the number of fibers, is required to obtain the iterative cross sectional forces, moments and the tangential stiffness tensors. The proposed method, even when inexact from the point of view of the elasticity theory, gives a computationally convenient way of approximating the strain-stress distribution in the section. Warping variables or iterative procedures for obtaining corrected strain fields are avoided in the present formulation. The resulting formulation is well suited for studying the constitutive and geometric nonlinear behavior of framed structures in the static and dynamic cases.

A mesh independent response is obtained by means of the regularization of the energy dissipated at constitutive level considering the characteristic length of the volume associated to a specific integration point and the fracture energy of the materials. Local and global damage indices have been developed based on the ratio between the visco elastic and nonlinear stresses. The proposed damage indices allow estimating the evolution of the global load carrying capacity of the structure and the damage state of the different members during dynamic actions.

The linearization of the virtual work functional (the weak form of the momentum balance equations) is performed in a manner consistent with the kinematical hypothesis of the rod theory and rate dependent inelasticity. An explicit expression for the objective measure of the strain rate

acting on each material point is deduced along with its linearized form. The procedure leads to the consistent deduction of the mass and viscous tangent components of the stiffness which are added to the material, geometric and loading dependent terms. Both, the material and spatial updating rule for rotations are considered. Due to the fact that the deformation map and their related dynamical variables belong to $\mathbb{R}^3 \otimes SO(3)$, an appropriated version of Newmark's scheme is used and details about the numerical implementation of the iterative updating procedure of the involved variables are also addressed. The time discretization of the linearized equations is carried out consistently with the iterative Newmark's scheme.

The space discretization of the linearized problem is performed using the standard Galerkin FE approach. The resulting model is implemented in a displacement based FE code. A Newton–Raphson type of iterative scheme is used for the step-by-step solution of the discrete problem. It is worth to note that even though using small time steps the numerical dissipation can be reduced, additional benefits in the numerical performance could be obtained employing energy-momentum conserving or variational based schemes, at least in the conservative limit of the problems.

An specific element for EDDs is developed, based on the rod model but releasing the rotational degrees of freedom. Appropriated constitutive relations are given for a wide variety of possible dissipative mechanisms including the corresponding integration algorithms.

If local geometric irregularities appear in a framed structure a two–scale, global and local, approach has been developed for studying its nonlinear response. At global scale level, all the elements of the model are 1D *i.e.* prismatic rods which consider the present extension to include an arbitrary distribution of inelastic composite materials in the cross sections of the geometrically exact formulation due to Reissner and Simo. For the geometric irregularity, an amplified view of the corresponding element is carried out, constructing a fully 3D model which constitutes the local scale level. The dimensional–coupling between scales is performed through surface–interfaces imposing the kinematic hypothesis assumed for the beam model. Starting from the full 3D stress state existing in the local model, cross sectional forces and moments, required at global level, are recovered by integrating at the surface–interface.

An iterative Newton–Raphson scheme based on the displacement method, which considers the interaction between scales is developed to obtain the response at the global level even in the nonlinear dynamic range. Equilibrium is checked at both, local and global levels, ensuring that compatible configurations are reached for the whole problem. The tangential stiffness of the local model is obtained numerically applying the perturbation method on the current configuration and obtaining the corresponding reaction forces reduced to the degree of freedom of the rod model. The computational implementation manages the problem by means of the *master–slave* approach. The global scale problem acts as the master, sending the iterative displacement/rotation fields to the local scale models which are the (slaves) and then receives the corresponding internal forces, moments and tangential tensors obtained by integration on the surface–interfaces. A parallelized computational implementation ensures a minimal intervention on specific codes for beams and solids is required.

Several numerical examples have been included for the validation of the proposed formulation. The examples include elastic and inelastic finite deformation response of framed structures with initially straight and curved beams. Viscous mechanisms of dissipation are included at constitutive level. The verification of the obtention of a mesh independent response for structures presenting softening behavior is carried out. Comparisons with existing literature is performed for the case of plasticity and new results are presented for degrading and composite materials. The geometric and constitutive nonlinear dynamic response of several 2D and 3D structures was computed for different constitutive models including composites. Those examples show how

the present formulation is able to capture different complex mechanical phenomena such as the uncoupling of the dynamic response from resonance due to inelastic incursions. Moreover, the present formulation which includes viscosity at material point level, suppress the high frequency content in the dynamic response which is a desirable characteristic of time stepping schemes.
The study of realistic flexible reinforced concrete framed structures subjected to static and dynamic actions is also carried out. The fully coupled constitutive and geometric behavior of the frames is compared for both cases. Detailed studies regarding to the evolution of local damage indices, energy dissipation and ductility demands were presented. Comparisons with experimental data are also provided. Those examples show how the present formulation is able to capture different complex mechanical phenomena such as the uncoupling of the dynamic response from resonance due to inelastic incursions. Other practical studies include the detailed study of seismic response of precast and cast in place concrete structures with energy dissipating devices. Advantages of the use of passive control are verified.
Finally, numerical examples are included showing the capabilities of the developed two–scale approach in predicting the elastic and inelastic dynamic responses of structures with local irregularities. The present formulation appears as a convenient approach for studying the dynamic nonlinear behavior or realistic RC structures where the response of the structure is dominated by local irregularities such as is the case of precast structures.

10.2 Further lines of research

Several lines of research can be opened from the results of the present work. A possible grouping of them is the following:

(i) **The extension of the Reissner–Simo theory for coupled thermic-mechanics problems**.
In the present formulation the adiabatic and isothermal case of the constitutive equations at material point level have been considered (see §4). Therefore, thermally loaded problems are not covered and coupled geometric-thermic-mechanic effects are not allowed. At the author knowledge, only a few works have been considered this case (see *e.g.* Simmonds [360] for an approximated version of the theory), and they are limited to theoretical developments in elastic range. In this manner, a possible contribution in further works can be given by the extension of the present formulation for including the full thermodynamical laws in the constitutive part of theory and the corresponding treatment in numerical simulations.

(ii) **Finite deformation models with enhanced kinematical assumptions**.
Several works have been devoted to the development of richer kinematics assumptions[1] incorporated in geometrically exact rod models; see *e.g.* [370, 323] for the inclusion of warping in elastic materials, [324] for anisotropic materials, [361, 151, 149] for the the case of plasticity with warping, among others. In any case, the reviewed works present one or more of the following limitations: (*a*) The out of plane component of the cross sectional displacement field is limited to the consideration of warping functions depending on the arch–length parameter. (*b*) Inelasticity is limited to plasticity. (*c*) A full 3D displacement field is added to the one derived from the plane assumption but the corresponding strain

[1] In the sense of improving the cross sectional displacement field obtained with the plane cross section assumption.

measures are simplified considering certain small strain assumptions. (d) General distribution of inelastic composite materials have not been considered.
Additional refinement in the displacement field can be obtained adding a general *distorting* 3D field $\hat{u} = u_i \hat{t}_i$ on the plane assumption as

$$\hat{x}(S, \xi_\beta, t) = \hat{\varphi}(S, t) + \xi_\beta \hat{t}_\beta(S, t) + u_i(S, \xi_\beta)\hat{t}_i(S, t), \tag{10.1}$$

in stead of Eq. (3.22). The distorting field $\hat{u}$ should be determined, even in the inelastic range, in a way such that the global equilibrium equations are fulfilled. In this case the deformation gradient $\mathbf{F}_f$ is the sum of the one obtained from plane case and the corresponding derived from the distorting field as

$$\mathbf{F}_f = \nabla_{X_i}(\hat{\varphi} + \hat{\mathscr{T}}) \otimes \hat{E}_i + \nabla_{X_i}(\hat{u}) \otimes \hat{E}_i = \mathbf{F}_p + \mathbf{F}_d. \tag{10.2}$$

Most of the theory for the plane case has been covered in the present work, therefore it remains opened to develop the same for the $\mathbf{F}_d$ yielding to additional equilibrium equations at the reduced level, an enhanced virtual work principle and so on. The rest of the usual procedures for proposing a numerical method for solving the new problem (constructing the distorting parts of the strain and strain rate field, linearization, space an time discretization, etc.) should be also be provided.
The main advantage of using the hypothesis of Eq. (10.1) is that a full strain field can be obtained on each material point on the cross section and, therefore, a larger set of constitutive equations can be employed.
Inspired in the work of Bairan and Mari [31, 32], which is limited to small strain assumption, it is possible to guess that the field $\hat{u}$ should be obtained by means of an appropriated cross sectional analysis enforcing the inter–fiber equilibrium through an iterative procedure. However, no attempts have been done in this line at the present.

(iii) **The use of variational integrators that preserve the geometric structure of the configuration manifold**.
As stated by West ([402], Ch. 1):

The variational method for deriving integrators means that the resulting algorithms automatically have a number of properties. In particular, they are symplectic methods, they exactly preserve momenta associated to symmetries of the system, and they have excellent longtime energy stability.

Therefore, the above mentioned properties make the variational methods a very useful tool for simulating flexible mechanisms made of rods which are either conservative or near-conservative. Moreover, the variational methodology allows to easily and cleanly derive good integrators even in highly complex geometries, such as the asynchronous space-time meshes. Variational methods preserve the geometry of the geometric structure of the continuum system. In any case, the method applies even when the system is not conservative. Additionally, this methodology provides an unifying framework from which to consider the Lagrangian side of symplectic integration theory.
In §6.3 and §6.5 a summary of the Hamiltonian formulation of the present rod theory as well as the firsts steps needed in developing a variational integrator (probably the simplest one) starting from the time discrete form of the Lagrangian were given. Only conservative systems were considered.
In any case, additional steps such as the linearization of the resulting (discrete) implicit equations and numerical verifications remain still uncompleted. Moreover, other integra-

tors of higher accurate order can be developed following analogous procedures. Moreover, the methodology could be extended to dissipative and forced systems.

(iv) **The extension of the present result to shell elements**.
Another type of structural element widely applied in several areas of engineering is the shell element. Geometrically exact models for shells (see [11, 188, 366, 367, 368] for the general theory; [76, 77, 369] for the case of variable thickness; the inclusion of inelasticity can be reviewed in [374]; a shell's formulation using *drilling* degrees of freedom can be consulted in [176, 177, 375]; the development of time–stepping schemes in [78, 80, 79, 373], among a really large list of works) share with the present rod model the fact that both formulations produce a nonlinear configuration manifold involving the rotation manifold (or the two-sphere in the case of shells). Particularly, the so called shell formulation with drilling rotations has the same number of degrees of freedom as the rod model and, therefore, are well suited to be combined in a computer code able to simulate the behavior of one and two dimensional structural elements. Typical examples of such structures are inflatable structures shear wall buildings, aircrafts with stiffener among many others.
An interesting possibility is given by the fact of extending the present formulation for composite materials to shell elements and combine them with rods for studying the previously described problems.

(v) **Effectiveness of using EDDs for seismic applications**.
The employment of EDDs in civil engineering structures has been verified through a set of numerical examples in the present work (see §9), however the benefits obtained depends of a large set of factors [382]: (i) The characteristics of the seismic action (duration, intensity, frequency content, etc.) (ii) The characteristics of the location of the building (solid type, possibility of liquefaction, etc.) (iii) The characteristic of the structure (eigenfrequencies of the modal shape which contributes to the response, local and global ductility, damage distribution, energy dissipation capacity, presence of second order effects or structural torsion, etc.); (iv) the possible (nonlinear) interaction between (i), (ii) and (iii); among others. Several methodologies has been proposed for the inclusion of passive EDDs in buildings (and other structures) (see *e.g.* [8, 129, 130]). However, none of them provides exhaustive design rules valid for the general case. It should be interesting to study the possibility of developing design criteria for buildings with EDDs based on energetic considerations based on the fracture energy of the materials such as those used in §4 and the correlation with the damage indices.

(vi) **Development of a two–scale shell–3D solid model**.
The two–scale model proposed in this work can be extended for considering shell–3D solid interaction. This extension can be useful for introducing the effects of local failures in the global mechanical response of composite structures (layered or not); the most important types of local failures are delamination and local fiber buckling. Due to the fact that usually real engineering structures require a large number of FE for a correct geometric description, it can be an interesting application in the study of the mechanical behavior of aircraft and aerospace structures made of composites.

Appendix A

Introduction to finite rotations

The main aim of the present appendix is to pave the way for the work in the next chapters concerning to the development of a geometrically exact theory 3D rods involving finite deformation, where rotations are coupled with translations. The results here presented naturally impacts on the description of the general motion, and several fields in theoretical and applied mechanics, such as analytical mechanics, structural dynamics, multi-body dynamics, flight mechanics, and so on, have profited from the results provided by the mathematicians or have contributed to develop theories for the accurate description of rotational motion [222].

First, we review some basic concepts associated with *large rotations* that will be required in the formulation of the kinematic hypothesis of a finite deformation theory for rods. The term *large* or *finite* rotation is normally employed in continuous mechanics as opposite to *small* or *infinitesimal* rotation, which are a set of rotations that can be described as elements of a vector space. Finite rotations, or more precisely the elements of the noncommutative transformation group, are an extensive and complex topic of mathematics, therefore, only the concepts and formalisms which are strictly necessaries for this work will be reviewed. However, more extensive and detailed works about the mathematical theory of finite rotations can be found in Refs. [15, 16, 28, 48] and on the application to beam, shell and flexible mechanism theories in [181, 179].

The outline of this appendix is as follows: firstly, the vector representation of a rotation is used to explain the noncommutative nature of general large rotations, which are classified as abstract elements of a noncommutative group isomorphic[1] to the orthogonal group of rotation tensors. Then a more formal definition of the rotation group in terms of differential manifolds is exposed, revealing a rich mathematical structure which corresponds to these of a Lie group under the usual matrix multiplication. Following, the so called spatial and material updating procedures for compound rotations is explained. A rigorous definition for the tangent space to the rotational manifold is presented in terms of the Lie algebra associated to the group of rotations. A rather detailed discussion about possible parameterizations of the rotational manifold is then described, addressing the practical advantages and limitations of using the vectorial ones. Finally, a configurational approach for describing large rotations in space is given along with the presentation of a set of operators relevant to the present theory.

[1] A rigorous definition of *isomorphisms* is the context of topology can be consulted in [285].

A.1 Large non-commutative rotations

In Fig. A.1 it is possible to see that the result of applying a set of large rotations on a body depends on the order in which they are applied. In this example three rotations of magnitude $\pi/2$ are arranged as the components of the *rotation vector* $\hat{\phi} = [\phi_{xx}, \phi_{yy}, \phi_{zz}]$ and then they are applied to a rigid box in two different orders, the final configuration of the box in general, will be different for each one of the options. Therefore, the three components of $\hat{\phi}$ do not represent uniquely to a given spatial rotation. Hence, rotations can not be treated as vectors due to they component do not commute, as it has been seen in the previous example or alternatively in Refs. [199, 363].

The *non–commutativity* of the components of the rotation vector implies that finite rotations are not elements of a *vectorial space*. From an algebraic point of view, a rotation $\boldsymbol{\beta}$ is a linear map or operator from $\mathbb{E}^3$, the 3D Euclidean vector space, to itself; that is to say, when a rotation is applied on a vector, the result always is a new vector, conserving the original length [48].

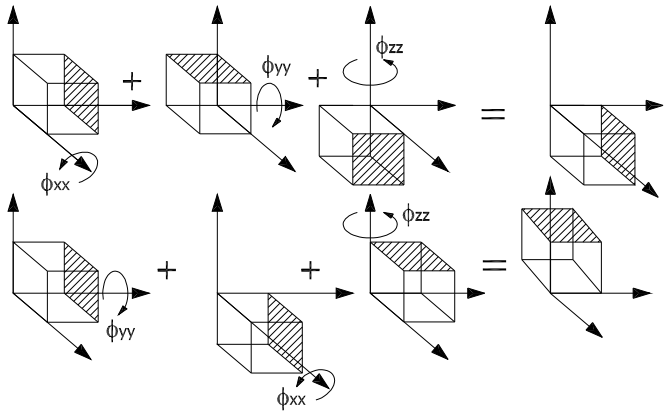

Figure A.1: Non-commutativity of the components of the *rotation vector* $\hat{\phi} = [\phi_{xx}, \phi_{yy}, \phi_{zz}]$.

Given the set $\mathfrak{R} = \{\boldsymbol{\beta} : \mathbb{E}^3 \to \mathbb{E}^3 \mid \boldsymbol{\beta} \text{ is a rotation operator}\}$, composed by all the finite rotations, it is possible to define an inner composition $\widetilde{\otimes}$ called *sum of rotations* in the following way

$$(\boldsymbol{\beta}_a \widetilde{\otimes} \boldsymbol{\beta}_b)(\hat{x}) \in \mathbb{E}^3 = \boldsymbol{\beta}_a(\boldsymbol{\beta}_b(\hat{x})) \quad \forall \quad \boldsymbol{\beta}_a, \boldsymbol{\beta}_b \in \mathfrak{R}, \quad \hat{x} \in \mathbb{E}^3 \tag{A.1}$$

where $\boldsymbol{\beta}_a$, $\boldsymbol{\beta}_b \in \mathfrak{R}$, are two consecutive rotations applied on the vector $\hat{x} \in \mathbb{E}^3$, and $\boldsymbol{\beta}_a(\boldsymbol{\beta}_b(\bullet)) \in \mathfrak{R}$ is the equivalent or *compound rotation* applied on $\hat{x}$. The set $\mathfrak{R}$ doted with the composition law $\widetilde{\otimes}$ posses the algebraic structure of *non-commutative group* (non–Abelian), which is formally defined [48] as

Definition A.1. ***Non-commutative group of rotations***

The set $\mathfrak{R}$ equipped with the internal operation $\widetilde{\otimes}$ is a non-commutative group if it is such that:

1. The internal operation is associative, *i.e.* $\boldsymbol{\beta}_a \widetilde{\otimes} (\boldsymbol{\beta}_b \widetilde{\otimes} \boldsymbol{\beta}_c) = (\boldsymbol{\beta}_a \widetilde{\otimes} \boldsymbol{\beta}_b) \widetilde{\otimes} \boldsymbol{\beta}_c$, $\forall \boldsymbol{\beta}_a, \boldsymbol{\beta}_b, \boldsymbol{\beta}_c \in \mathfrak{R}$.
2. There is a unique element $\mathbf{I} \in \mathfrak{R}$ called identity such that $\boldsymbol{\beta}_a \widetilde{\otimes} \mathbf{I} = \mathbf{I} \widetilde{\otimes} \boldsymbol{\beta}_a = \boldsymbol{\beta}_a$, $\forall \boldsymbol{\beta}_a \in \mathfrak{R}$.
3. For each $\boldsymbol{\beta}_a \in \mathfrak{R}$ there exist a unique element of $\mathfrak{R}$ called the inverse of $\boldsymbol{\beta}_a$ and denoted by $\boldsymbol{\beta}_a^{-1}$, such that $\boldsymbol{\beta}_a^{-1} \widetilde{\otimes} \boldsymbol{\beta}_a = \boldsymbol{\beta}_a \widetilde{\otimes} \boldsymbol{\beta}_a^{-1} = \mathbf{I}$.
4. The internal operation is non commutative *i.e.* $(\boldsymbol{\beta}_a \widetilde{\otimes} \boldsymbol{\beta}_b)(\hat{x}) \neq (\boldsymbol{\beta}_b \widetilde{\otimes} \boldsymbol{\beta}_a)(\hat{x})$.

For a detailed discussion about transformation groups see Refs. [246, 245, 285] ■

The group $\mathfrak{R}$ is isomorphic to the set composed by all the real and orthogonal matrices of order 3, with determinant equal to 1. The demonstration of this last result can be found, for example, in Ref. [321]. This isomorphism allow to identify each finite rotation with the corresponding orthogonal *rotation tensor* belonging to the *special orthogonal group* $SO(3)$ defined as

$$\mathcal{L}(\mathbb{E}^3) \supset SO(3) = \{\mathbf{\Lambda} \in \mathbf{M}_3(3) \;\; | \;\; \mathbf{\Lambda}^T\mathbf{\Lambda} = \mathbf{\Lambda}\mathbf{\Lambda}^T = \mathbf{I};\;\; |\mathbf{\Lambda}| = 1\} \tag{A.2}$$

where $\mathcal{L}(\mathbb{E}^3)$ is the space of linear transformations (or tensors) of $\mathbb{E}^3$, $\mathbf{I}$ is the identity matrix[2], $\mathbf{M}_3(3)$ is the set composed by all the 3×3 matrices with real coefficients, $\mathbf{\Lambda}$ is a *rotation tensor* and $|\bullet| = \text{Det}[\bullet]$ is the determinant operator. Therefore, $SO(3)$ is the set of all 3×3 real orthogonal matrices with unit determinant. It is not difficult to see that $SO(3)$ also have the structure of *smooth differentiable manifold* [119, 251], which is formally defined as

Definition A.2. ***Smooth n-manifolds***

A *smooth n–manifold* or manifold modeled in $\mathbb{R}^n$ is a set $\mathcal{M}$ such that:

1. For each element $P \in \mathcal{M}$ there is a subset $\mathcal{U}$ of $\mathcal{M}$ containing P and an one-to-one mapping called a *chart* or *coordinate system*, $\{x^\alpha\}$, from $\mathcal{U}$ onto an open set $\mathcal{V} \in \mathbb{R}^n$; x^α denote the components of this mapping ($\alpha = 1, 2, \ldots, n$).

2. If x^α and $\overline{x}^\alpha$ are two of such mappings, the change of coordinate functions $\overline{x}^\alpha(x^1, \ldots, x^n)$ are C^∞ (*i.e.* it is continuously differentiable as many times as required) ■

The definition of smooth manifold requires explicit expressions for the charts $\{x^\alpha\}$; in the case of the rotational manifold $SO(3)$ this aspect will be addressed in a next section devoted to its parametrization. A more extensive treatment about differential manifolds can be consulted in Refs. [255, 251]. It is also possible to show that the differential manifold $SO(3)$ under the usual matrix multiplication has the structure of a *Lie group*, which is defined as

Definition A.3. ***Lie groups***

A *Lie group* is a smooth n–dimensional manifold $\mathcal{M}^n$ endowed with the following two smooth mappings:

$$\begin{array}{rcll} \mathscr{F}_\alpha : \mathcal{M}^n \times \mathcal{M}^n & \rightarrow & \mathcal{M}^n & \\ (\boldsymbol{x}_1, \boldsymbol{x}_2) & \mapsto & \mathscr{F}_\alpha(\boldsymbol{x}_1, \boldsymbol{x}_2) = \boldsymbol{x}_1 \odot \boldsymbol{x}_2 & \text{Multiplication.} \end{array}$$

where $\boldsymbol{x}_1$, $\boldsymbol{x}_2 \in \mathcal{M}^n$, the symbol $\times$ is used to denote pairing between elements and the symbol $\odot$ is used to indicate an abstract operation (multiplication) between elements of the manifold $\mathcal{M}^n$. The second smooth mapping is:

$$\begin{array}{rcll} \mathscr{F}_\nu : \mathcal{M}^n & \rightarrow & \mathcal{M}^n & \\ \boldsymbol{x}_1 & \mapsto & \mathscr{F}_\nu(\boldsymbol{x}_1) = (\boldsymbol{x}_1)^{-1} & \text{Construction of the inverse element.} \end{array}$$

And having marked point $\boldsymbol{e} \in \mathcal{M}^n$ which satisfies together with $\mathscr{F}_\alpha$ and $\mathscr{F}_\nu$ the relations:

1. $\boldsymbol{x}_1 \odot (\boldsymbol{x}_2 \odot \boldsymbol{x}_3) = (\boldsymbol{x}_1 \odot \boldsymbol{x}_2) \odot \boldsymbol{x}_3$.

[2]Through the text the symbols $\mathbf{I}$, $\boldsymbol{I}$ and $\boldsymbol{i}$ are used to denote the identity element on a given set or metric space.

2. $\boldsymbol{e} \odot \boldsymbol{x}_1 = \boldsymbol{x}_1 \odot \boldsymbol{e} = \boldsymbol{x}$

3. $\boldsymbol{x} \odot \boldsymbol{x}^{-1} = \boldsymbol{x}^{-1} \odot \boldsymbol{x} = \boldsymbol{e}$ ■

Identifying $\boldsymbol{x}_i$ $(i = 1, 2, 3)$ with rotation operators as defined in Eq. (A.2), the operator $\mathscr{F}_\alpha = \odot$ with the usual matrix multiplication and the inverse matrix operator with $\mathscr{F}_\nu = (\bullet)^{-1}$, it is straightforward to see that $SO(3)$ posses the structure of a Lie group [319, 394]. It is also worth to note the parallelism between the definition of Lie group and the non-commutative group of rotations as presented above. For a more rigorous study of Lie groups it is recommendable to consult Refs. [119, 251, 285].
Let us recall that all the elements of $SO(3)$ entails the fundamental properties $\boldsymbol{\Lambda}^{-1} = \boldsymbol{\Lambda}^T$ and $|\boldsymbol{\Lambda}| = 1$. In the same manner, it is possible to identify the rotations $\boldsymbol{\beta}_a, \boldsymbol{\beta}_b, (\boldsymbol{\beta}_a \widetilde{\otimes} \boldsymbol{\beta}_b)$ and $(\boldsymbol{\beta}_b \widetilde{\otimes} \boldsymbol{\beta}_a) \in \mathfrak{R}$ with the corresponding operators: $\boldsymbol{\Lambda}_a, \boldsymbol{\Lambda}_b, \boldsymbol{\Lambda}_{ab}, \boldsymbol{\Lambda}_{ba} \in SO(3)$.
As it has been explained, rotations can be defined by means of rotation operators; the components of a given rotation operator depend on the reference frame adopted. On one hand, if two consecutive rotations $\boldsymbol{\beta}_a$ and $\boldsymbol{\beta}_b$, are composed to obtain $\boldsymbol{\beta}_a \widetilde{\otimes} \boldsymbol{\beta}_b$, two situations can happen:

- In the first case, the components of the rotation tensors representing the rotation $\boldsymbol{\beta}_a$ and $\boldsymbol{\beta}_b$, $\boldsymbol{\Lambda}_a$ and $\boldsymbol{\Lambda}_b \in SO(3)$, respectively, can be directly expressed in terms of a fixed [15], usually called spatial, reference frame and, therefore, the description employed for rotations is called *spatial description*[3].
  In this case, the vector $\hat{v}_c \in \mathbb{E}^3$ obtained by the application of a sequence of N rotations on a vector $\hat{v} \in \mathbb{E}^3$ can be seen as the result of the application of a *compound rotation* $\boldsymbol{\Lambda}_c \in SO(3)$ obtained by the consecutive application of the rotation tensors $\boldsymbol{\Lambda}_i \in SO(3)$ $(i = 1 \dots N)$ on the previous rotated vector, *i.e.*

$$\hat{v}_c = \boldsymbol{\Lambda}_N(\cdots(\boldsymbol{\Lambda}_i(\cdots(\boldsymbol{\Lambda}_1(\hat{v}))\cdots))\cdots) = \underbrace{\boldsymbol{\Lambda}_N \cdots \boldsymbol{\Lambda}_i \cdots \boldsymbol{\Lambda}_1}_{\boldsymbol{\Lambda}_c}(\hat{v}) \in \mathbb{E}^3. \tag{A.3}$$

  Therefore, the *inverse multiplicative rule* for rotation tensors is valid for the composition of rotations [321]. This is the typical case found in mechanics when a body attached frame is involved in describing the kinematics of material points [107] even when the components of the rotation tensors are given in a spatially fixed reference frame.

- In the second case, the rotation tensor $\boldsymbol{\Lambda}_a$, moves the reference frame and, therefore, the components of the rotation tensor $\boldsymbol{\Lambda}_b$ representing the second rotation $\boldsymbol{\beta}_b$ are expressed in the new rotated, or *updated*, reference frame. If several rotations are applied, the reference frame is transformed in a *rotating reference frame*.
  In this case, the *direct multiplicative rule* is valid for the composition of rotations, *i.e.*

$$\hat{v}_c = \boldsymbol{\Lambda}_1(\cdots(\boldsymbol{\Lambda}_i(\cdots(\boldsymbol{\Lambda}_N(\hat{v}))\cdots))\cdots) = \underbrace{\boldsymbol{\Lambda}_1 \cdots \boldsymbol{\Lambda}_i \cdots \boldsymbol{\Lambda}_N}_{\boldsymbol{\Lambda}_c}(\hat{v}) \in \mathbb{E}^3. \tag{A.4}$$

  Note that in Eq. (A.4) the components of each rotation tensor are referred to the corresponding updated reference frame. This kind of description of rotations is usually called *material description* and it is completely equivalent to the spatial one.

Identical results as those above explained can be reached by means of simple geometrical considerations; Fig. A.2 presents the result of applying two consecutive rotations $\boldsymbol{\theta}$ and $\boldsymbol{\phi}$ about

[3]Some authors [110, 199, 198, 200, 201] prefer to use the language of rigid-body dynamic employing the terms spatial and body attached coordinates in stead of material and spatial descriptions, respectively.

the axis Z and X respectively. In Figure A.2a the axis of rotation are fixed and the sequence of rotations is defined as: $\boldsymbol{\theta} \rightarrow \boldsymbol{\phi}$, first a rotation a rotation about Z is applied, followed by a rotation about X. On the contrary, in Fig. A.2b rotations are carried out in the inverse order, *i.e.* $\boldsymbol{\phi} \rightarrow \boldsymbol{\theta}$. In this case the second rotation $\boldsymbol{\theta}$ is carried out about the updated axis Z' obtained after applying the rotation $\boldsymbol{\phi}$ about X.

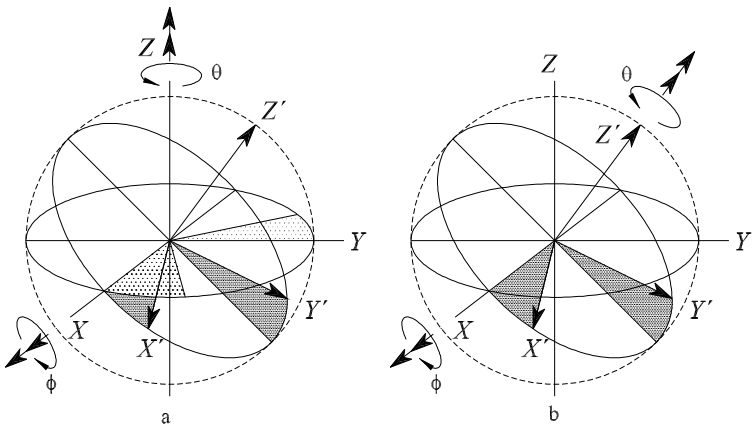

Figure A.2: Composition of rotations in the space. (a): Fixed base: $\boldsymbol{\theta} \rightarrow \boldsymbol{\phi}$. ($b$): Movable base: $\boldsymbol{\phi} \rightarrow \boldsymbol{\theta}$.

In both cases the resulting configuration is the same. Therefore, the composition of two or more rotations defined in terms of a spatially fixed reference frame is the same as these obtained applying the same sequence of rotations referred to a rotating frame but inverting the order of the composition. A more detailed introduction to the material and spatial descriptions of rotations and the related mathematical objects will be given in Section A.4.

A.2 Parametrization of the rotational manifold

Strictly, rotational motion can be regarded as the motion of particle within the nonlinear manifold $SO(3)$, therefore, it can not be described trivially by using standard coordinates as those commonly employed for motions in a linear space. As it has been previously described, rotations have to be parameterized using suitable charts [285, 394], some time called *quasi–coordinates*, which are inherently not global and/or non-singular [321]. Over the years, numerous techniques has been developed to cope with the description of rotational motion, following different approaches *e.g.* [321, 363, 394]. Among those we found the Cayley, or Gibbs, or Rodrigues parametrization [49]; the Milenkovic, or modified Rodrigues, or conformal rotation vector parametrization [283]; the Euler–Rodrigues, or unit quaternion parametrization [389], the Eulerian angles parametrization [148], (Euler angles are only one of several possible choices within this class, Cardan and Bryant angles being other choices); the Cayley–Klein parametrization [103]; the direction cosine parametrization [194]; and so on.
All these techniques show certain balance between advantages and drawbacks when compared each to other. Usually, both theoretical and computational issues can play a meaningful role in the choice, which is also influenced by the possible specific requirements of its application. According to Trainelli [394], within this somewhat unexpectedly large set, however, it is possible to draw a separation of the various techniques in two brad classes: the *vectorial* parameterizations, and the *non-vectorial* parameterizations.

The vectorial parameterizations feature a set of three or more parameters that define the cartesian components of a vector. This do not apply when dealing with non-vectorial techniques (*e.g.* Euler angles are three scalars that can not be understood as components of a geometric vector). Note that vector parameterizations can be *minimal, i.e.* are based on a smallest possible set of parameters, since the dimension of the $SO(3)$ is three. Non-minimal parameterizations include the Euler-Rodrigues and the Cayley-klein parameterizations (four scalar parameters related by and algebraic constrain) and the director cosine parametrization (nine scalar parameters related by six algebraic constrains).
In following we briefly describe the several choices for the parametrization of the rotational manifold, although in this work a part of the kinematics of rod elements is described using rotation tensors described by a minimal vectorial parametrization. Firstly, an intuitive geometrical deduction of an explicit expression for the rotation tensor in terms of the cartesian components of a rotation vector throughout the well known Euler's theorem [394] is presented and then its properties as well as other possible parameterizations are discussed.

A.2.1 The Euler´s theorem

The most used minimal vectorial parametrization of the rotation tensor is based by the *fundamental theorem of Euler* [394], which say: *The general displacement of a rigid body or vector, with one point fixed is a rotation about some axis which pases through that point.* A schematic representation of the theorem is shown in Fig. A.3 where $\hat{e} \in \mathbb{R}^3$ is the unit vector of the *axis of rotation* and $\theta = (\hat{\theta} \cdot \hat{\theta})^{1/2} \in [0, 2\pi]$ is the magnitude of the *rotation angle* with respect to a reference configuration[4]. By this way, the notion of a rotation vector $\hat{\theta} = \theta_i \hat{e}_i = \theta \hat{e}$, introduced in Section A.1 for describing rotations[5], is recovered.

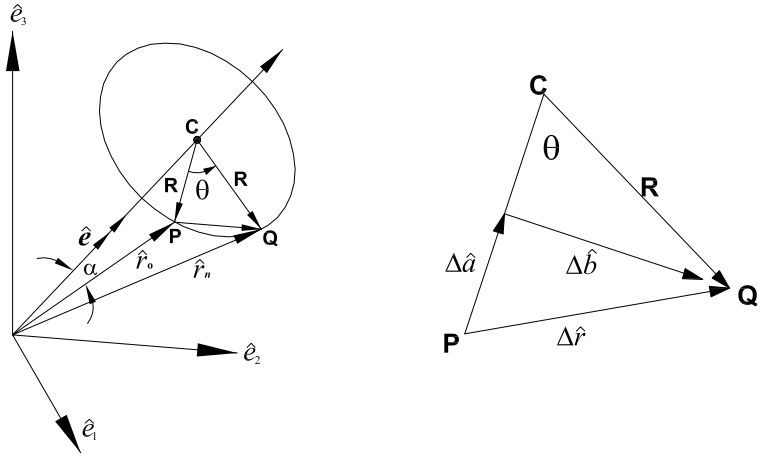

Figure A.3: Rotation vector.

Whenever $\theta = 0$ the axis $\hat{e}$ is not uniquely defined. Note that, since 2 scalar parameters are needed to represent a constat magnitude vector, such as $\hat{e}$, a generic rotation can be described at least with 3 scalar parameters, *i.e.* the dimension of the manifold $SO(3)$. Identical conclusions can be reached considering that the rotation tensor have nine independent components, which are reduced to three imposing the restriction associated to the manifold $SO(3)$, *i.e.* $\mathbf{\Lambda}\mathbf{\Lambda}^T = \mathbf{I}$

[4]The two quantities $(\hat{e}, \theta)$ are sometimes labeled as the *principal axis* of rotation and the *principal angle* of rotation, respectively [394].

[5]The vector $\hat{\theta}$ is some times called *pseudo–vector.*

and $\mathrm{Det}[\mathbf{\Lambda}] = 1$. By means of the Euler´s theorem, the two quantities $(\hat{e}, \theta)$ completely define the rotational displacement represented by the rotation tensor $\mathbf{\Lambda}$. Following geometrical reasonings from Fig. A.3 it is possible to see that

$$\Delta\hat{r} = \Delta\hat{a} + \Delta\hat{b} \tag{A.5}$$

where $\Delta\hat{b}$ is orthogonal to $\Delta\hat{a}$. The length of $\Delta\hat{b}$ is given by $\Delta \mathrm{b} = \mathrm{R}\sin(\theta)$, so that

$$\Delta\hat{b} = \frac{\Delta \mathrm{b}}{\|\hat{r}_o \times \hat{e}\|}(\hat{e} \times \hat{r}_o) = \frac{\mathrm{R}\sin(\theta)}{\|\hat{r}_o \times \hat{e}\|}(\hat{e} \times \hat{r}_o). \tag{A.6}$$

But, $\|\hat{r}_o \times \hat{e}\| = \|\hat{r}_o\| \sin\alpha = \mathrm{R}$, as it can be seen from Fig. A.3, so that Eq. (A.6) can be expressed as

$$\Delta\hat{b} = \sin(\theta)(\hat{e} \times \hat{r}_o) = \frac{\sin(\theta)}{\theta}(\hat{\theta} \times \hat{r}_o). \tag{A.7}$$

The vector $\Delta\hat{a}$ is orthogonal to both $\hat{e}$ and $\Delta\hat{b}$. Hence:

$$\begin{aligned}
\Delta\hat{a} &= \frac{\Delta \mathrm{a}}{\|\hat{e} \times \hat{r}_o\|} = (\hat{e} \times (\hat{e} \times \hat{r}_o)) = \frac{\Delta\hat{a}}{\mathrm{R}} = (\hat{e} \times (\hat{e} \times \hat{r}_o)) \\
\Delta \mathrm{a} &= \mathrm{R}(1 - \cos\theta) \\
\Delta\hat{a} &= \mathrm{R}(1 - \cos\theta)(\hat{e} \times (\hat{e} \times \hat{r}_o)) = \frac{1 - \cos\theta}{\theta^2}(\hat{\theta} \times (\hat{\theta} \times \hat{r}_o)).
\end{aligned} \tag{A.8}$$

Hence, from Eqs. (A.5), (A.7) and (A.8) we have

$$\hat{r}_n = \hat{r}_o + \Delta\hat{r} = \hat{r}_o + \frac{\sin(\theta)}{\theta}(\hat{\theta} \times \hat{r}_o) + \frac{(1 - \cos\theta)}{\theta^2}(\hat{\theta} \times (\hat{\theta} \times \hat{r}_o)). \tag{A.9}$$

Considering that $\hat{\theta} \times \hat{r}_o = \widetilde{\boldsymbol{\theta}}\hat{r}_o$, where $\widetilde{\boldsymbol{\theta}}$ the skew–symmetric tensor obtained from $\hat{\theta}$, *i.e.* $\hat{\theta} \times \hat{v} = \mathbf{\Pi}[\hat{\theta}]\hat{v} = \widetilde{\boldsymbol{\theta}}\hat{v}$, $\forall \hat{v} \in \mathbb{R}^3$, it is possible to recast Eq. (A.9) as

$$\hat{r}_n = \mathbf{\Lambda}(\hat{\theta})\hat{r}_o \tag{A.10}$$

where the rotation matrix $\mathbf{\Lambda}(\hat{\theta})$ is expressed according to the well known *Rodrigues's formula* [321, 394, 108]), which relates the *rotation vector* $\hat{\theta}$ with the associated *rotation tensor* $\mathbf{\Lambda}$ in the following form:

$$\mathbf{\Lambda} = \mathbf{I} + \frac{\sin\theta}{\theta}\widetilde{\boldsymbol{\theta}} + \frac{(1 - \cos\theta)}{\theta^2}\widetilde{\boldsymbol{\theta}}\widetilde{\boldsymbol{\theta}} = \mathbf{I} + \sin\theta\widetilde{\boldsymbol{e}} + (1 - \cos\theta)\widetilde{\boldsymbol{e}}\widetilde{\boldsymbol{e}}. \tag{A.11}$$

An alternative expression for Eq. (A.11) is

$$\mathbf{\Lambda} = \cos\theta\mathbf{I} + \sin\theta\widetilde{\boldsymbol{e}} + (1 - \cos\theta)(\widehat{e} \otimes \widehat{e}) \tag{A.12}$$

since $(\widetilde{\bullet})^2 = \bullet \otimes \bullet - |\bullet|^2\mathbf{I}, \quad \forall \bullet \in \mathbb{R}^3$.
Note that the rotation corresponding to $(-\theta, \hat{e})$ is equivalent to that corresponding to $(\theta, -\hat{e})$, hence it is represented by the tensor $\mathbf{\Lambda}^T = \mathbf{\Lambda}^{-1}$. It follows that the rotation tensor $\mathbf{\Lambda}$ rotates $\hat{e}$ on to itself, consequently,

$$\mathbf{\Lambda}(\hat{e}, \theta)\hat{e} - \hat{e} = \mathbf{\Lambda}(\hat{\theta})\hat{\theta} - \hat{\theta} = 0 \tag{A.13}$$

so that $\hat{e}$ is an eigenvector of $\mathbf{\Lambda}$ with positive unit eigenvalue. The other two eigenvectors and eigenvalues are easily determined using the orthogonality of $\mathbf{\Lambda}$ and considering that it is a real

operator with determinant equal to the 1. All the roots of the characteristic polynomial have a modulus equal to the unity. The other two roots are imaginary and conjugated, and it is possible to write their values as, $\lambda_1 = 1$, $\lambda_2 = e^{i\theta}$ and $\lambda_3 = e^{-i\theta}$. Having determined the roots, the general expression for the characteristic polynomial, $\wp$, of $\mathbf{\Lambda}$ is

$$\wp(\mathbf{\Lambda}) = \mathbf{\Lambda}^3 - \alpha_\wp \mathbf{\Lambda}^2 + \alpha_\wp \mathbf{\Lambda} - \mathbf{I} = 0 \tag{A.14}$$

where $\alpha_\wp$ is the trace of $\mathbf{\Lambda}$ and it is equal to $(1-\cos\theta)$ [321, 108]. Additionally, when two rotations $\mathbf{\Lambda}_a$, $\mathbf{\Lambda}_b$ are composed to obtain $\mathbf{\Lambda} = \mathbf{\Lambda}_b\mathbf{\Lambda}_a$, the quantities $(\theta, \hat{e})$ that are found applying Euler's theorem for the composed rotation $\mathbf{\Lambda}$ are related to $(\theta_a, \hat{e}_a)$, $(\theta_b, \hat{e}_b)$, *i.e.* the corresponding to $\mathbf{\Lambda}_a$ and $\mathbf{\Lambda}_b$ by [394]

$$\begin{aligned} \cos\frac{\theta}{2} &= \cos\frac{\theta_a}{2}\cos\frac{\theta_b}{2} - \sin\frac{\theta_a}{2}\sin\frac{\theta_b}{2}(\hat{e}_a \cdot \hat{e}_b) \\ \sin\frac{\theta}{2}\hat{e} &= \cos\frac{\theta_a}{2}\sin\frac{\theta_b}{2}(\hat{e}_b) + \cos\frac{\theta_b}{2}\sin\frac{\theta_a}{2}(\hat{e}_a) + \sin\frac{\theta_a}{2}\sin\frac{\theta_b}{2}(\hat{e}_b \times \hat{e}_a) \end{aligned} \tag{A.15}$$

A.2.2 Obtention the rotation pseudo–vector from rotation tensor

According to Eq. (A.11) and considering the symmetric part of the rotation tensor $\mathbf{\Lambda}$ [108]

$$\mathbf{\Lambda}^{\text{sym}} = \frac{1}{2}(\mathbf{\Lambda} - \mathbf{\Lambda}^T) = \sin\theta\widetilde{\boldsymbol{e}} = \frac{\sin\theta}{\theta}\widetilde{\boldsymbol{\theta}} \tag{A.16}$$

from which, knowing the skew–symmetric form of $\widetilde{\boldsymbol{\theta}}$, the terms $\hat{e}$ or θ can be obtained via:

$$\sin\theta\hat{e} = \frac{\sin\theta}{\theta}\frac{1}{2}\begin{bmatrix}\Lambda_{32} - \Lambda_{23} \\ \Lambda_{13} - \Lambda_{31} \\ \Lambda_{21} - \Lambda_{12}\end{bmatrix}. \tag{A.17}$$

This equation can be used provided $0 < \|\hat{\theta}\| < \pi$, but for outside of this range unicity is not ensured. A more accurate procedure for obtaining the pseudo-vector of rotation from the rotation tensor requires to employ a non minimal parametrization [108, 340, 341, 363] of the rotation as it will be discussed in the next sections.

A.2.3 Tangent space to the rotational manifold

Taking into account the orthogonality of $\mathbf{\Lambda}$, *i.e.* $\mathbf{\Lambda}\mathbf{\Lambda}^T = \mathbf{\Lambda}^T\mathbf{\Lambda} = \mathbf{I}$ and considering a variation[6] of $\mathbf{\Lambda}$, $\delta\mathbf{\Lambda}$, we have

$$\begin{aligned} \delta(\mathbf{\Lambda}\mathbf{\Lambda}^T) &= \delta\mathbf{\Lambda}\mathbf{\Lambda}^T + \mathbf{\Lambda}\delta\mathbf{\Lambda}^T = \widetilde{\boldsymbol{\phi}} + \widetilde{\boldsymbol{\phi}}^T = 0 \\ \delta(\mathbf{\Lambda}^T\mathbf{\Lambda}) &= \delta\mathbf{\Lambda}^T\mathbf{\Lambda} + \mathbf{\Lambda}^T\delta\mathbf{\Lambda} = \widetilde{\mathbf{\Phi}}^T + \widetilde{\mathbf{\Phi}} = 0. \end{aligned} \tag{A.18}$$

From Eq. (A.18) it is possible to deduce that the products $\delta\mathbf{\Lambda}\mathbf{\Lambda}^T$ and $\mathbf{\Lambda}^T\delta\mathbf{\Lambda}$ are *skew–symmetric operators* that will be denoted by $\widetilde{\boldsymbol{\phi}}$, $(\widetilde{\boldsymbol{\phi}}^T)$, and $\widetilde{\mathbf{\Phi}}$, $(\widetilde{\mathbf{\Phi}}^T)$, respectively. It is also possible to see that the variation of the rotation tensor is the product of one of this skew–symmetric tensors

[6] Observe that we have no defined explicit methods for calculating the linearized increments or the variations, however, for the purpose of introducing the the main ideas about tangent spaces to $SO(3)$ it is sufficient to suppose that we can calculate $\delta\mathbf{\Lambda}$. A detailed exposition about the calculus of variations on the rotational manifold is presented in next sections.

by the proper rotation tensor, according to

$$\delta\mathbf{\Lambda} = \widetilde{\boldsymbol{\phi}}\mathbf{\Lambda} = \mathbf{\Lambda}\widetilde{\mathbf{\Phi}}. \tag{A.19}$$

By other hand, if we take a point $\mathbf{\Lambda}_a \in SO(3)$ and let $\mathbf{\Lambda}(t)$ be any differentiable curve on $SO(3)$ parameterized in terms of a real parameter $t \in \mathbb{R}$, that passes through $\mathbf{\Lambda}_a$ at $t = 0$; that is $\mathbf{\Lambda}(0) = \mathbf{\Lambda}_a$, then the derivative with respect to t, $(\mathrm{d}/\mathrm{d}t[\mathbf{\Lambda}])|_{t=0}$, is said to be a *tangent vector* to $SO(3)$ at $\mathbf{\Lambda}_a$. The set of all tangent vectors at $\mathbf{\Lambda}_a$, denoted by $T_{\mathbf{\Lambda}_a}SO(3)$, forms a vector space called *tangent space* to $SO(3)$ at $\mathbf{\Lambda}_a$; formally we have the following definitions:

Definition A.4. ***Tangent space***

Let $\mathcal{M} \subset \mathbb{R}^n$ be an open set (manifold) and let $P \in \mathcal{M}$. The *tangent space* to $\mathcal{M}$ at P is simply the vector space $\mathbb{R}^n$ regarded as vectors emanating from P; this tangent space is denoted $T_P\mathcal{M}$ [251] (see Fig. A.4) ■

In the case of the rotational manifold, the tangent space at the identity $\mathbf{\Lambda}_a = \mathbf{I}$ is given a special name, the *Lie algebra* of $SO(3)$ and is denoted by $so(3)$. It has several important properties and in following we present a more rigorous definition:

Definition A.5. ***Lie algebra***

A *Lie algebra* ℓ of the Lie group L (see §A.1) is a tangent vector space at the identity, $T_{\mathbf{I}}L$, equipped with a bilinear, skew–symmetric brackets operator $[\![\cdot,\cdot]\!]$ satisfying *Jacobi's identity* [119, 285]. That is:

1. $[\![\boldsymbol{x}_a,[\![\boldsymbol{x}_b,\boldsymbol{x}_c]\!]]\!] + [\![\boldsymbol{x}_b,[\![\boldsymbol{x}_c,\boldsymbol{x}_a]\!]]\!] + [\![\boldsymbol{x}_c,[\![\boldsymbol{x}_a,\boldsymbol{x}_b]\!]]\!] = 0 \quad \forall \boldsymbol{x}_a,\boldsymbol{x}_b,\boldsymbol{x}_c \in \ell.$
2. The skew–symmetry means that $[\![\boldsymbol{x}_a,\boldsymbol{x}_b]\!] = -[\![\boldsymbol{x}_b,\boldsymbol{x}_a]\!] \quad \forall \boldsymbol{x}_a,\boldsymbol{x}_b \in \ell.$

Where the *Lie brackets* $[\![\cdot,\cdot]\!]$ can be obtained by differentiating the *Lie algebra adjoint transformation* Ad_G:

$$\begin{aligned} \mathrm{Ad}_G : \ell &\rightarrow \ell \\ \boldsymbol{x}_b &\mapsto \mathrm{Ad}_G[\boldsymbol{x}_b] := G\boldsymbol{x}_bG^{-1} \end{aligned}$$

where ℓ is a Lie algebra, $\boldsymbol{x}_b \in \ell$ and $G \in L$ a Lie group. The differentiation is carried out with respect to $G(\nu) \in L$ at the identity in the direction $\boldsymbol{x}_a \in \ell$ such that $G(\nu = 0) = \mathbf{I}$ and $\mathrm{d}G/\mathrm{d}\nu|_{\nu=0} = \boldsymbol{x}_a$ where $\nu \in \mathbb{R}$ is a parameter, giving:

$$[\![\boldsymbol{x}_a,\boldsymbol{x}_b]\!] \triangleq \frac{\mathrm{d}}{\mathrm{d}\nu}[G\boldsymbol{x}_bG^{-1}]\Big|_{\nu=0} = \Big[(\frac{\mathrm{d}}{\mathrm{d}\nu}G)\boldsymbol{x}_bG^{-1} + G\boldsymbol{x}_b\frac{\mathrm{d}}{\mathrm{d}\nu}(G^{-1})\Big]\Big|_{\nu=0} = \boldsymbol{x}_a\boldsymbol{x}_b - \boldsymbol{x}_b\boldsymbol{x}_a \qquad \blacksquare$$

Taking into account the above definition it is possible to show that $so(3)$ consist of the 3×3 skew–symmetric tensors. Differentiating both sides of $\mathbf{\Lambda}^T(t)\mathbf{\Lambda}(t) = \mathbf{I}$ and considering that $\mathbf{\Lambda}|_{(t=0)} = \mathbf{I}$ it follows that $(\mathrm{d}/\mathrm{d}t[\mathbf{\Lambda}^T]\mathbf{\Lambda})|_{t=0} + (\mathbf{\Lambda}^T\mathrm{d}/\mathrm{d}t[\mathbf{\Lambda}])|_{t=0} = 0$, so that the tensor elements of $so(3)$ have the form

$$\widetilde{\boldsymbol{\theta}} \triangleq \begin{bmatrix} 0 & -\theta_3 & \theta_2 \\ \theta_3 & 0 & -\theta_1 \\ -\theta_2 & \theta_1 & 0 \end{bmatrix}. \tag{A.20}$$

Note that an element $\widetilde{\boldsymbol{\theta}} \in so(3)$ can be represented by a vector $\hat{\theta} \in \mathbb{R}^3$ by means of the isomorphism established by the operator $\mathbf{\Pi} : \mathbb{R}^3 \rightarrow so(3)$ such that $\mathbb{R}^3 \ni \hat{\theta} \mapsto \mathbf{\Pi}[\hat{\theta}] = \widetilde{\boldsymbol{\theta}} \in T_{\mathbf{I}}SO(3)$. Thus, the skew–symmetric $\widetilde{\boldsymbol{\theta}}$ belongs to the tangent space of the rotation manifold $SO(3)$, denoted by $T_{\mathbf{I}}SO(3) = so(3)$ where the identity $\mathbf{I} \in SO(3)$ represent a base point on the rotational

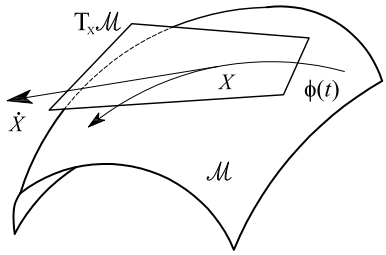

Figure A.4: Tangent vector $\dot{X} \in T_X\mathcal{M}$ to the manifold $\mathcal{M}$.

manifold. The following important relationships between the skew–symmetric tensor $\widetilde{\boldsymbol{\theta}} \in so(3)$ associated to the rotation vector $\widehat{\theta}_i \in \mathbb{R}^3$ are frequently found in the development of geometrically exact formulations for rods [285, 319, 394]

$$\widetilde{\boldsymbol{\theta}}_1\widetilde{\boldsymbol{\theta}}_2 = \hat{\theta}_1 \times \hat{\theta}_2 \tag{A.21a}$$
$$\widetilde{\boldsymbol{\theta}}_1\widetilde{\boldsymbol{\theta}}_2 = \hat{\theta}_2 \otimes \hat{\theta}_1 - \hat{\theta}_1 \cdot \hat{\theta}_2\mathbf{I} \tag{A.21b}$$
$$\widetilde{\boldsymbol{\theta}}_1\hat{\theta}_2 = -\widetilde{\boldsymbol{\theta}}_2\hat{\theta}_1 \tag{A.21c}$$
$$\hat{\theta}_1^T\widetilde{\boldsymbol{\theta}}_2 = -\hat{\theta}_2^T\widetilde{\boldsymbol{\theta}}_1 \tag{A.21d}$$
$$\widetilde{\boldsymbol{\theta}}\hat{\theta} = \hat{\theta}^T\widetilde{\boldsymbol{\theta}} \tag{A.21e}$$
$$\widetilde{\boldsymbol{\theta}}^{n+2} = -(\hat{\theta}^T\hat{\theta})\widetilde{\boldsymbol{\theta}}^n \quad (\text{for } n \geqslant 1) \tag{A.21f}$$
$$\boldsymbol{\Pi}(\widetilde{\boldsymbol{\theta}}_1\hat{\theta}_2) = \widetilde{\boldsymbol{\theta}}_1\widetilde{\boldsymbol{\theta}}_2 - \widetilde{\boldsymbol{\theta}}_2\widetilde{\boldsymbol{\theta}}_1 = \hat{\theta}_2 \otimes \hat{\theta}_1 - \hat{\theta}_1 \otimes \hat{\theta}_2 \tag{A.21g}$$

REMARK A.1. Taking into account the fact that $T_{\mathbf{I}}SO(3) \approx so(3)$ posses the formal structure of the Lie algebra of the Lie group $SO(3)$ it is possible to identify the corresponding *adjoint map* as follows: if $\boldsymbol{\Lambda}$ and $\widetilde{\boldsymbol{\theta}}$ are arbitrary elements of $SO(3)$ and $so(3)$, respectively; then $\boldsymbol{\Lambda}\hat{\theta}\boldsymbol{\Lambda}^{-1}$ is the corresponding adjoint map [246] which is another element of $so(3)$ and the following identity can be established: $\boldsymbol{\Lambda}\widetilde{\boldsymbol{\theta}}\boldsymbol{\Lambda}^T = \boldsymbol{\Pi}[\boldsymbol{\Lambda}\hat{\theta}]$ ■

REMARK A.2. In view of the above results, considering appropriate smoothness assumptions [285] and taking into account Eqs. (A.19) and (A.21g), the derivative of $\boldsymbol{\Lambda}(s)$ with respect to $s \in \mathbb{R}$ may be put in the well know form[7] $\boldsymbol{\Lambda}_{,s} = \widetilde{\boldsymbol{\omega}}_s\boldsymbol{\Lambda}$, where $\widetilde{\boldsymbol{\omega}}_s := \boldsymbol{\Lambda}_{,s}\boldsymbol{\Lambda}^T \in so(3)$, which is termed the *rotational vorticity* or *spin*. Combining this with the Rodrigues's formula of Eq. (A.11) and noting that $\dot{\hat{e}} \cdot \hat{e} = 0$ since $\hat{e}$ is a constant magnitude vector, the following expression is obtained

$$\hat{\omega}_s = \theta_{,s}\,\hat{e} + [\sin\theta\mathbf{I} + (1 - \cos\theta)\widetilde{\boldsymbol{e}}]\hat{e}_{,s} \tag{A.22}$$

where $\hat{\omega}$ is expressed in terms of $(\theta, \hat{e})$ and their derivatives ■

A.2.4 The exponential form of the rotation tensor

The exponential form of the rotation tensor is based on the specialization of the exponential map [48, 108, 394] defined by the tensorial power series

$$\exp[\bullet] := \sum_{k=0}^{\infty} \frac{(\bullet)^k}{k!} \tag{A.23}$$

[7] Here $(\bullet)_{,s}$ ('comma's) is used to denote partial differentiation of $(\bullet)$ with respect to $s \in \mathbb{R}$.

to the case of rotation,

$$\begin{aligned} \exp[\bullet] : so(3) \approx T_{\mathbf{I}}SO(3) &\rightarrow SO(3) \\ \widetilde{\boldsymbol{\theta}} &\mapsto \boldsymbol{\Lambda}(\widetilde{\boldsymbol{\theta}}) \equiv \exp[\widetilde{\boldsymbol{\theta}}]. \end{aligned} \tag{A.24}$$

That is to say that for any rotation vector $\hat{\theta} \in \mathbb{R}^3$, and hence any skew–symmetric tensor $\widetilde{\boldsymbol{\theta}} \in so(3)$, we get the rotation tensor $\boldsymbol{\Lambda}(\hat{\theta}) = \exp[\,] \circ \boldsymbol{\Pi} \circ \hat{\theta}$. For these reasons, the exponential parametrization of rotation and the associated rotation vector, appears as the most direct representation among all possible vectorial parameterizations which are discussed in following sections, and it is also addressed as the *natural* or *canonical* parametrization for $SO(3)$. The Rodrigues's formula is recovered from Eq. (A.23) taking into consideration the recursive property of the cross product:

$$\widetilde{\boldsymbol{\theta}}^{2m-a} = (-1)^{m-1}\theta^{2(m-1)}\widetilde{\boldsymbol{\theta}}^{a} \tag{A.25}$$

for any $m \in \mathbb{N}$ and $a \in \{1, 2\}$. Using the previous result we get

$$\exp[\widetilde{\boldsymbol{\theta}}] = \mathbf{I} + \sum_{m=1}^{\infty} \frac{(-1)^{m-1}\theta^{2(m-1)}}{(2m-1)!}\widetilde{\boldsymbol{\theta}} + \sum_{m=1}^{\infty} \frac{(-1)^{m-1}\theta^{2(m-1)}}{2m!}\widetilde{\boldsymbol{\theta}}^2 \tag{A.26}$$

and, therefore, Eq. (A.11) is recovered after recognition of the power expansions in terms of those for $\sin(\theta)$ and $\cos(\theta)$. Given a rotation tensor $\boldsymbol{\Lambda}$, the corresponding rotation vector $\hat{\theta}$ can be recovered by means of using the inverse formula

$$\hat{\theta} := \text{axial}[\text{Log}(\boldsymbol{\Lambda})] \tag{A.27}$$

where the logarithmic function is defined by the tensorial power series

$$\begin{aligned} \text{Log}[\bullet] : SO(3) &\rightarrow T_{\mathbf{I}}SO(3) \approx \mathbb{R}^3 \\ \boldsymbol{\Lambda}(\hat{\theta}) &\mapsto \text{Log}[\boldsymbol{\Lambda}] = \widetilde{\boldsymbol{\theta}} \approx \hat{\theta} \in \mathbb{R}^3 \end{aligned} \tag{A.28}$$

$$\text{Log}[\bullet] := -\sum_{k=0}^{\infty} \frac{1}{k!}(\mathbf{I} - \bullet)^k. \tag{A.29}$$

Note that, when applied to rotations, the $\exp[\bullet]$ and $\text{Log}[\bullet]$ maps are not one-to-one, therefore a restriction over all possible (∞) determinations of $\hat{\theta}$ for a given $\boldsymbol{\Lambda}$ must be imposed. This is accomplished selecting the *principal value* of $\hat{\theta}$, *i.e.* the single vector within all possible solutions of Eq. (A.25) that has a magnitude in $[0, 2\pi)$.

A.2.5 Differential map associated to $\exp[\bullet]$

The exponential map has associated the following differential map defined by tensorial power series [394],

$$\text{dexp}[\bullet] := \sum_{k=0}^{\infty} \frac{\bullet^k}{(k+1)!}. \tag{A.30}$$

The exponential map and its associated differential map enjoy remarkable properties, valid beyond the particular application to rotations presented here. Among those we recall:

$$\begin{aligned} \exp[\bullet] &= \text{dexp}[\bullet]\text{dexp}[-\bullet]^{-1} = \text{dexp}[-\bullet]^{-1}\text{dexp}[\bullet] \\ \text{dexp}[\bullet] &= \mathbf{I} + \bullet\text{dexp}[\bullet] = \mathbf{I} + \text{dexp}[\bullet]\bullet \end{aligned} \tag{A.31}$$

the second property of Eq. (A.31) expresses the *symbolical* definition of the associated differential map as the *derivative* of the exponential map in the neighborhood of the identity, *i.e.*

$$\operatorname{dexp}[\bullet] \overset{sym}{=} \frac{\exp[\bullet] - \mathbf{I}}{\bullet}. \tag{A.32}$$

The differential tensor associated to $\mathbf{\Lambda}(\hat{\theta})$ is denoted $D_{\mathbf{\Lambda}} = \operatorname{dexp}[\widetilde{\boldsymbol{\theta}}]$. A *finite form* formula similar to Eq. (A.11) for $\mathbf{\Lambda}$ holds for the differential tensor

$$D_{\mathbf{\Lambda}} = \mathbf{I} + \alpha_1 \widetilde{\boldsymbol{\theta}} + \alpha_2 \widetilde{\boldsymbol{\theta}}^2 \tag{A.33}$$

where the scalar coefficients α_1 and α_2, depending evenly on θ, are given by

$$\alpha_1 := \frac{(1-\cos\theta)}{\theta_2} = \frac{1}{2}\frac{\sin(\theta/2)}{(\theta/2)^2} \tag{A.34a}$$

$$\alpha_2 := \frac{(\theta-\sin\theta)}{\theta_3}. \tag{A.34b}$$

It is worth noting that $\operatorname{Det}(D_{\mathbf{\Lambda}}) = 2\alpha_1 = \sin^2(\theta/2)/(\theta/2)^2$, so that $D_{\mathbf{\Lambda}}$ is singular at $\theta = \pi$, while for $\theta = 0$ we get $D_{\mathbf{\Lambda}} = \mathbf{\Lambda}(\hat{\theta}) = \mathbf{I}$. The associated differential map relates the derivatives of the rotation vector with respect to a given scalar parameter $s \in \mathbb{R}$, $\hat{\theta}_{,s}$, with the corresponding skew–symmetric tensor $\widetilde{\boldsymbol{\omega}}_s$ depending on $\hat{\omega}_s$ is given by

$$\hat{\omega}_s = D_{\mathbf{\Lambda}}\hat{\theta}_{,s} = \operatorname{dexp}(-\widetilde{\boldsymbol{\theta}})\hat{\theta}_{,s} \quad \in \quad \mathbb{R}^3 \tag{A.35}$$

as can easily verified from Eq. (A.22). The inverse of the associated differential map can be expressed as the tensorial power series

$$D_{\mathbf{\Lambda}}^{-1} = \mathbf{I} + \frac{1}{2}\widetilde{\boldsymbol{\theta}} + \frac{1}{\theta^2}\Big(1 - \frac{1}{2}\frac{\sin\theta/\theta}{(1-\cos\theta)/\theta^2}\Big)\widetilde{\boldsymbol{\theta}}^2 = \mathbf{I} - \frac{1}{2}\widetilde{\boldsymbol{\theta}} + \frac{1}{\theta^2}\Big(1 - \frac{\theta/2}{\tan(\theta/2)}\Big)\widetilde{\boldsymbol{\theta}}^2. \tag{A.36}$$

For a detailed deduction of Eqs. (A.33), (A.34a) and (A.34b) see [394].

A.2.6 General minimal vectorial parametrization

The previously presented Rodrigues's formula provides a *vectorial parametrization* of the rotation tensor that is *minimal* in the sense that it is characterized by a minimal set of three parameters, which can be arranged as the pair $(\theta, \hat{e})$. In a more general case, this kind of vectorial minimal parametrization consists of the pair $(p, \hat{e})$ [394], where $p = p(\theta)$ is the *generating function* of the parametrization. The generating function must be an odd function of the rotation angle $\theta = |\hat{\theta}|$ and must to present the limit behavior: $\lim_{\theta\to 0} p(\theta)/\theta = k$, where $k \in \mathbb{R}$ is a constant called *normalization factor* of the parametrization. The parameters are used to construct the *rotation parameter vector* $\hat{p} = p\hat{e} \in \mathbb{R}$. We denote the *vectorial parametrization map of rotation* as

$$\begin{aligned} \operatorname{rot}[\bullet] : \mathbb{R}^3 &\rightarrow SO(3) \\ \mathbf{\Pi}[\hat{p}] = \widetilde{\boldsymbol{p}} &\mapsto \operatorname{rot}[\widetilde{\boldsymbol{p}}] = \mathbf{\Lambda}(\hat{p}). \end{aligned} \tag{A.37}$$

Thus, given a rotation parameter vector $\hat{p} \in \mathbb{R}^3$ and its associated skew–symmetric tensor $\widetilde{\boldsymbol{p}} \in so(3)$, we get a rotation tensor by $\mathbf{\Lambda} = \operatorname{rot}[\widetilde{\boldsymbol{p}}]$. The explicit expression of the vectorial

parametrization map is easily obtained from the Euler-Rodrigues formula, Eq. (A.11), as

$$\mathbf{\Lambda} = \mathbf{I} + P_1\widetilde{\boldsymbol{p}} + P_2\widetilde{\boldsymbol{p}}^2 \tag{A.38}$$

where the scalar coefficients P_1 and P_2, depending evenly on θ, read $P_1(\theta) := \frac{\sin\theta}{p(\theta)}$ and $P_2(\theta) := \frac{1-\cos\theta}{p(\theta)^2}$ ($p = |\hat{p}|$). We remark[8] that Eq. (A.38) holds also for the case $\hat{p} = 0$, yielding $\mathbf{\Lambda} = \mathbf{I}$. The eigenvalues $\lambda_{1,2}(\mathbf{\Lambda})$ are written in terms of P_1 and P_2 as

$$\lambda_{1,2}(\mathbf{\Lambda}) = (1 - p^2P_2) \pm ipP_1 \tag{A.39}$$

and $\mathrm{Det}[\mathbf{\Lambda}] = |\mathbf{\Lambda}| = (1 - p^2P_2)^2 + (pP_1)^2 = 1$.
As seen with the exponential parametrization, it is possible to associate a differential map $\mathrm{drot} : so(3) \mapsto \mathcal{L}(\mathbb{R}^3)$ to the minimal vectorial parametrization map such that, symbolically,

$$\mathrm{drot}[\bullet] \overset{sym}{=} \frac{\mathrm{rot}[\bullet] - \mathbf{I}}{\bullet} \tag{A.40}$$

and the following properties are satisfied:

$$\begin{aligned} \mathrm{rot}[\bullet] &= \mathrm{drot}[\bullet]\mathrm{drot}[-\bullet]^{-1} = \mathrm{drot}[-\bullet]^{-1}\mathrm{drot}[\bullet] \\ \mathrm{rot}[\bullet] &= \mathbf{I} + (\bullet)\mathrm{drot}[\bullet] = \mathbf{I} + \mathrm{drot}[\bullet](\bullet) \end{aligned} \tag{A.41}$$

in complete analogy with the exponential map. The explicit expression for the associated differential map is

$$H = \mu\mathbf{I} + H_1\widetilde{\boldsymbol{p}} + H_2\widetilde{\boldsymbol{p}}^2 \tag{A.42}$$

The coefficients μ, H_1 and H_2, depending evenly on θ, are defined as $\mu(\theta) = \frac{1}{p'(\theta)}$, $H_1(\theta) = \frac{1-\cos\theta}{p(\theta)^2}$ and $H_2(\theta) = \frac{\mu(\theta)p(\theta)-\sin\theta}{p(\theta)^3}$. With $p' := \mathrm{d}p/\mathrm{d}\theta$. Note that $H_1 = P_2$ and that $H_2 = (\mu - P_1)/p^2$.
The associated differential map relates the derivative $\hat{p}_{,s}$ ($s \in \mathbb{R}$) of the rotation parameter vector with the spin $\hat{\omega}_s$ as $\hat{\omega}_s = \mathrm{drot}(\hat{p})\hat{p}_{,s}$. The inverse of the associated differential tensor may be expressed as

$$H^{-1} = \frac{1}{\mu}\mathbf{I} - \frac{1}{2}\widetilde{\boldsymbol{p}} + \frac{1}{p^2}\left(\frac{1}{\mu} - \frac{1}{2}\frac{P_1}{P_2}\right)\widetilde{\boldsymbol{p}}^2 \tag{A.43}$$

Table A.1 show a summarization of the more commonly used minimal vectorial parameterizations.

Table A.1: Minimal parametrization of rotations employing *pseudo–vectors*.

Parametrization	$p(\theta)$	$\mathbf{\Lambda}(\hat{p})$ $(\hat{p} = p(\theta)\hat{e})$	$H(\hat{p})$
Natural	θ		
Linear	$\sin(\theta)$		
Cayley/Gibbs/Rodrigues	$2k\tan(\frac{\theta}{2})$	$\mathbf{I} + \frac{\sin(\theta)}{p(\theta)}\widetilde{\boldsymbol{p}}$	$\frac{1}{p'(\theta)}\mathbf{I} + \frac{1-\cos\theta}{p(\theta)^2}\widetilde{\boldsymbol{p}}$
Wiener/Milenkovic	$4k\tan(\frac{\theta}{4})$	$+\frac{(1-\cos(\theta))}{p(\theta)^2}\widetilde{\boldsymbol{p}}^2$	$+\frac{\mu(\theta)p(\theta)-\sin\theta}{p(\theta)^3}\widetilde{\boldsymbol{p}}^2$
Reduced Euler-Rodrigues	$2k\sin(\frac{\theta}{2})$		

[8] An alternative expression of the vectorial parametrization map [394] is: $\mathbf{\Lambda} = \mathbf{I} + [\gamma\mathbf{I} + \frac{1}{2}\nu\widetilde{\boldsymbol{p}}]\nu\widetilde{\boldsymbol{p}}$, where the scalar coefficients γ and ν, depending evenly on θ, are defined as: $\gamma(\theta) := \cos(\theta/2)$, $\nu(\theta) := 2\frac{\sin\theta/2}{p(\theta)}$. Clearly, $\gamma = P_1/\sqrt{2P_2}$, $\nu = \sqrt{2P_2}$ and $\mathrm{Det}[\mathbf{\Lambda}] = (1 - (\nu p)^2/2) + \gamma^2(\nu p)^2 = 1$.

A.2.7 Non–minimal vectorial parameterizations: quaternions

The minimal parameterizations show some limitations that stem from the use of pseudo–vectors, for example all those associated with the sine generating function has certain advantages but it is non-unique for angles greater than π, other of them became the rotation tensor or its differential map rank deficient for certain values of θ [321, 365, 108]. The problem can be overcame if four parameters, commonly called *normalized quaternion* or *Euler parameters*, are employed for parameterizing the rotation. With such a process in mind, it is possible to re-express Eq. (A.11) using half-angles so that:

$$\boldsymbol{\Lambda} = (\cos^2(\theta/2) - \sin^2(\theta/2))\mathbf{I} + 2\cos(\theta/2)\sin(\theta/2)\widetilde{\boldsymbol{\theta}} + 2\sin^2(\theta/2)\hat{e}\otimes\hat{e}. \tag{A.44}$$

In deriving Eq. (A.44) it has been made use of the half-angle formulae, but also the relationship $\widetilde{\boldsymbol{e}}\widetilde{\boldsymbol{e}} = \widetilde{\boldsymbol{e}}^2 = \hat{e}\otimes\hat{e} - \mathbf{I}$.
A *unit quaternion* is now defined using four Euler parameters, q_0– q_3, so that:

$$\hat{\mathrm{q}}_q = \cos(\theta/2) + \sin(\theta/2)\hat{e} = \begin{bmatrix} \hat{\mathrm{q}} \\ q_0 \end{bmatrix} = \begin{bmatrix} \sin(\frac{\theta}{2})\hat{e} \\ \cos(\frac{\theta}{2}) \end{bmatrix} = \begin{bmatrix} \frac{\hat{\psi}}{2} \\ \cos(\frac{\theta}{2}) \end{bmatrix} \tag{A.45}$$

where $\hat{\psi}$ is the reduced Euler Rodrigues pseudo–vector, see Table A.1, with $k = 1/2$. From Eq. (A.45), the *length* of $\hat{\mathrm{q}}$ is clearly unity with $\hat{\mathrm{q}}_q \cdot \hat{\mathrm{q}}_q = \mathrm{q}_0^2 + \mathrm{q}_1^2 + \mathrm{q}_2^2\mathrm{q}_3^2 = 1$.
Substituting from Eq. (A.45) into (A.44) leads to the relationship:

$$\boldsymbol{\Lambda}(\hat{\mathrm{q}}_q) = (\mathrm{q}_0^2 - \hat{\mathrm{q}}\cdot\hat{\mathrm{q}})\mathbf{I} + 2\hat{\mathrm{q}}\otimes\hat{\mathrm{q}} + 2\hat{\mathrm{q}}_0\widetilde{\boldsymbol{q}} = 2\begin{bmatrix} \mathrm{q}_0^2 + \mathrm{q}_1^2 - 1/2 & \mathrm{q}_1\mathrm{q}_2 - \mathrm{q}_3\mathrm{q}_0 & \mathrm{q}_1\mathrm{q}_3 + \mathrm{q}_2\mathrm{q}_0 \\ \mathrm{q}_2\mathrm{q}_1 + \mathrm{q}_3\mathrm{q}_0 & \mathrm{q}_0^2 + \mathrm{q}_2^2 - \frac{1}{2} & \mathrm{q}_2\mathrm{q}_3 - \mathrm{q}_1\mathrm{q}_0 \\ \mathrm{q}_3\mathrm{q}_1 - \mathrm{q}_2\mathrm{q}_0 & \mathrm{q}_3\mathrm{q}_2 + \mathrm{q}_1\mathrm{q}_0 & \mathrm{q}_0^2 + \mathrm{q}_3^2 - \frac{1}{2} \end{bmatrix} \tag{A.46}$$

REMARK A.3. The quaternion compound rotation is given by $\hat{\mathrm{q}}_{ab} = \hat{\mathrm{q}}_b\hat{\mathrm{q}}_a$, where $\hat{\mathrm{q}}_b\hat{\mathrm{q}}_a$ involves the quaternion product whereby:

$$\hat{\mathrm{b}}\hat{\mathrm{a}} = \mathrm{a}_0\mathrm{b}_0 - \hat{\mathrm{a}}\cdot\hat{\mathrm{b}} + a_0\hat{\mathrm{b}} + b_0\hat{\mathrm{a}} - \hat{\mathrm{a}}\times\hat{\mathrm{b}}$$

which is non-commutative because the inverse product is

$$\hat{\mathrm{a}}\hat{\mathrm{b}} = a_0b_0 - \hat{\mathrm{a}}\cdot\hat{\mathrm{b}} + a_0\hat{\mathrm{b}} + b_0\hat{\mathrm{a}} + \hat{\mathrm{a}}\times\hat{\mathrm{b}}$$

, $\forall$ quaternion $\hat{\mathrm{a}}$ and $\hat{\mathrm{b}} \in \mathbb{R}^4$. Analogous expressions can be obtained for $\boldsymbol{\Lambda}$ in terms of quaternion and other pseudo–vectors [108] ■

A.2.7.a Normalized quaternion from the rotation tensor

A general procedure for obtaining the rotation vector from the rotation tensor involves the computation of the Euler parameters, q_0–q_3. This can achieved via algebraic manipulations on the component of $\boldsymbol{\Lambda}$ as expressed in Eq. (A.46). The *Spurrier*'s algorithm [108, 365], which can be simply checked by working with the components for Eq. (A.46), involves:

$$a = \max\Big[\mathrm{Tr}[\boldsymbol{\Lambda}], \Lambda_{11}, \Lambda_{22}, \Lambda_{33}\Big] \tag{A.47a}$$

where $\mathrm{Tr}[\bullet] = \sum_i (\bullet)_{ii}$ is the trace operator[9] and

$$\begin{array}{lll} \text{if} & a = \mathrm{Tr}(\mathbf{\Lambda}) & \rightarrow \left\{ \begin{array}{ll} \mathrm{q}_0 = \frac{1}{2}(1+a)^{\frac{1}{2}} & \\ \mathrm{q}_i = (\Lambda_{kj} - \Lambda_{jk})/4q_0; & i = 1,3 \end{array} \right. \\ \text{else if} & a = \Lambda_{ii} & \rightarrow \left\{ \begin{array}{ll} \mathrm{q}_i = (\frac{1}{2}a + \frac{1}{4}\big[1 - \mathrm{Tr}[\mathbf{\Lambda}]\big]) & \\ \mathrm{q}_0 = \frac{1}{4}(\Lambda_{kj} - \Lambda_{jk})/q_i & \\ \mathrm{q}_l = \frac{1}{4}(\Lambda_{li} + \Lambda_{il})/q_i; & l = j,k \end{array} \right. \end{array} \tag{A.47b}$$

with i, j, k as the cyclic combination of $1, 2, 3$.
Allowing for the definition of q_0–q_3 in Eq. (A.45), Eq. (A.47b) coincide with the earlier relationship for $\hat{e}$ (or $\hat{\theta}$) in Eq. (A.17). Having obtained q_0–q_3 for rotations of magnitude less than π, the tangent scaled pseudo vector can be obtained from: $2\tan(\frac{\theta}{2})\hat{e} = \frac{2}{q_0}\hat{\mathrm{q}}$ (see Table A.1).

A.2.8 Non–vectorial parameterizations

This kind of parametrization can be minimal, *i.e.* 3 parameters or non-minimal, (> 3 parameters). Usually all them are based on the decomposition of a rotation in a set of simpler rotations about a specific reference frame which moves rigidly with the body [321]. Any rotation α is obtained composing sequentially the three elemental rotations, and its operator $\mathbf{\Lambda}_\alpha$ is obtained calculating the ordered product of the operators corresponding the elemental rotations. In following we describe briefly the more known of them[10].

A.2.8.a Euler angles

This set of angles (ϕ, θ, ψ) - *precession, nutation* and *proper rotation* - are corresponding to three successive and independent rotations about the axis OZ', OX' and OZ' of a movable triad rigidly attached to the solid. Fig. A.5 show the definition of the angles. If the rotation are small it is difficult to identify the angles ϕ and ψ due to almost there is not variation of the axis OZ with θ. In this cases the a coordinate system involving rotations about the three axis of the reference frame is preferable. This is the case of the Cardan's systems and it is described in the following section. The rotation operator $\mathbf{\Lambda}_E$ is obtained as

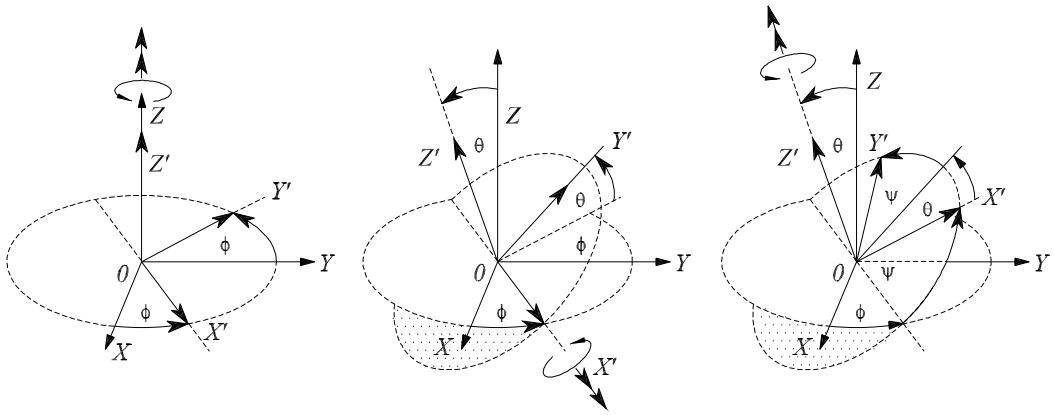

Figure A.5: Euler decomposition of angles.

[9] A more elaborated definition for the trace operator will be presented in the next sections.
[10] A more detailed discussion about non–vectorial parameterizations of rotations can be found in [321].

$$\mathbf{\Lambda}_E = \mathbf{\Lambda}_Z(\phi)\mathbf{\Lambda}_X(\theta)\mathbf{\Lambda}_Z(\psi) \qquad -\pi < \phi,\ \ \psi \leq \pi; \quad 0 \leq \theta \leq \pi \tag{A.48a}$$

with,

$$\mathbf{\Lambda}_Z(\phi) = \begin{bmatrix} \cos\phi & -\sin\phi & 0 \\ \sin\phi & \cos\phi & 0 \\ 0 & 0 & 0 \end{bmatrix} \mathbf{\Lambda}_X(\theta) = \begin{bmatrix} 1 & 0 & 0 \\ 0 & \cos\theta & -\sin\theta \\ 0 & \sin\theta & \cos\theta \end{bmatrix} \mathbf{\Lambda}_Z(\psi) = \begin{bmatrix} \cos\psi & -\sin\psi & 0 \\ \sin\psi & \cos\psi & 0 \\ 0 & 0 & 0 \end{bmatrix}$$

A.2.8.b Cardan angles

This system is defined by means of three angles (θ, φ, ϕ) around the axis OX', OY' and OZ' as it is shown[11] in Fig. A.6 In this case the rotation operator associated to the rotation $\boldsymbol{\alpha}_C$ is

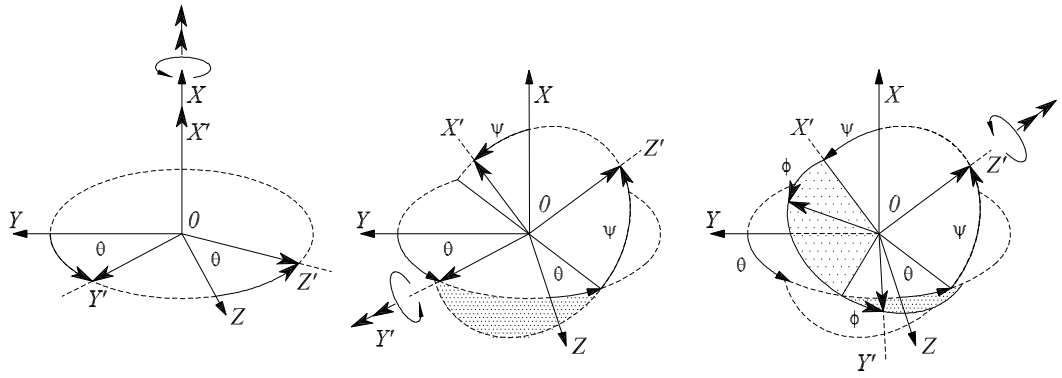

Figure A.6: Cardan decomposition of angles.

obtained as

$$\mathbf{\Lambda}_C = \mathbf{\Lambda}_X(\theta)\mathbf{\Lambda}_Y(\varphi)\mathbf{\Lambda}_Z(\phi) \qquad -\pi < \theta,\ \ \phi \leq \pi; \quad -\frac{\pi}{2} \leq \theta \leq \frac{\pi}{2} \tag{A.49a}$$

with $\mathbf{\Lambda}_\theta$ and $\mathbf{\Lambda}_\phi$ as in Eq. (A.48a) and $\mathbf{\Lambda}_Y(\varphi)$ as

$$\mathbf{\Lambda}_Y(\varphi) = \begin{bmatrix} \cos\varphi & 0 & \sin\varphi \\ 0 & 1 & 0 \\ -\sin\varphi & 0 & \cos\varphi \end{bmatrix}.$$

In the case of both Euler and Cardan systems it is necessary to employ a predefined sequence for the order in which the rotations are applied about the axis. This last characteristic involves additional problems for theoretical developments and numerical implementations [321].

A.3 Configurational description of motion

In this section a brief introduction to the *configurational approach* for the description of the motion of bodies is presented. The minimal amount of concepts is introduced to show a general framework of the theory. In the next sections the concepts here presented will be expanded for the case of motions involving large rotations. Some previous knowledge in differential geometry and continuous mechanics is required and, therefore, only a few preliminary concepts about tensors on manifolds will be addressed. Details about the configurational approach to the dynamics of bodies in the context of differential manifolds can be reviewed in Refs. [246, 251].

[11] Another common choice is OZ', OY' and OX'.

A.3.1 Preliminaries

In this section some preliminaries for an appropriated description of motion in terms of differentiable manifolds is given. Let to consider the set $\{x^j\}$ denoting a curvilinear coordinate system defined on an open subset of $\mathbb{R}^3$, $\{z^i\}$ and $\{\hat{\mathrm{I}}_i\}$ denoting the (canonical) Cartesian coordinate systems of $\mathbb{R}^3$ and the corresponding unit basis vectors, respectively; it is possible to see the z^i as function of x^j and vice–versa. Then, the following entities can be defined:

Definition A.6. ***Curvilinear basis vector***

The *curvilinear coordinate basis vector* $\hat{g}_j$ corresponding to x^i are defined by:

$$\hat{g}_j = \frac{\partial z^i}{\partial x^j}\hat{\mathrm{I}}_i, \qquad (i = 1, \ldots, 3)$$

and are tangent to the coordinate curves obtained from x^j. The *dual basis* $\hat{g}_j^*$ is defined by $\hat{g}_j^* \cdot \hat{g}_k = \delta_{jk}$. These two basis are said to be the dual each of the other ■

Definition A.7. ***Metric tensor***

The *metric tensor* $\boldsymbol{g}$ is defined as

$$g_{jk} = \frac{\partial z^i}{\partial x^j}\frac{\partial z^p}{\partial x^k}\delta_{ip}$$

and let $\boldsymbol{g}^* = \boldsymbol{g}^{-1}$ denote the inverse tensor of $\boldsymbol{g}$ then $\hat{g}_j^* = \boldsymbol{g}\hat{g}_j$ ■

Commonly, the vector $\hat{g}_j$ are called *co-variant* vectors and $\hat{g}_j^*$ contra–variant vectors or simply vectors. For more details about metric spaces consult [119, 251, 255, 285]. Let suppose that all the vector spaces considered in the study are equipped with a metric tensor. Therefore, all the involved spaces are metric vector spaces and all the finite–dimensional manifolds are Riemannian manifolds that are embedded in the Euclidean space. Additionally, we may identify a dual vector space by its primary vector space.

Definition A.8. ***Co–vector space***

The *co–vector space* $\mathcal{V}^*$ of the vector space $\mathcal{V}$ is defined by the space of linear maps $\mathcal{V} \to \mathbb{R}$, *i.e.* $\mathcal{V}^* := \mathfrak{L}(\mathcal{V}, \mathbb{R})$. These linear maps are represented by the dot product defined as

$$\begin{aligned} (\bullet \cdot \bullet) : \mathcal{V}^* \times \mathcal{V} &\to \mathbb{R} \\ (\hat{f}^*, \hat{a}) &\mapsto \hat{f}^* \cdot \hat{a} \in \mathbb{R} \end{aligned} \tag{A.50}$$

which is bilinear and well defined, *i.e.* if $\hat{f}^* \in \mathcal{V}^*$ is fixed and $\hat{f}^* \cdot \hat{a} = 0 \; \forall \, \hat{a} \in \mathcal{V}$, then $\hat{a} = 0$. Conversely, if $\hat{a} \in \mathcal{V}$ is fixed and $\hat{f}^* \cdot \hat{a} = 0 \; \forall \, \hat{f}^* \in \mathcal{V}^*$, then $\hat{f} = 0$. Note that the co–vector space is also a vector space satisfying the vector space properties. A vector and its co–vector spaces are *canonically isomorphic i.e.* $\mathcal{V} \approx \mathcal{V}^*$ ■

Definition A.9. ***Adjoint operator***

Let $\mathbf{F} \in \mathfrak{L}(\mathcal{V}, \mathcal{W})$ be a linear operator between the vector spaces $\mathcal{V} \to \mathcal{W}$. The *adjoint operator* $\mathbf{F}^* \equiv \mathrm{Ad}[\mathbf{F}] \in \mathfrak{L}(\mathcal{V}^*, \mathcal{W}^*)$ is defined with the aid of the dot product as

$$(\mathbf{F}^*\hat{w}^*) \cdot \hat{a} = \hat{w}^* \cdot (\mathbf{F}\hat{a}) \in \mathbb{R}, \qquad \forall \, \hat{a} \in \mathcal{V}, \; \hat{w}^* \in \mathcal{W}^* \tag{A.51}$$

where the first dot product is on the vector space $\mathcal{V}$ and the second one on the vector space $\mathcal{W}$, see Fig. A.7. The adjoint operator is also called a dual operator ■

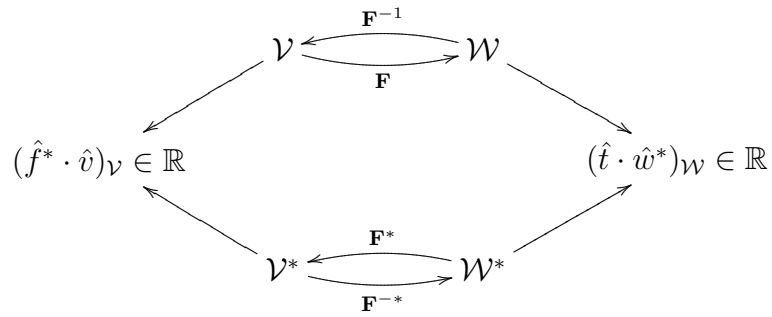

Figure A.7: Domains and ranges for the operator $\mathbf{F}$ and its adjoint operator $\mathbf{F}^*$.

Definition A.10. ***Inverse operator***

If the operator $\mathbf{F}$ is a linear bijection, $\mathbf{F} \in \mathfrak{L}(\mathcal{V}, \mathcal{W})$, the *inverse operator* $\mathbf{F}^{-1} \in \mathfrak{L}(\mathcal{W}, \mathcal{V})$ exist and is unique. The inverse operator is defined by means of the formulas $\mathbf{I} = \mathbf{F}^{-1}\mathbf{F}$ and $\mathbf{i} = \mathbf{F}\mathbf{F}^{-1}$, where $\mathbf{I} \in \mathfrak{L}(\mathcal{V}, \mathcal{V})$ is the identity on $\mathcal{V}$, and $\boldsymbol{i} \in \mathfrak{L}(\mathcal{W}, \mathcal{W})$ is the identity on $\mathcal{W}$. The inverse of the adjoint operator $\mathbf{F}^* \in \mathfrak{L}(\mathcal{V}^*, \mathcal{W}^*)$ is defined similarly as $\mathbf{i}^* = \mathbf{F}^{-*}\mathbf{F}^*$ and $\mathbf{I}^* = \mathbf{F}^*\mathbf{F}^{-*}$, where $\mathbf{i}^* \in \mathfrak{L}(\mathcal{W}^*, \mathcal{W}^*)$ is the identity on $\mathcal{W}^*$, and $\mathbf{I}^* \in \mathfrak{L}(\mathcal{V}^*, \mathcal{V}^*)$ is the identity on $\mathcal{V}^*$. Note that an inverse adjoint operator is an operator $\mathbf{F}^{-*} \in \mathfrak{L}(\mathcal{V}^*, \mathcal{W}^*)$ ■

Let the pairs $(\mathcal{V}, \boldsymbol{G})$ and $(\mathcal{W}, \boldsymbol{g})$ indicate metric vector spaces equipped with the metric tensor $\boldsymbol{G} \in \mathfrak{L}(\mathcal{V}, \mathcal{V}^*)$ and $\boldsymbol{g} \in \mathfrak{L}(\mathcal{W}, \mathcal{W}^*)$. Metric tensor are used for measuring distances and deformation, which, in general, is not possible without introducing a metric. Since manifolds are embedded in the Euclidean space we could choose metric tensor as the identity elements. This can be achieved by identifying the metric tensor spaces $(\mathcal{V}, \boldsymbol{G})$ and $(\mathcal{W}, \boldsymbol{g})$ with the Euclidean vector space.

Definition A.11. ***Inner product***

The *inner product* for a metric vector space $(\mathcal{V}, \boldsymbol{G})$ is defined by

$$\begin{aligned} \langle \cdot, \cdot \rangle_{\boldsymbol{G}} : \mathcal{V} \times \mathcal{V} &\to \mathbb{R} \\ (\hat{a}, \hat{b}) &\mapsto \langle \hat{a}, \hat{b} \rangle_{\boldsymbol{G}} := \boldsymbol{G}\hat{a} \cdot \hat{b} = \hat{a}^* \cdot \hat{b} \end{aligned} \tag{A.52}$$

where for simplicity the co–vector $\boldsymbol{G}\hat{a} = G_{ij}a^j$ is often denoted by $\hat{a}^*$ ■

Definition A.12. ***Transpose operator***

The *transpose operator* of the tensor operator $\mathbf{F} \in \mathfrak{L}\big((\mathcal{V}, \boldsymbol{G}), (\mathcal{W}, \boldsymbol{g})\big)$, denoted $\mathbf{F}^T$ is formally defined via the inner product as

$$\big\langle \mathbf{F}^T \hat{w}, \hat{v} \big\rangle_{\boldsymbol{G}} = \big\langle \hat{w}, \mathbf{F}\hat{v} \big\rangle_{\boldsymbol{g}} \qquad \forall \;\; \hat{w} \in \mathcal{W}, \;\; \hat{v} \in \mathcal{V}. \tag{A.53}$$

Hence, the transpose operator is a mapping $\mathbf{F}^T \in \mathfrak{L}(\mathcal{W}, \mathcal{V})$ ■

After the definition of he inner product, we found a relation between the transpose $\mathbf{F}^T$ and the adjoint operator $\mathbf{F}^*$, yielding $\mathbf{F}^T = \boldsymbol{G}^{-1}\mathbf{F}^*\boldsymbol{g}$. Note that the transpose operator depends on metric tensors on contrary to the adjoint operator and that in the case when $\boldsymbol{G} = \boldsymbol{I}$ and $\boldsymbol{g} = \boldsymbol{i}$ both operators are the same.

Definition A.13. ***Tensor product***

The *tensor product* between the vector $\hat{a} \in \mathcal{V}$ and the co–vector $\hat{f}^* \in \mathcal{W}^*$ is defined employing the dot product by

$$(\hat{a} \otimes \hat{f}^*) \cdot \hat{w} = (\hat{f}^* \cdot \hat{w})\hat{a} \in \mathcal{V} \quad \forall \ \ \hat{w} \in \mathcal{W} \tag{A.54}$$

where the tensor $\hat{a} \otimes \hat{f}^*$ belongs to the tensor space produced by $\mathcal{V}$ and $\mathcal{W}^*$, *i.e.* $\hat{a} \otimes \hat{f}^* \in \mathcal{V} \otimes \mathcal{W}^* = \mathfrak{L}(\mathcal{W}, \mathcal{V})$ ■

The tensor product is a linear mapping for each member separately and, therefore, a bilinear operator. The tensor is called a two–point tensor if it is defined on two different vector spaces.

Definition A.14. ***General two–point tensor space***

The *general two–point tensor space* $\mathfrak{F}$ can be denoted by

$$\mathfrak{F} := \underbrace{\mathcal{V} \otimes \cdots \otimes \mathcal{V}}_{r} \otimes \underbrace{\mathcal{V}^* \otimes \cdots \otimes \mathcal{V}^*}_{s} \otimes \underbrace{\mathcal{W} \otimes \cdots \otimes \mathcal{W}}_{t} \otimes \underbrace{\mathcal{W}^* \otimes \cdots \otimes \mathcal{W}^*}_{u}$$

that is a space of r-fold on the vector space $\mathcal{V}$, s-fold on the vector space $\mathcal{V}^*$, t-fold on the vector space $\mathcal{W}$ and u-fold on the vector space $\mathcal{W}^*$. This can be shortly denoted by the tensor space $\mathfrak{F}(r, s, t, u)$ ■

Permutation of vector spaces is allowed[12]. The tensor space is a vector space itself by satisfying all vector space properties [285]. The vectors can be considered as first order tensors and both of them can be characterized by studying if they are elements of corresponding vector or tensor spaces, respectively. A *general tensor* is defined as an element of a tensor space, thus the *two–point* tensor $\mathbf{T}$ of the tensor space $\mathfrak{F}(r, s, t, u)$ is the following multi–linear mapping:

$$\mathbf{T} : \big(\mathcal{V}^* \times \cdots \times \mathcal{V}^* \times \mathcal{V} \times \cdots \times \mathcal{V} \times \mathcal{W}^* \times \cdots \times \mathcal{W}^* \times \mathcal{W} \times \cdots \times \mathcal{W}\big) \to \mathbb{R}.$$

The two–point tensor $\mathbf{T}$ is an element of the two–point tensor space such that it assigns a tensor for its two–point domain.

Definition A.15. ***Trace operator***

The *trace of the tensor*, $\mathrm{Tr} \in \mathfrak{L}(\mathcal{V}^* \times \mathcal{V}^*, \mathbb{R})$ of the one point tensor $\hat{f}^* \otimes \hat{a} \in \mathcal{V}^* \times \mathcal{V}$ is a scalar–valued linear operator defined via the dot product

$$\mathrm{Tr}(\hat{f}^* \otimes \hat{a}) = \hat{f}^* \cdot \hat{a} \quad \in \mathbb{R} \tag{A.55}$$

Also the trace operation for the tensor on $\mathcal{V} \times \mathcal{V}^*$ can be applied noting $\mathcal{V} = \mathcal{V}^{**}$, but it is not defined for two–point tensors ■

An useful property of the trace operator is

$$\mathrm{Tr}\big[\mathbf{T}_1^T \mathbf{T}_2\big] = \mathrm{Tr}\big[\mathbf{T}_1 \mathbf{T}_2^T\big] \tag{A.56}$$

for any pair of second order Cartesian tensors $\mathbf{T}_1$ and $\mathbf{T}_2$.

Definition A.16. ***Double–dot product***

The *double–dot product* of the tensors $\hat{f}^* \otimes \hat{t}^* \in \mathcal{V}^* \otimes \mathcal{W}^*$ and $\hat{v} \otimes \hat{w} \in \mathcal{V} \otimes \mathcal{W}$ is defined via the

[12] The notation $\mathfrak{F}(1, 0, 0, 1)$ could mean the tensor spaces $\mathcal{V} \otimes \mathcal{W}^*$ or $\mathcal{W}^* \otimes \mathcal{V}$.

ordinary dot product as

$$(\hat{f}^* \otimes \hat{t}^*) : (\hat{v} \otimes \hat{w}) := (\hat{f}^* \cdot \hat{v})_{\mathcal{V}} \cdot (\hat{t}^* \cdot \hat{w})_{\mathcal{W}} \quad \in \mathbb{R} \tag{A.57}$$

where the subscripts indicate the vector space of the corresponding dot product. Therefore, the double–dot product is mapping $\mathfrak{L}(\mathcal{V}^* \times \mathcal{W}^* \times \mathcal{V} \times \mathcal{W}, \mathbb{R})$ that is a four order operator ■

Finally, a general tensor not necessarily can be represented by the by the tensor product of vectors, *e.g.* $\hat{f} \otimes \hat{a}$, frequently tensors are given as a set of components defined on certain basis vector of the tensor space. Let $\{\hat{G}_i\}$ be an ordered basis for the vector space $\mathcal{V}$ and let $\{\hat{g}_i\}$ be an ordered basis for the vector space $\mathcal{W}$, then we may present a general two-order two-point tensor $\mathbf{T} \in \mathcal{V} \otimes \mathcal{W}$ by the linear combination of the basis vector, namely

$$\mathbf{T} = \mathrm{T}_{ij} \hat{G}_i \otimes \hat{g}_j \tag{A.58}$$

where $\hat{G}_i \otimes \hat{g}_j \in \mathcal{V} \otimes \mathcal{W}$ corresponds to the basis vector of the tensor with coefficients $\mathrm{T}_{ij} \in \mathbb{R}$. The coefficient matrix $[\mathrm{T}_{ij}] \in \mathbb{R}^{3\times3}$ is called the component matrix of the tensor $\mathbf{T}$ with respect to the bases $\{\hat{G}_i\}$ and $\{\hat{g}_i\}$. Higher order tensors are represented in a similar way [285, 251]. In order to represent tensors in co–vector spaces it is necessary to define their bases.

Definition A.17. ***Dual bases***

The *dual bases* $\{\hat{G}_i^*\}$ and $\{\hat{g}_i^*\}$ on the co–vector spaces $\mathcal{V}^*$ and $\mathcal{W}^*$ are defined by the formulas

$$\hat{G}_i^* \cdot \hat{G}_j = \delta_{ij}, \quad \hat{g}_i^* \cdot \hat{g}_j = \delta_{ij} \tag{A.59}$$

then the tensor $\mathbf{T} \in \mathcal{V} \otimes \mathcal{W}^*$ may be represented by $\mathbf{T} = \mathrm{T}_{ij} \hat{G}_i \otimes \hat{g}_j^*$ ■

A.3.2 Current and initial reference placements

Let $\chi_t : \mathcal{B} \to \mathbb{R}^3$ be a smooth time–dependent embedding of the material body $\mathcal{B}$ into Euclidean space $\mathbb{R}^3$. For each fixed time $t \in \mathbb{R}^+$, the mapping $\chi(t, \cdot)$ is defined as the *current placement* of the body $\mathcal{B}$ along with the current place vector $\hat{x}$ of a body-point, namely

$$\mathcal{B}_t \subset \mathbb{R}^3 := \chi(\hat{X}, t), \quad \hat{x} := \chi(\hat{X}, t), \quad \forall \hat{X} \in \mathcal{B}. \tag{A.60}$$

The initial reference placement $\mathcal{B}_0$ is defined as the special case of the current placement $\mathcal{B}_t$ by setting $t = 0$, giving

$$\mathfrak{B}_0 := \chi(\mathcal{B}, t = 0), \quad \hat{X} := \chi(\hat{X}, t = 0) \quad \forall \hat{X} \in \mathcal{B} \tag{A.61}$$

where $\hat{X}$ is an *initial reference place* vector. Since the initial reference placement $\mathcal{B}_0$ is unaffected by observation transformation (see *e.g.* Ogden [300]), it is possible to call vectors and tensors defined on the initial reference placement $\mathcal{B}_0$ as *material quantities*. For example, the reference place $\hat{X}$ is called *material place vector*, and $\mathcal{B}_0$ the *material placement* of the body. Sometimes the material description is named a referential or *Lagrangian* description, and occasionally, some distinction has been accomplished between the phrases. Contrary to the material placement $\mathcal{B}_0$, the current placement $\mathcal{B}_t$ and vectors and tensors defined on it are concerned in the observation transformation. Vectors and tensors defined on the current placement $\mathcal{B}_t$ are called *spatial quantities*, *e.g.* a current place vector $\hat{x}$ is also named as a *spatial place vector*, and $\mathcal{B}_t$ as a *spatial placement*. A spatial description is sometimes called a *Eulerian* description.
In this work the terms *material* and *spatial* will be applied for placements, vectors, tensors,

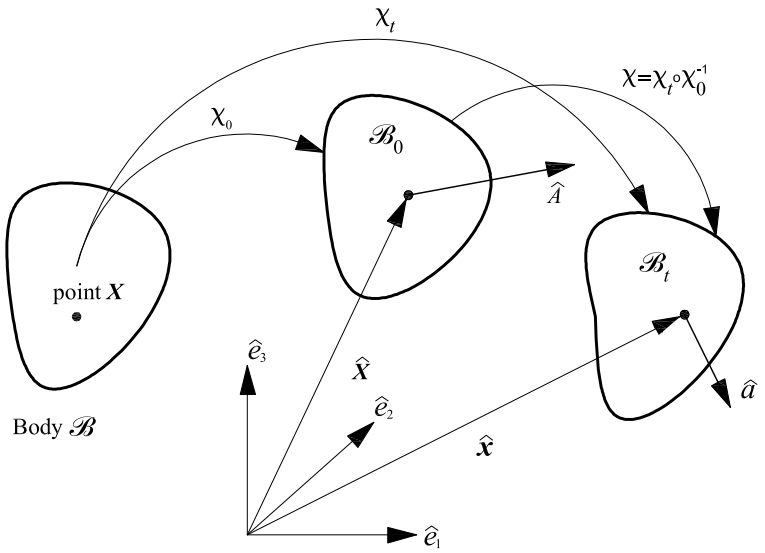

Figure A.8: Configurational description of the motion.

fields, spaces and descriptions. A geometric interpretation of the material body $\mathcal{B}$, the material placement $\mathcal{B}_0$, and the spatial placement $\mathcal{B}_t$, as well as for material/spatial vectors is given in Fig. A.8[13].

Fig. A.8 shows that a body–point $\hat{X} \in \mathcal{B}$, which is represented by a vector-valued mapping $\hat{X} := \chi(\hat{X})$, assigns a material vector $\hat{A}$ on the material placement $\mathcal{B}_0$. The material vector belongs to the tangent space of the material placement $\mathcal{B}_0$, namely $T_{\hat{X}}\mathcal{B}_0$, where $\hat{X}$ corresponds to the base point[14] of manifold. Correspondingly, the body–point $\hat{X} \in \mathcal{B}$, which is represented by the mapping $\hat{x} = \chi(\hat{X})$, assigns the spatial vector $\hat{a}$ on the spatial placement $\mathcal{B}_t$. The spatial vector belongs to the tangent space of the spatial placement $\mathcal{B}_t$, *i.e.* $\hat{a} \in T_{\hat{x}}\mathcal{B}_t$, where $\hat{x}$ represents a base point of on the manifold $\mathcal{B}_t$.

Defining $\mathcal{V} := T_{\hat{X}}\mathcal{B}_0$ and $\mathcal{W} := T_{\hat{x}}\mathcal{B}_t$ it is possible to construct multi–linear two–point operators, (or tensors), $\mathbf{T}$ at the body point $\hat{X} \in \mathcal{B}$, with mappings $\hat{X} = \chi_0(\hat{X})$ and $\hat{x} = \chi(\hat{X})$ as:

$$\begin{aligned} \mathbf{T} : T^*_{\hat{X}}\mathcal{B}_0 \times \ldots \times T_{\hat{X}}\mathcal{B}_0 \times \ldots \times T^*_{\hat{x}}\mathcal{B}_t \times \ldots \times \ldots \times T_{\hat{x}}\mathcal{B}_t &\rightarrow \mathbb{R} \\ (\hat{X}^{*1}, \ldots, \hat{X}^{*n}, \hat{X}_1, \ldots, \hat{X}_n, \ldots, \hat{x}^{*1}, \ldots, \hat{x}^{*n}, \ldots, \hat{x}_1, \ldots, \hat{x}_n) &\mapsto \mathbf{T}(\hat{X}^{*1}, \ldots, \hat{x}_1) \in \mathbb{R} \end{aligned}$$

where $T^*_{\hat{X}}\mathcal{B}_0$ and $T^*_{\hat{x}}\mathcal{B}_t$ are the co–vector tangent spaces[15] for the (vector) tangent spaces $T_{\hat{X}}\mathcal{B}_0$ and $T_{\hat{x}}\mathcal{B}_t$, respectively. The multi-linear operator $\mathbf{T}$ is an element of multi-linear operators denoted as $\mathbf{T} \in \mathfrak{L}(T^*_{\hat{X}}\mathcal{B}_0 \times \ldots T_{\hat{X}}\mathcal{B}_0 \times \ldots T^*_{\hat{x}}\mathcal{B}_t \times \ldots T_{\hat{x}}\mathcal{B}_t, \mathbb{R})$ (An extensive revision for tensorial calculus on manifolds can be found in [256]). Usually, the coefficients of tensor operators are described in the bases (see Eq. A.59) associated to the vector and co–vector spaces over they act. In the configurational description of continuous mechanics frequently appear this kind of mathematical objects.

It is possible to associate a symmetric positive-definite *metric tensor* to each vector or co–vector space, constructed from the corresponding vector bases. Let pairs $(\mathcal{V}, \mathbf{G})$ and $(\mathcal{W}, \mathbf{g})$ indicate

[13]Note that placements, likewise place vectors, should be regarded as mappings, not the image of these maps, according to [246].

[14]A base point is a point of the manifold where a tangent space is induced.

[15]The co–vector space $\mathcal{V}^*$ of the vector space $\mathcal{V}$, is bilinear and positive definite. The elements of co–vector space is said to be perpendicular to elements of the vector space [246, 256, 285].

metric vector spaces in the material and spatial configurations, with material metric tensor, (seen as bi-linear operator), $\mathbf{G} \in \mathfrak{L}(\mathcal{V}, \mathcal{V}^*)$ and the spatial metric tensor $\mathbf{g} \in (\mathcal{W}, \mathcal{W}^*)$. Metric tensors are used to measure distances and strains. A canonical representation for the metric tensor in material and spatial configurations is given by the identity $\mathbf{I} \in \mathbb{R}^3$, this metric tensor result of describing the points by means of Euclidean 3D coordinates.
Considering the previous content, in following formal definitions for the linear form corresponding to the virtual work principle is given in the context of differential calculus on finite and infinite–dimensional manifolds.

Definition A.18. ***Virtual work on finite–dimensional manifolds***

The *virtual work* on the tangent point bundle $T\mathcal{B}_0$ at fixed time $t = t_0$ and at the place vector $\hat{x}_0 := \hat{x}(t_0) \in \mathcal{B}_0$ is defined as a linear form by

$$G_{\mathscr{V}}(\hat{x}_0, \delta\hat{x}) := \hat{f}^* \cdot \delta\hat{x} \tag{A.62}$$

where $\delta\hat{x} \in T_{\hat{x}}\mathcal{B}_0$ is the *virtual displacement* and the force vector $\hat{f}^*(t_0, \hat{x}_0) \in T^*_{\hat{x}}\mathcal{B}_0$ belongs to the co–tangent point–space ■

In the case that the considered manifold is subjected to holonomic constraints, *i.e.* a constrained manifold, $\delta\hat{x} \in T_{\hat{x}}\mathcal{B}_0$ occupies the subspace of $\mathbb{R}^n$ which is the tangent space at the base point $\hat{x}_0$ with dimension $d < n$ [245] (see Fig. A.9).
By the other hand, forces can be classified, according to the *Newtonian mechanics*, into *external* and *inertial* forces when it has the general form $-m\ddot{\hat{x}}$, where m is a constant called *mass*. Inertial force may be regarded as an effective force, indeed, if an external force is acting on a particle, which is otherwise free, then the inertial force may be regarded as the reaction force, hence the force equilibrium in the dynamical sense is achieved in this mechanical system[16].

Definition A.19. ***Virtual work on infinite–dimensional manifold***

The virtual work on the tangent field bundle $T_{\hat{x}}\mathcal{C}_0$ at the fixed time $t = t_0$ and the place field $\hat{x}_0 := \hat{x}(t_0) \in \mathcal{C}_0$ is defined as an integral over the domain of the body $\mathcal{B}$

$$G_{\mathscr{V}}(\hat{x}_0, \delta\hat{x}) := \int_{\mathcal{B}} \hat{f}^* \cdot \delta\hat{x} \mathrm{d}V \tag{A.63}$$

where the virtual displacement field $\delta\hat{x} \in T_{\hat{x}}\mathcal{C}_0$ and the force field $\hat{f}^* = \hat{f}(t_0, \hat{x}_0) \in T^*_{\hat{x}}\mathcal{C}_0$ which belongs to the co–tangent field space. The tangent field space $T_{\hat{x}}\mathcal{C}_0$ is defined in Eq. (A.86). Similarly as in the finite–dimensional case, the same classification of forces can be done ■

A.4 Configurational description of compound rotations

As it has been introduced in §A.1 a compound rotation can be defined by two different way, nevertheless, equivalent ways: the *material* description, and the *spatial* description[17]. In view of that, in this section we perform a more formal description of compound rotations in terms of the configurational description of the rotational motion [247, 246].

[16] Another way to classify forces is used in *Lagrangian mechanics* where forces are separated into constraint and applied forces. Constraint forces can be verified with the aid of the virtual work since they are workless. Then we may note that constraint forces occupy $\hat{f}^{\mathrm{con}} \in T^*_{\hat{x}}\mathcal{B}_0^{\perp}$ that is orthogonal to $T_{\hat{x}}\mathcal{B}_0$ via duality pairing. Hence, we may neglect the constraint forces in the virtual work forms [245].

[17] A extensive introduction to the configurational approach of continuous mechanics can be reviewed in [256, 388].

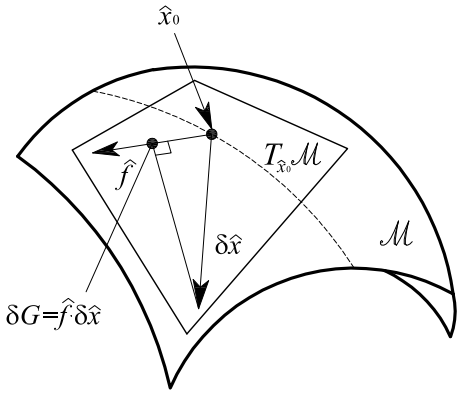

Figure A.9: Geometric representation of the virtual work principle on the manifold $\mathcal{M}$ with tangent space $T_{\hat{x}}\mathcal{M}$ at the base point $\hat{x}$; ($\hat{x}_0$: place vector, $\hat{f}$: force co–vector, $\delta\hat{x}$: virtual displacement, δW: virtual work).

To this end, let $\{\hat{E}_i\}$ and $\{\hat{e}_i\}$ be two spatially fixed (inertial) reference coordinate systems identified with the *material* and *spatial* coordinate system, respectively. Given two rotation vectors described these reference systems, *i.e.* $\hat{\Psi} = \Psi_i \hat{E}_i$ for material frame and $\hat{\psi} = \psi_i \hat{e}_i$ for spatial frame, it is possible to obtain $\mathbf{\Lambda} \in SO(3)$ by means of applying the exponential mapping as

$$\mathbf{\Lambda} = \exp[\widetilde{\mathbf{\Psi}}] = \exp[\widetilde{\boldsymbol{\psi}}] \tag{A.64}$$

with $\widetilde{\mathbf{\Psi}}$ and $\widetilde{\boldsymbol{\psi}}$ being the skew–symmetric tensors obtained from $\hat{\Psi}$ and $\hat{\psi}$, respectively. In this manner, the rotation tensor $\mathbf{\Lambda}$ is parameterized in the material or spatial description, although when the rotation tensor itself can be regarded as a two point operator [245].
If following, if a *rotation increment* is applied it is possible to obtain the new compound rotation according to Eq. (A.3), and employing Eq. (A.26) it is possible to define the material and spatial descriptions of the compound rotation as described below

A.4.1 Material description of the compound rotation

Given a material incremental rotation vector, $\hat{\Theta} = \Theta_i \hat{E}_i$, the new compound rotation tensor, $\mathbf{\Lambda}_c$, is defined by means of the *left translation mapping* defined as an operator with base point in $\mathbf{\Lambda} \in SO(3)$ and described by

$$\begin{aligned} \text{left}_{\mathbf{\Lambda}}(\bullet) : SO(3) &\rightarrow SO(3) \\ \exp[\widetilde{\mathbf{\Theta}}] &\mapsto \mathbf{\Lambda}_c = \mathbf{\Lambda}\exp[\widetilde{\mathbf{\Theta}}] = \mathbf{\Lambda}\mathbf{\Lambda}_n^{\text{mat}} \end{aligned} \tag{A.65}$$

where $\widetilde{\mathbf{\Theta}} \in so(3)$ is the skew–symmetric tensor obtained from $\hat{\Theta}$ and $\mathbf{\Lambda}_n^{\text{mat}} = \exp[\widetilde{\mathbf{\Theta}}]$ is the material form of the incremental rotation operator. It is worth to note that the left translation map is defined as acting on an element of $so(3)$ but the final updating procedure requires the specification of a point $\mathbf{\Lambda}$ on the rotational manifold $SO(3)$. This description is called material since the incremental rotation operator acts on a material vector space.

REMARK A.4. Note that the updating rule of Eq. (A.65) can be identified with the *material updating rule* of §A.1 ■

A.4.2 Spatial description of the compound rotation

Given a spatial incremental rotation vector, $\hat{\theta} = \theta_i \hat{e}_i$, the description of the new compound rotation tensor, $\mathbf{\Lambda}_c$, can be defined by means of the *right translation mapping*, with base point in $\mathbf{\Lambda} \in SO(3)$, defined as

$$\begin{aligned} \text{right}_{\mathbf{\Lambda}}(\bullet) : SO(3) &\rightarrow SO(3) \\ \exp[\widetilde{\boldsymbol{\theta}}] &\mapsto \mathbf{\Lambda}_c = \exp[\widetilde{\boldsymbol{\theta}}]\mathbf{\Lambda} = \mathbf{\Lambda}_n^{\text{spa}}\mathbf{\Lambda} \end{aligned} \tag{A.66}$$

where $\widetilde{\boldsymbol{\theta}} \in so(3)$ is the skew–symmetric tensor obtained from $\hat{\theta}$ and $\Lambda_n^{\text{spa}} = \exp[\widetilde{\boldsymbol{\theta}}]$ is the spatial form of the incremental rotation operator. The right translation map is also defined as acting on an element of $so(3)$ but the final updating procedure requires the specification of a point $\mathbf{\Lambda}$ on the rotational manifold $SO(3)$. This description is called spatial since the incremental rotation operator acts on a spatial vector space.

REMARK A.5. Note that the updating rule of Eq. (A.66) can be identified with the *spatial updating rule* of §A.1 ■

The material and spatial descriptions of the incremental rotation tensor, generically designed as $\mathbf{\Lambda}_n$ omitting the super-scripts mat and spa, and the incremental rotation vectors and skew–symmetric tensors are related by [245, 363]

$$\hat{\theta} = \mathbf{\Lambda}\hat{\Theta} \tag{A.67a}$$

$$\widetilde{\boldsymbol{\theta}} = \mathbf{\Lambda}\widetilde{\mathbf{\Theta}}\mathbf{\Lambda}^T \tag{A.67b}$$

$$\mathbf{\Lambda}_n^{\text{spa}} = \mathbf{\Lambda}\mathbf{\Lambda}_n^{\text{mat}}\mathbf{\Lambda}^T \tag{A.67c}$$

where the first relation, Eq. (A.67a), is called a *Lie algebra adjoint transformation*[18] on the Euclidean space with the vectors cross product as the Lie algebra $(\mathbb{R}^3, \cdot \times \cdot)$, the second relation of Eq. (A.67b) is the Lie Algebra adjoint transformation on $so(3)$, $\text{Ad}_{\mathbf{\Lambda}}(\widetilde{\mathbf{\Theta}}) = \mathbf{\Lambda}\widetilde{\mathbf{\Theta}}\mathbf{\Lambda}^T$; and the last relation, Eq. (A.67c), is an inner automorphism that is an isomorphism onto itself, [246, 244].

REMARK A.6. At it has be shown in §A.2.3 $\exp[\widetilde{\mathbf{\Theta}}] \in SO(3)$, with $\widetilde{\mathbf{\Theta}}$ being the skew–symmetric tensor obtained from $\hat{\Theta} \in \mathbb{R}^3$ that belongs to the tangential space of $SO(3)$ at the identity on $SO(3)$; *i.e.* $\widetilde{\mathbf{\Theta}} \in so(3) \approx T_{\mathbf{I}}SO(3)$ ■

A.4.3 Material tangent space to $SO(3)$

Taking the directional (Fréchet) derivative of the compound rotation, *i.e.* differentiating the perturbed configuration of the material form of the compound rotation $\mathbf{\Lambda}\exp[\nu\widetilde{\mathbf{\Theta}})]$ with respect to the scalar parameter ν and setting $\nu = 0$, yields to the *material tangent space* to $SO(3)$ at the base point $\mathbf{\Lambda}$, which is formally defined as [246]

$$T_{\mathbf{\Lambda}}^{\text{mat}}SO(3) := \{\widetilde{\mathbf{\Theta}}_{\mathbf{\Lambda}} := (\mathbf{\Lambda}, \widetilde{\mathbf{\Theta}}) \;\big|\; \mathbf{\Lambda} \in SO(3),\ \widetilde{\mathbf{\Theta}} \in so(3)\} \tag{A.68}$$

where an element of the material tangent space $\widetilde{\mathbf{\Theta}}_{\mathbf{\Lambda}} \in T_{\mathbf{\Lambda}}^{\text{mat}}SO(3)$ is a skew–symmetric tensor, *i.e.* $\widetilde{\mathbf{\Theta}} \in so(3)$. The notation $(\mathbf{\Lambda}, \widetilde{\mathbf{\Theta}})$ is used for indicating the pair formed by the rotation tensor $\mathbf{\Lambda}$ and the skew–symmetric tensor $\widetilde{\mathbf{\Theta}}$, representing the material tangent tensor, at the base point $\mathbf{\Lambda} \in SO(3)$ [246]. See Fig. A.10. For simplicity it is possible to omit the base point $\mathbf{\Lambda}$ by denoting $\widetilde{\mathbf{\Theta}}\mathbf{\Lambda} \in T_{\mathbf{\Lambda}}^{\text{mat}}SO(3)$ if there is no danger of confusion.

[18] This concept has been defined in Remark A.1 (pp. 262) of the §A.2.3.

A.4.3.a Spatial tangent space to $SO(3)$

Respectively, the *spatial tangent space* on the rotation manifold $SO(3)$, at any base point $\mathbf{\Lambda}$, can be defined as

$$T^{\text{spa}}_{\mathbf{\Lambda}}SO(3) := \{\widetilde{\boldsymbol{\theta}}_{\mathbf{\Lambda}} := (\mathbf{\Lambda}, \widetilde{\boldsymbol{\theta}}) \;\big|\; \mathbf{\Lambda} \in SO(3),\ \widetilde{\boldsymbol{\theta}} \in so(3)\} \tag{A.69}$$

By analogy with the material case, an element of the spatial tangent space $\widetilde{\boldsymbol{\theta}}_{\mathbf{\Lambda}} \in T^{\text{spa}}_{\mathbf{\Lambda}}SO(3)$ is a skew–symmetric tensor belonging to $so(3)$. Again, omitting the base point $\mathbf{\Lambda}$, it is possible to write $\widetilde{\boldsymbol{\theta}}\mathbf{\Lambda} \in T^{\text{spa}}_{\mathbf{\Lambda}}SO(3)$.

REMARK A.7. The elements of the Lie group $SO(3)$ can be alternatively defined as linear operators $\mathbf{\Lambda} \in \mathfrak{L}(\mathbb{R}^3, \mathbb{R}^3)$ providing another interpretation for a rotation, *i.e.* it is an *adjoint transformation* between the material and spatial tangent spaces, see Eqs. (A.67a) to (A.67c). Additionally, a rotational motion induces a rotation operator, since the rotation operator maps the *material place* vector $\hat{X} \in \mathcal{B}_0$ to the *spatial place* vector $\hat{x} \in \mathcal{B}_t$ by means of the transformation $\hat{x}(t) = \mathbf{\Lambda}(t)\hat{X}$, *i.e.* $\mathbf{\Lambda} \in \mathfrak{L}(\mathcal{B}_0, \mathcal{B}_t)$. More generally, rotation operators transform material vectors into spatial vectors, that is $\mathbf{\Lambda} \in \mathfrak{L}(T_{\hat{X}}\mathcal{B}_0, T_{\hat{x}}\mathcal{B}_t)$ ■

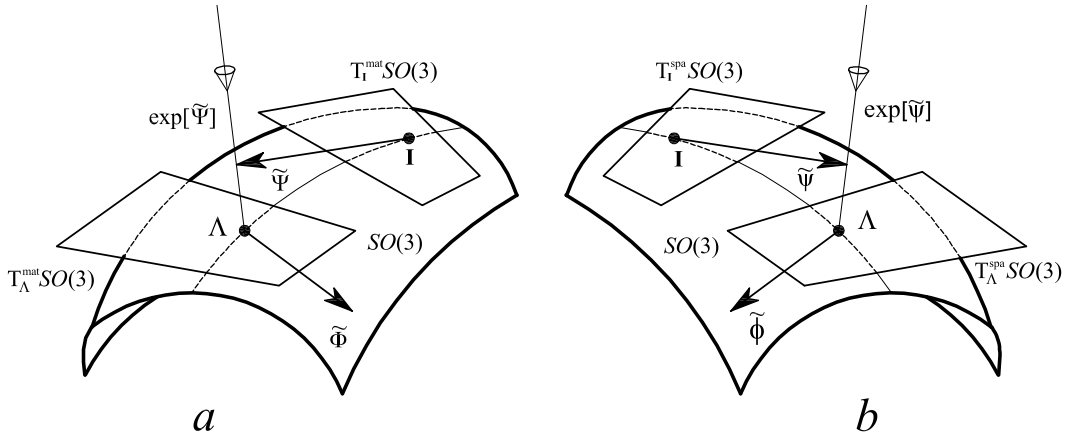

Figure A.10: Geometric representation of the tangent spaces on the rotational manifold $SO(3)$. (a): Material. (b): Spatial.

A.4.4 Incremental additive rotation vectors

Consider a rotation tensor $\mathbf{\Lambda}_0 \in SO(3)$ which can be indistinctly parameterized (minimally) by using the spatial or material vectors $\hat{\psi} = \psi_i \hat{e}_i$ and $\hat{\Psi} = \Psi_i \hat{E}_i$, respectively; *i.e.* we have $\mathbf{\Lambda}_0 = \exp[\widetilde{\boldsymbol{\psi}}] = \exp[\widetilde{\mathbf{\Psi}}]$.

A.4.4.a Spatial description

Consider a *spatial incremental rotation* of magnitude $\delta\theta$ which is applied on $\mathbf{\Lambda}_0$. The increment of rotation is described by the (spatial) *incremental rotation vector* $\delta\hat{\theta} = \delta\theta_i \hat{e}_i$ and the corresponding incremental rotation tensor can be determined using Eqs. (A.11), (A.12) or its equivalent exponential form $\mathbf{\Lambda}_\theta = \exp[\delta\widetilde{\boldsymbol{\theta}}]$. Then we obtain the *compound* or *updated* rotation $\mathbf{\Lambda} = \mathbf{\Lambda}_\theta \mathbf{\Lambda}_0 \in SO(3)$, which is the result of two consecutive rotations parameterized by $\hat{\psi}$ and

$\delta\hat{\theta}$, respectively [228].
Consider now the new compound rotation vector $\hat{\psi} + \delta\hat{\psi}$ which parameterizes $\mathbf{\Lambda}$, with $\delta\hat{\psi}$ the additive increment of the rotation vector $\hat{\psi}$; in general we have

$$\exp[\widetilde{\boldsymbol{\psi}} + \delta\widetilde{\boldsymbol{\theta}}] \neq \exp[\widetilde{\boldsymbol{\psi}} + \delta\widetilde{\boldsymbol{\psi}}] = \exp[\widetilde{\boldsymbol{\theta}}]\exp[\widetilde{\boldsymbol{\psi}}]. \tag{A.70}$$

It is possible to see that $\delta\widetilde{\boldsymbol{\psi}}$ is the linear additive increment of $\widetilde{\boldsymbol{\psi}}$ because they belong to the same tangent space $T^{\text{spa}}_{\mathbf{I}}SO(3)$, in contrast with $\delta\widetilde{\boldsymbol{\theta}} \in T^{\text{spa}}_{\exp[\widetilde{\boldsymbol{\psi}}]}SO(3)$. One can observe that, because of $\delta\widetilde{\boldsymbol{\theta}}$ being skew–symmetric, the spatial form of the linearized increment or admissible variation of the rotation tensor, $\delta\mathbf{\Lambda}$, is no longer orthogonal. In fact, $\delta\widetilde{\boldsymbol{\theta}}$ belongs to the tangential space of the rotation tensor $\mathbf{\Lambda} \in SO(3)$.
The linearized relation between $\delta\hat{\psi}$ and $\delta\hat{\theta}$ is obtained as follows: construct a perturbed configuration of $\mathbf{\Lambda}$ depending on a scalar parameter $\varepsilon \in \mathbb{R}^3$ as

$$\mathbf{\Lambda}_\varepsilon = \mathbf{\Lambda}_{\varepsilon\theta}(\varepsilon\delta\widetilde{\boldsymbol{\theta}})\mathbf{\Lambda}_0(\widetilde{\boldsymbol{\psi}}) = \exp[\varepsilon\delta\widetilde{\boldsymbol{\theta}}]\mathbf{\Lambda}_0 = \exp[\widetilde{\boldsymbol{\psi}} + \varepsilon\delta\widetilde{\boldsymbol{\psi}}] \tag{A.71}$$

considering the fact that $\exp[\widetilde{\boldsymbol{\psi}}]^{-1} = \exp[-\widetilde{\boldsymbol{\psi}}]$ one obtains

$$\exp[\varepsilon\delta\widetilde{\boldsymbol{\theta}}] = \exp[\widetilde{\boldsymbol{\psi}} + \varepsilon\delta\widetilde{\boldsymbol{\psi}}]\exp[-\widetilde{\boldsymbol{\psi}}]. \tag{A.72}$$

Taking the derivative of Eq. (A.72) with respect to ε and setting $\varepsilon = 0$, it is possible, using the Rodrigues's formula, obtain the linearized relation between the incremental rotation vector $\delta\hat{\theta}$ and the increment of the rotation vector, $\delta\hat{\psi}$, [178, 182, 365] as

$$\delta\hat{\theta} = D\mathbf{\Lambda}_{\varepsilon\theta}\cdot\delta\hat{\psi} = \frac{\mathrm{d}}{\mathrm{d}\varepsilon}\Big[\exp[\varepsilon\delta\widetilde{\boldsymbol{\theta}}]\Big]\Big|_{\varepsilon=0} \tag{A.73a}$$

$$= \frac{\mathrm{d}}{\mathrm{d}\varepsilon}\Big[\exp[\widetilde{\boldsymbol{\psi}} + \varepsilon\delta\widetilde{\boldsymbol{\psi}}]\exp[-\widetilde{\boldsymbol{\psi}}]\Big]\Big|_{\varepsilon=0} = \mathbf{T}_{\theta\psi}\delta\hat{\psi} \tag{A.73b}$$

where the *spatial tangential transformation tensor* $\mathbf{T}_{\theta\psi}$ is given by

$$\mathbf{T}_{\theta\psi} = \mathbf{T}_{\theta\psi}(\hat{\psi}) = \frac{\sin\psi}{\psi}\mathbf{I} + \frac{1-\cos\psi}{\psi^2}\widetilde{\boldsymbol{\psi}} + \frac{\psi-\sin\psi}{\psi^3}\hat{\psi}\otimes\hat{\psi} \tag{A.74}$$

with determinant[19] $\mathrm{Det}[\mathbf{T}_{\theta\psi}] = 2(1-\cos\psi)/\psi^2$. Therefore, $\delta\hat{\psi} \neq \delta\hat{\theta}$ for general 3D rotations unless $\delta\hat{\theta}$ and $\delta\hat{\psi}$ are coaxial. Besides, when $\psi = 2k\pi$ for $k \in \mathbb{N}$, $\mathbf{T}_{\theta\psi}$ becomes rank deficient, which may imply problems in the numerical implementations.
Also it is possible to define the inverse transformation [228, 178, 365]

$$\delta\hat{\psi} = \mathbf{T}_{\psi\theta}\delta\hat{\theta} \tag{A.75}$$

where

$$\mathbf{T}_{\psi\theta} = \mathbf{T}_{\psi\theta}(\hat{\psi}) = \mathbf{T}^{-1}_{\theta\psi}(\hat{\psi}) = \frac{\psi/2}{\tan(\psi/2)}\mathbf{I} - \frac{1}{2}\widetilde{\boldsymbol{\psi}} + \frac{1}{\psi^2}\Big[1 - \frac{\psi/2}{\tan(\psi/2)}\Big]\hat{\psi}\otimes\hat{\psi}. \tag{A.76}$$

[19] For a detailed deduction of the tensors $\mathbf{T}_{\theta\psi}$ and $\mathbf{T}_{\psi\theta}$ see Refs. [104, 105, 178, 182, 365].

To avoid the singularity due to the use of the rotation vector to parameterize the rotation tensor, a re-scaling remedy is available [182, 181] as follows: when $\theta > \pi$ is identified:

$$\psi^* = \psi - 2n\pi i_\psi \tag{A.77}$$

where $n = \text{int}[(\psi + \pi)/2\pi]$, the number of full–cycle rotations. This remedy makes sure $\psi^* \in [-\pi, \pi]$ and therefore overcome the singularity.

REMARK A.8. Note that the transformation $\mathbf{T}_{\theta\psi}$ has an effect on the base points, changing the base point from $\mathbf{I}$ to $\exp(\widetilde{\psi})$. The tangential transformation $\mathbf{T}_{\theta\psi}(\hat{\psi})$, $\mathbf{\Lambda}(\hat{\psi})$ and the skew–symmetric tensor $\widetilde{\psi}$ have the same eigenvectors. Hence, $\mathbf{T}_{\theta\psi}(\hat{\psi})$, $\mathbf{\Lambda}(\hat{\psi})$ and $\widetilde{\psi}$ are commutative [178] ■

A.4.4.b Material description

Analogously as for the case of spatial description, if we start from the material description of the compound rotation tensor $\mathbf{\Lambda} = \exp[\widetilde{\mathbf{\Psi}} + \delta\widetilde{\mathbf{\Psi}}] = \exp[\widetilde{\mathbf{\Psi}}]\exp(\delta\widetilde{\mathbf{\Theta}})$, it is possible to see that $\widetilde{\mathbf{\Psi}}$ and its linear increment $\delta\widetilde{\mathbf{\Psi}}$ belong to the same tangent space of rotation, *i.e.* $T^{\text{mat}}_{\mathbf{I}}SO(3)$. However[20], the skew–symmetric tensor $\delta\widetilde{\mathbf{\Theta}}$ belongs $T^{\text{mat}}_{\exp[\widetilde{\mathbf{\Psi}}]}SO(3)$ and therefore, in general we have

$$\exp[\widetilde{\mathbf{\Psi}}]\exp[\delta\widetilde{\mathbf{\Theta}}] = \exp[\widetilde{\mathbf{\Psi}} + \delta\widetilde{\mathbf{\Psi}}] \neq \exp[\widetilde{\mathbf{\Psi}} + \delta\widetilde{\mathbf{\Theta}}]$$

due to that both tangent tensors belong to different linear spaces. It is worth to note that $\hat{\Psi} = \Psi_i\hat{E}_i$, $\delta\hat{\Psi} = \delta\Psi_i\hat{E}_i$ and $\delta\hat{\Theta} = \delta\Theta_i\hat{E}_i$ are the material axial vectors obtained from $\widetilde{\mathbf{\Psi}}$, $\delta\widetilde{\mathbf{\Psi}}$ and $\delta\widetilde{\mathbf{\Theta}}$, respectively.
Therefore, in an analogous manner as for the spatial case, constructing a perturbed configuration on $\mathbf{\Lambda}_0$, the following result is obtained

$$\exp[\varepsilon\delta\widetilde{\mathbf{\Theta}}] = \exp[-\widetilde{\mathbf{\Psi}}]\exp[\widetilde{\mathbf{\Psi}} + \varepsilon\delta\widetilde{\mathbf{\Psi}}]. \tag{A.78}$$

Taking the derivative of Eq. (A.78) with respect to ε and setting $\varepsilon = 0$, it is possible, using the Rodrigues's formula, obtain the linearized relation between the incremental rotation vector $\delta\hat{\Theta}$ and the linearized increment of the rotation vector, $\delta\hat{\Psi}$, [178, 182, 365] as

$$\delta\hat{\Theta} = D\mathbf{\Lambda}_{\varepsilon\Theta}\cdot\delta\hat{\Psi} = \frac{\mathrm{d}}{\mathrm{d}\varepsilon}\Big[\exp[\varepsilon\delta\widetilde{\mathbf{\Theta}}]\Big]\Big|_{\varepsilon=0} \tag{A.79a}$$

$$= \frac{\mathrm{d}}{\mathrm{d}\varepsilon}\Big[\exp[-\widetilde{\mathbf{\Psi}}]\exp[\widetilde{\mathbf{\Psi}} + \varepsilon\delta\widetilde{\mathbf{\Psi}}]\Big]\Big|_{\varepsilon=0} = \mathbf{T}_{\Theta\Psi}\delta\hat{\Psi} \tag{A.79b}$$

where $\mathbf{T}_{\Theta\Psi}(\hat{\Psi})$ defines the *material tangential transformation tensor* and the following identity holds

$$\delta\hat{\Theta} = \mathbf{T}_{\Theta\Psi}\delta\hat{\Psi} = \mathbf{T}^T_{\theta\psi}\delta\hat{\Psi}. \tag{A.80}$$

Then, $\mathbf{T}_{\Theta\Psi}(\hat{\Psi})$ is a linear mapping between the material tangent spaces $T^{\text{mat}}_{\mathbf{I}} \mapsto T^{\text{mat}}_{\exp(\widetilde{\mathbf{\Psi}})}$. On other hand, it is also valid that

$$\delta\hat{\Psi} = \mathbf{T}_{\Psi\Theta}\delta\hat{\Theta} = \mathbf{T}^{-1}_{\Theta\Psi}\delta\hat{\Theta} = \mathbf{T}^{-T}_{\theta\psi}\delta\hat{\Theta}. \tag{A.81}$$

[20] Here the symbol δ is used to denote a rather *small* or linearized increment.

Additionally, considering $\delta\hat{\Psi} = \mathbf{I}\delta\hat{\psi}$ and $\delta\hat{\theta} = \mathbf{\Lambda}\delta\hat{\Theta}$ one obtains that

$$\mathbf{T}_{\Theta\Psi} = \mathbf{\Lambda}^T\mathbf{T}_{\theta\psi} \quad \text{and} \quad \mathbf{T}_{\Psi\Theta} = \mathbf{T}_{\theta\psi}^{-1}\mathbf{\Lambda} = \mathbf{T}_{\psi\theta}\mathbf{\Lambda}.$$

REMARK A.9. Note that the transformation $\mathbf{T}_{\Theta\Psi}$ has an effect on the base points, changing the base point from $\mathbf{I}$ to $\exp(\widetilde{\mathbf{\Psi}})$. It is worth also noting that the tangential transformation $\mathbf{T}_{\Theta\Psi}(\hat{\Psi})$, the corresponding rotation tensor $\mathbf{\Lambda}(\hat{\Psi})$ and the skew–symmetric tensor $\widetilde{\mathbf{\Psi}}$ have the same eigenvectors. Hence, $\mathbf{T}_{\Theta\Psi}(\hat{\Psi})$, $\mathbf{\Lambda}(\hat{\Psi})$ and $\widetilde{\mathbf{\Psi}}$ are commutative [178] ■

A.4.5 Vector spaces on the rotational manifold

A.4.5.a Material vector space

According to the previous results, it is possible to define the *material vector space* on the rotation manifold at the base point $\mathbf{\Lambda}$ as

$$T_{\mathbf{\Lambda}}^{\text{mat}} := \{\hat{\Theta}_{\mathbf{\Lambda}} := (\hat{\Psi}, \hat{\Theta}) \big| \mathbf{\Lambda} = \exp[\widetilde{\mathbf{\Psi}}] \in SO(3), \hat{\Theta} \in \mathbb{R}^3\} \tag{A.82}$$

where an element of the material vector space is $\hat{\Theta}_{\mathbf{\Lambda}} \in T_{\mathbf{\Lambda}}^{\text{mat}}$, which is an affine space with the rotation vector $\hat{\Psi}$ as a base point and the incremental rotation vector $\hat{\Theta}$ as a tangent vector.
Hence, the tangential transformation $\mathbf{T}_{\Theta\Psi}$ is a mapping $\mathbf{T}_{\Theta\Psi} : T_{\mathbf{I}}^{\text{mat}} \mapsto T_{\mathbf{\Lambda}}^{\text{mat}}$. The elements of this material vector space can be added by the parallelogram law only if they occupy the same affine space, *i.e.* if their associated skew–symmetric tensors belongs to the same tangent space of the rotation manifold, [246]. The definition of Eq. (A.82) gives a practical notation for sorting rotation vectors in different tangent spaces.

A.4.5.b Spatial vector space

By analogy with the material case, the *spatial vector space* on the rotation manifold at any point $\mathbf{\Lambda}$ is defined as

$$T_{\mathbf{\Lambda}}^{\text{spa}} := \{\hat{\theta}_{\mathbf{\Lambda}} := (\hat{\psi}, \hat{\theta}) \big| \mathbf{\Lambda} = \exp(\widetilde{\boldsymbol{\psi}}) \in SO(3), \hat{\theta} \in \mathbb{R}^3\} \tag{A.83}$$

An element of the spatial vector space is $\hat{\theta}_{\mathbf{\Lambda}} \in T_{\mathbf{\Lambda}}^{\text{spa}}$ and the tangential operator $\mathbf{T}_{\psi\theta} : T_{\mathbf{I}}^{\text{spa}} \mapsto T_{\mathbf{\Lambda}}^{\text{spa}}$ is the transposed as in the material form, Eq. (A.80).
The spatial and material vector spaces are related by the rotation tensor as given in Eq. (A.67a), from which follows that with the base point $\mathbf{I} \in SO(3)$, $(\hat{\Psi} \in T_{\mathbf{I}}^{\text{mat}})$

$$\hat{\psi}_{\mathbf{I}} = \mathbf{I}\hat{\Psi}_{\mathbf{I}} \rightarrow \hat{\psi}_{\mathbf{I}} = \hat{\Psi}_{\mathbf{I}} \tag{A.84}$$

where '=' denotes the canonical isomorphism between the spatial and material vector spaces. The identity $\mathbf{I}$ maps between the vector fields $T_{\mathbf{I}}^{\text{mat}} \rightarrow T_{\mathbf{I}}^{\text{spa}}$. Now the relation between spatial and material vectors can be given as $(\hat{\psi}, \hat{\theta}) = (\mathbf{I}\hat{\Psi}, \mathbf{\Lambda}\hat{\Theta})$, where $\hat{\psi}$ and $\hat{\Psi}$ represent the base point in the spatial and material vector spaces, respectively.
This notation can be written more compactly as $\hat{\theta}_{\mathbf{\Lambda}} = \mathbf{\Lambda}\hat{\Theta}_{\mathbf{\Lambda}}$, called the *push–forward*[21] of $\hat{\Theta}_{\mathbf{\Lambda}}$ by $\mathbf{\Lambda}$, where the rotation tensor should be considered as a mapping between the material and spatial vector spaces of rotation, $\mathbf{\Lambda} : T_{\mathbf{\Lambda}}^{\text{mat}} \rightarrow T_{\mathbf{\Lambda}}^{\text{spa}}$, see Fig. A.11. A push–forward operator maps a material vector space into a spatial vector space. It makes sense since rotation operator is a two-point tensor. Note that the push–forward operator $\mathbf{\Lambda}$ has no influence on the base point of

[21] Detailed formalism about pullback and push–forward operator will be given in the next sections.

the rotation manifold, another push–forward for rotation tensors is $\widetilde{\boldsymbol{\theta}}_{\boldsymbol{\Lambda}} = \boldsymbol{\Lambda}\widetilde{\boldsymbol{\Theta}}_{\boldsymbol{\Lambda}}\boldsymbol{\Lambda}^T$ is a mapping between the material and spatial tangent spaces of rotation $\boldsymbol{\Lambda}(\bullet)\boldsymbol{\Lambda}^T : T^{\text{mat}}_{\boldsymbol{\Lambda}}SO(3) \rightarrow T^{\text{spa}}_{\boldsymbol{\Lambda}}SO(3)$. Fig. (A.11) shows a scheme of the connections between spatial and material configurations.

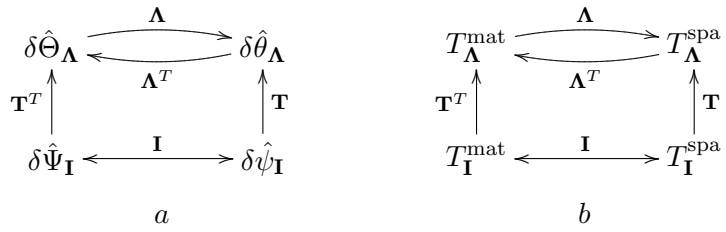

Figure A.11: Commutative diagrams. (a): Configurational description of vectors. (b): Corresponding vector spaces.

A.5 Variation, Lie derivative and Lie variation

In previous sections definitions for manifolds and tangent spaces have been given for the finite–dimensional case *i.e.* any element of the tangent space can de constructed by means of a combination of a finite number of elements called basis. By contrast, the placement field of continuous mechanics takes values in a *Hilbert* space which is formally defined as

Definition A.20. ***Hilbert space***

A *Hilbert space* is a complete inner-product space, and here specially a complete infinite-dimensional inner-product vector-valued function space. For a detailed presentation of functional analysis in continuous mechanics see [251, 255] ■

In a Hilbert space chart parametrization maps vector-values functions into vector–valued functions. The placement field needs an infinite number of basis functions in order to present an arbitrary placement field on continuum, yielding infinite–dimensional manifolds.
In this section a definition for *variation*, *Lie derivative* and *Lie variation* in the context of the configurational approach of continuous mechanics will be given, *i.e.* for manifolds modeled in infinite-dimensional Hilbert spaces, called field manifolds. The concepts of *pullback* and *push–forward* operators are essential for the understanding of Lie derivative and variation [251, 255, 245]. Some previous definitions are required:

Definition A.21. ***Fréchet derivative and differential***

The Fréchet derivative of the vector $\hat{f} : \mathcal{H} \subset \mathcal{H}_1 \rightarrow \mathcal{H}_2$ at fixed $\hat{x} \in \mathcal{H}$, with $\mathcal{H}, \mathcal{H}_1$ and $\mathcal{H}_2$ being Hilbert spaces, is defined as the following continuous linear operator:

$$D\hat{f}(\hat{x}) : \mathcal{H}_1 \rightarrow \mathcal{H}_2 \quad \text{such that} \quad \hat{f}(\hat{x}+\hat{u}) - \hat{f}(\hat{x}) = D\hat{f}(\hat{x}) \cdot \hat{u} + r(\hat{x},\hat{u})$$

where the remainder obeys the condition $lim_{\hat{u}\mapsto 0}\frac{\|r(\hat{x},\hat{u})\|_{\mathcal{H}_\in}}{\|\hat{u}\|_{\mathcal{H}_\infty}} = 0$. $D\hat{f}(\hat{x})$ is called *Fréchet differential*. A vector is called Fréchet differentiable if its Fréchet derivative exists. The derivative is also a linearized form ■

Definition A.22. ***Gâteaux differential***

The *Gâteaux differential* of the vector $\hat{f} : \mathcal{H} \subset \mathcal{H}_1 \rightarrow \mathcal{H}_2$ at fixed $\hat{x} \in \mathcal{H}$ ($\beta \in \mathbb{R}$) is defined as

the limit:

$$D\hat{f}(\hat{x})\cdot\hat{u} := \lim_{\beta\mapsto 0}\frac{\hat{f}(\hat{x}+\beta\hat{u})-\hat{f}(\hat{x})}{\beta} = \frac{\mathrm{d}\hat{f}(\hat{x}+\beta\hat{u})}{\mathrm{d}\beta}\Big|_{\beta=0}$$

where the limit is to be interpreted in the norm of $\mathcal{H}_2$ ■

The formula of the present definition is a practical and simple way to compute the directional derivative that is the term $D\hat{f}(\hat{x})\cdot\hat{u}$ where $\hat{u}\in\mathcal{H}_1$ indicates the direction.

Definition A.23. ***Field manifold***

A infinite–dimensional *field manifold* is a set $\mathcal{C}$ of a Hilbert space $\mathcal{H}_1$, $(\mathcal{C}\subset\mathcal{H}_1)$, is defined as a infinite–dimensional manifold in analogous way that for the finite–dimensional case, excepting that the points $x\in\mathcal{C}$ are vector valued fields and it can depend also on time $t\in\mathbb{R}^+$. A manifold at a fixed time $t=t_0$ is denoted by $\mathcal{C}_0$ ■

Definition A.24. ***Tangent field bundle***

A *tangent field bundle* is a virtual displacement field $\delta\hat{x}$ at any place field $\hat{x}\in\mathcal{C}_0$ and for a fixed time $t=t_0$ is defined as

$$T\mathcal{C}_{t_0} := \{(\hat{x},\delta\hat{x})\in\mathcal{H}_1\times\mathcal{H}_1 \,\big|\, \hat{x}\in\mathcal{C}_{t_0},\, D_{\hat{x}}h(t_0,\hat{x})\cdot\delta\hat{x}=0,\, D_{\hat{x}}h \text{ is surjection}\} \tag{A.85}$$

where $D_{\hat{x}}h$ is the Fréchet partial derivative of any kind of holonomic constrain with respect to $\hat{x}$ at $t=t_0$ ■

Definition A.25. ***Tangent field space***

For a fixed time $t=t_0$, a *tangent field space* at the base point $\hat{x}_0\in\mathcal{C}_0$ is defined as

$$T_{\hat{x}_0}\mathcal{C} := \{\delta\hat{x}\in\mathcal{H}_1 \mid (\hat{x}_0,\delta\hat{x})\in T\mathcal{C}_{t_0}\} \tag{A.86}$$

where $T\mathcal{C}_{t_0}$ is the tangent field bundle ■

Definition A.26. ***Velocity field space***

A *velocity field space* is closely related with the tangent field space and is defined by formula

$$T_{\hat{x}}\mathcal{C} := \{\dot{\hat{x}}\in\mathcal{H}_1 \,\big|\, (\hat{x},\dot{\hat{x}})\in T\mathcal{C}\} \tag{A.87}$$

where now time is free, not fixed, like in the virtual displacement. The velocity field that is an element of the velocity field–space is also denoted by $\hat{v} := \dot{\hat{x}}\in T_{\hat{x}}\mathcal{C}$ ■

A.5.1 Variation operator

The variation operator δ is defined as the special case of Fréchet differential at fixed $t=t_0$ by

$$\delta h(t_0,\hat{x},\hat{v}) := D_{\hat{x}}h(t_0,\hat{x},\hat{v})\cdot\delta\hat{x} + D_{\hat{v}}h(t_0,\hat{x},\hat{v})\cdot\delta\hat{v} \tag{A.88}$$

where $\hat{x}\in\mathcal{C}_{t_0}$ is a place field, $\delta\hat{x}\in T_{\hat{x}_0}\mathcal{C}$ is a virtual displacement field, $\hat{v}\in T_{\hat{x}}\mathcal{C}$ is a velocity field, and $\delta\hat{v} := \delta\dot{\hat{x}}\in T_{\hat{x}_0}\mathcal{C}$ is a virtual velocity filed. Moreover, $D_{\hat{x}}$, $D_{\hat{v}}$ are the Fréchet partial derivative with respect to place and velocity, respectively.

A.5.2 Pullback operator

Let the operator $\mathscr{R} : T_{\hat{X}}\mathcal{B}_0 \mapsto T_{\hat{x}}\mathcal{B}$ be an invertible linear mapping between the tangent spaces of material and spatial manifolds. The material manifold is denoted by $\mathcal{B}_0$ and the spatial manifold by $\mathcal{B}$. Moreover, let $\{\hat{g}_i\}$ and $\{\hat{G}_i\}$ be the bases for the spatial and material tangent spaces $T_{\hat{X}}\mathcal{B}_0$ and $T_{\hat{x}}\mathcal{B}$, respectively, and let $\{\hat{g}_i^*\}$ and $\{\hat{G}_i^*\}$ be the corresponding dual bases for the spatial and material cotangent spaces $T^*_{\hat{X}}\mathcal{B}_0$ and $T^*_{\hat{x}}\mathcal{B}$.
The *pullback* operator by $\mathscr{R} \in \mathfrak{L}(T_{\hat{X}}\mathcal{B}_0, T_{\hat{x}}\mathcal{B})$ for the spatial vector $\hat{a} = a^i\hat{g}_i \in T_{\hat{x}}\mathcal{B}$ is defined by

$$\overleftarrow{\mathscr{R}}\,(\hat{a}) := a^i(\mathscr{R}^{-1}\hat{g}_i) \in T_{\hat{X}}\mathcal{B}_0 \tag{A.89}$$

where $\mathscr{R}^{-1} \in \mathfrak{L}(T_{\hat{x}}\mathcal{B}, T_{\hat{X}}\mathcal{B}_0)$ is the inverse of the operator $\mathscr{R}$.
The pullback operator by $\mathscr{R} \in \mathfrak{L}(T_{\hat{X}}\mathcal{B}_0, T_{\hat{x}}\mathcal{B})$ for the spatial co–vector $\hat{f}^* = f_i^*\hat{g}_i^* \in T^*_{\hat{x}}\mathcal{B}$ is defined by

$$\overleftarrow{\mathscr{R}}\,(\hat{f}^*) := f_i^*(\mathscr{R}^*\hat{g}_i^*) \in T^*_{\hat{X}}\mathcal{B}_0 \tag{A.90}$$

where $\mathscr{R}^* \in \mathfrak{L}(T^*_{\hat{x}}\mathcal{B}, T^*_{\hat{X}}\mathcal{B}_0)$ is the adjoint operator of $\mathscr{R}$ (see Def. A.9 in pp. 269). The definition for pullback operator for vectors or co–vectors is different. A pullback operator maps spatial vector into material vectors, and spatial co–vectors into material co–vectors, therefore, it is possible to see the pullback operator as a *materializer* operator.

A.5.3 Push forward operator

The *push forward* operator by $\mathscr{R} \in \mathfrak{L}(T_{\hat{X}}\mathcal{B}_0, T_{\hat{x}}\mathcal{B})$ for the material vector $\hat{A} = A^i\hat{G}_i \in T_{\hat{X}}\mathcal{B}_0$ is defined by

$$\underrightarrow{\mathscr{R}}(\hat{A}) := A^i(\mathscr{R}\hat{G}_i) \in T_{\hat{x}}\mathcal{B}. \tag{A.91}$$

The push forward operator by the isomorphism $\mathscr{R} \in \mathfrak{L}(T_{\hat{X}}\mathcal{B}_0, T_{\hat{x}}\mathcal{B})$ for the material co–vector $\hat{F}^* = F_i^*\hat{G}_i^* \in T^*_{\hat{X}}\mathcal{B}_0$ is defined by

$$\underrightarrow{\mathscr{R}}(\hat{F}^*) := F_i^*(\mathscr{R}^{-*}\hat{G}_i^*) \in T^*_{\hat{x}}\mathcal{B} \tag{A.92}$$

where $\mathscr{R}^{-*} \in \mathfrak{L}(T^*_{\hat{X}}\mathcal{B}_0, T^*_{\hat{x}}\mathcal{B})$ is the inverse of $\mathscr{R}^*$.
If the operator $\mathscr{R}$ is invertible between the material and spatial tangent spaces, $\mathscr{R} \in \mathfrak{L}(T_{\hat{X}}\mathcal{B}_0, T_{\hat{x}}\mathcal{B})$, then its adjoint, its inverse and the inverse of the adjoint operators are $\mathscr{R}^* \in \mathfrak{L}(T^*_{\hat{x}}\mathcal{B}, T^*_{\hat{X}}\mathcal{B}_0)$, $\mathscr{R}^{-1} \in \mathfrak{L}(T_{\hat{x}}\mathcal{B}, T_{\hat{X}}\mathcal{B}_0)$ and $\mathscr{R}^{-*} \in \mathfrak{L}(T^*_{\hat{X}}\mathcal{B}_0, T^*_{\hat{x}}\mathcal{B})$, respectively.
Clearly the push forward operator is different for the case of vectors or co-vectors. The push forward operator maps the material (co)vectors into the spatial (co)vectors. The pullback or push forward operators for higher order tensor are defined such as the pullback or push forward operator for each basis vector separately.
For example, the push forward of the second order tensor $\mathfrak{G} \in \mathfrak{L}(T^*_{\hat{X}}\mathcal{B}_0, T^*_{\hat{X}}\mathcal{B}_0)$, the material form of the metric tensor, by the isomorphism $\mathbf{F} \in \mathfrak{L}(T_{\hat{X}}\mathcal{B}_0, T_{\hat{x}}\mathcal{B})$, the *deformation gradient* [251], is

$$\begin{aligned}\underrightarrow{\mathbf{F}}(\mathfrak{G}) &= \underrightarrow{\mathbf{F}}(\mathfrak{G}_{ij}\hat{G}_i^* \otimes \hat{G}_j^*) \\ &= \mathfrak{G}_{ij}(\mathbf{F}^{-*}\hat{G}_i^*) \otimes (\mathbf{F}^{-*}\hat{G}_j^*) = \mathbf{F}^{-*}\mathfrak{G}\mathbf{F}^{-1} \in \mathfrak{L}(T_{\hat{X}}\mathcal{B}_0, T^*_{\hat{x}}\mathcal{B})\end{aligned} \tag{A.93}$$

where the identity $\hat{a} \otimes \mathbf{F}\hat{b} = (\hat{a} \otimes \hat{b}\mathbf{F}^*)$, $\forall\ \hat{b} \in T_{\hat{X}}\mathcal{B}_0$, has been used. The resulting spatial tensor $\mathbf{F}^{-*}\mathfrak{G}\mathbf{F}^{-1}$ corresponds to the *Cauchy deformation tensor* often denoted by $\boldsymbol{c}$[22].

A.5.4 Lie derivative

The *Lie derivative* $\mathrm{L}_{\mathscr{R}}(\mathbf{c})$ of the general tensor $\mathbf{c}(\eta) \in \mathcal{C}$ with respect to the isomorphic mapping $\mathscr{R}(\eta) \in \mathfrak{L}(T_{\hat{X}}\mathcal{B}_0, T_{\hat{x}}\mathcal{B})$ and the parameter $\eta \in \mathbb{R}$ is defined by

$$\mathrm{L}_{\mathscr{R}}(\mathbf{c}) := \underset{\rightarrow}{\mathscr{R}}\Big(\frac{\mathrm{d}}{\mathrm{d}\eta}\Big[\overset{\leftarrow}{\mathscr{R}}\,(\mathbf{c}(\eta))\Big]\Big) \tag{A.94}$$

The pullback operator $\overset{\leftarrow}{\mathscr{R}}$ materializes the spatial components of the general tensor $\mathbf{c}$. It is well known that the derivative of an objective material tensor is an objective tensor [300], therefore, if the pulled back tensor is objective, its derivative in the material configuration will be as well. The push–forward operator $\underset{\rightarrow}{\mathscr{R}}$ is considered as the inverse of the pullback operation where the resulting Lie derivative tensor $\mathrm{L}_{\mathscr{R}}(\mathbf{c})$ belongs to the same tensor space $\mathcal{C}$ as the original $\mathbf{c}$.

A.5.5 Lie variation

The *Lie variation* $\delta_{\mathscr{R}}(\mathbf{c})$ of a general tensor $\mathbf{c} \in \mathcal{C}$ with respect to the isomorphic mapping $\mathscr{R} \in \mathfrak{L}(T_{\hat{X}}\mathcal{B}_0, T_{\hat{x}}\mathcal{B})$ is defined by

$$\delta_{\mathscr{R}}(\mathbf{c}) := \underset{\rightarrow}{\mathscr{R}}(\delta[\overset{\leftarrow}{\mathscr{R}}\,(\mathbf{c}(\eta))]) \tag{A.95}$$

where the variation operator correspond to these given in Eq. (A.88), which is accomplished at the fixed time $t = t_0$. As for the case of the Lie derivative, the Lie variation is an objective quantity if the original tensor is objective. The definition of Lie variation is connected with a *virtual displacement* [245]. This last affirmation can be seen by writing the Lie variation with the aid of the Gâteaux differential at the point $(\hat{x}, \hat{v})$ at fixed time $t = t_0$

$$\delta_{\mathscr{R}}(\mathbf{c}) = \underset{\rightarrow}{\mathscr{R}}\Big[\frac{\mathrm{d}(\overset{\leftarrow}{\mathscr{R}}\,(\mathbf{c}))}{\mathrm{d}\eta}\Big]\Big|_{\eta=0} \tag{A.96}$$

where the tensor $\mathbf{c}(t_0, \hat{x} + \eta\delta\hat{x}, \hat{v} + \eta\delta\hat{v})$ and the operator $\mathscr{R}(t_0, \hat{x} + \eta\delta\hat{x}, \hat{v} + \eta\delta\hat{v})$ depends on the virtual displacement $\delta\hat{x}$ and the virtual velocity $\delta\hat{v}$[23].
An important result in rod theory is the calculation of the Lie variation of the deformation gradient, (two–point tensor), $\mathbf{F} = F_{ij}\hat{g}_i \otimes \hat{G}^*_j \in T_{\hat{x}}\mathcal{B} \times T^*_{\hat{X}}\mathcal{B}_0$, by the rotation operator $\boldsymbol{\Lambda} \in T_{\hat{X}}\mathcal{B}_0 \times T_{\hat{x}}\mathcal{B}$, which reads

$$\delta_{\boldsymbol{\Lambda}}\mathbf{F} = \underset{\rightarrow}{\boldsymbol{\Lambda}}\big[\delta(\overset{\leftarrow}{\boldsymbol{\Lambda}}\,\mathbf{F})\big] = \boldsymbol{\Lambda}(\delta(\boldsymbol{\Lambda}^T\mathbf{F})) = \boldsymbol{\Lambda}(\delta\boldsymbol{\Lambda}^T\mathbf{F} + \boldsymbol{\Lambda}^T\delta\mathbf{F}) = \delta\mathbf{F} + \boldsymbol{\Lambda}\delta\boldsymbol{\Lambda}^T\mathbf{F}. \tag{A.97}$$

[22] If the tensor are expressed in the Euclidean space then the metric $\mathfrak{G} = \mathbf{I}$, and the adjoint operator is identified with the transpose of the gradient tensor, *i.e.* $\mathbf{F}^{-*} = \mathbf{F}^{-T}$, yielding to $\boldsymbol{c} = \mathbf{F}^{-T}\mathbf{F}^{-1}$.

[23] Note that the virtual displacement belongs to the tangent point-space $T_{\hat{x}_0}\mathcal{M}$ in the finite–dimensional case and to the tangent field–space $T_{\hat{x}_0}\mathcal{C}$ in the infinite–dimensional case.

The variation of the rotation operator using both, the material and spatial updating rules are

$$\delta\mathbf{\Lambda} = \frac{\mathrm{d}}{\mathrm{d}\eta}\mathbf{\Lambda}\exp[\eta\delta\widetilde{\mathbf{\Theta}}]\Big|_{\eta=0} = \mathbf{\Lambda}\delta\widetilde{\mathbf{\Theta}} \tag{A.98a}$$

$$\delta\mathbf{\Lambda} = \frac{\mathrm{d}}{d\eta}\exp[\eta\delta\widetilde{\boldsymbol{\theta}}]\mathbf{\Lambda}\Big|_{\eta=0} = \delta\widetilde{\boldsymbol{\theta}}\mathbf{\Lambda}, \tag{A.98b}$$

respectively; hence the term $\mathbf{\Lambda}\delta\mathbf{\Lambda}^T$ in Eq. (A.97) is equal to $-\delta\widetilde{\boldsymbol{\theta}}$ in both descriptions because $\delta\widetilde{\boldsymbol{\theta}} = \mathbf{\Lambda}\delta\widetilde{\mathbf{\Theta}}\mathbf{\Lambda}^T$. Finally, the Lie variation of the deformation tensor $\mathbf{F}$ with respect to the rotation operator $\mathbf{\Lambda}$ is written as

$$\delta_{\mathbf{\Lambda}}\mathbf{F} = \delta\mathbf{F} - \delta\widetilde{\boldsymbol{\theta}}\mathbf{F} \quad \in (T_{\hat{x}}\mathcal{B} \otimes T^*_{\hat{X}}\mathcal{B}_0) \tag{A.99}$$

which is a *co–rotational operator*, (see Refs. [362, 228] for a physical interpretation of co–rotated magnitudes). Although the spatial virtual rotation tensor $\delta\widetilde{\boldsymbol{\theta}}_{\mathbf{\Lambda}} \in T^{\mathrm{spa}}_{\mathbf{\Lambda}}SO(3)$, *i.e.* it occupies a spatial tangent space, it is also an element of the tensor–space $(T_{\hat{x}}\mathcal{B} \otimes T^*_{\hat{X}}\mathcal{B}_0)$.

A.5.6 Co–rotated derivatives

In this section an important result related to the derivatives of spatial vectors described in a moving frame induced by rotational motion will be presented. The *co–rotated derivative* of a vector described in the moving reference frame will be deduced. This kind of derivative will be latter employed in formulation of a geometrically exact theory for rods.

Let suppose two spatially fixed axes $\{\hat{E}_i\}$ employed to describe the material configuration of a body, $\mathcal{B}_0$, and $\{\hat{e}_i\}$ to describe the spatial configuration at time t of the body during motion $\mathcal{B}_t$. Additionally, let suppose a spatial moving axis $\{\hat{t}_i\}$ obtained by means of the operation of a two–point rotation tensor $\mathbf{\Lambda} = [\Lambda_{ij}]_{\hat{e}_i\otimes\hat{E}_j}$ acting on the material reference frame, according to: $\hat{t}_i = \Lambda_{ij}\hat{E}_j$. Note that the induced moving frame correspond to the push–forward by the rotation tensor of the material reference frame to the spatial placement.

Any spatial vector $\hat{v}$ belonging to the tangent space of $\mathcal{B}_t$ at $\hat{x}(\hat{X}, t)$ can be described in any of the two spatial reference frames, $\{\hat{e}_i\}$ or $\{\hat{t}_i\}$, according to $\hat{v} = \bar{v}_i\hat{t}_i = \bar{v}_i\mathbf{\Lambda}\hat{E}_i = \mathbf{\Lambda}\hat{V}$ and $\hat{v} = v_i\hat{e}_i$. It is interesting to note that the components of the spatial vector $\hat{v}$ expressed in the moving frame $\{\hat{t}_i\}$ are identical to the components of the material vector, $\hat{V}$ obtained by its pullback to the (material) reference configuration $\{\hat{E}_i\}$,

$$\widehat{V} = \mathbf{\Lambda}^T\hat{v} = \bar{v}_i\mathbf{\Lambda}\hat{E}_i = \bar{v}_i\hat{E}_i. \tag{A.100}$$

Let suppose that the spatial vector and the rotation tensor are implicitly parameterized in terms of $S \in \mathbb{R}$, *i.e.* $\hat{v} = \hat{v}(S)$ and $\mathbf{\Lambda} = \mathbf{\Lambda}(S)$. Taking the derivative of $\hat{v}$ with respect S we have [251, 228]

$$\begin{aligned}\hat{v}_{,S} &= \mathbf{\Lambda}_{,S}\,\hat{\bar{v}} + \mathbf{\Lambda}\hat{\bar{v}}_{,S} = (\mathbf{\Lambda}_{,S}\,\mathbf{\Lambda}^T)(\mathbf{\Lambda}\hat{\bar{v}}) + \mathbf{\Lambda}(\mathbf{\Lambda}^T\hat{v})_{,S} \\ &= \widetilde{\boldsymbol{\omega}}_{\mathbf{\Lambda}}\hat{v} + \mathbf{\Lambda}(\mathbf{\Lambda}^T\hat{v})_{,S}\end{aligned} \tag{A.101}$$

It is worth to note that in the deduction of Eq. (A.101) the pullback by $\mathbf{\Lambda}$ of the spatial vector $\hat{v}$ has been performed and the definition of *angular velocity* $\widetilde{\boldsymbol{\omega}}_{\mathbf{\Lambda}}$ (see §A.5.7) has been used considering the derivative with respect to the scalar parameter S. From Eq. (A.101) it is possible to define the following derivative:

Definition A.27. ***Co–rotated derivative***

The co–rotated derivative of the spatial vector $\hat{v}(S)$ $(S \in \mathbb{R})$ with respect to the scalar parameter

S as the following operator:

$$\begin{aligned} \overset{\triangledown}{(\bullet)}_{,S} : T_{\hat{x}}\mathcal{B}_t &\rightarrow T_{\hat{x}}\mathcal{B}_t \\ \hat{v} &\mapsto \overset{\triangledown}{\hat{v}}_{,S} \equiv \boldsymbol{\Lambda}\hat{V}_{,S} \equiv \hat{v}_{,S} - \widetilde{\boldsymbol{\omega}}_{\boldsymbol{\Lambda}}\hat{v} \equiv \hat{v}_{,S} - \hat{\omega}_{\boldsymbol{\Lambda}} \times \hat{v} \end{aligned} \tag{A.102}$$

The definition of the co–rotated derivative implies that it is a particular case of the Lie derivative applied to a spatial vector described in a rotating frame and the corresponding pullback/push forward operations are performed by the same rotation tensor as these that define the moving frame $\{\hat{t}_i\}$ ■

Additionally, Eq. (A.102) gives a new explicit expression for this particular Lie derivative:

$$\overset{\triangledown}{v}_{,S} \equiv \mathrm{L}_{\boldsymbol{\Lambda}}(\hat{v}) = \hat{v}_{,S} - \hat{\omega}_{\boldsymbol{\Lambda}} \times \hat{v} \tag{A.103}$$

The physical meaning of co–rotated derivative is that the derivative of a spatial object is taken by an observer fixed in the moving frame, *only on the components* referred to the corresponding moving frame. An observed who stays still in the fixed spatial frame needs to pullback the object to the material form $\hat{\bar{v}} = \boldsymbol{\Lambda}^T\hat{v}$ to perform the usual derivative operation and then push forward to the spatial form $\boldsymbol{\Lambda}\hat{\bar{v}}_{,S}$. Equivalently, the observer needs to subtract the *spin effect* $\hat{\omega}_{\boldsymbol{\Lambda}} \times \hat{v}$ from the usual derivative $\hat{v}_{,S}$ to have the same *objective* observation as by the observer fixed in the moving frame, [362, 228].
On other hand, for any spatial second order tensor $\mathbf{T} = \bar{\mathrm{T}}_{ij}\hat{t}''_i \otimes \hat{t}'_j$ that defines a transformation, $\hat{v}'' = \mathbf{T}\hat{v}'$ between vectors $\hat{v}' = \hat{\bar{v}}'\hat{t}'_j \in T_x\mathcal{B}_{t'}$ at any time t' and $\hat{v}'' = \hat{\bar{v}}''_i\hat{t}_i \in T_x\mathcal{B}_{t''}$ at any time t'' associated with the rotation tensors $\boldsymbol{\Lambda}' = \hat{t}'_i \otimes \hat{E}_i \in SO(3)$ and $\boldsymbol{\Lambda}'' = \hat{t}''_i \otimes \hat{E}_i \in SO(3)$ of the same material point and the corresponding material objects $\hat{\bar{v}}'$, $\hat{\bar{v}}''$ and $\bar{\mathbf{T}}$, one may define the corresponding co–rotated derivative as

$$\begin{aligned} \overset{\triangledown}{(\bullet)}_{,S} : (T_x\mathcal{B}_{t''} \times T^*_x\mathcal{B}_{t'}) &\rightarrow (T_x\mathcal{B}_{t''} \times T^*_x\mathcal{B}_{t'}) \\ \bar{\mathbf{T}}_{(\hat{t}''_i \otimes \hat{t}'_j)} &\mapsto \overset{\triangledown}{\mathbf{T}}_{,S} \end{aligned}$$

where

$$\overset{\triangledown}{\mathbf{T}}_{,S} \equiv \bar{\mathbf{T}}_{ij,S}\,\hat{t}''_i \otimes \hat{t}'_j \equiv \boldsymbol{\Lambda}''[(\boldsymbol{\Lambda}'')'\mathbf{T}\boldsymbol{\Lambda}']_{,S}\,(\boldsymbol{\Lambda}')^T \equiv \boldsymbol{\Lambda}''\bar{\mathbf{T}}_{,S}\,(\boldsymbol{\Lambda}')^T \equiv \mathbf{T}_{,S} - (\widetilde{\boldsymbol{\omega}}''_{\boldsymbol{\Lambda}}\mathbf{T} - \mathbf{T}\widetilde{\boldsymbol{\omega}}'_{\boldsymbol{\Lambda}}) \tag{A.104}$$

In analogous manner as in the case of vectors the co–rotated derivative of a second order tensor can be rewritten as

$$\overset{\triangledown}{\mathbf{T}}_{,S} \equiv \mathrm{L}_{\boldsymbol{\Lambda}''}(\mathbf{T}) = \mathbf{T}_{,S} - (\widetilde{\boldsymbol{\omega}}''_{\boldsymbol{\Lambda}}\mathbf{T} - \mathbf{T}\widetilde{\boldsymbol{\omega}}'_{\boldsymbol{\Lambda}}) \tag{A.105}$$

And the chain rule holds for the co-rotated derivative operation [228]:

$$\overset{\triangledown}{\hat{v}}''_{,S} = \overset{\triangledown}{\mathbf{T}}_{,S}\,\hat{v}' + \mathbf{T}\,\overset{\triangledown}{v}'_{,S}\,. \tag{A.106}$$

A.5.7 Configurational description of variations and derivatives

Supposing that the orientation tensor $\boldsymbol{\Lambda} \in SO(3)$ is given in term of one independent variable $x \in \mathbb{R}$, and following analogous procedures as those described in Eqs. (A.73a) and (A.79a), we

can consider the linearized increments $\delta_x\mathbf{\Lambda}$[24] which allow to obtain

$$\delta_x(\mathbf{\Lambda}\mathbf{\Lambda}^T) = \delta_x\mathbf{\Lambda}\mathbf{\Lambda}^T + \mathbf{\Lambda}\delta_x\mathbf{\Lambda}^T = \delta\widetilde{\boldsymbol{w}}_x + \delta\widetilde{\boldsymbol{w}}_x^T = \delta_x\mathbf{I} = 0 \tag{A.107a}$$

$$\delta_x(\mathbf{\Lambda}^T\mathbf{\Lambda}) = \delta_x\mathbf{\Lambda}^T\mathbf{\Lambda} + \mathbf{\Lambda}^T\delta_x\mathbf{\Lambda} = \delta\widetilde{\boldsymbol{W}}_x + \delta\widetilde{\boldsymbol{W}}_x^T = \delta_x\mathbf{I} = 0 \tag{A.107b}$$

where the skew–symmetric tensors $\delta\widetilde{\boldsymbol{w}}_x \in T^{\text{spa}}_{\mathbf{\Lambda}}SO(3)$ and $\delta\widetilde{\boldsymbol{W}}_x \in T^{\text{mat}}_{\mathbf{\Lambda}}SO(3)$ are some times called the *spin* tensors [363, 228]. The following relationships are also valid

$$\widetilde{\boldsymbol{w}}_{\delta x} \equiv \mathbf{\Lambda}\widetilde{\mathbf{W}}_{\delta x}\mathbf{\Lambda}^T, \qquad \widetilde{\mathbf{W}}_{\delta x} \equiv \mathbf{\Lambda}^T\widetilde{\boldsymbol{w}}_{\delta x}\mathbf{\Lambda}. \tag{A.108}$$

The associated material and spatial axial vectors are: $\delta\hat{W}_x \in T^{\text{mat}}_{\mathbf{\Lambda}}$ and $\delta\hat{w}_x \in T^{\text{spa}}_{\mathbf{\Lambda}}$ respectively.

A.5.7.a Derivatives

If instead of the linearized form the *derivative* form is calculated, it is possible to obtain

$$\widetilde{\mathbf{\Omega}}_x \equiv \mathbf{\Lambda}^T\mathbf{\Lambda}_{,x} \quad \in T^{\text{mat}}_{\mathbf{\Lambda}}SO(3) \tag{A.109a}$$

$$\widetilde{\boldsymbol{\omega}}_x \equiv \mathbf{\Lambda}_{,x}\,\mathbf{\Lambda}^T = \mathbf{\Lambda}\widetilde{\mathbf{\Omega}}_x\mathbf{\Lambda}^T \quad \in T^{\text{spa}}_{\mathbf{\Lambda}}SO(3) \tag{A.109b}$$

which are also called *spin* tensors as x varies [362, 182], associated with the following material and spatial axial vectors

$$\hat{\omega}_x = \omega_{xj}\hat{t}_j \qquad \in T^{\text{spa}}_{\mathbf{\Lambda}} \tag{A.110a}$$

$$\hat{\Omega}_x = \Omega_{xj}\hat{t}_j \qquad \in T^{\text{mat}}_{\mathbf{\Lambda}}. \tag{A.110b}$$

By other hand, considering the spatial updating of the compound rotation defined in Eq. (A.66) $\mathbf{\Lambda} = \mathbf{\Lambda}_n\mathbf{\Lambda}_0$ and using the chain rule of partial derivatives, we have

$$\mathbf{\Lambda}_{,x} = \mathbf{\Lambda}_{n,x}\,\mathbf{\Lambda}_0 + \mathbf{\Lambda}_n\mathbf{\Lambda}_{0,x} \tag{A.111}$$

Therefore, the spatial form of the spin tensor as x varies is described by

$$\begin{aligned}\widetilde{\boldsymbol{\omega}}_x &= \mathbf{\Lambda}_{,x}\,\mathbf{\Lambda}^T = \mathbf{\Lambda}_{n,x}\,\mathbf{\Lambda}_0\mathbf{\Lambda}^T + \mathbf{\Lambda}_n\mathbf{\Lambda}_{0,x}\,\mathbf{\Lambda}^T \\ &= \mathbf{\Lambda}_{n,x}\,\mathbf{\Lambda}_n^T + \mathbf{\Lambda}_n\mathbf{\Lambda}_{0,n}\,\mathbf{\Lambda}_0^T\mathbf{\Lambda}_n^T \qquad (A.112)\\ &= \widetilde{\boldsymbol{\omega}}_{nx} + \mathbf{\Lambda}_n\widetilde{\boldsymbol{\omega}}_{0x}\mathbf{\Lambda}_n^T \quad \in so(3) \qquad (A.113)\end{aligned}$$

where the skew–symmetric tensor $\widetilde{\boldsymbol{\omega}}_{nx} = \mathbf{\Lambda}_{n,x}\,\mathbf{\Lambda}_n^T \in T^{\text{spa}}_{\mathbf{\Lambda}}SO(3)$ is spatial description of the *incremental spin* tensor. The corresponding material description of the incremental spin tensor is obtained by means of applying the pullback operator by the rotation tensor $\mathbf{\Lambda}$ to the spatial description of the incremental spin tensor according to

$$\begin{aligned}\widetilde{\mathbf{\Omega}}_{nx} &= \overleftarrow{\mathbf{\Lambda}}\,[\widetilde{\boldsymbol{\omega}}_{nx}] = \mathbf{\Lambda}^T\widetilde{\boldsymbol{\omega}}_{nx}\mathbf{\Lambda} = \mathbf{\Lambda}^T[\widetilde{\boldsymbol{\omega}}_x - \mathbf{\Lambda}_n\widetilde{\boldsymbol{\omega}}_{0x}\mathbf{\Lambda}_n^T]\mathbf{\Lambda} \qquad (A.114a)\\ &= \mathbf{\Lambda}^T\mathbf{\Lambda}_{,x} - \mathbf{\Lambda}_0^T\mathbf{\Lambda}_{0,x} \qquad (A.114b)\\ &= \widetilde{\mathbf{\Omega}}_x - \widetilde{\mathbf{\Omega}}_{0x} = \mathbf{\Lambda}_0^T\widetilde{\boldsymbol{\omega}}_x^T\mathbf{\Lambda}_0 \quad \in T^{\text{mat}}_{\mathbf{\Lambda}_n}SO(3) \qquad (A.114c)\end{aligned}$$

The associated axial vectors are $\hat{\omega}_{nx} \in T^{\text{spa}}_{\mathbf{\Lambda}_n} \cong \mathbb{R}^3$ for the spatial description and $\widehat{\Omega}_{nx} \in T^{\text{mat}}_{\mathbf{\Lambda}_n} \cong \mathbb{R}^3$ for the material description. Additionally, the following spatial and material forms are

[24] The subscript x is used to highlight that the linearized increment in $\mathbf{\Lambda}$ is due to a linear increment in $x \in \mathbb{R}$.

obtained

$$\widetilde{\boldsymbol{\omega}}_{0x} = \boldsymbol{\Lambda}_{0,x}\,\boldsymbol{\Lambda}_0^T \qquad \in T^{\rm spa}_{\boldsymbol{\Lambda}_0} SO(3) \tag{A.115a}$$

$$\widetilde{\boldsymbol{\Omega}}_{0x} = \boldsymbol{\Lambda}_0^T \widetilde{\boldsymbol{\omega}}_{0x} \boldsymbol{\Lambda}_0 = \boldsymbol{\Lambda}_0^T \boldsymbol{\Lambda}_{0,x} \qquad \in T^{\rm mat}_{\boldsymbol{\Lambda}_0} SO(3) \tag{A.115b}$$

Eq. (A.113) implies that the spatial spin tensors cannot be obtained by a simple addition of an incremental spin relative to the previous configuration; It is necessary to align the spin of the previous configuration to the current one by applying the corresponding *relative rigid–body rotation*. A similar effect has to be accounted for constructing an additive rule for the axial vector associated to Eq. (A.113) *i.e.*

$$\widehat{\omega}_x = \widehat{\omega}_{nx} + \boldsymbol{\Lambda}_n \widehat{\omega}_{0x} \qquad \in T^{\rm spa}_{\boldsymbol{\Lambda}} \cong \mathbb{R}^3. \tag{A.116}$$

It is straightforward to confirm that a simple addition for spin tensors and the corresponding axial vectors can be performed in the material form according to:

$$\widetilde{\boldsymbol{\Omega}}_x = \widetilde{\boldsymbol{\Omega}}_{nx} + \widetilde{\boldsymbol{\Omega}}_{0x} \qquad \in T^{\rm mat}_{\boldsymbol{\Lambda}} SO(3) \tag{A.117}$$

$$\widehat{\Omega}_x = \widehat{\Omega}_{nx} + \widehat{\Omega}_{0x} \qquad \in T^{\rm mat}_{\boldsymbol{\Lambda}} \cong \mathbb{R}^3 \tag{A.118}$$

If the material description is preferred, *i.e.* $\boldsymbol{\Lambda} = \boldsymbol{\Lambda}_0 \boldsymbol{\Lambda}^{\rm m}_n$, we obtain the following results:

$$\begin{aligned} \widetilde{\boldsymbol{\omega}}_x &= \boldsymbol{\Lambda}_{,x}\,\boldsymbol{\Lambda}^T = [\boldsymbol{\Lambda}_{0,x}\,\boldsymbol{\Lambda}^{\rm m}_n + \boldsymbol{\Lambda}_0 \boldsymbol{\Lambda}^{\rm m}_{n,x}]\boldsymbol{\Lambda}^{{\rm m}T}_n \boldsymbol{\Lambda}_0^T \\ &= \boldsymbol{\Lambda}_{0,x}\,\boldsymbol{\Lambda}_0^T + \boldsymbol{\Lambda}_0 \boldsymbol{\Lambda}^{\rm m}_{n,x}\,\boldsymbol{\Lambda}^{{\rm m}T}_n \boldsymbol{\Lambda}_0^T \\ &= \widetilde{\boldsymbol{\omega}}_{0x} + \boldsymbol{\Lambda}_0 \widetilde{\boldsymbol{\omega}}^{\rm m}_{nx} \boldsymbol{\Lambda}_0^T \quad \in T^{\rm spa}_{\boldsymbol{\Lambda}} SO(3) \end{aligned} \tag{A.119a}$$

$$\begin{aligned} \widetilde{\boldsymbol{\Omega}}_x &= \overleftarrow{\boldsymbol{\Lambda}}\,[\widetilde{\boldsymbol{\omega}}_x] = \boldsymbol{\Lambda}^T \widetilde{\boldsymbol{\omega}}_x \boldsymbol{\Lambda} \\ &= \boldsymbol{\Lambda}^{{\rm m}T}_n \boldsymbol{\Lambda}_0^T [\boldsymbol{\Lambda}_{0,x}\,\boldsymbol{\Lambda}_0^T + \boldsymbol{\Lambda}_0 \boldsymbol{\Lambda}^{\rm m}_{n,x}\,\boldsymbol{\Lambda}^{{\rm m}T}_n \boldsymbol{\Lambda}_0^T] \boldsymbol{\Lambda}_0 \boldsymbol{\Lambda}^{\rm m}_n \\ &= \boldsymbol{\Lambda}^{{\rm m}T}_n \widetilde{\boldsymbol{\Omega}}_{0x} \boldsymbol{\Lambda}^{\rm m}_n + \widetilde{\boldsymbol{\Omega}}^{\rm m}_{nx} \quad \in T^{\rm mat}_{\boldsymbol{\Lambda}} SO(3) \end{aligned} \tag{A.119b}$$

where $\widetilde{\boldsymbol{\Omega}}_{0x} = \boldsymbol{\Lambda}_0^T \boldsymbol{\Lambda}_{0,x} \in T^{\rm mat}_{\boldsymbol{\Lambda}_0} SO(3)$, $\widetilde{\boldsymbol{\omega}}_{0x} = \boldsymbol{\Lambda}_{0,x}\,\boldsymbol{\Lambda}_0^T \in T^{\rm spa}_{\boldsymbol{\Lambda}_0} SO(3)$, $\widetilde{\boldsymbol{\Omega}}^{\rm m}_{nx} = \boldsymbol{\Lambda}^{{\rm m}T}_n \boldsymbol{\Lambda}^{\rm m}_{n,x} \in T^{\rm mat}_{\boldsymbol{\Lambda}_n} SO(3)$, $\widetilde{\boldsymbol{\omega}}^{\rm m}_{nx} = \boldsymbol{\Lambda}^{\rm m}_{n,x}\,\boldsymbol{\Lambda}^{{\rm m}T}_n \in T^{\rm spa}_{\boldsymbol{\Lambda}_n} SO(3)$ with their corresponding axial vectors: $\hat{\Omega}_x \in T^{\rm mat}_{\boldsymbol{\Lambda}}$, $\hat{\omega}_x \in T^{\rm spa}_{\boldsymbol{\Lambda}}$, $\hat{\Omega}_{0x} \in T^{\rm mat}_{\boldsymbol{\Lambda}_0}$, $\hat{\omega}_{0x} \in T^{\rm spa}_{\boldsymbol{\Lambda}_0}$, $\hat{\Omega}^{\rm m}_{nx} \in T^{\rm mat}_{\boldsymbol{\Lambda}_n}$, $\hat{\omega}^{\rm m}_{nx} \in T^{\rm spa}_{\boldsymbol{\Lambda}_n}$, which are related by

$$\hat{\omega}_x = \hat{\omega}_{0x} + \boldsymbol{\Lambda}_0 \hat{\omega}^{\rm m}_{nx} \tag{A.119c}$$

$$\hat{\Omega}_x = \boldsymbol{\Lambda}^{{\rm m}T}_n \hat{\Omega}_{0x} + \hat{\Omega}^{\rm m}_{nx} \quad \in T^{\rm mat}_{\boldsymbol{\Lambda}} SO(3) \tag{A.119d}$$

REMARK A.10. Results obtained in Eqs. (A.119a), (A.119b), (A.119c) and (A.119d) are completely equivalent to those obtained in Eqs. (A.109a)–(A.118) replacing $\boldsymbol{\Lambda}^{\rm m}_n = \boldsymbol{\Lambda}^T \boldsymbol{\Lambda}_n \boldsymbol{\Lambda}$ ■

Corresponding material and spatial *angular vectors* are given in terms of total rotation vector

$$\hat{\Omega}_{\boldsymbol{\Lambda}} = \mathbf{T}(\hat{\Psi})\dot{\hat{\Psi}}, \qquad \hat{\Omega} \in T^{\rm mat}_{\boldsymbol{\Lambda}}, \qquad \dot{\hat{\Psi}}, \hat{\Psi} \in T^{\rm mat}_{\mathbf{I}} \tag{A.120a}$$

$$\hat{\omega}_{\boldsymbol{\Lambda}} = \mathbf{T}(\hat{\psi})\dot{\hat{\psi}}, \qquad \hat{\omega} \in T^{\rm spa}_{\boldsymbol{\Lambda}}, \qquad \dot{\hat{\psi}}, \hat{\psi} \in T^{\rm spa}_{\mathbf{I}} \tag{A.120b}$$

The time derivative of the material/spatial angular velocity tensor or vector is known as mate-

rial/spatial *angular acceleration tensor* or *vector* respectively, and is given by

$$\begin{aligned}
\widetilde{\boldsymbol{A}}_{\boldsymbol{\Lambda}} &:= \dot{\widetilde{\boldsymbol{\Omega}}}_{\boldsymbol{\Lambda}}, \quad \widetilde{\boldsymbol{A}}_{\boldsymbol{\Lambda}} \in T^{\mathrm{mat}}_{\boldsymbol{\Lambda}} SO(3) \\
\hat{A}_{\boldsymbol{\Lambda}} &:= \dot{\hat{\Omega}}_{\boldsymbol{\Lambda}}, \quad \hat{A}_{\boldsymbol{\Lambda}} \in T^{\mathrm{mat}}_{\boldsymbol{\Lambda}} \\
\widetilde{\boldsymbol{\alpha}}_{\boldsymbol{\Lambda}} &:= \dot{\widetilde{\boldsymbol{\omega}}}_{\boldsymbol{\Lambda}}, \quad \widetilde{\boldsymbol{\alpha}}_{\boldsymbol{\Lambda}} \in T^{\mathrm{spa}}_{\boldsymbol{\Lambda}} SO(3) \\
\hat{\alpha}_{\boldsymbol{\Lambda}} &:= \dot{\hat{\omega}}_{\boldsymbol{\Lambda}}, \quad \hat{\alpha}_{\boldsymbol{\Lambda}} \in T^{\mathrm{spa}}_{\boldsymbol{\Lambda}}
\end{aligned} \tag{A.121}$$

where $\hat{A}_{\boldsymbol{\Lambda}}$ and $\hat{\alpha}_{\boldsymbol{\Lambda}}$ are the material and spatial angular acceleration vector at the base point $\boldsymbol{\Lambda} \in SO(3)$.
It is worth to note that the material incremental rotation vector $\hat{\Theta}_{\boldsymbol{\Lambda}}$, the angular velocity vector $\hat{\Omega}_{\boldsymbol{\Lambda}}$ and the material angular acceleration vector $\hat{A}_{\Lambda}$ belong to the same vector space on the rotation manifold, *i.e.* $\hat{\Theta}_{\boldsymbol{\Lambda}}$, $\hat{\Omega}_{\boldsymbol{\Lambda}}$, $\hat{A}_{\boldsymbol{\Lambda}} \in T^{\mathrm{mat}}_{\boldsymbol{\Lambda}}$ with the base point $\boldsymbol{\Lambda} = \exp(\widetilde{\boldsymbol{\Psi}})$.
As the time, t, changes, these vectors occupy different tangent spaces because the rotation operator depends on time, namely $\boldsymbol{\Lambda} = \boldsymbol{\Lambda}(t)$, therefore, the base point is moving permanently. Vector quantities of this type are known in mechanics as *spin vectors*. Spin vectors are rather tricky in numerical sense as they occupy a distinct vector space on the manifold. Correspondingly, the *spatial spin vectors* are $\hat{\theta}_{\boldsymbol{\Lambda}}$, $\hat{\omega}_{\boldsymbol{\Lambda}}$, $\hat{\alpha}_{\boldsymbol{\Lambda}} \in T^{\mathrm{spa}}_{\boldsymbol{\Lambda}}$.
Angular velocity and acceleration vectors and time derivatives of total rotation vector are related by

$$\begin{aligned}
\hat{A}_{\boldsymbol{\Lambda}} &= \mathbf{T} \cdot \ddot{\hat{\Psi}} + \dot{\mathbf{T}} \cdot \dot{\hat{\Psi}}, \qquad \hat{A}_{\boldsymbol{\Lambda}} \in T^{\mathrm{mat}}_{\boldsymbol{\Lambda}}; \quad \hat{\Psi}, \dot{\hat{\Psi}} \ddot{\hat{\Psi}} \in T^{\mathrm{mat}}_{\mathbf{I}} \\
\hat{\alpha}_{\Lambda} &= \mathbf{T}^T \cdot \ddot{\hat{\psi}} + \dot{\mathbf{T}}^T \cdot \dot{\hat{\psi}}, \quad \hat{\alpha}_{\boldsymbol{\Lambda}} \in T^{\mathrm{spa}}_{\boldsymbol{\Lambda}}; \quad \hat{\psi}, \dot{\hat{\psi}} \ddot{\hat{\psi}} \in T^{\mathrm{spa}}_{\mathbf{I}}
\end{aligned} \tag{A.122}$$

where the tangential transformation depends on the total rotation vector and the rotation operator is $\boldsymbol{\Lambda} = \exp(\widetilde{\boldsymbol{\Psi}}) = \exp(\widetilde{\boldsymbol{\psi}})$. The deduction of the time derivative of the tangential transformation, $\mathbf{T}(\bullet)$, involves a large and tedious algebraic work and it can be found in [246, 338] and references therein, its final expression is

$$\begin{aligned}
\dot{\mathbf{T}}(\dot{\hat{\Psi}}, \hat{\Psi}) &= c_1(\hat{\Psi} \cdot \dot{\hat{\Psi}})\mathbf{I} - c_2(\hat{\Psi} \cdot \dot{\hat{\Psi}})\widetilde{\boldsymbol{\Psi}} + c_3(\hat{\Psi} \cdot \dot{\hat{\Psi}})\hat{\Psi} \otimes \hat{\Psi} \\
&+ c_4(\dot{\hat{\Psi}} \cdot \hat{\Psi})\dot{\hat{\Psi}} + c_5(\dot{\hat{\Psi}} \otimes \hat{\Psi} + \hat{\Psi} \otimes \dot{\hat{\Psi}})
\end{aligned} \tag{A.123}$$

where the coefficients c_i, $(\Psi = |\hat{\Psi}|)$, are

$$\begin{aligned}
c_1 &:= \frac{\Psi \cos\Psi - \sin\Psi}{\Psi^3}; \qquad c_2 := \frac{\Psi \sin\Psi + 2\cos\Psi - 2}{\Psi^4}; \\
c_3 &:= \frac{3\sin\Psi - 2\Psi - \Psi\cos\Psi}{\Psi^5}; \qquad c_4 := \frac{\cos\Psi - 1}{\Psi^2}; \quad c_5 := \frac{\Psi - \sin\Psi}{\Psi^3}
\end{aligned}$$

Appendix B

Additional results

In this appendix some additional rather extensive results that were excluded from the main body of the text for facilitating the reading are given.

B.1 Reduced linear–elastic constitutive relations

In this appendix the explicit expressions for the coefficients of the reduced linear-elastic constitutive relations for rod cross sections composed of not necessarily homogeneous nor isotropic hyperelastic materials are provided.
Considering that $\hat{n}^{\mathrm{m}} = \mathbf{C}^{\mathrm{me}}_{nn}\hat{\mathcal{E}}_n + \mathbf{C}^{\mathrm{me}}_{nm}\hat{\Omega}_n$ and $\hat{m}^{\mathrm{m}} = \mathbf{C}^{\mathrm{me}}_{mn}\hat{\mathcal{E}}_n + \mathbf{C}^{\mathrm{me}}_{mm}\hat{\Omega}_n$ in the material form and Eq. (3.162) we have [228]:

$$
\begin{aligned}
C^{\mathrm{me}}_{nnij} &= \mathcal{C}^{\mathrm{me0}}_{ij}\bar{\mathcal{A}}^{*} && \text{(B.1a)}\\
C^{\mathrm{me}}_{nmi1} &= \mathcal{C}^{\mathrm{me0}}_{i3}\bar{\mathcal{S}}^{*}_{3} - \mathcal{C}^{\mathrm{me0}}_{i2}\bar{\mathcal{S}}^{*}_{2} && \text{(B.1b)}\\
C^{\mathrm{me}}_{mn1j} &= \mathcal{C}^{\mathrm{me0}}_{3j}\bar{\mathcal{S}}^{*}_{3} - \mathcal{C}^{\mathrm{me0}}_{2j}\bar{\mathcal{S}}^{*}_{2} && \text{(B.1c)}\\
C^{\mathrm{me}}_{nmi2} &= \mathcal{C}^{\mathrm{me0}}_{i1}\bar{\mathcal{S}}^{*}_{2} && \text{(B.1d)}\\
C^{\mathrm{me}}_{mn2j} &= \mathcal{C}^{\mathrm{me0}}_{1j}\bar{\mathcal{S}}^{*}_{2} && \text{(B.1e)}\\
C^{\mathrm{me}}_{nmi3} &= -\mathcal{C}^{\mathrm{me0}}_{i1}\bar{\mathcal{S}}^{*}_{3} && \text{(B.1f)}\\
C^{\mathrm{me}}_{nm3j} &= -\mathcal{C}^{\mathrm{me0}}_{1j}\bar{\mathcal{S}}^{*}_{3} && \text{(B.1g)}\\
C^{\mathrm{me}}_{mm11} &= \mathcal{C}^{\mathrm{me0}}_{22}\bar{\mathcal{I}}^{*}_{22} + \mathcal{C}^{\mathrm{me0}}_{33}\bar{\mathcal{I}}^{*}_{33} - (\mathcal{C}^{\mathrm{me0}}_{23}\bar{\mathcal{I}}^{*}_{23} + \mathcal{C}^{\mathrm{me0}}_{32}\bar{\mathcal{I}}^{*}_{32}) && \text{(B.1h)}\\
C^{\mathrm{me}}_{mm22} &= \mathcal{C}^{\mathrm{me0}}_{11}\bar{\mathcal{I}}^{*}_{22} && \text{(B.1i)}\\
C^{\mathrm{me}}_{mm33} &= \mathcal{C}^{\mathrm{me0}}_{11}\bar{\mathcal{I}}^{*}_{33} && \text{(B.1j)}\\
C^{\mathrm{me}}_{mm12} &= \mathcal{C}^{\mathrm{me0}}_{31}\bar{\mathcal{I}}^{*}_{32} - \mathcal{C}^{\mathrm{me0}}_{21}\bar{\mathcal{I}}^{*}_{22} && \text{(B.1k)}\\
C^{\mathrm{me}}_{mm21} &= \mathcal{C}^{\mathrm{me0}}_{13}\bar{\mathcal{I}}^{*}_{32} - \mathcal{C}^{\mathrm{me0}}_{12}\bar{\mathcal{I}}^{*}_{22} && \text{(B.1l)}\\
C^{\mathrm{me}}_{mm13} &= \mathcal{C}^{\mathrm{me0}}_{21}\bar{\mathcal{I}}^{*}_{23} - \mathcal{C}^{\mathrm{me0}}_{31}\bar{\mathcal{I}}^{*}_{33} && \text{(B.1m)}\\
C^{\mathrm{me}}_{mm31} &= \mathcal{C}^{\mathrm{me0}}_{12}\bar{\mathcal{I}}^{*}_{23} - \mathcal{C}^{\mathrm{me0}}_{13}\bar{\mathcal{I}}^{*}_{33} && \text{(B.1n)}\\
C^{\mathrm{me}}_{mm23} &= -\mathcal{C}^{\mathrm{me0}}_{11}\bar{\mathcal{I}}^{*}_{23} && \text{(B.1o)}\\
C^{\mathrm{me}}_{mm32} &= -\mathcal{C}^{\mathrm{me0}}_{11}\bar{\mathcal{I}}^{*}_{32} && \text{(B.1p)}
\end{aligned}
$$

with,

$$\bar{\mathcal{A}}^* = \int_{\mathcal{A}} g_0^{-1}\bar{\alpha}d\xi_2 d\xi_3 \tag{B.2a}$$

$$\bar{\mathcal{S}}_2^* = \int_{\mathcal{A}} g_0^{-1}\bar{\alpha}\xi_3 d\xi_2 d\xi_3 \tag{B.2b}$$

$$\bar{\mathcal{S}}_3^* = \int_{\mathcal{A}} g_0^{-1}\bar{\alpha}\xi_2 d\xi_2 d\xi_3 \tag{B.2c}$$

$$\bar{\mathcal{I}}_{22}^* = \int_{\mathcal{A}} g_0^{-1}\bar{\alpha}(\xi_3)^2 d\xi_2 d\xi_3 \tag{B.2d}$$

$$\bar{\mathcal{I}}_{33}^* = \int_{\mathcal{A}} g_0^{-1}\bar{\alpha}(\xi_2)^2 d\xi_2 d\xi_3 \tag{B.2e}$$

$$\bar{\mathcal{I}}_{23}^* = \bar{\mathcal{I}}_{32}^* = \int_{\mathcal{A}} g_0^{-1}\bar{\alpha}\xi_2\xi_3 d\xi_2 d\xi_3. \tag{B.2f}$$

Note that the reduced elasticity constants have an overall symmetry for any hyperelastic material due to the fact that $\mathcal{C}_{ij}^{\text{me0}} = \mathcal{C}_{ji}^{\text{me0}}$. For other materials the symmetry may not hold because of non-existence of the strain energy functional of Eq. (3.149). In general, the coupling exist, such as stretch-bending coupling, stretch-torsion coupling and torsion-bending coupling, etc.
On other hand, we may align the rod reference curve so that $\bar{\mathcal{S}}_2^* = \bar{\mathcal{S}}_3^* = 0$. This means that the cross section elasticity centroid line does not coincide with the mass centroid line for a general curved rod even though the rod material is homogeneous because the initial curvature correction term g_0 appears as the numerator in the integrals of the inertia constants while it appears as the denominator for the elasticity constants.
The coefficients in the case of the spatial form of the constitutive tensors are the same as given in Eqs. (B.1a) to (B.2f) due to the fact that material tensors have the same components in the material frame as their co–rotated counterparts in $\{\hat{t}_i \otimes \hat{t}_j\}$.

B.2 Additive Increment of the Rotational Strain

In this section the method proposed by Simo and Vu-Quoc [363], for calculating an explicit expression for the term $(\mathrm{d}(\exp[\widetilde{\Theta}])/\mathrm{d}S)\exp[-\widetilde{\Theta}]$, where the skew–symmetric tensor $\widetilde{\Theta}(S)$ and its associated axial vector $\hat{\theta}(S)$ in spatial form are related by $\widetilde{\Theta}\cdot\hat{v} = \hat{\theta}\times\hat{v},\ \forall\,\hat{v}\in\mathbb{R}^3$, is summarized. Alternatively, the material description can be employed considering that $\hat{\psi} = \Lambda^T\hat{\theta}$ or $\widetilde{\Psi} = \Lambda^T\widetilde{\Theta}\Lambda$. Therefore, given a rotation vector $\hat{\theta}(S)$ which parameterize the rotation tensor $\exp[\widetilde{\Theta}(S)]$ follow the steps:

□ **Compute axial vectors**

$$\begin{aligned}
\hat{e} &= \hat{\theta}/\|\hat{\theta}\| \\
\bar{\theta} &= \tan(\frac{1}{2}\|\hat{\theta}\|)\hat{e} \\
\bar{\theta}' &= \frac{1}{2}\frac{\tan(\frac{1}{2}\|\hat{\theta}\|)}{\frac{1}{2}\|\hat{\theta}\|}\Big[\hat{\theta}' - \big(1 - \frac{\|\hat{\theta}\|}{\sin(\|\theta\|)}\big)(\hat{e}\cdot\hat{\theta}')\hat{e}\Big]
\end{aligned}$$

where $\widetilde{\Theta} \triangleq \mathrm{d}\widetilde{\Theta}/\mathrm{d}S$ and $\bar{\theta}$ is the axial vector of $\widetilde{\Theta}$.

□ **Compute exponential and derivative**

$$\begin{aligned}\exp[\widetilde{\Theta}] &= \mathbf{I} + \frac{2}{1+\|\bar{\theta}\|^2}(\widetilde{\bar{\Theta}} + \widetilde{\bar{\Theta}}^2) \\ \frac{\mathrm{d}}{\mathrm{d}S}\exp[\widetilde{\Theta}(S)] &= \frac{2}{1+\|\bar{\theta}\|^2}\Big[\widetilde{\bar{\Theta}}' + \widetilde{\bar{\Theta}}'\widetilde{\bar{\Theta}} + \widetilde{\bar{\Theta}}\widetilde{\bar{\Theta}}' - \frac{2\bar{\theta}\cdot\bar{\theta}'(\widetilde{\bar{\Theta}} + \widetilde{\bar{\Theta}}^2)}{1+\|\bar{\theta}\|^2}\Big].\end{aligned}$$

Upon noting the identity

$$\widetilde{\bar{\Theta}}^3 = -\|\bar{\theta}\|^2\widetilde{\bar{\Theta}}$$

A lengthy but straightforward manipulation yields the result

$$\Big(\frac{\mathrm{d}(\exp[\widetilde{\Theta}])}{\mathrm{d}S}\Big)\exp[-\widetilde{\Theta}] = \frac{2}{1+\|\bar{\theta}\|^2}(\widetilde{\bar{\Theta}}' + \widetilde{\bar{\Theta}}'\widetilde{\bar{\Theta}} - \widetilde{\bar{\Theta}}\widetilde{\bar{\Theta}}' + A)$$

where A is given by

$$A \equiv -\bar{\theta}\cdot\bar{\theta}'(\widetilde{\bar{\Theta}} - \widetilde{\bar{\Theta}}^2) - \widetilde{\bar{\Theta}}\widetilde{\bar{\Theta}}'\widetilde{\bar{\Theta}} + \widetilde{\bar{\Theta}}\widetilde{\bar{\Theta}}'\widetilde{\bar{\Theta}}^2.$$

It remains to show that indeed $A \equiv 0$. This follows at once from the identities

$$\widetilde{\bar{\Theta}}\widetilde{\bar{\Theta}}'\widetilde{\bar{\Theta}} \equiv -(\bar{\theta}\cdot\bar{\theta}')\widetilde{\bar{\Theta}}, \qquad \widetilde{\bar{\Theta}}\widetilde{\bar{\Theta}}'\widetilde{\bar{\Theta}}^2 \equiv -(\bar{\theta}\cdot\bar{\theta}')\widetilde{\bar{\Theta}}^2$$

which finally gives

$$\begin{aligned}\Big(\frac{\mathrm{d}(\exp[\widetilde{\Theta}])}{\mathrm{d}S}\Big)\exp[-\widetilde{\Theta}] &= \frac{2}{1+\|\bar{\theta}\|^2}(\widetilde{\bar{\Theta}}' + \widetilde{\bar{\Theta}}'\widetilde{\bar{\Theta}} - \widetilde{\bar{\Theta}}\widetilde{\bar{\Theta}}') \qquad \text{Spatial Form} \\ \exp[-\widetilde{\Psi}]\Big(\frac{\mathrm{d}(\exp[\widetilde{\Psi}])}{\mathrm{d}S}\Big) &= \frac{2}{1+\|\bar{\psi}\|^2}(\widetilde{\bar{\Psi}}' + \widetilde{\bar{\Psi}}'\widetilde{\bar{\Psi}} - \widetilde{\bar{\Psi}}\widetilde{\bar{\Psi}}') \qquad \text{Material Form}\end{aligned}$$

□ **Compute the axial vector**.
In addition, it is also noted that the axial vector $\hat{\beta}$ of $(\mathrm{d}(\exp[\widetilde{\Theta}])/\mathrm{d}S)\exp[-\widetilde{\Theta}]$ is given by the expression

$$\hat{\beta} = \frac{2}{1+\|\bar{\psi}\|^2}\left[\bar{\theta}' + (\bar{\theta}\times\bar{\theta}')\right]$$

or equivalently,

$$\hat{\beta} = \frac{\sin\|\hat{\theta}\|}{\|\hat{\theta}\|}\hat{\theta}' + \Big(1 - \frac{\sin\|\hat{\theta}\|}{\|\hat{\theta}\|}\Big)\Big(\frac{\hat{\theta}\cdot\hat{\theta}'}{\|\hat{\theta}\|}\Big)\frac{\hat{\theta}}{\|\hat{\theta}\|} + \frac{1}{2}\Big(\frac{\sin\frac{1}{2}\|\theta\|}{\frac{1}{2}\|\hat{\theta}\|}\Big)^2\hat{\theta}\times\hat{\theta}'$$

we observe that $\hat{\beta} \approx \hat{\theta}'$ for $\|\hat{\theta}\|$ small, *i.e.*, $\hat{\theta}'$ is the first approximation of $\hat{\beta}$.

Bibliography

[1] Aagaard BT. *Finite-Element Simulations of Earthquakes*, PhD Thesis, California Institute of Technology, Pasadena, (2000).

[2] Abichou H, Zahrouni H, Potier-Ferry M. Asymptotic numerical method for problems coupling several nonlinearities, *Computer Methods in Applied Mechanics and Engineering*. 191 (2002) 5795-5810.

[3] Ahmadi HR, Muhr AH. Modelling dynamic properties of filled rubber, *Plastics, Rubber and Composites Processing and Applications*. 26 (1997) 451-461.

[4] Aiken I. Passive energy dissipation hardware and applications, *Proceedings, Los Angeles County and Seaosc Symposium on Passive Energy Dissipation Systems for New and Existing Buildings*, Los Angeles, (1996).

[5] Aiken I. Testing of seismic isolators and dampers - considerations and limitations, *Proceedings, Structural Engineering World Congress*, San Francisco, California, (1998).

[6] Aiken I, Kelly JM, Pall AS. Seismic response of a nine-story steel frame with friction damped cross-bracing, *Proceedings, Ninth World Conference on Earthquake Engineering*, Tokyo and Kyoto, Japan, (1988).

[7] Aiken I, Kelly JM. Cyclic dynamic testing of fluid viscous dampers, *Proceedings, Caltrans Fourth Seismic Research Workshop*, California Departament of Transportation, Sacramento, California, USA, (1996).

[8] Akiyama H. *Metodología de proyecto sismoresistente de edificios basada en el balance energético*, Editorial Reverté, SA. (2003).

[9] Aköz Y, Kadioğlu F. The mixed finite element method for the quasi-static and dynamic analysis of viscoelastic Timoshenko beams, *International Journal of Numerical Methods for Engineering*. 44 (1999) 1909–1932.

[10] Ambrósio J. Efficient kinematic joint descriptions for flexible multibody systems experiencing linear and non-linear deformations, *International Journal of Numerical Methods for Engineering*. 56 (2003) 1771-1793.

[11] Antman SS. *Nonlinear problems of elasticity*, Springer-Velag (107), 1991.

[12] Antman SS. Dynamical problems for geometrically exact theories of nonlinearly viscoelastic rods, *Journal of Nonlinear Science*. 6 (1996) 1-18.

[13] Antman SS. Invariant dissipative mechanisms for the spatial motion of rods suggested by artificial viscosity, *Journal of Elasticity*. 70 (2003) 55–64.

[14] Arfiadi Y, Hadi MNS. Passive and active control of three-dimensional buildings, *Earthquake Engineering and Structural Dynamics*. 29 (2000) 377–396.

[15] Argyris J. An excursion into large rotations, *Computer Methods in Applied Mechanics and Engineering*. 32 (1982) 85–155.

[16] Argyris J, Poterasu VF. Large rotations revisited application of Lie algebra, *Computer Methods in Applied Mechanics and Engineering*. 103 (1993) 11–42.

[17] Aristizabal-Ochoa JD. Large deflection and postbuckling behavior of Timoshenko beam-columns with semi–rigid connections including shear and axial effects, *Engineering Structures*. 29 (2007) 991-1003.

[18] Armero F. Large-scale modeling of localized dissipative mechanisms in a local continuum: applications to the numerical simulation of strain localization in rate-dependent inelastic solids *Mechanics of Cohesive-Frictional Materials*. 4 (1999) 101-31.

[19] Armero F, Romero I, On the objective and conserving integration of geometrically exact rod models, *Trends in Computational Structural Mechanics*, Lake Constance, Austria, May 2001.

[20] Armero F, Romero I. On the formulation of high-frequency dissipative time-stepping algorithms for nonlinear dynamics. Part I: Low-order methods for two model problems and nonlinear elastodynamics, *Computer Methods in Applied Mechanics and Engineering*. 190 (2001) 2603–2649.

[21] Armero F, Romero I, On the formulation of of high-frequency dissipative time-stepping algorithms for nonlinear dynamics. Part II: second-order methods, *Computer Methods in Applied Mechanics and Engineering*. 190 (2001) 6783–6824.

[22] Armero F. On the characterization of localized solutions in inelastic solids: an analysis of wave propagation in a softening bar, *Computer Methods in Applied Mechanics and Engineering*. 191 (2001) 181–213.

[23] Armero F, Romero I. Energy–dissipating momentum–conserving time–stepping algorithms for the dynamic of nonlinear Cosserat rods, *Computational Mechanics*. 31 (2003) 3–26.

[24] Armero F, Ehrlich D. An analysis of strain localization and wave propagation in plastic models of beams at failure, *Computer Methods in Applied Mechanics and Engineering*. 193 (2004) 3129-3171.

[25] Armero F, Ehrlich D. Numerical modeling of softening hinges in the Euler–Bernoulli beams, *Computers and Structures*. 84 (2005) 641–656.

[26] Armero F, Ehrlich D. Finite element methods for the analysis of softening plastic hinges in beams and frames, *Computational Mechanics*. 35 (2005) 237-264.

[27] Asano M, Masahiko H, Yamamoto M. The experimental study on viscoelastic material dampers and the formulation of analytical Model, *Proceedings of the 12th World Conference on Earthquake Engineering*. (2001) Paper No 1535.

[28] Atluri SN, Cazzani A. Rotations in computational solid mechanics, *Archives of Computational Methods in Engineering*. 2 (1995) 49–138.

[29] Atluri SN, Vasudevan S. A consistent theory of finite stretches and finite rotations, in space–curved beams of arbitrary cross section, *Computational Mechanics*. 27 (2001) 271–281.

[30] Ayoub A, Filippou FC. Mixed formulation of nonlinear steel-concrete composite beam element, *Journal of Structural Engineering*. 126 (2000) 0371-0381.

[31] Bairan Garcia JM, Mari Bernat AR. Coupled model for the non-linear analysis of anisotropic sections subjected to general 3D loading. Part 1: Theoretical formulation, *Computers and Structures* 84 (2006) 2254-2263.

[32] Bairan Garcia JM, Mari Bernat AR. Coupled model for the nonlinear analysis of sections made of anisotropic materials, subjected to general 3D loading. Part 2: Implementation and validation, *Computers and Structures* 84 (2006) 2264-2276.

[33] Bak T. *Lecture notes–modeling of mechanical system*, Technical Report, Aalborg University, Department of Control Engineering, (2002).

[34] Bangash T, Munjiza A. Experimental validation of a computationally efficient beam element for combined finite–discrete element modeling of structures in distress, *Computational Mechanics*. 30 (2003) 366–373.

[35] Barbat AH, Rodellar J, Ryan EP, Molinares N. Active control of nonlinear base-isolated buildings, *Journal of Engineering Mechanics*. 121 (1995) 676–684.

[36] Barbat AH, Oller S. Hanganu A., Oñate E., Viscous damage model for Timoshenko beam structures, *International Journal for Solids and Structures*. 34 (1997) 3953–3976.

[37] Barbat AH, Oller S, Mata P, Vielma JC. Computational simulation of the seismic response of buildings with energy dissipating devices, *Proceedings of the* COMPDYN 2007, *First International Conference on Computational Methods in Structural Dynamics and Earthquake Engineering*, Rethymno, Crete, Greece, June, 13^{th}–15^{th}, (2007).

[38] Barbat AH, Oller S, Mata P, Vielma JC. Numerical modeling of the seismic response of buildings with energy dissipators, COMPDYN 2007, *First International Conference on Computational Methods in Structural Dynamics and Earthquake Engineering*, Rethymno, Crete, Greece, June, 13^{th}–15^{th}, (2007) (Keynote Lecture).

[39] Barham WS, Aref AJ, Dargush GF. Flexibility–based large increment method for analysis of elastic-perfectly plastic beam structures, *Computers and Structures*. 83 (2005) 2453-2462.

[40] Barroso LR, Breneman SE, Smith HA. Performance evaluation of controlled steel frames under multilevel seismic loads, *Journal of Structural Engineering*. 128 (2002) 1368–1378.

[41] Bathe KJ, Bolourchi S. Large displacement analysis of three-dimensional beam structures, *International Journal of Numerical Methods in Engineering*. 14 (1979) 961–986.

[42] Bathe KJ. *Finite element procedures*, Prentice Hall, Inc. 1996.

[43] Batista Marques de Sousa Jr J, Barreto Caldas R. Numerical analysis of composite steel–concrete columns of arbitrary cross section, *Journal of Engineering Mechanics*. 131 (2005) 1721–1730.

[44] Battini JM, Pacoste C. Plastic instability of beam structures using co-rotational elements, *Computer Methods in Applied Mechanics and Engineering*. 191 (2002) 5811-5831.

[45] Battini JM, Pacoste C. Co-rotational beam elements with warping effects in instability problems, *Computer Methods in Applied Mechanics and Engineering*. 191 (2002) 1755-1789.

[46] Bauchau OA, Theron NJ. Energy decaying scheme for non-linear beam models, *Computer Methods in Applied Mechanics and Engineering*. 134 (1996) 37–56.

[47] Bauchau OA, Bottasso CL. On the design of energy preserving and decaying schemes for flexible, nonlinear multi-body systems, *Computer Methods in Applied Mechanics and Engineering*. 169 (1999) 61–79.

[48] Bauchau O, Trainelli L. The Vectorial Parametrization of Rotation, *Nonlinear Dynamics*. 32 (2003) 71–92.

[49] Bauchau OA, Choi JI. The vector parameterization of motion, *Nonlinear Dynamics*. 33 (2003) 165–188.

[50] Bayrak O, Sheikh SA. Plastic hinge analysis, *Journal of Structural Engineering*. 127 (2001) 1092–1100.

[51] Bažant Z.P. Asymptotic matching analysis of scaling of structural failure due to softening hinges. II: Implications, *Journal of Engineering Mechanics*. 6 (2003) 651–654.

[52] Bažant Z.P. Asymptotic matching analysis of scaling of structural failure due to softening hinges. I: Theory, *Journal of Engineering Mechanics*. 6 (2003) 641–650.

[53] Behdinans K, Tabarrok B. A finite element formulation for sliding beams, part I, *International Journal for Numerical Methods in Engineering*. 43 (1998) 1309–1333.

[54] Benavent-Climent A. Shaking table tests of reinforced concrete wide beam-column connections, *Earthquake Engineering and Structural Dynamics*. 34 (2005) 1833-1839.

[55] Benavent-Climent A. Influence of hysteretic dampers on the seismic response of reinforced concrete wide beamcolumn connections, *Engineering Structures*. 28 (2006) 580-592.

[56] Bentz EC. *Sectional analysis of reinforced concrete members*, PhD Thesis, University of Toronto, (2000).

[57] Betsch P, Steinmann P. Frame–indifferent beam finite element based upon the geometrically exact beam theory, *International Journal for Numerical Methods in Engineering*. 54 (2002) 1775–1788.

[58] Betsch P, Menzel A, Stein E. On the parametrization of finite rotations in computational mechanics. A classification of concepts with application to smooth shells, *Computer Methods in Applied Mechanics and Engineering*. 155 (1998) 273–305.

[59] Betsch P, Steinmann P. Conservation properties of a time FE method. Part I: time-stepping schemes for N-body problems, *International Journal for Numerical Methods in Engineering*. 49 (2000) 599–638.

[60] Betsch P, Steinmann P. Conservation properties of a time FE method—part II: Time-stepping schemes for non-linear elastodynamics, *International Journal for Numerical Methods in Engineering*. 50 (2001) 1931–1955.

[61] Betsch P, Steinmann P. Conservation properties of a time FE methodpart III: Mechanical systems with holonomic constraints, *International Journal for Numerical Methods in Engineering*. 53 (2002) 2271-2304.

[62] Betsch P, Steinmann P. Constrained dynamics of geometrically exact beams, *Computational Mechanics*. 31 (2003) 49–59.

[63] Blanco PJ, Feijóo RA, Urquiza SA. A unified variational approach for coupling 3D–1D models and its blood flow applications, *Computer Methods in Applied Mechanics and Engineering*. 196 (2007) 4391-4410.

[64] Blandford GE. Large deformation analysis of inelastic space truss structures, *Journal of Structural Engineering*. 122 (1996) 407–415.

[65] Blandford GE. Review of progressive failure analyses for truss structures, *Journal of Structural Engineering*. 123 (1996) 122–129.

[66] Bonet J, Wood RD.*Nonlinear continuum mechanics for finite element analysis*, Cambridge University Press, (1997).

[67] Borri M, Mello F, Atluri SN. Variational approaches for dynamics and time-finite-elements: numerical studies, *Computational Mechanics* 7 (1990) 49–76.

[68] Borri M, Trainelli L, Croce A. The embedded projection method: a general index reduction procedure for constrained system dynamics, *Computer Methods in Applied Mechanics and Engineering*. 195 (2006) 6974–6992.

[69] Bottasso CL, Borri M. Energy preserving/decaying schemes for non-linear beam dynamics using the helicoidal approximation, *Computer Methods in Applied Mechanics and Engineering* 143 (1997) 393-415.

[70] Bottasso CL, Borri M, Trainelli L. Integration of elastic multibody systems by invariant conserving/dissipating algorithms. II. Numerical schemes and applications, *Computer Methods in Applied Mechanics and Engineering* 190 (2001) 3701–3733.

[71] Bottasso CL, Borri M, Trainelli L. Geometric invariance, *Computational Mechanics* 129 (2002) 163-169.

[72] Boutyour EH, Azrar L, Potier-Ferry M. Vibration of buckled elastic structures with large rotations by an asymptotic numerical method, *Computers and Structures*. 84 (2006) 93–101.

[73] Boyer F, Primault D. Finite element of slender beam in finite transformation: A geometrically exact approach, *International Journal of Numerical Methods in Engineering*. 59 (2004) 669–702.

[74] Bozzo LM, Barbat AH. *Diseño sismoresistente de edifcios. Técnicas convencionales y avanzadas*, Editorial Reverté SA, (2000).

[75] Braga F, Faggella M, Gigliotti R, Laterza M. Nonlinear dynamic response of HDRB and hybrid HDRB-friction sliders base isolation systems, *Bulletin of Earthquake Engineering*. 3 (2005) 333–353.

[76] Brank B, Ibrahimbegović A. On the relation between different parametrizations of finite rotations for shells, *Engineering Computations*. 18 (2001) 950–973.

[77] Brank B, Korelc J, Ibrahimbegović A. Nonlinear shell problem formulation accounting for through-the-thickness stretching and its finite element implementation, *Computers and Structures*. 80 (2002) 699–717.

[78] Brank B, Korelc J, Ibrahimbegović A. Dynamics and time-stepping schemes for elastic shells undergoing finite rotations, *Computers and Structures*. 81 (2003) 1193–1210.

[79] Brank B, Korelc J, Ibrahimbegović A. Dynamics and time-stepping schemes for elastic shells undergoing finite rotations, *Computers and Structures*. 81 (2003) 1193–1210.

[80] Brank B, Mamouri S, Ibrahimbegović A. Constrained finite rotations in dynamics of shells and Newmark implicit time-stepping schemes, *International Journal for Computed-Aided Engineering and Software*. 22 (2005) 505–535.

[81] Bratina S, Saje M, Planinc I. On materially and geometrically non-linear analysis of reinforced concrete planar frames, *International Journal of Solids and Structures*. 41 (2004) 7181-7207.

[82] Briseghella L, Majorana CE, Pellegrino C. Conservation of angular momentum and energy in the integration of non-linear dynamic equations, *Computer Methods in Applied Mechanics and Engineering*. 179 (1999) 247–263.

[83] Bruneau M, Vian D. Experimental investigation of P–Δ effects to collapse during earthquakes, 12^{th} *European Conference on Earthquake Engineering*, Elsevier Science Ltd. Paper Ref. 021.

[84] Budd CJ, Iserles A. Geometric integration: numerical solution of differential equations on manifolds, *The Royal Society*. 357 (1999) 945–956.

[85] Buonsanti M, Royer–Carfagni G. From 3-D nonlinear elasticity theory to 1–D bars with nonconvex energy, *Journal of Elasticity*. 70 (2003) 87–100.

[86] Burlion N, Gatuingt F, Pijaudier-Cabot G, Daudeville L. Compaction and tensile damage in concrete: constitutive modelling and application to dynamics, *Computer Methods in Applied Mechanics and Engineering*. 183 (2000) 291–308.

[87] Cao DQ, Dongsheng L, Wang CHT. Three dimensional nonlinear dynamics of slender structures: Cosserat rod element approach, Lancaster University, Department of Physics, *short technical report* (2005).

[88] Cardona A, Gerardin M. A beam finite element non-linear theory with finite rotations, *International Journal of Numerical Methods in Engineering*. 26 (1988) 2403–2438.

[89] Cardona A, Huespe A. Evaluation of simple bifurcation points and post-critical path in large finite rotations problems, *Computer Methods in Applied Mechanics and Engineering*. 175 (1999) 137–156.

[90] Car E, Oller S, Oñate E. An anisotropic elasto plastic constitutive model for large strain analysis of fiber reinforced composite materials, *Computer Methods in Applied Mechanics and Engineering*. 185 (2000) 245–277.

[91] Car E. *Modelo constitutivo continuo para el estudio del comportamiento mecánico de los materiales compuestos*, PhD Thesis, Universidad Politécnica de Cataluña. (2000).

[92] Celledoni E, Owren B. Lie group methods for rigid body dynamics and time integration on manifolds, *Computer Methods in Applied Mechanics and Engineering*. 192 (2003) 421–438.

[93] Cesnik CES, Sutyrint VG, Hodges DH. Refined theory of composite beams: the role of short–wavelength extrapolation, *International Journal of Solids and Structures*. 33 (1988) 1387–1408.

[94] Chopra AK. *Dynamics of structures: theory and applications to earthquake engineering*, Prentice Hall, (2000).

[95] Christenson RE. *Semiactive control of civil structures for natural hazard mitigation: analytical and experimental studies*, PhD Thesis, University of Notre Dame, Indiana (2001).

[96] Clark P, Aiken I, Ko E, Kasai K, Kimura I. Design procedures for buildings incorporating hysteretic seismic devices. *Proceedings*, 68^{th} *Annual Convention Santa Barbara*, California, Structural Engineering Association of California, October (1999).

[97] Cocchetti G, Maier G. Elastic-plastic and limit-state analyses of frames with softening plastic–hinge models by mathematical programming, *International Journal of Solids and Structures*. 40 (2003) 7219–7244.

[98] Coleman J, Spacone E. Localization issues in force-based frame elements, *Journal of Structural Engineering*. 127 (2001) 1257–1265.

[99] Connes A. C^* algebras and differential geometry, *C.R. Acad. Sci.* Paris, Ser. A-B, 290, (1980).

[100] Connor JJ, Wada A, Iwata M, Huang YH. Damage-controlled structures. I: Preliminary design methodology for seismically active regions, *Journal of Structural Engineering*. 123 (1997) 423–431.

[101] Cosenza E, Manfredi G, Damage indices and damage measures, *Progress in Structural Engineering Materials*. 2 (2000) 50–59.

[102] Cosenza E, Manfredi G, Verderame GM. A fibre model for push–over analysis of underdesigned reinforced concrete frames. *Computers and Structures* 84 (2006) 904-916.

[103] Cottingham WN, Doyle DD. The rotational dynamics of rigid bodies implemented with the Cayley Klein parametrization, *Molecular Physics*. 99 (2001) 1839–1843.

[104] Courtois P, Ibrahimbegović A. Vecteur de rotation incrémental pour les coques non-linéaires en grandes rotations, 16*ème Congrès Franais de Mécanique*, Nice, France. (2003) 1–6, (In French).

[105] Courtois P, Ibrahimbegović A. Implantation numérique pour le vecteur de rotation incrémental en coques non-linéaires soumises à de grandes rotations, 16*ème Congrès Franais de Mécanique*, Nice, France. (2003) 1–6, (In French).

[106] Crisfield MA, Galvanetto U, Jelenič G. Dynamics of 3-D co-rotational beams, *Computational Mechanics*. 20 (1997) 507–519.

[107] Crisfield MA. *Non-linear finite element analysis of solids and structures*, (Vol. 1), John Wiley & Sons. (1998).

[108] Crisfield MA. *Non-linear finite element analysis of solids and structures*, (Vol. 2), John Wiley & Sons. (1998).

[109] Crisfield MA, Wills J. Solution strategies and softening materials, *Computer Methods in Applied Mechanics and Engineering*. 66 (1988) 267–289.

[110] Crisfield MA. Jelenič G. Objectivity of strain measures in the geometrically exact three-dimensional beam theory and its finite-element implementation, *The Royal Society*. 455 (1999) 1125–1147.

[111] CSI *Analysis Reference Manual For* SAP2000®, ETABS®, *and* SAFE™, Computers and Structures, Inc. Berkeley, California, USA, (2004).

[112] Das S, Hadi MNS. Non–linear finite element analysis of reinforced concrete members using MSC/NASTRAN, MSC *World User's Conference*, Newport Beach, CA, June (1996).

[113] Davenne L, Ragueneau F, Mazar J, Ibrahimbegović A. Efficient Approaches to Finite Element Analysis in Earthquake Engineering, *Computers and Structures*. 81 (2003) 1223–1239.

[114] Davenne L. Macro-element analysis in earthquake engineering, *Conference on multi–physics and multi–scale computer models in non–linear analysis and optimal design of engineering structures under extreme conditions*, Slovenia, June 13–17, (2004).

[115] De La Llera JC, Vásquez J, Chopra AK, Almazán JL. A macro–element model for inelastic building analysis, *Earthquake Engineering and Structural Dynamics*. 29 (2000) 1725–1757.

[116] Dichmann DJ, Maddocks JH, Pego RL. Hamiltonian dynamics of an elastica and the stability of solitary waves, *Archive for Rational Mechanics and Analysis*. 135 (1996) 357-396.

[117] Dides MA, De La Llera JC. A comparative study of concentrated plasticity models in dynamic analysis of building structures, *Earthquake Engineering and Structural Dynamics*. 34 (2005) 1005–1026.

[118] Driemeier L, Baroncini SP, Alves M. A contribution to the numerical non-linear analysis of three-dimensional truss system considering large strains, damage and plasticity, *Communications in Nonlinear Science and Numerical Simulation*. 10 (2005) 515–535.

[119] Dubrokin BA, Fomenko AT, Nóvikov SP. *Geometría moderna. Métodos y aplicaciones*. Vols 1 & 2. Ed. URSS, Moscú, (2000).

[120] EC8, Eurocode No 8. Design of structures for earthquake resistance. European Committee for standardization, 3rd Draft, prEN 1998-1-1:2001, May 2001.

[121] Ehrlich D, Armero F. Finite element methods for the analysis of softening plastic hinges in beams and frames, *Computational Mechanics*. 35 (2005) 237–264.

[122] Elliott KS. Research and development in precast concrete framed structures, *Progress in Structural Engineering and Materials*. 2 (2000) 405–428.

[123] Elnashai AS, Mwafy AM, Overstrength and force reduction factors of multistorey reinforced concrete buildings, *The Structural Design of Tall Buildings*. 11 (2002) 329–351.

[124] Ericksen JL, Truesdell C. Exact theory of stress and strain in rods and shells, *Archive for Rational Mechanics and Analysis*. 1 (1957) 295–323.

[125] European Committee for Standaridization. *Eurocode 8: Design of structures for earthquake resistance–Part 1: General rules, seismic actions and rules for buildings*. Final Draft, Ref No: prEN 1998-1:2003 E. (2003).

[126] Fajfar P, Fifchinger M, Dolšek M. Macro-models and simplified methods for efficient structural analysis in earthquake engineering, *Conference on multi–physics and multi–scale computer models in non–linear analysis and optimal design of engineering structures under extreme conditions*. Slovenia, June 13–17, (2004).

[127] Fantilli AP, Ferretti D, Iori I, Vallini P. Flexural deformability of concrete beams, *Journal of Structural Engineering* 124 (1998) 1041–1049.

[128] Fardis MN. Seismic analysis of RC structures, *Construction Research Communications Limited*. 1 (1997) 57–67.

[129] Federal Emergency Management Agency, *Prestandard and Commentary for the Seismic Rehabilitation of Buildings*, Report 356, Washington, DC: FEMA. (2000).

[130] Federal Emergency Management Agency, NEHRP *Recommended Provisions for Seismic Regulations for New Buildings and Other Structures*, Report 368, Washington, DC: FEMA. (2000).

[131] Felippa CA, Crivelli LA, Haugen B. A survey of the core-congruential formulation for geometrically nonlinear TL finite elements, *Archives of Computational Methods in Engineering*. 1 (1994) 1–48.

[132] Fialko S. Aggregation multilevel iterative solver for analysis of large–scale finite element problems of structural mechanics: linear statics and natural vibrations, *Parallel Processing and Applied Mathematics: 4th International Conference*, PPAM 2001 Na: czów, Poland, September 9-12, (2001).

[133] Flores P, Ambrósio J. Revolute joints with clearance in multibody systems, *Computers and Structures*. 82 (2004) 1359-1369.

[134] Fraternali F, Bilotti G. Nonlinear elastic stress analysis in curved composite beams, *Computers and Structures*. 62 (1997) 837–859.

[135] Freddi L, Morassi A, Paroni R. Thin-walled beams: the case of the rectangular cross-section, *Journal of Elasticity*. 76 (2004) 45-66.

[136] Friedemann S. A variational approach to obstacle problems for shearable nonlinearly elastic rods, *Archives of Rational Mechanics*, 140 (1997) 103–159.

[137] Fu Y, Kasai K. Comparative study of frames using viscoelastic and viscous dampers, *Journal of Structural Engineering*. 124 (1998) 513–522.
[138] Fu F, Lam D, Ye J. Parametric study of semi–rigid composite connections with 3-D finite element approach, *Engineering Structures*. 29 (2007) 888-898.
[139] Galucio AC, Deü JF, Ohayon R. Finite element formulation of viscoelastic sandwich beams using fractional derivative operators, *Computational Mechanics*. 33 (2004) 282-291.
[140] Garusi E, Tralli A. A hybrid stress-assumed transition element for solid-to-beam and plate-to-beam connections, *Computers and Structures*. 80 (2002) 105-115.
[141] Gebbeken N. A refined numerical approach for the ultimate-load analysis of 3-D steel rod structures, *Engineering Computations*. 15 (1998) 312–344.
[142] Gerardin M, Cardona A. Kinematics and dynamics of rigid and flexible mechanisms using finite elements and Quaternion algebra, *Computational Mechanics*. 4 (1989) 115–135.
[143] Gluck N, Reinhorn AM, Gluck J, Levy R. Design of supplemental damping for control of structures, *Journal fo Structural Engineering*. 122 (1996) 1394–1399.
[144] Goicolea JM, García Orden JC. Dynamic analysis of rigid and deformable multibody systems with penalty methods and energy-momentum schemes, *Computer Methods in Applied Mechanics and Engineering* 188 (2000) 789–804.
[145] Gonzalez O, Simo JC. On the stability of symplectic and energy-momentum algorithms for non-linear Hamiltonian systems with symmetry, *Computer Methods in Applied Mechanics and Engineering*. 134 (1996) 197–222.
[146] Gopalakrishnan S, Doyle JF. Spectral super–elements for wave propagation in structures with local non–uniformities, *Computer Methods in Applied Mechanics and Engineering*. 121 (1995) 77–90.
[147] Göttlicher B, Schweizerhof K. Analysis of flexible structures with occasionally rigid parts under transient loading, *Computers and Structures* 83 (2005) 2035-2051.
[148] Grassia FS. Practical parameterization of rotations using the exponential map, *Journal of Graphics Tools*. 3 (1998) 29–48.
[149] Gruttmann F, Sauer R, Wagner W. A geometrical nonlinear eccentric 3-D beam element with arbitrary cross sections. *Computer Methods in Applied Mechanics and Engineering*. 160 (1998) 383–400.
[150] Gruttmann F, Sauer R, Wagner W. *Shear stresses in prismatic beams with arbitrary crosssections*, Technical Report, Universität Karlsruhe (TH), Institut für Baustatik, (1998).
[151] Gruttmann F, Sauer R, Wagner W. Theory and numerics of three-dimensional beams with elasto-plastic material behavior, *International Journal of Numerical Methods in Engineering*, 48 (2000) 1675–1702.
[152] Gupta A, Krawinkler H. Dynamic P-Delta effects for flexible inelastic steel structures, *Journal of Structural Engineering*. 126 (2000) 145–154.
[153] Gruttmann F, Wagner W. *Shear correction factors in Timoshenko's beam theory for arbitrary shaped crosssections*, Technical report, Universität Karlsruhe (TH), Institut für Baustatik, (2001).
[154] Hailu D, Zekaria A, Kassegne AK. A new efficient multiple-node constraint approach for FEA analysis of radius-cut RBS moment frames in highly seismic areas, *Proceedings of the Joint EACE-AAU International Conference on Computational Mechanics. Structures and Earthquake Engineering*, January 9–10, Addis Ababa, Ethiopia, (2003).
[155] Hajjar JF, Schiller PH, Molodan A. A distributed plasticity model for cyclic analysis of concrete–filled steel tube beam-columns and composite frames, *Engineering Structures*. 20 (1998) 398–412.
[156] Hajjar JF, Schiller PH, Molodan A. A distributed plasticity model for concrete-filled steel tube beam-colum with interlayer slip, *Engineering Structures*. 20 (1998) 663–676.
[157] Hajjar JF. Concrete-filled steel tube columns under earthquake loads, *Progress in Structural Engineering Materials*. 2 (2000) 72–81.
[158] Halliday PJ, Grosh K. Dynamic response of complex structural intersections using hybrid methods. *Journal of Applied Mechanics*. 66 (1999) 653–659.
[159] Hanganu AD, Barbat AH, Oñate E. *Metodología de Evaluación del Deterioro en Estructuras de Hormigón Armado*, International Center for Numerical Methods in Engineering, CIMNE, Technical report. 39 (1997).
[160] Hanganu AD, Oñate E, Barbat AH. Finite element methodology for local/global damage evaluation in civil engineering structures, *Computers and Structures*. 80 (2002) 1667–1687.

[161] Hanson RD, Aiken ID, Nims DK, Ritchter PJ, Batchman RE. State of the art and state of the practice in seismic engineering dissipation, *Procedings, ATC-17-1. Seminar on seismic isolation, passive energy dissipation and active control.* Applied Technology Council, San Francisco, California, March, (1993).

[162] Healey TJ, Mehta PG. Straightforward computation of spatial equilibria of geometrically exact cosserat rods, *International Journal of Bifurcation and Chaos in Applied Sciences and Engineering.* 15 (2005) 949–966.

[163] Highway Innovative Technology Evaluation Center (HITEC). A service center of the Civil Engineering Research Foundation (CERF). *Guidelines for the Testing of Seismic Isolation and Energy Dissipaton Devices.* Technical Evaluation Report No 96-02, (1996).

[164] Highway Innovative Technology Evaluation Center (HITEC). A service center of the Civil Engineering Research Foundation (CERF). *Summary of the evaluation findings for the testing of seismic isolation and passive energy dissipating devices*, Technical Evaluation Report No 40404, (1999).

[165] Hjelmstad KD, Taciroglu E. Mixed variational methods for finite element analysis of geometrically non-linear, inelastic BernoulliEuler beams, *Communications in Numerical Methods in Engineering.* 19 (2003) 809-832.

[166] Holden T, Restrepo J, Mander HJ. Seismic performance of precast reinforced and prestressed concrete walls, *Journal of Structural Engineering.* 126 (2003) 286–296.

[167] Hori A, Sasagawa A. Large deformation of inelastic large space frame. I: analysis, *Journal of Structural Engineering*, 126 (2000) 580-588.

[168] Hori A, Sasagawa A. Large deformation of inelastic large space frame. II: application, *Journal of Structural Engineering*, 126 (2000) 589-595.

[169] Hsiao KM, Lin JY, Lin WY. A consistent co–rotational finite element formulation for geometrically nonlinear dynamic analysis of 3-D beams, *Computer Methods in Applied Mechanics and Engineering.* 169 (1999) 1–18.

[170] Hughes TJR. *The finite element method. Linear static and dynamic finite element analysis.* Dover Publishers, New York, (2000).

[171] Hutchinson JR. Shear coefficients for Timoshenko beam theory, *Journal of Applied Mechanics.* 68 (2001) 87–92.

[172] Hwang JS, Ku SW. Analytical modelling of high damping rubber bearings, *Journal of Structural Engineering.* 123 (1997) 1029–1036.

[173] Iaura M, Atluri SN. Dynamic analysis of planar flexible beams with finite rotations by using inertial and rotating frames, *Computers and Structures.* 55 (1993) 453–462.

[174] Iaura M, Atluri SN. On a consistent theory, and variational formulation of finitely stretched and rotated 3-D space-curved beams, *Computational Mechanics.* 4 (1989) 73–78.

[175] Ibrahimbegović A, Frey F. Finite element analysis of linear and non–linear planar deformations of elastic initially curved beams, *International Journal for Numerical Methods in Engineering.* 36 (1993) 3239–3258.

[176] Ibrahimbegović A. Stress resultant geometrically nonlinear shell theory with drilling rotations-Part I. A consistent formulation, *Computer Methods in Applied Mechanics and Engineering.* 118 (1994) 265–284.

[177] Ibrahimbegović A, Frey F. Stress resultant geometrically nonlinear shell theory with drilling rotations-Part II. Computational aspects, *Computer Methods in Applied Mechanics and Engineering.* 118 (1994) 285–308.

[178] Ibrahimbegović A. On the element implementation of geometrically nonlinear Reissners beam theory: three-dimensional curved beam elements, *Computer Methods in Applied Mechanics and Engineering.* 122 (1995) 11–26.

[179] Ibrahimbegović A, Frey F, Kožar I. Computational aspects of vector–like parametrization of three-dimensional finite rotations, *International Journal for Numerical Methods in Engineering.* 38 (1995) 3653–3673.

[180] Ibrahimbegović A, Shakourzadeh H, Batoz JL, Al Mikdad M, Ying-Qiao G. On the role of geometrically exact and second-order theories in buckling and post-buckling analysis of three-dimensional beam structures, *Computers and Structures.* 61 (1996) 1101–1114.

[181] Ibrahimbegović A. On the choice of finite rotation parameters, *Computer Methods in Applied Mechanics and Engineering.* 149 (1997) 49–71.

[182] Ibrahimbegović A, Mazen AM. Finite rotations in dynamics of beams and implicit time-stepping schemes, *International Journal of Numerical Methods in Engineering*. 41 (1998) 781–814.

[183] Ibrahimbegović A, Al Mikdad M. Finite rotations in dynamics of beams and implicit time-stepping schemes, *International Journal for Numerical Methods in Engineering*. 41 (1998) 781–814.

[184] Ibrahimbegović A, Mamouri S. Nonlinear dynamics of flexible beams in planar motion: formulation and time–stepping scheme for stiff problems, *Computers and Structures*. 70 (1999) 1–22.

[185] Ibrahimbegović A, Mamouri S. On rigid components and joint constraints in nonlinear dynamics of flexible multibody systems employing 3D geometrically exact beam model, *Computer Methods in Applied Mechanics and Engineering*. 188 (2000) 805–831.

[186] Ibrahimbegović A, Mamouri S, Taylor RL, Chen AJ. Finite element method in dynamics of flexible multibody system: modeling of holonomic constrains and energy conserving integration schemes, *Multibody System Dynamics*. 4 (2000) 195–223.

[187] Ibrahimbegović A, Al Mikdad M. Quadratically convergent direct calculation of critical points for 3D structures undergoing finite rotations, *Computer Methods in Applied Mechanics and Engineering*. 189 (2000) 107–120.

[188] Ibrahimbegović A, Brank B, Courtois P. Stress resultant geometrically exact form of classical shell model and vector-like parametrization of constrained finite rotations, *International Journal of Numerical Methods in Engineering*. 52 (2001) 1235–1252.

[189] Ibrahimbegović A, Mamouri S. Energy conserving/decaying implicit scheme for nonlinear dynamics of three-dimensional beams undergoing finite rotations, *Computer Methods in Applied Mechanics and Engineering*. 191 (2002) 4241–4258.

[190] Ibrahimbegović A, Taylor RL. On the role of frame-invariance in structural mechanics models at finite rotations, *Computer Methods in Applied Mechanics and Engineering*. 191 (2002) 5159–5176.

[191] Ibrahimbegović A, Taylor RL, Lim H. Non–linear dynamics of flexible multibody systems, *Computers and Structures*. 81 (2003) 1113–1132.

[192] Ibrahimbegović A. On the geometrically exact formulation of structural mechanics and its applications to dynamics, control and optimization, Comptes Rendus *Mecanique*. 331 (2003) 383-394.

[193] Ibrahimbegović A, Knopf-Lenoir C, Kučerová A, Villon P. Optimal design and optimal control of structures undergoing finite rotations and elastic deformations, *International Journal for Numerical Methods in Engineering*. 61 (2004) 2428–2460.

[194] Innocenti C, Paganelli D. Determining the 3×3 rotation matrices that satisfy three linear equations in the direction cosines, *Advances in Robot Kinematics Mechanisms and Motion*, Springer (2006).

[195] Irago H. Deduction of Saint-Venant's principle for the asymptotic residue of elastic rods, *Journal of Elasticity* 57 (1999) 55-83.

[196] Isobe D, Tsuda M. Seismic collapse analysis of reinforced concrete framed structures using the finite element method, *Earthquake Engineering and Structural Dynamics*. 32 (2003) 2027–2046.

[197] Izzuddin, BA. Conceptual issues in geometrically nonlinear analysis of 3D framed structures, *Computer Methods in Applied Mechanics and Engineering*. 191 (2001) 1029–1053.

[198] Jelenič G, Saje M. A kinematically exact space finite strain beam model-finite element formulation by generalized virtual work principle, *Computer Methods in Applied Mechanics and Engineering*. 120 (1995) 131–161.

[199] Jelenič G, Crisfield MA. Geometrically exact 3D beam theory: implementation of a strain-invariant finite element for static and dynamics, *Computer Methods in Applied Mechanics and Engineering*. 171 (1999) 141–171.

[200] Jelenič G, Crisfield MA. Dynamic analysis of 3D beams with joints in presence of large rotations, *Computer Methods in Applied Mechanics and Engineering*. 190 (2001) 4195–4230.

[201] Jelenič G, Crisfield MA. Problems associated with the use of Cayley transform and tangent scaling for conserving energy and momenta in Reissner-Simo beam theory, *Communications in Numerical Methods in Engineering*. 18 (2002) 711–720.

[202] Jelenič G, Different aspects of invariance and shear locking in 3D beam elements, *Advanced Research Workshop: Multi-physics and Multi-scale Computer Models in Non-linear Analysis and Optimal Design of Engineering Structures Under Extreme Conditions*, Bled, Slovenia, June 13–17, (2004).

[203] Jiang WG, Henshall JL. A coupling cross-section finite element model for torsion analysis of prismatic bars, *European Journal of Mechanics A/Solids*. 21 (2002) 513-522.

[204] Jung SN, Nagaraj VT, Chopra I. Refined structural model for thin–and thick–walled composite rotor blades, *Journal of the American Institute of Aeronautics and Astronautics*. 40 (2002) 105–116.

[205] Kachanov L. Time of rupture process under creep conditions, *Izvestia Akademii Nauk*. 8 (1958) 26–31.

[206] Kane C, Marsden JE, Ortiz M, West M. Variational integrators and the Newmark algorithm for conservative and dissipative mechanical systems, *International Journal for Numerical Methods in Engineering*. 49 (2000) 1295–1325.

[207] Kapania RK, Li J. On a geometrically exact curved/twisted beam theory under rigid cross-section assumption, *Computational Mechanics*. 30 (2003) 428–443.

[208] Kapania RK, Li J. A formulation and implementation of geometrically exact curved beam elements incorporating finite strains and finite rotations, *Computational Mechanics*. 30 (2003) 444–459.

[209] Kappos AJ. Seismic damage indices for RC buildings: evaluation of concepts and procedures, *Progress in Structural Engineering and Materials*. 1 (1997) 78–87.

[210] Kasai K, Fu Y, Watanabe A. Passive control systems for seismic damage mitigation, *Journal of Structural Engineering*. 124 (1998) 501–512.

[211] Kelly JM. *Earthquake-resistant design with rubber*, *Springer-Verlag*; 2^{nd} Edition, (1997).

[212] Kelly JM. The role of damping in seismic isolation, *Earthquake Engineering and Structural Dynamics*. 28 (1999) 3–20.

[213] Kikuchi M, Aiken I. An analytical hysteresis model for elastomeric seismic isolation bearings, *Earthquake Engineering and Structural Dynamics*. 26 (1997) 215–231.

[214] Kim JK, Lee TG. Failure behavior of reinforced concrete frames by the combined layered and nonlayered method, *Computers and Structures*. 48 (1993) 819–825.

[215] Kojima H, Yoshihide Y. Performance, durability of high damping rubber bearings for earthquake protection, *Rubber World*. 202 (4) (1990).

[216] Krysl P, Endres L. Explicit Newmark/Verlet algorithm for time integration of the rotational dynamics of rigid bodies, *Short Communication*, University of San Diego, (2004).

[217] Krysl P. Direct time integration of rigid body motion with discrete-impulse midpoint approximation: Explicit Newmark algorithms, *Communications in Numerical Methods in Engineering*. 22 (2005) 441–451.

[218] Kwak HG, Filippou FC. *Finite element analysis of reinforced concrete structures under monotonic loads*, Technical Report, No UCB/SEMM–90/14, University of California, Berkeley, California, USA, (1990).

[219] Kwak HG, Kim SP. Nonlinear analysis of RC beam subject to cyclic loading, *Journal of Structural Engineering*. 127 (2001) 1436–1444.

[220] Lafortune S, Goriely A, Tabor M. The dynamics of stretchable rods in the inertial case, *Nonlinear Dynamics*. 43 (2006) 173-195.

[221] Lee SS, Moon TS. Moment-rotation model of semi–rigid connections with angles, *Engineering Structures*. 24 (2002) 227-237.

[222] Lee T, Leok M, McClamroch NH. Lie group variational integrators for the full body problem, *Computer Methods in Applied Mechanics and Engineering*. 196 (2007) 2907–2924.

[223] Lee D, Taylor DP. Viscous damper development and future trends, *The Structural Design of Tall Buildings*. 10 (2001) 311–320.

[224] Lefik M, Schrefler BA. 3-D finite element analysis of composite beams with parallel fibre, based on homogenization theory, *Computational Mechanics*. 14 (1994) 2–15.

[225] Lens EV, Cardona A, Géradin M. Energy preserving time integration for constrained multibody systems, *Multibody System Dynamics*. 11 (2004) 41-61.

[226] Lew A, Marsden JE, Ortiz M, West M. *An overview of variational integrators, Finite element methods: 1970's and beyond*, L.P. Franca Ed., CIMNE, Barcelona, Spain, (2003).

[227] Lew A, Marsden JE, Ortiz M, West M. Variational time integrators, International Journal for Numerical Methods in Engineering. 60 (2004) 153-212 .

[228] Li J. *A geometrically exact curved beam theory and its finite element formulation/implementation*, MSc Thesis, Virginia Polytechnic Institute and State University, (2000).

[229] Lim CW, Chung TY, Moon SJ. Adaptive bang-bang control for the vibration control of structures under earthquakes, *Earthquake and Structural Dynamics*. 32 (2003) 1977–1994.

[230] Lin YY, Chang KC. Study on damping reduction factors for buildings under earthquake ground motions, *Journal of Structural Engineering*. 129 (2003) 206–214.

[231] Lin WH, Chopra AK. Asymmetric one-storey elastic system with non-linear viscous and viscoelastic dampers: Symplified analysis and supplemental damping system design, *Earthquake Engineering and Structural Dynamics*. 32 (2003) 579–596.

[232] Lin WH, Chopra AK. Asymmetric one–storey elastic system with non–linear viscous and viscoelastic dampers: Earthquake response, *Earthquake Engineering and Structural Dynamics*. 32 (2003) 555–577.

[233] Liu JY, Hong JZ. Dynamics of three-dimensional beams undergoing large overall motion, *European Journal of Mechanics A/Solids*. 23 (2004) 1051-1068.

[234] Love AEHA. *Treatise on the mathematical theory of elasticity*, Dover: New York, (1996).

[235] Lu Y. Comparative study of seismic behavior of multistory reinforced concrete framed structures, *Journal of Structural Engineering*. 128 (2002) 169–178.

[236] Lubliner J. On the thermodynamic foundations of non–linear solid mechanics, *International Journal of Non-Linear Mechanics*. 7 (1972) 237-254.

[237] Lubliner J. *Thermomechanics of Deformable Bodies*, Departament of Civil Engineering, Technical Report, University of California, Berkeley, (1985).

[238] Lubliner J, Oliver J, Oller S, Oñate E. A plastic-damage model for concrete, *International Journal of Solids and Structures*. 25 (1989) 299–326.

[239] Lubliner J. *Plasticity Theory*. Dover Publications, (2008).

[240] Luccioni B, Oller S, Danesi R. Coupled plastic-damaged model, *Computer Methods in Applied Mechanics and Engineering*. 129 (1996) 81–89.

[241] Luccioni BM, Rougier VC. A plastic damage approach for confined concrete, *Computers and Structures*. 83 (2005) 2238-2256.

[242] Łuczko J. Bifurcations and internal resonances in space-curved rods, *Computer Methods in Applied Mechanics and Engineering*. 191 (2002) 3271-3296.

[243] Magalhães de Souza R, Filippou FC, Maués Brabo Pereira A, Aranha Jr GYR. Force formulation of a non–prismatic Timoshenko beam finite element for dynamic analysis of frames, CILAMNE, XXIV *Iberian Latin–American Congress on Computational Methods in Engineering*, Ouro Preto/MG Brasil, (2003).

[244] Mäkinen J. Critical study of Newmark-scheme on manifold of finite rotations, *Computer Methods in Applied Mechanics and Engineering*. 191 (2001) 817–828.

[245] Mäkinen J. *A Formulation for flexible multibody mechanics. Lagrangian geometrically exact beam elements using constrain manifold parametrization*, PhD Thesis, Tampere University of Technology, Institute of Applied Mechanics and Optimization, 3 (2004).

[246] Mäkinen J, Marjamäki H. Total Lagrangian parametrization of rotation manifold, ENOC-2005, *Fifth EUROMECH Nonlinear Dynamics Conference*, Eindhoven, Netherlands, 7-12 August, (2005) 522–530.

[247] Mäkinen J. Total Lagrangian Reissners geometrically exact beam element without singularities, *International Journal of Numerical Methods in Engineering*. 70 (2007) 1009–1048.

[248] Makris N, Burton SA, Hill D, Jordan M. Analysis and design of ER damper for seismic protection of structures, *Journal of Mechanics Engineering*. 122 (1996) 1003–1011.

[249] Makris N, Changt SP. Effect of viscous, viscoplastic and friction damping on the response of seismic isolated structures, *Earthquake Engineering and Structural Dynamics*. 29 (2000) 85–107.

[250] Malvern LE. *Introduction to the mechanics of a continuous medium*, Prentice-Hall, Inc. (1969).

[251] Marsden JE, Hughes TJR. *Mathematical foundations of elasticity*, Prentice-Hall, California, (1983).

[252] Marsden JE, Wendlandt JM. Mechanical systems with symmetry, variational principles, and integration algorithms in *Current and Future Directions in Applied Mathematics*, Alber M, Hu B, Rosenthal J, Eds. Birkhäuser, (1997) 219-261.

[253] Marsden JE, Pekarsky S, Shkoller S, West M. Variational methods, multisymplectic geometry and continuum mechanics, *Journal of Geometry and Physics*. 38 (2001) 253–284.

[254] Marsden JE, West M. Discrete mechanics and variational integrators, *Acta Numerica*. (2001) 357–514.

[255] Marsden JE, Ratiu TS. *Introduction to mechanics and symmetry*, Springer-Velarg, 17 (2002).

[256] Martínez Franklin CE. *A theoretical and numerical evaluation of nonlinear beam elements*, MSc Thesis, Massachusetts Institute of Technology, (1997).

[257] Martinez X, Oller S, Rastellini F, Barbat AH, Numerical procedure for the computation of RC structures reinforced with FRP using the serial/parallel mixing theory, *Computers and Structures*. (2008) (In Press).

[258] Mata P, Oller S, Barbat AH. Static analysis of beam structures under nonlinear geometric and constitutive behavior, *Computer Methods in Applied Mechanics and Engineering*. 196 (2007) 4458–4478.

[259] Mata P, Boroschek R, Barbat AH, Oller S. High damping rubber model for energy dissipating devices, *Journal of Earthquake Engineering*. 11 (2) (2007) 231–256.

[260] Mata P, Oller S, Barbat AH. Dynamic analysis of beam structures considering geometric and constitutive nonlinearity, *Computer Methods in Applied Mechanics and Engineering*. 197 (2008) 857–878.

[261] Mata P, Barbat AH, Oller S, Boroschek R. Nonlinear seismic analysis of RC structures with energy dissipating devices, *International Journal for Numerical Methods in Engineering*. (2008) (Submitted).

[262] Mata P, Barbat AH, Oller S, Boroschek R. Computational models for the seismic response of reinforced concrete buildings with energy dissipating devices, *Archives of Computational Methods in Engineering*. (2008) (Submitted).

[263] Mata P, Barbat AH, Oller S. Two–scale approach for the nonlinear dynamic analysis of RC structures with localized irregularities, *Engineering Computations*. (2008) (Submitted).

[264] Mata P, Barbat AH, Oller S. Multiscale modelling of the seismic response of precast buildings, USNCCM, IX 9$^{\text{th}}$ US *National Congress on Computational Mechanics*, (Technical presentation) San Francisco, California. July 23–26, (2007).

[265] Mata A. P, Boroschek K, R. Caracterización mecánica de una goma de alto amortiguamiento para el desarrollo de disipadores de energía, 2$^{\text{do}}$ *Congreso Ibero americano de Ingeniería Antisísmica*, Madrid, España, 16–19 de Octubre, (2001).

[266] Mata P, Barbat AH, Oller S. Mejoras en el Comportamiento sísmico de estructuras prefabricadas por medio de disipadores de energía, *Congresso de Métodos Computacionais em Engenharia*, Portugal, Lisboa, 31 de Maio–2 de Junio, (2004).

[267] Mata P, Boroschek R, Barbat AH. Analytical model for high damping elastomers applied to energy dissipating devices. Numerical study and experimental validation, 3CSC *Third European conference on Structural Control*, Vienna, July 12–15, (2004).

[268] Mata P, Barbat AH, Oller S. Improvement of the seismic behavior of precast concrete structures by means of energy dissipating devices, 3CSC *Third European conference on Structural Control*, Vienna, July 12–15, (2004).

[269] Mata P, Barbat AH, Oller S. Seismic analysis of structures incorporating energy dissipating devices by means of numerical methods, *Computational Civil Engineering, International Symposium*, Iasi, România, May 26, (2006).

[270] Mata P, Barbat AH, Oller S. Numerical Simulation of the Seismic behavior of passively controlled precast concrete buildings, *Computational Civil Engineering, International Symposium*, Iasi, România, May 26, (2006).

[271] Mata P, Oller S, Barbat AH, Boroschek R. Numerical code for seismic analysis of structures incorporating energy dissipating devices, *First European Conference on Earthquake Engineering and Seismology*, ECEES, Geneva, Switzerland, 3–8 September, (2006).

[272] Mata P, Barbat AH, Oller S, Boroschek R. Evaluation of the seismic behavior of precast concrete buildings with energy dissipating devices, *First European Conference on Earthquake Engineering and Seismology*, ECEES, Geneva, Switzerland, 3–8 September, (2006).

[273] Mata P, Boroschek R, Barbat AH, Oller S. Numerical–experimental study of high damping elastomers for energy dissipating devices, *First European Conference on Earthquake Engineering and Seismology*, ECEES, Geneva, Switzerland, 3–8 September, (2006).

[274] Mata P, Oller S, Barbat AH, Boroschek R. Nonlinear constitutive formulation for a finite deformation beam model based on the mixing rule for composites, ECCOMAS 2007, *Thematic Conference, Mechanical Response of Composites*, Porto, Portugal, 12^{th}–14^{th} September, (2007).

[275] Mata P, Barbat AH, Oller S, Boroschek R. Desarrollo de un código numérico para el análisis no lineal de estructuras sometidas a acciones sísmicas, 3er *Congreso Nacional de Ingeniería Sísmica*, España, Gerona, May 8–11, (2007).

[276] Mata P, Barbat AH, Oller S, Boroschek R. Simulación numérica de la respuesta sísmica nolineal de edificaciones prefabricadas con disipadores de energía, 3er *Congreso Nacional de Ingeniería Sísmica*, España, Gerona, May 8–11, (2007).

[277] Mata P, Barbat AH, Oller S, Boroschek R. Evaluación del comportamiento sísmico de estructuras basado en la evolución de índices de daño, 3er *Congreso Nacional de Ingeniería Sísmica*, España, Gerona, May 8–11, (2007).

[278] Mazars J, Kotronis P, Ragueneau F, Casaux G. Using multifiber beams to account for shear and torsion. Applications to concrete structural elements, *Computer Methods in Applied Mechanics and Engineering*. 195 (2006) 7264-7281.

[279] Mazzolani FM. Passive control technologies for seismic-resistant buildings in Europe, *Progress in Structural Engineering and Materials*. 3 (2001) 277–287.

[280] McCune RW, Armstrong CG, Robinson DJ. Mixed–dimensional coupling in finite element models. *International Journal for Numerical Methods in Engineering*. 49 (2000) 725–750.

[281] Mcrobie FA, Lasenby J. Simo-Vu Quoc rods using Clifford algebra, *International Journal for Numerical Methods in Engineering*. 45 (1999) 377–398.

[282] Meek JL, Loganathan S. Large displacement analysis of space-frame structures, *Computer Methods in Applied Mechanics and Engineering*. 72 (1989) 57–75.

[283] Milenkovic VJ, Milenkovic V. Rational orthogonal approximations to orthogonal matrices, *Computational Geometry: Theory and Applications*. 7 (1997) 25–32.

[284] Shugyo M. Elastoplastic large deflection analysis of three-dimensional steel frames, *Journal of Structural Engineering*. 129 (2003) 1259–1267.

[285] Mishchenko A, Fomenko A. *A course of differential geometry and topology*, Mir Publisher, Moscow, (1988).

[286] Mitsugi J. Direct strain measure for large displacement analyses on hinge connected beam structures, *Computers and Structures*. 64 (1997) 509–517.

[287] Miyazakyi M, Mitsusaka Y. Design of a building with 20% or greater damping, *Tenth World Conference on Earthquake Engineering*, Madrid, Spain, (1992) 4143–4148.

[288] Mohd Yassina AY, Nethercotb DA. Cross-sectional properties of complex composite beams, *Engineering Structures*. 29 (2007) 195-212.

[289] Mokos VG, Sapountzakis EJ. A BEM solution to transverse shear loading of composite beams, *International Journal of Solids and Structures* 42 (2005) 3261-3287.

[290] Molta GF, Crisfield MA. A finite element formulation for 3-D continua using the co-rotational technique, *International Journal for Numerical Methods in Engineering*. 3 (1996) 3775–3792.

[291] Monaghan DJ, Doherty IW, Mc Court D, Armstrong GC. Coupling 1D beams to 3D bodies, *Proceedings*, 7th *International Meshing Roundtable*, Sandia National Lab, October (1998) 285–293.

[292] Monaghan DJ, Lee KY, Armstrong CG, Ou H. Mixed dimensional finite element analysis of frame models. *Proceedings* 10^{th} ISOPE *Conference*, May 28–June 2, Seattle, USA, 4 (2000) 263–269.

[293] Monti G, Spacone E. Reinforced concrete fiber beam element with bond-slip. *Journal of Structural Engineering*. 126 (2000) 654-661.

[294] Müller A, Maiβer P. A Lie-group formulation of kinematics and dynamics of constrained MBS and its application to analytical mechanics, *Multibody System Dynamics*. 9 (2003) 311-352.

[295] Nadler B, Rubin MB. Post-buckling behavior of nonlinear elastic beams and three-dimensional frames using the theory of Cosserat point, *Mathematics and Mechanics of Solids*. 9 (2004) 369–398.

[296] Neuenhofer A, Filippou FC. Evaluation of the nonlinear frame finite-element models, *Journal of Structural Engineering*. 123 (1997) 958–966.

[297] Neuenhofer A, Filippou FC. Geometrically nonlinear flexibility–based frame finite element, *Journal of Structural Engineering*. 124 (1998) 704–711.

[298] Noels L, Stainier L, Ponthot JP. Energy conserving balance of explicit time steps to combine implicit and explicit algorithms in structural dynamics, *Computer Methods in Applied Mechanics and Engineering*. 195 (2006) 2169-2192.

[299] Nukala PKVV, White DW. A mixed finite element for three-dimensional nonlinear analysis of steel frames, *Computer Methods in Applied Mechanics and Engineering*. 193 (2004) 2507–2545.
[300] Ogden RW. *Non-linear elastic deformations*, Dover Publications, Inc. (1997).
[301] Oliver J, Cervera M, Oller S, Lubliner J. Isotropic damage models and smeared crack analysis of concrete, *Proceedings* 2^{tnnd} ICCAADCS, Zell Am See, Austria, Pineridge Press. 2 (1990) 945–958.
[302] Oliver J. Modelling strong discontinuities in solid mechanics via strain softening constitutive equations. Part 1: Fundamentals. *International Journal for Numerical Methods in Engineering*. 39 (1996) 3575-600.
[303] Oliver J, Huespe AE, Continuum approach to material failure in strong discontinuity settings, *Computer Methods in Applied Mechanics and Engineering*. 193 (2004) 3195-3220.
[304] Oller S, Luccioni B, Barbat AH, Un método de evaluación del daño sísmico en pórticos de hormigón armado, *Revista internacional de métodos numéricos para cálculo y diseño en ingeniería*. 12 (1996) 215–238.
[305] Oller S, Oñate E, Miquel J, Botello S. A plastic damage constitutive model for composites materials, *International Journal of Solids and Structures*. 33 (1996) 2501–2518.
[306] Oller S, Oñate e, Miquel J. Mixing anisotropic formulation for the analysis of composites, *Communications in Numerical Methods in Engineering*. 12 (1996) 471–482.
[307] Oller S. *Fractura mecánica. Un enfoque global*, International Center for Numerical Methods in Engineering, CIMNE. 1 (2001).
[308] Oller S, Canet JM, Zalamea F. Composite material behavior using a homogenization double scale method, *Journal of Engineering Mechanics*. 131 (2005) 65-79.
[309] Oller S, Barbat AH. Momentcurvature damage model for bridges subjected to seismic loads, *Computer Methods in Applied Mechanics and Engineering*. 195 (2006) 4490–4511.
[310] Oñate E. Cálculo de estructuras por el método de los elementos finitos, *International Center for Numerical Methods in Engineering* CIMNE. 1 (1992).
[311] O'Reilly OM. On constitutive relations for elastic rods, *International Journal of Solids and Structures*. 35 (1998) 1009–1024.
[312] Ovesy HR, Loughlan J, GhannadPour SAM. Geometric non-linear analysis of channel sections under end shortening, using different versions of the finite strip method, *Computers and Structures*. 84 (2006) 855-872.
[313] Owen DRJ, Hilton E. *Finite elements in plasticity*, Pineridge Press Ltd, I. (1986).
[314] Pajunen S, Large elasto–plastic analysis of beams using kinematically exact elements, *Communications in Numerical Methods in Engineering*. 16 (2000) 497–504.
[315] Pampanin S. Alternative design philosophies and seismic response of precast concrete buildings. *Structural Concrete*. 4 (2003) 203–211.
[316] Pampanin S, Amaris A, Akguzel U, Palermo A. Experimental investigations on high–performance jointed ductile connections for precast frames. *First European Conference on Earthquake Engineering and Seismology*, Geneva, Switzerland, 3–8 September (2006). (Paper No 2038).
[317] Papaioannou I, Fragiadakis M, Papadrakakis M. Inelastic analysis of framed structures using the fiber approach, *Proceedings of the* 5^{th} *International Congress on Computational Mechanics* (GRACM 05), Limassol, Cyprus, 29 June 1 July, (2005).
[318] Park MS, Lee BC. Geometrically non-linear and elastoplastic three-dimensional shear flexible beam element of Von-Mises-type hardening material, *International Journal for Numerical Methods in Engineering*. 39 (1996) 383–408.
[319] Park FC, Ravani B. Smooth invariant interpolation of rotations, ACM *Transactions on Graphics*. 16 (1997) 277–295.
[320] Parulekar YM, Reddy GR, Vaze KK, Kushwaha HS. Lead extrusion dampers for reducing seismic response of coolant channel assembly, *Nuclear Engineering and Design*. 227 (2004) 175-183.
[321] Pérez Morán A. *Formulaciones tangente y secante en análisis no lineal de vigas de Cosserat*, PhD Thesis, Universitat Politècnica de Catalunya, Spain, (2005).
[322] Petrolo AS, Casciaro R. 3D beam element based on Saint Venànt's rod theory, *Computers and Structures* 82 (2004) 2471-2481.
[323] Petrov E, Géradin M. Finite element theory for curved and twisted beams based on exact solutions for three-dimensional solids. Part 1: Beam concept and geometrically exact nonlinear formulation, *Computer Methods in Applied Mechanics and Engineering*. 165 (1998) 43–92.

[324] Petrov E, Géradin M. Finite element theory for curved and twisted beams based on exact solutions for three-dimensional solids. Part 2: Anisotropic and advanced beam models, *Computer Methods in Applied Mechanics and Engineering*. 165 (1998) 93–127.

[325] Pi YL, Bradford MA. Elasto-plastic buckling and postbuckling of arches subjected to a central load, *Computers and Structures*. 81 (2003) 1811-1825.

[326] Pielorz A. Nonlinear equations for a thin beam, *Acta Mechanica*. 167 (2004) 1–12.

[327] Popescu B, Hodges DH. On asymptotically correct Timoshenko-like anisotropic beam theory, *International Journal of Solids and Structures*. 37 (2000) 535–558.

[328] Posbergh TA. *Modelling and control of mixed and flexible structures*, PhD Thesis, University of Maryland, (1988).

[329] Powanusorn S. *Effect of confinement on shear dominated reinforced concrete elements*, PhD Thesis, Texas A&M University, (2003).

[330] Rasouli SK, Yahyai M. Control of response of structures with passive and active tuned mass dampers, *The Structural Design of Tall Buildings*. 11 (2002) 1–14.

[331] Reismann, H. Finite deformation of slender beams, ZAMM -*Journal of Applied Mathematics and Mechanics*. 81 (2001) 481488.

[332] Reissner E. On one–dimensional finite–strain beam theory: the plane problem, *Journal of Applied Mathematics and Physics*. 23 (1972) 795–804.

[333] Reissner E. On one–dimensional large-displacement finite-strain beam theory, *Studies in Applied Mathematics*, LII. (1973) (2) 87–95.

[334] Rey S. *Symmetry breaking, averaging and elastic rods with high intrinsic twist*, PhD Thesis, Faculté sciences de base, École Polytechnique Fédérale de Lausanne, (2002).

[335] Reznikov BS. Analysis of the nonlinear deformation of composites with allowance for finite rotations of structural elements. Translated from *Zhurnal Prikladnoi Mekhaniki i Tekhnicheskoi Fiziki* Novosibirsk, URSS. 4 (1991) 161–165.

[336] Rhim J, Lee SW. A vectorial approach to computational modeling of beams undergoing finite rotations, *International Journal for Numerical Methods in Engineering*. 41 (1998) 527–540.

[337] Riley MA, Sadek F, Mohraz B. Guidelines for testing passive energy dissipation devices, *Proceedings, U.S./Japan Bridge Engineering Workshop*, 15^{th}, Tsukuba city, Japan, (1999).

[338] Ritto-Corrëa M, Camotin D. On the differentiation of the Rodriguez formula and its significance for the vector-like parametrization of Reissner-Simo beam theory, *International Journal for Numerical Methods in Engineering*. 55 (2002) 1005–1032.

[339] Robinson WH, Greenbank LR. An extrusion energy absorber suitable for the protection of structures during an earthquake, *Earthquake Engineering and Structural Dynamics*. 4 (2006) 251–259.

[340] Romero I, Armero F. An objective finite element approximation of the kinematics and geometrically exact rod and its use in the formulation of an energy-momentum conserving scheme in dynamics, *International Journal for Numerical Methods in Engineering*. 54 (2002) 1683–1716.

[341] Romero I. The interpolation of rotations and its application to finite element models of geometrically exact rods, *Computational Mechanics*. 34 (2004) 121–133.

[342] Rosen A, Sabag M, Givoli G. A general nonlinear structural model of a multirod (multibeam) system-I. Theoretical derivations, *Computers and Structures* 61 (1996) 617–632.

[343] Rubin MB. On the theory of a Cosserat point and shear locking in thin beams, *Communications in Numerical Methods in Engineering*. 17 (2001) 201–213.

[344] Rubin MB. A simplified implicit Newmark integration scheme for finite rotations, *Computers and Mathematics with Applications*. 53 (2007) 219–231.

[345] Ryan KR, Chopra AK. Estimating the seismic displacement of friction pendulum isolators based on non-linear response history analysis, *Earthquake Engineering and Structural Dynamics*. 33 (2004) 359–373.

[346] Saje M, Planinc I, Turk G, Vratanar B. A kinematically exact finite element formulation of planar elastic-plastic frames, *Computer Methods in Applied Mechanics and Engineering*. 144 (1997) 125–151.

[347] Saje M, Turk G, Kalagasidu A, Vratanar B. A kinematically exact finite element formulation of elastic-plastic curved beams, *Computers and Structures*. 67 (1998) 197–214.

[348] Saje M, Planinc I, Bratina S. Large displacements and instability of beam-like structural systems, *Advanced Research Workshop: Multi-physics and Multi-scale Computer Models in Non-linear Analysis and Optimal Design of Engineering Structures Under Extreme Conditions*, Bled, Slovenia, June 13–17, (2004).

[349] Sansour C, Sansour J, Wriggers E. A finite element approach to the chaotic motion of geometrically exact rods undergoing in-plane deformations, *Nonlinear Dynamics*. 11 (1996) 189–212.

[350] Sansour C, Wagner W. Multiplicative updating of the rotation tensor in the finite element analysis of rods and shells a path independent approach, *Computational Mechanics*. 31 (2003) 153-162.

[351] Schclar NL. Computational Mechanics Publications, Topics in Engineering V. 20. *Anisotropic Analysis Using Boundary Elements*, (1994).

[352] Schimizze AM. *Comparison of P–Δ analyses of plane frames using commercial structural analysis programs and current AISC design specifications*, MSc Thesis, Virginia Polytechnic Institute and State University, USA, (2001).

[353] Schulz M, Filippou F. Non-linear spatial Timoshenko beam element with curvature interpolation, *International Journal for Numerical Methods in Engineering*. 50 (2001) 761–785.

[354] Scott MH, Fenves GL. Plastic hinge integration methods for the force-based beam-column elements, *Journal of Structural Engineering*. 132 (2006) 244–252.

[355] Shao Y, Aval S, Mirmiran A. Fiber-element model for cyclic analysis of concrete-filled fiber reinforced polymer tubes, *Journal of Structural Engineering*. 131 (2005) 292–303.

[356] Shen KL, Soong TT. Design of energy dissipation devices based on concept of damage control, *Journal of Structural Engineering*. 122 (2005) 76–82.

[357] Shi G, Atluri SN, Elasto–plastic large deformation analysis of space–frames: a plastic hinge and stress–based explicit derivation of tangent stiffness, *International Journal of Numerical Methods in Engineering*. 26 (1988) 589–615.

[358] Shim KW, Monaghan DJ, Armstrong CG. Mixed dimensional coupling in finite element stress analysis, 10^{th} *International Meshing Roundtable*, Sandia National Laboratories, Newport Beach, California. (2001) 269–277.

[359] Shim KW, Monaghan DJ, Armstrong CG. Mixed dimensional coupling in finite element stress analysis, *Engineering with Computers*. 18 (2002) 241-252.

[360] Simmonds JG. A simple nonlinear thermodynamic theory of arbitrary elastic beams, *Journal of Elasticity*. 81 (2005) 51-62.

[361] Simo JC, Hjelmstad KD, Taylor RL. Numerical simulations of elasto–viscoplastic response of beams accounting for the effect of shear, *Computer Methods in Applied Mechanics and Engineering*. 42 (1984) 301–330.

[362] Simo JC. A finite strain beam formulation. The three-dimensional dynamic problem. Part I, *Computer Methods in Applied Mechanics and Engineering*. 49 (1985) 55–70.

[363] Simo JC, Vu-Quoc L. A three-dimensional finite-strain rod model. Part II: Computational aspects, *Computer Methods in Applied Mechanics and Engineering*. 58 (1986) 79–116.

[364] Simo JC, Ju J. Strain and stress based continuum damage models–Part I: formulation, *International Journal of Solids and Structures*. 23 (1987) 281–301.

[365] Simo JC, Vu-Quoc L. On the dynamics in space of rods undergoing large motions - A geometrically exact approach, *Computer Methods in Applied Mechanics and Engineering*. 66 (1988) 125–161.

[366] Simo JC, Fox DD. On a stress resultant geometrically exact shell model. Part I: Formulation and optimal paramtrization, *Computer Methods in Applied Mechanics and Engineering*. 72 (1989) 267–364.

[367] Simo JC, Fox DD, Rifai MS. On a stress resultant geometrically exact shell model. Part II: Linear theory; computational aspects, *Computer Methods in Applied Mechanics and Engineering*. 73 (1989) 53–92.

[368] Simo JC, Fox DD, Rifai MS. On a stress resultant geometrically exact shell model. Part III: Computational aspects on the nonlinear theory, *Computer Methods in Applied Mechanics and Engineering*. 79 (1990) 21–70.

[369] Simo JC, Rifai MS, Fox DD. On a stress resultant geometrically exact shell model. Part IV: Variable thickness shells with through-the-thickness stretching, *Computer Methods in Applied Mechanics and Engineering*. 81 (1990) 91–126.

[370] Simo JC, Vu-Quoc L. A geometrically-exact rod model incorporating shear and torsion-warping deformation, *International Journal of Solids and Structures*. 27 (1991) 371–393.
[371] Simo JC. The (symmetric) Hessian for geometrically nonlinear models in solid mechanics: Intrinsic definition and geometric interpretation, *Computer Methods in Applied Mechanics and Engineering*, 96 (1992) 189–200.
[372] Simo JC, Tarnow N, Wong KK. Exact energy-momentum conserving algorithms and symplectic schemes for nonlinear dynamics, *Computer Methods in Applied Mechanics and Engineering*. 100 (1992) 63–116.
[373] Simo JC, Tarnow N, Doblare M. Non–linear dynamics of three-dimensional rods: exact energy and momentum conserving algorithms, *International Journal for Numerical Methods in Engineering*. 34 (1992) 117–164.
[374] Simo JC, Kennedy JG. On a stress resultant geometrically exact shell model. Part V. Nonlinear plasticity: formulation and integration algorithms, *Computer Methods in Applied Mechanics and Engineering*. 96 (1992) 133–171.
[375] Simo JC. On a stress resultant geometrically exact shell model. Part VII. Shell intersections with 5/6 DOF finite element formulations, *Computer Methods in Applied Mechanics and Engineering*. 108 (1993) 319–339.
[376] Simo JC, Rifai MS, Fox DD. Stress resultant geometrically exact shell model. Part VI: Conserving algorithms for nonlinear dynamics, *International Journal for Numerical Methods in Engineering*. 38 (1995) 1431–1473.
[377] Simo JC, Hughes TJR. *Computational Inelasticity*, Springer Velag, 7 (1997).
[378] Sivaselvan MV, Reinhorn AM. Collapse analysis: large inelastic deformations analysis of planar frames, *Journal of Structural Engineering*. 128 (2002) 1575–1583.
[379] Smith LM, Griffiths DV. *Programming the finite element method*, (2^{th} Ed.) John Wiley & Sons Ltd, (1988).
[380] Smoleński WM. Statically and kinematically exact nonlinear theory of rods and its numerical verification, *Computer Methods in Applied Mechanics and Engineering*. 178 (1999) 89–113.
[381] Snir M, Otto S, Huss-Lederman S, Walker D, Dongarra J. MPI *The complete reference* Vol. 1, *The* MPI *Core*, 2nd Ed. Massachusetts Institute of Technology, (1998).
[382] Soong TT, Dargush GF. *Passive energy dissipation systems in structural engineering*, John Wiley & Soms, Ltd. (1997).
[383] Soong TT, Spencer JBF. Supplemental energy dissipation: state-of-the-art and state-of-the-practice, *Engineering Structures*. 24 (2002) 243-259.
[384] Spacone E, El-Tawil S. Nonlinear analysis of steel–concrete composite structures: state of the art, *Journal of Structural Engineering*. 130 (2004) 159–168.
[385] Spencer Jr BF, Nagarajajah S. State of the art of structural control, *Journal of Structural Engineering*. 129 (2003) 845–856.
[386] Spiliopoulos KV, Lykidis GCh. An eficient three-dimensional solid finite element dynamic analysis of reinforced concrete structures, *Earthquake Engineering and Structural Dynamics*. 35 (2) (2005) 137–157.
[387] Stammers CW, Sireteanu T. Control of building seismic response by means of three semi-active friction dampers, *Journal of Sound and Vibration*. 237 (2000) 745–759.
[388] Steinmann P. On the spatial and material settings of thermo-hyperelastodynamics, *Journal of Elasticity*. 66 (2002) 109–157.
[389] Stuelpnagel J. On the parametrization of the three-dimensional rotation group, SIAM *Review*. 6 (1964) 422–430.
[390] Taucer FF, Spacone E, Filipou FC. *A fiber beam-column element for seismic response analysis of reinforced concrete structures*, Technical Report No UCB/EERC-91/17. Earthquake Engineering Research Center, University of California, Berkeley, (1991).
[391] Teh LH, Clarke MJ. Symmetry of tangent stiffness matrices of 3D elastic frame, *Journal of Engineering Mechanics*. 125 (1999) 0248-0251.
[392] Thanoon WA, Hamed AMM, Noorzaei J, Jaafar MS, Al-Silayvani BJ. Inelastic analysis of composite sections, *Computers and Structures*. 82 (2004) 1649-1656.
[393] Towashiraporn P, Park J, Goodno BJ, Craig JI. Passive control methods for seismic response modification, *Progress in Structural Engineering and Materials*. 4 (2002) 47–86.

[394] Trainelli L. *The vectorial parametrization of rotation and motion*, Technical Report, Politecnico di Milano, Dipartimento de Ingegneria Aerospaziale, (2002).

[395] Tso WK, Moghadam AS. Pushover procedure for seismic analysis of buildings, *Progress in Structural Engineering and Materials* 3 (1998) 337–344.

[396] Turkalj G, Brnic J, Prpic-Orsic J, ESA formulation for large displacement analysis of framed structures with elastic–plasticity, *Computers and Structures*. 82 (2004) 2001–2013.

[397] Wada A, Huang YH, Iwata M. Passive damping technology for buildings in Japan, *Progress in Structural Engineering and Materials*. 2 (2000) 335–350.

[398] Wagner W, Gruttmann F. Finite element analysis of Saint-Venant torsion problem with exact integration of the elastic-plastic constitutive equations. *Computer Methods in Applied Mechanics and Engineering*. 190 (2001) 3831–3848.

[399] Wen Yu, Hodges DH, Volovoi V, Cesnik CES. On Timoshenko-like modeling of initially curved and twisted composite beams, *International Journal of Solid and Structures*. 39 (2002) 5101–5121.

[400] Wenzel M. Consistent transition of beam–shell structures within the FE method. PAMM *Proceedings in Applied Mathematics & Mechanics*. 3 (2003) 320-321.

[401] Wen YK. Method for Random Vibration of Hysteretic Systems, *Journal of the Engineering Mechanics Division*. 102 (1976) 249–263.

[402] West M. *Variational integrators*, PhD Thesis, California Institute of Technology, USA, (2004).

[403] Williamson EB. Evaluation of damage and P-Δ effects for systems under earthquake excitation, *Journal of Structural Engineering*. 129 (2003) 1036–1046.

[404] Wisniewski K. Finite rotation quadrilateral element for multi-layer beams, *International Journal of Solid and Structures*. 44 (1999) 405–431.

[405] Wolfe RW, Masri SF, Caffrey J. Some structural health monitoring approaches for nonlinear hydraulic dampers, *Journal of Structural Control*. 9 (2002) 5–18.

[406] Yang YB, Leu LJ. Constitutive laws and force recovery procedures in nonlinear analysis of trusses, *Computer Methods in Applied Mechanics and Engineering*. 92 (1991) 121–131.

[407] Yang JN, Kim YH, Agrawal AK. Resseting semiactive stiffness damper for seismic response control, *Journal of Structural Engineering*. 126 (2000) 1427–1433.

[408] Yeung N, Pan ADE. The effectiveness of viscous-damping walls for controlling wind vibrations in multi-story buildings, *Journal of Wind Engineering and Industrial Aerodynamics*. (77–78) (1998) 337–348.

[409] Youssef N. Viscous dampers at multiple levels for the historic preservation of the Los Angeles City Hall, *The Structural Design of Tall Buildings*. 10 (2001) 339–350.

[410] Yu W, Hodges DH. Elasticity solutions versus asymptotic sectional analysis of homogeneous, isotropic, prismatic beams, *Journal of Applied Mechanics*. 71 (2004) 15–23.

[411] Yu AM, Yang XG, Nie GH, Generalized coordinate for warping of naturally curved and twisted beams with general cross–sectional shapes, *International Journal of Solids and Structures*. 43 (2006) 2853–2867.

[412] Yu W, Volovoi VV, Hodges DH, Hong X. Validation of the variational asymptotic beam sectional analysis, *Journal of the American Institute of Aeronautics and Astronautics*. 40 (2002) 2105–2112.

[413] Yu W, Hodges DH, Volovoi V, Cesnik CES. On Timoshenko-like modeling of initially curved and twisted composite beams, *International Journal of Solids and Structures*. 39 (2002) 5101–5121.

[414] Yu W, Hodges DH. Elasticity solutions versus asymptotic sectional analysis of homogeneous, isotropic, prismatic beams, *Journal of Applied Mechanics*. 71 (2004) 15–23.

[415] Uriz P, Whittaker AS. Retrofit of the pre-Northridge steel moment-resisting frames using fluid viscous dampers, *The Structural Design of Tall Buildings*. 10 (2001) 371–390.

[416] Valles RE, Reinhorn AM, Kunnath SK, Li C, Madan A. IDARC 2D Version 4.0: *A Program for the Inelastic Damage Analysis of Buildings*, Technical Report No NCEER-96-0010. National center for earthquake engineering research, State University of New York at Buffalo, January 8, (1996).

[417] Vieira EW. *A three dimensional setting for strong discontinuities modelling in failure mechanics*, PhD Thesis, Technical University of Catalonia, (2003).

[418] Vignjevic R. A hybrid approach to the transient collapse analysis of thin walled frameworks I, *Computer Methods in Applied Mechanics and Engineering*. 148 (1997) 407–421.

[419] Vignjevic R. A hybrid approach to the transient collapse analysis of thin walled frameworks II, *Computer Methods in Applied Mechanics and Engineering*. 148 (1997) 423–437.

[420] Volovoia VV, Hodges DH, Berdichevsky VL, Sutyrin VG. Asymptotic theory for static behavior of elastic anisotropic I–beams, *International Journal of Solids and Structures*. 36 (1999) 1017–1043.

[421] Vu-Quoc L, Li S. Dynamics of sliding geometrically-exact beams: large angle maneuver and parametric resonance, *Computer Methods in Applied Mechanics and Engineering*. 120 (1995) 65–118.

[422] Vu-Quoc L. Deng H, Ebcioğlu IK. Multilayer beams: A geometrically exact formulation, *Journal of Nonlinear Science*. 6 (1996) 239-270.

[423] Vu-Quoc L. Deng H. Dynamics of geometrically-exact sandwich beams/1-D plates: computational aspects, *Computer Methods in Applied Mechanics and Engineering*. 146 (1997) 135–172.

[424] Xue Q, Meek JL. Dynamic response and instability of frame structures, *Computer Methods in Applied Mechanics and Engineering* 190 (2001) 5233–5242.

[425] Zamm ZA, Itzkov M. The derivative with respect to a tensor: some theoretical aspects and applications, *Mathematical Mechanics*. 82 (2002) 535–544.

[426] Zhi-da C. On the Representation of finite rotation in nonlinear field theory of continuum mechanics, *Applied Mathematics and Mechanics*. 7 (1986) 1017–1026.

[427] Živković M, Kojić M, Slavković R, Grujović N. A general beam finite element with deformable cross-section, *Computer Methods in Applied Mechanics and Engineering*. 190 (2001) 2651–2680.

[428] Ziyaeifara M, Noguchi H. A refined model for beam elements and beam–column joints, *Computers and Structures*. 76 (2000) 551–564.

[429] Zupan D, Saje M. Finite-element formulation of geometrically exact three-dimensional beam theories based on interpolation of strain measures, *Computer Methods in Applied Mechanics and Engineering*. 192 (2003) 5209-5248.

[430] Zupan D, Saje M. The three-dimensional beam theory: Finite element formulation based on curvature, *Computers and Structures*. 81 (2003) 1875-1888.

[431] Zupan D, Saje M. Analytical integration of stress field and tangent material moduli over concrete cross-sections, *Computers and Structures*. 83 (2005) 2368–2380.

[432] Zupan D, Saje M. The linearized three-dimensional beam theory of naturally curved and twisted beams: The strain vectors formulation, *Computer Methods in Applied Mechanics and Engineering*. 195 (2006) 4557-4578.

Technical University of Catalonia, UPC, Barcelona, Spain, February, 2008.